CRANFIELD UNIVERSITY

SCHOOL OF MECHANICAL ENGINEERING

SIMON JAMES BOURNE

NOVEL HYDROPHILIC POLYMER COUPLANT FOR APPLICATION IN ULTRASONIC NON DESTRUCTIVE TESTING

PHD THESIS

CRANFIELD UNIVERSITY

SCHOOL OF MECHANICAL ENGINEERING

ACADEMIC YEAR 1997-2001

SIMON JAMES BOURNE

NOVEL HYDROPHILIC POLYMER COUPLANT FOR APPLICATION INULTRASONIC NON DESTRUCTIVE TESTING

PhD THESIS

SUPERVISORS: MARCUS NEWBOROUGH

DONALD HIGHGATE

SPONSORS: SONATEST PLC

Abstract

Ultrasonic Non Destructive Testing (NDT) is used to inspect materials and structures for defects. Water is commonly used in NDT as a couplant to improve ultrasonic transfer between an interrogating probe and test piece. Unfortunately, the presence of water can cause corrosion and/or degradation of the test piece material. The aim of this investigation was to evaluate hydrated cross-linked hydrophilic polymers as candidate solid contact ultrasonic couplant for use in the field of ultrasonic NDT.

The fact that hydrophilic polymers can absorb and retain large quantities of water suggested that they might demonstrate the desirable ultrasonic properties of water without the risks associated with conventional water coupling. To test this, the ultrasonic properties of a range of hydrophilic polymers were assessed. Excellent results were achieved, attenuation as low as 0.36 and 0.71dB mm^{-1} at 5 and 10MHz respectively being measured. Great potential for efficient coupling was established due to acoustic impedance in the region of 1.8MN s m^{-3}.

A polymer dependant coupling pressure of less that 1kg cm^{-2} was required to achieve optimum coupling to a smooth steel block. Mechanical longevity, evaluated by life testing, showed that polymers of up to 70% equilibrium water content were best suited for dynamic testing applications. Temperature was shown to effect ultrasonic properties; a drop from 5 to -12°C caused an increase in attenuation of 3dB mm^{-1} and velocity of 350m s^{-1}. Pressure demonstrated no influence on attenuation but affected an increase in velocity of 44m s^{-1} per kg cm^{-2}. Further investigation into the unique ultrasonic properties of hydrophilic polymers showed that the water sorption process caused an increase in attenuation prior to saturation being reached. This was attributed to the absorption of sound during the polymer transformation from the glassy to rubbery condition observed during hydration. Dehydration from 100 to 37% saturation in a 60% equilibrium water content polymer caused an increase in attenuation of 1.8dB mm^{-1} at 5MHz.

The research concluded with the design and development of a prototype wheel probe employing hydrophilic polymer as the tyre. Operation at 5MHz in pulse echo mode demonstrated results competitive to conventional immersion testing. An MMA-VP cross-linked hydrophilic polymer of approximately 60% equilibrium water content was found most suitable to this application.

This thesis suggests that there is a clear role for hydrophilic polymers in ultrasonic NDT. The success of the wheel probe design developed as a result of this research has resulted in patent application in both the UK and USA.

Table of Contents

List of Figures

Chapter 5

List of Tables

Notation

B_D	Beam diameter	m
C	Plate thickness	m
D	Transducer crystal diameter	m
E	Young's modulus	N m^{-2}
f	Frequency	Hz
F	Focal length	m
F_Z	Focal zone	m
N	Near field length	m
V	Velocity of sound	m s^{-1}
V_C	Velocity of a compression wave	m s^{-1}
V_S	Velocity of a shear wave	m s^{-1}
Z	Acoustic Impedance	N s m^{-3}

Greek Symbols

α	Beam divergence half angle	o
α_i	Angle of incidence	o
α_s	Reflected shear wave angle	o
β_c	Refracted compression wave angle	o
β_s	Refracted shear wave angle	o
δ	Partial charge	+/-
λ	Wavelength	m
μ	Attenuation	dB mm^{-1}
ρ	Density	kg m^{-3}
σ	Poission's ratio	

Acronyms

AN	Acrylonitrile
FFT	Fast Fourier Transform
HEMA	Hydroxyethylmethacrylate
MMA	Polymethylmethacrylate
NDT	Non Destructive Testing
QA	Quality Assurance
SDMS	Sonatest Data Management Software
VP	Vinyl Pyrrolidone

Chapter 1 : The Project

1.1 Introduction

The inspection of materials is becoming an ever more important topic as the range of applications to which they are put continues to increase. In particular there is a growing trend for the use of composites in safety critical structures in the aerospace industry. This has resulted in a demand for new tools and techniques that allow the inspection of such structures, both during manufacture and in service, for unwanted defects. Historically, quality assurance (QA) involved destructive testing, which even where it is applicable is time-consuming, wasteful and expensive. Today, a wide range of non-destructive testing (NDT) techniques including ultrasonics, eddy current, radiography, magnetic particle, acoustic emission, dye penetrant and thermal imaging are at the disposal of QA and condition monitoring personnel, helping to make material inspection more reliable and economic. Ultrasonic testing is one of the most commonly used NDT techniques and it is to this field that this work aims to contribute.

1.1.1 Ultrasonic Testing and the Importance of a Couplant

Ultrasonic testing involves the generation of mechanical vibrations in a transmitting probe and their propagation through the component under test (test piece). The regular motion of these vibrating particles is measured in terms of frequency (in Hertz). If the frequency is above 20,000 Hz, the mechanical vibrations (sound waves) are referred to as ultrasound. As the ultrasound travels through the test piece, it undergoes a degree of modification before reception by the transmitting or dedicated receiver probe. It is the extent and nature of modification that is influenced by the host material and used to assess the material condition.

Efficient transfer of ultrasound between the probe and test piece is critical for reproducible ultrasonic testing. The interface between an ultrasonic probe and test piece held in pressed contact is mainly occupied by air, with contact being made only over very small areas. This situation is exacerbated by particularly rough surfaces. The transmission of ultrasound across such an interface is extremely inefficient owing to the large acoustic impedance mismatch between air and solid materials. This problem is usually overcome by the employment of a liquid coupling media (e.g. water) between the probe and test piece; most commonly by the application of a gel or by submersion of the entire test piece in a water tank. In this way ultrasonic transfer is

immensely improved as the coupling media fills the air gaps between the probe and test piece.

Coupling gels are used for manual testing where point measurements are required. A typical application would be thickness metering, routinely carried out as a manufacturing process and on many structures including storage vessels, ship hulls and pipelines. Where a greater portion of the test piece is to be interrogated, a degree of scanning is required of the probe. This is most efficiently achieved by immersing the probe and test piece in water. In this way complex geometries can be accommodated and the probe may be scanned over the test piece without making physical contact. The water ensures a very consistent level of ultrasound transfer as it flows readily into surface undulations. A full review of ultrasonic NDT is provided in Appendix A.

1.1.2 Current Limitations

Water is and will remain an excellent couplant because of its superior ultrasonic properties but its use with many materials including modern composite systems poses great problems:

- Practically it involves immersion of the complete test piece, which is both expensive and difficult to achieve in large structures such as aircraft wings and helicopter rotors.

- Prolonged contact can cause contamination and/or degradation of the test piece material.

- Composite structures frequently fail by delamination, which is detectable by ultrasound because of the resulting air filled gap. The materials are not electrically conducting and are therefore not suitable for eddy current or magnetic examination. Ultrasonic inspection is ideal but if water couplant is used it often finds its way into the delamination and both prevents detection and prejudices any attempt at rectification.

It is therefore clear that a new approach to non-liquid couplants is essential.

1.1.3 Potential of Solid Couplants

Solid contact couplants potentially offer a means for overcoming the limitations associated with liquid couplants. Flexible solids are able to

conform to surface undulations when put under moderate pressure and thus exclude air greatly enhancing the area of contact between two solid surfaces. This offers great scope for improved ultrasonic transmission between a probe and test piece without the risks suffered with fluid couplants. Unfortunately, compliance is achieved at the expense of mechanical longevity. In addition, many conventional materials exhibiting the high level of flexibility required for coupling applications tend also to exhibit high attenuation of ultrasound. Devices incorporating solid couplants tend to employ stiff rubbers in order to achieve good resistance to wear. However, the ultrasonic properties of these materials are poor, greatly reducing the usefulness of the devices. Solid couplants that provide relatively little attenuation would be most advantageous.

1.1.4 Hydrophilic Polymers

Cross-linked hydrophilic polymer technology represents an entirely new approach to the production of a high water content material of controllable elastic properties. Originally developed between 1965 and 1980 for biomedical applications, the material consists of a polymer skeleton containing chemical sites to which water molecules are attracted ionically. The result is a family of polymeric materials characterised by the ability to take in (by absorption and adsorption) up to 95% water by wet weight.

In this form, they are soft, elastic and conformable and while largely comprised of water it is in a form which cannot be squeezed out. For these reasons hydrophilic polymers appeared to be candidates for the development of a novel couplant system sharing the ultrasonic properties of water but free from the problems associated with the use of liquid water.

1.2 Aims and Objectives

The aim of this project was to research the ultrasonic properties of a range of hydrophilic polymers and consider the feasibility of employing them as novel, solid contact ultrasonic couplants. This involved researching:

- The acoustic properties of a range of hydrophilic polymers with respect to ultrasound transmission,

- The material properties relevant to the transmission of ultrasound across interfaces of industrial interest,

- The potential for manipulation of polymer properties and their affects on ultrasound transmission,

- The optimal polymer(s) for specific NDT applications,

- The method(s) of polymer application,

- The design options for an ultrasonic probe employing hydrophilic polymers.

This project was sponsored by Sonatest PLC who supplied all of the ultrasonic equipment used (see Appendix B)

Chapter 2: Hydrophilic Polymers as Prospective Ultrasonic Couplants

2.1 Introduction to Hydrophilic Polymers

Cross-linked hydrophilic polymers are described as macromolecular networks that swell but do not dissolve in water [Highgate, 1989 and Mathur, 1996]. This is an apparently contradictory condition, as the material may consist mainly of water, yet it is in solid form and dry to the touch. Hydrophilic polymers achieve this situation by combining hydrophilic (water soluble) and hydrophobic (water insoluble) monomers into a cross linked structure. The ability of hydrophilic polymers to absorb water arises from hydrophilic functional groups attached to the polymeric backbone, while their resistance to dissolution is due to cross-links between the network chains [Kalal, J. Circa. 1980]. When dehydrated the polymers are hard with typical machining properties characteristic of the hydrophobic component (Perspex in the case of MMA-VP copolymers). Placing them in water allows them to hydrate over time until they reach equilibrium [Maffezzoli et al, 1996 and Maffezzoli et al. 1998].

Cross-linked hydrophilic polymers are available in both homopolymer and copolymer forms. Homopolymers are single molecular species and are restricted to relatively low water uptake. Hydrophilic copolymers are essentially made up of two monomer constituents – hydrophilic and hydrophobic. The hydrophobic part (e.g. MMA) provides the long-term structure of the final material whereas the hydrophilic part provides hydration sites (e.g. OH or N). It is to these sites that water bonds. In addition, an amount of free water enters the inter-molecular voids caused by the initial hydration expansion of the polymer. The amount of water absorbed by a hydrophilic copolymer is dictated by the ratio of hydrophilic to hydrophobic components and the degree of cross-linking.

Complete hydration is reached after a period depending on the final water uptake capacity of the polymer together with the surface area to volume ratio. Water advances through the polymer as a front leaving two clearly defined regions (hydrated and dehydrated) [Maffezzoli, et al, 1996]. The water acts as a plasticiser causing the polymer to expand and become flexible. The polymers resistance to dissolution will be discussed in more detail in section 2.1.2. Suffice to say that cross-links play the largest role in the materials investigated in this research. The cross-links also guarantee a predictable expansion ratio.

An important practical aspect of hydrophilic polymer technology is the associated chemical flexibility. As the quantity of the hydrophilic component of a copolymer may be easily controlled, the ultimate water content on full hydration may be accurately defined. Similarly, the hydrophobic (or backbone) component can comprise of a number of different polymers providing alternative mechanical properties for the final hydrated material. Indeed, conventional hydrophilic polymers have low notch-tear strength. Suitable choice of monomer system and polymer fabrication method can dramatically improve tear strength and therefore the longevity in arduous environments [Highgate, 1974 and 1975]. The same authors have shown that repeated hydration and dehydration cycles do not result in any degradation of the polymer structure.

2.1.1 The Definition of 'Hydrophilic'

A chemical will be a solvent to another material if the attraction between it and the material is stronger than the mutual attraction (i.e. solvent-solvent and material-material). Therefore, a polymer will be soluble in water if the water-polymer attractions are greater than the polymer-polymer and water-water attractions. On the other hand, a polymer will be insoluble in water if the polymer-polymer and water-water attractions are stronger than those between the water-polymer are. The intermediate case is where there are water-polymer, water-water and polymer-polymer attractions and sufficient cross-links to define a stable long range structure. It is these types of polymer that swell when immersed in water and are termed hydrophilic [Highgate, 1989].

2.1.2 Intermolecular Attractions

Attractions between polymer molecules and water molecules arise due to partial negative and partial positive charges associated with different atoms in the system. These charges arise owing to polarity in certain covalent bonds. The polarity exists because atoms of high electronegativity attract the bond electrons closer to them, setting up an uneven distribution of electrons. For example oxygen and nitrogen atoms adopt a partial negative charge when covalently bonded to carbon or hydrogen atoms which by definition causes the carbon or hydrogen atoms to adopt a partially positive charge. It is the partial charge of an atom on one molecule that is attracted to an oppositely partially charged atom on another molecule that is the basis of ionic bonding between the polymer chains and water molecules.

This same process also accounts for a degree of natural intermolecular attraction between hydrophilic polymer molecules. However, the most significant bonding between the polymer chains is that of chemical cross-links, the density and length of which are of prime importance. These bonds are one or two orders of magnitude stronger than ionic bonds between polymer and water molecules. As a result, hydrophilic polymers can be dried out (in a vacuum oven) and subsequently rehydrated without degradation of the polymers. Physical entanglements of the polymer chains due to high molecular weight can also contribute to apparent intermolecular attraction.

It may therefore be said that if partial positive and partial negative charges exist in polymer molecules, their density together with the nature of the polymer-polymer attractions described above, will dictate if the polymer is soluble or not in water. If the polymer swells in water, then these factors will ultimately control the extent.

Two classes of hydrophilic material, which differ by virtue of their water attracting centres (i.e. the polar bonds), are discussed. The first group relies on the electronegativity of oxygen to provide the water-attracting sites. Such a system is polyhydroxyethylmethacrylate (HEMA) the most significant part of the repeating polymer unit is represented in Figure 2.1. The δ symbol represents the partial charges.

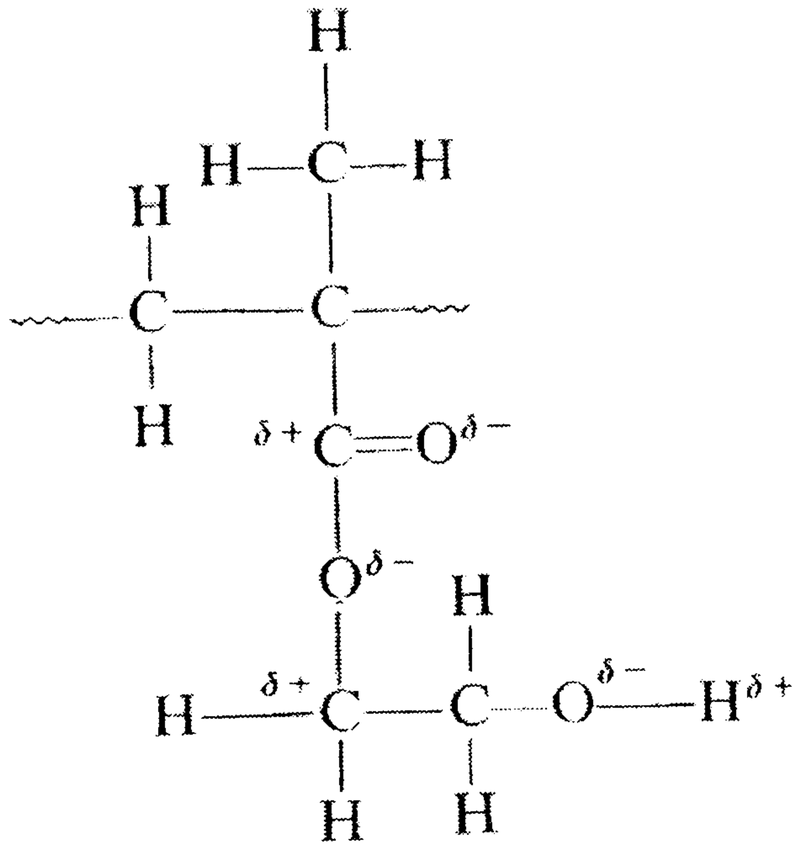

Figure 2.1 Repeat polymer unit of HEMA showing the partial positive and negative charges.

The water and polymer attracting sites are the partial positive and partial negative charges. These centres are those which will attract opposite partial charges on the water molecule. The oxygen and hydrogen atoms are especially important due to their exposed nature and attraction with opposite partial charges in different parts of the polymer molecule which controls the

water attraction. This is shown schematically in Figure 2.2 a) and b), the dotted lines in which represent hydrogen bonds. Although only one bond is shown per atom, in reality, many would exist owing to bonding occurring in three dimensions.

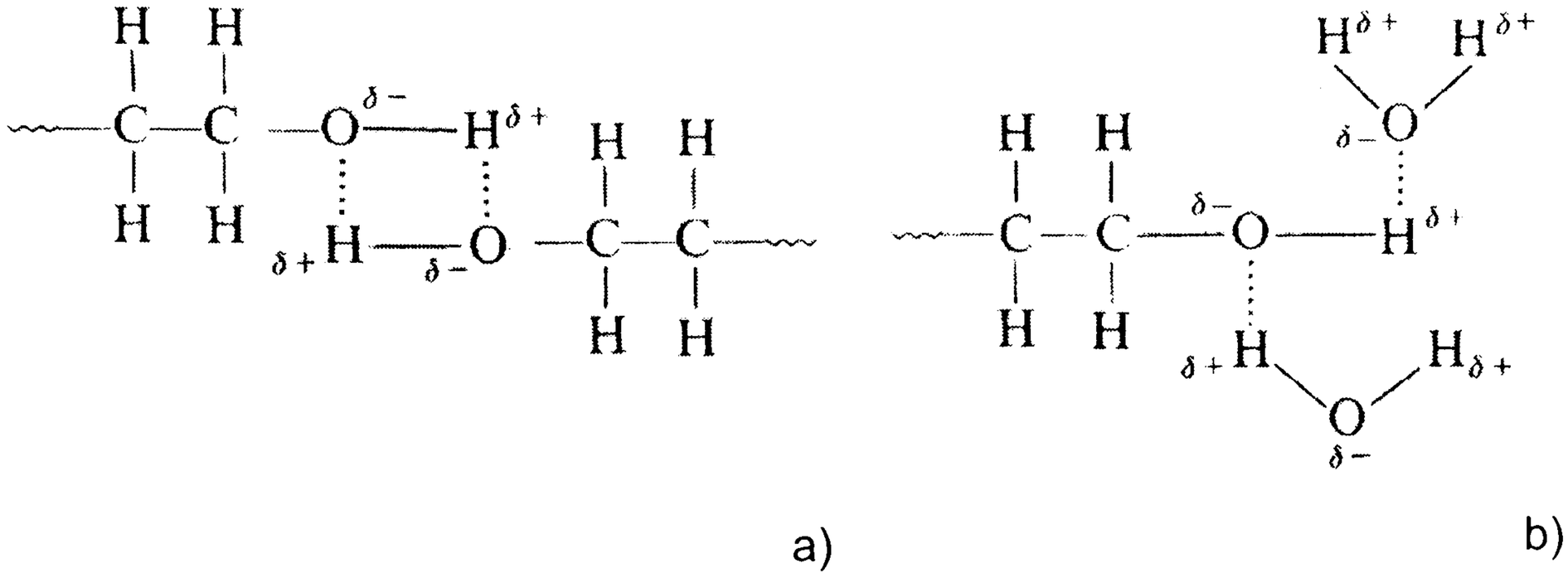

a) b)

Figure 2.2 Intermolecular attractions, a) polymer-polymer and b) polymer-water, in HEMA

Although the carbon-oxygen double bond is polar, its effect on inter-polymer and polymer-water attraction is insignificant in comparison with the O-H function and may be neglected [Gehrke, 1993]. The stability of these polymers is achieved by cross-linking rather than relying solely on the hydrogen bonds between the polymer chains. A further form of this material is shown in Figure 2.3.

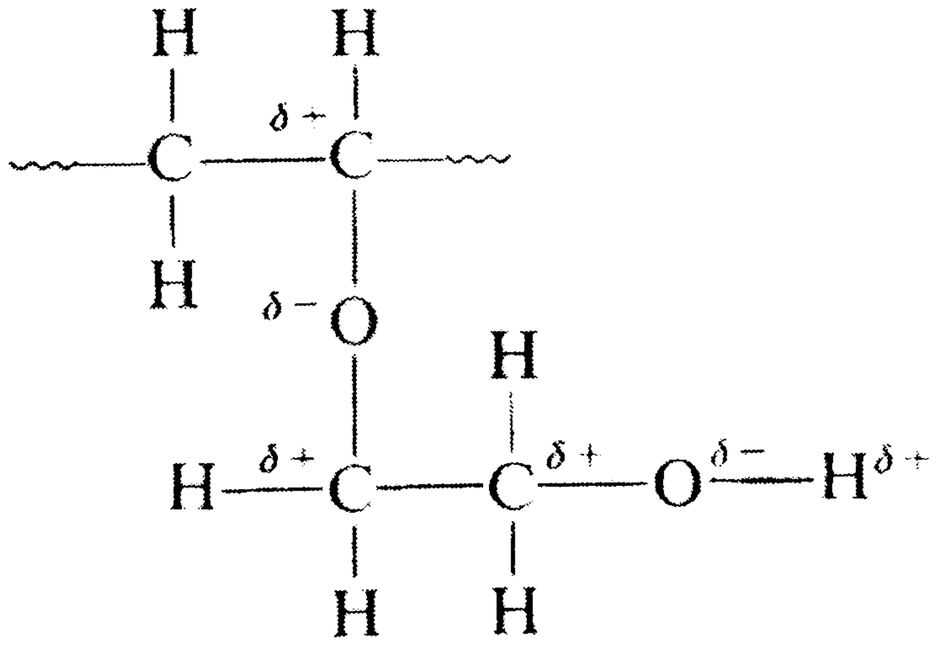

Figure 2.3 Alternative form of HEMA showing partial positive and negative charges.

The second group of materials relies on the polarity of the carbon-nitrogen bond in N-vinyl, 2, pyrrolidone as the main water-attracting centre. Again the carbon-oxygen double bond contributes little to the polymer-polymer and polymer-water attractions and may be ignored. The partial negative charge of the nitrogen atom is relatively shielded and the pyrrolidone group is

non-flexible and bulky. Therefore, there is a reduction in polymer-polymer attractions, but not in polymer-water attractions. In fact, this material is soluble in water unless it is (i) cross-linked, (ii) has a very high molecular weight, or (iii) polymerised with a hydrophobic monomer, which reduces the density of the pyrrolidone rings. A combination of cross-linking and co-polymerisation is normally used to control the final water content and physical properties of these materials when wet. The significant repeat unit is shown in Figure 2.4.

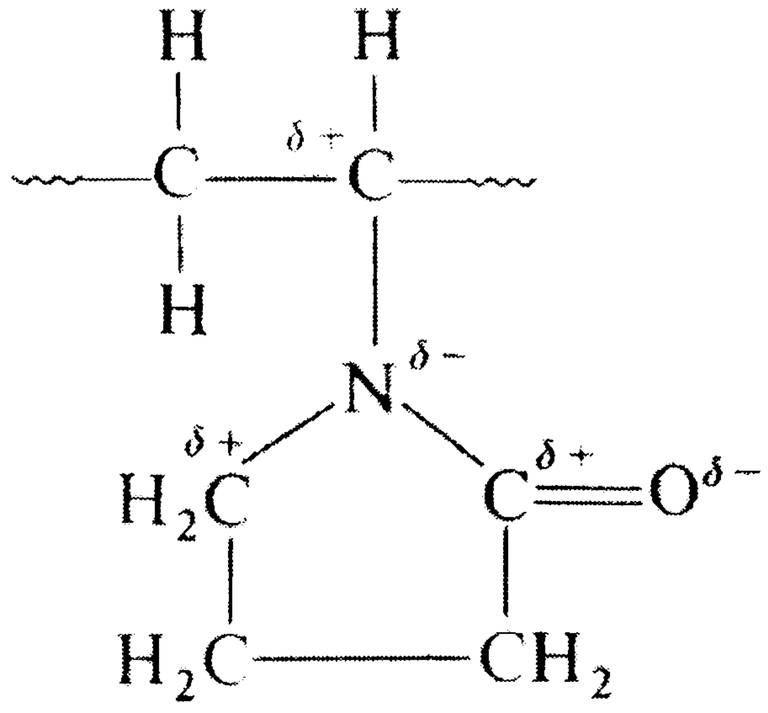

Figure 2.4 Repeat unit in N-Vinyl, 2, pyrrolidone showing partial positive and negative charges.

2.1.3 Hydration Mechanisms

The hydration characteristics of these materials (i.e. their water uptake and consequent linear expansion) are related to the chemical structure as follows:

(a) The water-attracting centres, within the polymer system, give rise to what is described as 'bound' water. This is that part of the total water content which is absorbed most readily: it enters the material at an early stage in hydration and is the most difficult to remove subsequently.

(b) A second important factor is the extent of the polymer-polymer interactions (both polar attractions and chemical cross-links) and also the size and flexibility of any side groups attached to the polymer backbone. It is generally held that strong polar interactions and/or the high density of short cross-links and small flexible side groups give rise to small polymer-free zones. These limit the volume available for the simple absorption of water, as opposed to the moisture that is chemically bound in the structure. Such unattached moisture is generally known as 'free' water and occupies the polymer-free zones around the polymer molecules. It is part of the total

moisture content that partakes in osmotic reactions and most easily moves into, or out of, the hydrated hydrophilic material.

2.1.4 Hydrophilic Polymer Fabrication

The co-polymerisation of a bulk monomer-liquid mixture may be performed by one of three routes – chemical, irradiation or ultra violet. The chemical route necessitates the use of a suitable initiator and cross-linking agent [Kudela, 1990]. The mix is placed into a disposable plastic mould and heated (as it is usual for the initiator to be temperature activated). The reaction is exothermic which frequently necessitates water cooling [Gehrke, 1993].

Alternatively, irradiation may be used. This approach just requires that the two liquid monomers are well mixed. Irradiating with electron beam or γ radiation generates free radical sites which facilitate polymerisation and cross-linking on recombination.

Both chemical and irradiation techniques result in a solid material confined to its mould. Blanks are small stubs/sections cut from a larger cast cylinder. These blanks may be in turn machined to specified dimensions. If however, accurate sacrificial moulds are used, only minor finishing steps such as edge buffing may be required. If this process can be optimised, it makes for a highly efficient route to finished component production. [Kudela, 1990]

The use of ultra-violet irradiation for the polymerisation of hydrophilic polymers is quite limited due to their low penetrating power compared with electron beam or γ radiation. Therefore, this technique tends to be used solely for the polymerisation of thin membrane components of less than 1mm thickness. Typically the monomer mix is spread externally onto a suitably shaped mould and subjected to ultraviolet rays for a time sufficient to allow suitable penetration [Kalal, Circa 1980].

The chemical and irradiation routes are the most commonly used. However, they both place constraints on the size of the final product. The only difference between the two routes is the homogeneity of the polymer. The radiation is of sufficient power to pass straight through the mixture resulting in a uniform product. The chemical route may yield slight variations owing to temperature gradients within the reaction vessel [Shah, 1991]. However, as long as the reactions were successful, materials formulated using either technique will absorb comparable amounts of water, given substantially the same ratio of initial monomers.

2.1.5 Hydrophilic Polymer History

Hydrophilic polymers were discovered in the mid 1960s at the Institute for Macromolecular Chemistry in Czechoslovakia [Gehrke, 1993]. They have subsequently been developed primarily for use as soft contact lenses. The original material was polyhydroxyethylmethacrylate (HEMA) produced by bulk polymerisation resulting in an optically clear solid. On hydration, the pure material was able to absorb 38% water by weight, offering an expansion ratio of 1.2 [Highgate, 1989]. This can be varied by adding vinyl pyrrolidone or methacrylic acid.

In the early stages of development the Czech army undertook a project using HEMA as contact lenses to be worn for ten days and nights without removal. The purpose was to correct eyesight while permitting a conventional gas mask to be worn for long periods. As the eye has no blood vessels supplying oxygen to the cornea, oxygen is absorbed by diffusion with the surrounding air. Therefore if a contact lens is designed to be worn for a long period, oxygen must be supplied by an alternative mechanism. Rigid contact lenses were traditionally designed to flush a film of tear fluid under the contact lens each time the eye blinked, supplying oxygen. This was suitable for rigid lenses during daytime use when eye movement was high, but unsuitable for soft flexible lenses. Therefore an alternative approach was taken focussing on the development of a suitably transparent material with high gas permeability, enabling absorption of oxygen directly from the environment. The HEMA used in the project had a low water content (38%) and did not yield the desired gas permeability resulting in the project being scrapped.

Since this time, hydrophilic polymers have been used extensively in medicine, mainly owing to their high water contents and associated reduced risk of rejection. HEMA has had the longest period of service of any hydrophilic material and has been accepted for opthalmic use by the Food and Drug Administration of the USA. The other main medical use is in oral drug release mechanisms.

More recent developments have concentrated on co-polymers of vinyl pyrrolidone and other structural units, including methylmethacrylate, styrene and nylon. These have resulted in a range of materials exhibiting controllable mechanical and physical properties. Thus it is now possible to produce high water content systems, which are strong and elastic or stiff and semi-rigid.

Medical research is currently underway into the use of such materials as structural supports for the urethra to help prevent problems associated with prostate inflammation. Potential for contraception applications are also being

explored where a hydrophilic plug is used to block fallopian tubes. For many of these applications, the ability of the material to hydrate/swell in situ is considered a major asset.

Non medical uses have included nutrient release into soil for growing plants and water absorption in nappies and sanitary products. Hydrophilic polymers have not been used practically in the field of ultrasonic NDT until this time. Patent application covering this wide area of application has resulted from this research project [Bourne et al, US-09/396,435 & UK 9921846.3].

2.2 Basic Properties of Hydrophilic Polymers

Investigations conducted as part of this research focussed initially on four different hydrophilic polymers believed to represent a cross section of the different water uptake levels available. These materials were specified as having equilibrium water contents of 38, 50, 60 and 75% water by weight once fully hydrated. These shall be referred to as Batches A, B, C and D respectively. Batches B, C and D are cross-linked copolymers consisting of polymethylmethacrylate and vinyl pyrollidone. Batch A is HEMA (polyhydroxyethylmethacrylate) a cross-linked homopolymer.

2.2.1 Hydration

The polymers were supplied in the form of cast rods, approximately 10mm in diameter. Sections of four different thicknesses were initially cut from each batch and submerged in water at the same moment. The dry thicknesses were calculated from the expansion ratios measured from previously hydrated test samples. The aim was to have all the polymers hydrating to a range of equal thickness for easy comparison. The surfaces of the samples were lightly ground and polished to remove any machining marks and ensure both faces were parallel. The different dry and subsequent fully hydrated thicknesses are listed in Table 2.1.

A		**B**		**C**		**D**	
Thickness (mm)		Thickness (mm)		Thickness (mm)		Thickness (mm)	
Dry	Hydrated	Dry	Hydrated	Dry	Hydrated	Dry	Hydrated
0.87	1.02	0.75	0.97	0.72	1.00	0.62	0.91
2.57	3.04	2.25	2.88	2.20	2.94	1.86	2.85
4.22	5.04	3.79	-----	3.66	4.91	3.11	4.76
8.39	10.00	7.55	9.62	7.27	9.77	6.23	9.53

Table 2.1 Thickness of a range of hydrophilic polymers before and after hydration in water.

The rate of hydration was monitored by removing each sample from the water, blotting them dry and weighing them at set time intervals before re-submerging them. The measured change in weight was translated into percentage weight of water as described in Equation 2.1.

$$wt\% = \frac{(W_H - W_D)}{W_H} \times 100 \qquad \textbf{Equation 2.1}$$

where W_H and W_D are the weights of the polymer when hydrated and dehydrated respectively. The results are shown in Figures 2.5 to 2.8.

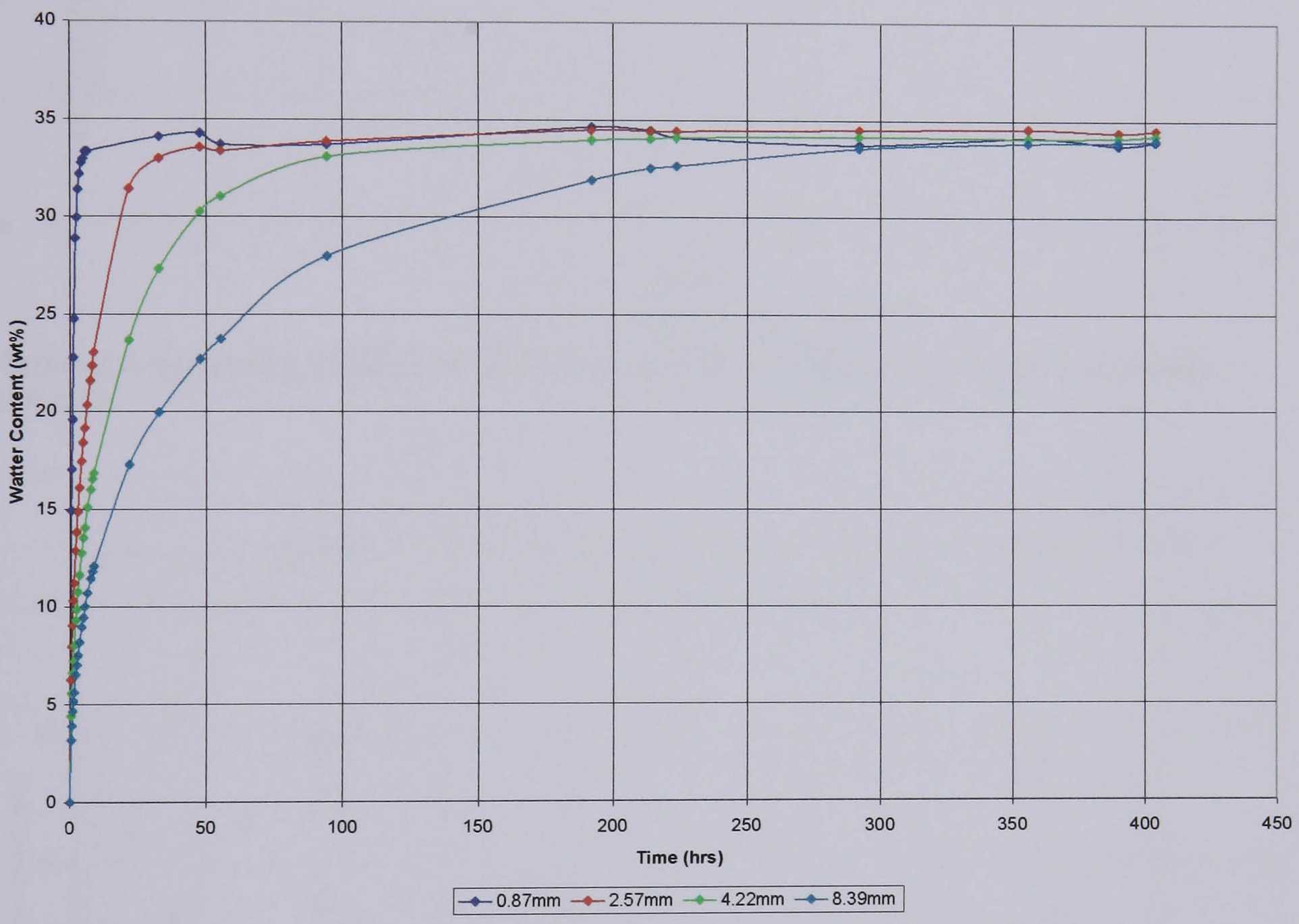

Figure 2.5 Hydration profiles for different dry thicknesses of hydrophilic polymer – Batch A

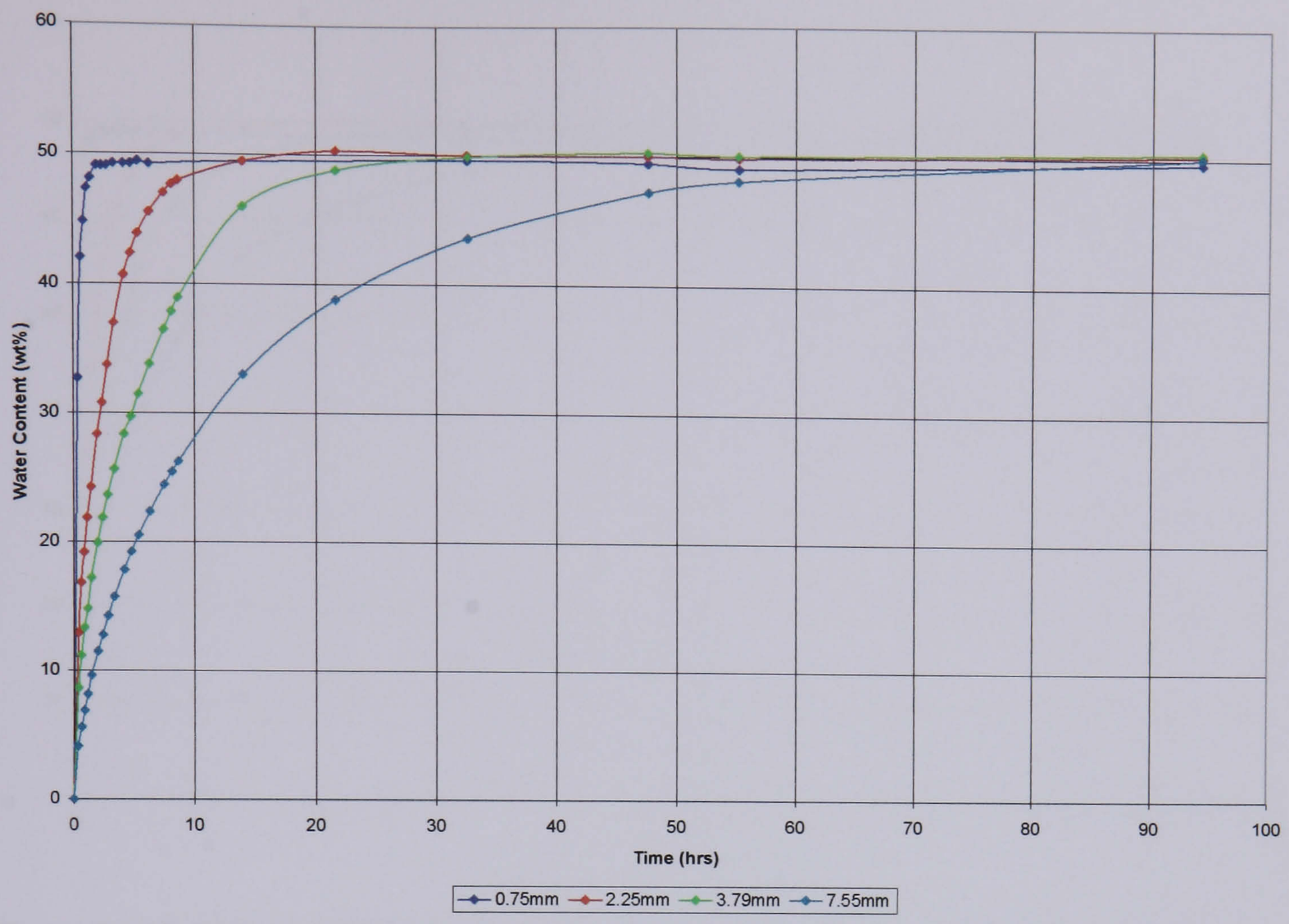

Figure 2.6 Hydration profiles for different dry thicknesses of hydrophilic polymer – Batch B

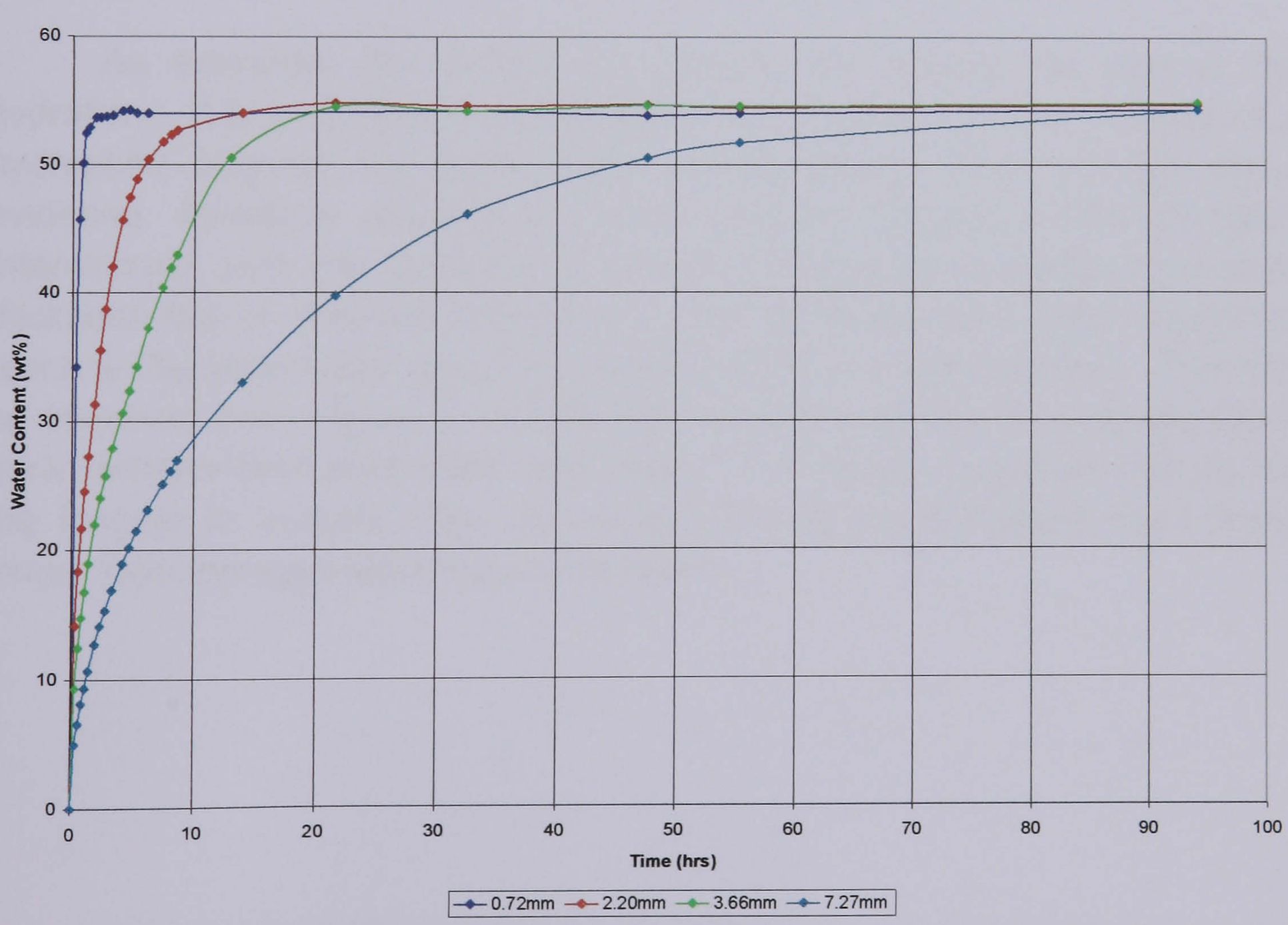

Figure 2.7 Hydration profiles for different dry thicknesses of hydrophilic polymer – Batch C

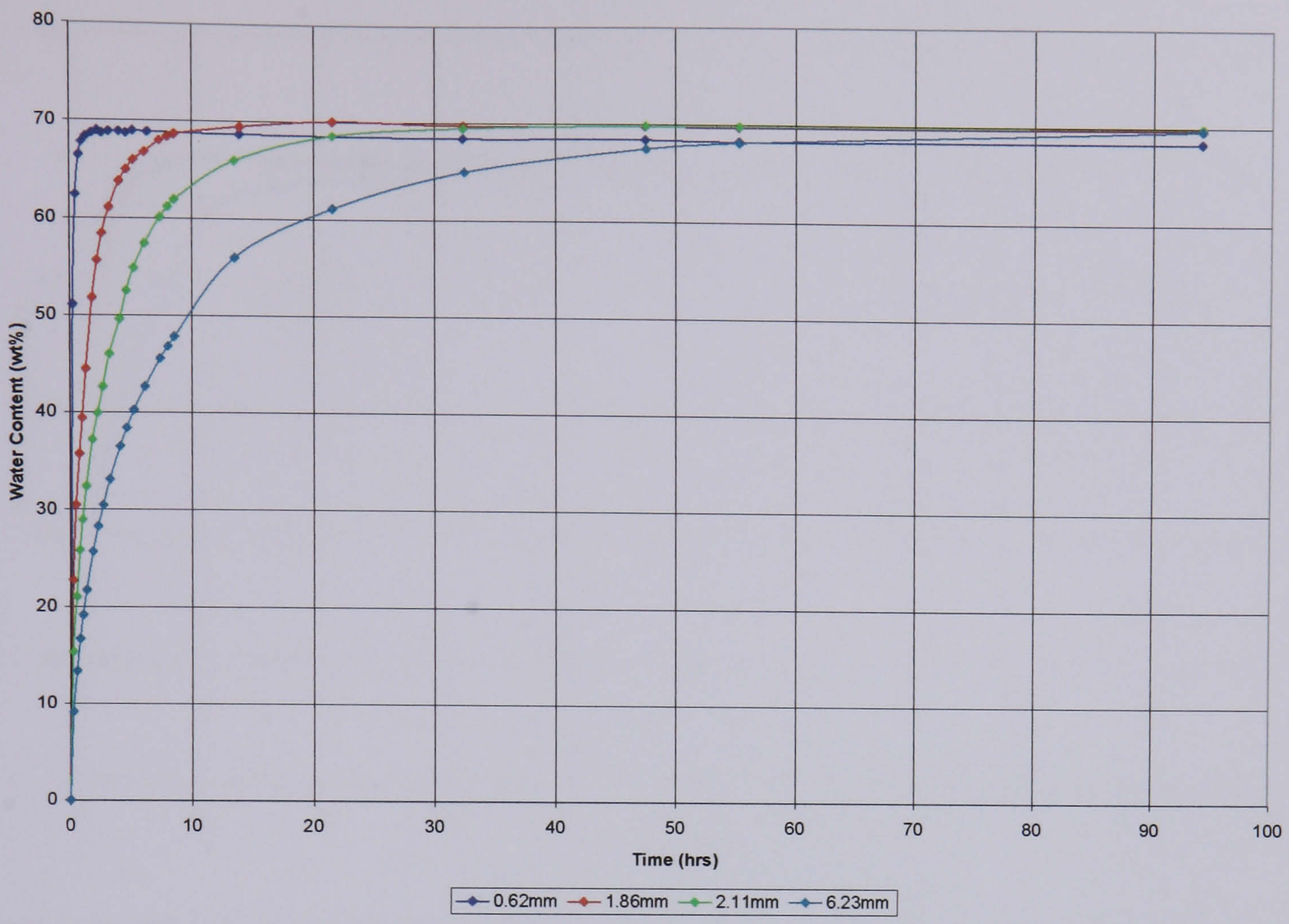

Figure 2.8 Hydration profiles for different dry thicknesses of hydrophilic polymer – Batch D

As expected, the thicker the sample, the greater the time to full hydration. It is also clear that the higher the equilibrium water content of a hydrophilic polymer, the faster it will absorb water. From this and other evidence, hydration appears to be a Fickian diffusion limited process. Interestingly, with the exception of Batch A, hydrophilic polymers of similar thickness but of different batches (i.e. different equilibrium water contents) reach full hydration after about the same amount of immersion time. This can be observed from Figure 2.9 where the hydration profiles of nominally 2mm thick samples from each Batch are shown. The Batch A polymer took by far the longest to hydrate fully, one sample taking approximately eight times longer than the equivalent Batch D polymer.

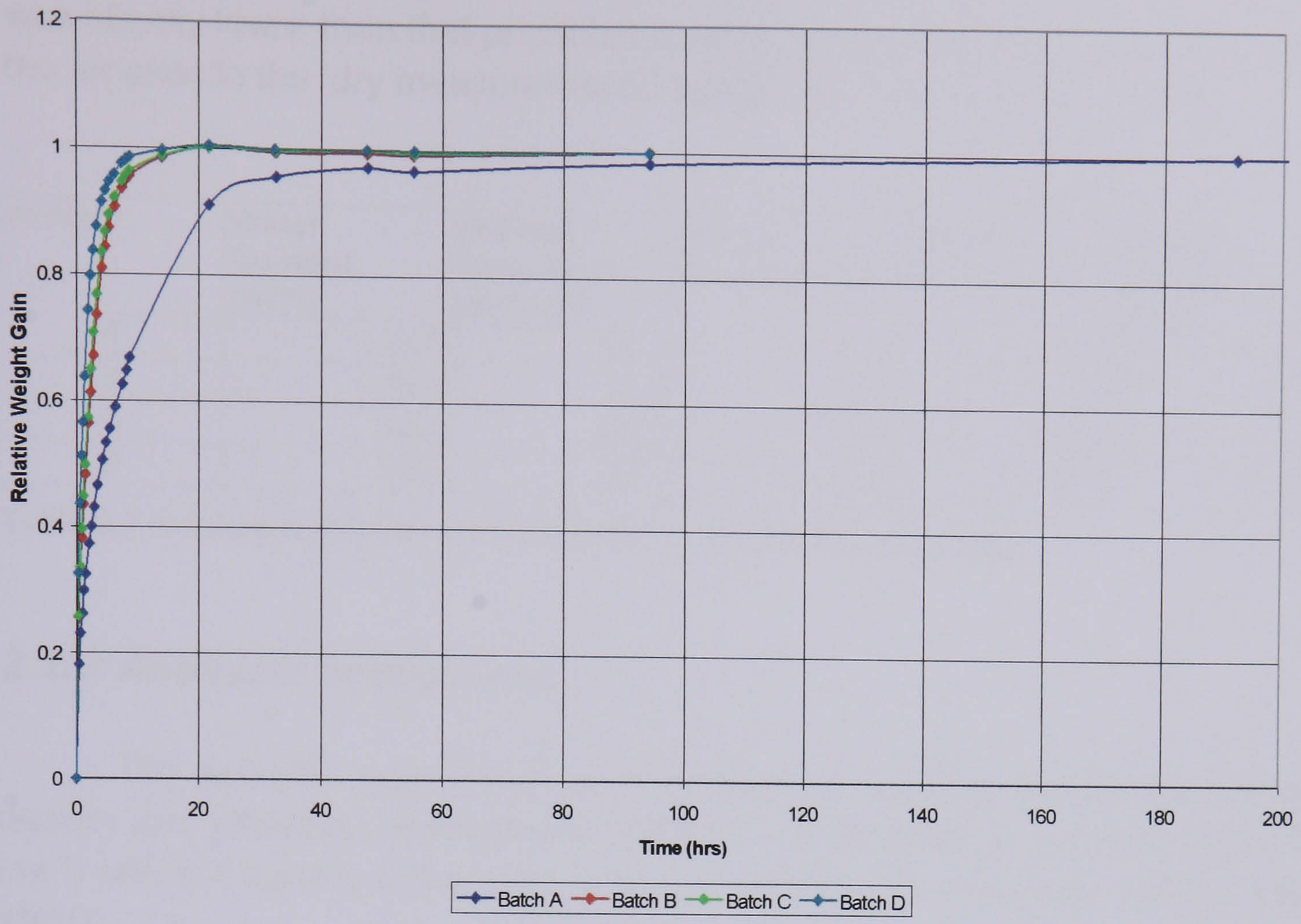

Figure 2.9 Relative hydration profiles of different hydrophilic polymers. Nominal 2mm dry thickness.

2.2.2 Expansion Characteristics

As the polymers begin to take on water, an obvious volume increase is observed. During this phase, two clearly defined regions are visible: the outer flexible zone and the dry, glassy inner zone (the cylindrical samples employed in these tests took three to four days to fully hydrate). By touch alone, samples from Batches D and A appeared most compliant followed by C then B.

Indeed, Maffezzoli et al [1996] found that ultrasound is capable of distinguishing between the two zones of a part-hydrated hydrophilic polymer, as a portion of ultrasound is reflected from the boundaries between them. Maffezzoli used this technique to map the progression of the water front through the material during hydration. This shall be discussed further in Chapter 5.

Table 2.2 lists the hydration data achieved for Batches A to D. Making accurate dimensional measurements on soft, flexible materials proved subjective. To ensure that the measurements were as reliable as possible, each was carefully taken three times with digital vernier callipers and the averages used. It is evident that the ultimate water content of all the polymers

was slightly lower than that predicted by the supplier. Moisture absorbed from the air prior to the 'dry measurements' being taken may account for this.

Sample	Water Content (wt%)	Volume Occupied by Water (%)	Weight Increase (%)	Volume Increase (%)	Linear Expansion Ratio
A	35.5	42.1	55.2	72.6	1.25
B	49.0	52.9	96.3	113.7	1.31
C	53.4	57.4	114.6	134.9	1.33
D	66.1	69.2	195.0	225.0	1.49

Table 2.2 Average hydration data for different hydrophilic polymers.

2.2.3 Acoustic Impedance

The acoustic impedance of a material is equal to the product of its density and ultrasonic transmission velocity. This yields an odd unit (kg m^{-3}, ms^{-1}) which is usually referred to as N s m^{-3} or Rayl [Krautkramer, 1983 & Silk, 1984].

The velocity of ultrasound in the hydrated samples was determined by transmitting an ultrasonic pulse into a sample of known thickness and measuring the time taken for it to reflect from the opposite face and return to its point of entry. A digital ultrasonic flaw detector and a single crystal compression wave probe operating at 10MHz (SLP10-10) were used for the measurements. Under normal circumstances, a velocity measurement of this nature would be conducted by pressing the ultrasonic probe onto the surface of the test piece to ensure good contact. However, as hydrated hydrophilic polymers are very flexible, great care was taken to ensure that the samples were not compressed while the measurement was taken. Should this have happened, the samples would reduce in thickness and an erroneous velocity measurement would be calculated. The most reproducible method proved to involve placing the probe upside down on the bench and placing the polymer sample on top with a little water at the interface. This guaranteed as much as possible that the polymer samples were not deformed from their natural dimensions. The ultrasonic velocity results were subsequently confirmed by repeating the procedure with a smaller 10MHz, TMP3 probe.

The density was calculated from dimensional measurements and weight. Each measurement was taken three times and the average used to increase accuracy and repeatability.

There are two important trends and one exception to be observed from Table 2.3. Both the density and ultrasonic transmission velocity of hydrated

hydrophilic polymers decrease with increasing water content, tending towards the value of pure water. The exception is the sample from Batch A, which has an ultrasound transmission velocity that is lower than other samples of higher water contents. It is suggested that this is because Batch A Polymer is inherently a different material to the others. This implies that while it is obvious water content influences density, ultrasonic transmission velocity and acoustic impedance, the host polymer network also plays an important contribution.

As expected, the acoustic impedance is highest in materials of lower water content. However, the difference between the four hydrophilic polymer samples as shown in Table 2.3 is quite small (0.47 N s m^{-3}). It is noteworthy that all four of the hydrophilic polymers examined in this investigation offer higher acoustic impedance than both water and natural rubber. This suggests they would all perform more efficiently as ultrasonic couplant than water and natural rubber when used with materials of industrial interest (assuming identical surface contact).

Sample	Density (kgm^{-3})	Ultrasonic Velocity ($m\ s^{-1}$)	Acoustic Impedance (N s m^{-3}) $x10^6$
A	1149.62	1627.53	1.87
B	1119.39	1673.35	1.87
C	1085.68	1679.12	1.82
D	1077.74	1619.27	1.75
Distilled Water*	998.20	1482.30	1.48
Natural Rubber*	909.50	1600.00	1.46
Perspex*	1185.00	2700.00	3.20

Table 2.3 Acoustic impedance of different hydrated hydrophilic polymers along with commonly encountered materials in ultrasonic testing at room temperature. * Kaye & Labby, 1975.

2.2.4 Frequency Spectra

Of key importance to the project aim is the range of frequencies different hydrophilic polymers are able to transmit. Exploration of this involves a number of stages. Firstly, an ultrasonic pulse must be introduced to the material under test. This is done by coupling an ultrasonic probe to the surface. The pulse must then be captured after passage through the material. One method, known as through transmission may be used where a second probe is coupled to the opposite surface of the test piece and acts as a receiver. An alternative approach, and the one adopted in this study, is the pulse echo method. Here, the transmitting probe also receives the ultrasonic pulse that is reflected from the opposite side of the test piece (back wall echo). Secondly, the captured pulse must then be analysed. This is achieved

by performing a Fast Fourier Transform (FFT). From this data, much relevant information may be derived.

A theoretical 'acoustically transparent' material would not effect the ultrasonic pulse as it travelled through it. However, in the vast majority of materials, this is not the case. As the pulse moves through a material it is effectively filtered, reducing in amplitude owing to scattering and absorption. It is usual for higher frequencies to be attenuated the most.

2.2.4.1 Test Probe Characteristics

To assess hydrophilic materials over a wide range of frequencies a high frequency ultrasonic probe was selected and used. This was a TMP3 which is a 10MHz compression wave probe. A TMP3 is a delay line type probe used mainly in the aerospace industry for high resolution, near surface material inspection. It has a single lead metaniobate crystal of 6mm diameter. In its normal mode of operation its rexolite delay block would be fitted. However, in this particular case it was not used. This ensured that no 'filtering' of the ultrasonic pulse took place in the delay block itself. For this probe to be used to characterise the ultrasonic performance of the hydrophilic polymers, the characteristics of the probe itself must first be determined.

During manufacture, a parallel-sided 25mm thick steel test block (IIW-A2) is used in the evaluation of this probe. Steel is known to have very little attenuation to ultrasound and is therefore often assumed to be an 'acoustically transparent' material. Therefore, a pulse of ultrasound which (i) is introduced to the test block from the probe under test, (ii) propagates to the opposite surface where it is reflected back and, (iii) received again by the probe, can be assumed to be unaffected by its passage through the test block. It is therefore assumed that the characteristics of the received pulse represent the characteristics of the pulse generated by the probe. A digital ultrasonic flaw detector was used to drive the probe.

The received pulse was transferred from the ultrasonic flaw detector to a desktop PC where it was analysed using Microsoft Excel. The macros used in Excel for this purpose were written specifically for this study. Previous attempts were made using Fortran and MathCad, but Excel proved to be the quickest and most reliable technique[A]. The sponsors wish to keep the specific code used in their testing system confidential, but the main component used

[A] It should be noted that these analysis tools are now used as the basis for the probe characterisation and certification system now used at Sonatest PLC and sold as an independent product. The finished system was developed in conjunction with Rizwan Latif as part of his MSc project. [Latif, 2000]

for calculation of the frequency spectrum is shown in Appendix C. The analysis is performed in seven main stages:

- The ultrasonic pulse displayed on the screen of the ultrasonic flaw detector is made up of 250 vertical lines (in each pixel column) with respect to time, each of which has a maximum and minimum amplitude value. The average of these values is determined for each column and the receiver gain used to calculate the time amplitude of each point in mV.
- A Fourier Analysis is performed on the data, yielding an array containing real and imaginary parts.
- Both the real and imaginary parts are squared, added together and the square root established. This represents the vector amplitude.
- This amplitude data is then converted into a logarithmic scale and normalised. Finding the maximum amplitude and then subjecting each amplitude data (A) to Equation 2.2 performs this. The process presents the maximum amplitude at 0dB and all other data below it.

$$dB = 20 \times \log\left(\frac{A}{\max}\right) \qquad \textbf{Equation 2.2}$$

- The frequency increment between each amplitude point is determined by performing the calculation described by Equation 2.3, where 'range' is the range of the ultrasonic flaw detector (μs) when the pulse was captured.

$$MHz = \frac{250}{512 \times range} \qquad \textbf{Equation 2.3}$$

- The frequency increments are added together to generate the frequency scale.
- Frequency and amplitude scales are plotted to show the full frequency spectrum.

The peak frequency is easily determined by finding the corresponding frequency to the amplitude data of the greatest value. In the case of the TMP3 probe, this was 10.50MHz; showing that the probe is operating well within its design tolerance of ± 10%. There is another characteristic, known as the bandwidth, which is also very important here. The bandwidth represents the frequency range over which the probe may be feasibly used. It is determined by firstly locating the points on the frequency curve either side of the peak frequency that are 6dB lower (i.e. half) in amplitude. The corresponding frequencies are then subtracted from each other to yield the bandwidth (Equation 2.4). The TMP3 probe had upper and lower –6dB points of 13.45 and 8.52MHz respectively. This represents a relatively narrow bandwidth of 4.93MHz (or 47% of the peak frequency), and a centre frequency of 8.09MHz calculated via equation 2.5. Therefore, if this probe

were to be used for the evaluation of the frequency characteristics of hydrophilic polymers, they would only be effectively interrogated over the 8.52 to 13.45MHz frequency range at a maximum.

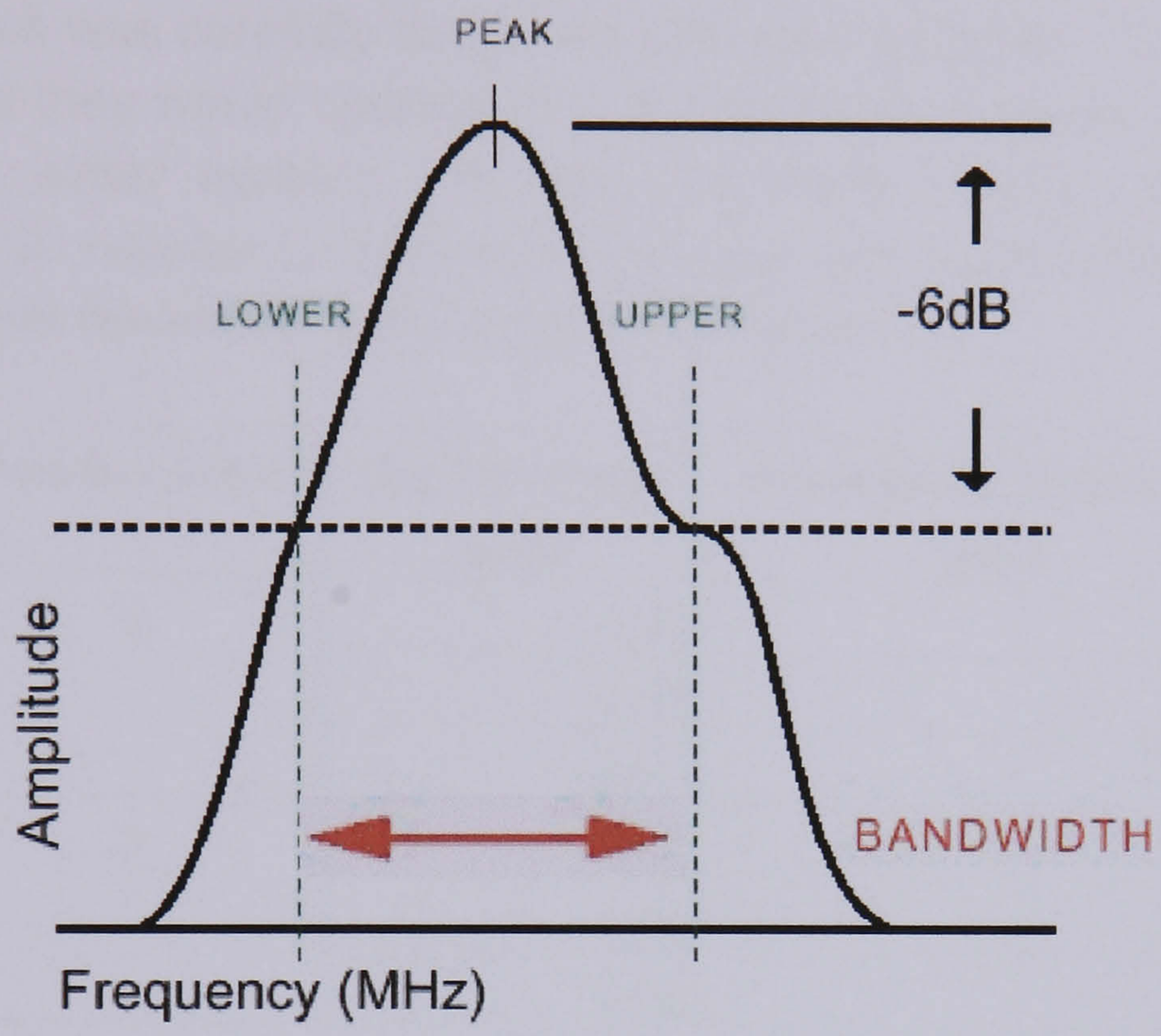

Figure 2.10 Representation of a frequency spectrum defining bandwidth.

$$Bandwidth = \left(-6dB_{Upper}\right) - \left(-6dB_{Lower}\right) \qquad \textbf{Equation 2.4}$$

$$CentreFrequency = \sqrt{\left(-6dB_{Upper}\right) \times \left(-6dB_{Lower}\right)} \qquad \textbf{Equation 2.5}$$

In an attempt to increase the bandwidth of the probe and hence the range of frequencies propagated through the hydrophilic polymers, the configuration of the ultrasonic flaw detector was altered. The main change was to remove the filterbands that were acting to promote the 10MHz target frequency of the probe by attenuating frequencies below 7 and above 13MHz. In addition, the rate at which the crystal was fired (TX width) was adjusted from its natural position of 250ns to 110ns. This had the effect of reducing the pulse generated by the probe from three cycles to one, which in turn increased the bandwidth. The new upper and lower –6dB points shifted to 13.14 and 4.98MHz, representing a new bandwidth of 8.17MHz or 78%. The test certificate produced for this TMP3 probe operated with the modified configuration can be seen in Appendix D. All settings were logged and used for all frequency determination studies documented in this Chapter.

2.2.4.2 Sample Preparation

Specimens were cut from each of the four batches of hydrophilic polymers. Each was carefully sectioned with parallel faces. Their thicknesses were such that they would hydrate to 3, 5 and 10mm nominal thickness when at equilibrium water content. In this way each polymer batch could be investigated with respect to thickness and also with each other. The dry and hydrated sample thicknesses are outlined in Table 2.4.

Polymer Batch	Dry Thickness (mm)	Equilibrium Thickness (mm)
A	2.16	3.26
	4.30	5.34
	8.91	10.66
B	2.42	3.08
	4.00	5.19
	7.99	9.93
C	2.30	3.04
	3.77	5.04
	7.55	9.96
D	2.03	3.02
	3.34	4.96
	6.58	9.94

Table 2.4 Dry and hydrated thicknesses of different hydrophilic polymers used for frequency evaluation.

2.2.4.3 Testing

The TMP3 probe was coupled to each sample in turn with a very small amount of oil. Great care was taken to ensure that complete coupling was achieved while not compressing the material, which would effectively reduce its thickness and potentially impact on the results. This was accomplished easily for the lower water content and thinner samples, as they were stiffer. The Batch D samples were more of a challenge. However, as the materials are translucent, it was possible to look through the material to the surface where the probe was coupled. Regions of non-contact were clearly visible in contrast to regions of intimate contact with the probe face. This made it possible to apply the lowest possible coupling pressure whilst ensuring full acoustic contact was made with the probe. An additional consideration was one of 'over coupling'. If too much coupling fluid was used, it could run down the side of the sample and find its way onto the bottom surface. When this happened, a noticeable portion of the ultrasound incident on the back wall of

the sample was transmitted into the bench, reducing the amplitude of that returned to the probe. On occasions where this occurred, erroneous readings were recorded and the test had to be redone.

With the probe in contact with a sample, the controls on the ultrasonic flaw detector were adjusted so that the first back wall echo was expanded to fill the screen. The gain was adjusted so that the signal was full on the screen but not clipped. In each case, the previously determined optimum probe calibration was used to ensure the enhanced bandwidth was utilised. The signal was then captured and transferred to Excel where the analysis macros performed their function.

2.2.4.4 Results

With the data calculated, the frequency spectra from each thickness of a particular hydrophilic polymer batch were plotted together for comparison. These can be seen in Figure 2.11 to Figure 2.14. In each case, it is clear that the thinner samples transmit the ultrasound from the probe much more readily. Of key importance is that the overall amplitude is higher for the thinner samples and that it is the higher frequencies that are attenuated to the greatest extent from passage through thicker samples. It is concluded from this that for all four batches of hydrophilic polymer, the overall absorption of ultrasound is directly proportional to the thickness. Frequency spectra for the same thicknesses of Perspex were also determined for comparative purposes. These are shown in Figure 2.15.

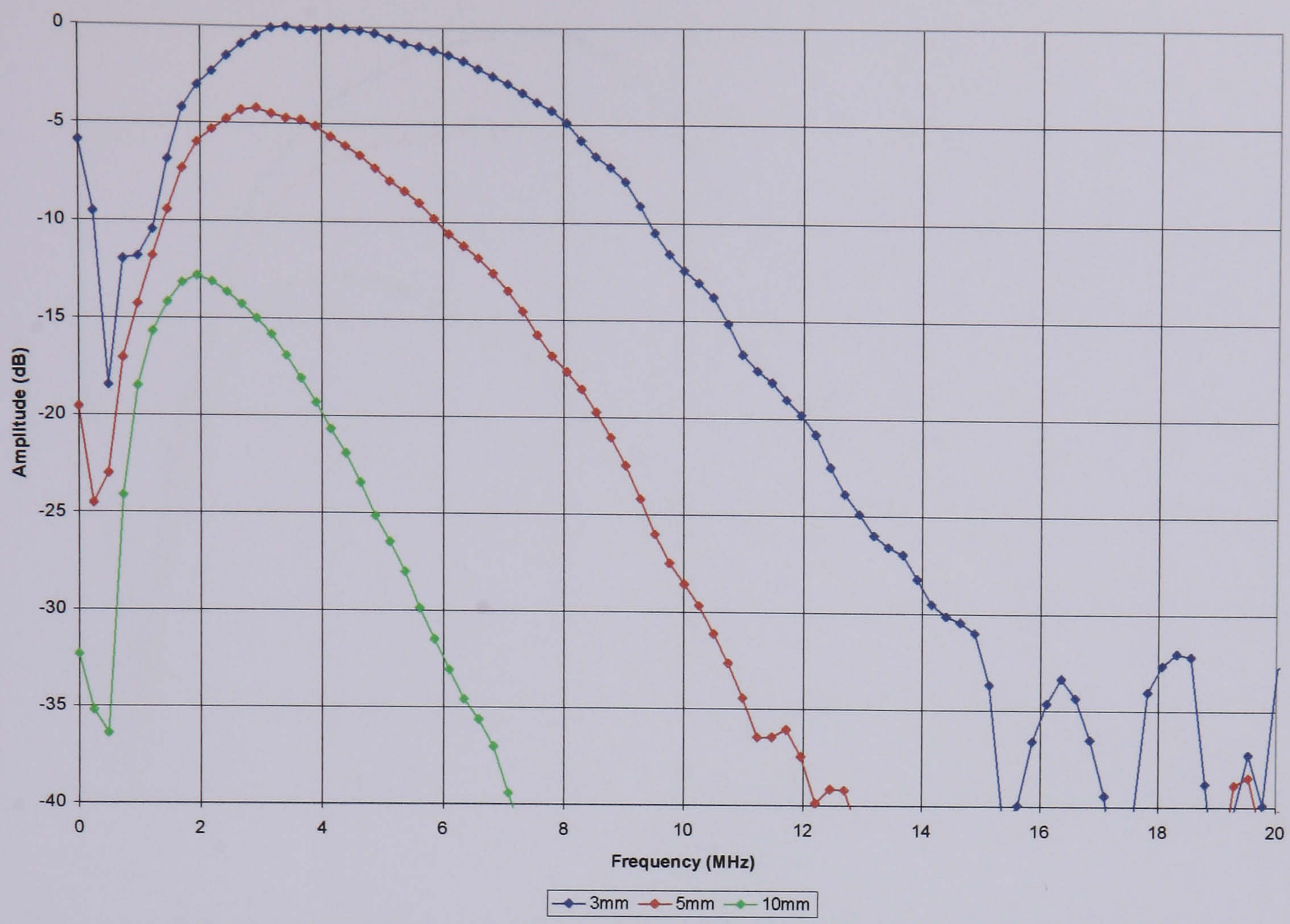

Figure 2.11 Frequency spectra of a nominally 10MHz broadband pulse having propagated through different thicknesses of hydrated hydrophilic polymer from Batch A. Pulse echo measurement was used.

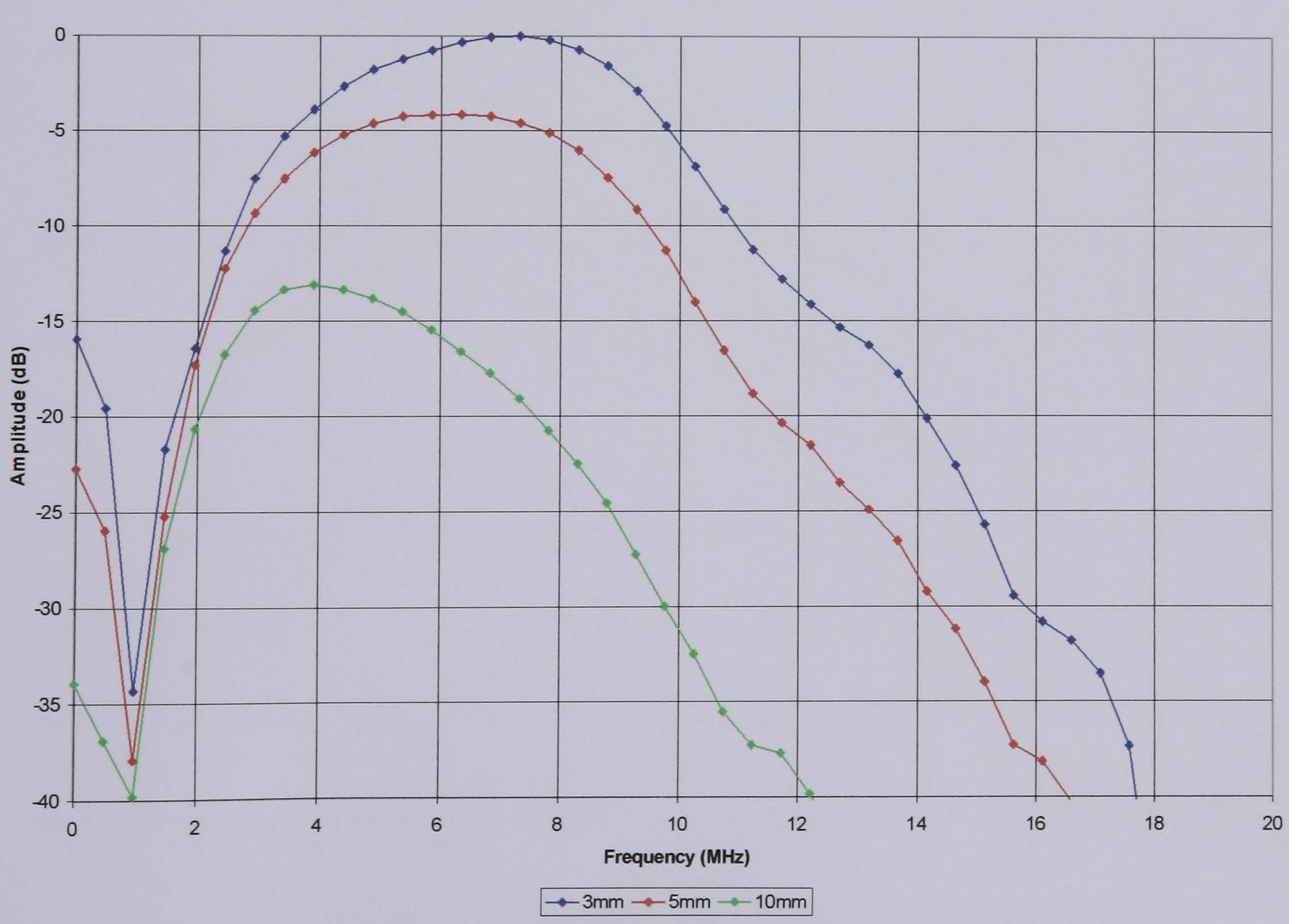

Figure 2.12 Frequency spectra of a nominally 10MHz broadband pulse having propagated through different thicknesses of hydrated hydrophilic polymer from Batch B. Pulse echo measurement was used.

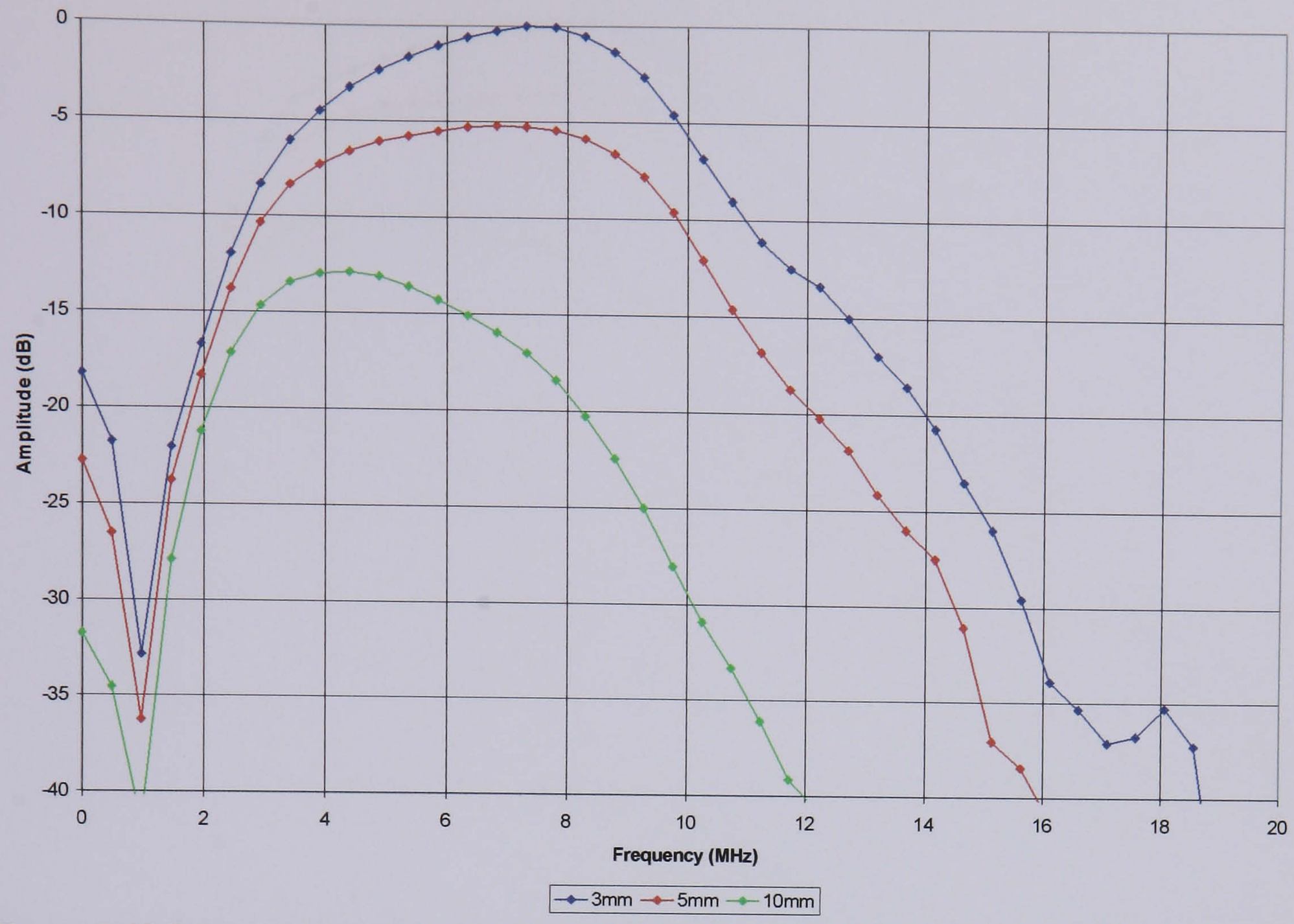

Figure 2.13 Frequency spectra of a nominally 10MHz broadband pulse having propagated through different thicknesses of hydrated hydrophilic polymer from Batch C. Pulse echo measurement was used.

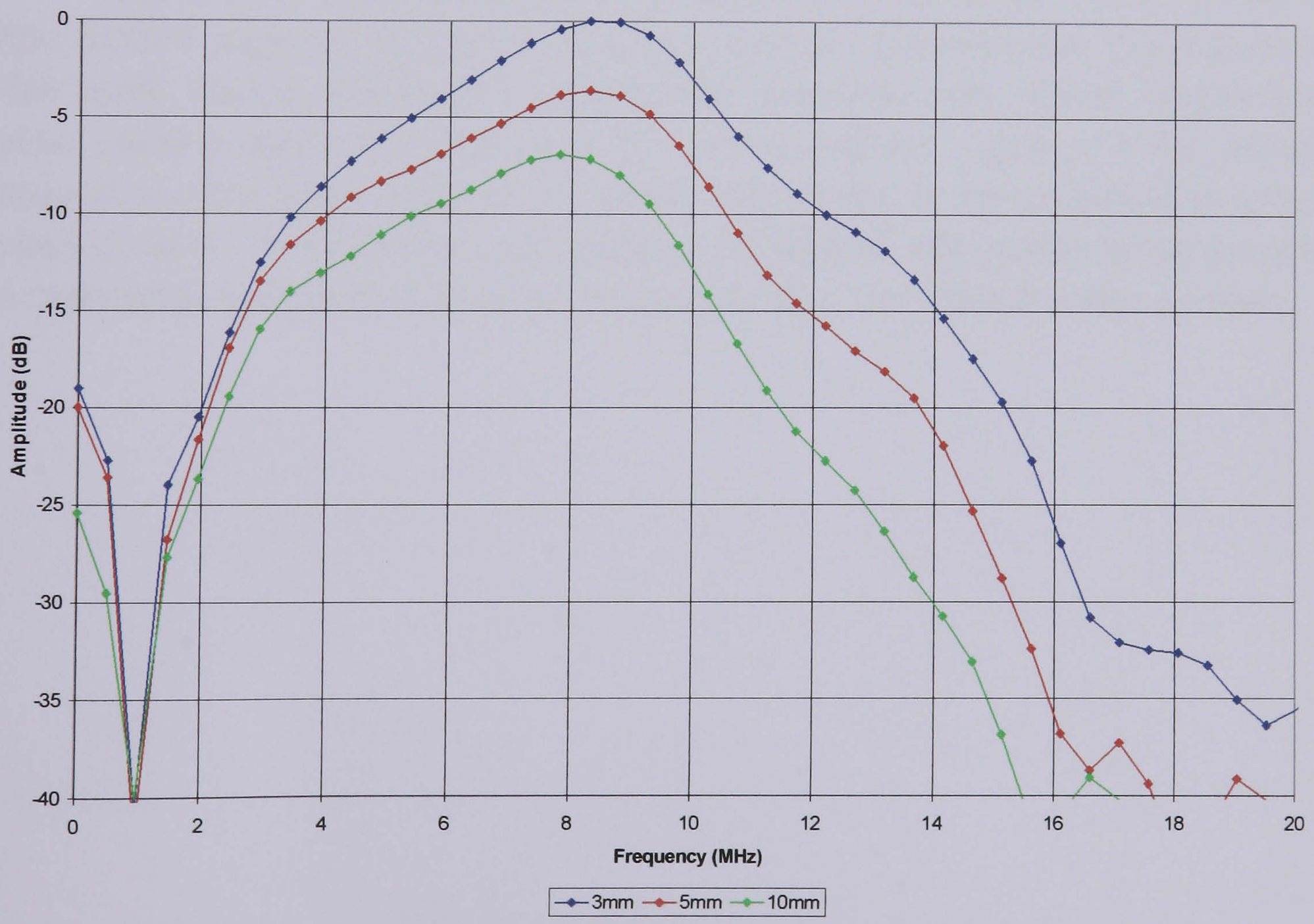

Figure 2.14 Frequency spectra of a nominally 10MHz broadband pulse having propagated through different thicknesses of hydrated hydrophilic polymer from Batch D. Pulse echo measurement was used.

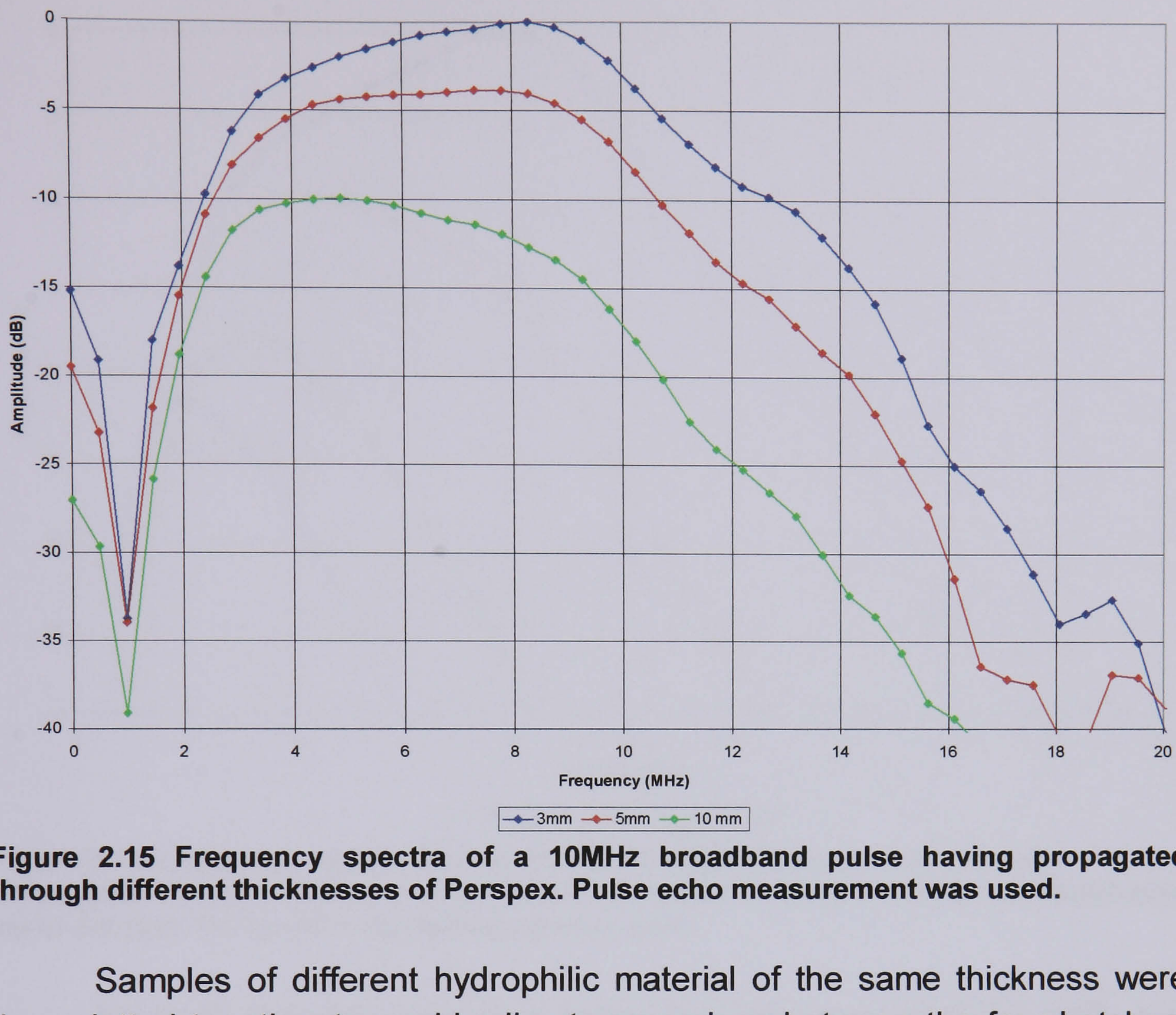

Figure 2.15 Frequency spectra of a 10MHz broadband pulse having propagated through different thicknesses of Perspex. Pulse echo measurement was used.

Samples of different hydrophilic material of the same thickness were then plotted together to enable direct comparison between the four batches. This quite clearly shows that hydrophilic polymers with higher equilibrium water content attenuate ultrasound to a lesser degree. Again, it is the higher frequencies that have been preferentially attenuated in the polymers of lower water content. It is therefore concluded that the bulk attenuation of ultrasound in hydrophilic polymers is inversely proportional to equilibrium water content.

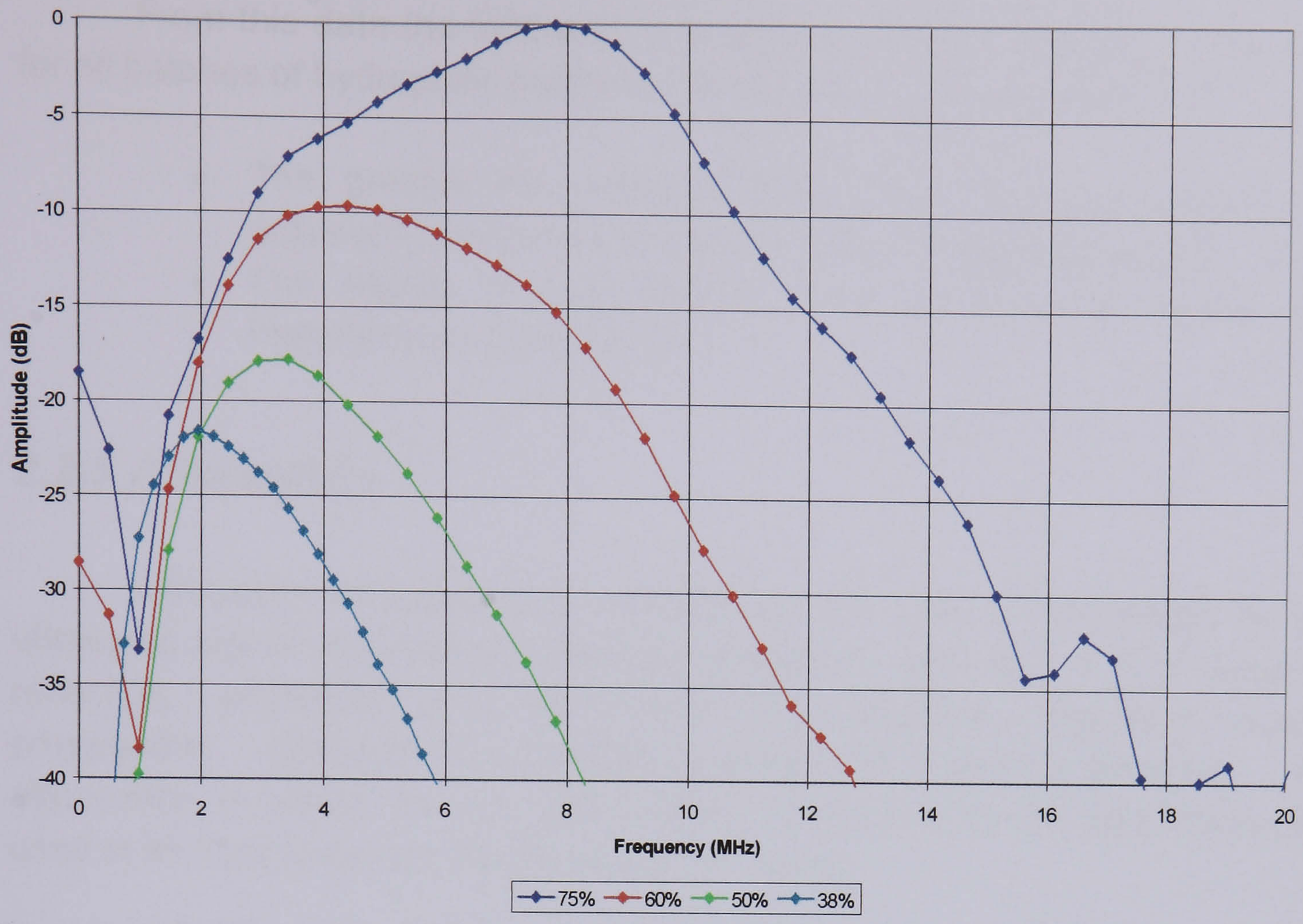

Figure 2.16 Frequency spectra of a nominally 10MHz broadband pulse having propagated through 10mm thicknesses of hydrophilic polymers of different equilibrium water content. Pulse echo measurement was used.

From all the data captured during the frequency analysis trials, key figures were calculated and are presented in Table 2.5.

Material	Thickness (mm)	-6dB Lower (MHz)	-6dB Upper (MHz)	Bandwidth (MHz)	Centre Freq. (MHz)	Peak Freq. (MHz)
38% HP	3.26	1.59	8.12	6.53	3.59	3.42
	5.34	1.28	6.31	5.03	2.84	2.93
	10.66	0.96	3.73	2.77	1.89	1.95
50% HP	3.08	3.26	10.05	6.80	5.72	7.32
	5.19	2.79	9.50	6.71	5.15	6.35
	9.93	2.15	7.33	5.18	3.97	3.91
60% HP	3.04	3.43	10.07	6.65	5.87	7.32
	5.04	2.81	10.07	7.27	5.32	6.84
	9.96	2.23	7.93	5.70	4.21	4.39
75% HP	3.02	4.93	10.75	5.83	7.28	8.30
	4.96	4.21	10.46	6.25	6.64	8.30
	9.94	3.98	10.02	6.04	6.31	7.81
Perspex	2.99	2.97	10.93	7.96	5.70	8.30
	4.98	2.62	10.62	8.00	5.28	7.32
	10.04	2.27	9.70	7.43	4.69	4.88

Table 2.5 Hydrophilic polymer frequency data resulting from ultrasonic analysis with a nominally 10MHz broadband probe. Perspex is also included as a datum.

From this data the following conclusions can be made which hold true for all batches of hydrophilic polymers investigated in this research:

- The greater the physical thickness of hydrated hydrophilic polymers, the lower the signal frequency and bandwidth.
- The higher the equilibrium water content, the higher the frequency and bandwidth.

2.2.5 Attenuation

Ultrasonic attenuation is defined as the loss in amplitude of an ultrasonic signal per distance travelled through a material. It is a result of reflection, scattering and absorption of ultrasound occurring during propagation. Attenuation is usually described in terms of dB mm^{-1}. As attenuation is known to vary with respect to frequency, the test frequency used in its measurement should always be stated.

2.2.5.1 Review of Techniques

i) Multiple Reflection Method

To establish the attenuation in a particular material, it is ideal to have a number of samples of different thickness. However, often such samples are not readily available. In this situation a multiple reflection method is often used [Salgueiro da Silva, et al, 1992, Abd El-Malak, 1997 and Sheffield City Polytechnic, JDB: EXP-10.22]. This approach requires only one sample with parallel sides. Instead of monitoring only the first back wall echo, the technique requires the amplitude of two or more repeat echoes to be considered. Repeat echoes arise from the ultrasound being reflected back and forth from each parallel side of the sample. Each repeat echo represents the ultrasonic signal having travelled through the material an additional time to the one previous. For example, in the case of a 10mm thick sample, the first back wall echo represents the signal that has travelled 20mm through the sample. The second back wall echo represents the signal has travelled 40mm and so on. In this way pulses that have travelled through thicker samples are in effect simulated. The two most common approaches for the determination of the amplitude from different back wall echoes in this method is to either:

- Use the gain controls on the flaw detector to adjust each echo in turn to a specific amplitude on the screen. For example, if first back wall echo

requires 50dB of gain to be 50% full screen height and the second requires 60dB to be at the same level, the increased travel distance has imposed a 10dB attenuation. Or,

- Adjust the gain until the first back wall echo is at 100% full screen height. Note the amplitude of each subsequent repeat echo in terms of % full screen height (see Figure 2.17). Convert the differences between the first back wall echo and each subsequent repeat echo to decibels using Equation A.15 in Appendix A.

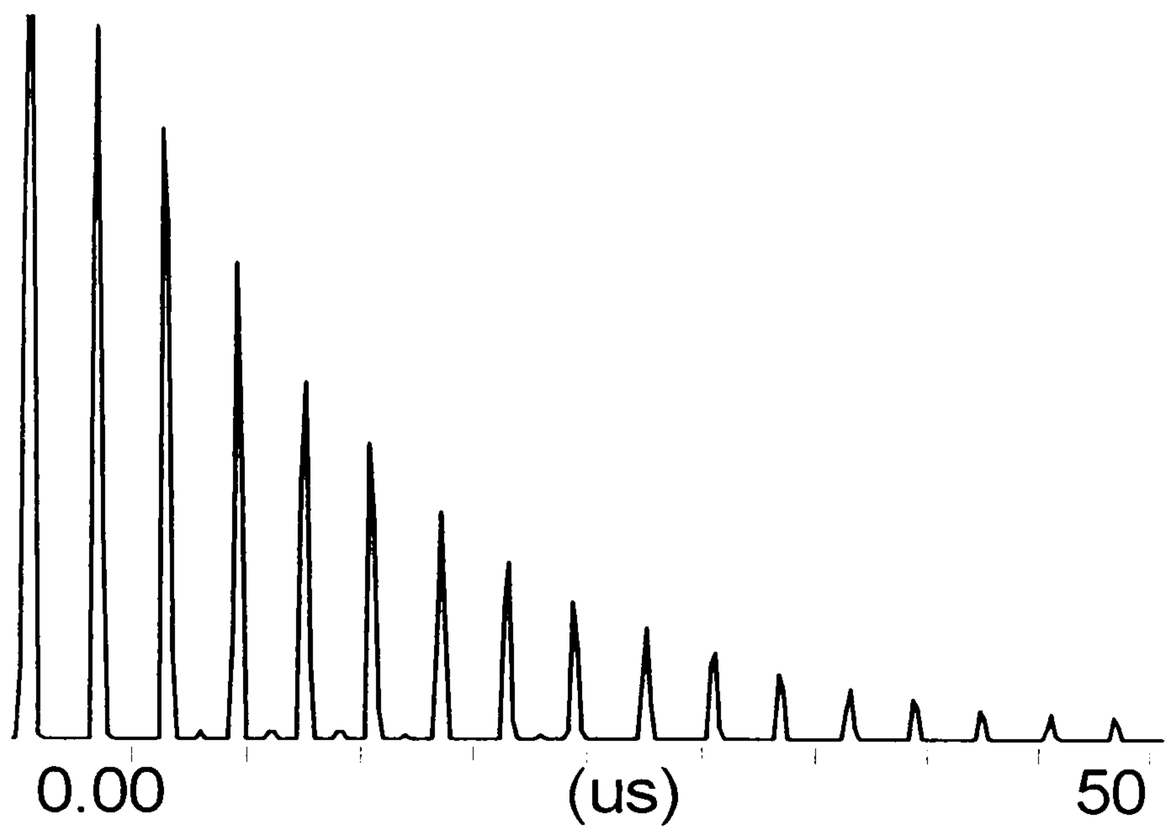

Figure 2.17 A-scan showing multiple repeat echoes through a 10mm thick aluminium sample. The probe used was 10MHz narrow band, the A-scan was captured using Sonatest Data Management Software (SDMS).

Whichever approach is used, the most effective way to establish the attenuation is to plot the changes in amplitude (dB) against the corresponding increase in travel distance. The result should be a straight-line graph, the gradient of which is the attenuation in dB mm^{-1} (see Figure 2.18).

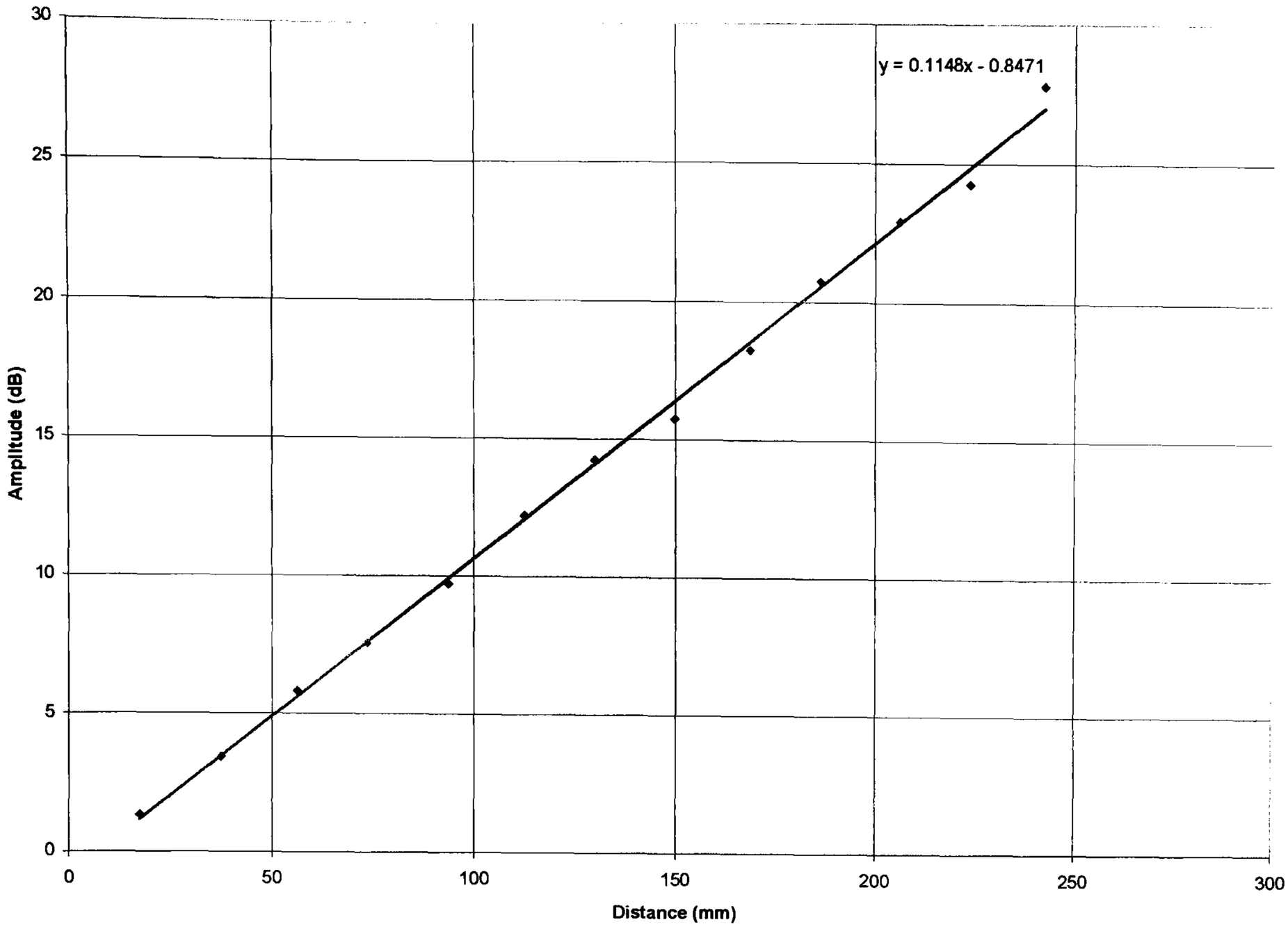

Figure 2.18 Determination of attenuation in aluminium using the multiple repeat echo technique. Drop in amplitude Vs ultrasonic travel distance.

In the example shown in Figure 2.17 and Figure 2.18, a 10mm aluminium plate was used. The attenuation measured using the multiple reflection technique was 0.1148dB mm^{-1}. The probe used was 10MHz and therefore, this experiment has measured the attenuation in aluminium to be 0.11dB mm^{-1} at 10MHz. This is in good agreement with Cartz [1995], who quotes attenuation in aluminium as 0.09dB mm^{-1} albeit measured at 2.25MHz. These tests were conducted by coupling the probe directly to the aluminium. It is possible for the multiple reflection method to be performed via immersion testing. However, in this case, the losses due to acoustic impedance mismatch between the aluminium and the water must be considered [Smith et al, 1998].

The deficiency in the multiple echo technique which limits its accuracy is the assumption that the ultrasound is 100% reflected each time it is incident onto a surface of the sample. We know this to be true for the sample-air interface owing to the massive acoustic impedance between air and solid materials. However, the side with the probe coupled is responsible for the absorption of a small portion of ultrasonic energy from each reflection. This is due to a portion of the sound propagating into the probe each time. It is known that this happens otherwise the returning multiple echoes would not be detected. In fact, this rate of absorption from the material to the probe will also vary from different sample materials owing to differing acoustic

impedance mismatches between the sample material and the transducer crystal of the probe. This additional reduction of energy from the sample causes the ultrasonic signal to appear to be decaying in amplitude at a rate quicker than that owing solely to the attenuation in the sample. Hence, attenuation data achieved by the multiple echo technique tends to produce pessimistic results.

ii) Multiple Sample Method

An alternative technique for attenuation determination that is generally regarded as being more accurate requires samples of different thickness [Hull, 1996]. In this case both through transmission and pulse echo methods may be employed. The amplitude of the first back wall echo (or transmission signal in the case of through transmission) is determined for each thickness of material by adjusting the gain of the ultrasonic flaw detector until the back wall echo is at a given percentage of full screen height (e.g. 80%). This essentially works in the same way as the multiple echo technique only eliminating the influence of additional signal decay resulting from transmission of ultrasound into the probe on each round trip through the sample. Unfortunately, there is still an element of error common to both this and the multiple echo method caused by beam spreading. As ultrasound is passed through any material, the sound beam undergoes a degree of spreading, hence introducing an element of natural amplitude decay. Therefore, even perfect samples of zero attenuation would display some loss in amplitude.

iii) Double Through Transmission Method

The final technique to be discussed here is known as the double through transmission method [Drinkwater and Cawley, 1994 and Smith, et al, 1998]. This approach necessitates the use of an immersion tank and requires the material samples to be in plate form – the width and length being considerably larger than the thickness. This method is believed to be very accurate as it ensures 100% coupling and like the multiple thickness method, eliminates the cumulative erroneous multiple reflection factors. Its drawbacks are that it requires extensive equipment and may not be suitable for materials that are susceptible to water ingress or cannot be prepared to appropriate dimensions. An immersion transducer transmits an ultrasonic pulse into the water, which is reflected by a reflector (usually a plate of glass) back to the probe where the amplitude is recorded. The test sample is then supported in the path of the ultrasonic beam and the modified amplitude from the glass reflector is noted. A number of considerations and corrections are required to the raw data acquired here. Firstly, loss of signal amplitude owing to acoustic impedance mismatch between the water and the sample must be

compensated for. In addition, the attenuation in water, shift in probe focal distance and possible non-linear propagation through the water must also be understood. These issues are discussed at length by Smith, et al, 1998.

A pulse of ultrasound generated by an ultrasonic probe consists of a spectrum of frequencies. As the pulse travels through a material the frequency spectrum will undergo modification. Therefore, it cannot be assumed that the component of the frequency spectrum with the highest amplitude (peak frequency) will be the same frequency both before and after propagation through a test piece material. With this in mind it can be seen that using the amplitude of the signal alone as a measure of attenuation often leads to inaccurate results. For example, Figure 2.19 represents the frequency spectra of two identical pulses generated by a 10MHz probe having travelled through 6 and 20mm of Perspex (i.e. pulse echo through 3 and 10mm samples). If the amplitude of the signals were used without considering the change in peak frequency (frequency downshift) the attenuation would be assumed to be approximately 9.75dB over the 14mm and therefore 0.7dBmm^{-1} at 10MHz. However, the true attenuation at 10MHz is the difference in amplitude between the 10MHz components in the frequency spectra. This generates a different value of 1dBmm^{-1} at 10MHz. This is a reasonable consideration and it is surprising that it is so frequently omitted.

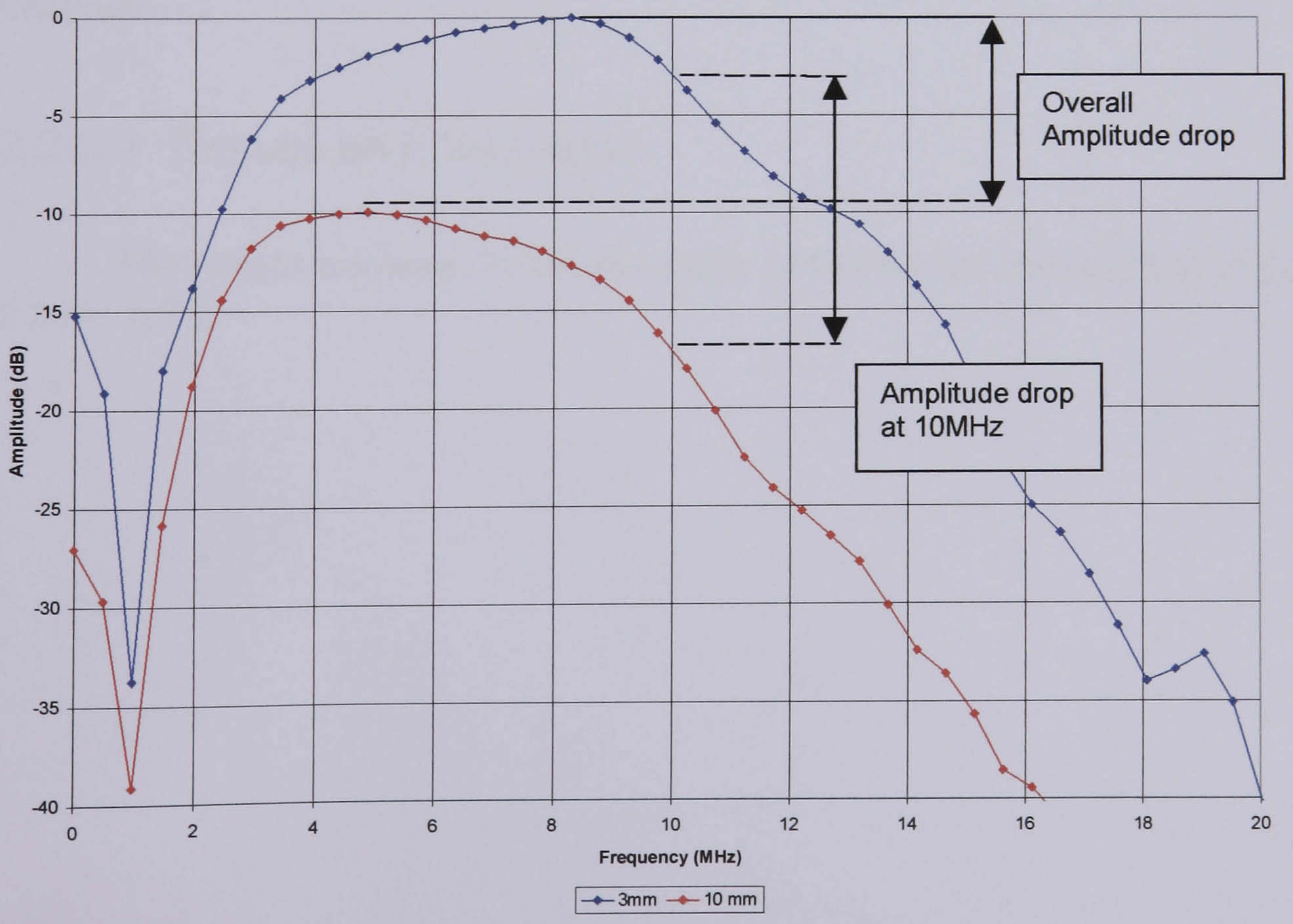

Figure 2.19 Frequency spectra of same nominally 10MHz pulse having propagated 'pulse echo' through 3 and 10mm samples of Perspex. Potential inaccuracies in attenuation measurement are marked.

2.2.5.2 Test Procedure

In this study, the multiple thickness method was used to establish attenuation in the four different hydrophilic polymer: Batches A-D. For optimum accuracy, a direct comparison between the frequency spectra of the ultrasonic signals was performed. This was achieved by subtracting the amplitude of each frequency from a given thickness from that of a thinner one. Dividing the amplitude difference by the difference in travel distance produced the attenuation in dB mm^{-1} with respect to frequency. This eliminates underestimation of attenuation caused by frequency downshift.

TMP3 probe was used with the optimum configuration settings on the ultrasonic flaw detector determined earlier. This enabled the attenuation to be investigated over a greater frequency range. For each hydrophilic polymer, samples of 3, 5 and 10mm thickness were used. The choice of thin samples was made to keep errors due to beam spreading to a minimum. This was made possible by the use of such a high frequency probe as the TMP3, lower frequencies would have necessitated much thicker samples. The attenuation was calculated three times for each polymer, taking the different responses from the 3 and 5mm samples, 5 and 10mm samples and finally the 3 and 10mm samples. The 3-10mm comparison is expected to have given the greatest degree of accuracy as it involved the largest variance in propagation distance.

2.2.5.3 Results and Discussion

The results achieved from this round of testing are displayed in Figure 2.20 to 2.23.

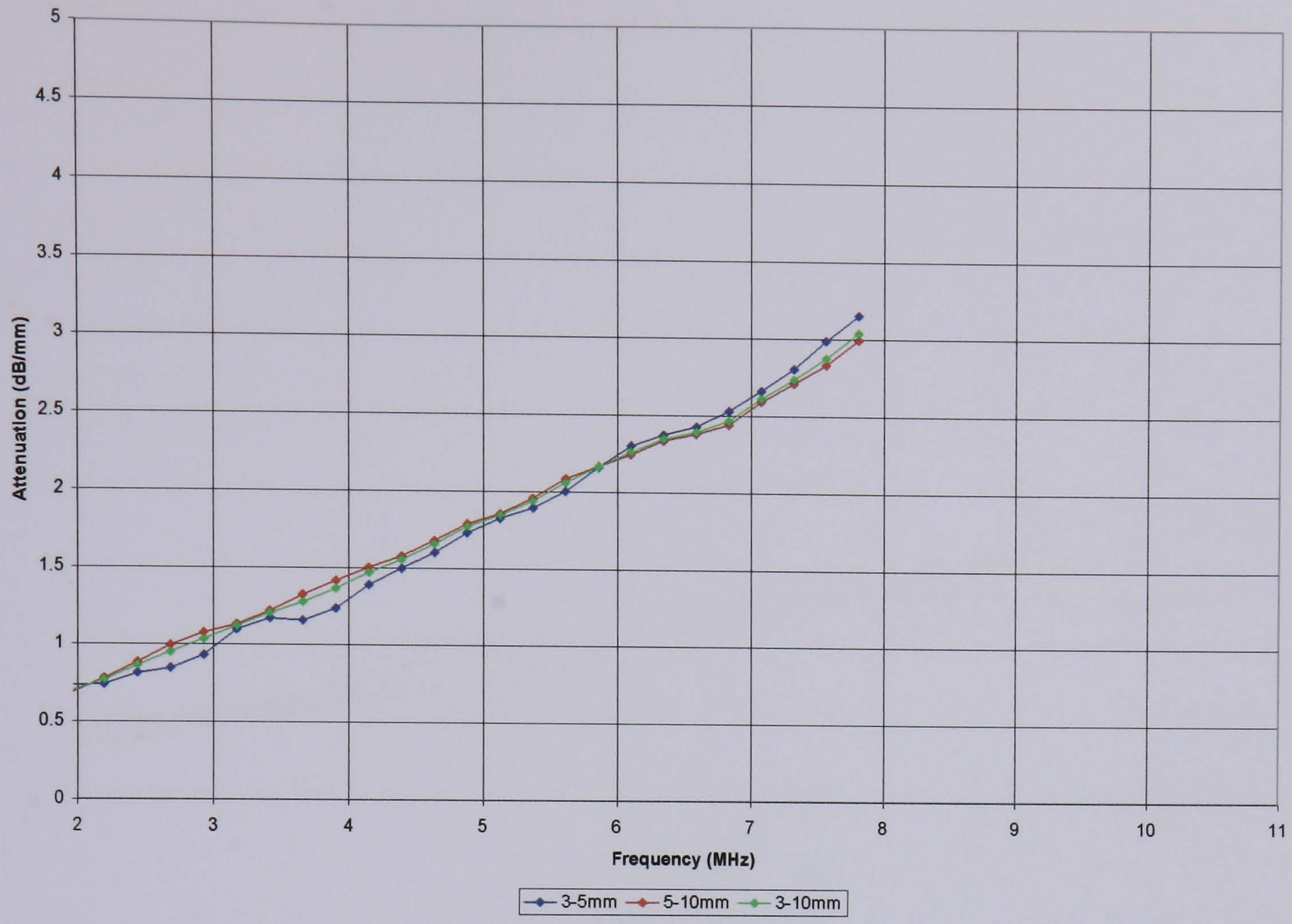

Figure 2.20 Attenuation (dB/mm) Vs Frequency (MHz) for a Batch A hydrated hydrophilic polymer.

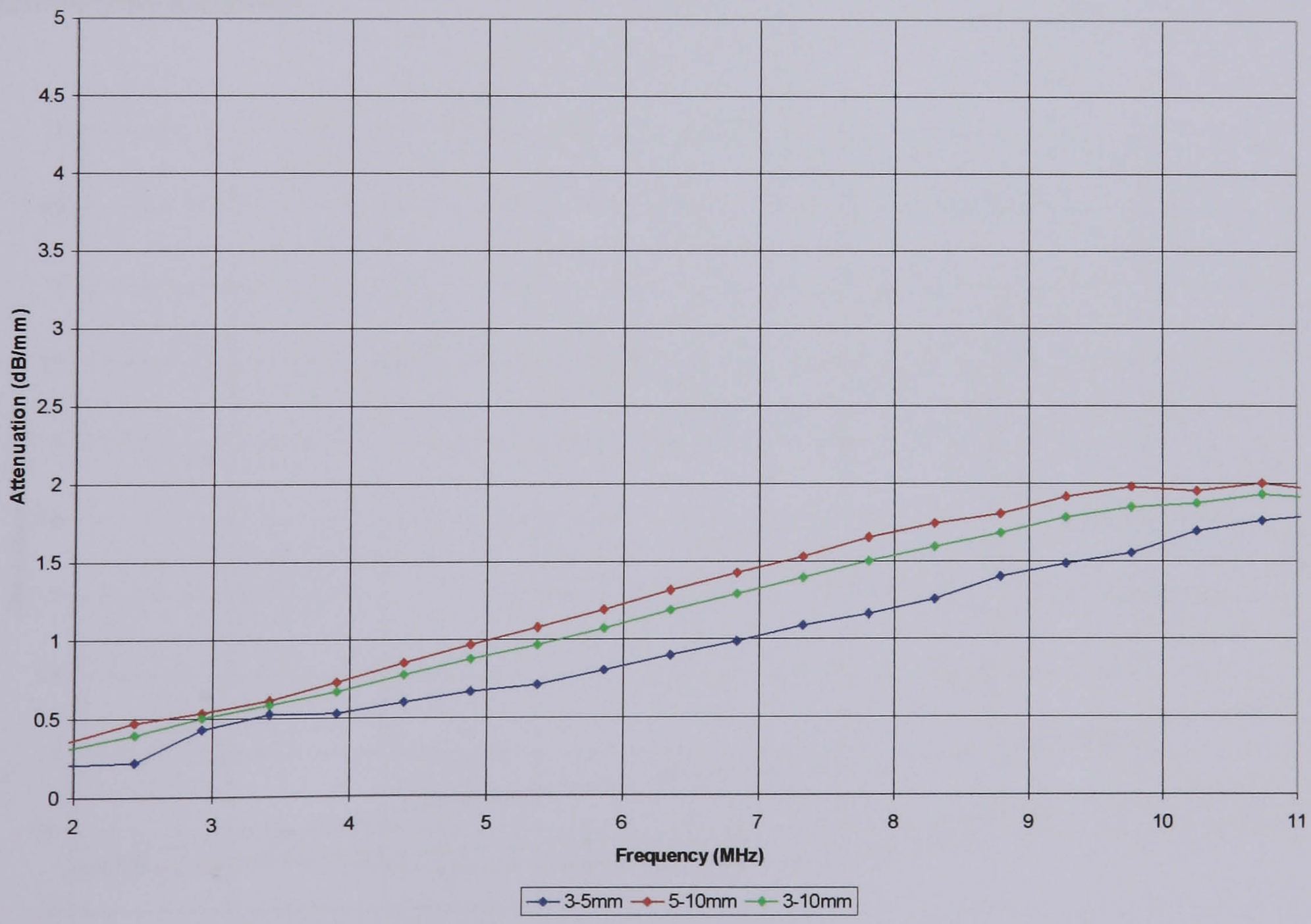

Figure 2.21 Attenuation (dB/mm) Vs Frequency (MHz) for a Batch B hydrated hydrophilic polymer.

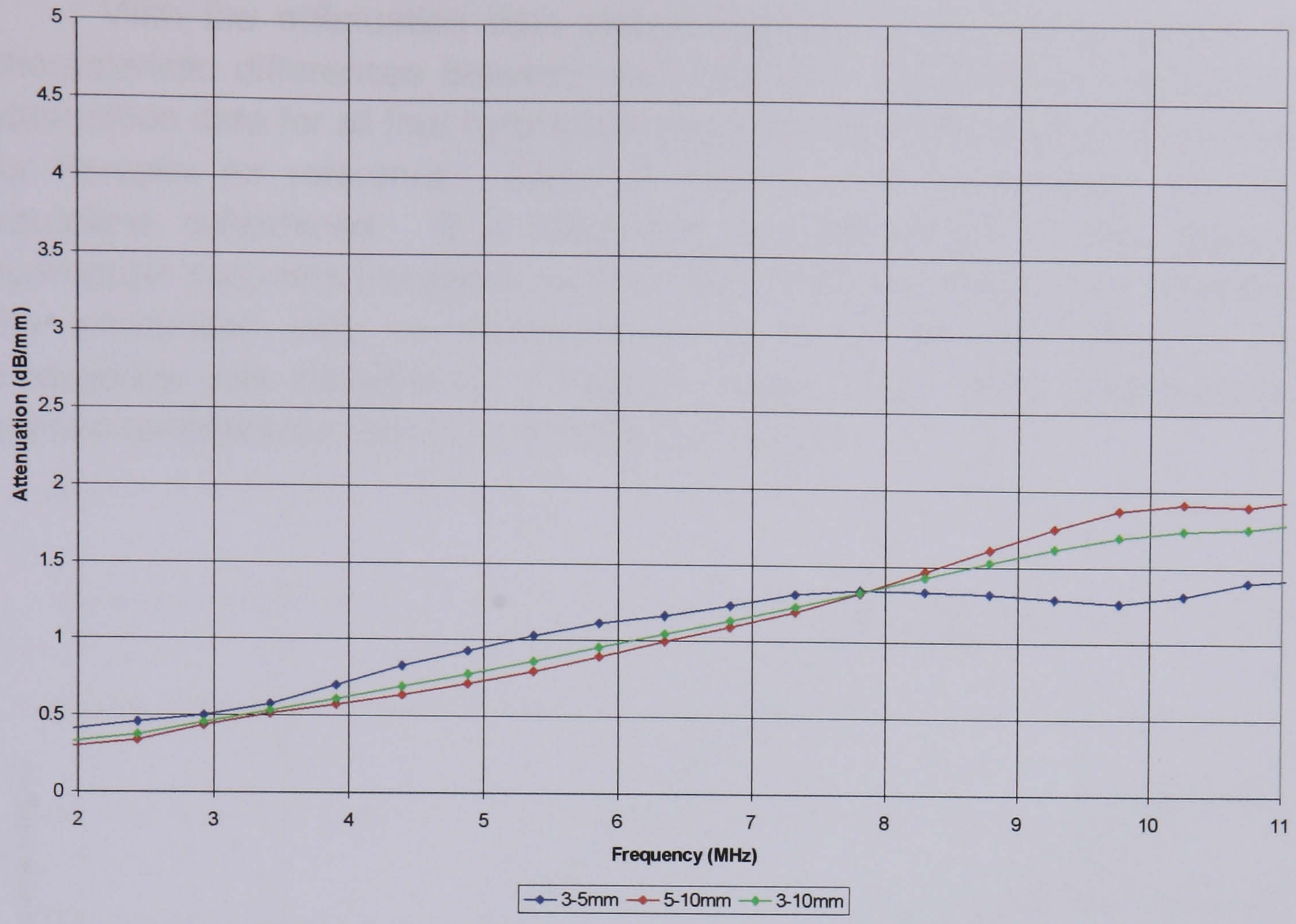

Figure 2.22 Attenuation (dB/mm) Vs Frequency (MHz) for a Batch C hydrated hydrophilic polymer.

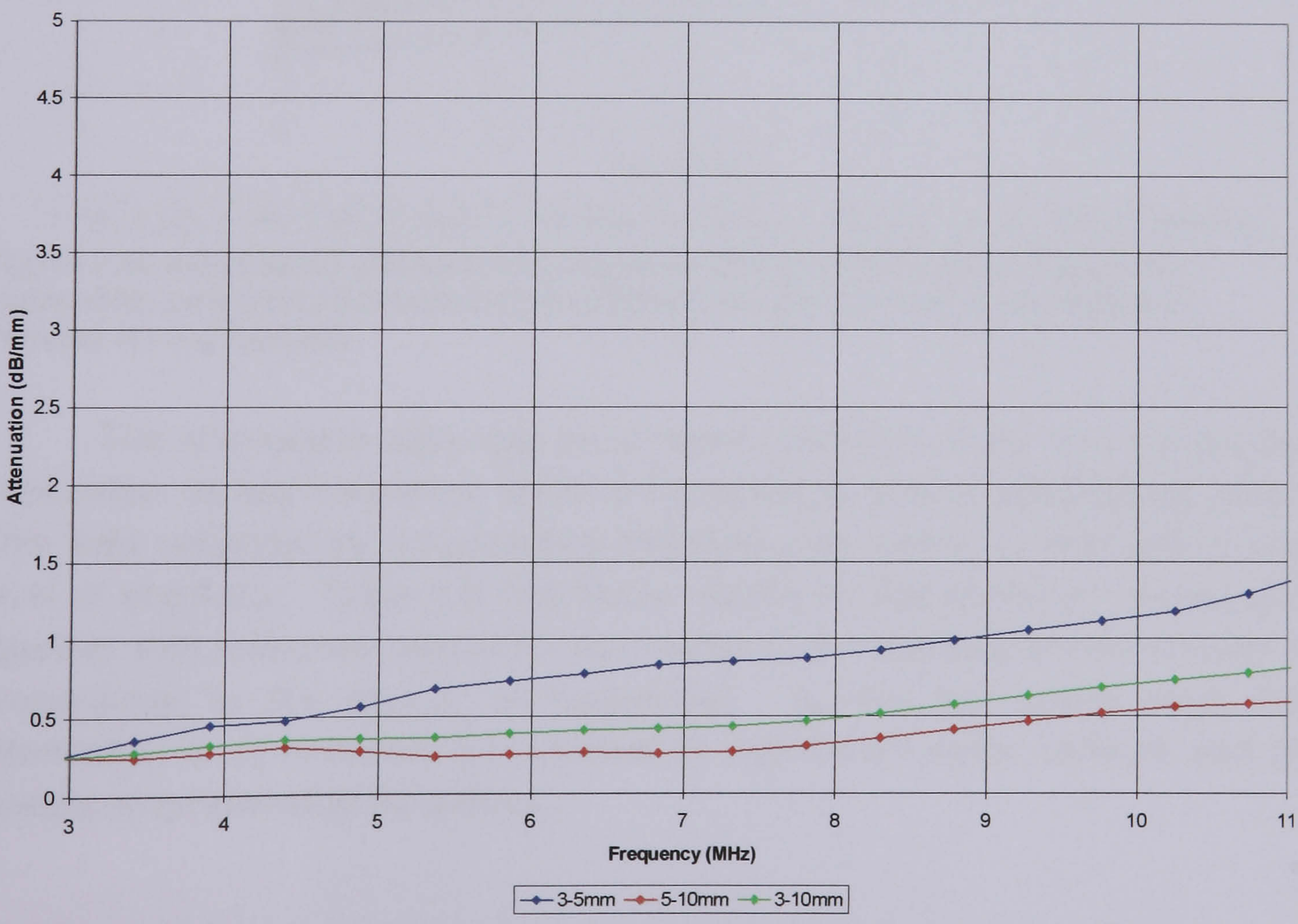

Figure 2.23 Attenuation (dB/mm) Vs Frequency (MHz) for a Batch D hydrated hydrophilic polymer.

With the attenuation data plotted together, it is easy to identify the characteristic differences between each polymer. Figure 2.24 illustrates the attenuation data for all four hydrophilic polymers together with that determined for Perspex for reference. Lines of best fit have been drawn and their equations determined. It is clear that the attenuation in fully hydrated hydrophilic polymers increases linearly with increasing frequency. Therefore, the attenuation may be expressed in terms of dB mm^{-1} MHz^{-1}. The emergence and consistency of logical trends in the data generated has earned confidence in the experimental procedure.

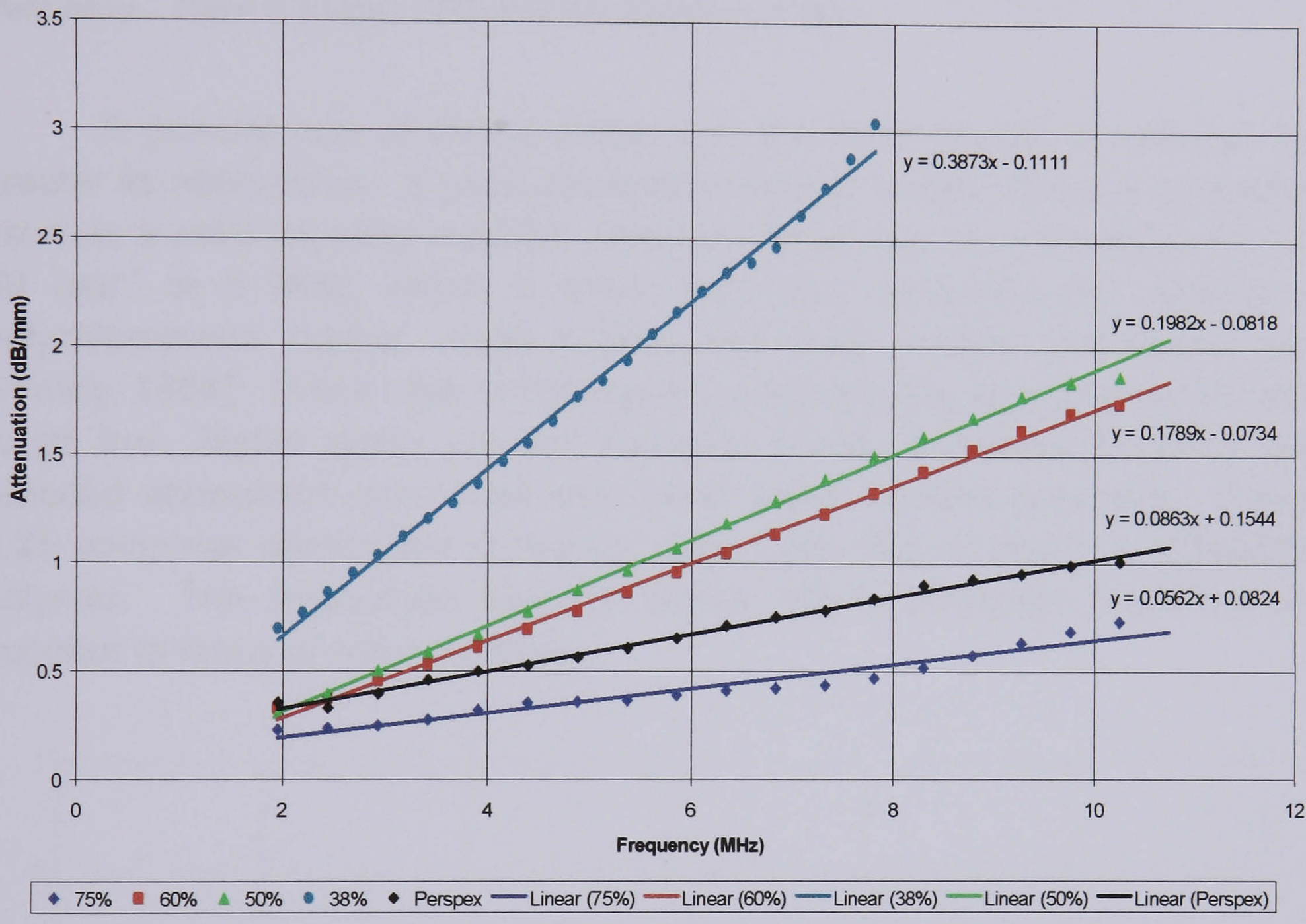

Figure 2.24 Attenuation (dB/mm) Vs Frequency (MHz) for the range of hydrated hydrophilic polymers (Batches A-D) of different equilibrium water contents and Perspex for comparison.

The attenuation data may be analysed further to determine the precise attenuation at any frequency within the bandwidth of the interrogating probe. This was achieved by interpolating between data points to maintain a high level of accuracy. Table 2.6 lists these results for the materials investigated together with reference values for pure water (note that attenuation in water is proportional to the square of frequency). It may be clearly seen that attenuation is (i) inversely proportional to equilibrium water content, and (ii) directly proportional to frequency.

Material	Attenuation @ 2.5MHz (dB/mm)	Attenuation @ 5MHz (dB/mm)	Attenuation @ 10MHz (dB/mm)	Attenuation (dB/mm /MHz)
A	0.89	1.81	3.76*	0.39
B	0.41	0.90	1.86	0.20
C	0.38	0.80	1.72	0.18
D	0.24	0.36	0.71	0.06
Perspex	0.34	0.58	1.00	0.09
Water ▪	1.36×10^{-3}	5.43×10^{-3}	21.72×10^{-3}	2.1715×10^{-4} $dBmm^{-1} MHz^{-2}$

Table 2.6 Attenuation data for a range of hydrophilic polymers, Perspex and water. *Calculated from linear regression, as ultrasonic signal deteriorated at required frequency. ▪ Kaye & Labby, 1975 and Krautkramer, 1983.

A general rule of thumb states that the more flexible a material, the greater its attenuation. A good example is natural rubber, which is commonly used as a solid coupling material. Natural rubber has an attenuation of 3.75 dB mm^{-1} at 5 MHz, which is lower than that measured on samples of polychloroprene rubber, nitrile rubber and butyl rubber [Drinkwater and Cawley, 1994]. In the case of hydrophilic polymers, the opposite can be said to be true, higher water content polymers having increased flexibility with reduced attenuation compared with lower water content polymers. Figure 2.25 compares attenuation in natural rubber with that of Batch D hydrophilic polymer. The hydrophilic polymer clearly offers ultrasonic properties far superior to those of natural rubber.

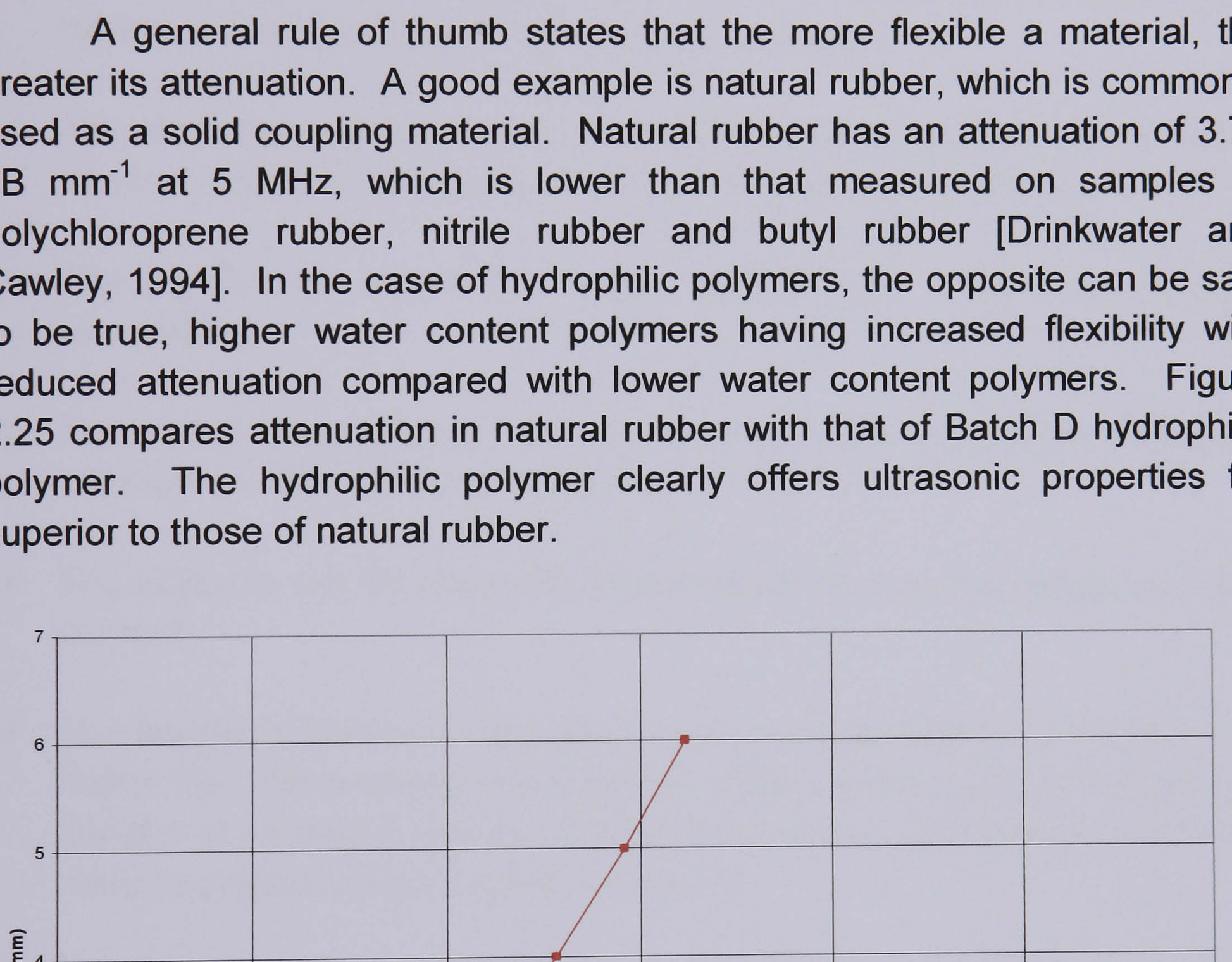

Figure 2.25 Comparison between attenuation of natural rubber interpreted from Drinkwater & Cawley [1994] and a Batch D hydrophilic polymer against frequency.

2.3 Conclusion

From these initial investigations it is clear that hydrophilic polymers demonstrate excellent acoustic properties and offer tremendous potential for novel, solid contact ultrasonic couplants. Points of particular note include,

- A soft and flexible nature, offering potential to conform to uneven surfaces, eliminating air, promoting the correct conditions for ultrasonic coupling.

- The ability to transmit high frequencies – evidence of transmission above 10MHz being demonstrated. This is a significant benefit over natural rubber, a commonly used solid couplant material.

- The demonstration of very low attenuation to ultrasound for a rubbery class of material. (ranging from 1.81 to 0.36 dB mm^{-1}at 5MHz).

- The higher the equilibrium water content, the lower the ultrasonic attenuation.

- The higher the equilibrium water content, the more gradual the increase in attenuation with respect to frequency.

- The ability to vary the acoustic properties by altering the equilibrium water content.

- The benefit of having an acoustic impedance approximately 1.8 MN s m^{-3} higher than those of water and natural rubber, which implies more efficient transfer of ultrasonic energy into materials of industrial interest (assuming identical surface contact can be achieved).

- The potential to vary the mechanical properties by substituting alternative 'backbone hydrophobic' monomers.

Chapter 3: Literature Review

3.1 Problems and Opportunities - The Current Situation

Immersion testing is arguably the most reproducible method of ultrasonic examination, not least because of the consistent level of coupling. However, there are a number of disadvantages associated with this well used technique. Firstly, cost. Immersion tanks are very expensive, the simple three-axis example in Figure A.28 in Appendix A cost £56,000 (bought by the Defence Clothing and Textiles Agency, 1995 from Meccasonics). Secondly, an immersion tank places limits on the size of the test piece – large objects require large immersion tanks. British Aerospace use a tank that is 20 feet long, 10 feet wide and 10 feet deep for the examination of aeroplane wing panels. In addition, immersion tanks are not portable – the test piece requires detachment from any other structure and transportation to the tank. This is often impractical and extends inspection time. The third disadvantage is one of contamination. Obviously, an immersion test necessitates the complete saturation of the test piece with water. This is often not acceptable to a number of materials. Composites in particular are sensitive to the presence of free water. This was described by Taylor [1997] who found the deterioration in impact properties of ultra high molecular weight polyethylene panels (UHMWPE) was proportional to the time spent submerged in water. Similarly, materials susceptible to corrosion or those with open cell structures, for example, are unable to be evaluated via this method (see Figure 3.1 and Figure 3.2). An additional issue concerns the diffusion of water by capillary action into defects such as delaminations in composites. This often has the effect of filling the air cavity with water, a medium that transmits sound readily. The result is a defect that would normally prevent the passage of ultrasound, suddenly transmitting sound as a defect free region of the sample would. This has huge implications for the reliable detection of defects in components ultrasonically evaluated with the immersion technique.

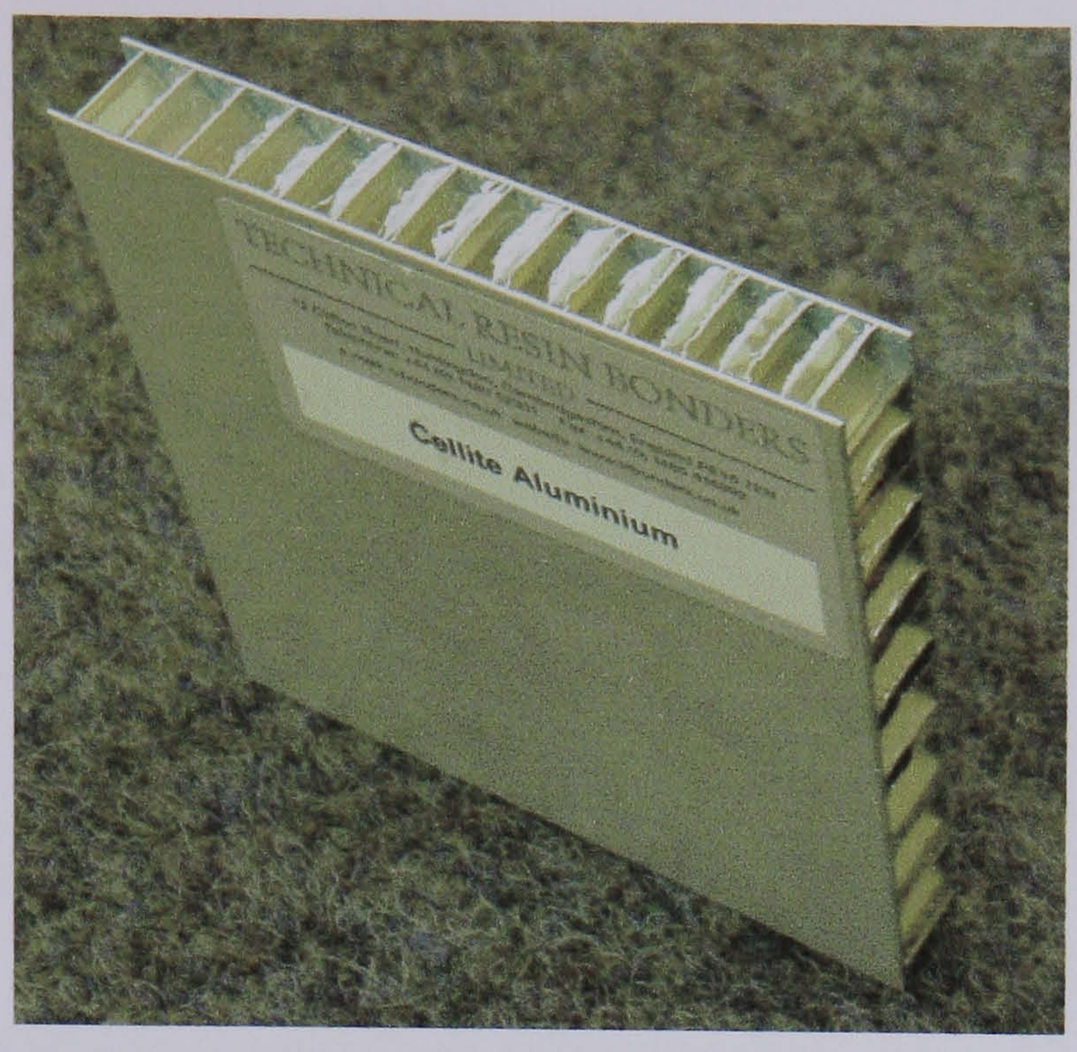

Figure 3.1 Aluminium honeycomb similar to that used on Concorde. An example of an open cell structure that cannot be subjected to immersion testing due to risk of water ingress.

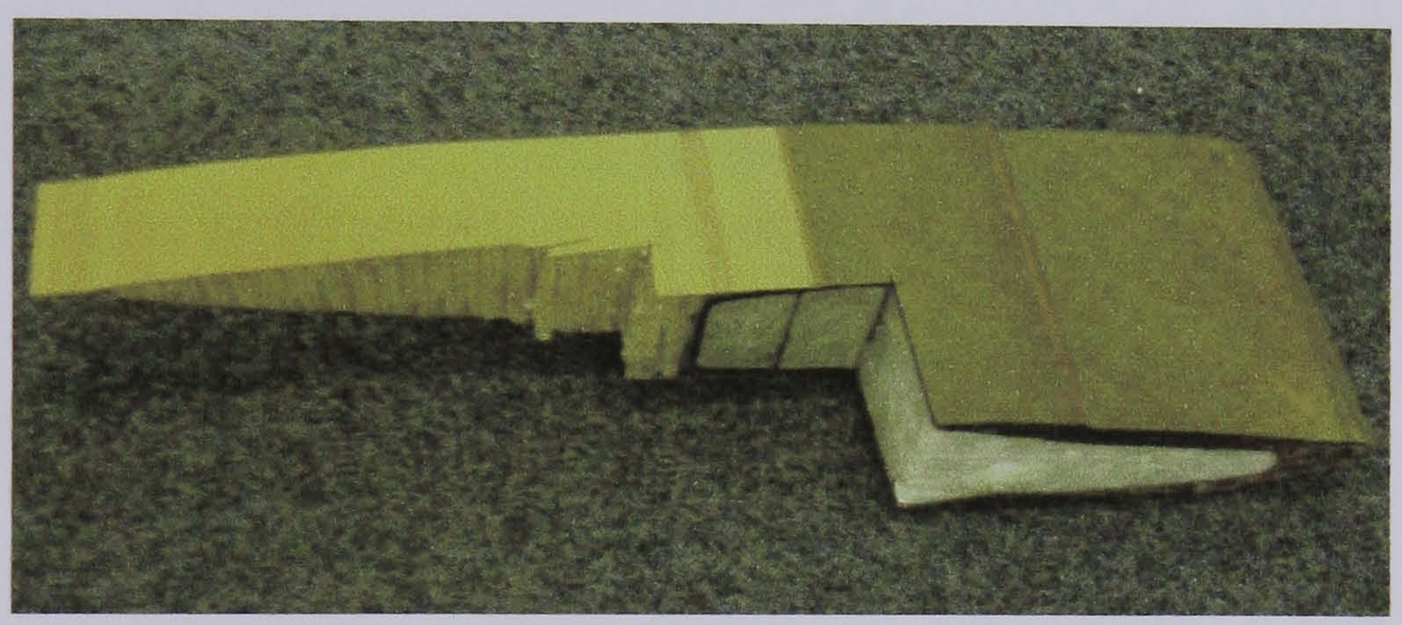

Figure 3.2 Section from a helicopter rotor blade. Material samples of this nature cannot be subjected to immersion testing, particularly at part-manufacture stages.

As with immersion testing, the jet probe approach has its own restrictions. Cost is again a major issue as expensive water collection and pumping equipment is required to maintain the water jet. The consistency of coupling is not as effective as that achieved through immersion testing. This is in part due to the inclusion of air bubbles in the jet stream, which are very difficult to avoid. In addition, there still remains the issue of saturation with water, which is not suitable for many materials. A general point is that both immersion and in particular jet probe systems tend not to be very user friendly, mainly due to the huge amounts of water that need to be handled.

So, the restricting factors in automated NDT can be summarised as follows:

- Threat of contamination/corrosion due to saturation with water,
- Unreliable detection of defects due to water absorption,
- The cost of the equipment required,
- The inability to conduct examinations in-situ,

- Limitations on the size of test piece examinable,

Of all of these, it is felt that the absorption of water is the most serious as it gives rise to both contamination and an associated risk of negative defect detection. This is particularly important in the case of composites. Indeed, with the increasing use of composite materials in safety critical structures for example aerospace, there is growing need for clean and reliable methods of NDT.

3.2 Existing Technology

The concerns described above have been in the minds of practitioners and research and development engineers alike for many years, resulting in a number of alternative methods for the ultrasonic inspection of a range of materials. As is usually the case, different advantages and disadvantages must be traded off against one another to establish preferred compromises. Below is a summary of some of the main techniques developed to overcome the need for the application of a liquid couplant and the associated limitations.

3.2.1 Air Coupling

An ideal ultrasonic system would be non-contact, operating in air. Interesting research has been conducted on air-coupled probes by Yano et al [1987] and Manthey et al [1992] and more recently, Grandia, et al [1994]. Unfortunately, to overcome the severe attenuation imposed by air to high frequency sound, air-coupled probes must operate at relatively low frequencies (typically 50 – 400kHz) in comparison with conventional contact probes. This places limitations on resolution and their use in practical environments.

To improve the signal to noise ratio, air coupled probes are not damped. In other words the transducer crystal rings for a long time after firing. Probes of this type are often termed 'resonant transducers'. This means that such systems must operate in through transmission mode, the main implications being that (i) the position of a detected defect cannot be given in relation to the surface of the test piece, and (ii) there must be access to both sides of the test piece. A general explanation of the differences between an air-coupled system and the approach of conventional ultrasonic NDT is given by Bourne, et al [2000a] where discussion focuses on technique development with a Sonda 007CXL Airscan system from QMI.

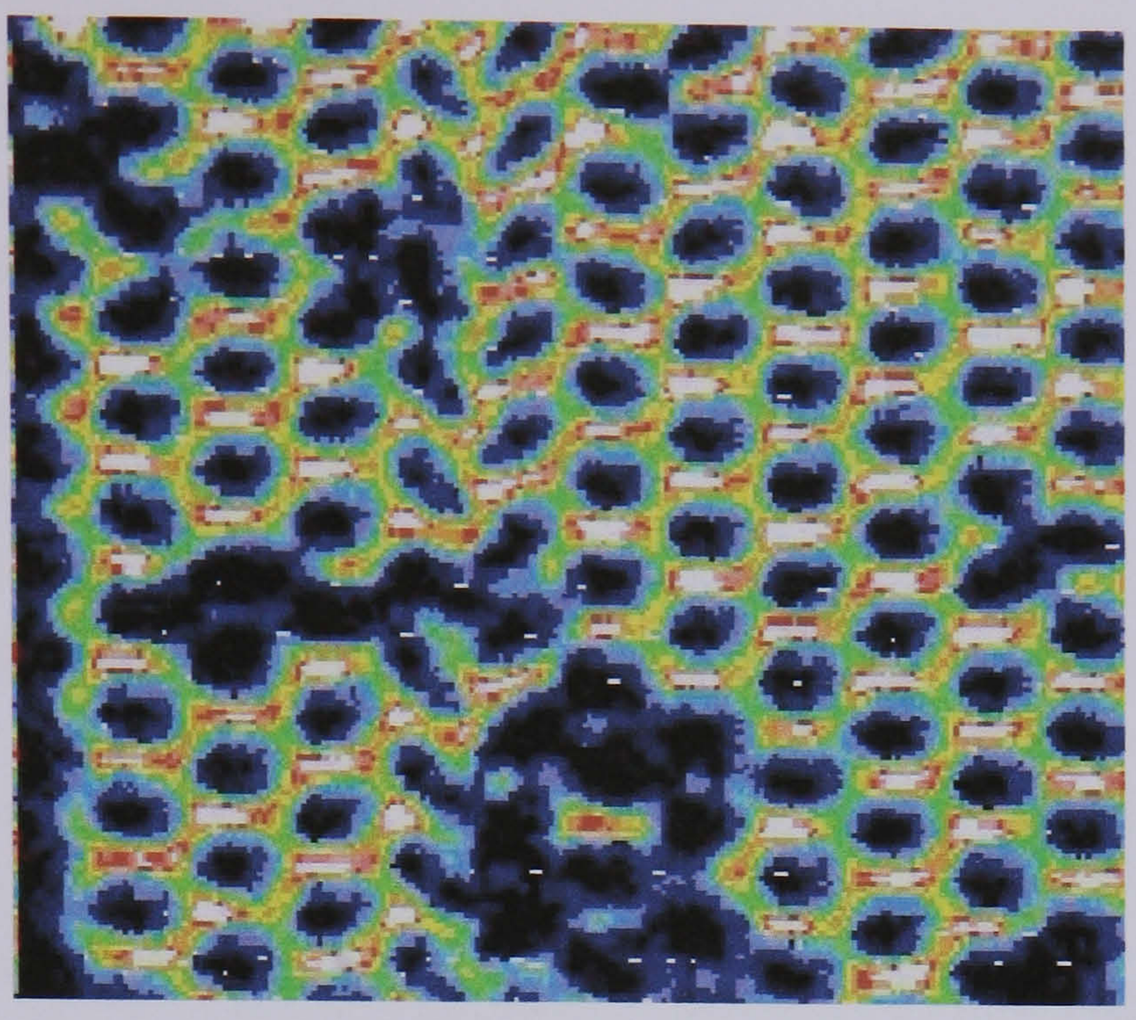

Figure 3.3 C-scan image of a metal honey comb structure with composite skins used for a space application. Damaged cells are clearly visible as dark regions. [Buckley and Loertscher, 1999].

Recently, investigations have been made into methods for increasing resolution without the need for using higher frequency probes [Buckley and Loertscher 1999]. Techniques include the use of focussed probes together with offsetting probe alignment, hence reducing the 'effective beam diameter' enabling the detection of smaller defects. Defects of down to 2mm in diameter have been detected with 400kHz probes under optimal conditions.

3.2.2 Laser Generated Ultrasound

Much work has been focussed on the development of techniques for the generation and detection of ultrasound via lasers [Hutchins, 1988]. Again, the main advantage of such techniques is the ability to operate without making direct contact with the test piece, enabling measurements to be conducted on hot materials. A good example being the measurement of the velocity of sound in liquid lead at 2000°C [Cadler and Wilcox, 1980].

It is convenient to consider two cases for the generation of ultrasound. The first relies on a laser as a source of thermoelastic energy whereby a laser pulse introduces a sudden deposition of thermal energy into a restricted volume at the test piece surface [Ready, 1971]. The rise in temperature is accompanied by an equally rapid thermal expansion, resulting in mechanical vibration in the test piece [Scruby et al, 1981]. This process generates ultrasound that radiates into the test piece in a very different way to conventional piezoelectric sources, offering scope for special applications. The second method involves the use of a higher power laser to deposit sufficient heat into the test piece surface to raise the temperature to the

boiling point causing some of the heated region to ablate (boil off). In this case, the laser is operating as a source of elastic energy. This generally causes a metal plasma to form over the surface of the test piece. As a result, the effect of the laser beam becomes very complex. The relationship between the energy in the laser beam and the amplitude of the resultant ultrasound for this mode of generation has been investigated by Krehl et al, [1975]. The direction of propagation is preferentially normal to the test piece surface in the case of compression waves [Scruby, et al, 1981 and Miller & Pursey, 1954].

The ultrasound may be detected by the use of laser interferometers. In principle, a coherent optical beam reflected from the test piece under examination is allowed to interfere with another part of the beam split off and reflected from a fixed reflector. Small movements in the surface of the test piece (caused by an ultrasonic pulse) may therefore be detected by changes in the interference conditions between the beams.

Despite the effective generation of ultrasound via lasers, the complete system is let down by the detection techniques [e.g. Bandarenko, et al, 1976], which are relatively inefficient in comparison to conventional piezoelectric methods. This area has however been the subject of recent research by Klein, et al [2000]. Additional disadvantages include the high cost of such systems and the risk of damaging the test piece surface as a result of the high energies required, all of which place great limitations on their practical application at this time. The technique is however being evaluated for wide spread use in the aerospace industry [Petillion, et al, 1998].

3.2.3 Electro Magnetic Acoustic Transducers (EMAT's)

EMAT's are non-contact transducers, therefore requiring no coupling fluid [Thompson, 1990]. They function by inducing eddy currents in the surface of the test piece using an energised flat coil within the body of the probe. If the region containing the eddy currents is placed in a magnetic field the Lorentz force between the current and magnetic fields induces stresses in the surface of the test piece. These stresses generate a mechanical wave in the test piece. The process of reception is the direct inverse of the effect described above [Silk, 1984].

As an EMAT's may be held just off the surface of the test piece, they are particularly useful for the inspection of hot test pieces and are not hindered by surfaces covered in protective coatings. The main disadvantages of these devices in comparison to piezoelectric transducers, is that they are relatively less efficient (loss of amplitude in the region of 50dB) [Silk, 1984]

offering lower sensitivity [Billson and Hutchins, 1993]. In addition, EMAT's are very sensitive to probe lift-off, the amplitude of the generated ultrasonic signal suffering large fluctuation from very minor changes in probe to test piece distance. The nature by which eddy currents are generated in the test piece is itself a limiting factor, restricting the use of such devices to the generation and detection of ultrasound in electrically conducting materials. Some work has been done by Hsu et al, 1999 exploring the potential for generating ultrasonic waves in non-conducting composites with EMAT's by adhering a removable aluminium foil tape to the sample surface.

3.2.4 Solid Couplants

An alternative approach is to employ a solid-contact coupling medium between the probe and test piece. Unlike the other alternative techniques described, this requires contact with the test piece, but still does not pose a threat of contamination. There are two common designs of solid coupled probes. The first is a manual (or static) probe onto which a rubber tip is attached to the front of a standard contact probe which is then pressed against the surface of the test piece, coupling being provided by the rubber tip. The second is the wheel probe in which a standard transducer crystal is attached to the axle of a wheel that rolls over the surface of the test piece, coupling being provided by the rubber tyre. Probes of this nature have been in existence for some time [Dickson, 1982, Billson and Hutchins 1993 and Drinkwater and Cawley 1994]. Such devices offer the following potential advantages:

- The process is clean – eliminating potential couplant contamination of the test piece,
- No additional equipment is required (e.g. immersion tank),
- No limit is placed on the size of the test area,
- The technique is portable, allowing scope for in-situ examinations, reducing down time,
- There is no need to carry large quantities of coupling fluid should the examination be mobile (e.g. railway line examinations).

However, there are a number of technical obstacles. The solid coupling material would ideally be sufficiently compliant to conform to the uneven surfaces encountered in practical inspection while not imparting a high

level of ultrasonic attenuation. Unfortunately, these two demands are almost mutually exclusive in conventional materials. A general 'rule of thumb' is that as the flexibility of a material increases, so does its attenuation to ultrasound. For this reason, and in an attempt to increase the life of the solid couplant, stiff rubbers such as natural rubber have often been chosen for this application in the past. As a result, a high level of pressure is required when coupling to surfaces that are anything other than mirror smooth. Similarly, the attenuation in the material is quite high, restricting practical use to low frequencies, typically below 2MHz. This has forced undesirable designs such as the use of resonant transducers for increased signal amplitude. This limits their use to through transmission, severely restricting usefulness. In addition, a small amount of coupling fluid is often required to assist coupling, which re-introduces a risk of test piece contamination. In this sense, such solid couplants can be said to reduce the amount of liquid couplant required but not eliminate it altogether. Therefore, the limitations of conventional solid couplant may be summarised as follows:

- An inability to conform to rough surfaces,
- High attenuation to ultrasound,
- Low frequency operation,
- Through transmission only.

3.3 Literature Review

With a general picture of the limitations facing conventional ultrasonic inspection of materials and structures, together with an appreciation of the main techniques and alternative approaches developed to enable ultrasonic evaluation to continue to advance, time was spent exploring the literature. This focused on developments in solid couplant and their employment in practical applications.

3.3.1 Solid Coupled Through Transmission Probes

The earliest reference to solid coupled ultrasonic probes is believed to be that of John Dickson who presented a paper at the 10th World Conference on NDT in 1982 entitled 'Dry coupling ultrasonic method of inspection on composite and metallic honeycomb panels on aircraft structures'.

Dickson went onto develop both static and wheel probes incorporating solid couplant. Both employed a low frequency resonant transducer crystal between 0.5 and 2MHz and so were used as pairs, most commonly in through transmission. A schematic of the static probe is shown in Figure 3.4. The transducer crystal is held in pressed contact with a contact shim by a simple spring. The shim is in turn pressed against the solid rubber tip.

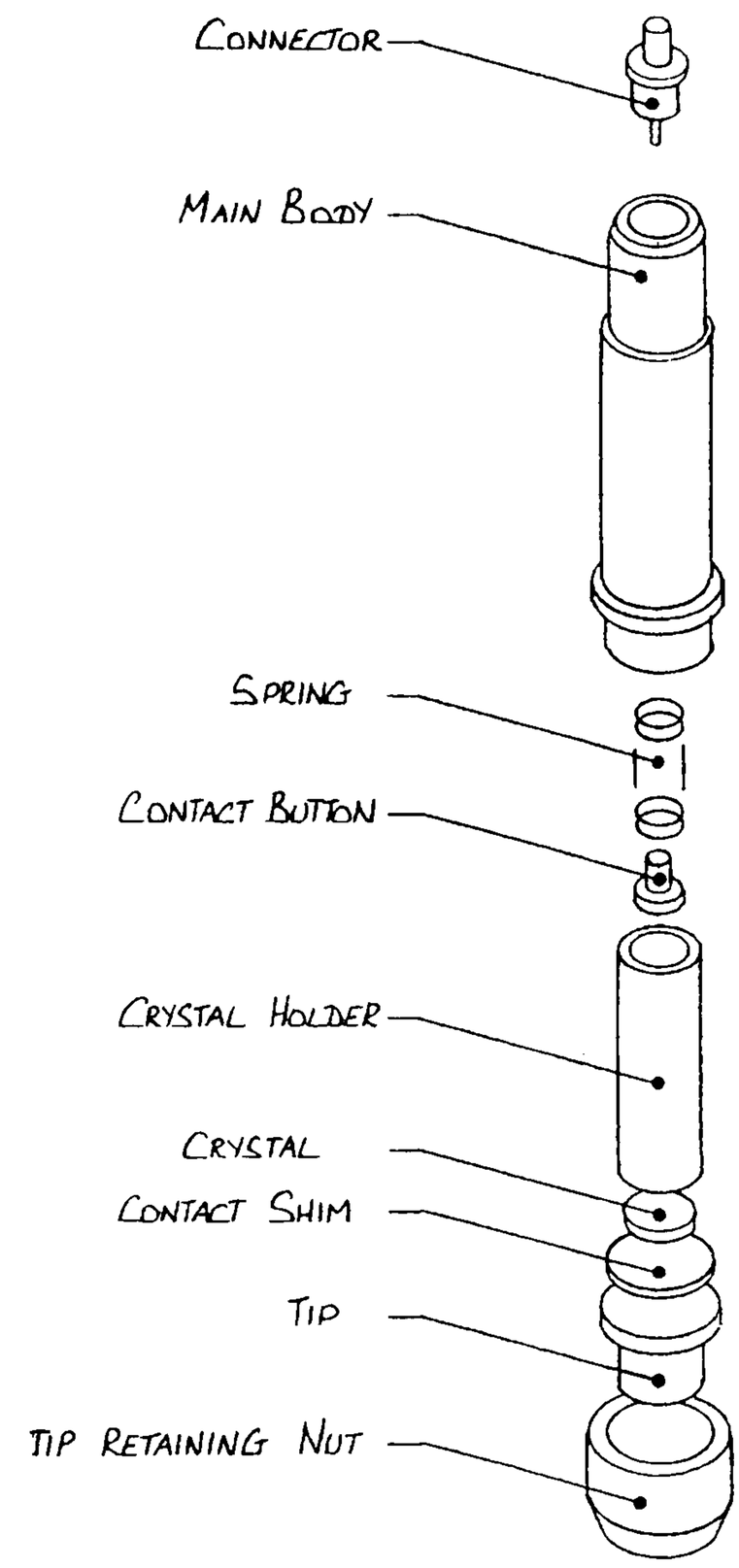

Figure 3.4 Schematic of a solid coupled static ultrasonic probe developed at Sonatest by Dickson, circa 1980. These devices are still commercially available.

The design of the wheel probe is more complex (see Figure 3.5). This is mainly due to the mechanical issues involved in keeping the ultrasound beam perpendicular to the test piece while enabling the wheel to rotate. This forced an undesirable design to be implemented. A low frequency resonant transducer crystal is bonded to an aluminium stub at the centre of the axle. The stub has a convex radius to enable it to fit snugly inside the wheel. This has the effect of diverging the ultrasound beam, resulting in a very broad sound field. This is effectively the opposite of focussing, having a negative effect on beam definition. The curved aluminium stub is fixed in the centre of the wheel, with the sound beam facing towards the test piece. This sub assembly is surrounded by a reservoir of oil, which is contained by an outer Perspex shell. It is this outer shell that is free to rotate and onto which the thin

rubber tyre fits. Coupling to the test piece is achieved by pressed contact with the tyre. Of key importance here is the high number of interfaces the ultrasound must cross inside the body of the probe before being propagated into the test piece material:

1. Crystal to aluminium
2. Aluminium to oil
3. Oil to Perspex
4. Perspex to rubber
5. Rubber to test piece

By applying Equation A.5 from Appendix A it may be shown that approximately 55% of the ultrasound generated by the transducer crystal is propagated into the tyre of the wheel probe. This accounts for a large 7.6dB loss in signal amplitude (excluding attenuation) before the sound has even reached the test piece material. This is the main reason for using a resonant transducer crystal, generating a significantly higher amplitude signal than a conventional damped device, flooding the test piece material with non-directional ultrasound. The side effect of this is of course the long ringing signals generated, necessitating the use of a second device as a receiver. Both the solid coupled static and wheel probes developed by Dickson could be driven by a conventional ultrasonic flaw detector. However, a custom designed drive unit was developed by Sonatest known as the Dryscan UFD 200 which enabled much more efficient use. The main difference over a conventional ultrasonic flaw detector was the incorporation of lower frequency filterbands and a tuneable receiver frequency.

The first few references addressed here (Circa 1980's) used these probes or ones developed in parallel using the same design philosophy.

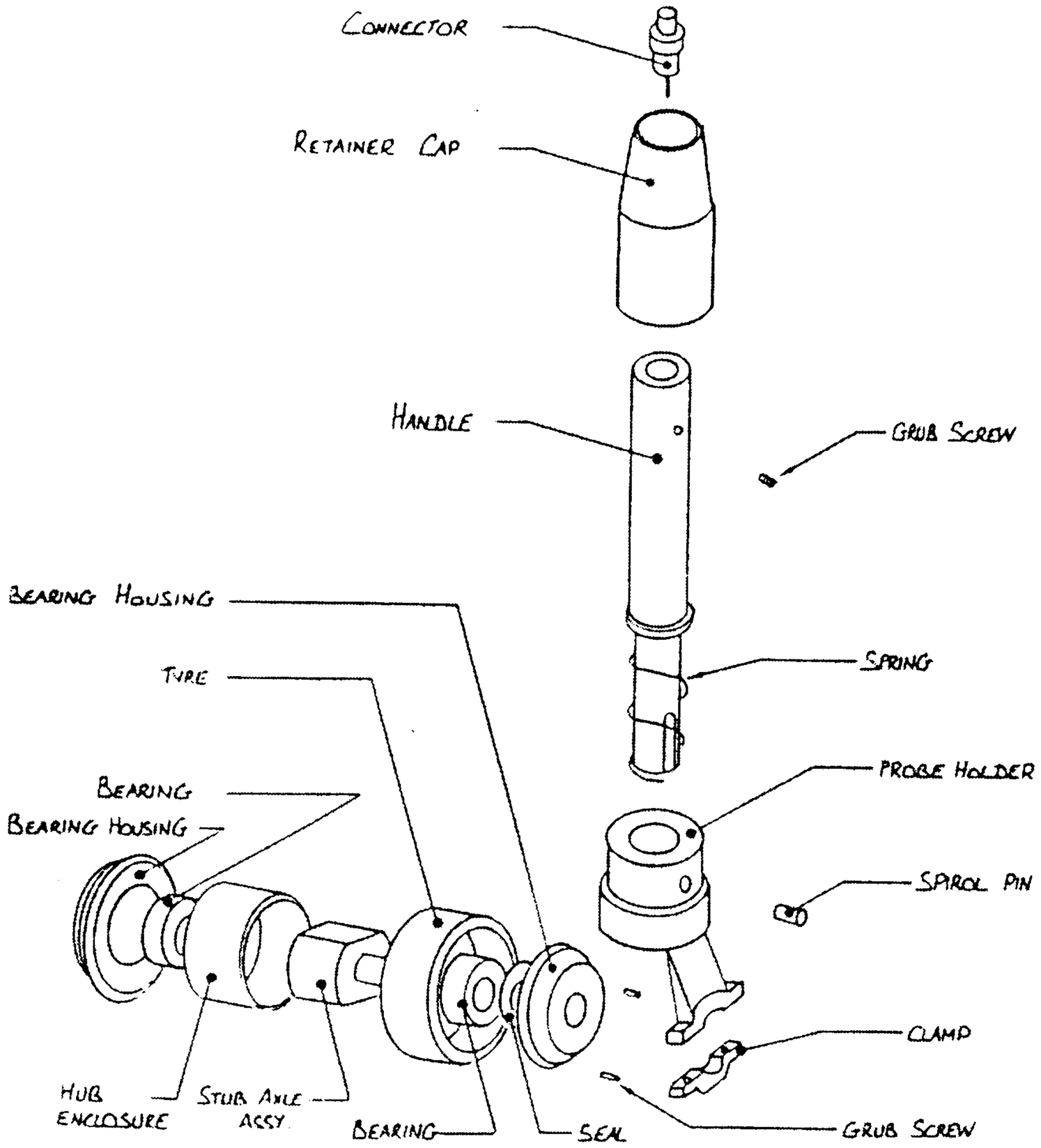

Figure 3.5 Schematic of a solid coupled ultrasonic wheel probe developed at Sonatest by Dickson, circa 1980. These devices are still commercially available.

Lecru [1987] described the need for a solid coupled ultrasonic technique for the inspection of bonded composite assemblies in aircraft structures. His reasons overlap with observations already discussed; namely the desire to eliminate coupling fluid, increased inspection speed and ease of interpretation of ultrasonic results.

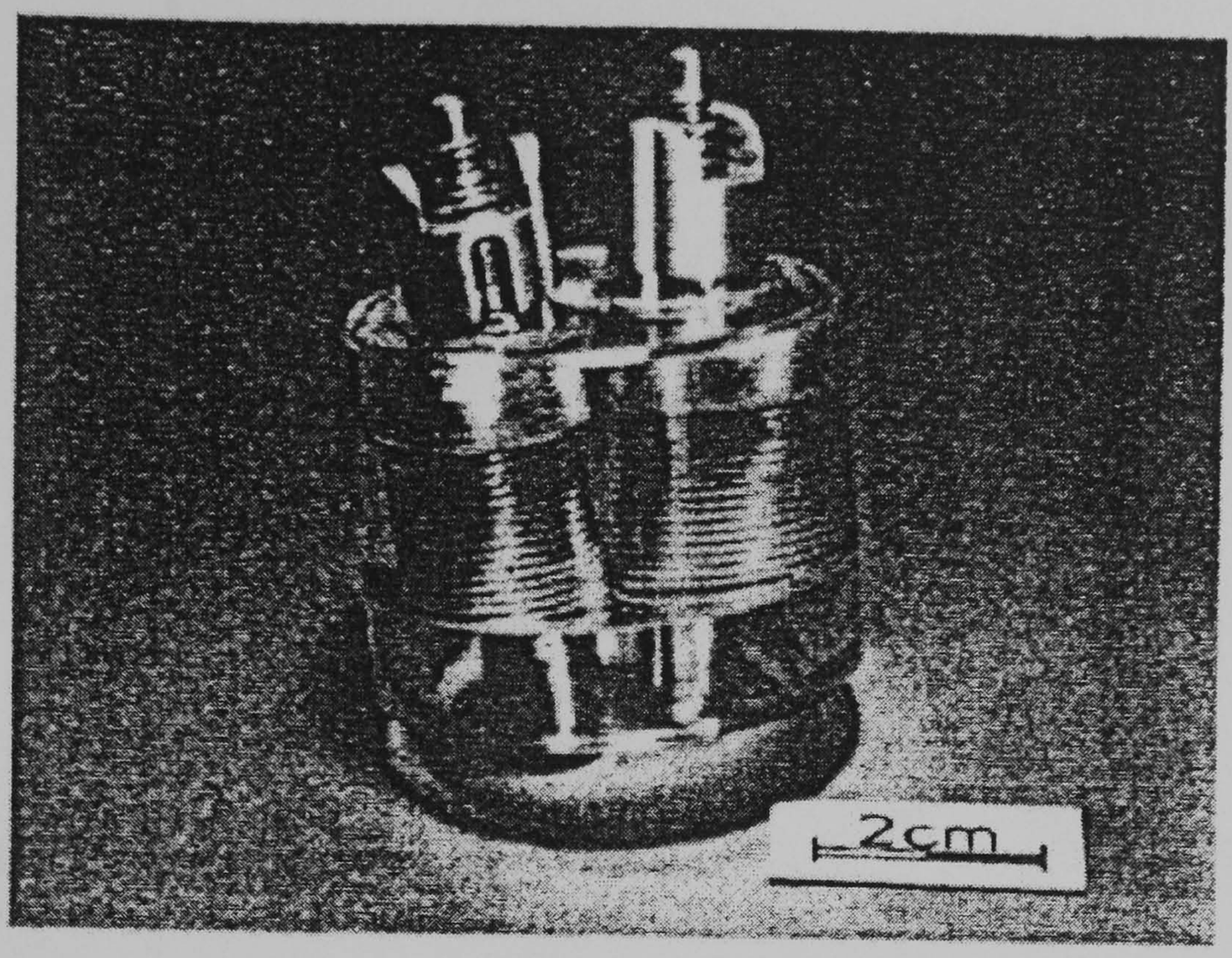

Figure 3.6 Solid coupled twin probe arrangement used by Lecru [1987].

For this application two low frequency, straight beam ultrasonic compression probes were used in tandem. One transmitted ultrasound of around 1.5MHz and the other received. Two probes were required because the transducer crystals in the probes were resonant. This increased the amount of energy produced by the probe but resulted in long ringing signals. This means that a long time must pass before a resonant probe having just transmitted a pulse of ultrasound has stopped ringing sufficiently to be ready for reception of the returning pulse. In this application, as with many others, this was not feasible owing to the travel time of the pulse through the sample being shorter than the transducer 'ring down' time. Hence two probes were utilised in this case on the same side of the test piece, separated by a distance of approximately 10mm. Coupling was achieved to the test piece via 'a soft rubber end piece' whose composition and ultrasonic properties were not disclosed. The test piece itself was described as two thin sheets bonded on top of each other.

The technique worked by saturating the test piece with ultrasound from one probe and monitoring the amplitude received by the other. The principle being that if there was no bond between the top and bottom sheets, then all the energy would stay in the top sheet resulting in a high received amplitude. If however the bond between the two sheets was good, some of the energy would be propagated into the bottom sheet resulting in a reduced amplitude detected. The technique having been proven by the static probe approach, roller probes were developed capable of producing the same results but allowing the inspection to be conducted even faster by permitting rapid scanning.

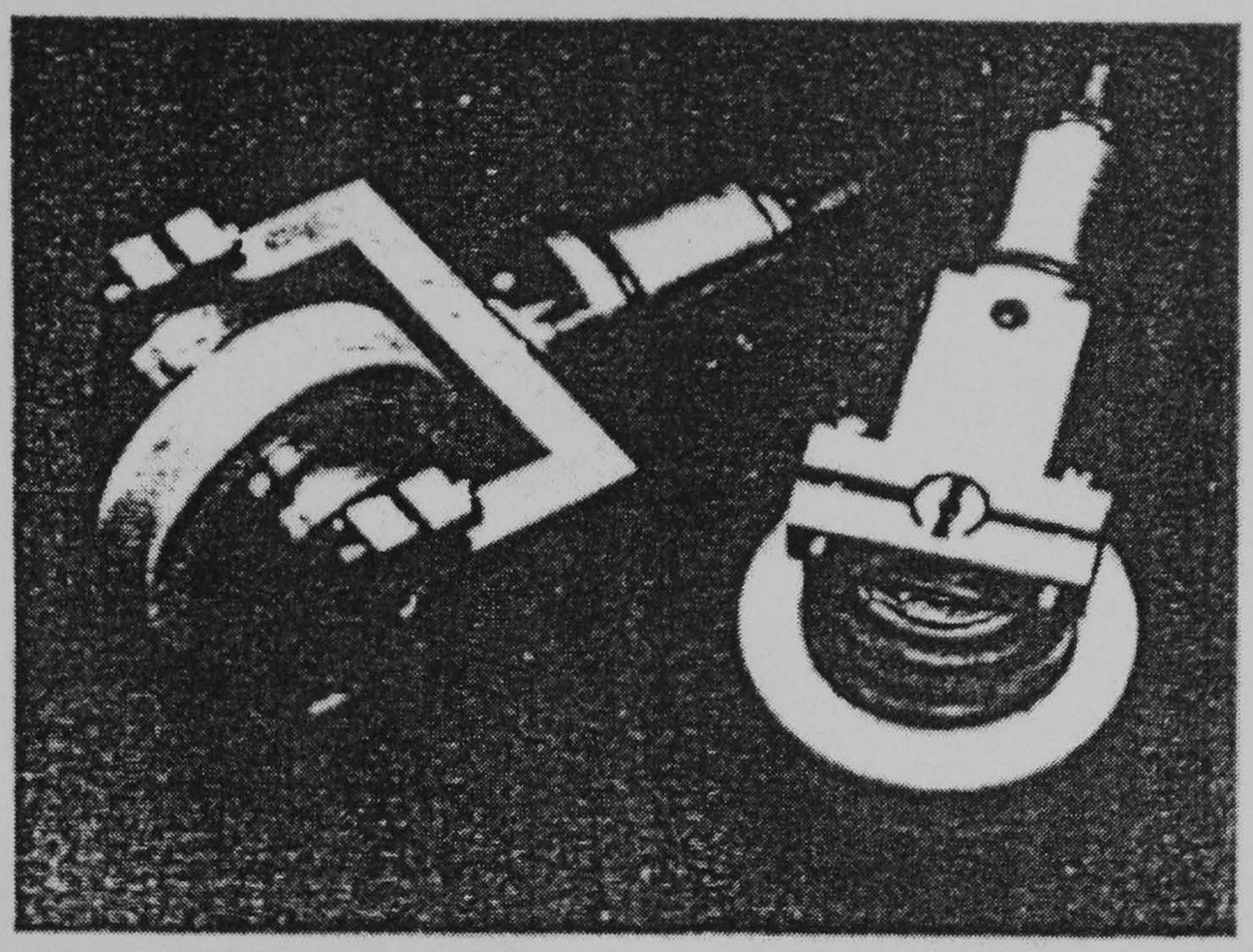

Figure 3.7 Solid coupled wheel probes used in tandem to generate C-scan images of disbonding in composite panels. [Lecru, 1987]

The technique was taken a stage further by integrating the roller probes with a C-scan system, results producing strong indications of large disbonded areas. The system was found to be insensitive to sheet thickness or paint film thickness, which was a major asset for inspection of ageing aircraft. However the limitations of the technique were significant. It was noted that the technique was only capable of identifying 'significant bonding defects' i.e. the presence of an air layer between the two sheets, which meant that the quality of the bond could not be graded. The smallest areas of disbond reported were 10mm in diameter, which is not sufficiently sensitive for many inspections. In addition, inspection of composites was inconclusive, showing a marked relation to the orientation of the fibres in the top sheet layer. This is a key point as the use of composites is on the increase in aerospace and other safety critical structures.

Thavasimuthu, et al [1989] evaluated the use of solid coupled ultrasonic probes for the inspection of abrasive wheels. Again the presence of couplant was cited as a nuisance, soaking into the small pores in the wheels and necessitating its subsequent removal. The inspection method adopted was very similar to that described by Lecru, employing two probes, one for transmission and the other reception. Coupling was achieved by 'rubberised pads connected intimately with the probes'. No description of the material or its ultrasonic properties was given although it is suspected to be that developed by Dickson. Both probes were positioned on the same side of the test piece rather than used in through transmission mode. It is clear from the figures of the received ultrasound, that the crystals were resonant. Both 0.5 and 1.25MHz probes were evaluated; the latter demonstrating the greatest signal change when placed over an area containing a defect.

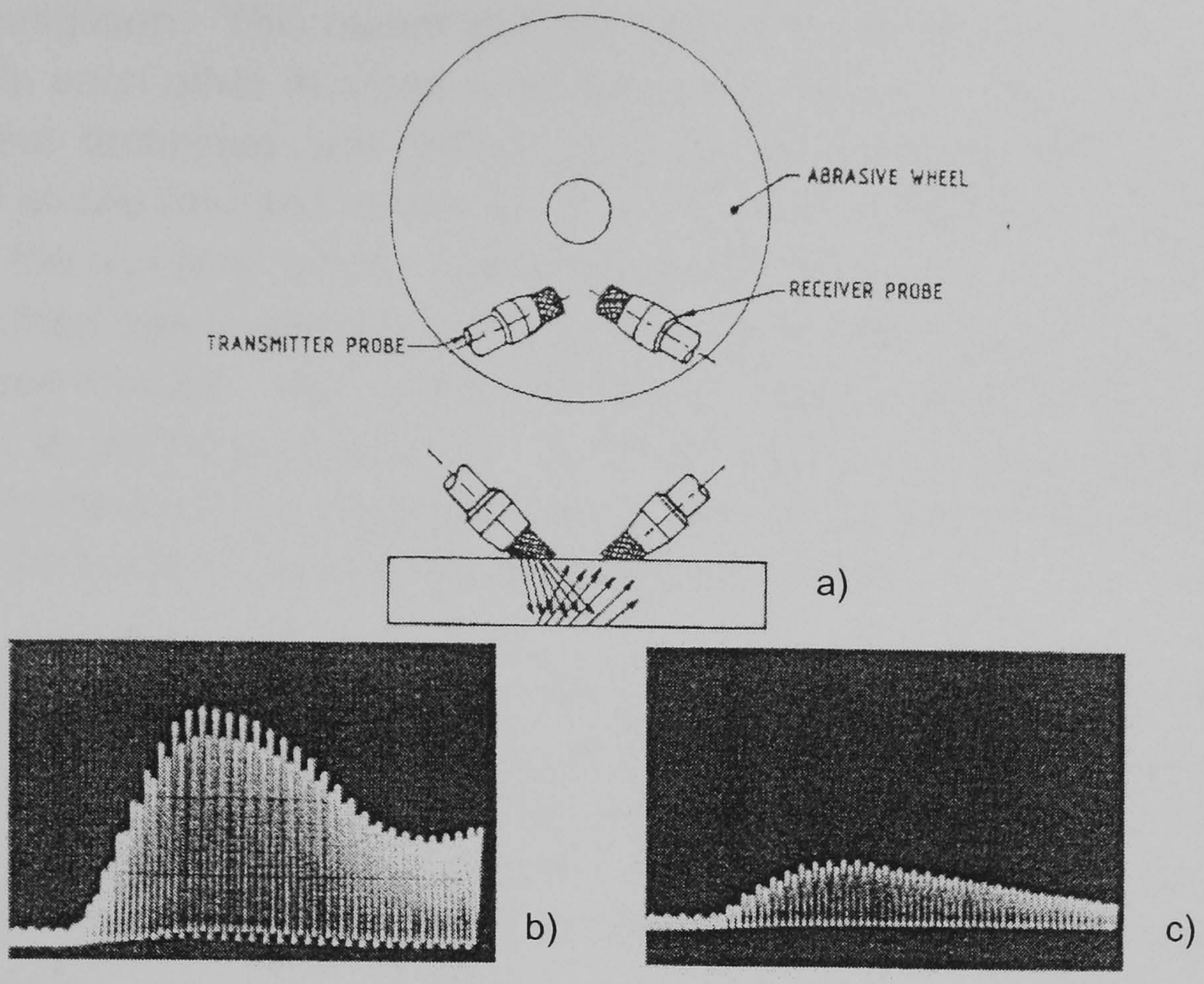

Figure 3.8 A) Probe arrangement and typical ultrasonic signals generated by solid coupled probes over B) a good area, and C) an area containing defects. [Thavasimuthu, 1989]

The technique worked by transmitting ultrasound into the wheel via probe 1, where it is reflected from the rear side of the test piece and detected by probe 2. A defect free region was typified by a strong returning signal. A region containing a defect such as a crack produced a signal of significantly lower amplitude, the ultrasound being scattered away from its path towards the receiving probe. While the signals reported show a clear distinction between the good and bad regions, practical experience has proven that small variations in amplitude can be caused by a number of factors the most significant being minor misalignment of the probes. In fact, results from this inspection method required confirmation by radiography. Thus quantification of defects located with this solid coupled technique is not sufficiently reproducible for practical application.

Thavasimuthu, et al [1990] again used a solid coupled ultrasonic technique for the inspection of rivets in a steam turbine. This time, two 1.25MHz resonant probes were used in tandem in through transmission from the cap of the rivet to the turbine blade. The main driver for the use of solid coupled transducers in this case was not concern of contamination by liquid couplant, but remote access. The complex geometry of the test piece ruled out the use of conventional ultrasonic probes.

Thavasimuthu claimed that precise positioning of the solid coupled probes onto the test piece was not critical so long as they bridged the region

under investigation. This meant that the probes could be positioned at right angles from each other in areas were there was access. This was possible because the technique was being used to saturate the test piece with ultrasound at one end and to monitor the amplitude of that which propagated through to the receiving probe. The amplitude of the sound received from the receiving probe was monitored and used to estimate the integrity of the region it had passed through. High amplitude corresponded to good integrity (i.e. no obstruction to sound propagation). A defect such as a crack reducing the effective diameter of the rivet neck under test would reduce the amount of ultrasound transmitted, causing a low amplitude reading.

The severity of the damage was graded by comparison to amplitude readings taken from samples of known levels of damage. Therefore this technique had to be tailored to each specific application. Quantification of amplitude variations due to different coupling pressures was not given. Neither was proof that probe positions did not significantly effect amplitude measurements.

The instrumentation used in this study was a Dryscan UFD 200 produced by Sonatest. Although it is not stated, the results achieved by Lecru are so similar that it is believed the same equipment was believed to be utilised. At the time of publication the only solid coupled system commercially available was that developed by Dickson.

3.3.2 Solid Coupled Static Pulse Echo Probes

Billson and Hutchins [1993] reported the development of a static, solid coupled probe operating at a centre frequency of 5MHz using a new 'low loss' synthetic rubber coupling medium. No indication was given as to what the rubber consisted of or how it was fabricated. The description given of the prototype probe developed incorporating their coupling rubber strongly suggests that it consisted of a conventional 5MHz, damped transducer with the rubber held in pressed contact with the probe face. This is an important point as the attenuation in the new rubber was low enough to enable the use of a conventional (damped) probe in the prototype, permitting operation in pulse echo mode.

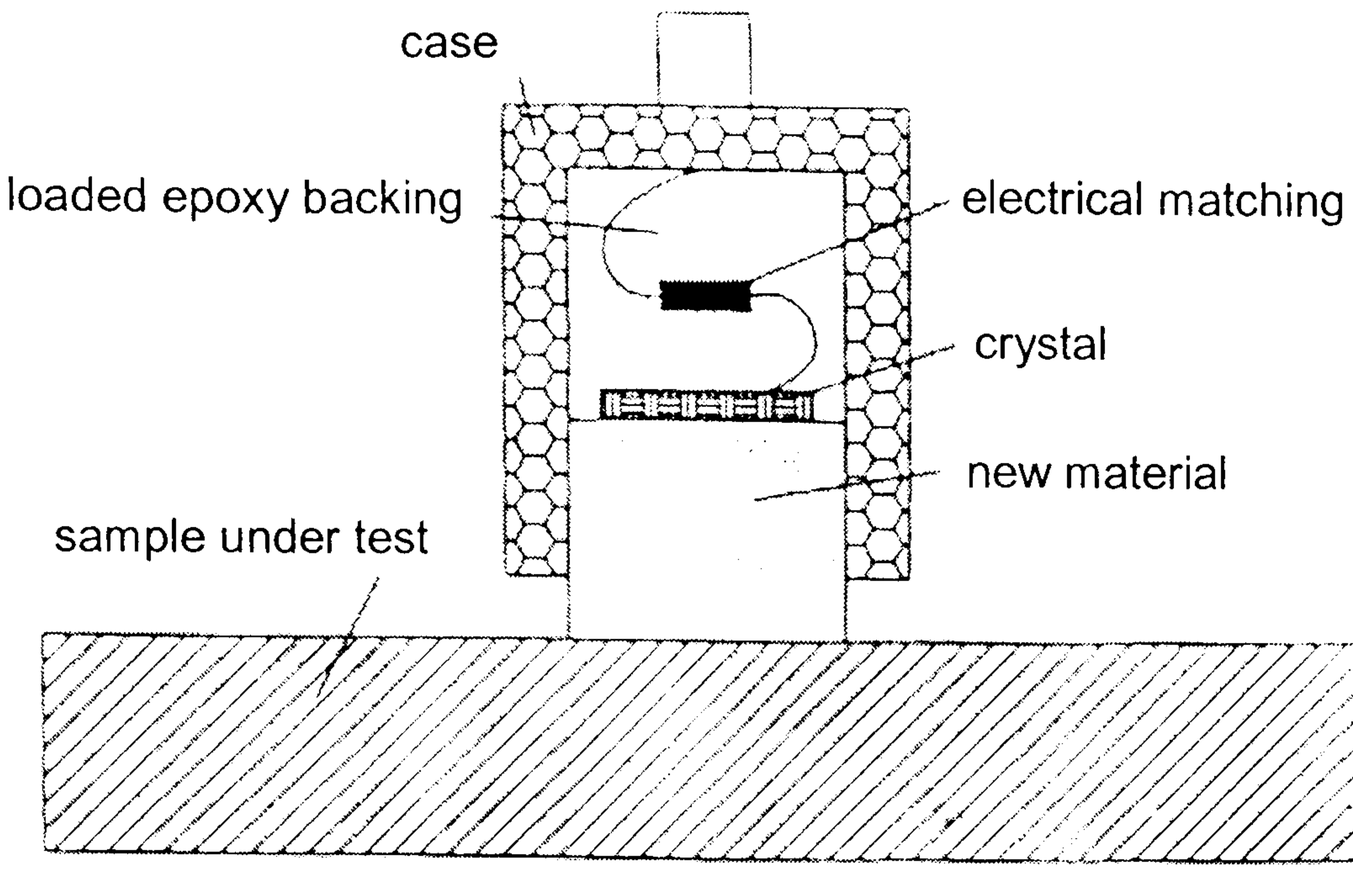

Figure 3.9 Schematic of prototype solid coupled static probe developed by Billson and Hutchins [1993].

Billson and Hutchins performed a basic analysis of the ultrasonic characteristics of their rubber by transmitting an ultrasonic pulse from a high damped 5MHz probe through 26mm sections of aluminium and natural rubber and comparing the back wall echoes with those from their new rubber. Aluminium proved to impart virtually no attenuation to the ultrasonic signals and so it was used as a datum. The backwall echo from the new rubber was visibly higher in amplitude than that from the natural rubber (see Figure 3.10A). However, arbitrary units were used for plotting the information and so a direct comparison is difficult. It appears, the amplitude from the new rubber was approximately 12dB higher than that from the natural rubber over the 52mm travelled (26 x 2) through the samples. This implies that the attenuation of the new rubber is superior to that of natural rubber by approximately 0.23dB mm^{-1}, based on amplitude alone.

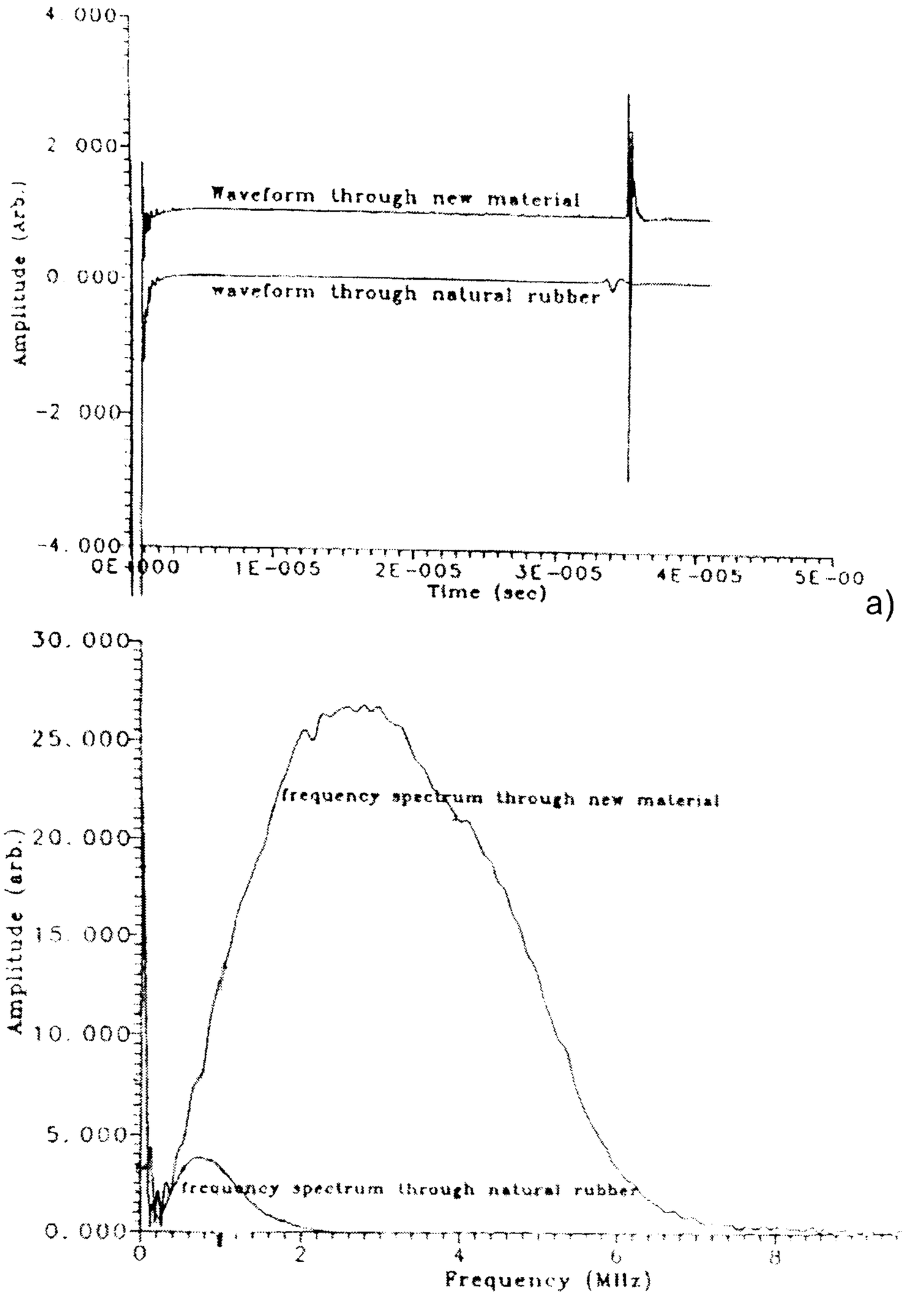

Figure 3.10 A) Ultrasonic pulses, and B) Frequency spectra generated by a 5MHz probe having been propagated through natural rubber and the new solid couplant material evaluated by Billson and Hutchins [1993].

The frequency spectra of the natural rubber and the new rubber also show the large difference in amplitude, but again, arbitrary units are used for the amplitude scale. In this case the amplitude difference appears to be approximately 16dB. What can be clearly determined from the plots is that the centre frequency of the pulse transmitted through the natural rubber has dropped significantly down to about 1MHz. The pulse transmitted through the new rubber has also dropped in frequency, but only as far as about 3MHz. Nevertheless, this is a significant drop from the 5MHz centre frequency of the transmitting probe.

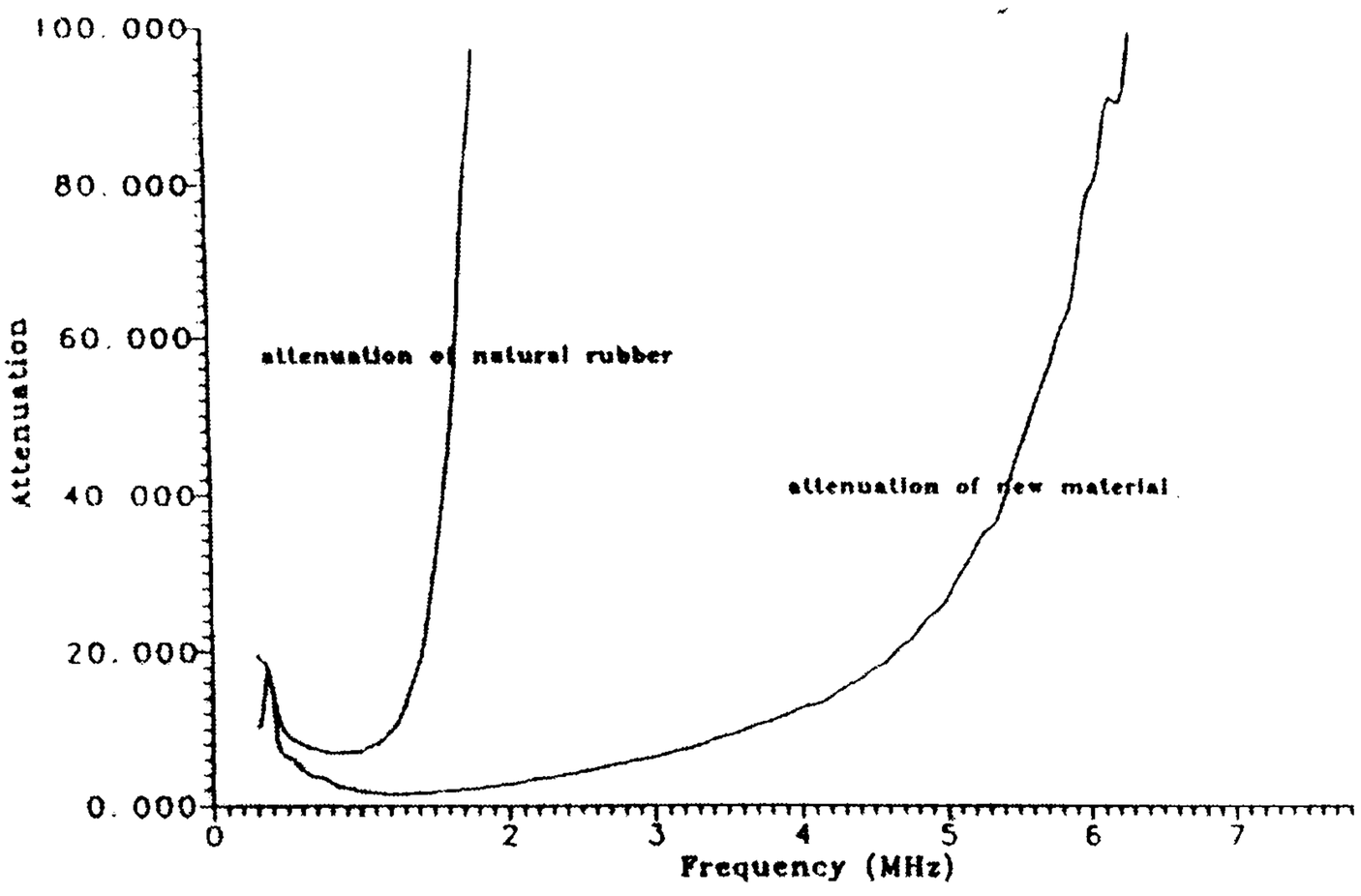

Figure 3.11 Plot of ultrasonic attenuation in the new solid couplant material evaluated by Billson and Hutchins [1993]. Attenuation of natural rubber is included for reference.

Plots of attenuation through the natural and new rubbers were obtained by dividing their frequency spectra by that of the aluminium sample. This is a very effective method as it removes the influence of the transmitting probe from the results and ensures that the attenuation at particular frequencies can be determined as discussed in section 2.2.5. Unfortunately, no units were given on the graph plotted for attenuation. However, it can be seen that the attenuation increases with increasing frequency. In the case of natural rubber, the attenuation can be seen to begin a steep increase at all frequencies higher than 1MHz. The new rubber shows a lower attenuation than the natural rubber above 0.5MHz. Attenuation in the new rubber does not increase as sharply with frequency as it does though the natural rubber. It can be seen that the attenuation in the new rubber at just over 3MHz is at the same level as the attenuation in natural rubber at 1MHz.

Billson and Hutchins demonstrated the performance of their prototype device by showing A-scan results from materials such as thin plates of steel, titanium and carbon reinforced plastic. Multiple back wall echoes were clear, but the amount of gain supplied to the pulser is not given and so the true amplitude of the signals is unknown. The last example given by them is the A-scan of a 3mm diameter hole 43mm below the surface of an aluminium sample. This too looks clear, but again signal amplitude is not given. Another key issue is to do with how much pressure needs to be applied to the probe in order to achieve these signals. This was not discussed in the paper. Billson and Hutchins add in their conclusion that plans were afoot to commercialise the probe and that work was underway on producing a wheel probe using the

new rubber as a solid coupling tyre. As these have not been seen in the industry and no follow up paper was ever written on the wheel probe, it can only be assumed that this attempt was either abandoned or unsuccessful.

Drinkwater and Cawley have produced many papers on the topic of solid couplant and have been an excellent source of reference. In 1997b, they described a similar static probe device to that of Billson and Hutchins, only operating at a centre frequency of 7MHz in pulse echo mode. The solid couplant was described as a 'low loss rubber'. No indication as to its formulation or method of fabrication was given. Again, the prototype device incorporated a conventional probe with the low loss rubber attached to the front face. The design was more sophisticated than that of Billson and Hutchins as it included an adjustable spring loaded collar to ensure that a reproducible amount of pressure was applied when measurements were taken. This indicates that Drinkwater and Cawley appreciated that the level of coupling achieved varied with the amount of pressure applied to the probe. In this particular paper the only information given regarding the ultrasonic properties of the low loss rubber was that its attenuation is similar to that of Perspex. This permitted the use of a 'thick' rubber tip, similar to a conventional Perspex delay line.

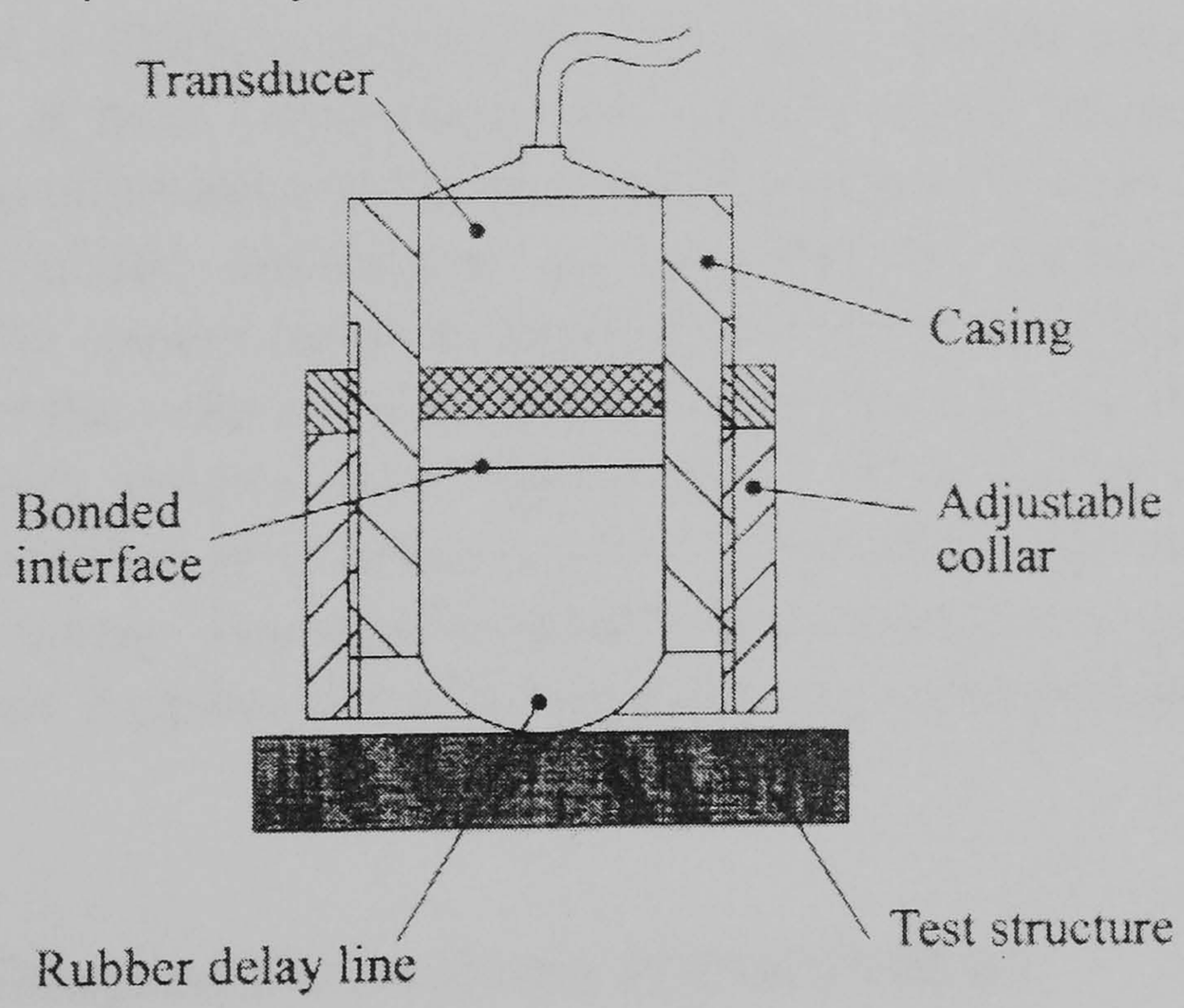

Figure 3.12 Schematic of prototype solid coupled static probe, developed by Drinkwater and Cawley [1997b].

A typical application for the prototype device is described as thickness gauging of materials with rough surfaces. Drinkwater and Cawley suggest the use of the device as a composite system, employing oil together with the rubber tip to achieve coupling. An A-scan is shown in the paper representing the front and back wall echoes from a 20mm thick steel plate achieved with the static solid coupled probe, the rubber tip 'smeared with oil prior to testing'.

The steel plate was described as moderately rough with mildly corroded surfaces of roughness average R_a = 5.9μm. The A-scan plot gives a linear scale of amplitude and so the true amplitude cannot be determined. Indeed, the front wall echo goes off the scale (clipped) and so even a comparison between the two cannot be made. It is explained that if no oil were applied to the rubber tip prior to testing, the steel back wall echo, although still visible, is only 7% of that when oil is applied. This implies a massive amplitude loss of 23dB on this particular sample if oil is not used to assist coupling. Drinkwater and Cawley go on to state that sufficient energy could be propagated into a 4mm thick iron sample of roughness average of R_a = 17.6 μm to enable thickness metering to be performed. Again, oil was used to assist the coupling provided by the rubber tip. The authors stressed that the amount of oil couplant required with their prototype device was much less than that used with conventional gel coupled probes, 'one wipe with an oil soaked cloth being sufficient for a number of point measurements'. It was felt that the rubber tip conformed around the large 'peaks' of the roughness while the oil filled out the smaller irregularities and 'valleys'. Therefore, the rougher the surface, the more oil required to achieve tolerable coupling. No indication as to the level of pressure applied was given.

Dixon, et al [2000] reported use of a highly flexible solid couplant for the generation of both compression and angled shear waves in steel and aluminium. The attenuation of the coupling material is not given but from data that is, the acoustic impedance is calculated as being approximately 1MN s m^{-3}. The experimental arrangement involved a 2.6mm thick, 15mm diameter disk of the solid couplant being fixed to the face of an 'off-the-shelf' 5MHz probe with double sided sticky tape. This set-up permitted the successful introduction of ultrasound into a 'rough aluminium surface' with an applied load of 0.5kg. The material itself is described as not being physically robust. However, it carries the advantage of being cold-castable into complex shapes.

3.3.3 Solid Coupled Pulse Echo Wheel Probes

Further details of the acoustic properties of the low loss rubber reported by Drinkwater and Cawley [1997b] are given in a previous paper [1994]. Its attenuation was derived using the double through transmission method, where a probe is placed within an immersion tank normal to a glass plate. The frequency spectrum of the echo from the glass is taken and divided by the frequency spectrum of the glass echo when a sample of the rubber is placed between the probe and glass. This is the same principle as the technique used by Billson and Hutchins. The plot of attenuation with respect to

frequency is shown in Figure 3.13. It includes plots of natural rubber, Perspex and the new low loss rubber for comparison. At 5MHz, the attenuation in the natural rubber is seen to be 3.75dB mm^{-1}, Perspex 0.53dB mm^{-1} and the new low loss rubber 0.31dB mm^{-1}. This is a very low attenuation for a rubber. The authors claim that the low loss rubber demonstrates a similar level of compliance in comparison with other rubbers and that 'satisfactory transmission of ultrasound across an interface between the new rubber and a metal or plastic can be achieved with very modest coupling pressures'.

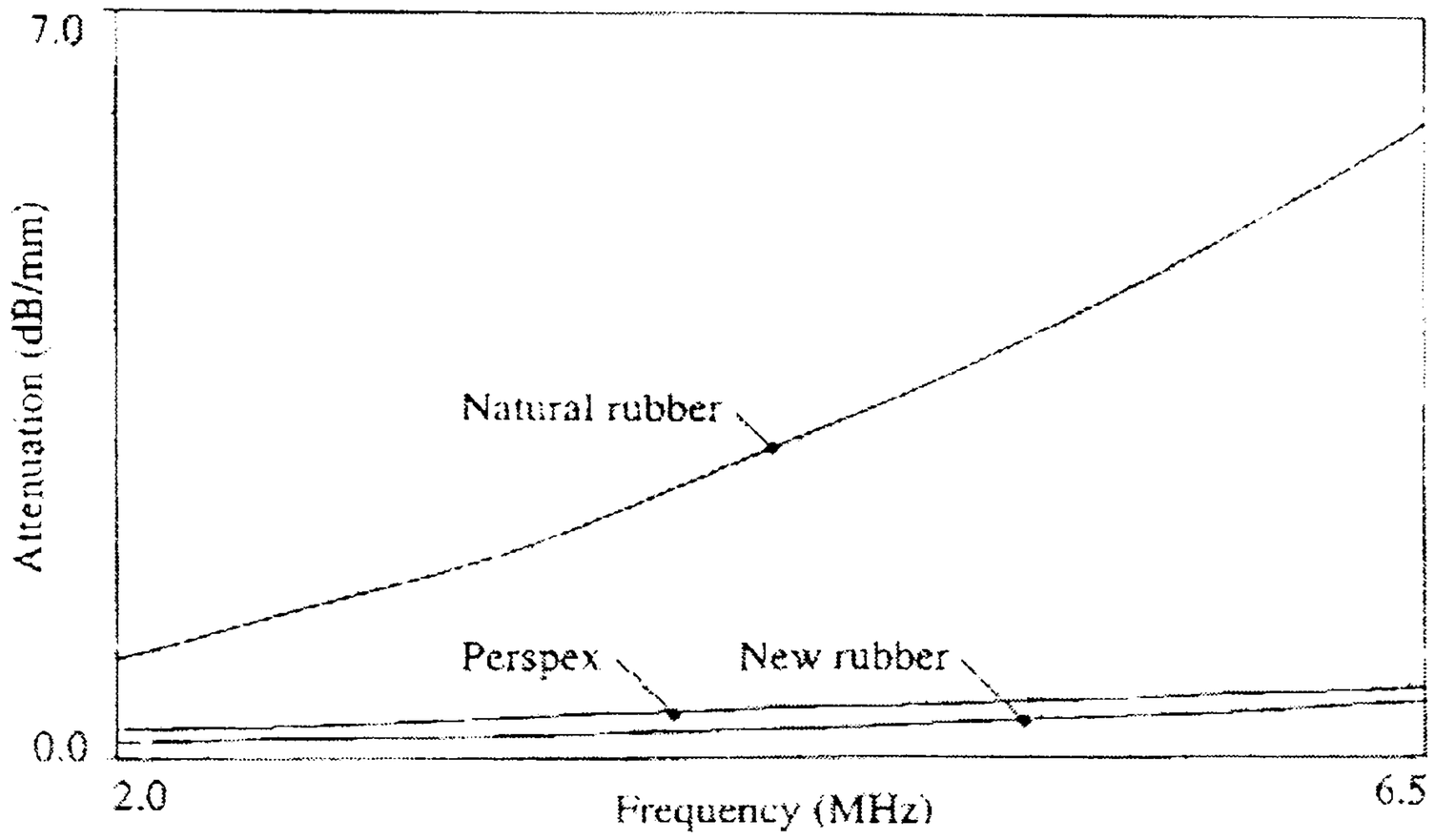

Figure 3.13 Attenuation of solid coupling rubber labelled as 'New Rubber' used by Drinkwater and Cawley [1994] plotted with respect to frequency. Perspex and natural rubber are also shown for comparison.

Drinkwater and Cawley manufactured tyres from the new low loss rubber for fitting to a prototype wheel probe. The device is centred on a conventional 5MHz immersion probe at the centre, coupling being provided to the test piece by the tyre (see figure 3.14). Contrary to conventional wheel probes, the tyre consists of a thick (approximately 12mm) section. Therefore the tyre acts as a delay line. It was reported that an applied load of approximately 1kg was required to maintain consistent coupling. The device yielded typical signals of 300mV at an attenuation setting of 30dB on an old Wells Krautkramer HIS-1 ultrasonic flaw detector. The paper includes a plot of the A-scan generated by the device when placed in contact with 4.5mm thick cross-plied carbon fibre reinforced plastic laminate. Of particular interest is that the front wall echo is only about 6dB higher than the back wall echo. This implies very good coupling between the tyre and plastic sample. The frequency spectrum of the front wall echo gives a peak amplitude of 3.8MHz compared with 4.8MHz when the same transducer was used with immersion coupling. This shows that despite its low attenuation, the coupling rubber had preferentially attenuated the higher frequency components of the ultrasonic pulse.

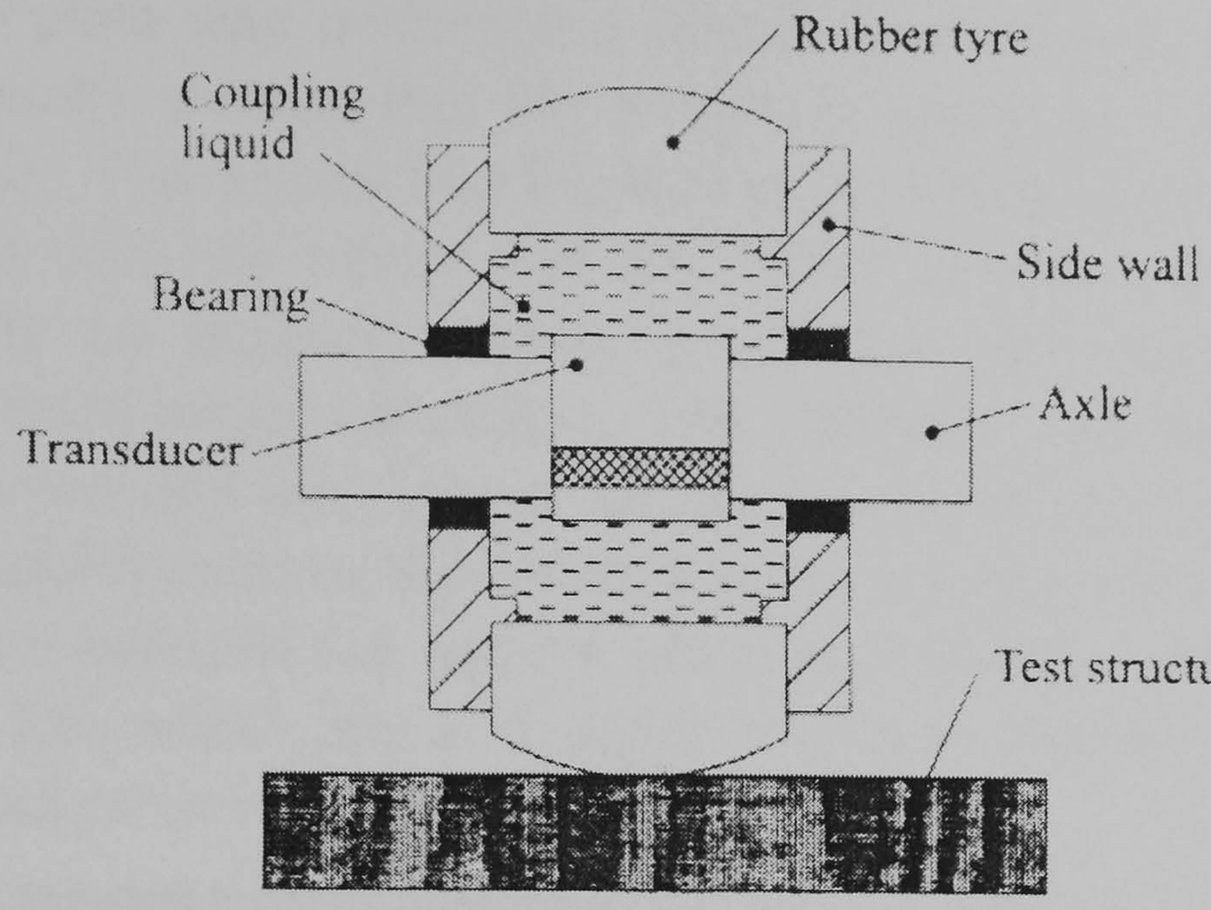

Figure 3.14 Schematic of solid coupled wheel probe developed by Drinkwater and Cawley [1997b].

To prove the practical application of this device, the authors chose to inspect the afore mentioned carbon fibre composite containing known areas of impact damage with the prototype wheel probe. This was done by monitoring the amplitude of the composite back wall echo. The same region of the sample was then scanned a second time using conventional immersion testing for comparison. The resultant C-scans in the paper appear to have been achieved using different scanning indexes, resulting in one image being slightly distorted when compared to the other. In addition, the immersion test was performed using a 10MHz probe while the wheel probe employed a 5MHz probe. This makes direct comparison more difficult. However, excellent agreement was demonstrated. An additional scan was performed of the same composite using the wheel probe. This time the amplitude of echoes from the area between the front and back wall echoes was monitored. The resulting C-scan represents the echoes from the delamination itself, demonstrating that the pulses generated by the wheel probe device are sufficiently short in duration to be capable of defect detection in pulse echo mode. This is the first application of this kind of a solid coupled wheel probe utilising a thick rubber tyre section.

Drinkwater and Cawley discuss what appears to be the same wheel probe further in a subsequent paper in 1997[c]. This is the same paper that discloses the 7MHz static solid coupled device previously discussed. The diameter of the wheel is 70mm and the width 40mm. The tyre thickness is 12mm. The liquid couplant inside the wheel that couples the immersion probe to the inside of the tyre is described as 'acoustically matched to the rubber'. In an attempt to address the issue of coupling consistency of the wheel to the test piece, the authors performed a C-scan of a uniform 3mm thick aluminium plate. The purpose was to monitor the amplitude of the aluminium back wall

echo. As the plate was uniform the amplitude should be the same at any point. The results showed that the amplitude varied by ± 6% of the mean signal (±0.5dB). This shows that the limit of accuracy for absolute amplitude measurements with this device will be limited to ±6%. Immersion testing suffers virtually no coupling variations whereas gel coupled probes can demonstrate much larger variations. The variations reported for this wheel probe are very low and the authors felt that they would not greatly restrict the bulk of applications as most frequently it is the presence or not of a signal or the time interval between two signals which is of interest. Therefore in terms of sensitivity, this wheel probe is better than gel coupled probes used for scanning but not as good as immersion testing.

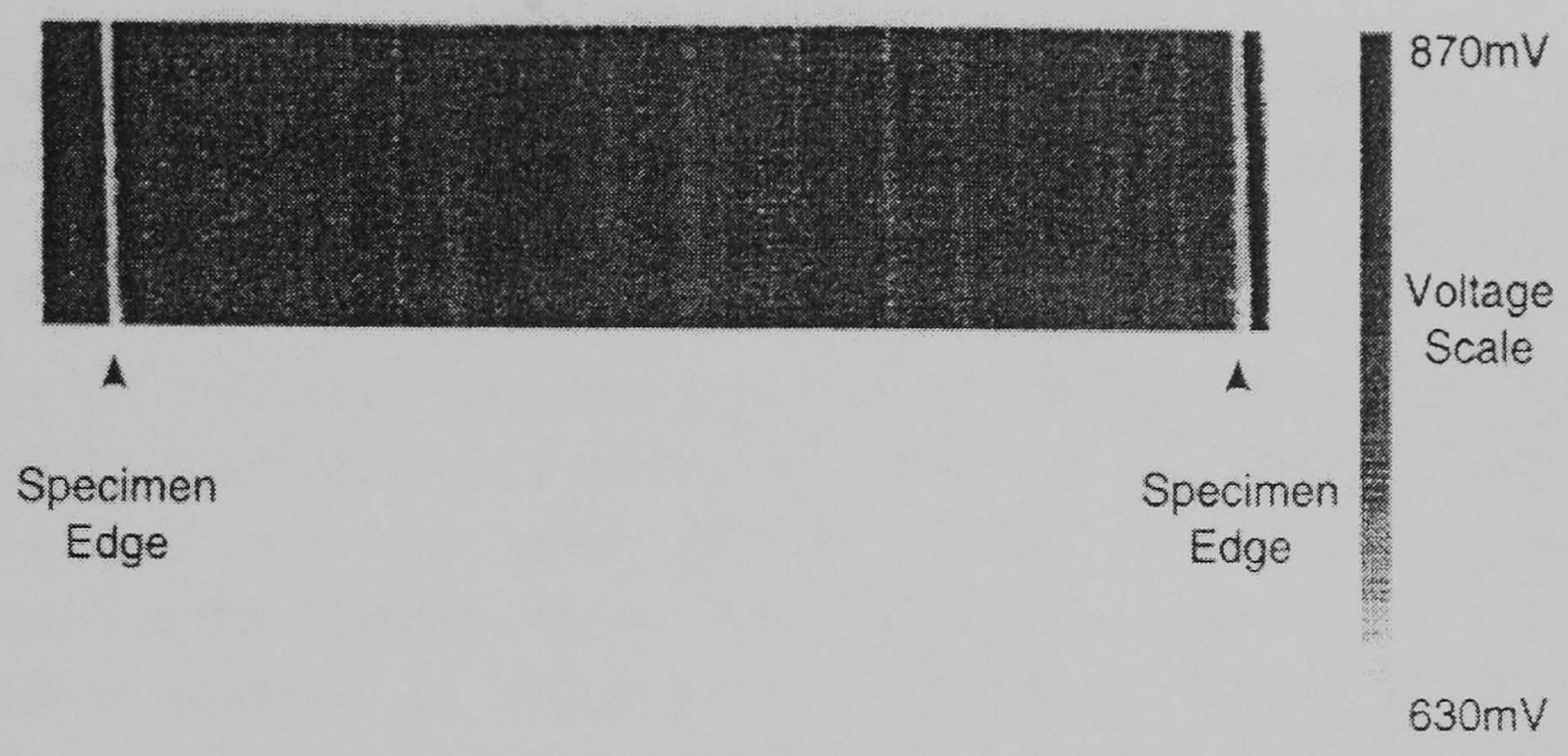

Figure 3.15 Amplitude C-scan of 3mm thick aluminium plate recorded with prototype wheel probe reported by Drinkwater and Cawley [1997b]. Variations in coupling are observed as vertical strips.

The amplitude variations can be seen to manifest themselves as stripes on the C-scan. The amplitude reaching the outer surface of the tyre was found to be consistent all around the tyre, which means that the amplitude variations were due to coupling variations. As the tyre rotates over the sample, a given point on the circumference of the tyre makes contact with the plate at the same horizontal position on each horizontal pass. This explains why the amplitude variations took the form of vertical stripes and means that these variations are due to the tyre. Further investigation by the authors showed that parts of the tyre always produced slightly lower signals when in contact with the plate than other parts. The precise cause of this is unknown but is suspected to be due to surface contamination of the tyre during the moulding process.

Results from three trial applications for the wheel probe are also described. The first was to identify gross disbonds in automotive adhesive joints. The inspection involved scanning a thin aluminium plate of about 1.2mm thickness. Half of the underside of the plate was coated with adhesive. As the plate was very thin a frequency of over 5MHz would be

required to separate the repeat echoes in the time domain. The current device operates at 3.8MHz and therefore not offering the required resolution, and so a different approach was adopted. This involved analysing the rate of decay of the ringing signal within the aluminium. Where the plate was coated with adhesive, some ultrasound would be transmitted into it causing the reverberations to die down quicker. In the areas where there was no backing on the plate, the ultrasound would reverberate within the plate for much longer resulting in a much lower decay constant. This approach proved to be successful for the detection of large area disbonds. However, it would be a huge advantage if a higher frequency could be used to enable the resolution of the repeat echoes.

The second application again focuses on the detection of gross disbonds, this time between a stainless steel rail and aluminium inner. A similar approach was used as with the automotive adhesive joint; removing a portion of the aluminium inner simulated a defect. Therefore the test was to determine the difference between a portion of stainless steel with aluminium bonded to the back of it and a portion where it was not. Many repeat echoes were observed over the area with no bond as the ultrasound freely reverberated in the stainless steel. The area with a good bond showed much fewer repeat echoes as much of the ultrasound had 'leaked' into the aluminium. Again, the approach of monitoring the amplitude of the last few repeat echoes proved acceptable. What was of note with this application was that the surface of the stainless steel was very rough (R_a=7.2μm), this had contributed to the low amplitude of signals received which in turn caused a degree of noise to be introduced to the system. No indication was given as to the amount of pressure applied to achieve coupling in this test.

The final application involved the inspection of a prototype heat exchanger. This involved transmitting through outer carbon tiles and then into an internal copper pipe. The inner wall of the copper pipe has castellations that act as fins to improve cooling. The amplitude of the stepped inner of the copper pipe was monitored. The resultant C-scan showed the castellations and a low amplitude region that might have represented a defective bond or carbon tile.

These three trial applications demonstrate the potential of the solid coupled wheel probe. However, the device described by Drinkwater and Cawley still suffers from relatively low frequency operation and a need for either high coupling pressures and/or additional liquid coupling. Recently, Robinson et al [2000] has begun to address the shortcomings by building on the wheel probe developed by Drinkwater and Cawley as a basis to explore use at higher frequencies. This has involved the fitting of a 10MHz probe and

use with a sophisticated PC based ultrasonic flaw detector that is described as being capable of performing on-line advanced signal processing tasks. Promising results have been reported for use on automotive adhesively bonded joints using what is described as 'inverse adaptive filtering' to characterise bond quality. In addition, impressive results have been achieved with the system when used to rapidly inspect a 100μm thick sealant layer in an aerospace wet wing structure. While excellent results have been reported in this paper, it must be remembered that the wheel probe is operating as a component of a sophisticated system. Much analysis and filtering of the signals recorded by the wheel is undertaken which is key to defect detection in these challenging applications. With regard to the wheel alone, the advancement reported here is the increase in operating frequency from nominally 5 to nominally 10MHz by the substitution of the initial immersion probe. To assist with reaching higher frequencies, the thickness of the tyre has been reduced to 10mm to reduce attenuation and a curvature of 14mm radius added to the tyre to concentrate contact pressure.

Of particular interest is the plot of attenuation with respect to frequency provided by Robinson. This shows natural rubber, Perspex and the new rubber for comparison. Unlike the plot offered in Drinkwater [1994], which represented attenuation over the 2 – 6.5MHz range, this time the broader range of 3 – 13MHz is provided. Although the units have changed from dB mm^{-1} to Neper m^{-1} a conversion can be readily made. A feature not portrayed in the earlier paper is that a crossover is reached at about 6MHz beyond which the new rubber imparts a higher attenuation than Perspex. Therefore, the attenuation in the new rubber increases more rapidly with frequency than Perspex does. Figure 3.16 shows an attenuation plot of the new rubber interpreted from Robinson et al. This data has been converted to $dBmm^{-1}$ and plotted with the attenuation data achieved for the range of hydrophilic polymers evaluated in Chapter 2.

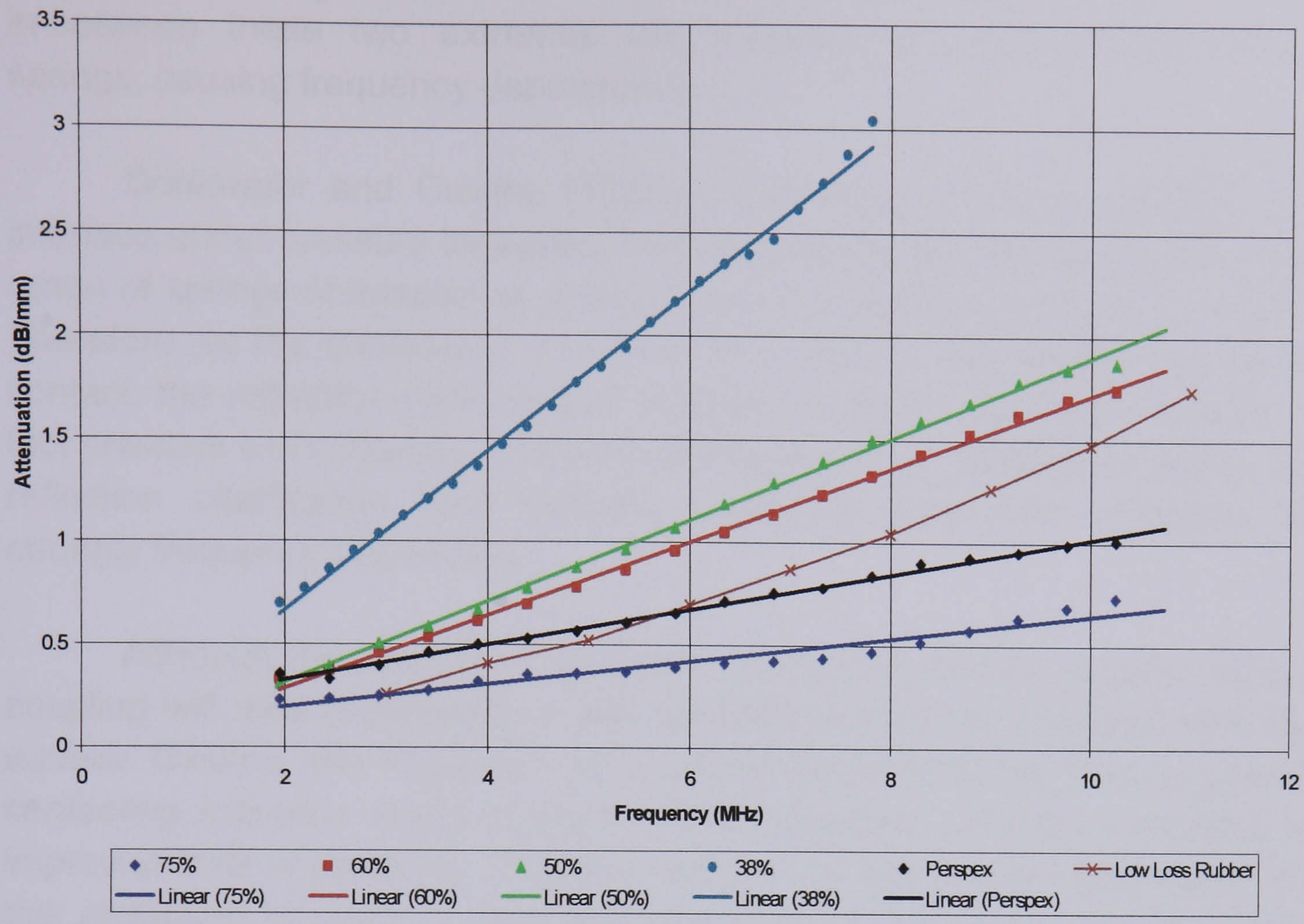

Figure 3.16 Attenuation of new rubber (interpreted from Robinson et al [2000]) for use as a high frequency solid couplant. Data for hydrophilic polymers and Perspex determined in Chapter 2 have also been included.

It is clear from the data shown in Figure 3.16 that the attenuation of the low loss rubber is similar to that of Perspex and sits partway between the different hydrophilic polymer Batches C-D. Interestingly, the rate of attenuation increase with respect to frequency appears greater than all of the hydrophilic polymers except Batch A. This implies that for high frequency applications, hydrophilic polymers B, C and D would be more suitable.

3.3.4 Transmission Across Partially Contacting Surfaces

For all of these solid coupled devices, the ability to make surface contact between the solid couplant and test piece remains of key importance. Analysis of reflection coefficients is an important method of characterising such partially contacting interfaces. Experimental and theoretical studies have led to the development of the generally accepted spring and mass-spring models [Baik and Thompson, 1984]. Such models involve likening the interface between two materials to a spring of a given stiffness. Poor contact is modelled by a very soft spring, resulting in almost complete reflection at all frequencies. Perfect contact is modelled by a very stiff spring, giving a reflection coefficient similar to the 'perfect contact reflection coefficient' described by Equation A.6 (Appendix A) at all frequencies. Interfaces that are

in-between these two extremes are modelled by intermediate stiffness springs, causing frequency dependence.

Drinkwater and Cawley [1997a] summarise well the scenario of an interface under pressure by saying that such interfaces may be modelled by a range of springs of increasing stiffness corresponding to increasing pressure. Therefore, as the pressure is increased from zero to that required for perfect contact, the reflection coefficient is expected to be frequency dependent. In fact previous work [Haines, 1980 and Drinkwater et al, 1996a] has shown that reflection coefficients from partially contacting solid-solid interfaces are strongly frequency dependant.

Although the amount of pressure required to achieve a given level of coupling will vary depending on the conformance of the materials and their surface finishes, the frequency of a sound beam reflected from a partially contacting interface would increase with increasing pressure indicating an improved level of coupling. This is in addition to the familiar observation that the amplitude of such a reflected beam would decrease with increasing pressure also implying improved coupling.

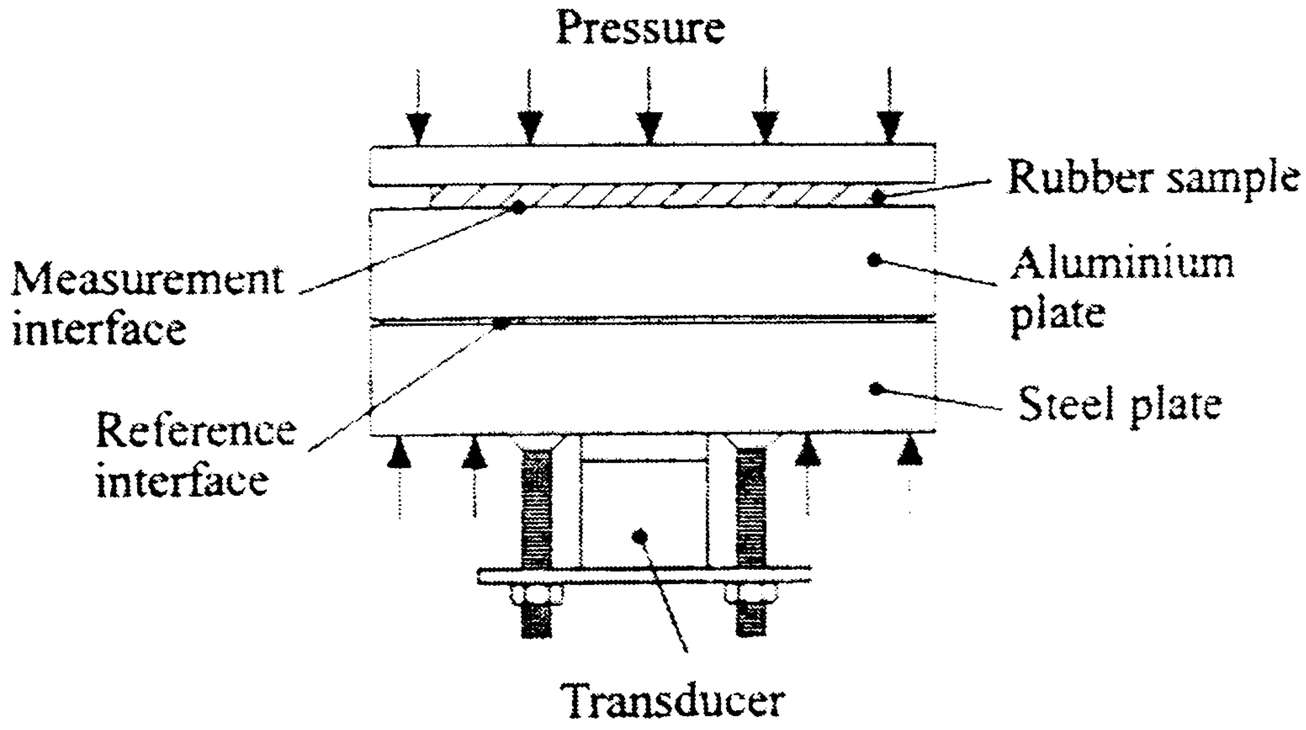

Figure 3.17 Representation of rig used to monitor the reflection coefficient from a material interface under varying degrees of pressure. Drinkwater and Cawley [1997c].

Drinkwater and Cawley [1997c] investigated these two indicators together. Four scenarios were investigated (i) a glass epoxy adhesive joint, (ii) an aluminium and rubber sheet under pressure, (iii) an aluminium sheet to rubber cylinder, and (iv) two aluminium plates under pressure. In all cases the amplitude data showed the expected trend, high amplitude at low pressure, steadily decreasing as the pressure increased. However, the frequency data did not reflect that described by the theory [Haines, 1980], showing unexpected frequency independence as pressure at the interface was increased. This was traced to subtle flaws in the experimental design. Issues

of extreme sensitivity to misalignment, large ultrasonic beam focal diameter and large scale surface irregularities were blamed.

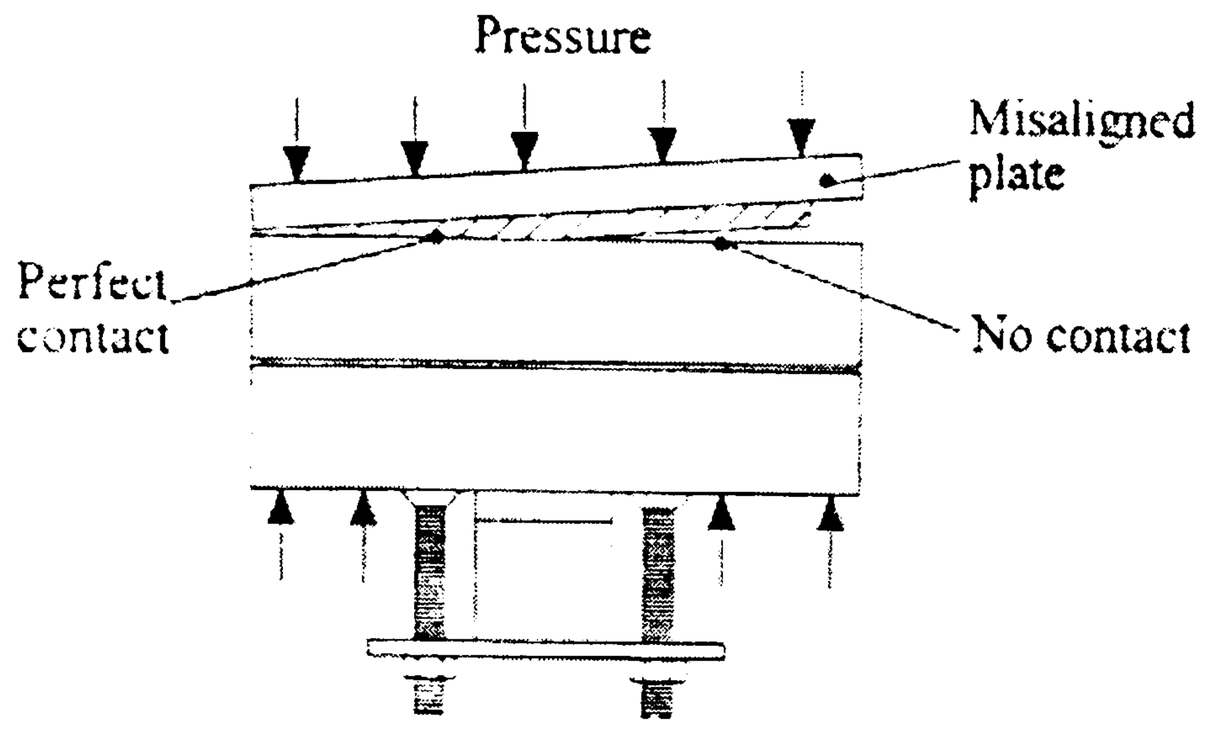

Figure 3.18 Exaggeration of misalignment in plates used in investigation into coupling across a solid-rubber interface. Drinkwater and Cawley [1997c].

In essence their explanation of this observation was that the ultrasonic beam 'illuminates' a region of the interface in which there is an area of perfect contact, an area of no contact and a very small area of intermediate contact. The areas of perfect and no contact are frequency independent (either reflecting or transmitting ultrasound at all frequencies). As these areas are large in comparison to the small area of intermediate contact, they dominate the overall 'bulk' measurement of that region.

After taking further steps to overcome these issues, frequency dependence was observed between two (machined flat and grit blasted) aluminium plates as pressure was varied. From these experiences it may be stated that investigations into coupling efficiency with respect to pressure necessitate the acquisition and agreement of both frequency and amplitude data before confidence can be placed in test conclusions. This lesson is very important, as coupling efficiency will have to be determined for the hydrophilic polymers under investigation in this research.

Drinkwater and Cawley [1996b and 1997a] went a stage further by considering the effect of surface roughness in the case of coupling between a soft rubber and a solid surface. Reasonable agreement was found with theory and the results were used to predict the level of pressure that would be required to effectively couple the particular rubber investigated and surfaces of known roughness.

A similar paper by Drinkwater et al [1996a] centred on the interaction of ultrasound with a partially contacting aluminium-aluminium interface which showed an additional phenomenon specific to solid-solid interfaces. When

the pressure applied to the interface was repeatedly cycled (i.e. applied and removed several times) a hysteresis effect could be seen between the reflection coefficient and the contact pressure. There was a large difference between the first loading and unloading cycle, which diminished as the process was repeated. It was hypothesised that this was down to an 'asperity shakedown' process whereby plastic deformation occurred, enabling the two solids to fit together snugly. It is interesting that this occurred at pressures as low as 10% of the yield stress as this suggests that much higher pressures were placed upon the small asperities.

3.3.5 Patents

Patent surveys were conducted on the topic of coupling ultrasound between an ultrasonic probe and a test piece. These were conducted firstly by on-line searches using QPat-US and IBM IP Network. QPat-US is a database containing the front page of all patents filed in the US since 1974. The IBM IP Network is a database of all US patents since 1971 and all European and world patents since 1978. A more comprehensive survey was then conducted by the British Patent Office and the United States Department of Commerce. This followed a provisional patent application covering the use of hydrophilic polymers as solid contact ultrasonic couplants in these territories [US-09/396,435 and UK9921846.3 Bourne, et al]

Of the 36 patents uncovered by the survey, 15 were irrelevant, 6 were concerned with ultrasonic transmission and reception of ultrasound but far removed from the focus of this work, 9 related to ultrasonic contact being made via a flexible solid and 6 specifically mentioned hydrophilic polymers. Of the 9 concerned with flexible contact, there was a large amount of similarity. In fact 5 were granted to the same two people, namely Pagano and Bull. The most common theme was use of polyurethane to achieve ultrasonic contact with the addition of a small quantity of conventional coupling fluid. The patents suggest that the main field of application was in the rail industry. A focussed search for any technical papers from these authors has proved negative. The 6 that expressly mentioned hydrophilic polymers are dealt with in turn, starting with the most relevant.

Soloway, 1973 [US 3921442] claims the use of a hydrophilic polymer attached to the front of an ultrasonic static probe. No details of the hydrophilic polymer are given. It is known that at the time the patent was filed, hydrophilic polymer technology was in its early stages, the only material available being HEMA, which is homopolymer limited to 38% hydration with water (shown in this study to possess the poorest ultrasonic properties). Therefore it is

reasonable to state that the other, more advanced hydrophilic copolymers investigated in this study were not available at that time. In fact there is strong reason to suggest that the device claimed by Soloway was never actually produced, as claims are made that the hydrophilic polymer was capable of absorbing oil. This is patently not true as only polar fluids such as water may be absorbed.

The following patents are concerned with medical applications and with the exception of Richardson, the means of hydrophilic application is extremely simplistic, made by producing a sheet and holding it in pressed contact with the patient.

Richardson et al, 1984 [US 4459854] claims the use of hydrophilic material for the coupling of an ultrasonic probe to vascular vessels for the measurement of blood flow. In particular, hydrophilic polymers of between 75 to 90% water are claimed. Richardson goes even further by specifying ultrasonic properties as either (i) attenuation of less than 0.2dB mm^{-1} at a frequency of 5MHz, (ii) longitudinal velocity of sound approximately equal to $1500ms^{-1}$, and (iii) acoustic impedance of about 1.5M N s^{-3}. Although extremely vague and all encompassing, this is the only reference to ultrasonic properties of hydrophilic materials found in the patent literature.

Wokalek et al, 1990 [US 4905700] claims the use of a hydrophilic material consisting of over 90% water for the transmission of ultrasound into a patient for medical diagnostic applications. The hydrophilic material being in a simple sheet form. It is known from practical work conducted in this research that hydrophilic polymers of such high water content are extremely weak and disintegrate very easily when handled.

Orr et al, 1995 [US 5394877] and Montecalvo, 1996 [US 5522878] both describe use of a hydrophilic sheet seemingly identical to that of Wokalek's which functions as an ultrasonic couplant when pressed in contact with the skin. Orr claims that the sheet adheres inherently to the skin.

Larson et al, 2000 [US 6039694] again claims the use of a thin sheet of hydrophilic polymer this time in the form of a sheath. The sheath is for enveloping a medical ultrasonic probe, permitting insertion into the body without risk of contamination from instrumentation and/or coupling fluids. The hydrophilic polymer is almost identical to that claimed by Wokalek, Orr and Montecalvo in both water content and form, being ideally between 70 and 95% water.

There is no credible patent disclosing the use of any hydrophilic material as an aid to ultrasonic inspection of materials. Even in the medical field where hydrophilics have made an appreciable impact, there is no mention of a wheel type arrangement for the multi-point ultrasonic interrogation of the patient.

3.4 The Desired Properties of Ultrasonic Couplant

Having established the limitations of conventional ultrasonic couplant and discussed the current state of the art, a 'wish list' of all properties that would constitute an ideal ultrasonic couplant was generated. It is appreciated that satisfying all of these ideals is not possible, as many of them are mutually exclusive.

- Most importantly, it should be capable of removing air from the probe – test piece interface. This is essential as air acts as a reflector to high frequency ultrasound, greatly reducing its transfer between materials. Hence, the couplant should be able to flow/conform to surface undulations/roughness.

- A couplant should be capable of transmitting a wide range of frequencies. This improves the potential for a greater number of applications.

- The couplant should offer low attenuation to ultrasound. This reduces the gain (signal amplification) required hence providing greater test penetration and improving the signal to noise ratio.

- Ideally, there should be a low acoustic impedance mismatch between the couplant and the test piece. The lower the mismatch, the greater the transfer of ultrasound (assuming identical contact).

- Minimal risk of couplant penetration into test piece defects that could lead to non detection.

- It is important that the couplant does not contaminate or degrade the test piece in any way, affecting its performance after the test has been conducted.

- The ability to function over a range of temperatures and in the presence of oil and grease would be an advantage.

3.5 Conclusions

Immersion testing is generally accepted as being the most reproducible method of ultrasonic examination, owing to its consistent level of coupling. Unfortunately, this approach requires expensive systems, which are often impractical to use and pose serious threats of both test piece damage and inspection integrity.

Several ultrasonic NDT techniques have been developed in an attempt to address the limitations associated with liquid coupling for both manual and automated techniques. However, despite a high level of sophistication, the alternative inspection methods all have serious drawbacks including, cost, practicality and quality of results. There remains significant scope for improvement of solid coupled ultrasonic probes. Despite recent research and development within the NDT community, it is the solid couplant materials themselves that remain a limiting factor in the performance of such devices.

An enhanced solid contact ultrasonic couplant would have tremendous scope for many applications in NDT. It is anticipated that its greatest utilisation would be in automated ultrasonic NDT, applied as part of a novel wheel probe.

The desired properties for an ideal solid contact ultrasonic couplant have been established.

Chapter 4: Evaluation Programme for Hydrophilic Polymers

4.1 Review of Research Objectives

The literature review confirmed that there is widespread need for improved solid contact ultrasonic couplants. The preliminary investigations into basic ultrasonic properties reported in Chapter 2 justified the view that hydrophilic polymers can in principle satisfy these requirements. A novel wheel probe device employing hydrophilic polymer as solid couplant would offer an alternative to problematic immersion testing and therefore is the prototype design to focus on.

These considerations appeared to justify a full-scale research programme into the ultrasonic performance of hydrophilic polymers over a range of physical and environmental conditions. A design study into a wheel probe device was also warranted with the ultimate aim of quickening the design and realisation of practical application of hydrophilic polymers.

This Chapter seeks to confirm initial results and to investigate in more depth the ultrasonic properties of hydrophilic polymer systems in practical coupling situations. In addition, an assessment of mechanical longevity was conducted.

4.2 Coupling Efficiency

It is evident from practitioners that the ability of a solid material to form good surface contact with both the test piece material and probe is paramount if it is to function successfully as an ultrasonic couplant. For a solid coupled probe to be used for ultrasonic inspection, it is equally important to achieve given levels of contact consistently, promoting reliable, quantitative results. The ability to accomplish suitable levels of contact for ultrasound transmission at low contact pressures would also be a practical advantage. Existing solid coupled probes demonstrate large signal fluctuations with respect to coupling pressure, often requiring very high loads in practice.

Therefore, the nature of how candidate flexible solid materials form surface contact with test piece materials holds many of the key issues that will describe their performance as ultrasonic couplants. The first half of this Chapter therefore includes an assessment of surface contact between the

range of four hydrophilic polymers (Batch A and Batch D) under investigation in this study and a steel test piece selected by the sponsors to represent the typical condition of test structures encountered in the field of ultrasonic inspection.

4.2.1 Testing Programme

In order to fully explore the nature of coupling behaviour demonstrated by hydrophilic polymers when in contact with a typical test piece sample, a testing programme was prepared. Its main aims were to:

- Explore the relationship between the pressure applied to the interface between different hydrophilic polymers and a defined test piece with respect to the resulting ultrasonic coupling efficiency,

- Determine the optimum pressure for ultrasound transmission from a range of hydrophilic polymers into a defined test piece, and

- Investigate the effect of pressure on the ultrasonic transparency of hydrophilic polymers.

After consideration, it was felt that the most effective way to meet these aims was to mimic the practical situation experienced in real pulse echo testing. This involved transmitting ultrasound from an ultrasonic probe, through the solid couplant under evaluation, into the test piece where it was reflected from the back wall. The reflected sound beam passed back through the solid couplant layer to the probe where it was detected. The condition of the echo signal was used as a guide to the coupling efficiency between the polymer and test piece. This approach was different to that adopted by Drinkwater and Cawley [1997a,c] who during their studies of the interaction of ultrasound with partially contacting interfaces, elected to monitor the reflection coefficient from the couplant/test piece interface, comparing their findings with the predictions of numerical contact and spring models. In our case, the main reason for opting to transmit through the interface, as illustrated in Figure 4.1, was to reproduce the conditions encountered in real testing, enabling the rapid translation of results to practical devices such as manual (static) probes and wheel (scanning) probes. The practicalities described in the literature [Drinkwater et al, 1994, 1996a, 1997a,c] relating to accurate measurement of coupling behaviour were used to guide against experimental pitfalls. To that end coupling efficiency was assessed in terms of both signal amplitude and frequency.

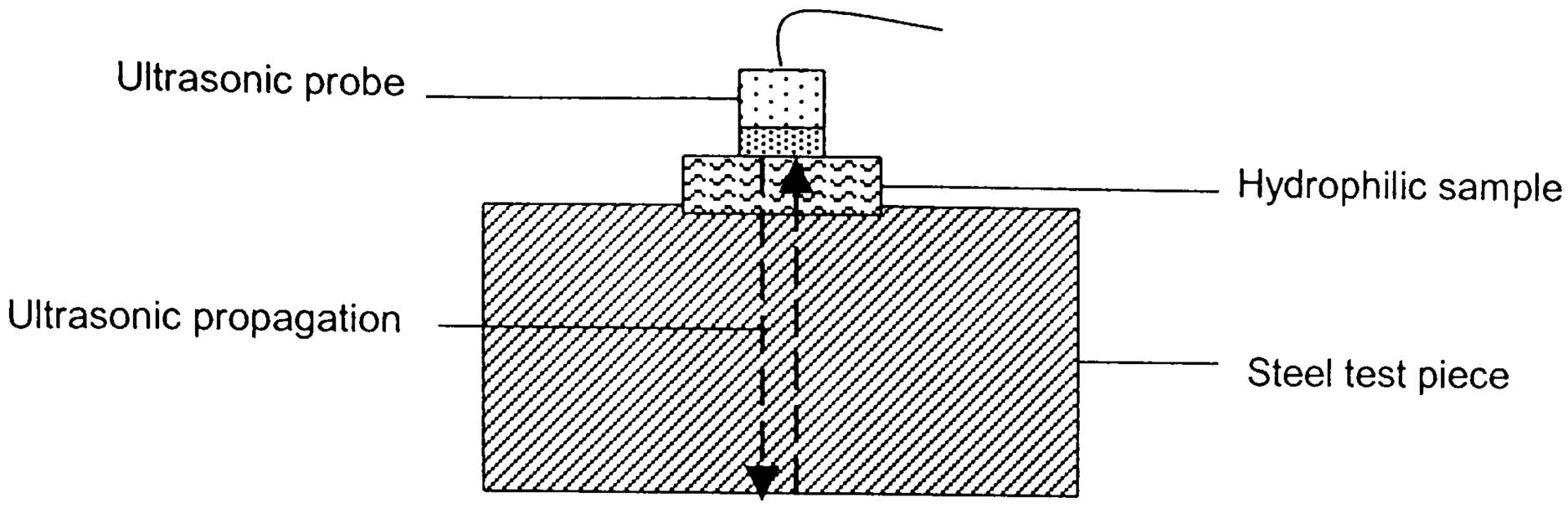

Figure 4.1 Schematic of test set up showing the path of ultrasound propagation

4.2.2 Experimental Procedure

To achieve the situation illustrated in Figure 4.1 the development of a reliable test rig was required. This had to be capable of providing the following:

- Reproducible, but easily varied degrees of load to the polymer/test piece interface,

- A means of accurately measuring the applied load, and

- Constraints to limit probe misalignment that would have a detrimental effect on measurement accuracy.

Such a test rig was developed consisting of a free-standing frame enabling a plunger to be raised and lowered by turning a knob. The position of the plunger may be locked by tightening a securing screw. The plunger was fitted with a key which mates with a special steel sleeve machined to house the test probe. This ensures that the probe is securely attached to the plunger, unable to tilt away from the normal. This was a key design aim as the effect of tilting on the ultrasonic readings would be detrimental.

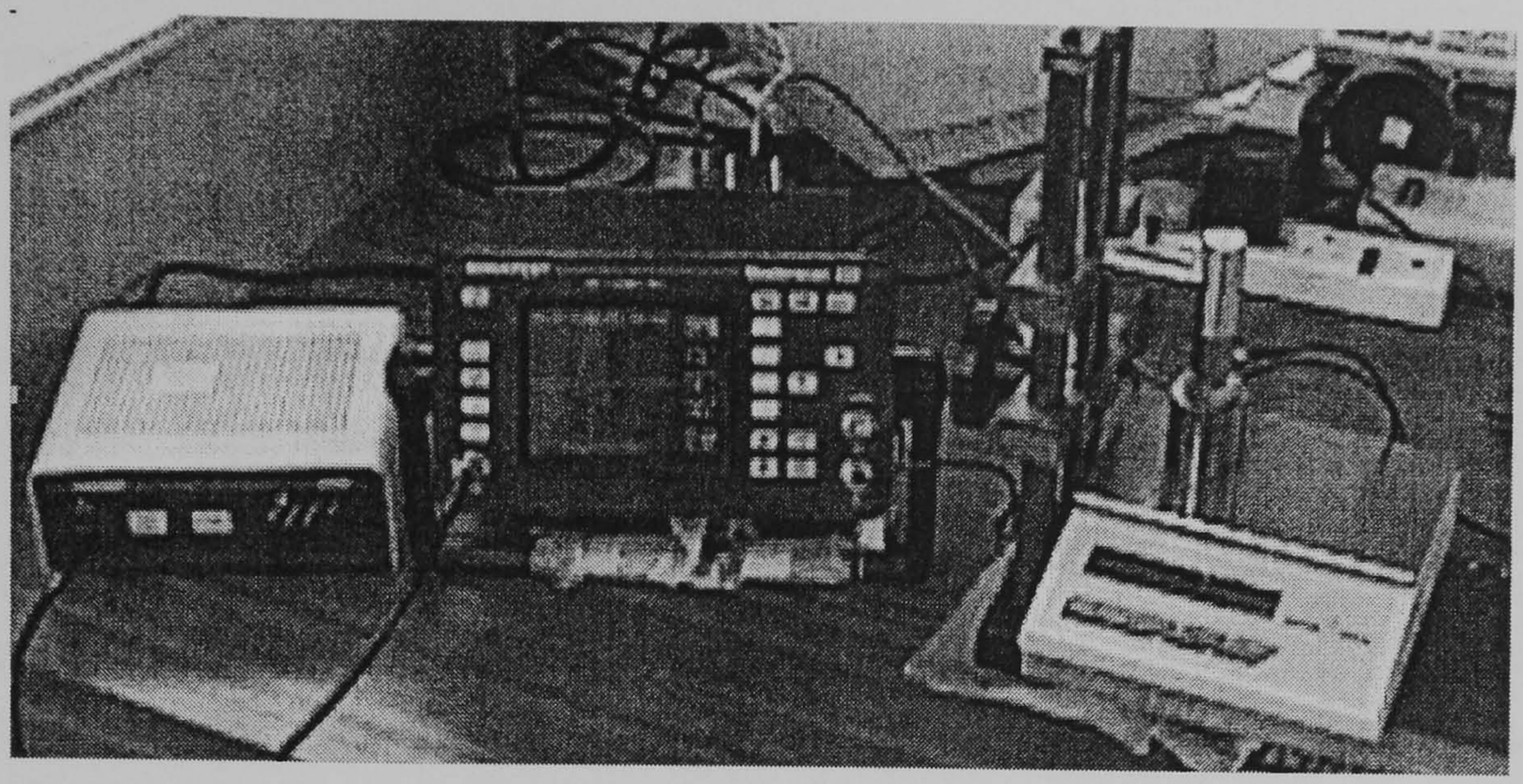

Figure 4.2 Picture of test set up used for coupling efficiency evaluation programme. From left to right – charger, ultrasonic flaw detector, test rig, test piece and balance.

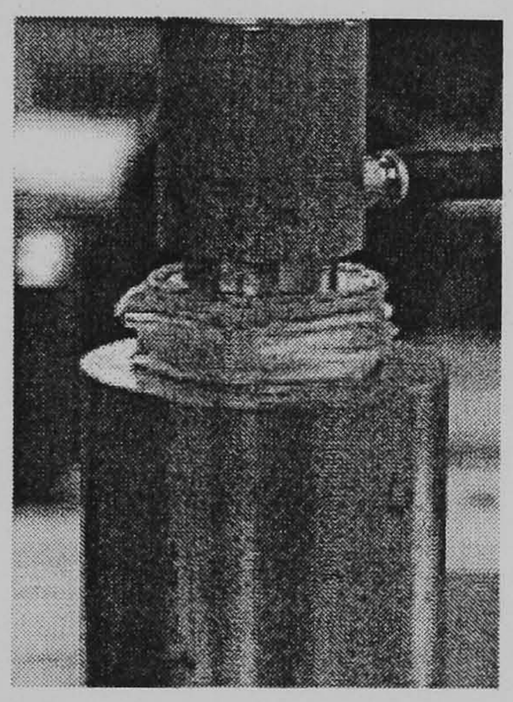

Figure 4.3 Close up of probe/polymer and polymer/test piece interface as seen in coupling efficiency test rig.

The test piece itself was a steel cylinder of 40mm diameter by 70mm in length. Its surface finish was smooth with some light scratches. The sponsors selected it as being of typical material and surface finish to that experienced in practice. Steel was a particularly good choice of test piece material as its ultrasonic properties are well defined and understood to remain unchanged over the range of pressures applied in this investigation. It would have been of interest to investigate coupling behaviour between hydrophilic polymers and composite materials, but the ultrasonic properties of such materials are known to undergo changes as a result of pressure and are particularly sensitive to environmental conditions. Therefore, use of a steel test piece (and suitable test rig) ensured in so far as was possible that as coupling pressure was varied, changes in the measured ultrasonic signals were caused only by physical changes at the interface between the hydrophilic polymer and test piece.

A digital balance was placed at the base of the rig onto which the test piece was placed. The hydrophilic sample (in the form of a disc) was then placed centrally on the top of the test piece and the balance zeroed. The

probe may be carefully lowered until it makes contact with the hydrophilic sample.

This scenario allows the probe to be placed in pressed contact with the solid couplant; the applied load exerted by the rig being read off directly from the balance. The test piece back wall echo was monitored on the ultrasonic instrument and stored digitally for later analysis. Two drops of water were applied to the interface between the probe and hydrophilic polymer to eliminate the presence of air and maintain consistent coupling. This ensures that signal variations are the result of the behaviour of the hydrophilic polymer/test piece interface only.

The probe used in this testing programme was an SLP10-10, containing a 10MHz highly damped 10mm diameter lead metaniobate crystal. An SLP10-10 is a common, plain longitudinal transducer, typically used for manual (static) testing. The overall diameter of the probe is 17mm. The centre frequency was found to be 5.8MHz with a bandwidth of 1.5 – 10MHz, when driven in wide band mode (i.e. no filterbands on the ultrasonic flaw detector). Due to this lower than expected centre frequency, the probe was found to give stronger output signal when used in 5MHz narrowband mode on the ultrasonic flaw detector. As a result of this, the coupling efficiency tests were conducted using this set up. Certificates of the probe driven at both 10 and 5MHz narrow band settings can be seen in Appendix D. The pulse and frequency spectrum are presented in Figure 4.4.

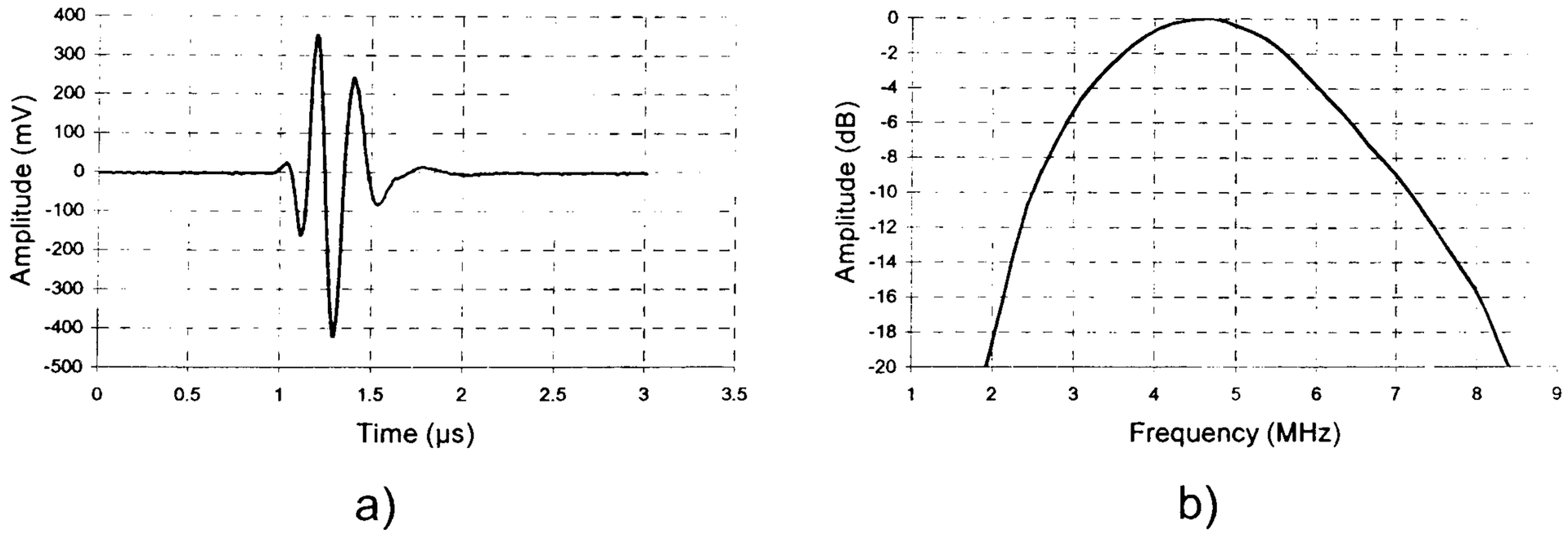

Figure 4.4 A) Pulse and B) frequency spectrum of SLP10-10 probe driven with the ultrasonic flaw detector using a 5MHz narrowband.

The hydrated hydrophilic samples evaluated in this study were approximately 28mm in diameter and 10mm thick. This thickness was chosen as it ensured that the echo signal from the back wall of the steel test piece fell centrally between the repeat echoes from the polymer itself, as illustrated schematically in Figure 4.5. This guaranteed that the signal of interest was always clearly visible even while the samples were under maximum compression.

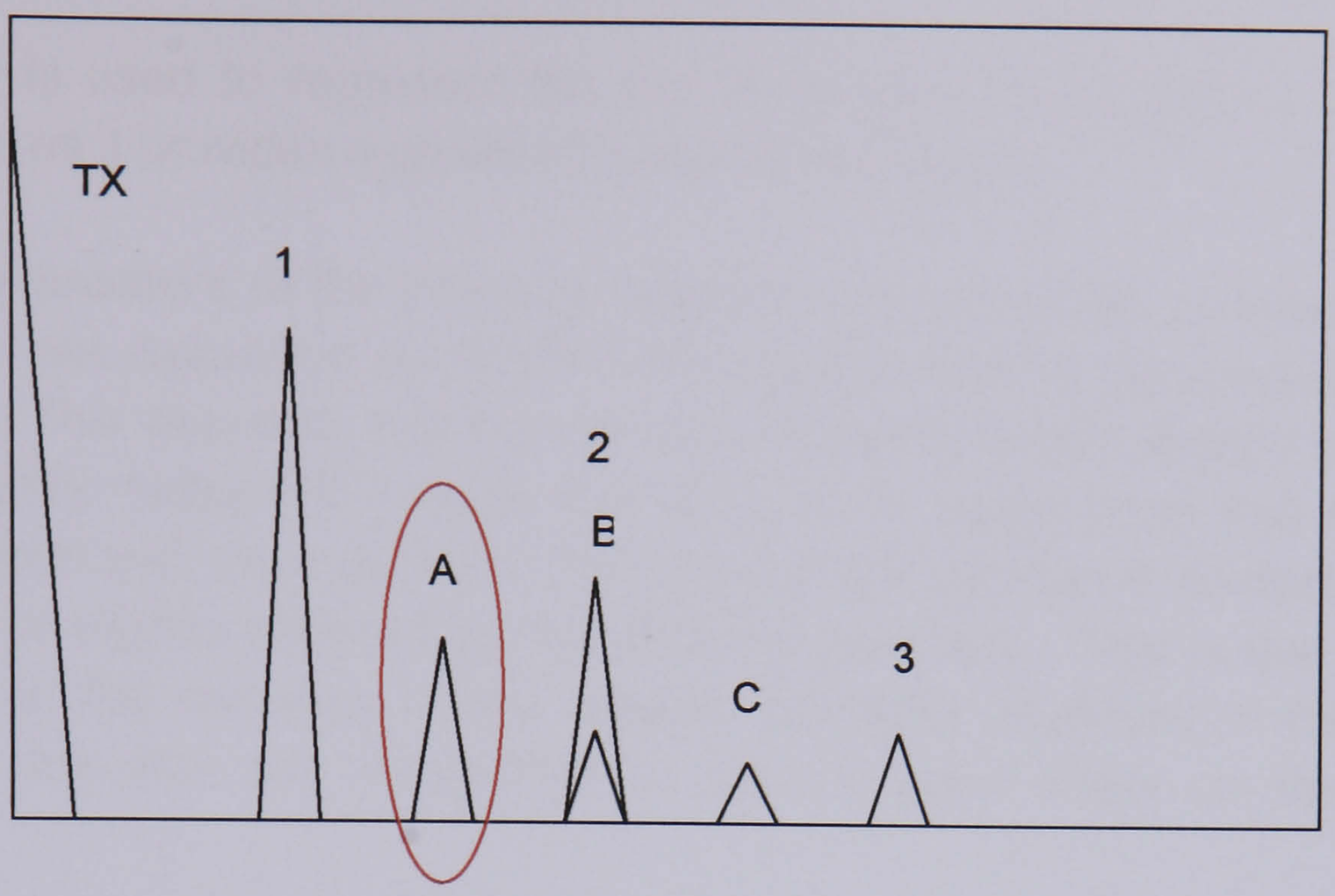

Figure 4.5 Schematic of echo locations on the screen of the ultrasonic flaw detector. Echoes 1, 2 and 3 are repeat echoes from the hydrophilic sample. Echoes A, B and C are repeat echoes from the steel test piece. The first steel back wall echo monitored in this study is highlighted.

4.2.3 Measurements

The amplitude of the echo signal was readily measured. It involved using the gain control on the ultrasonic flaw detector (minimum step is 0.5dB) to adjust the signal height to just under 100% full screen height to eliminate clipping, and then noting the gain value. An electronic gate positioned over the signal was used to determine the exact percentage of full screen height the signal achieved. Equation A.15, Appendix A was utilised to calculate the additional gain that would be required to achieve full screen height. This value is then added to the recorded gain and represents the gain required to increase the signal to exactly 100% screen height – which was treated as the reference height. This method yields higher gain resolution than the ultrasonic unit is capable of providing, assisting in the reduction of errors. Note that a low gain corresponds to an echo of high amplitude or vice versa.

The method used to determine the signal frequency was similar to that described in Chapter 2. However, this phase of experimentation was conducted prior to the development of the analysis macros that enabled semi-automated frequency calculation in Excel. A Mathcad program designed specially for this application was used[B]. This required manual measurements from the frequency spectra to be made with cross-hairs and so the data analysis phase of these tests accounted for a significant portion of the project time. The Mathcad program used is listed in Appendix C. The centre

[B] With valuable input from Dennis Cuttler (a colleague at Sonatest Plc)

frequency is used to represent the test frequency as opposed to the peak frequency, as it provides a greater frequency resolution.

The pressure at the interface between the hydrophilic polymer and the test piece was calculated by dividing the applied load by the contact area of the probe. This assumes that the pressure is concentrated directly under the probe, rapidly falling off outside this area. It is appreciated that this is a potential source of error as the surface area of the polymer in contact with the test piece is slightly different for the different polymers. This is due to slight variations in the diameter of the polymer samples employed in this study. However, this was not anticipated to have a great effect on the results achieved.

It is also accepted that the pressure distribution in the polymers while under test will not be 100% uniform. Modelling the pressure distribution in the hydrophilic polymer would be very complex so it is more constructive to consider the effects that the extremes of either high or low pressure may have on practical application. Very low loads would reduce the pressure, spreading the load over a wider area than the probe diameter, amplifying the effects of small undulations in the polymer surface. Very high loads would result in the load being focussed on the area directly under the probe. These considerations suggest that the actual pressure is more accurately described at higher loads. In both conditions, the spreading of load over an area greater than the probe diameter would result in pressure calculations always being slightly pessimistic. However, the range of applied loads employed within this test was considered to be between the two extremes and the actual effect on results caused due to pressure variations was expected to be negligible.

4.2.4 Initial Results

The first hydrophilic polymer to be evaluated was from Batch A. The interface between the polymer and steel was dry, therefore coupling was provided solely by the hydrophilic sample. The retaining screw was loosened, and the probe lowered onto the surface of the hydrophilic sample. The settings on the ultrasonic unit were adjusted to home in on the first steel back wall echo. The echo was captured and stored in the memory of the ultrasonic flaw detector with only the weight of the probe pressing onto the hydrophilic sample. Subsequent echoes were captured after imparting a higher load onto the interface between the hydrophilic sample and the test piece. The retaining screw was always tightened before an echo was captured, to ensure that the applied load was constant. The load applied by the test rig can be read directly off the balance at all times. It should be noted that adjustments to the

ultrasonic unit settings were required at each measurement load. This was due to the hydrophilic sample compressing under the increased load, resulting in the echoes from the test piece moving left on the screen towards the TX pulse.

Analysis of the amplitude data generated an unexpected result. The echo amplitude was seen to initially increase with increasing pressure until it reached approximately 0.75kg cm^{-2} where it levelled off and began to decrease after 1.5kg cm^{-2}. Analysis of the frequency data revealed a similar anomaly, increasing initially before dropping. This suggested there was something incorrect with the measurement process.

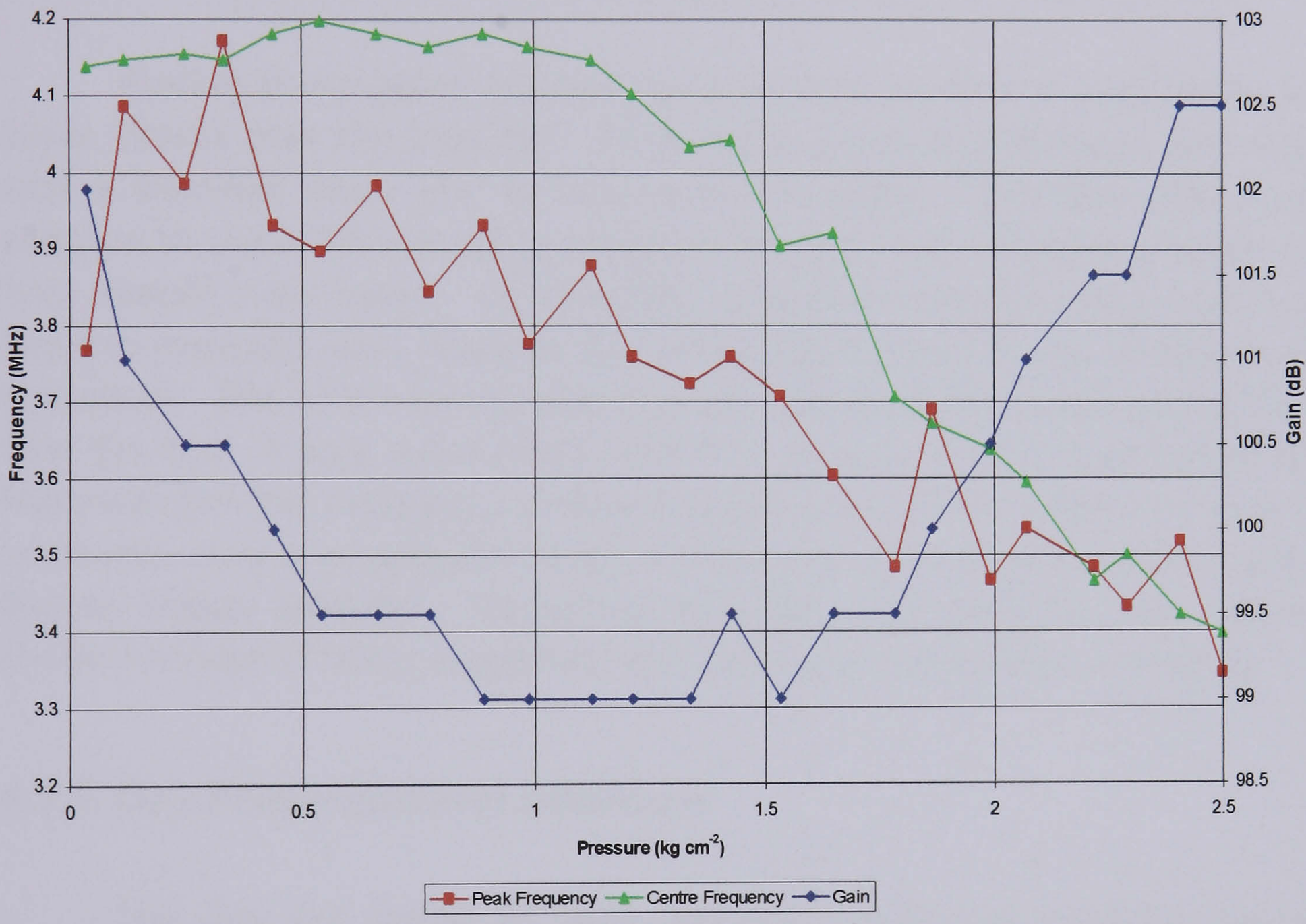

Figure 4.6 Amplitude and frequency data plotted against increasing coupling pressure. Unexpected downturn in both amplitude (signified by an increase in receiver gain) and frequency at high pressures is observed. Batch A hydrophilic polymer.

Close inspection of the testing equipment revealed an oversight in the rig design. It was noticed that the test piece was not positioned directly over the load cell in the balance. As a result, the balance pan was beginning to tilt very slightly once the applied load was sufficient. This had the effect of upsetting the parallel arrangement between the probe face and the surfaces of the test piece causing the ultrasound incident on the test piece back wall to be reflected back at an angle. Therefore, only a portion of the total reflected ultrasound was actually incident on the probe when pan tilting occurred. Figure 4.7 illustrates this schematically.

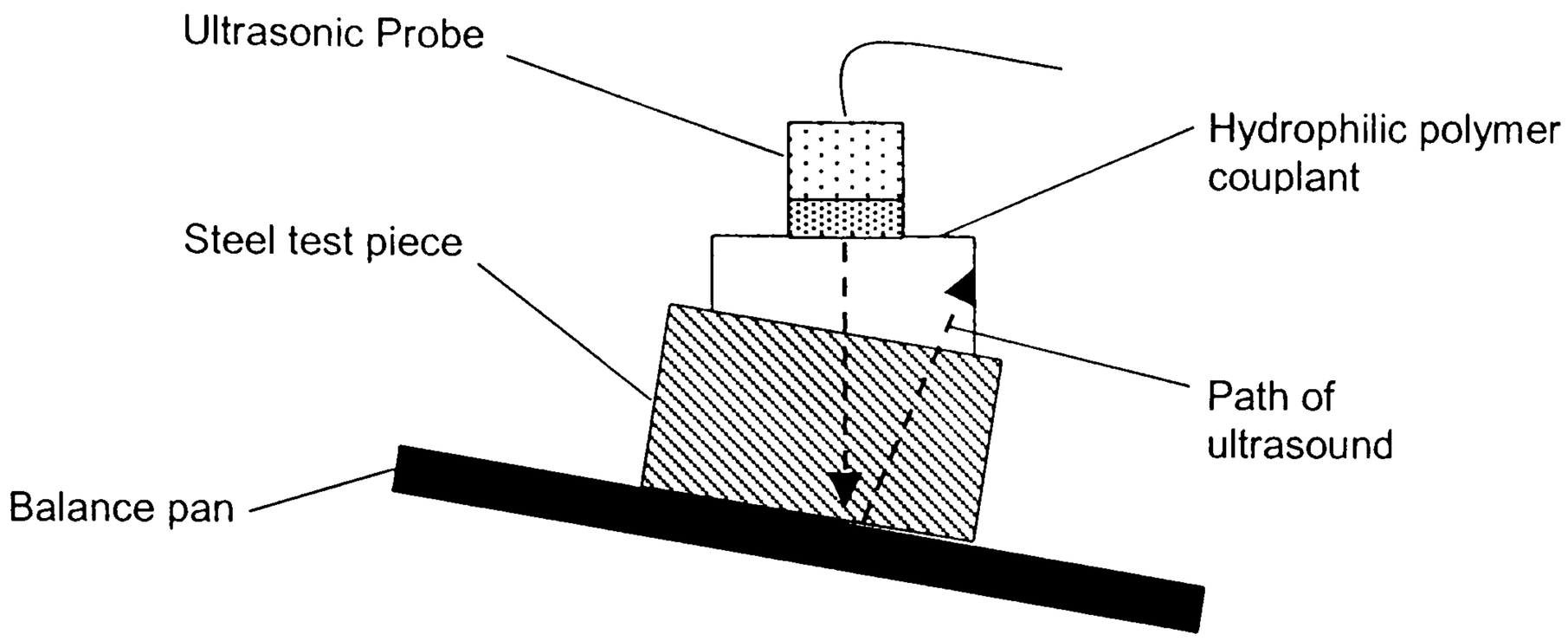

Figure 4.7 Exaggerated schematic of balance pan tilt at high coupling pressures.

Further investigation showed that it was not possible to position the test piece directly over the load cell. As a result, a new balance was purchased with a stainless steel pan, far less prone to tilting. With this unit, it was possible to place the test piece on top of the load cell, minimising deviations from normal even further. By doing this, significant practical steps had been taken to eliminate false readings due to misalignment of the probe face to the test piece. The new balance also had the benefit of finer resolution (0.01g) than the first. It was surprisingly difficult to procure such an instrument with fine resolution but retaining a sufficient maximum load to enable testing to be conducted over a meaningful range of pressures. The device selected was a Mettler Toledo BD6000. Repeating the initial tests with this new balance showed no sign of tilting suggesting that the problem had been overcome.

4.2.5 Dry Polymer/Steel interface

The first full round of tests conducted with the modified test rig concentrated on hydrated polymers coupling to steel in the absence of any free water. The amplitude and frequency were measured at different pressures both when force was being applied to and removed from the interface, hence generating additional data which will permit the exploration of the loading and unloading cycles. All four batches of polymer (A – D) were subjected to this testing programme. Tests were conducted six times for each polymer to explore the reproducibility of the experimental procedure.

Amplitude data acquired for all four hydrophilic polymers from each round of testing is shown in Figure 4.8 to Figure 4.11.

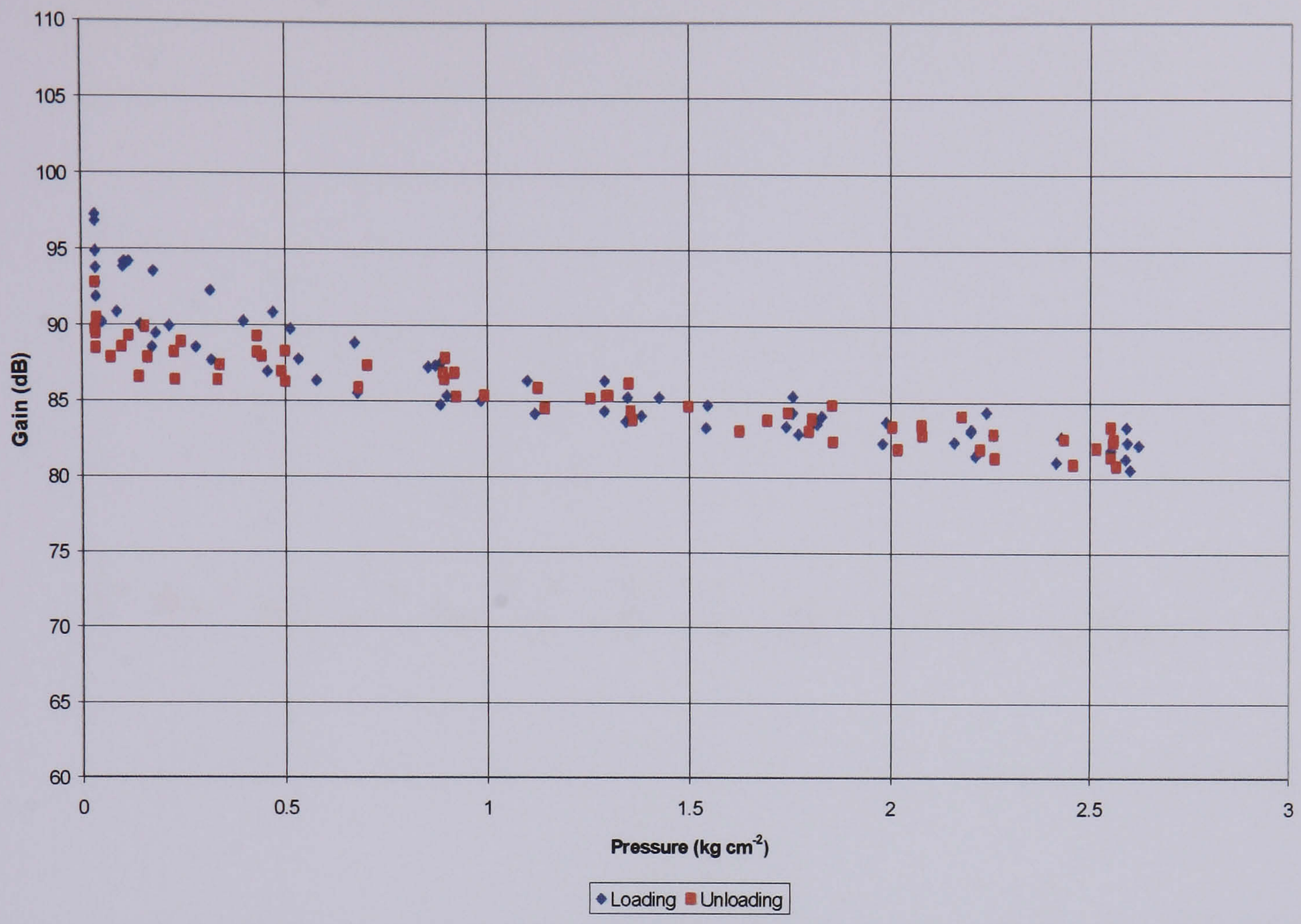

Figure 4.8 Amplitude data acquired via a Batch A hydrophilic polymer during loading and unloading cycles of a coupling efficiency evaluation programme.

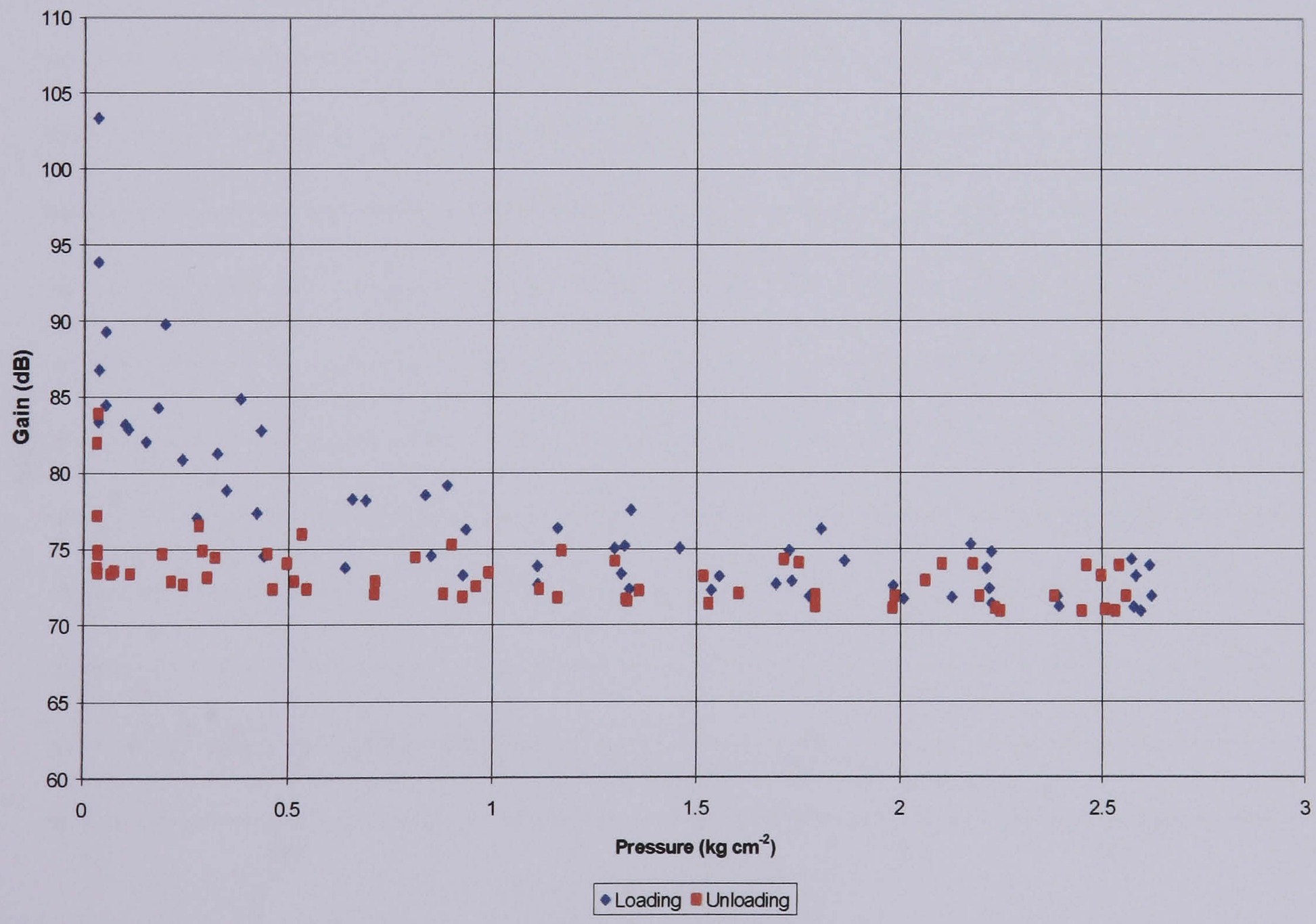

Figure 4.9 Amplitude data acquired via a Batch B hydrophilic polymer during loading and unloading cycles of a coupling efficiency evaluation programme.

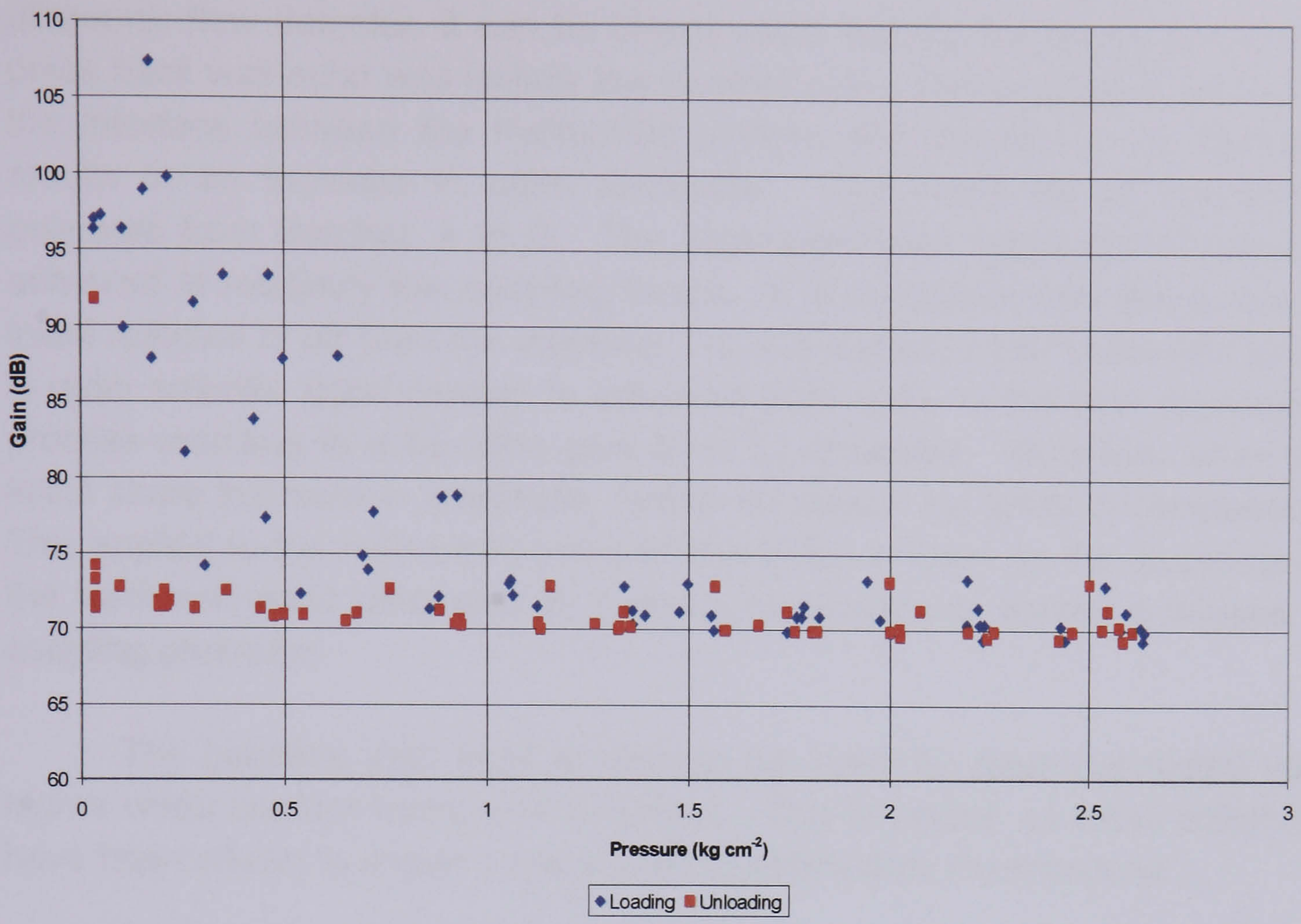

Figure 4.10 Amplitude data acquired via a Batch C hydrophilic polymer during loading and unloading cycles of a coupling efficiency evaluation programme.

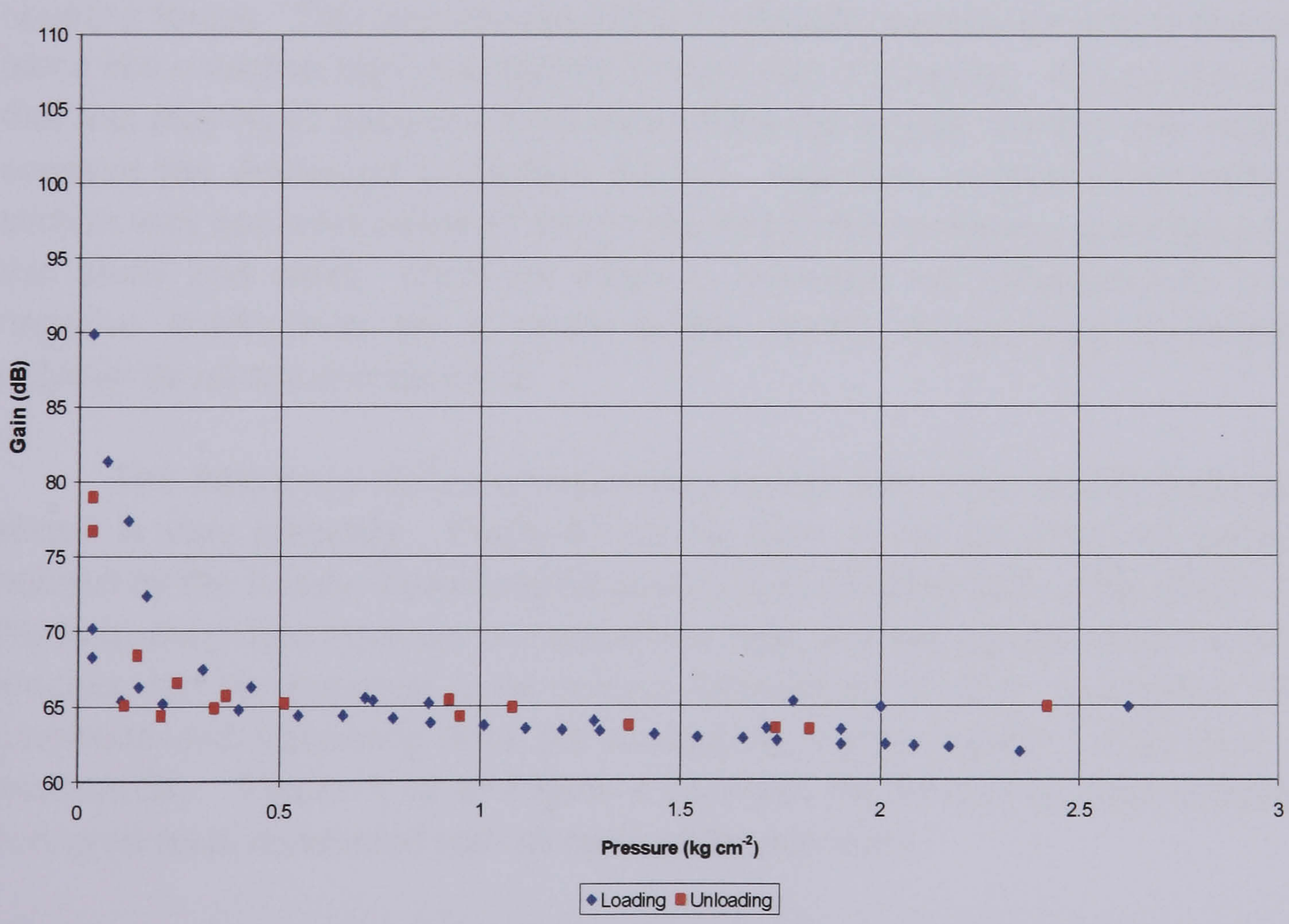

Figure 4.11 Amplitude data acquired via a Batch D hydrophilic polymer during loading and unloading cycles of a coupling efficiency evaluation programme.

Remembering that the gain is the amount of amplification required to increase the steel back wall echo to full screen height on the screen of the

ultrasonic flaw detector, it can be clearly seen that the amplitude of the test piece back wall echo was initially low in amplitude. The application of load to the interface between the hydrophilic sample and the test piece interface results in an increase in echo amplitude. This holds for all hydrophilic polymers from Batches A to D. The most significant amplitude increase is achieved at relatively low coupling forces. It is suggested that this is due to initial removal of air from the interface. As the surface finish of the test piece is quite smooth, good contact is achieved quite early in the load application process resulting in a baseline gain level as observed. Therefore, after the initial sharp increase in amplitude, further increases are small in comparison. This applied to the hydrophilic sample from Batch A least, as the amplitude of the back wall echo continued to increase markedly with further increases in coupling pressure.

The baseline gain level is seen to be lower for tests conducted with higher water content hydrophilic polymers. This is logical, as these polymers have been shown to impart a lower level of attenuation to ultrasound.

During the unloading cycles, the amplitude does not follow the same pattern as the loading cycles. Instead the amplitude remains high at very low coupling forces. This was likened to the hydrophilic sample sticking to the test piece like a suction cup, maintaining a high level of coupling. It is conceivable that this may have occurred if the face of the hydrophilic sample was slightly concave (as discussed in Section 4.2.11). However, in practice no natural stiction was apparent between any of the hydrophilic polymers investigated in this study and steel. Such an effect is therefore not considered to have negative implications for a wheel probe device incorporating hydrophilic polymer as ultrasound couplant.

The frequency data corresponding to the amplitude results displayed above is very pleasing. Firstly it can be seen to be following the pattern defined by the theory; increasing frequency with increasing coupling force. As the frequency data matches the amplitude data, the test rig and measurement process can be assumed to be correct [Drinkwater, 1997c]. Secondly, both amplitude and frequency data are consistent, demonstrating a high level of repeatability. Figure 4.12 to Figure 4.15 show the frequency data acquired during all tests conducted with all hydrophilic polymers.

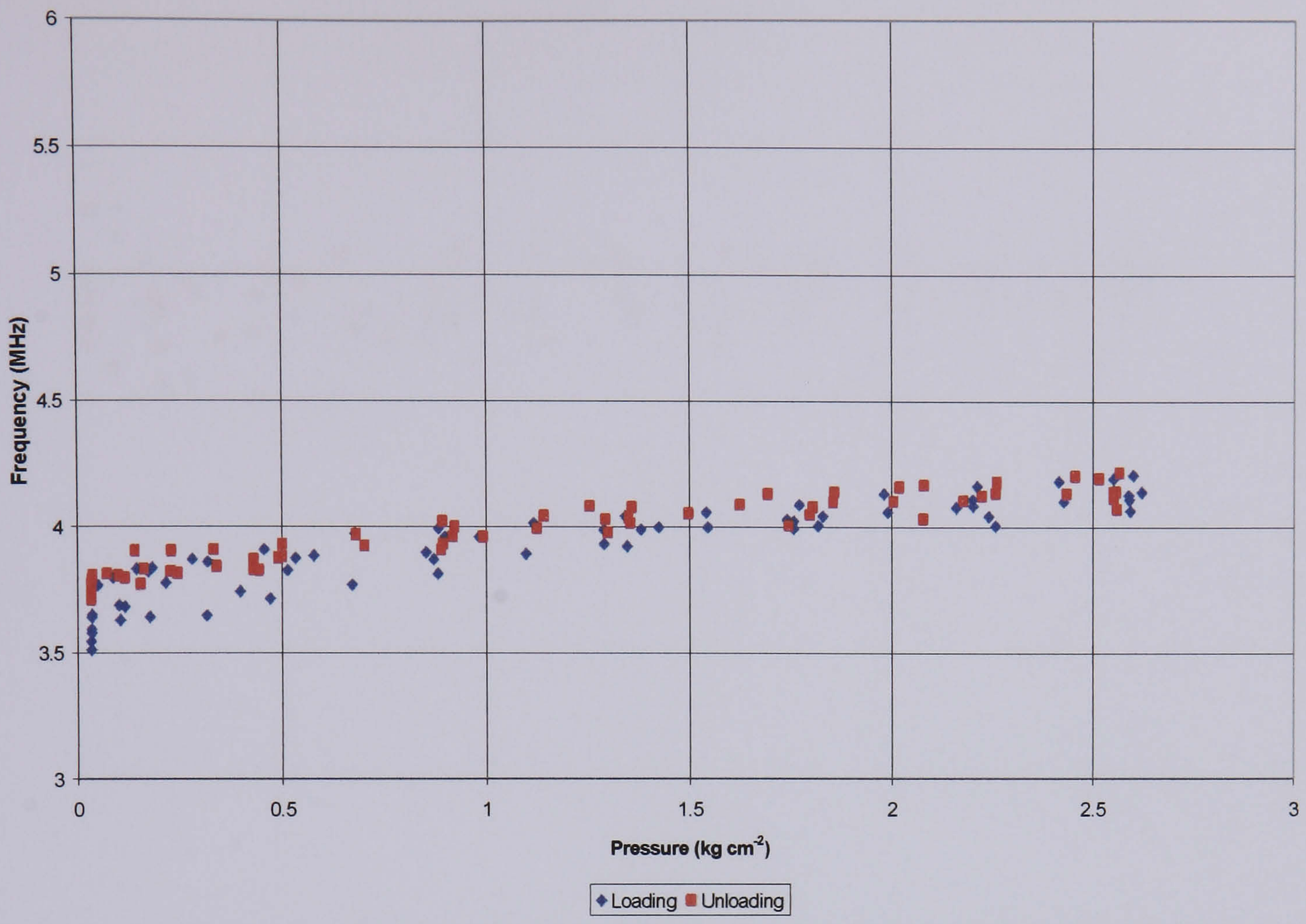

Figure 4.12 Frequency data acquired via a Batch A hydrophilic polymer during repeated loading and unloading cycle of a coupling efficiency evaluation programme

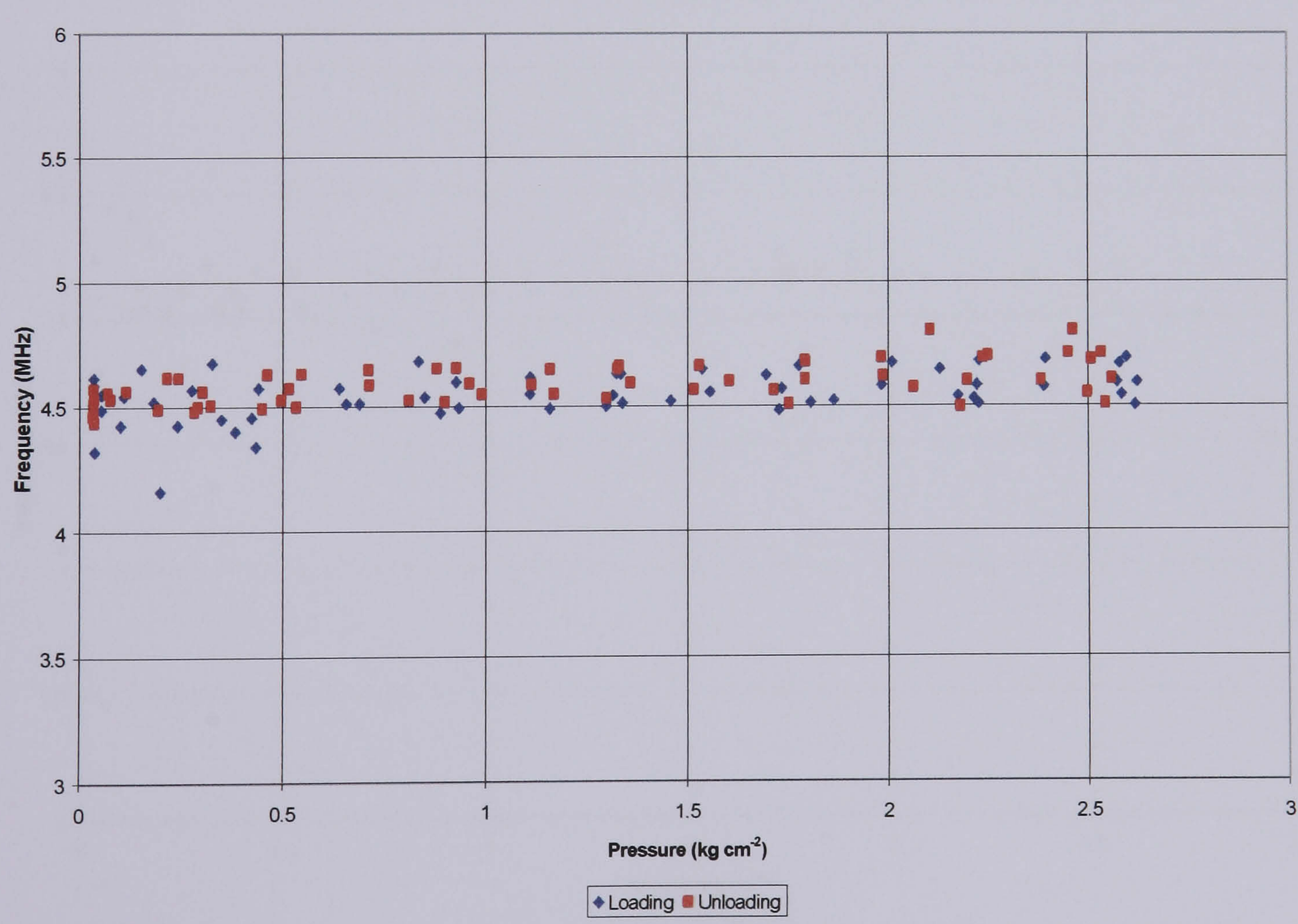

Figure 4.13 Frequency data acquired via a Batch B hydrophilic polymer during repeated loading and unloading cycle of a coupling efficiency evaluation programme.

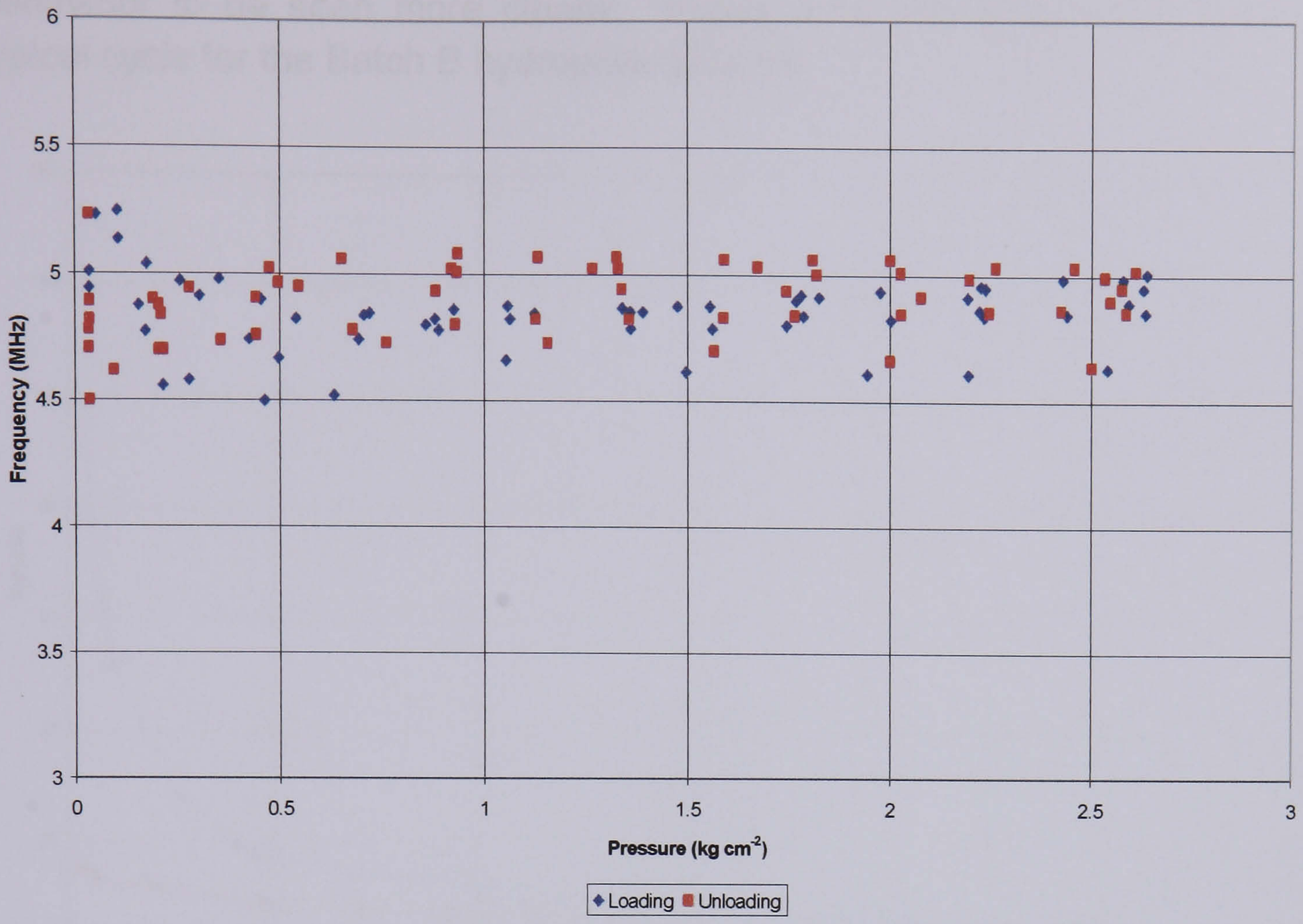

Figure 4.14 Frequency data acquired via a Batch C hydrophilic polymer during repeated loading and unloading cycle of a coupling efficiency evaluation programme.

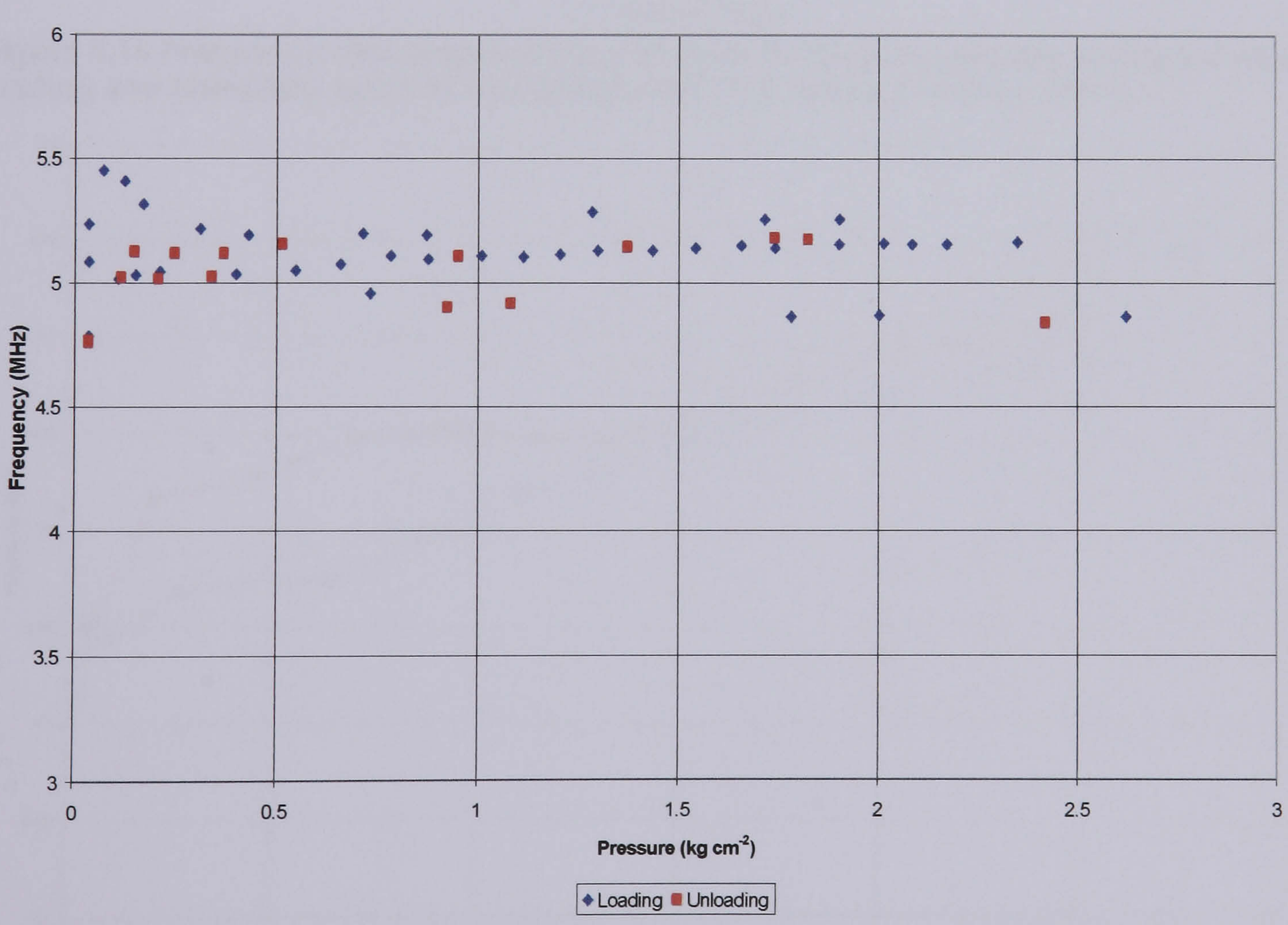

Figure 4.15 Frequency data acquired via a Batch D hydrophilic polymer during repeated loading and unloading cycle of a coupling efficiency evaluation programme.

The data displayed above represents all the results from each round of tests. Considering just one loading and unloading cycle enables the coupling

behaviour to be seen more clearly. Figure 4.16 and Figure 4.17 show a typical cycle for the Batch B hydrophilic polymer.

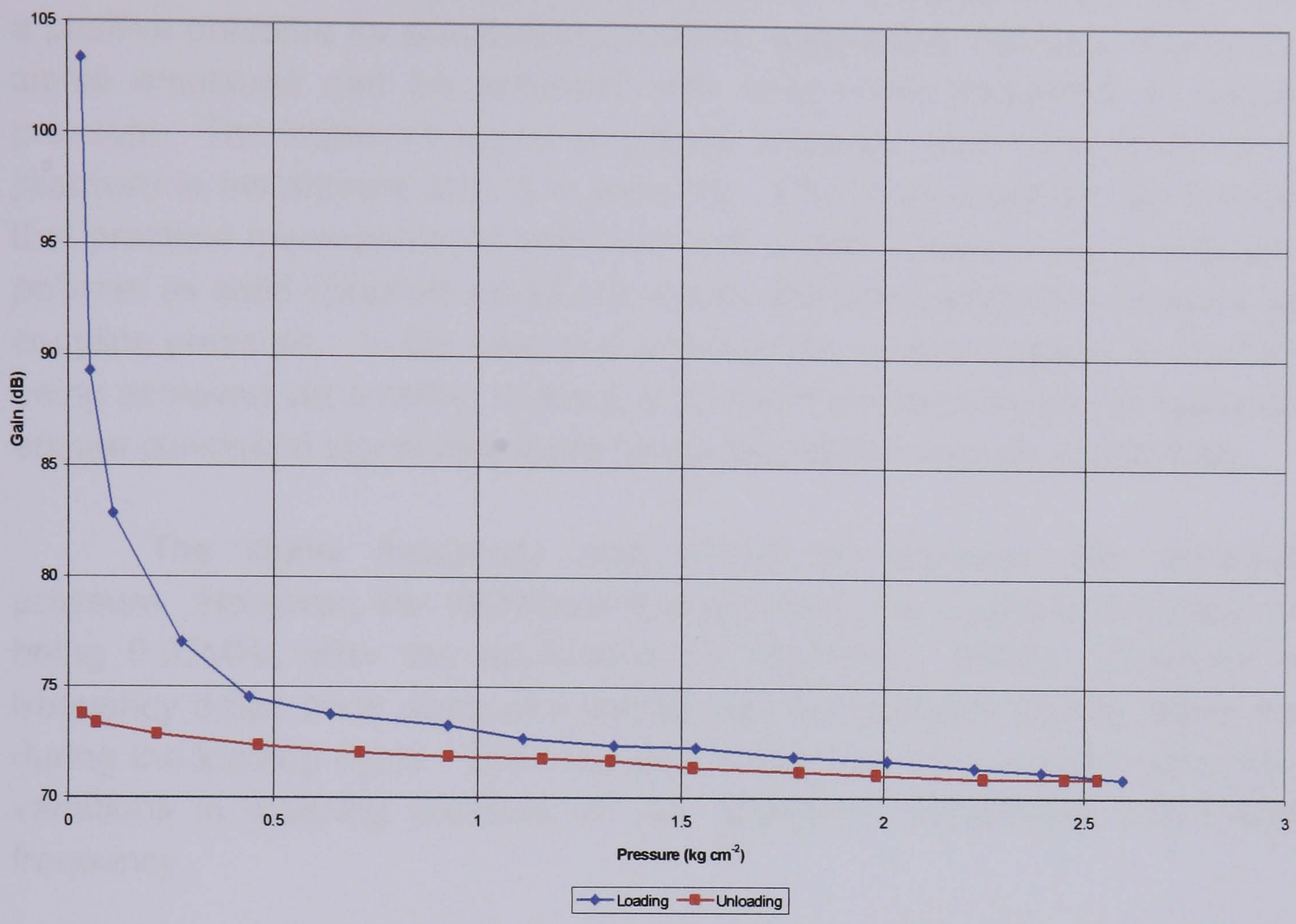

Figure 4.16 Frequency data acquired via a Batch B hydrophilic polymer during a single loading and unloading cycle of a coupling efficiency evaluation programme.

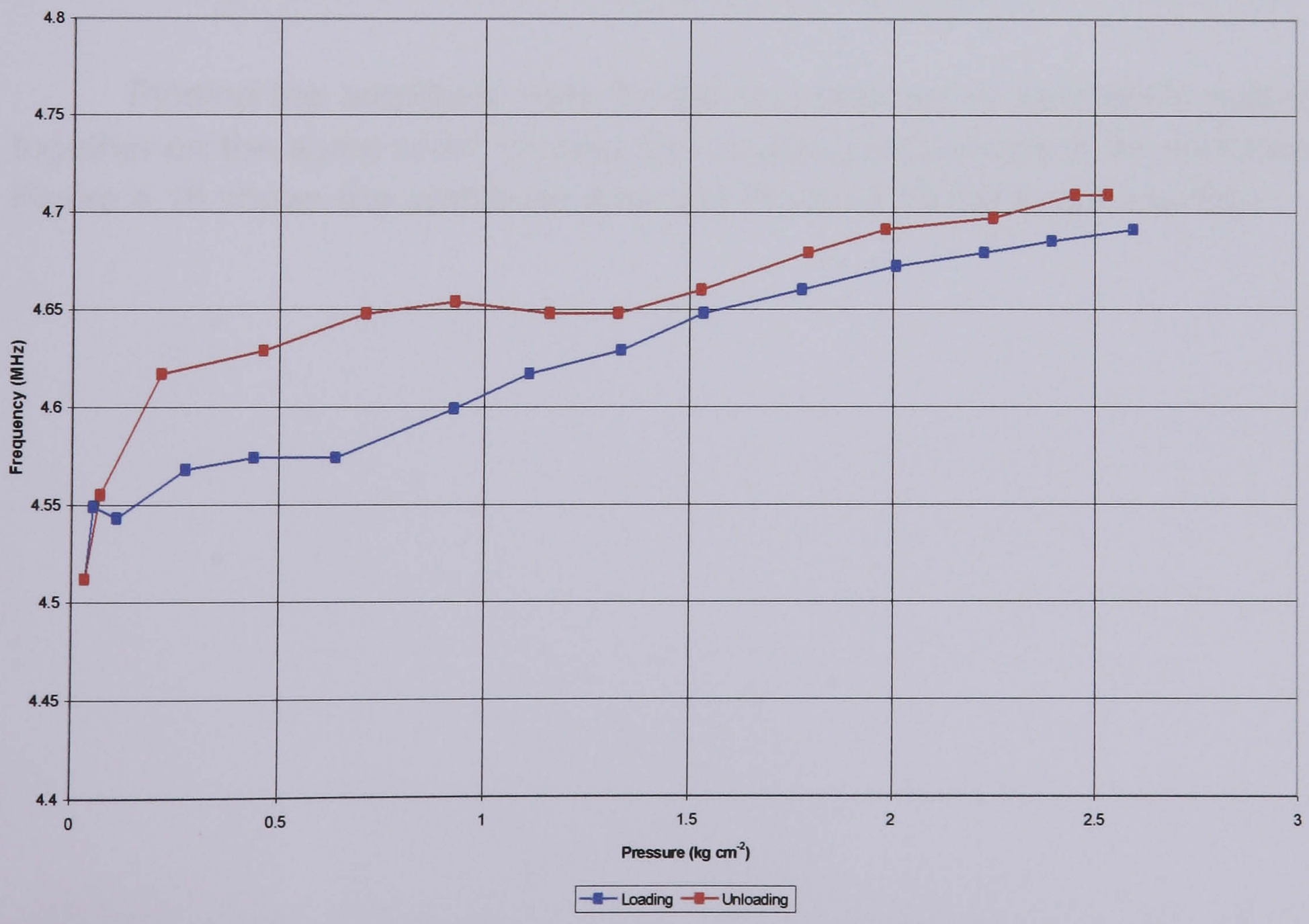

Figure 4.17 Frequency data acquired via a Batch B hydrophilic polymer during a single loading and unloading cycle of a coupling efficiency evaluation programme.

This shows a marked increase in amplitude during loading, the example in Figure 4.16 being approximately 29dB following the application of just 0.4kg cm^{-2} which equates to an applied load of approximately 1kg. This is a positive outcome for practical application, suggesting that large increases in signal amplitude can be achieved with very minor increases in coupling pressure. The improved signal amplitude achieved after initial application of pressure is maintained after it is reduced. This is also positive as it implies that practical measurements achieved with a static probe using a hydrophilic polymer as solid couplant would not require the application of a constant high coupling pressure. In the case of a wheel probe, where coupling is constantly being achieved via a rolling contact, a constant pressure would be required to ensure consistent signal amplitude (assuming similar surface conditions).

The signal frequency also shows an increase with increasing pressure. However, the difference is very minor, the example in Figure 4.17 being 0.03MHz after the application of 1kg load. During unloading, the frequency drops back down at a similar rate, but remains slightly higher than during the loading cycle. This was also interpreted as a positive outcome as variations in coupling pressure do not appear to significantly effect signal frequency.

4.2.6 Comparison Between Candidate Hydrophilic Polymers

Plotting the amplitude data for the four batches of hydrophilic polymer together on the same chart enables the coupling behaviours to be compared. Figure 4.18 shows the amplitude data and Figure 4.19 the frequency data.

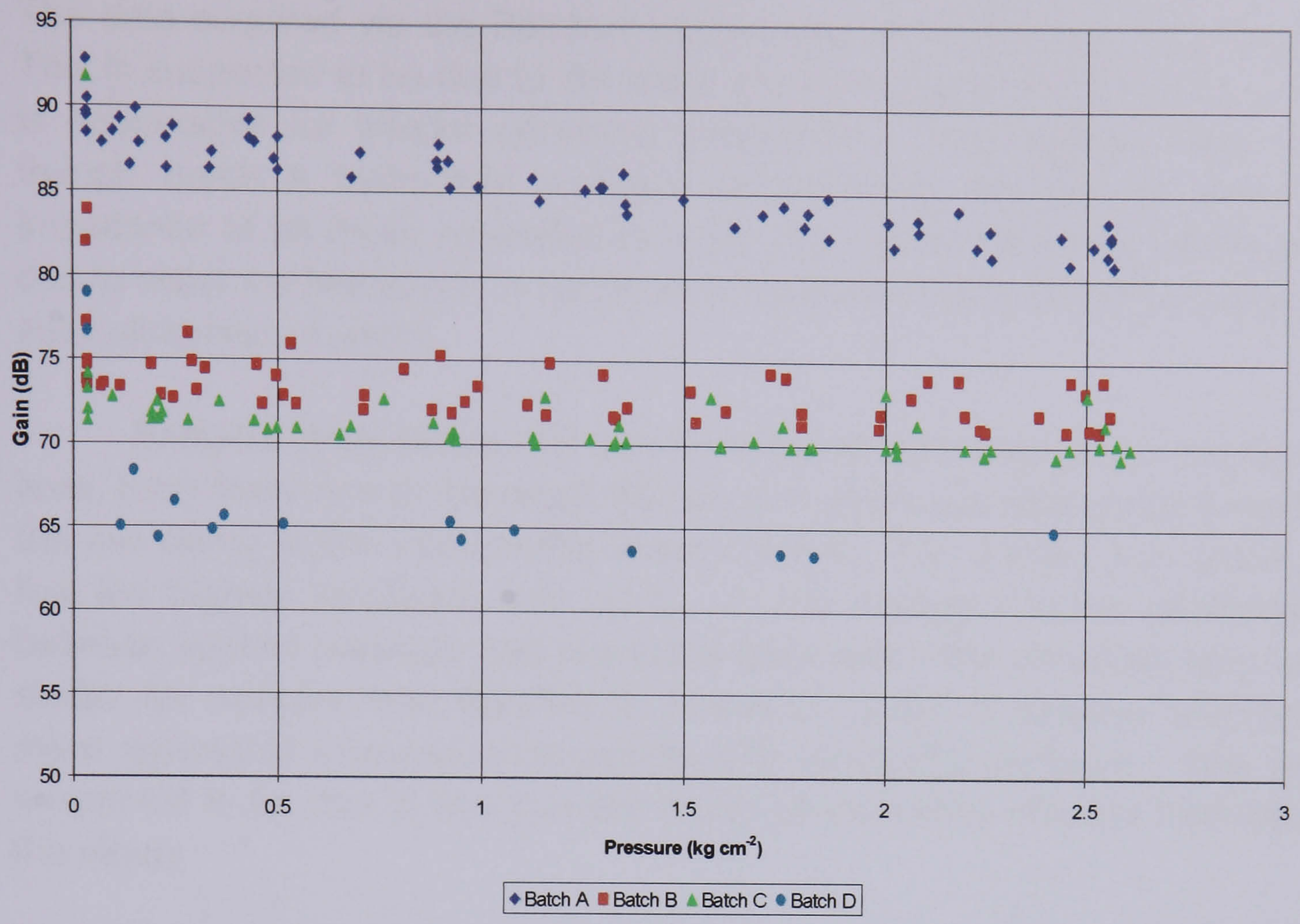

Figure 4.18 Amplitude data for different hydrophilic polymers during unloading cycles of a coupling efficiency evaluation programme.

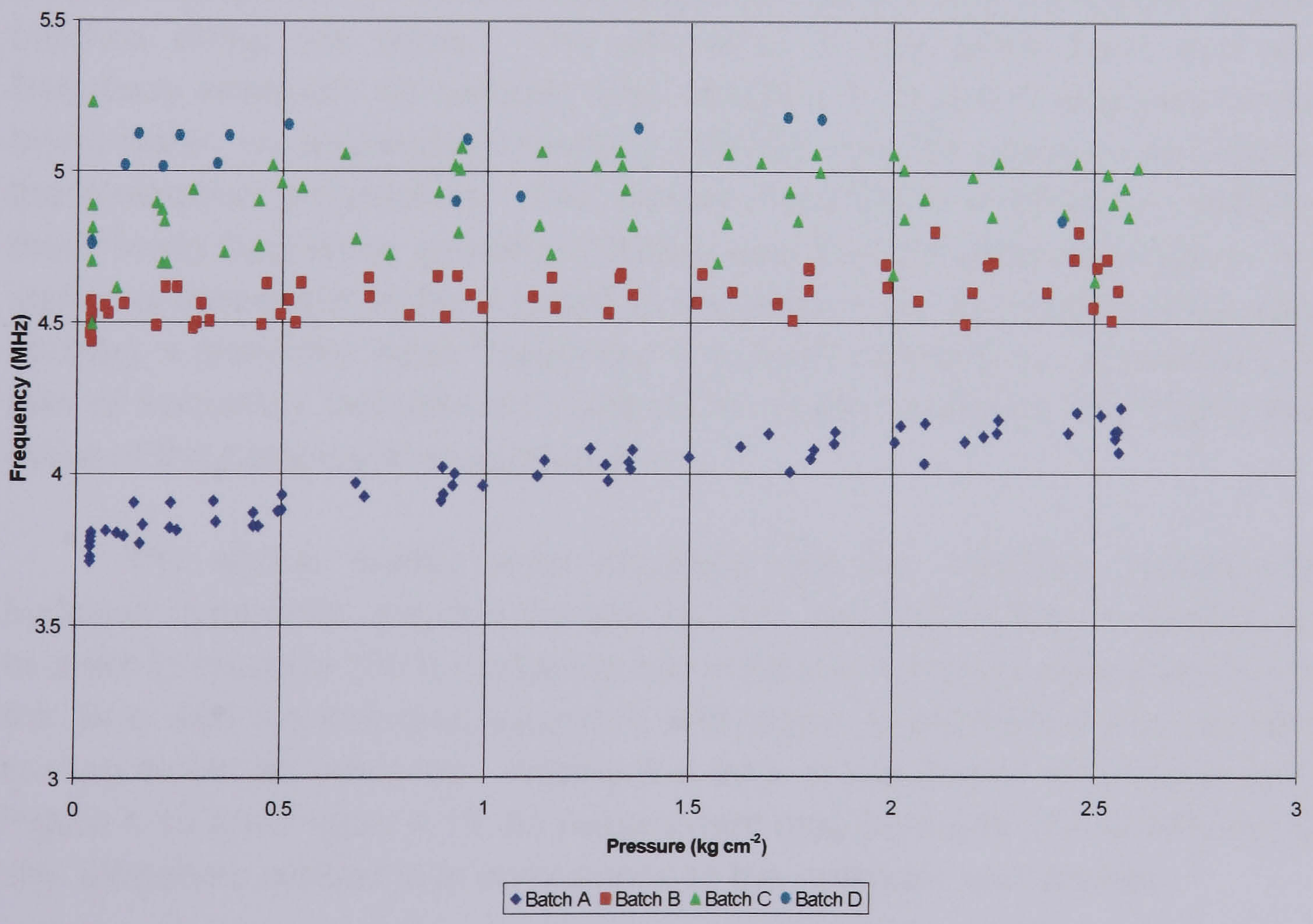

Figure 4.19 Frequency data for different hydrophilic polymers during unloading cycles of a coupling efficiency evaluation programme.

Beyond the gradual increase in signal amplitude with pressure, there is an additional trend – the higher the equilibrium water content of the hydrophilic polymer, the higher the amplitude of the test piece back wall echo.

The data acquired via the Batch A sample has by far the lowest amplitude. This is suspected to be due to the lower water content of this material, which is responsible for inferior ultrasonic properties. This suggests that even though Batch A hydrophilic samples demonstrated the greatest acoustic impedance of all those evaluated thus far, the overall ultrasonic attenuation due to water content played a much more significant role in its performance as solid ultrasonic couplant.

Samples from Batches B and C demonstrated very similar amplitude level, most likely due to the small difference in ultrasonic attenuation between the two owing to the comparable water content. The sample from Batch D has the highest amplitude data of all. It was noticed that the relationship between applied pressure and test piece back wall echo amplitude was very similar for samples from Batches B, C and D. Batch A however showed a more noticeable increase in amplitude with increasing pressure. This was suspected to be due to this polymer being an inherently different material to the others.

The frequency data behaved in a very similar way to the amplitude data already discussed, the relationship between the different hydrophilic polymer batches being the same. The difference in test piece back wall echo frequency achieved via samples from Batches A, B and C was very similar, being within an approximate range of 0.8MHz over the pressure employed in the evaluation programme. The sample from Batch A however, yielded a much lower frequency, typically 0.7MHz lower than the other data series. This again, is suspected to be a result of the differences in material attenuation, causing a generally larger frequency downshift in Batch A. In addition, the rate of frequency increase with respect to applied pressure was higher than those of the samples from batches B – D.

The above results were obtained with the interface between the hydrated hydrophilic polymer sample and the steel test piece completely dry. In order to emulate 100% contact at this interface, the tests were repeated but this time with the interface saturated with water, guaranteeing that complete contact would be achieved. Adding this data to the scatter data presented in Figure 4.18 and Figure 4.19; an assessment may be made of how efficient the 'dry' ultrasonic contact is in comparison to the optimum 'wet' contact.

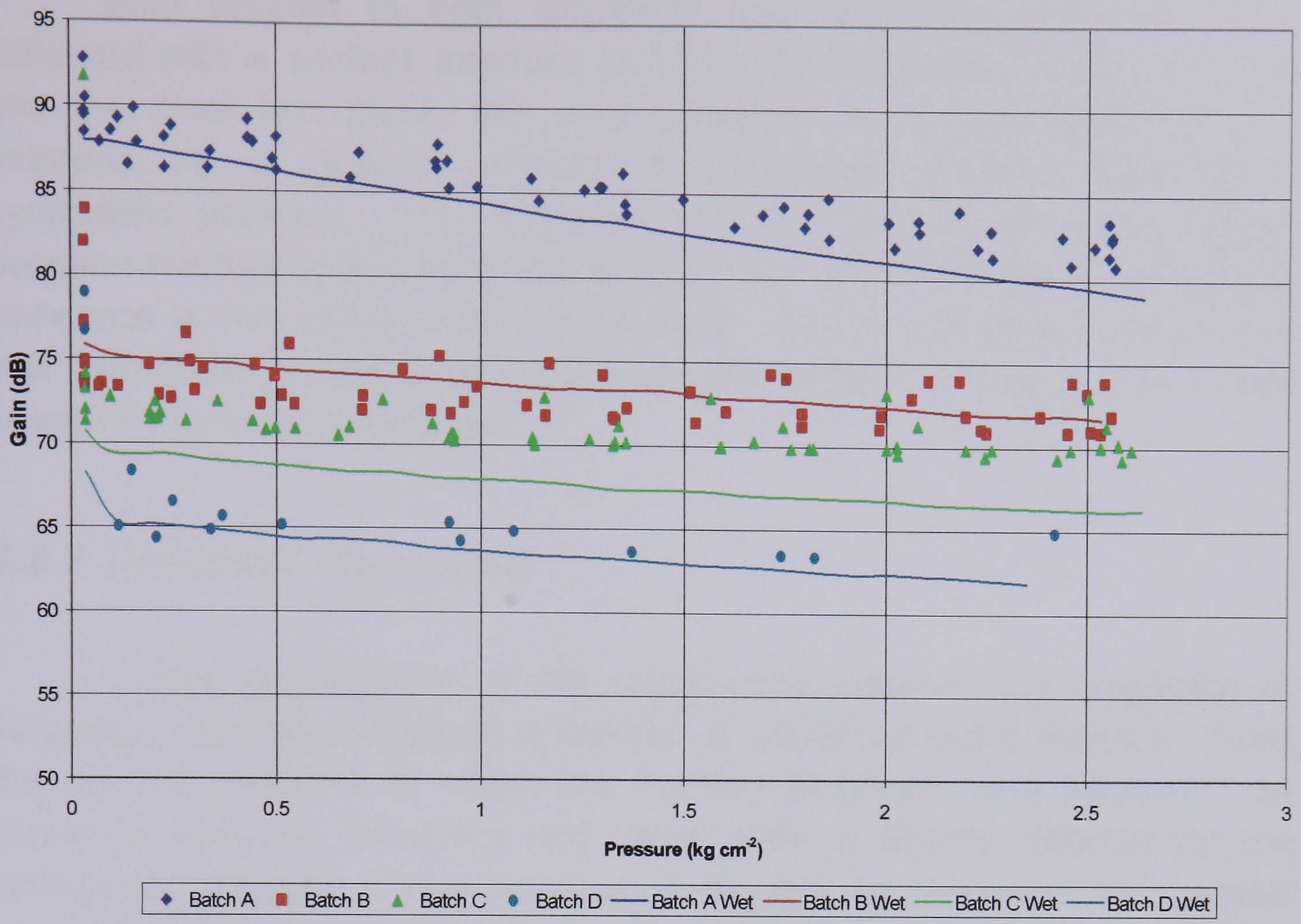

Figure 4.20 Amplitude data for different hydrophilic polymers during unloading cycles of a coupling efficiency evaluation programme. Amplitude data acquired with saturated interfaces to emulate 100% coupling is also shown for comparison.

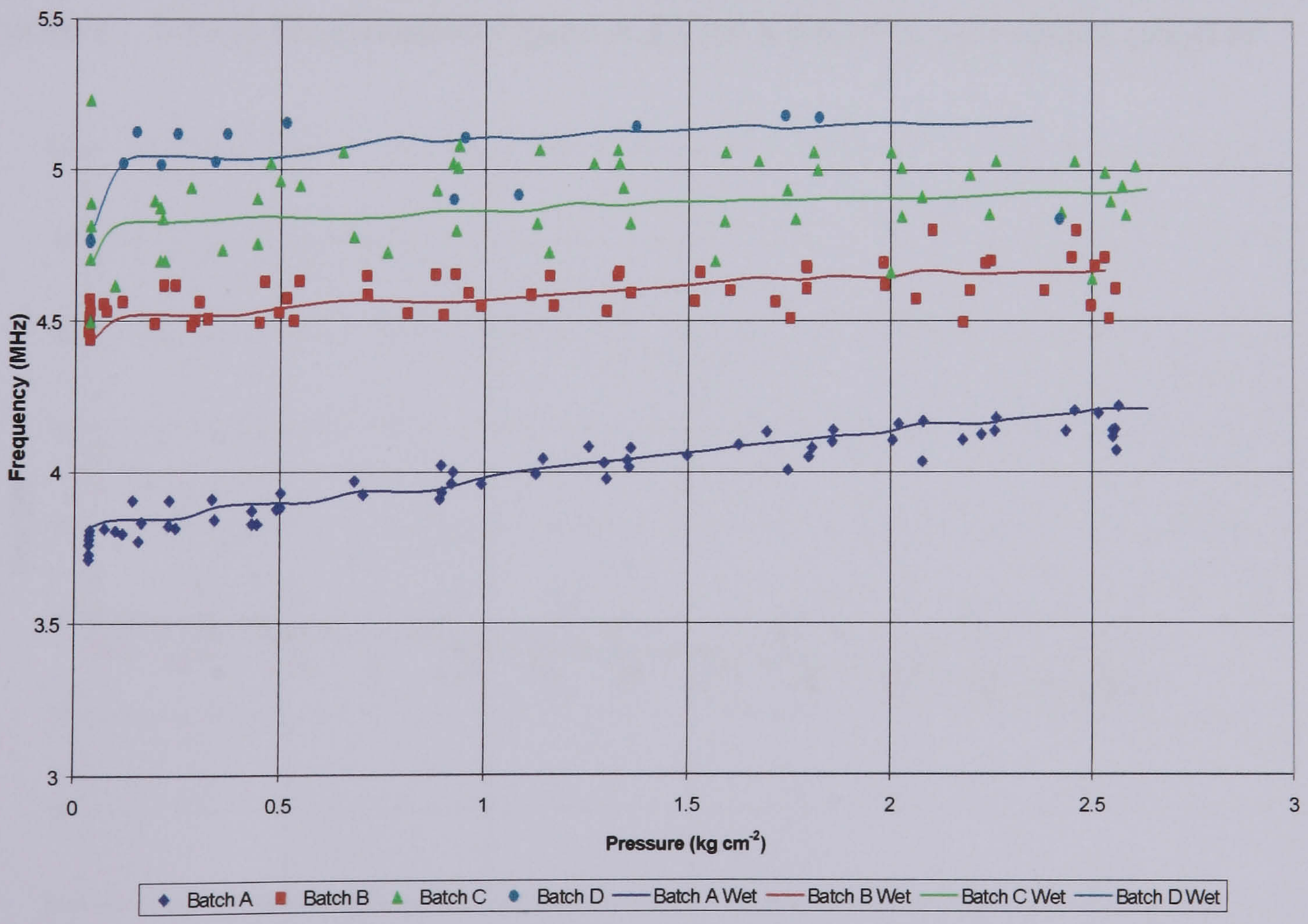

Figure 4.21 Frequency data for different hydrophilic polymers during unloading cycles of a coupling efficiency evaluation programme. Frequency data acquired with saturated interfaces to emulate 100% coupling is also shown for comparison.

With respect to both amplitude and frequency data, the results achieved with a 'perfect' interface between the hydrophilic polymer samples and the steel test piece, are very similar to those achieved with a dry interface, i.e. a situation whereby coupling was provided solely by the hydrophilic polymer. This suggests that the level of ultrasonic coupling between the hydrophilic polymers evaluated in this study and a smooth steel test piece is very close to that of the ideal. This is a good thing as it shows that hydrophilic polymers do not require the addition of free water to couple effectively to smooth surfaces.

4.2.7 Pressure Threshold

Closer investigation of the relationship between the amplitude and frequency data sets revealed a number of additional characteristics. Firstly, the applied pressure at which the loading amplitude and frequency data converge with the unloading and 'ideal' data is slightly different for each hydrophilic polymer. This process is thought to represent the pressure required to remove air from the interface between the polymer and the test piece. As would logically be expected, the most flexible polymer samples achieve this at lower pressures. This equates directly to the equilibrium water content. This is illustrated in Figure 4.22 for a Batch B hydrophilic polymer.

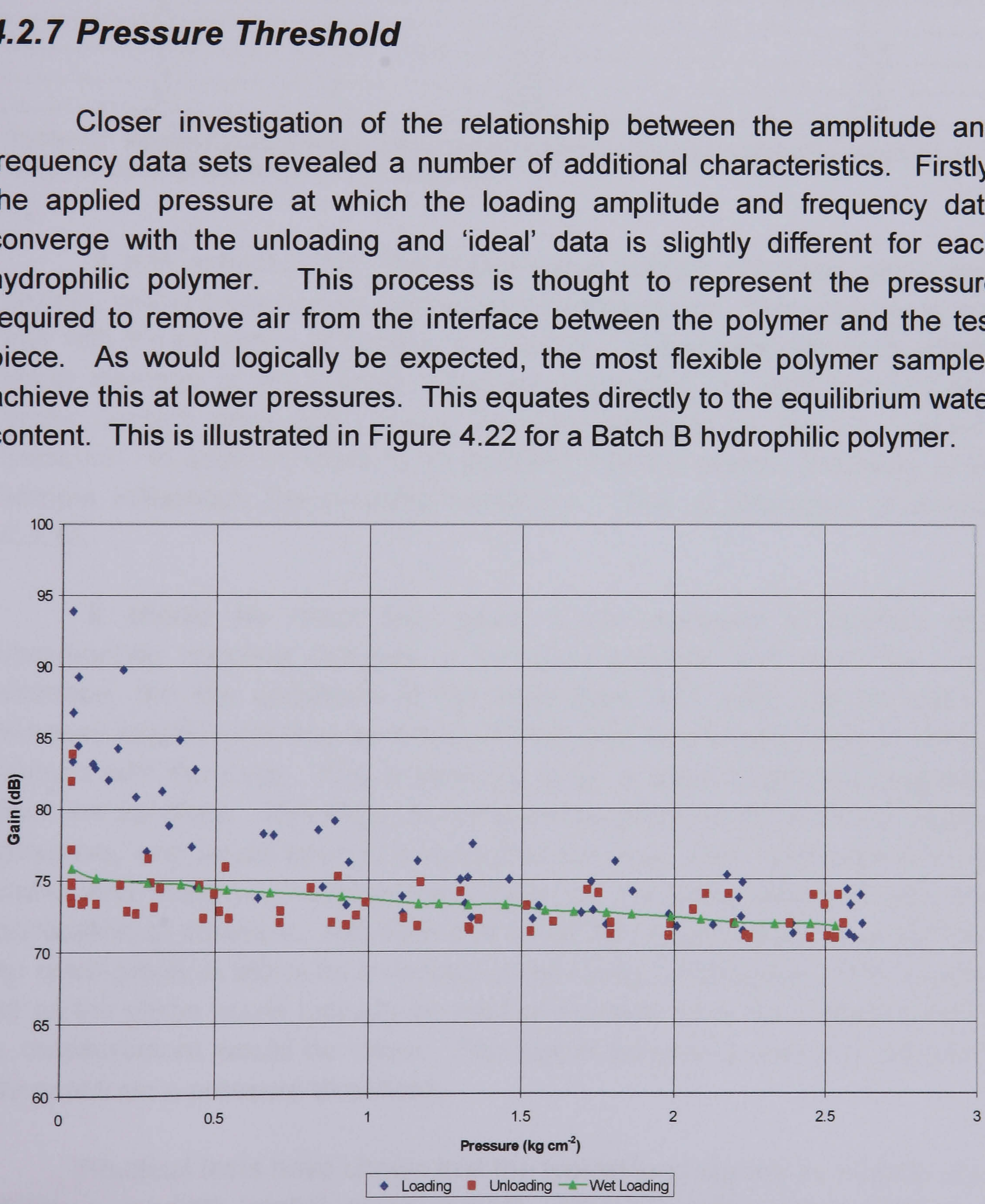

Figure 4.22 Amplitude comparison between loading and unloading cycles of a Batch B hydrophilic polymer during a coupling efficiency evaluation programme.

The dry loading data appear to converge on the unloading and wet data from approximately 0.5kg cm^{-2} onwards. This indicates that the efficiency of ultrasound transfer will not continue to increase at the same rate with further increases in pressure, representing an optimum pressure for practical use. Similar pressure threshold estimates can be made from analysing the data from the other polymers tested. These are listed in Table 4.1 together with the corresponding applied load for practical interpretation. The Batch D polymers did not demonstrate an obvious pressure threshold.

Hydrophilic Polymer Batch	Pressure Threshold (kg cm^{-2})	Applied Load (kg)
A	0.5	1.1
B	0.4	0.9
C	0.9	2.0
D	N/A	N/A

Table 4.1 Approximate pressure threshold at which optimum ultrasonic coupling via a range of hydrophilic polymers is achieved.

It was expected that the higher water content polymers, being more flexible, would demonstrate lower pressure thresholds. This appears to hold true with the exception of the Batch C sample. This is attributed to the slightly larger diameter of this sample, effectively spreading the applied load over a larger contact area and causing an over estimate of the true coupling pressure. In addition, there is a possibility that the surface geometry of the sample influenced the coupling behaviour. This is discussed in Section 4.3.10.

It should be noted that when a low pressure is applied while investigating coupling between a hydrated polymer and steel via a dry interface, the low amplitude of the steel back wall echo can be seen to increase slightly with time as if the polymer was slowly increasing its surface contact with the steel. This is believed to be a result of gas diffusing away from the interface. Therefore, to compare the pressure threshold of different polymers, one would have to ensure that the tests were conducted over the same time scale i.e. measurements taken at the same period of time after application of pressure. Although this effect has been noticed, it would have no great practical effect for a contact probe using a hydrophilic solid couplant tip as the probe would typically be held on location for a few moments before a measurement would be taken. The signal frequency does not appear to demonstrate a pressure threshold.

Practical tests have shown that the typical load applied to a probe while taking a manual (static) measurement, although varying form person to person, is approximately 2kg. Such a load equates to an approximate pressure of 0.9kg cm^{-2} for the probe employed in these tests, suggesting that

maximum signal amplitude may be achieved without the need for coupling pressures greater that those typically used for conventional liquid coupled probes. Indeed, it may be more practical to momentarily apply a pressure beyond the pressure threshold of the polymer before easing off to allow the measurement to be taken ensuring optimal signal amplitude.

4.2.8 Coupling Characteristics

The scatter data achieved from the repeated tests conducted with a dry interface between the hydrated polymer and steel test piece was used to determine trend data. A line of best fit was calculated and used to define coupling characteristics for the different hydrophilic polymers investigated. Firstly, the intercept values with the Y-axis were calculated. This provided an indication of the frequency and amplitude at a theoretical zero pressure for rapid comparison. Secondly, the gradients of the trend lines were calculated, providing information concerning the change in amplitude and frequency per unit pressure (see Table 4.2).

Hydrophilic polymer Batch	Frequency		Amplitude	
	MHz/kg cm^{-2}	MHz @ 0kg	dB/kg cm^{-2}	dB @ 0kg
A	0.15	3.81	2.95	89.05
B	0.05	4.53	0.93	74.15
C	0.04	4.84	0.75	71.89
D	0.03	5.00	1.04	65.89

Table 4.2 Trend data from different hydrophilic polymers acting as solid contact ultrasonic couplant during unloading cycles.

4.2.9 Influence of Sample Compression

The purpose of testing the polymers with wet interfaces was to attempt to hold constant the area of contact between the polymer and the steel (the criterion which is believed to play the governing role in ultrasonic transfer between materials) while varying the pressure applied to the interface. Thus, no changes in signal amplitude and frequency were expected. However, both amplitude and frequency proved to still be influenced by pressure. Therefore, with the effect of coupling eliminated, this is suspected to be the result of physical changes occurring within the polymers while under compression. Figure 4.23 and Figure 4.24 show the amplitude and frequency data acquired with saturated interfaces where this effect can be seen readily.

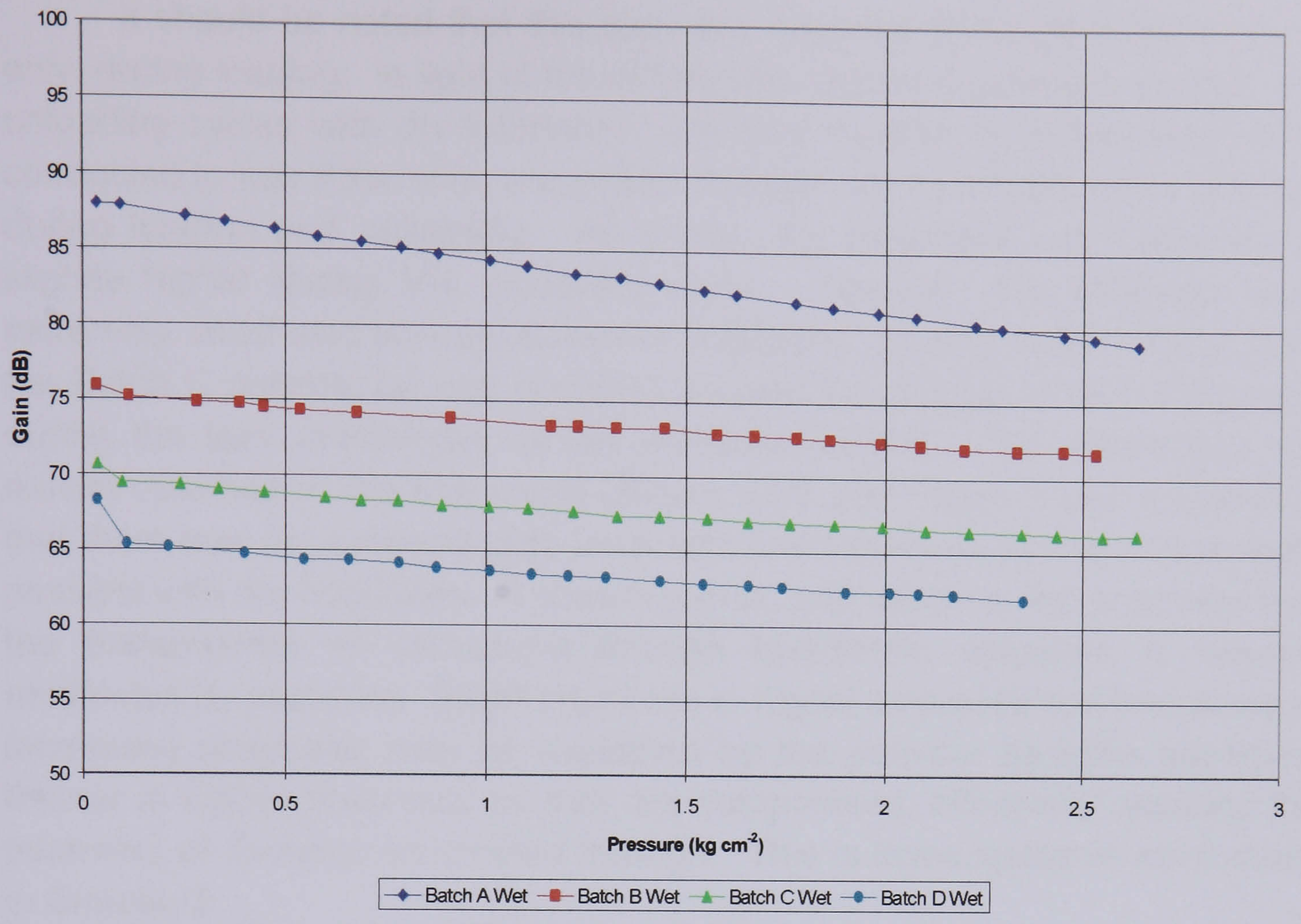

Figure 4.23 Amplitude data for different hydrophilic polymers during a loading cycle of a coupling efficiency evaluation programme. Data was acquired with saturated interfaces to emulate 100% coupling.

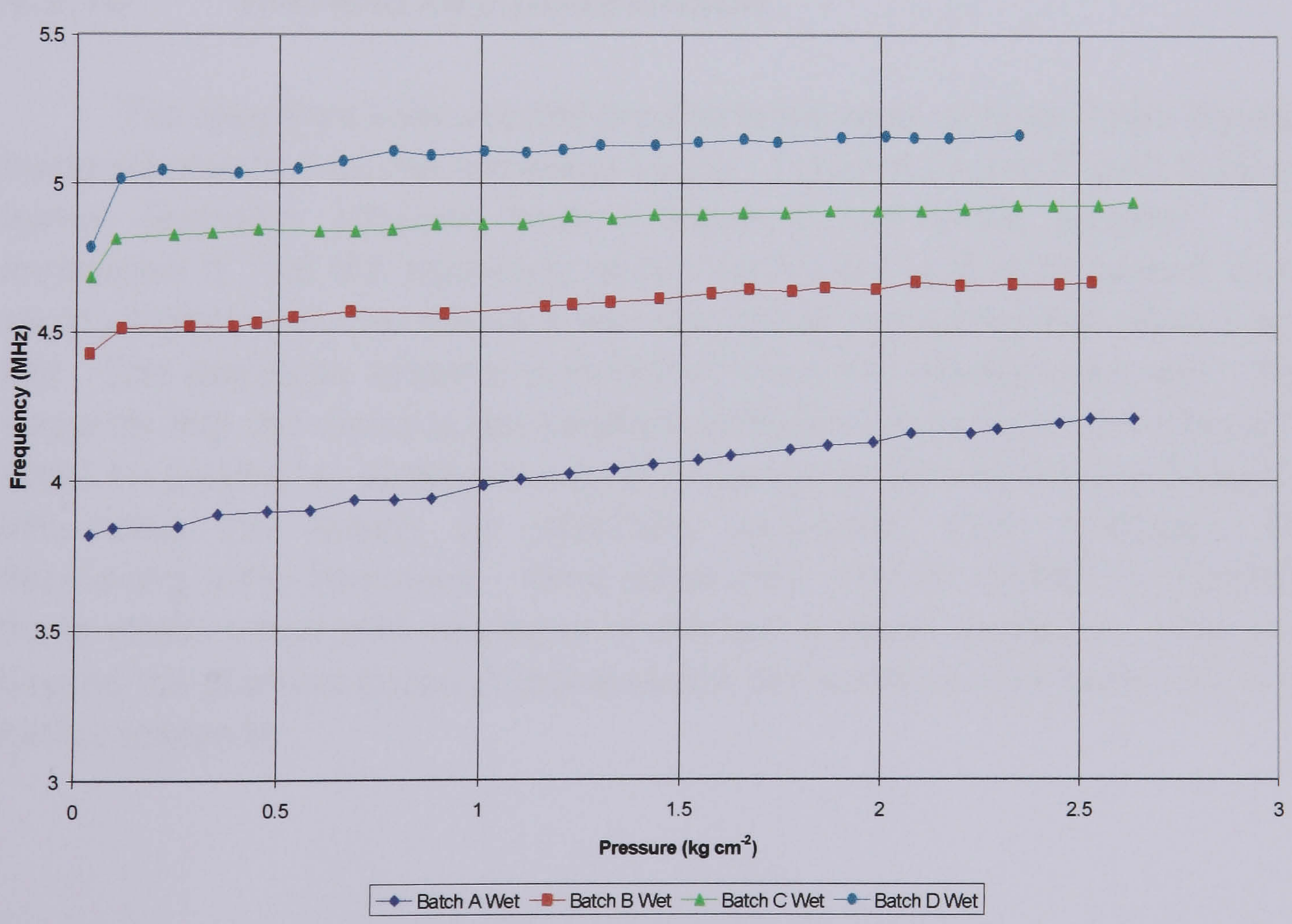

Figure 4.24 Frequency data for different hydrophilic polymers during a loading cycle of a coupling efficiency evaluation programme. Data was acquired with saturated interfaces to emulate 100% coupling.

It should be noted that this data was acquired from one round of tests only, during loading. In light of the differences observed between loading and unloading cycles with dry interfaces, a limited number of control tests were conducted to see if the echo properties, through wet interfaces, were different during loading and unloading. As a rule, the amplitude and frequency is slightly higher during the unloading cycle. However, the difference was extremely small and so was assumed negligible. During these control tests the Batch C polymer on one occasion showed no change at all in frequency during the test, irrespective of the pressure applied. This challenges the results obtained in the first round (Figure 4.23 and Figure 4.24), suggesting that there may be a repeatability issue with wet interfaces just as was thought possible with dry interfaces. It does however, add weight to the argument that the transmission of ultrasound through hydrophilic polymers is virtually unaffected by pressure. Slight increases in signal amplitude and frequency at increasing pressures may be explained by the polymer samples becoming thinner at higher pressures as they are compressed, effectively reducing the thickness of material transmitted through. This is investigated in more detail in Chapter 5.

4.2.10 Wet and Dry Comparison

The data from both wet and dry interfaces were compared (the dry data being represented by the unloading cycle). Figure 4.25 and Figure 4.26 are typical examples obtained from a Batch C hydrophilic polymer. The implication is that the frequency of the steel back wall echo tended to be slightly higher when the interface was dry (during unloading) than when it was wet. The amplitude however was higher when the interface was wet. This suggests that the water at the interface between the polymer and test piece might be playing an additional role to ensuring continuous surface contact – influencing the results by effectively increasing echo amplitude and decreasing echo frequency. More information may be gained by exploring these relationships with interfaces of different surface roughness. This runs beyond the practical scope of this research but would be a candidate topic for further research.

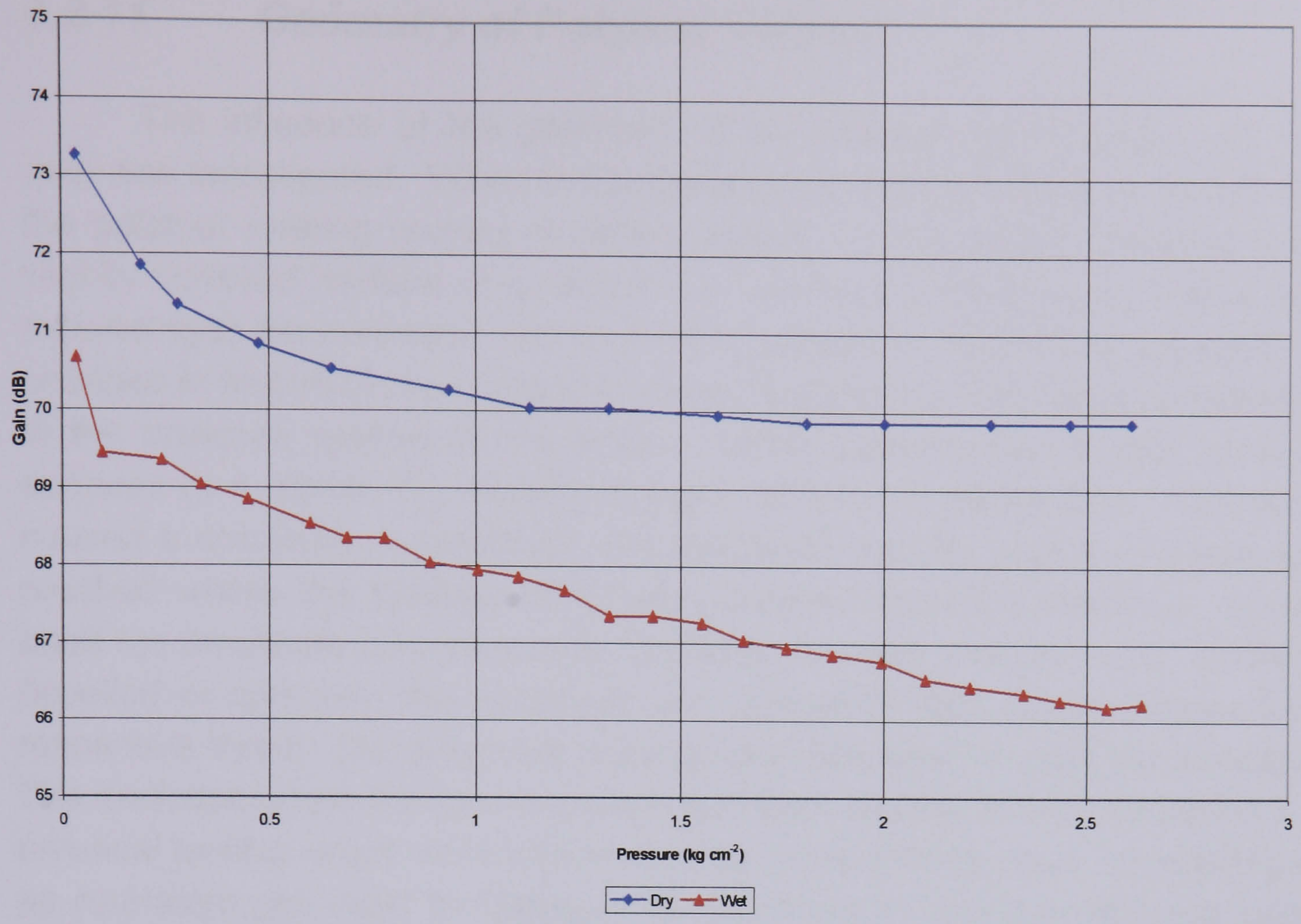

Figure 4.25 Amplitude of pulse echo signal through a Batch C hydrophilic polymer of different interface conditions.

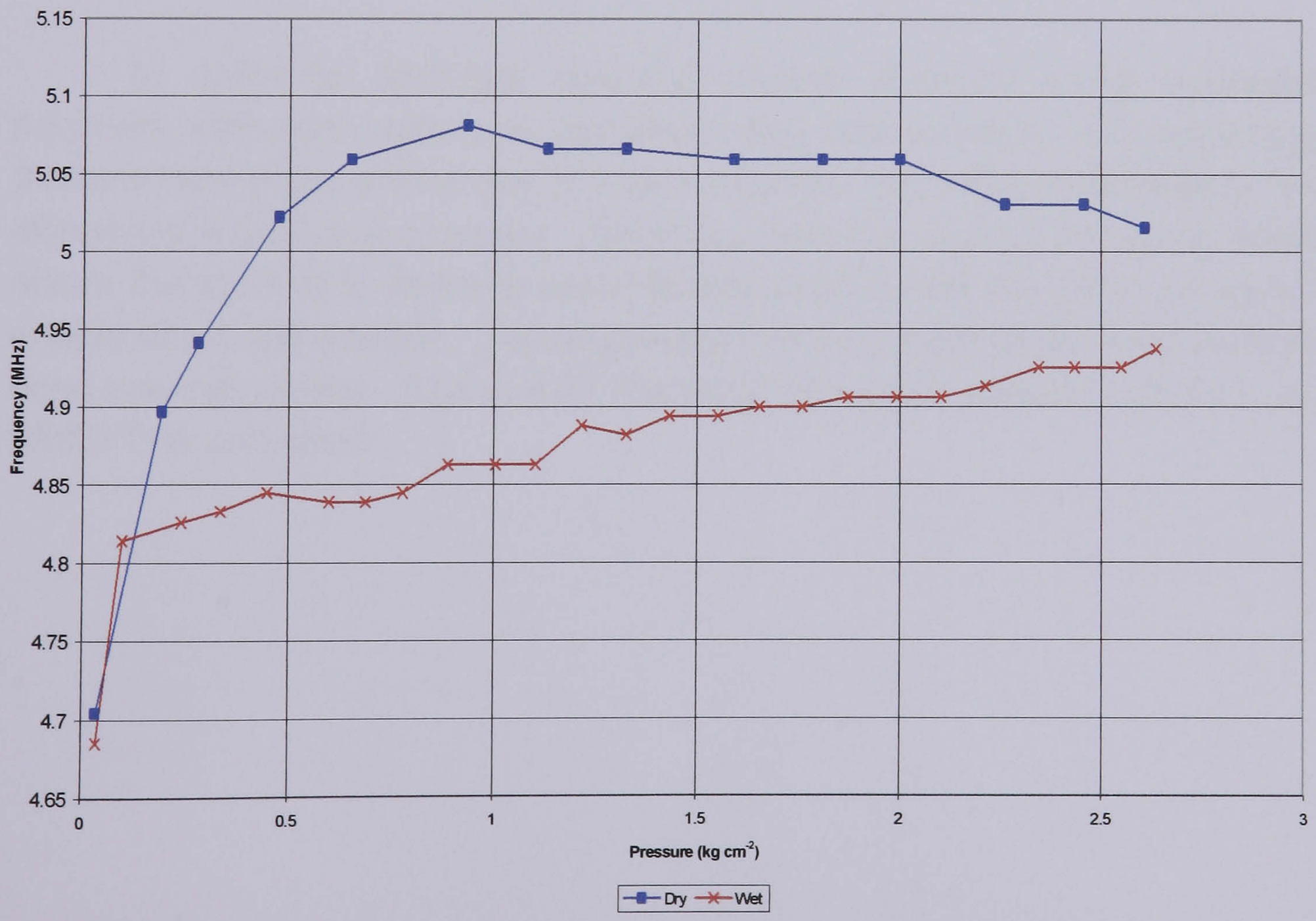

Figure 4.26 Frequency of pulse echo signal through a Batch C hydrophilic polymer of different interface conditions.

4.2.11 *Geometry of Polymer Surface*

The influence of the geometry of the polymer surface upon the test data was investigated. When the polymer is placed onto the steel, the area of the polymer making contact is clearly visible. Some of the samples had a slightly bevelled surface (e.g. Batch A) – making contact in the centre first, expanding to the perimeter with increasing pressure. With these samples, the changes in amplitude and frequency were predictable, both being proportional to the pressure applied to the probe. Other samples had slightly concave surfaces (e.g. Batch C), making contact around the edges first. This often caused a decrease in amplitude and frequency initially, until a pressure was reached where the majority of air was expelled from the interface. At this point the amplitude and frequency began to increase with pressure. Whether bevelled or concave, the amplitude and frequency data always followed the respective trend. (All polymers were ground flat when in their dry condition. The deviations from this geometry resulted from slightly uneven hydration.) In practical testing, slight variations in surface contact would have no real impact as operators are used to taking a few moments to achieve optimum signal when using conventional couplant.

4.2.12 *Comparison with Immersion Testing*

In order to compare coupling results obtained using hydrophilic polymers with pure water, an immersion test was required. By submerging the steel test piece and probe in a tank of water, the hydrophilic polymer was effectively substituted for water. Care was taken to position the probe directly above the steel at a distance equal to that used during the polymers tests to enable direct comparison. The amplitude and frequency of the steel back wall echo was calculated. Figure 4.27 illustrates the pulse shape (captured using WinDFD © software).

Figure 4.27 Steel back wall echo obtained from immersion test of steel component. 1 div. = 0.2μs.

The frequency of the pulse was 5.32MHz. The gain required to achieve full screen height (RF mode) was 59.85dB. This represents a signal greater in amplitude than the strongest signal obtained with any of the hydrophilic samples. This was expected, as the attenuation in the polymers is greater than in water. The Batch D sample gave the largest signal amplitude of all the hydrophilic polymer batches, being only 3.5dB lower in amplitude than the water couplant. It was not expected however that the signal frequency achieved via the water would be lower than that achieved by the Batch D polymer. The difference was 0.131MHz.

This proves that in absolute terms, the hydrophilic polymer is functioning at a very similar efficiency to pure water with regard to ultrasound transmission, giving further firm evidence that these materials are serious candidates for solid contact ultrasonic couplants, capable of offering results comparable to those achieved through immersion testing.

4.2.13 Summary

The evaluation programme involved using a range of hydrated hydrophilic polymers as solid couplant between a 5MHz probe and a smooth steel test piece. It was clear that the greater the equilibrium water content of the polymer, the greater the measured amplitude and frequency of the steel back wall echo at all pressures employed. Increases in pressure resulted in very small increases in signal frequency (Table 4.2), whereby the greatest change was demonstrated by the Batch A polymer. Increases in pressure resulted in significant increases in signal amplitude until a threshold was reached (Table 4.1). The application of additional pressure beyond this level did not generate a significant increase in measured signal amplitude. The pressure thresholds were approximately 0.5, 0.4 and 0.9kg cm^{-2} for the Batch

A, B and C polymers respectively. The Batch D polymer did not appear to display a pressure threshold, possibly due to its very flexible nature. During unloading, the signal amplitude was not affected when the pressure threshold was passed, continuing on a straight-line extrapolation. The Batch A polymer demonstrated the greatest change in signal amplitude with increasing pressure.

The evaluation programme included a comparison study between the coupling behaviour of hydrated hydrophilic polymers and a smooth steel test piece across two interface conditions; (i) completely devoid of free water – 'dry' and, (ii) saturated with free water – 'wet'. The purpose of the wet interface tests was to emulate perfect contact. Signal amplitude proved to be greatest across a wet interfaces whereas signal frequency was slightly higher across a dry interfaces. The signal amplitude data obtained across wet interfaces was for the main, well within the scatter data acquired from repeated tests across dry interfaces. The Batch C polymer showed the greatest discrepancy, the wet data generating a steel back wall echo amplitude 4dB greater than the nearest dry data point at its most extreme. This may have been due to the slightly larger diameter of this sample, effectively reducing the applied pressure. The signal frequency data obtained across the wet interfaces was always within the scatter data from the dry interface tests. Both the signal amplitude and frequency considerations indicate that the hydrophilic polymers are able to achieve near perfect contact with a smooth steel surface without the need for the application of free water.

The tests conducted with wet interfaces showed and unexpected increase in both signal amplitude and frequency with increasing pressure. The change was not significant, yet it suggested that the hydrophilic polymers themselves may undergo a slight modification of ultrasonic properties when under pressure. This effect is considered to be due to the 'squashing' of the polymer, effectively reducing the thickness of the sample. In this situation, there is less polymer for the ultrasound to pass through, therefore imparting less attenuation on the signal. This was confirmed by further experimentation reported in Chapter 5 where the reduction in sample thickness was compensated for and revealed no change in ultrasonic properties.

The Batch D polymer was unable to withstand the pressures placed upon it during the course of these tests. Cracks around the edges of the sample propagated towards the centre following the repeated application and removal of pressure.

The coupling performance of the hydrophilic polymers was compared to pure water by performing an immersion test with the same probe and test

piece. The measured signal frequency achieved from the immersion test was 5.32MHz requiring a gain of 59.85dB to reach full screen height (ultrasonic flaw detector in RF mode with the 5MHz narrowband enabled). This is the benchmark coupling performance and underlines the high coupling performance achieved by the hydrophilic polymers employed in these tests as they have generated signals of similar amplitude and frequency. Signal frequencies of over 5MHz were achieved from both Batch C and D hydrated hydrophilic polymers, with dry interfaces, under pressures of 0.5kg cm^{-2} (equivalent to a load of 1kg). In fact, frequencies slightly above those achieved via immersion testing have been accomplished with a Batch D polymer across a dry interface. The signal amplitude achieved via the immersion test was greater than that achieved by all of the hydrophilic polymers tested. The difference is however, only 4dB greater than the Batch D polymer with wet interfaces. Full screen height can be achieved from a dry contact Batch D polymer using a gain of approximately 65dB and below. Similarly, a gain of 70dB is required through a Batch C polymer coupling across a dry interface. This shows that hydrophilic polymers have a coupling performance (with smooth steel) comparable to pure water as used in immersion testing. This is a very positive outcome.

4.3 Life Testing

It is understood that hydrophilic polymers loose water through evaporation over time. What is not known is how quickly and by how much. In the light of previous results, it is anticipated that such a loss of water would have a detrimental effect on the ability of polymers to transmit ultrasound as it has been shown that ultrasonic transparency decreases with decreasing equilibrium water content. It is also reasonable to suggest that as a polymer dehydrates, it becomes stiffer and hence less able to conform to uneven surfaces which would be detrimental to acoustic coupling. At this stage in the research, the relationship between surface area to volume ratio and the rate of dehydration has not been investigated.

The target application for hydrophilic polymers is for use as part of a wheel probe where the polymer forms the tyre. It seems plausible that when operating in such a dynamic situation, the rate of dehydration of different hydrophilic polymers will be increased in comparison to that when the polymers are at rest. This would be very important when considering practical application of such a device as it would limit the length of time the probe would be capable of operating before the hydrophilic tyre became unsuitable for use.

In addition to the ultrasonic implications, there is also the issue of longevity. It is important to assess how the hydrophilic polymers will degrade with use. Indeed, a method was established to monitor the dehydration rates of different hydrophilic polymers while in rolling contact with a test surface. It also proved to be an effective, non-subjective method of assessing candidate hydrophilic polymers for suitability to the roller application.

4.3.1 Experimental Procedure

With the expansion ratios of the hydrophilic polymers from dry to hydrated known, small tyres were machined which would hydrate to the size of the rubber tyres employed on one currently used wheel probe (schematic in Figure 3.5). This allowed hydrophilic polymers to be used in the place of the conventional rubber. Note that the conventional wheel probe was not being used to evaluate the change in ultrasonic performance as the hydrophilic tyres dehydrated, it was simply a method for subjecting them to conditions similar to those which it is envisaged they would experience in practice.

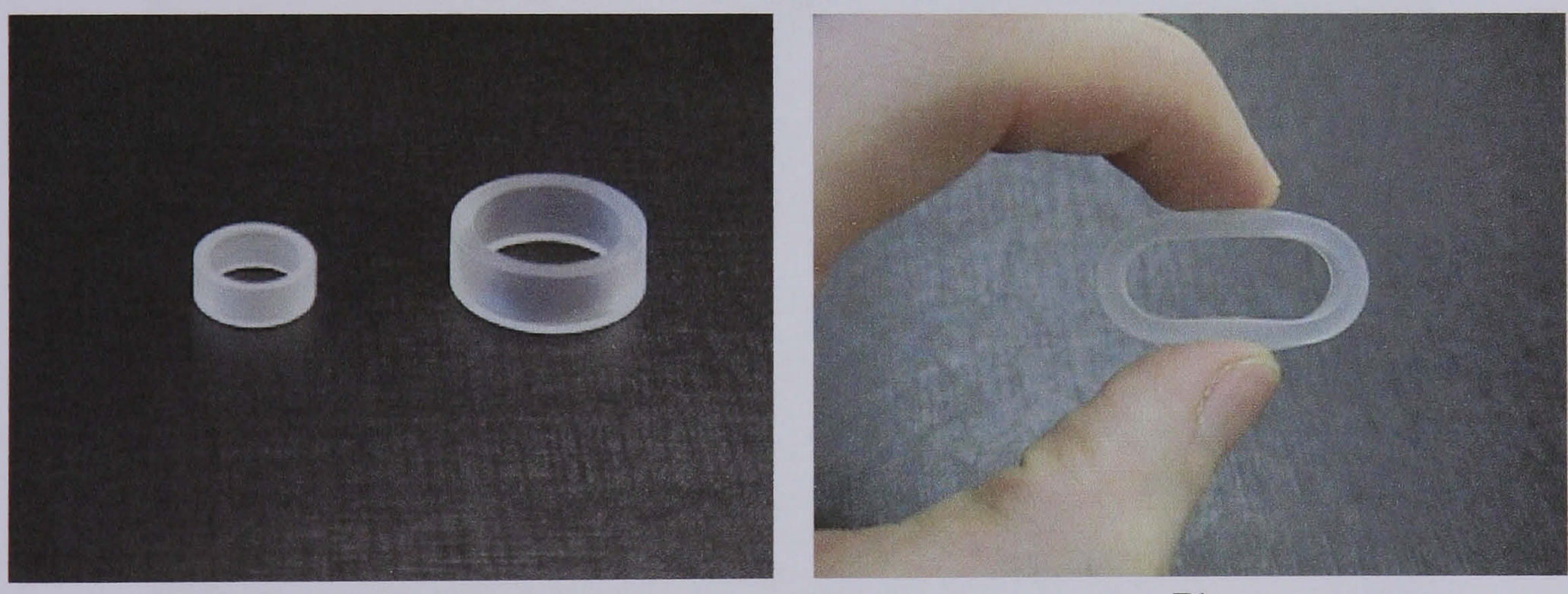

A) B)

Figure 4.28 A) Wheel probe tyres in both dry and hydrated states. B) Once hydrated, the tyre becomes very flexible.

The experiments were based on a test rig providing a continuously moving surface. A smooth Perspex rod of 32.9mm diameter was clamped in the chuck of a lathe as shown in Figure 4.29. The wheel probe with hydrophilic tyre was held in the tool turret and pressed against the rod as it rotated. The handle of the wheel probe was spring loaded. During the tests, the spring was compressed about 50% imparting a load of approximately 1.5kg. This represented a pressure on the footprint in excess of the pressure threshold observed of the polymers explored earlier which was generated by a 2kg load over a larger contact area. The Perspex rod was rotated at 260rpm, generating a surface speed of approximately 1mph.

The tyres were blotted dry before being fitted to the wheel probe. At set time intervals, the wheel probe was removed from the rig and weighed. The change in weight reflects the weight of water lost through evaporation during the trial. Photographs were also taken to document the mechanical degradation of the tyres. Each polymer was tested three times to validate the reproducibility of the procedure. Note that there was no free water involved in these tests at all, i.e. the tests were performed using hydrated polymers with a completely dry interface with the rod.

As the test piece used here is curved (Perspex rod), the nature of the contact with the tyre is different than it would be against a flat test piece. This has the effect of increasing the stresses in the tyre. This represents a safety factor.

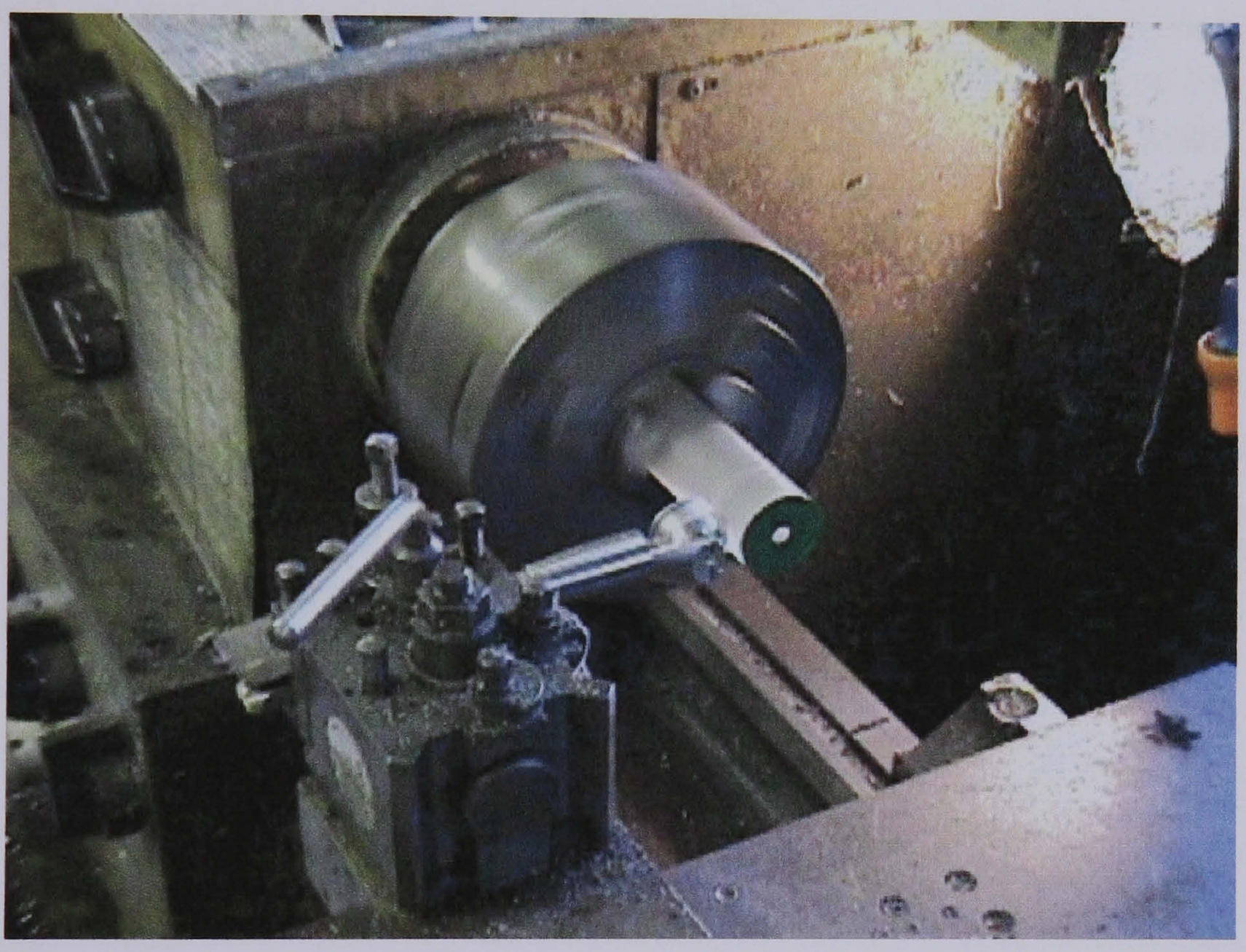

Figure 4.29 Life test in progress. Test rig was based around a lathe, providing a continuous rolling contact.

4.3.2 Hydrophilic Polymer Selection

As a result of receiving numerous research samples from the supplier, eight different hydrophilic polymer samples were believed to be at our disposal. They included:

1. 85% water by weight PMMA-VP
2. 75% water by weight PMMA-VP
3. 65% water by weight PMMA-VP
4. 60% water by weight PMMA-VP
5. 50% water by weight PMMA-VP

6. 38% water by weight HEMA
7. 40% water by weight High Strength Acrylonitrile-VP
8. 35% water by weight High Strength Acrylonitrile-VP

The percentages given are the anticipated water uptake of the polymers after reaching hydraulic equilibrium in water. It equates to the weight percent of the hydrated polymer that is accounted for by water. Polymers 1, 3, 7 & 8 had not been evaluated previously and are therefore outside the initial batch of four polymers described thus far.

4.3.3 Hydration

Before the tests could begin, the tyres required hydration. This was achieved by submerging them in water and allowing sufficient time to reach equilibrium. At regular time intervals, the tyres were removed from the water, blotted dry and weighed before being dropped back into the water. This allowed the rate of hydration to be monitored. In line with previous tests, the polymers capable of absorbing relatively higher quantities of water tended to have the greatest rate of hydration.

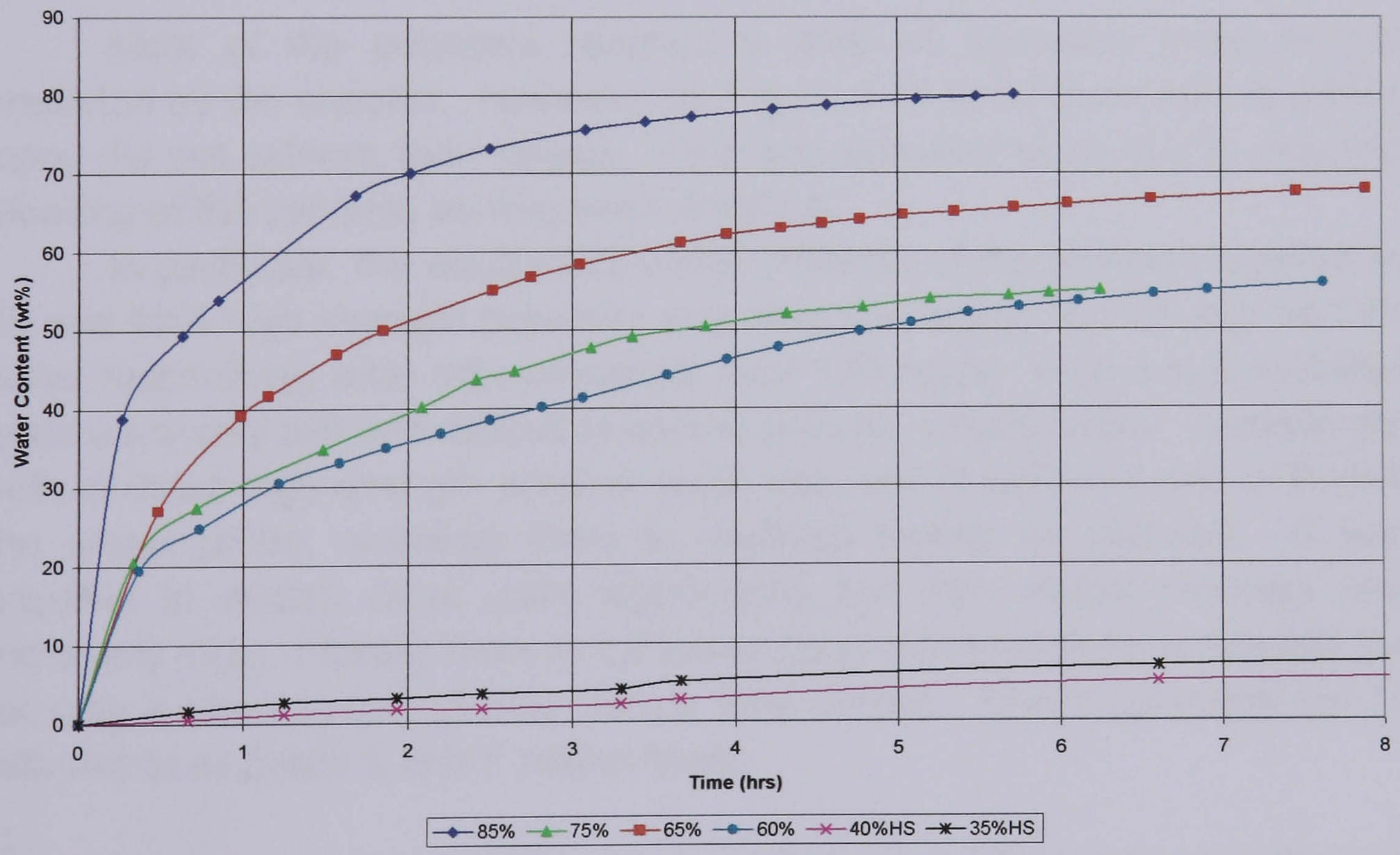

Figure 4.30 Hydration of different hydrophilic polymer tyres in water at room temperature. Legend indicates anticipated equilibrium water content.

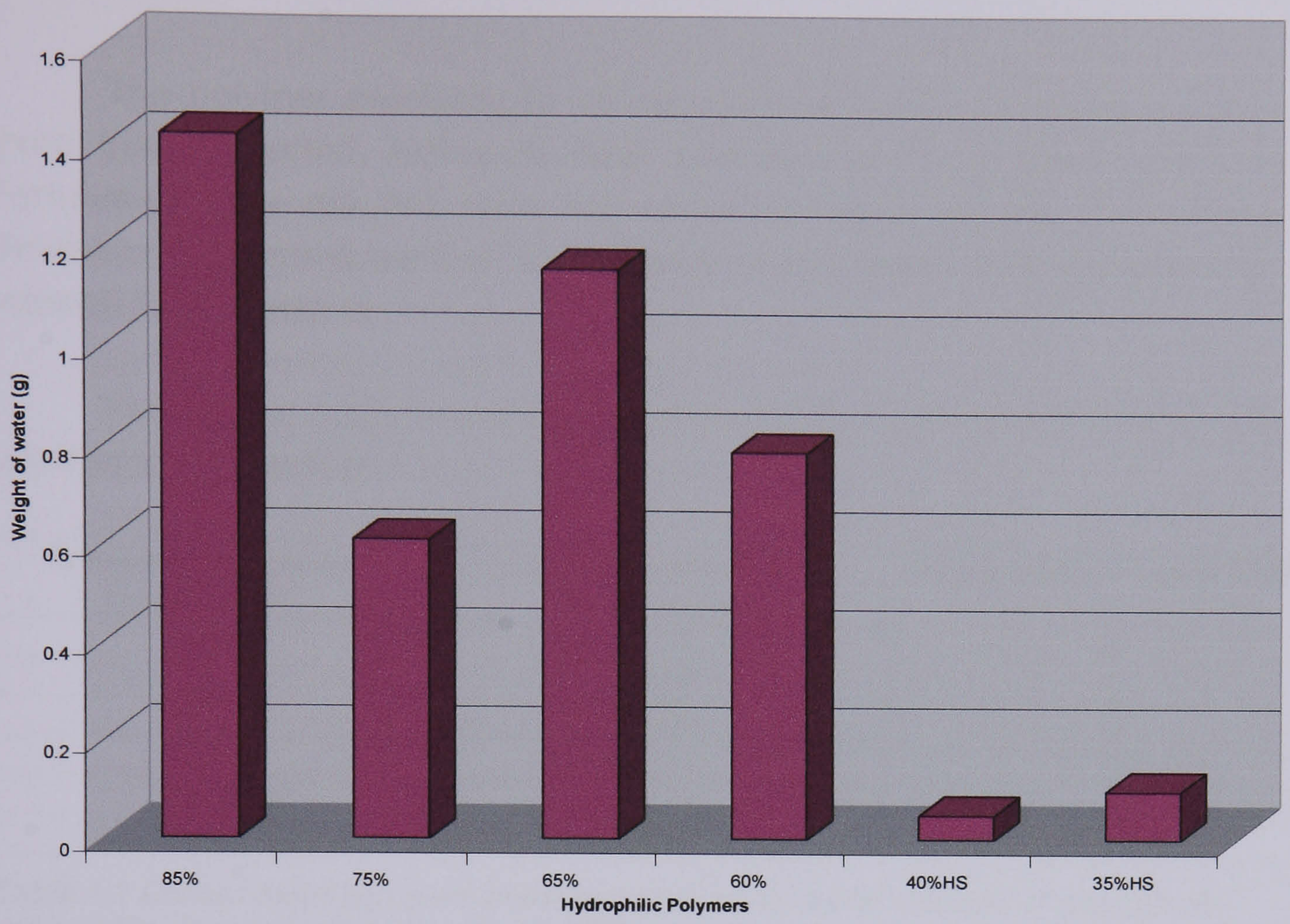

Figure 4.31 Weight of water absorbed by different hydrophilic polymers after submersion for 4 hours. Anticipated equilibrium water contents are shown.

Most of the polymers reached a level of hydration close to that predicted by the supplier. However, as Figure 4.30 and Figure 4.31 illustrate, many did not achieve their targets. This was assumed to be due to incorrect labelling of the samples as they were supplied.

In particular, the equilibrium water contents of the samples labelled as 35 and 40% high strength polymers was very low, being 18.14% and 14.14% water respectively after submersion for over 100 hours. As a result, hydrated tyres were very stiff and difficult to secure onto the wheel probe. Interestingly, both of these high strength polymer tyres were still of sufficient size to fit onto the wheel probe, enabling them to undergo testing as planned. It was possible to stretch them quite significantly but their elastic recovery was extremely slow. Placing them in hot water made them much more flexible, but for only a short period of time before they cooled. These polymers will be referred to as Batch E and F respectively.

It was suspected that the polymer labelled as 75% by the supplier was actually 60% polymer (Batch C) in light of its hydration characteristics. This resulted in a batch of six polymer tyres being machined that after hydration were too small for substitution onto the current wheel probe for testing. This meant that no Batch D (75%) polymers could be evaluated in these tests. Although inconvenient, this did not pose much threat to this testing programme, as the Batch D polymer (being one of the weakest) was not expected to withstand use on a wheel probe for any length of time.

The polymer predicted to absorb 65% water on equilibrium absorbed more than expected, taking its final hydrated wt % of water up to 70%. Fortunately, this did not have too great an effect on the final hydrated dimensions, enabling tests of this polymer to go ahead. This polymer shall be referred to as Batch G.

Finally, the polymer consisting of over 80% water at equilibrium will be referred to as Batch H

Predicted Hydration (wt.% water)	Actual Hydration (wt.% water)	Hydrophilic Polymer Batch
85	81.19	H
75	57.97	C
65	70.09	G
60	59.07	C
40HS	14.14	F
35HS	18.14	E

Table 4.3 Comparison between predicted and actual water content of a range of hydrophilic polymers at hydraulic stability.

4.3.4 Life Tests - Dehydration

The Batch H polymer proved too weak to test properly as many tyres were split completely trying to fit them onto the wheel probe. Due to the incorrect labelling of the research samples shipped by the supplier, no trials of the Batch D polymer could be conducted during this phase of testing. However, one test was conducted previously with such a polymer as part of the test validation procedure. In this case the effective surface speed was equal to 0.154mph and even then the tyre split after only 15 minutes.

The remainder of the polymers were life tested for 4 hours. Three tyres from each batch were evaluated to allow experimental reproducibility to be monitored. Figure 4.32 and Figure 4.33 illustrate the dehydration characteristics of the Batch G hydrophilic polymer tyres.

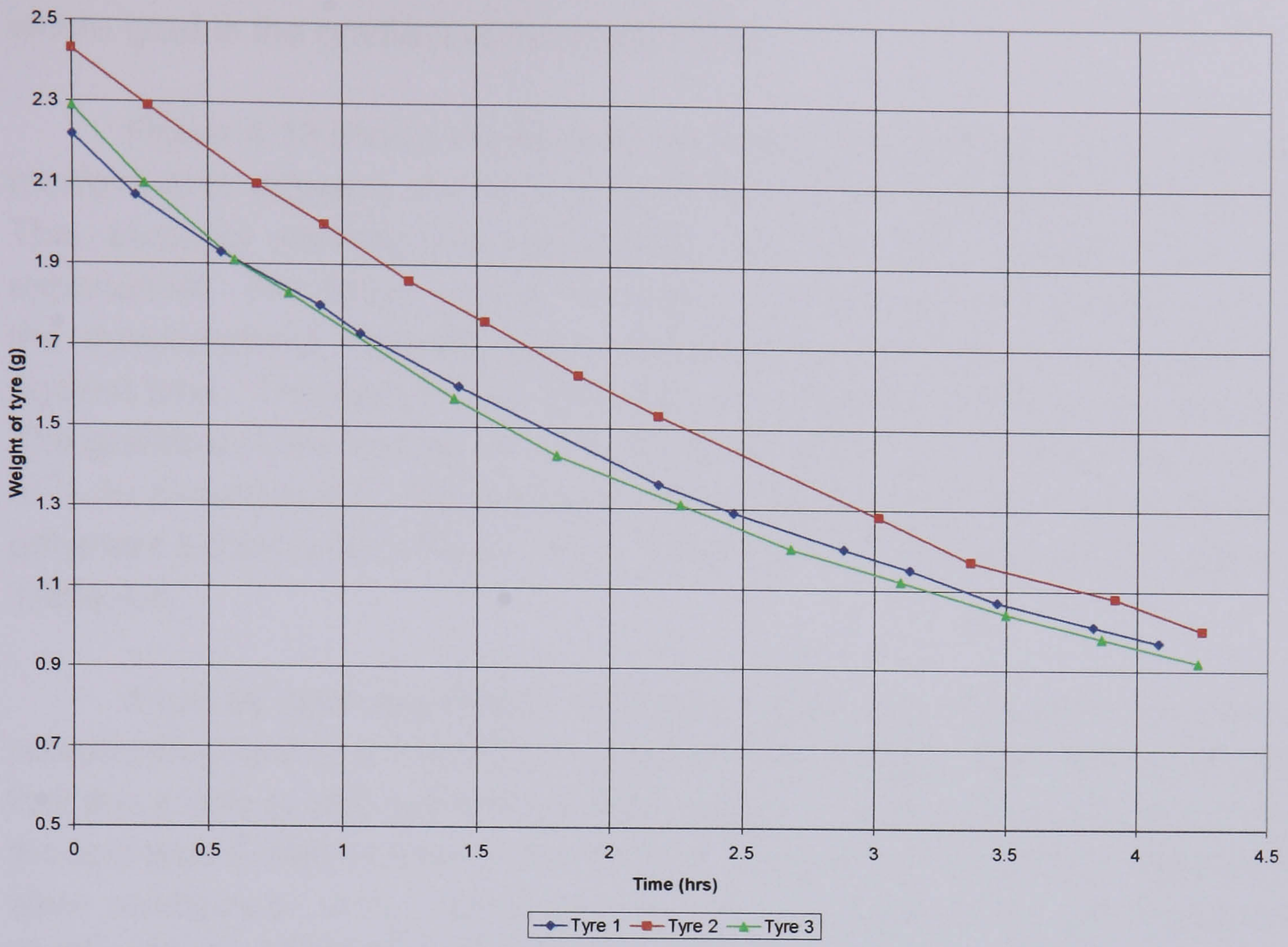

Figure 4.32 Dehydration data of three Batch G hydrophilic polymer tyres during 4-hour life tests.

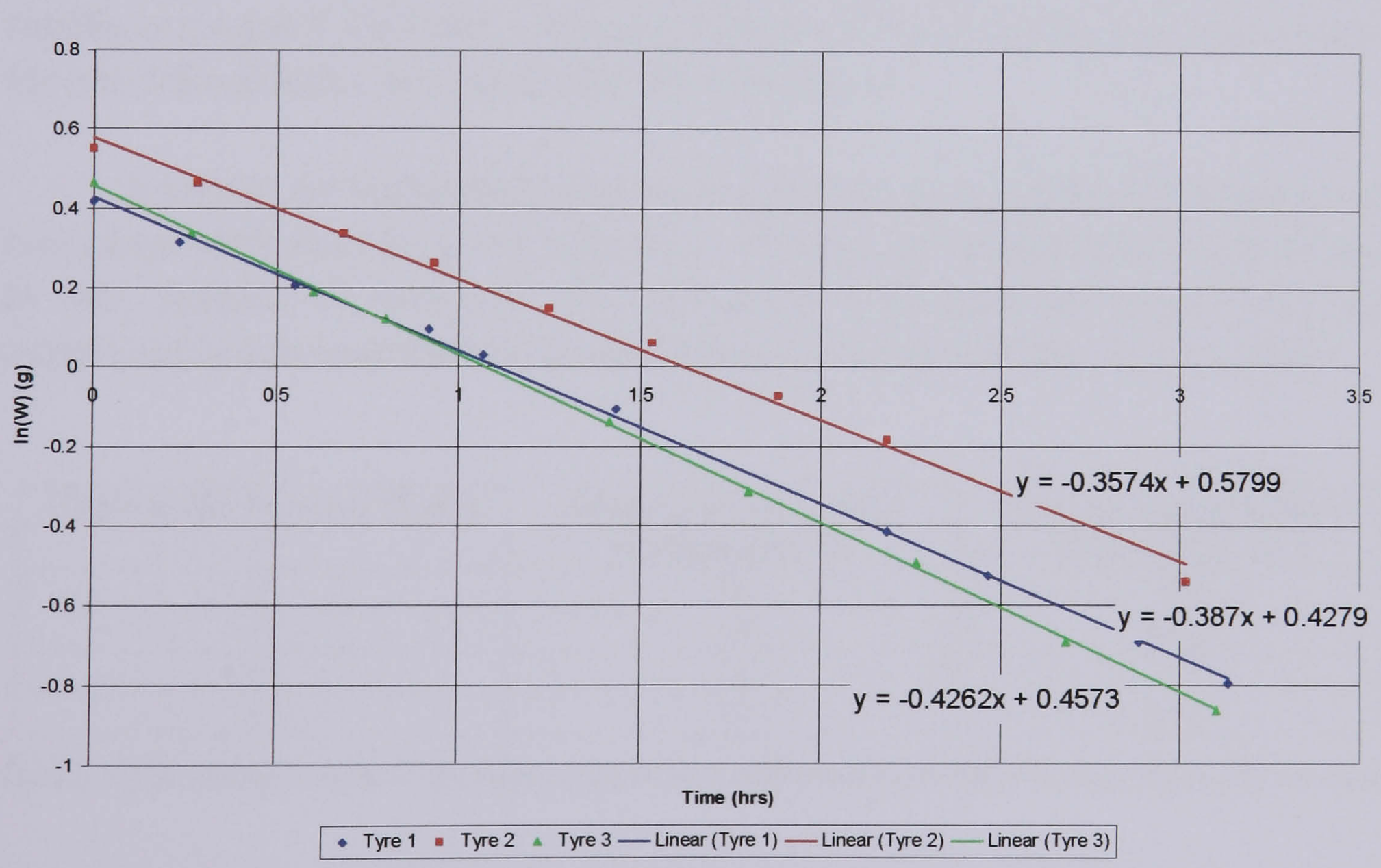

Figure 4.33 Dehydration of the same three Batch G hydrophilic tyres. ln(W) Vs time, where W equals the weight of water in the tyre. The gradient of the line of best fit for each set of data provides the rate of dehydration for each tyre (see Equation 4.1).

$$\text{Water loss per hour}\,(\text{wt}\%) = \left(1 - e^{(grad)}\right) \times 100 \qquad \textbf{Equation 4.1}$$

where grad is the gradient of the straight line.

Figure 4.33 shows the same dehydration data as Figure 4.3.2 only after manipulation, allowing the rate of water loss to be determined more easily. This involved making the assumption that the rate of water loss was exponential. The natural log of the weight of water in each tyre was taken at the measurement intervals during the test and plotting as a straight line against time. The data fit was good indicating that the assumption was valid. The gradient of the line can be used to calculate the rate of dehydration (wt.% hr^{-1}) via Equation 4.1. The average rate of water loss from the three Batch G polymers tested is 32.28% per hour. Data from the other polymers is listed in Table 4.4.

It can be seen from Figure 4.32 and Figure 4.33, that one of the traces, representing tyre 2, is translated upwards from the other two. It is most likely that this is due to that tyre being a little heavier. The rate of weight loss during the test was similar to that of the other two suggesting that the measurements were unaffected. It is notable that the reproducibility of the procedure was good, with results from similar tyres being very similar to each other.

Somewhat predictably, the higher water content tyres dehydrated more rapidly during the life tests. All tyres remained intact during the tests except for one from Batch C that split after 73 minutes.

It should be highlighted that the measured dehydration of the tyres may have been influenced by the high level of mechanical degradation observed. In one attempt to minimise this, dehydration calculations were based on weight reduction over the test period where minimal damage was recorded.

Hydrophilic Polymer Batch	Actual polymer water content (wt.%)	Average Dehydration Rate (wt.% hr^{-1})
G	70	32.3
C	59	30.5
F	14	7.2
E	18	7.3

Table 4.4 Average rates of dehydration of the different hydrophilic polymers life tested.

4.3.5 Life Tests – Mechanical Degradation

Photographs were taken of the tyres after being subjected to the same life test conditions for a similar length of time. It was hoped that these might be compared to give a basic contrast between the ware properties of each hydrophilic polymer tested.

4.3.5.1 Batch G, PMMA-VP

Figure 4.34 The three Batch G hydrophilic polymers life tested for 4 hours each. Clockwise from top: tyre 1, tyre 2 and tyre 3.

The Batch G tyres all developed many small splits around the edges as the tests progressed. Tyres 2 and 3 both worked their way onto the lip of the probe and so suffered significant damage. In hindsight, this may have caused a small amount of material loss. This in turn may have influenced the measured dehydration rates discussed in section 4.5.4. In this sense, the results in Table 4.4 can be assumed to be pessimistic.

It was noticed that the surface of the tyres became stiffer with time indicating that the surface of the tyre had a lower water content compared to the inner surface, which appeared to maintain its flexibility. This suggests that water is lost from the surface at a faster rate than it is diffused from high to low water concentrations. This has repercussions that impact upon the design of the final device developed as part of this work, described in Chapter 7.

None of the Batch G tyres split during these tests. The tyres required rehydrating in order to make them flexible enough to remove from the wheel probe and even this did not cause them to split.

4.3.5.2 Batch C, PMMA-VP

Figure 4.35 Three Batch C hydrophilic tyres after 4 hours life testing. Clockwise from top: tyre1, tyre2 and tyre3.

The Batch C polymer tyres did not develop as many splits as the Batch G tyres. However, the splits that did occur tended to be much larger, propagating over half way across the tyre. Tyre 1 failed after 73 minutes from one such split. It can be seen that these tyres did not work their way over the lip of the wheel probe, resulting in less overall damage. The same stiffening of the surface layer was observed as with the Batch G polymer already discussed.

It seems plausable that the process of tyre dehydration and resultant stiffening acts to retard split propagation. Thus, if the split achieves a critical length in a critical period of time (i.e. before dehydration has a dominant influence on split propagation) then catastrophic failure will occur.

4.3.5.3 Batch F, High Strength AN-VP

Figure 4.36 Tyre 3 – Batch F high strength polymer after 4.4 hours of life testing.

None of the Batch F tyres changed significantly in appearance during the tests. There were no signs of cracking or wear of any kind. The polymers felt very hard and inflexible, not at all suitable for conforming to surface undulations as would be require in practical application.

4.3.5.4 Batch E High Strength AN-VP

Figure 4.37 Tyre 1 – Batch E high strength polymer after 6 hours life testing.

Figure 4.37 illustrates the Batch E tyre after six hours of life testing. There were no signs of crack propagation or any mechanical wear. Soon after the test had begun, the tyre felt hard like Perspex. The Batch E tyre, like those from Batch F, felt too rigid for practical application as a solid couplant being unable to make good contact with the test piece.

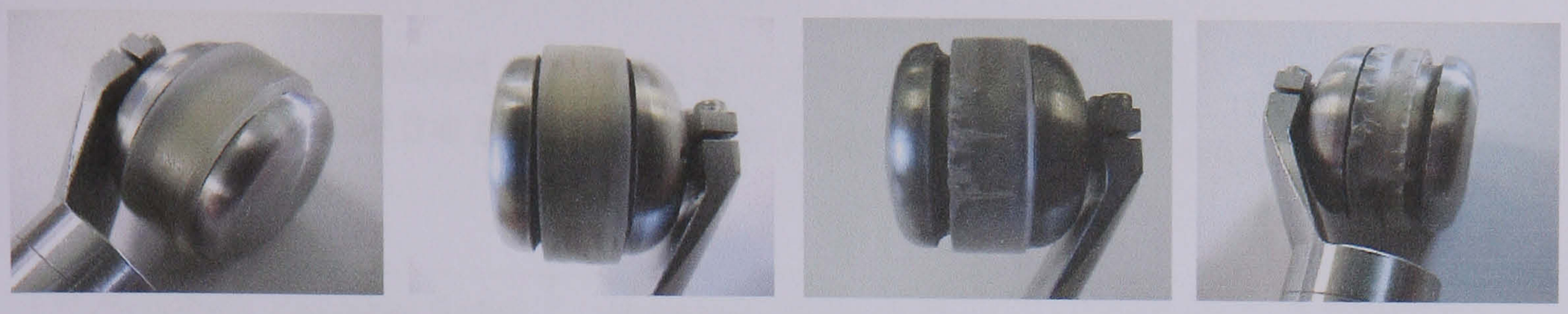

Figure 4.38 From left to right: Batch E, F, C and G hydrophilic tyres after life testing.

4.3.6 Standing Dehydration

As a control datum, one tyre from each batch was allowed to dehydrate on the wheel probe at room temperature while not being subjected to life testing. At set time intervals, the tyres were weighed enabling the dehydration rate to be monitored. During this process, all the tyres (except the Batch E and F) were fitted onto the wheel probe to mimic the same conditions as the life test. The Batch E and F tyres were not on the wheel probe because (i) it was feared that the compressive forced generated as they dehydrated and contracted would be sufficient to damage the wheel probe, and (ii) it increased the number of tests that could be conducted simultaneously.

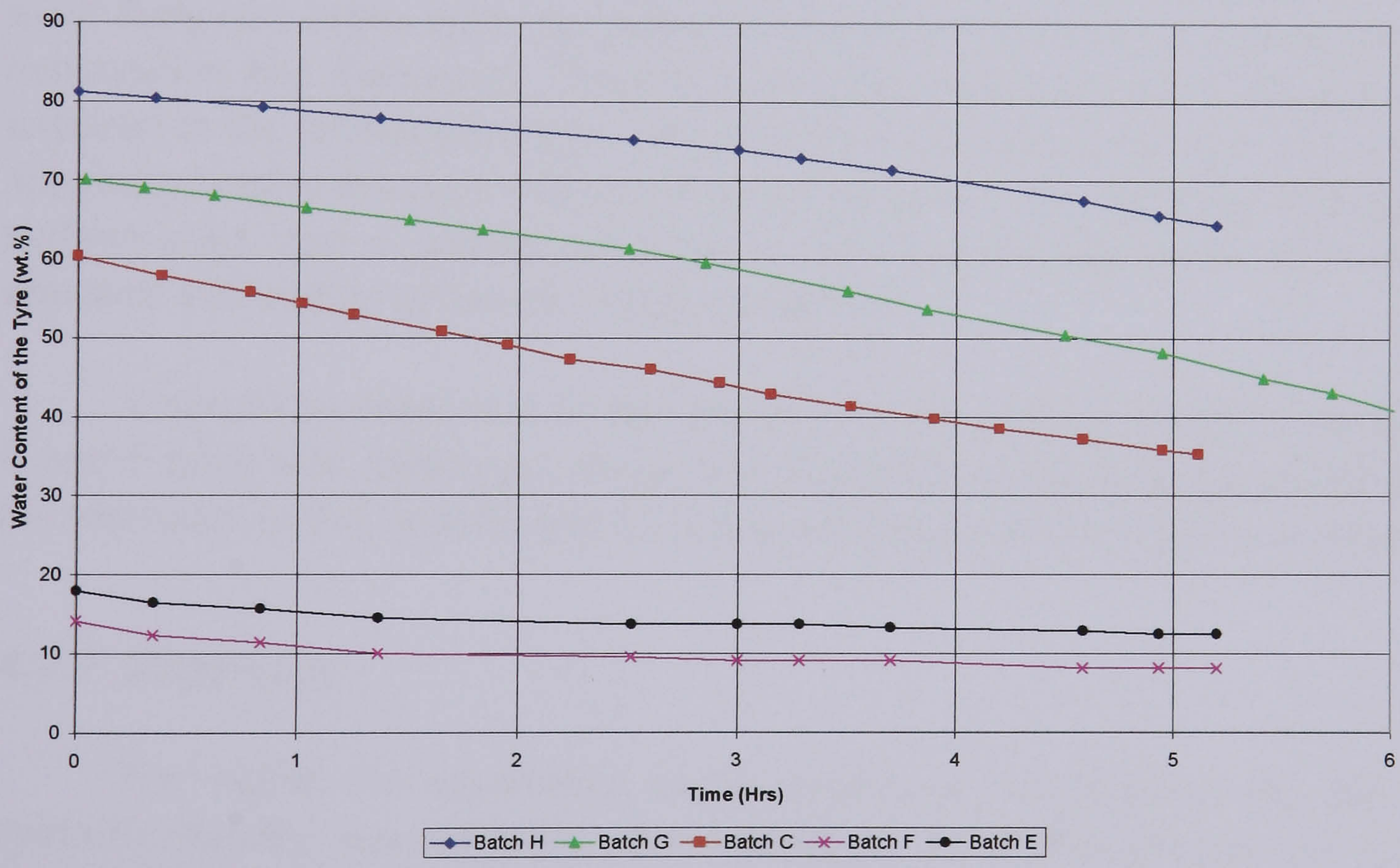

Figure 4.39 Chart displaying the dehydration characteristics of five different hydrophilic tyres. This data was achieved by letting the tyres dehydrate on a stationary wheel probe at room temperature, not by life testing.

The rate of dehydration that occurred during life testing was obviously different to that which occurred when the wheel was at rest (i.e. standing dehydration). To enable direct comparison between these rates, the percentage of water lost over a four hour period was calculated. The results

for all the tyres tested are listed in Table 4.5. Note that the life testing data is an average of all the tyres tested for a specific polymer batch.

Hydrophilic Polymer Batch	Standing Dehydration (wt.% lost over 4 hours)	Life Testing Dehydration (wt.% lost over 4 hours)
H	11.19	------
G	16.59	40.95
C	21.36	30.36
F	5.39	4.67
E	4.94	4.21

Table 4.5 Comparison between the percentage water lost from hydrophilic polymers left standing and under life test conditions over a 4 hour period.

It would be expected that the tyres dehydrate more rapidly when under life testing conditions, and this is observed for the Batch C and G polymers. However, the results also show that the Batch E and F polymers dehydrated more slowly when subjected to life testing than when standing still. This is most likely due to the tyres not being on the wheel probe when the standing dehydration was measured. Therefore, the tyres had additional surface area exposed to the environment from which water could evaporate. It is therefore suggested that in the case of Batch E and F polymers, the additional exposed surface area, had a greater influence on the rate of dehydration than the pressure and motion of the life testing conditions.

It should be noted that as the amounts of water evaporating from Batch E and F tyres was particularly small, the resolution of the data depended on the resolution of the balance and so is less accurate and more prone to error.

4.3.7 Summary

The higher the equilibrium water content of the polymer, the faster hydraulic stability was achieved upon hydration. All PMMA-VP tyres of size suitable for substitution onto the current wheel probe used in these tests, hydrated in less than one day (regardless of final water content). The higher water content tyres (e.g. Batch H) only required submersion in water for approximately five hours at room temperature to reach full hydration. The Batch E and F high strength tyres (AN-VP) only reached hydraulic stability after 100 hours submersion in water.

Generally, the higher the water content of the polymers tested the greater the rate of dehydration observed. This held true whether the tyres

were subjected to life testing or just left stationary. Dehydration rates for all PMMA-VP polymers were greater when subjected to life testing than when stationary. The greatest rate of dehydration measured from this programme was that of the Batch G polymer, being 32.28 wt % per hour when subjected to life testing. Even at this rate, the actual amount of water lost over three hours was less than 1g. This implies that only small quantities of 'make up' water would be required to maintain hydration during operation.

The Batch E and F high strength polymer tyres (18 and 14% water respectively) withstood life testing, showing no signs of wear. However, they were too stiff to conform to the surface of the test piece properly, which in practice would seriously impair ultrasonic transfer. The level of stiffness was so great that it would not require separate coupling efficiency tests to validate. Therefore, at this level of hydration the AN-VP polymers are unsuitable for practical use a solid ultrasonic couplant. However, AN-VP polymers of higher water content (presumably having increased flexibility) could have great potential for compatibility with a wheel probe type application, possibly offering higher wear resistance with acceptable ultrasonic properties.

The Batch C and G polymer tyres (59 and 70% water respectively) behaved quite differently. The tyres made from Batch C polymer developed fewer splits during life testing than those made from Batch G polymer. However, the splits in the Batch C polymer tyres were much longer, usually stretching over half of the width of the tyre. The Batch G polymer tyres were more likely to develop many small splits. From the different hydrophilic polymers evaluated thus far in the research, Batch C and G were emerging as the most suitable for a wheel probe type application as they demonstrated a good balance between reasonable resistance to degradation, while having good ultrasonic properties and the ability to conform to a test piece surface.

The Batch D and H polymers may be eliminated from future trials, as they appear too weak to be useful with a wheel probe type application. They may however, be suitable contenders for other, less physically demanding applications within ultrasonic NDT such as alternatives to the soft tips of manual (static) and spot weld probes.

4.4 Conclusions

Tests have been conducted into the ability of a range of hydrophilic polymers to transmit ultrasound into a smooth steel test piece under varying levels of applied pressure. Performance was assessed by measuring the amplitude and frequency of the steel back wall echo. It was found that:

- The higher the water content, the greater the signal amplitude and frequency over all pressures (0 to 2.5kg cm^{-2}).

- Both signal amplitude and frequency increased with increasing pressure.

- Samples of Batch A, B and C polymers, displayed evidence of a pressure threshold, beyond which the application of additional pressure had a reduced influence on signal amplitude.

- Signal amplitude remained high after the reduction of applied pressure below the threshold.

- Signal amplitude and frequency achieved from coupling via hydrophilic polymer samples compared well with that achieved from immersion testing, being very similar in frequency, and only 4dB lower in amplitude at best.

- The presence of free water at the interface between hydrophilic polymer and the test piece had negligible effects on the signal.

A study into how different hydrophilic polymer samples withstand application in a harsh rolling contact application has been conducted. Hydrophilic polymers were machined and hydrated to enable fixture to an existing wheel probe with which the testing was conducted. The rate of dehydration was determined by measuring the weight loss of the tyre at set time intervals. Mechanical degradation was graded by physical appearance. From this study it was found that:

- The higher the water content of the polymer, the greater its rate of dehydration.

- Small quantities of water (<1g) were lost during three to four hour testing periods.

- The higher the water content of the polymer, the greater the extent of degradation over the same testing period.

- Polymers of very low water content, although mechanically resilient, were unable to make good contact with the surface of the test piece.

- Polymers of over 70% water, can be excluded from the wheel probe application on grounds of being mechanically too weak.

At this juncture in the research, there is nothing to suggest that hydrophilic polymers cannot meet the objectives of the project.

Chapter 5: Investigation of Material Parameters Relevant to Ultrasound Transmission

5.1 Primary Material Properties Relevant to Ultrasonic NDT

Hydrophilic polymers have been shown through a series of practical experimentation to demonstrate both ultrasonic and mechanical properties suitable for their implementation in ultrasonic NDT. However, consideration of the practical environment in which they might be used suggests performance criteria that need to be considered specifically. It is necessary to establish the modification of ultrasonic properties with respect to changes in environmental temperature and variation in applied coupling pressure. Similarly, there will be a need for a means of establishing the frequency downshift in inspection frequency when using different hydrophilic polymers as couplant. Determination of such parameters will help define the practical limitations of hydrophilic polymer application in the field of ultrasonic NDT.

5.2 Influence of Temperature

All preceding experimentation has been performed at room temperature at approximately 25°C. The ability of hydrophilic polymers to function effectively as couplant at temperatures below room temperature would be a considerable advantage. Indeed any deterioration with respect to temperature reduction must be quantified.

5.2.1 Establishing a Testing Programme

A testing programme was designed to enable ultrasonic properties to be explored over the temperature range –20 to 25°C. It aimed to cool a hydrated sample to –20°C in a chiller and then measure its ultrasonic properties as a function of time as it warmed up. So that measurements could be achieved at known temperatures, the warming profile of the sample was determined. It was appreciated that the surface of the sample would most likely warm faster than the core. Therefore, it was necessary to establish the temperature at both regions to determine the extent of the thermal gradient. This was achieved by attaching two thermocouples, one embedded in the centre of the sample and the other fixed to the surface. The former was glued

into a 1mm diameter hole drilled halfway into the sample when in its dry condition. The second was attached to the surface with glue.

The sample was then wrapped in cling film for two purposes. Firstly, the cling film would eliminate dehydration of the sample during extended thermal testing. Should this have happened during the experiment, any change in ultrasonic properties measured may have been due to changes in temperature or changes in water content. Fixing one of these constant, permits the other to be investigated with increased confidence. Secondly, the cling film prevented frost forming on the sample surface. Frost would make the surface of the sample uneven and could have modified the coupling efficiency between the probe and sample. Therefore, certainty that any apparent change in ultrasonic properties was due to temperature rather than coupling efficiency caused by frost could not have been achieved.

The temperatures experienced by the thermocouples were displayed on a Newport digital thermometer, accurate to 0.1°C. With the sample cooled to -20°C, it was removed from the chiller and placed in air. Its warming profile was measured and plotted in Figure 5.1, showing core, surface and average temperatures.

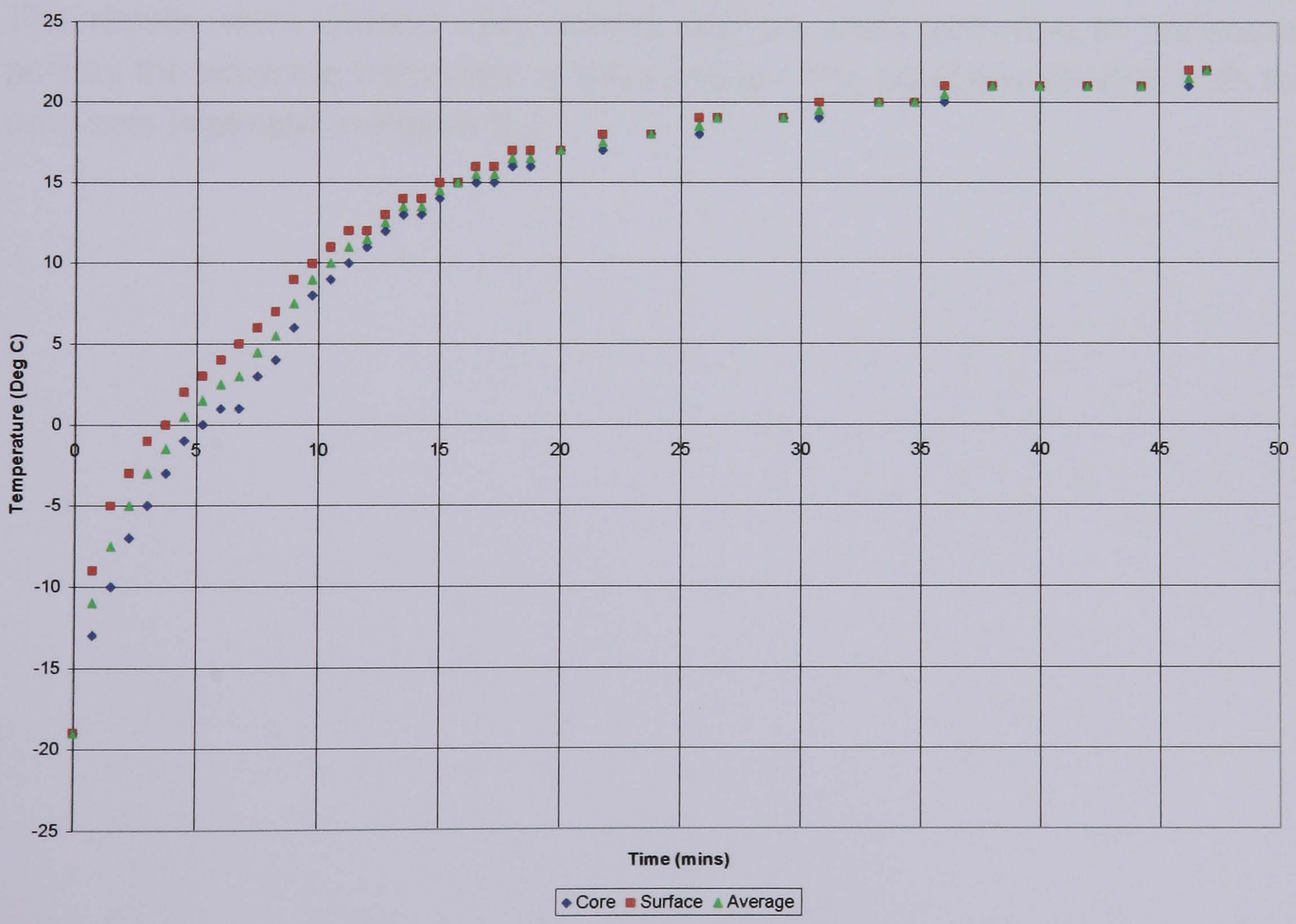

Figure 5.1 Warming profile of a Batch C hydrophilic polymer sample in air at 25°C.

The resultant warming profile is not desirable. It shows that the average temperature rises from –19 to 0°C in just over four minutes. This

would permit (at best) the acquisition of only one or two ultrasonic measurements over that temperature range which would be insufficient for adequate resolution. In addition, the difference between the surface and core temperatures was as large as 5°C, reducing confidence that a measurement taken in this scenario would reflect the true ultrasonic behaviour of the sample at a specific temperature. Even the calculation of the average temperature and the assumption that it represents the true temperature is not sufficiently accurate. In light of this, it was felt that the rate of warming effected by this process was too fast, not permitting sufficient readings to be taken and raising concerns over the effect of a large temperature gradient within the sample.

In an attempt to overcome these issues, an alternative warming process was explored. This involved chilling the sample a second time and placing it within an insulated container. When removed from the chiller on this occasion, the sample warmed much more slowly. This had the effect of reducing the difference between the surface and core temperatures to an acceptable level (lower than 0.2°C). Also, the slower warming rate afforded the time required to take ultrasonic measurements at sensible temperature intervals (-20 to 0°C in 90 minutes). This warming test was performed an additional time to ensure the warming profile was legitimate and reproducible. The results were indeed very similar and so were assumed to accurately portray the warming behaviour of the sample. The trend line fitted to both the data sets is plotted in Figure 5.2.

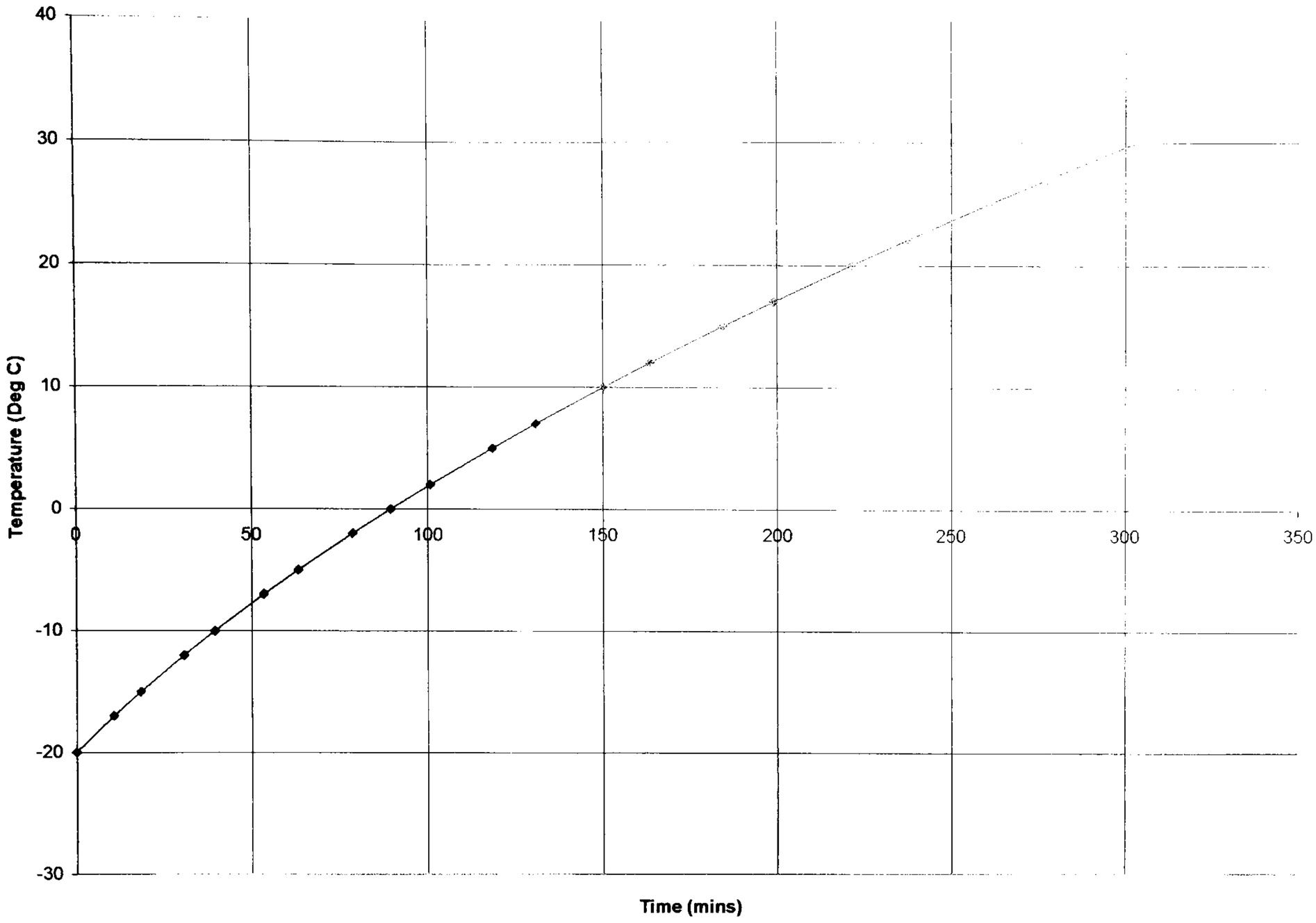

Figure 5.2 Warming behaviour of a Batch C hydrophilic sample in an insulated container. Data achieved by conducting two identical warming tests and averaging the results.

With the warming profile established, a testing programme can be created. Measurements were taken at 5°C intervals, in the range –20 up to +25°C. In an attempt to reduce the warming influence of the ultrasonic probe on the sample, the low temperature measurements (less that -10°C) were carried out in the chiller with the ultrasonic probe pre-cooled to approximately the same temperature. The intermediate temperature tests (-10 to 0°C) were conducted with the probe cooled in a domestic freezer to approximately -5°C. Tests conducted between 0 and 10°C were accomplished with the probe cooled to approximately 5°C in a domestic fridge. No chilling of the probe was done for tests conducted above 10°C.

The manufacturers of the ultrasonic probe used in these tests state that the ultrasonic performance is not affected over the range of temperatures employed in these tests. However, a standing echo was observed in the approximate region the sample back wall echo when cooled to –20°C. This was most likely due to a reflection internal to the probe, from the transducer crystal backing. Therefore, measurements taken at this temperature may have been influenced by the interference of this echo, raising doubt over its accuracy. Measurements performed at all other temperatures in the test were believed to remain uninfluenced by this echo.

5.2.2 Attenuation Results

The ultrasonic tests were performed as quickly as possible to minimise deviations from the predicted warming behaviour shown in Figure 5.2. In addition, insulated gloves were used at all times. The capture of the sample back wall echo was accompanied by a velocity measurement, taken by measuring the time interval between two repeat back wall echoes. The memory settings of the ultrasonic flaw detector were used to full effect to minimise the time the probe was required in contact with the sample.

The sample with the two thermocouples attached was allowed to warm alongside the sample under ultrasonic test. This enabled it to be used as a control for temperature. While it was appreciated that the temperature of the two samples would not have been exactly the same, it served as a useful check on whether handling the samples for measurement purposes caused the warming behaviour to deviate significantly from that presented in Figure 5.2 and assumed to be the case. It was reassuring to see that throughout all stages of the test, the temperature was extremely close to that predicted, the largest deviation being less than 2°C occurring at 10°C.

The back wall echoes were subjected to the Fast Fourier analysis macro shown in Appendix C to generate frequency spectra. Each frequency spectra was subtracted from that generated by the sample at room temperature and divided by the ultrasonic travel time. Finally, adding the attenuation of the sample at room temperature, yielded series of data describing the attenuation with respect to frequency at each measurement temperature. The result is illustrated in Figure 5.3.

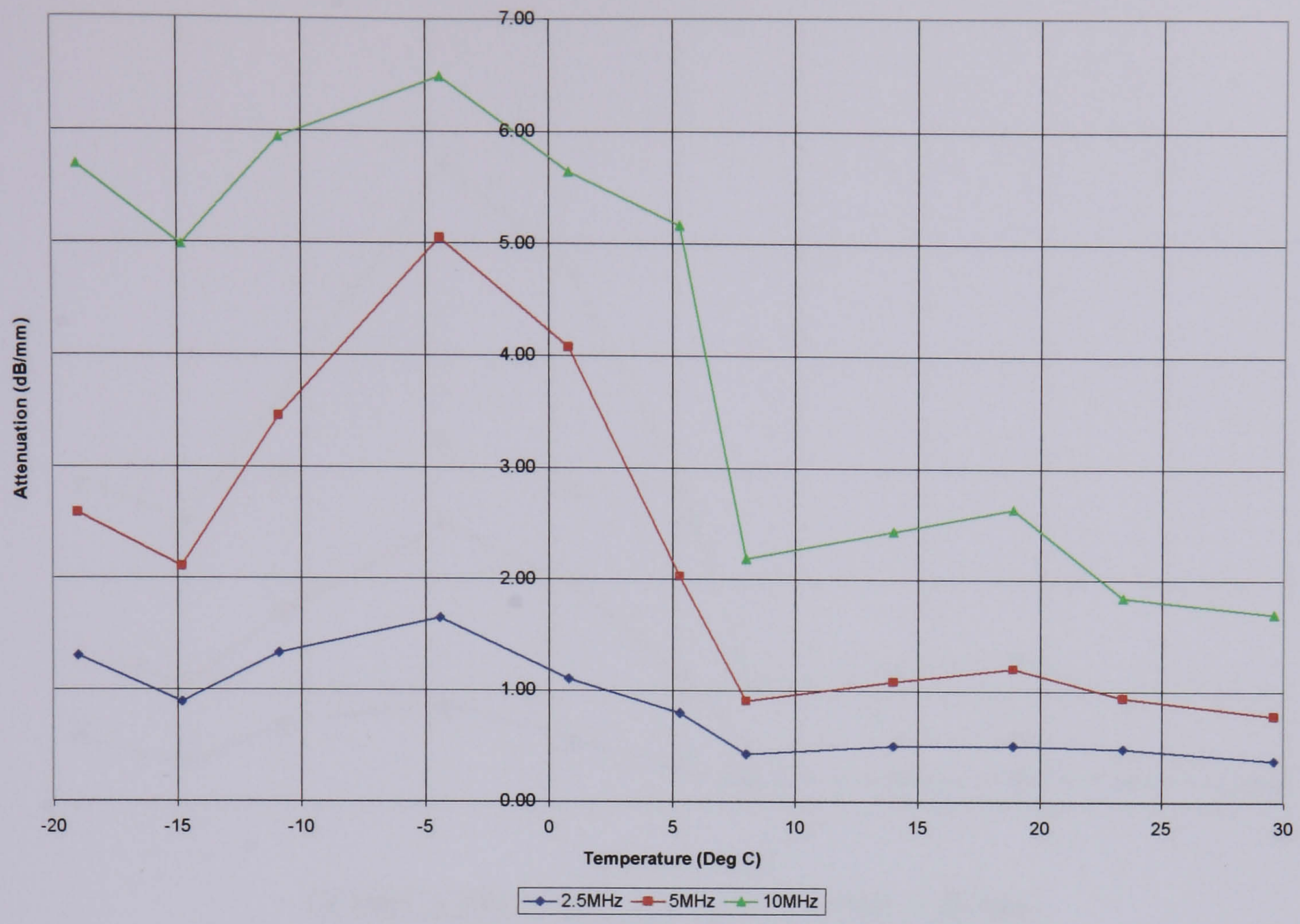

Figure 5.3 Attenuation in a Batch C hydrophilic polymer with respect to temperature. Attenuation at three different frequencies are shown.

Some noteworthy characteristics are demonstrated. Firstly the higher the frequency, the greater the attenuation at all temperatures. This is expected. Attenuation appears to increase as the sample warms, reaching a peak around -4°C. The attenuation is then seen to rapidly decrease until about 8°C where it levels off, undergoing minimal change until room temperature is reached. The -20°C result will be ignored in this analysis due to the aforementioned uncertainties regarding probe performance at this temperature.

Close inspection of the frequency and attenuation spectra shows that for many of the temperatures (particularly around -5°C where attenuation peaks), the amplitudes of frequency components above 5MHz are in the noise level. As a result, the attenuation at 10MHz taken directly from the measured data and plotted in Figure 5.3 is likely to be false. The only way to overcome this is to plot straight lines of best fit to the attenuation spectra for all the eleven measurement temperatures. Determination of the equations of these lines provides a route to calculating (essentially extrapolating) the attenuation at specific frequencies. In this way the 'true' attenuation at 10MHz was determined. Figure 5.4 show the measured attenuation together with that calculated from the attenuation equations.

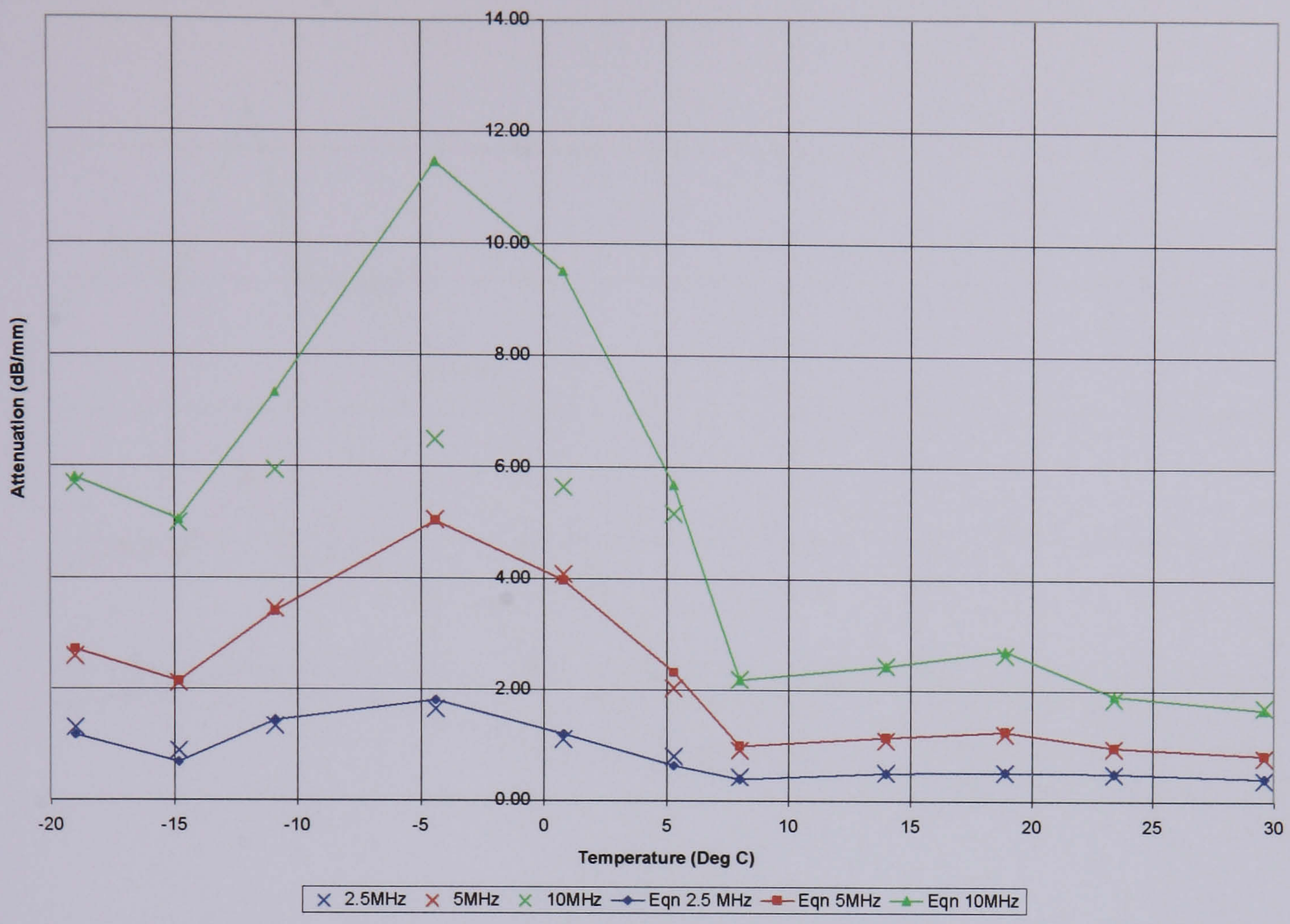

Figure 5.4 Attenuation in a Batch C hydrophilic polymer with respect to temperature. Attenuation at three different frequencies are shown. Solid lines represent the calculated attenuation. Crosses represent measured attenuation.

It is clear that the attenuation profiles for both 2.5 and 5MHz agree very closely with the calculated attenuation values. This is a good thing and shows accuracy in the calculation process. As suspected however, the attenuation calculated for the 10MHz profile differs greatly from that measured. Predictably this is amplified at around -5°C where the attenuation was greatest. The calculated profiles are felt to represent the true attenuation as they compensate for the almost complete loss of higher frequency components from the signal. The agreement of the measured and calculated attenuation profiles for frequencies within the useable bandwidth of the signal, has boosted confidence in their accuracy.

To assess the repeatability of the attenuation measurement at temperatures below room temperature, and to challenge the data acquired in this experiment, the test was repeated twice more. Once with the same sample and once with a new sample that has not been subjected to a freeze thaw cycle. With the experimental procedure honed, the opportunity to acquire additional measurements was taken. Figure 5.5 shows the results achieved for the repeat test on the first sample. The results were derived from the attenuation equations determined via the method described above. This permits direct comparison with data in Figure 5.4.

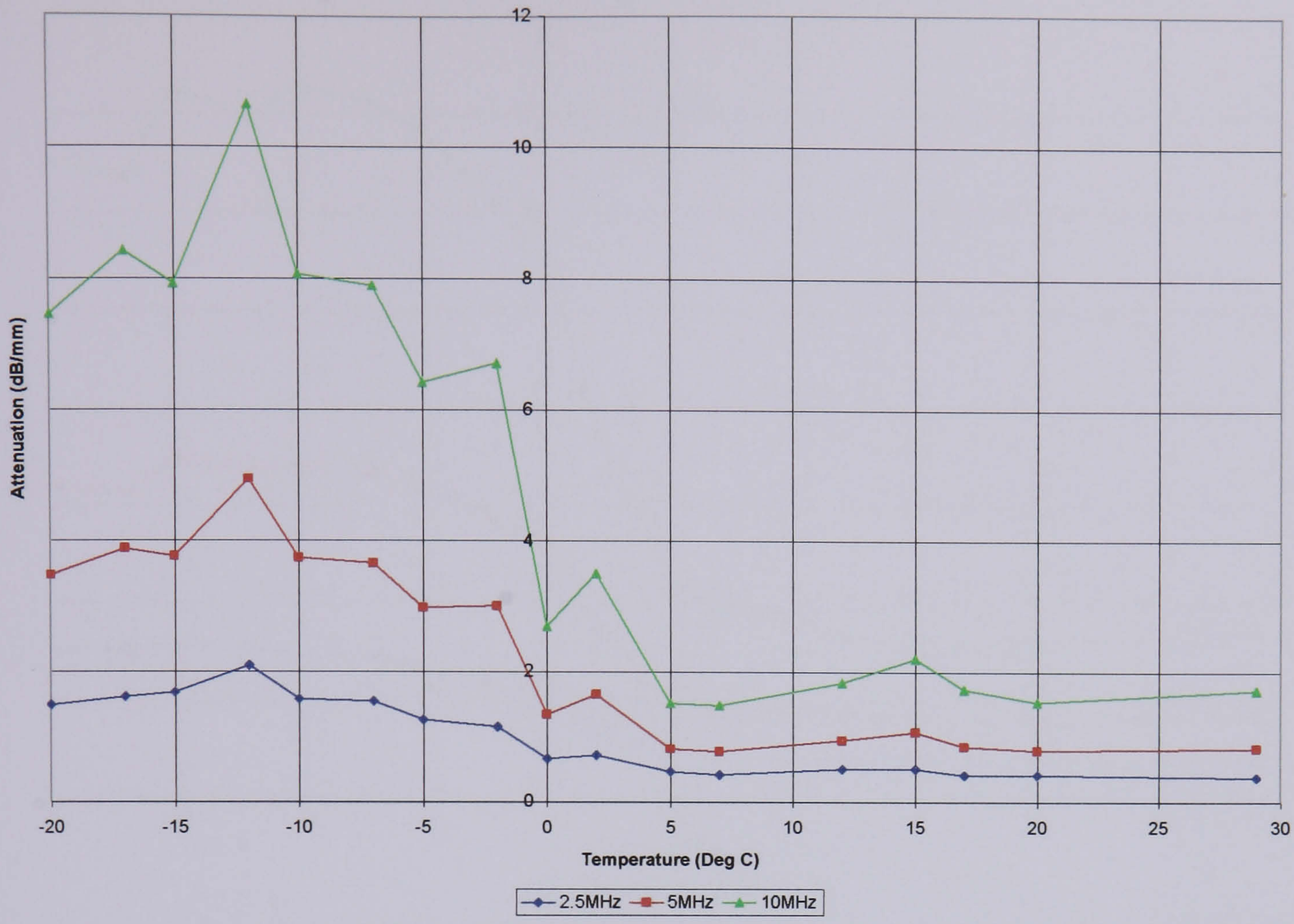

Figure 5.5 Attenuation in the same Batch C hydrophilic polymer sample with respect to temperature. Attenuation at three different frequencies are shown. The data was determined from practical measurement and calculation.

Again, obvious trends are evident that match with the first test. The attenuation increases slightly as the temperature rises, peaking at approximately -12°C. As the temperature continues to rise the attenuation falls off, reaching a minimum at about 5°C, beyond which no significant variations are observed.

Similar profiles were observed when the test was conducted with a new sample. The results are plotted in Figure 5.6.

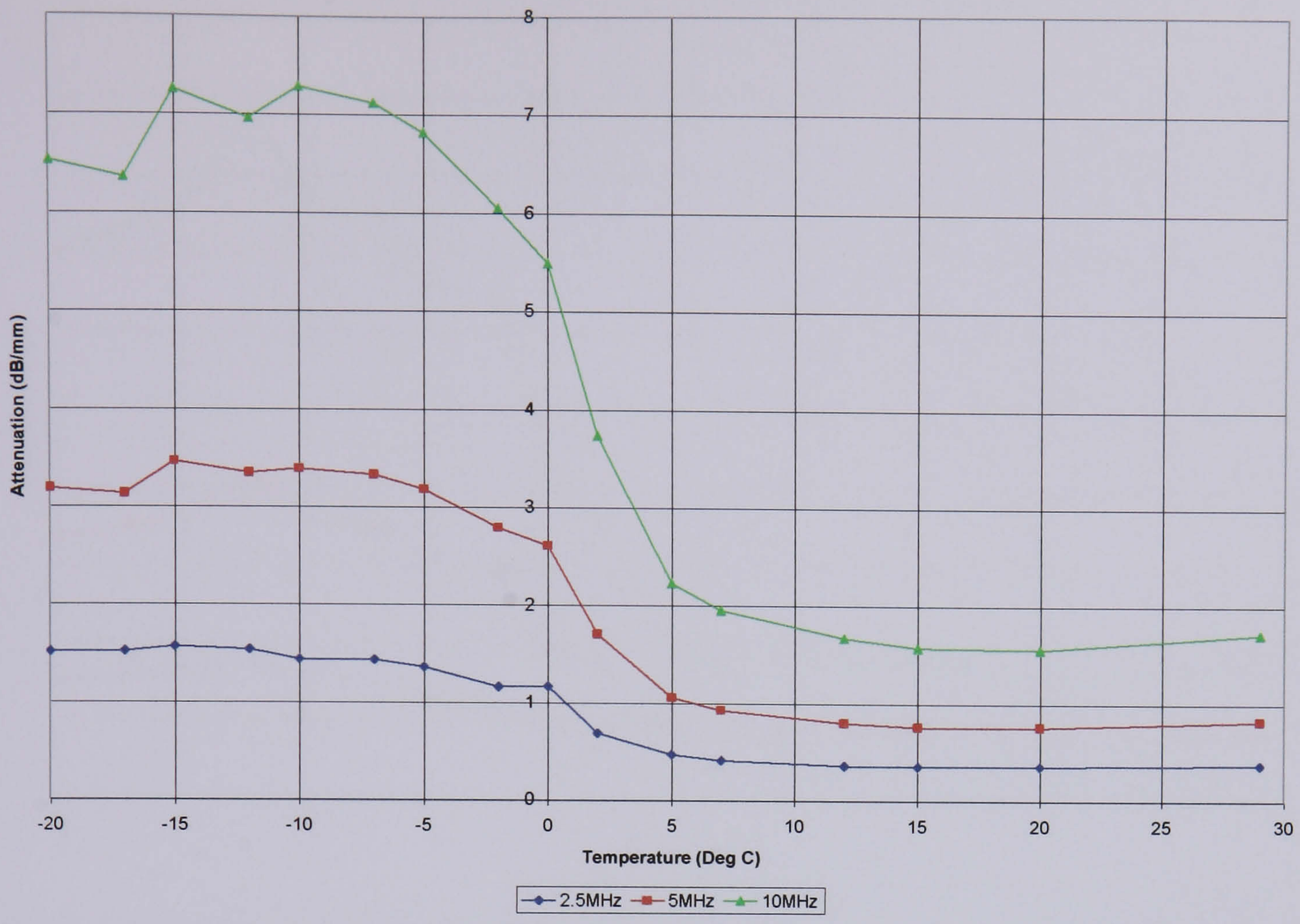

Figure 5.6 Attenuation in the a new hydrophilic polymer sample from Batch C with respect to temperature. Attenuation at three different frequencies are shown. The data was determined from practical measurement and calculation.

Similar traits are again observed. At all three frequencies, the attenuation established from this sample is slightly lower than that from the previous sample. Other than that, the profile adopts a very similar form. The consistency in the results acquired on different days with different samples has placed confidence in the experimental procedure and results.

The average attenuation was calculated from that determined for both samples. The result, shown in Figure 5.7, is believed to be an accurate representation of the attenuation characteristics of a hydrophilic polymer from Batch C, having an approximate equilibrium water content of 60% by weight. In establishing this data, steps have been taken to reduce error resulting from the following:

- experimental reproducibility,
- sample batch variations,
- loss of accurate data outside of the bandwidth of the back wall echo,
- temperature gradients through the sample,
- dehydration of the sample,
- frost formation on the sample surface,
- undesirable warming effects due to equipment and environment.

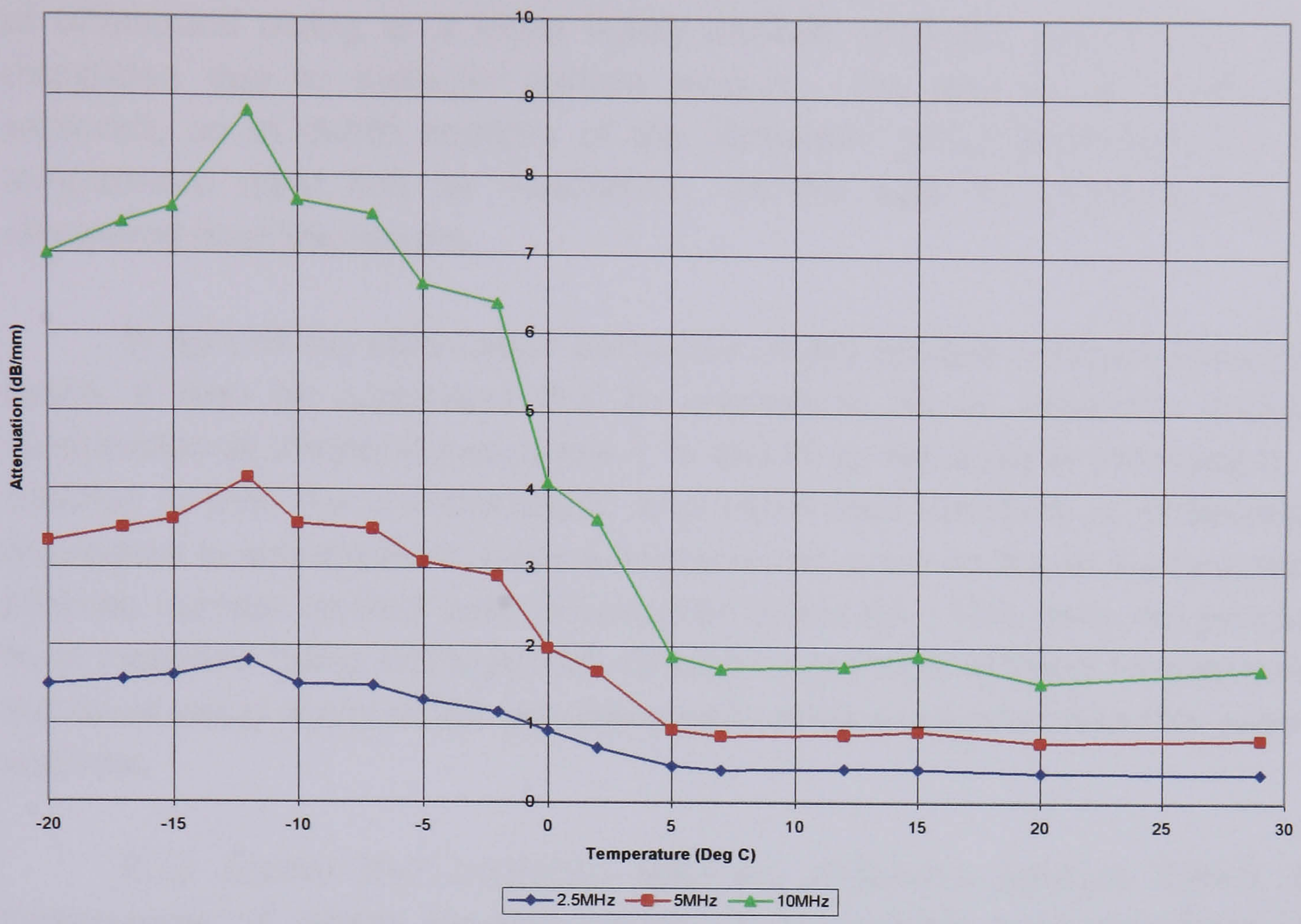

Figure 5.7 Average attenuation with respect to temperature, calculated from the data acquired from two independent tests on two different samples. Attenuation at three different frequencies are shown.

5.2.3 Discussion

During these low temperature tests a number of practical observations were made. Firstly, at temperatures below 2°C the sample took on a milky appearance. It is logical to suggest that frozen water within the polymer structure was responsible for this. This ties in neatly with the levelling out of the low-level attenuation observed when the sample is warming. It is therefore suggested that when water within the hydrophilic polymer freezes, attenuation in heightened. As the attenuation does not undergo an abrupt drop during warming, this would suggest that the thawing process is a gradual one. If the onset of attenuation decrease is assumed to match the moment when thawing begins, then this process begins at approximately -12°C.

As concerns were raised over the reliability of the ultrasonic measurements made at -20°C; there is reluctance to assign behaviour to describe the impact on the results achieved. It is likely that the standing echo observed in the ultrasonic probe at low temperatures modified the back wall echo, impacting on the results at this temperature only. This may be responsible for the slight downturn in attenuation observed at this temperature range. The sample did however, take on a more rigid form when milky in appearance. It is possible that this may have affected a more efficient transfer

of ultrasound owing to a more tightly packed structure, less energy being dissipated due to inelastic particle motion. For this to be exhaustively explored, an in depth analysis of the ultrasonic probe behaviour over low temperature must first be conducted. In this way, its influence may be eliminated from the results.

In light of the attenuation behaviour of this specific hydrophilic polymer batch, it may be concluded that its usefulness as an ultrasonic couplant deteriorates at temperatures below 5°C due to an increase in attenuation. In addition to this, the transformation to a more rigid structure as temperature decreases is anticipated to have a negative influence on the ability to achieve intimate surface contact with non-smooth materials. This does not preclude such materials being employed as ultrasonic couplants at these temperatures, but takes away many of the appealing properties associated with this class of material.

It is known that hydration with an antifreeze solution lowers the temperature at which freezing occurs in hydrophilic polymers [Highgate, 1989]. This is a plausible route towards extending the range of low temperatures over which hydrophilic polymers may operate successfully as ultrasonic couplant. Time constraints prevented this being investigated within this programme.

5.2.4 Velocity Results

The velocity of ultrasound propagation through the sample was determined over the range of temperatures employed in this study. As described, the ultrasonic travel time between two repeat back wall echoes was measured using the ultrasonic flaw detector. From this and the sample thickness readings taken simultaneously with the digital vernier callipers, the ultrasonic velocity was established. Figure 5.8 shows the average velocity calculated from two different samples.

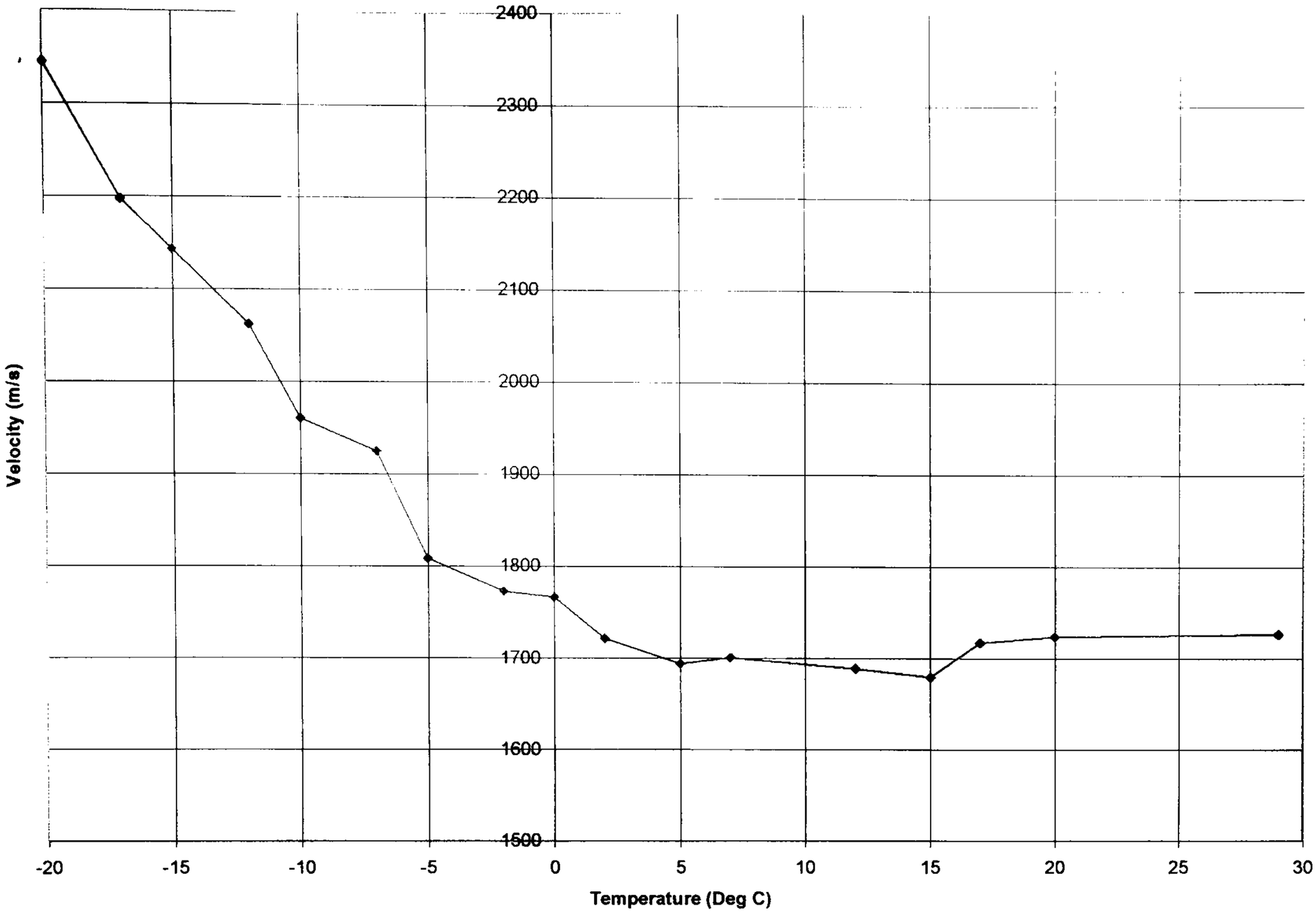

Figure 5.8 Velocity of ultrasound propagation through a Batch C hydrophilic polymer with respect to temperature.

Interestingly, the velocity demonstrates a marked trend, decreasing as the sample warms. The velocity is seen to drop from 2345ms^{-1} at -20°C to 1722ms^{-1} at 2°C. At this point it levels off undergoing no significant modification until room temperature is reached. It is interesting to note that at temperatures below -12°C the sample was measured as being slightly greater in thickness. Other than this effect, a genuine change in ultrasonic travel time was observed at temperatures below 2°C, having the greatest influence on the velocity profile. The velocity profile matches quite well with that of attenuation, both levelling off slightly above 0°C.

The change in ultrasonic velocity is important for ultrasonic applications where a hydrophilic material may be used to generate a beam of ultrasound in a test piece material at an angle other than 90°. As the angle of the refracted beam in the test piece is defined by Snell's Law, changes in velocity of the hydrophilic material would influence the angle of the ultrasound beam generated. By way of example, at room temperature, an angle of incidence of 22° in a Batch C hydrophilic polymer would generate a shear wave in steel at 45°. At -20°C however, the same angle of incidence would generate a shear wave of 31° in steel. This would be an unacceptable change for reliable flaw detection.

Typically angle probes made with a Perspex shoe come from the manufacturer with a statement of angle accuracy of ± 2° or less. For a Batch C hydrophilic polymer the same level of accuracy would necessitate a velocity window of 1665ms^{-1} (47° in steel) to 1786ms^{-1} (43° in steel). From the effect of temperature on ultrasonic velocity, this equates to a minimum temperature of -7°. As the relation between ultrasonic velocity and temperature has not been explored above room temperature, an upper limit has not been defined. It should also be noted however that increases in temperature may not necessarily result in the further reduction in ultrasonic velocity.

Below 0°C, the relationship between ultrasonic velocity and temperature appears to be linear. A line of best fit produces the formula $y = -30.431x + 1703.5$. This represents the sharp change in ultrasonic velocity with respect to changes in temperature. The beam angle would be pushed beyond the ±2° accuracy window over a temperature range of less than 4°C when below 0°C. This is an important limitation for hydrophilic polymer application, implying that for reliable generation of angled shear wave beams, the temperature must either be known to be (i) always above 0°C, or (ii) constantly within a 4°C window if below 0°C.

5.3 Influence of Pressure

It was concluded from coupling efficiency experimentation reported in Chapter 4, that hydrophilic polymers used as solid contact ultrasonic couplants achieved better coupling at higher pressures. This was observed from increases in both signal amplitude and frequency. This was believed to result from increased surface contact at higher pressures. However, when the tests were repeated with the interface between the polymer and test piece saturated with water (to emulate 100% surface contact) the amplitude and frequency still demonstrated an increase with respect to pressure. This may have been an effect of the ultrasonic properties of the polymers undergoing slight change when in a compressed condition.

This too is an important characteristic to be able to quantify. Practical use of any solid couplant be it for manual, point measurement or automated use incorporated in a wheel probe arrangement, would be subjected to a range of pressures. This could result from a number of reasons ranging from differences between operators to changes in test piece geometry.

5.3.1 Testing Programme

The experimental set up was a modified version of the test rig used for the initial coupling tests. A glass test piece was substituted for the steel and the ultrasonic probe was driven with the 10MHz filterbands selected rather than 5MHz as was the case previously. This afforded a bandwidth of 4.3MHz (see Appendix D) permitting ultrasonic performance to be observed over a usefully greater frequency range. Also the interface between the polymer and test piece was kept saturated with water at all times to emulate 100% contact. This assured, as much as possible, that the coupling efficiency remained unchanged over the range of coupling pressures applied. The reflection from the polymer – test piece interface was monitored rather than the test piece back wall echo. With the coupling efficiency held constant, any changes in ultrasonic signals observed when the polymer was subjected to varying levels of pressure were expected to result from changes in properties within the hydrophilic polymer brought on by the compression itself. In this way, the effect of pressure on the ultrasonic properties of hydrophilic polymers was investigated.

Load was applied in approximate steps of 500g increasing to 5500g (limit of the balance) generating a maximum pressure of 2.5kg cm^{-2}. This produced eleven readings per cycle. At each pressure, the interface echo was captured and stored in the ultrasonic flaw detector. Also, the ultrasonic travel time in the polymer was recorded by taking an echo to echo measurement between two polymer repeat echoes. For later calculation of the ultrasonic velocity, the compression of the polymer was also required precisely when each travel time measurement was taken. This was achieved in two parts by measuring directly from the rig with digital vernier calipers. Firstly the distance moved by the interrogating probe (through which the pressure was delivered) from its starting point at zero pressure was established. This included the compression of the polymer sample and also the deflection of the balance pan. Secondly, after the experiment was complete the relationship between the applied pressure and the amount by which the balance pan was deflected was measured. This was achieved by taking measurements directly from the rig (without the polymer samples present), pressure being applied via the probe. The relationship between applied pressure and balance pan deflection was determined by plotting them against one another. As is clearly shown by Figure 5.9, the relationship was linear. This meant that an equation could be easily determined and used to calculate the amount of balance pan compression at any pressure. With this known, it was subtracted from the overall measured compression to determine sample compression alone.

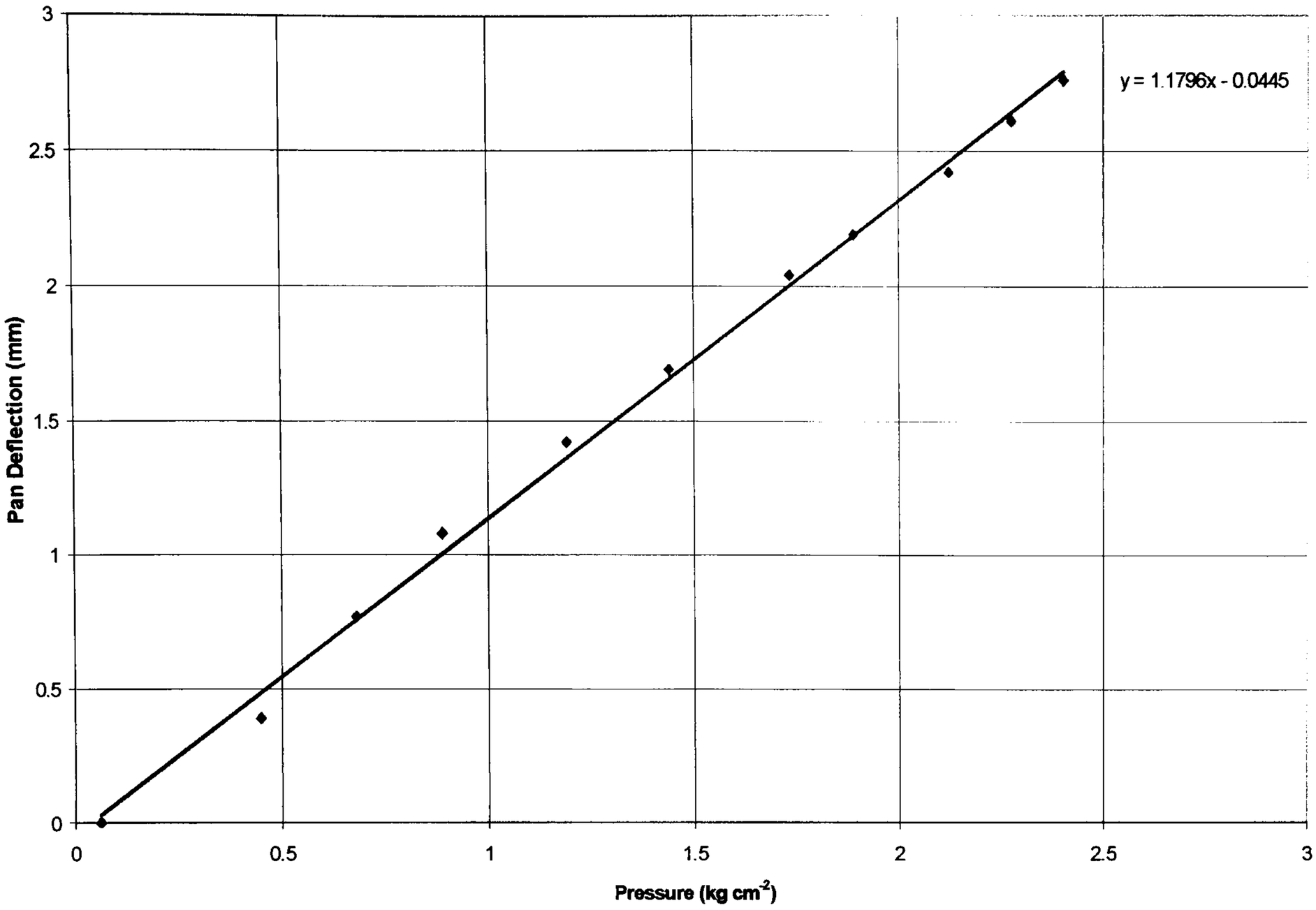

Figure 5.9 Deflection of balance pan at different applied pressures.

5.3.2 Results

With the influence of the balance pan deflection on earlier measurements determined, the sample thickness was calculated at all measurement pressures by simple subtraction. The result is plotted in Figure 5.10. This data can be used again in turn to establish the ultrasonic velocity at each measurement pressure as shown in Figure 5.12. The relationship between applied pressure and sample compression is shown in Figure 5.11.

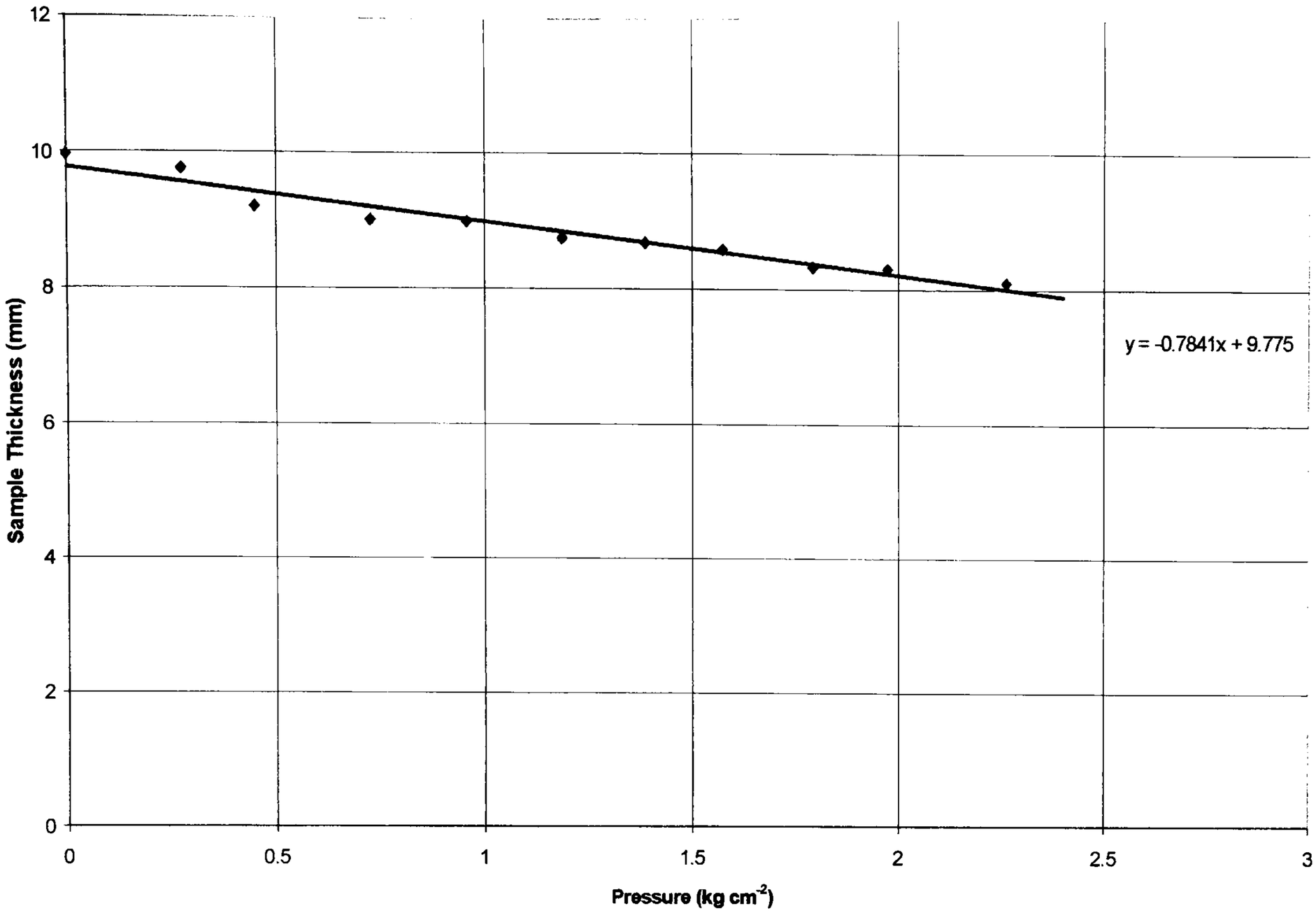

Figure 5.10 Change in thickness of a Batch C hydrophilic polymer sample under different pressures.

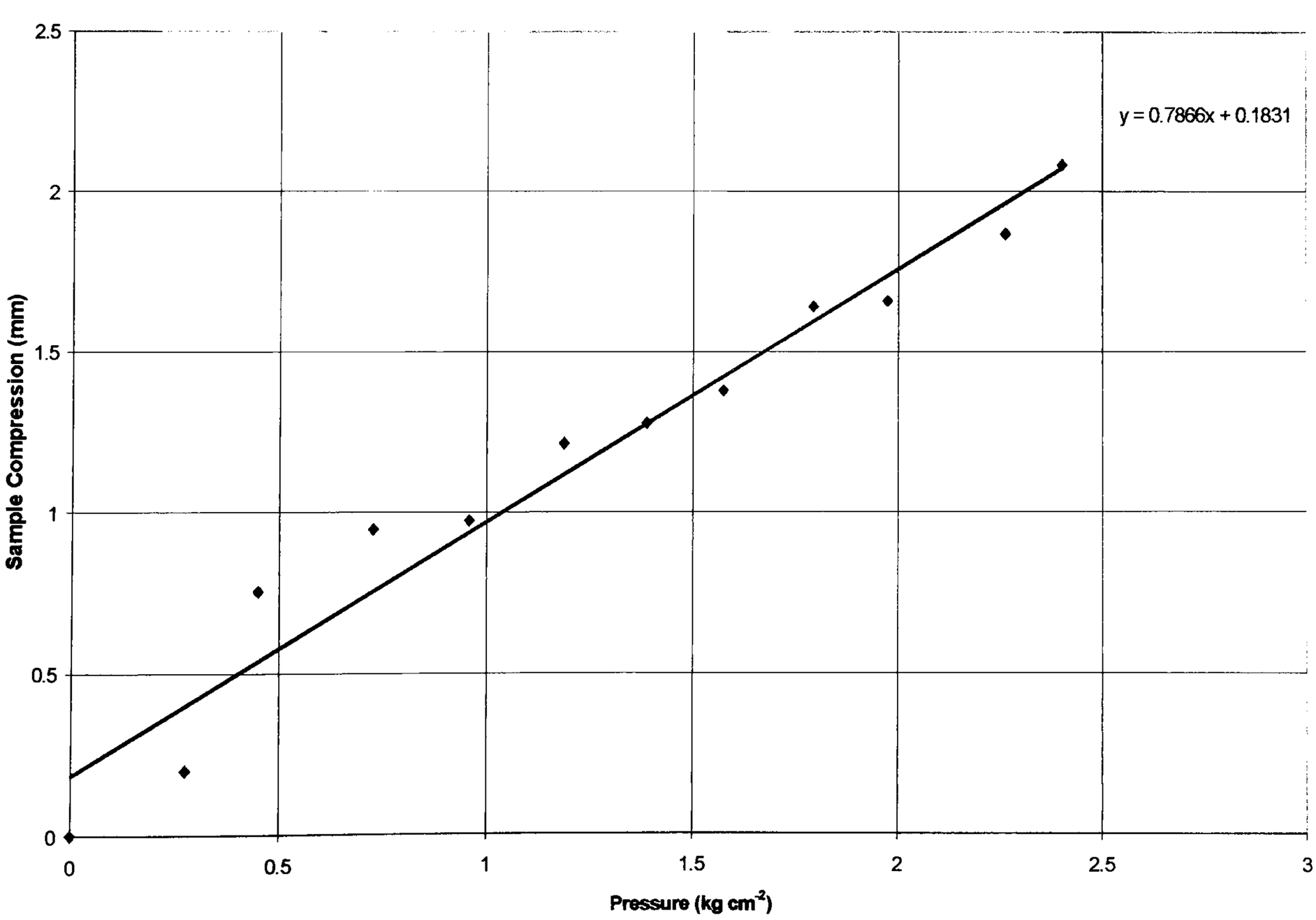

Figure 5.11 Compression of a Batch C hydrophilic polymer sample under different pressures.

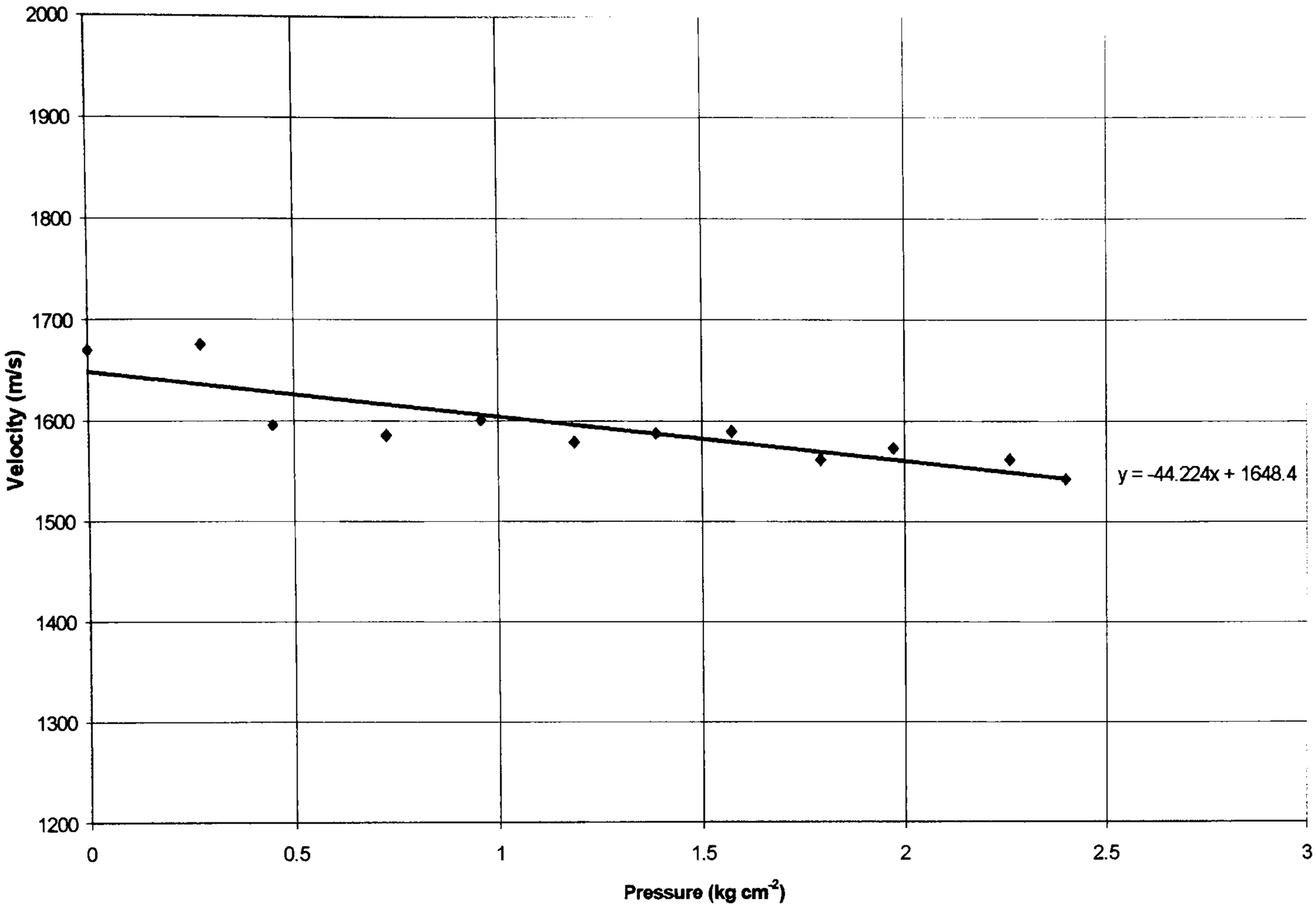

Figure 5.12 Change in ultrasonic velocity in a Batch C hydrophilic polymer under different pressures.

From this data it can be clearly seen that the sample suffers approximately 0.79mm compression per kg cm^{-2} pressure (0.4mm compression per kg applied load), which is quite small. The velocity of sound in the sample decreased with increasing pressure at a rate of $44ms^{-1}$ per kg cm^{-2} pressure ($23ms^{-1}$ per kg), which could be significant over a large pressure range.

The ultrasonic attenuation with respect to applied pressure was calculated from the echo data captured at each inspection pressure. The calculation process was the same as that described previously. Surprisingly, the attenuation profiles produced at each pressure were almost identical. These are shown in Figure 5.13 and indicate that (i) ultrasonic attenuation was independent to the range of pressure applied in this test, and (ii) the experimental rig produced very reliable and reproducible results. This is a positive outcome in both respects.

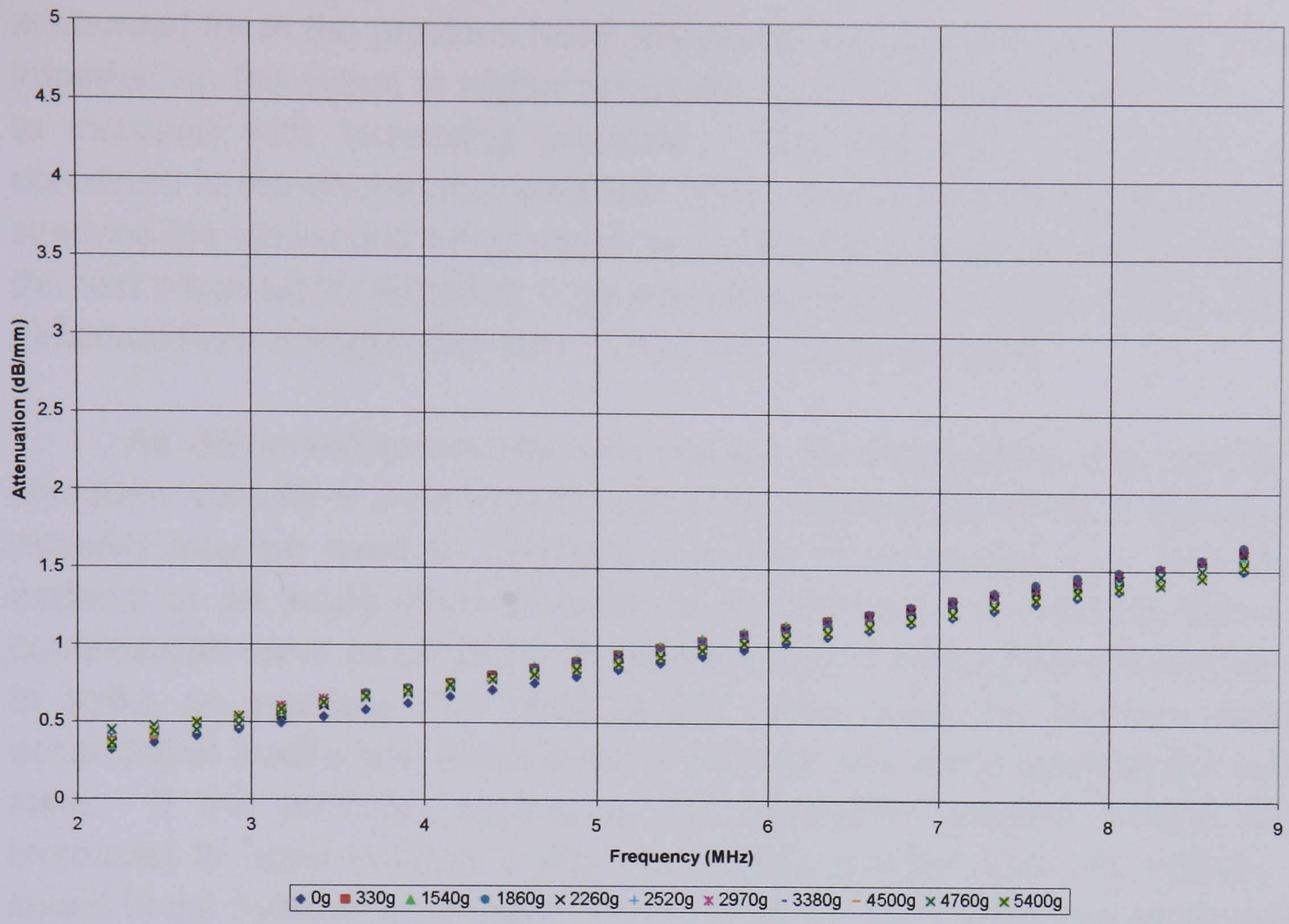

Figure 5.13 Attenuation profiles of a Batch C hydrophilic polymer under different loads representing a pressure range of 0 to 2.4kg cm^{-2}.

5.3.3 Implications

The fact that attenuation of the Batch C hydrophilic polymer sample remains unchanged over the range of pressures employed in these tests bodes well for practical use in ultrasonic NDT. Any modification in attenuation would cause signal amplitudes to vary. This would introduce an error factor to absolute amplitude measurements, seriously impairing inspections such as porosity grading, which are sensitive to such fluctuations.

This discovery suggests that the increases in amplitude and frequency observed of the steel back wall echo during the application of pressure in the coupling efficiency tests reported in Chapter 4, must have come from a factor other than changes in ultrasonic properties occurring within the hydrophilic material and coupling efficiency, as both held constant in this more recent test. Should the material properties or coupling efficiency have changed as a function of pressure during this experiment, the attenuation profiles would deviate from the near identical behaviour observed in Figure 5.13. This clearly did not happen. Similarly, peak frequency was seen to remain constant in this test whereas slight increases were observed in previous tests where the steel back wall echo was analysed. Therefore, it is concluded that changes in polymer thickness as a result of applied pressure, which were not

accounted for in the previous tests, effectively reduced the actual attenuation imparted on the signal at higher pressures, causing amplitude and frequency to increase with increasing pressure. The only other factor that may contribute to the discrepancy depends on the fact that the first method, which involved the ultrasound beam crossing the interface between the sample and the test piece twice, imparted a greater influence on the pulse than could be observed from a single reflection as was the case in this test.

As discussed previously with respect to temperature, the change in ultrasonic velocity is important for ultrasonic applications where a hydrophilic material may be used to generate a beam of ultrasound in a test piece material at an angle other than 90° to the surface. In practical terms, a compression wave propagating through a Batch C hydrophilic polymer so as to strike an interface with steel at 22° while under no pressure would, according to Snell's law, result in the production of a shear wave at 45° in the steel. If the pressure applied to the hydrophilic polymer wedge were increased to approximately 2.4kg cm^{-2} (5.5kg applied load) the velocity of sound in the hydrophilic polymer would increase. As a result, the same angle of incidence would generate a shear wave of 50° in the steel. This is a significant change in beam angle with the potential to place limitations on the utilisation of hydrophilic polymers for this application. Therefore it is suggested that if such materials were to be used for this purpose, a constant known pressure must be applied, possibly by a spring-loaded rig.

Normally angle probes are defined by the angle of the shear wave they generate in steel. A tolerance of ±2° on the beam angle is usual. For this to be achieved with a hydrophilic polymer as the wedge material, Snell's law shows that the velocity in the polymer must not vary by more than 117ms^{-1}. Using the line of best fit plotted in Figure 5.12, this translates to a pressure range of approximately 2.2kg cm^{-2} or 5kg applied load. In reality this range must be reduced to compensate for variations in velocity due to batch differences and machining tolerances. However, this is a particularly large pressure range and is significantly greater than the approximate 2kg applied load likely to be used during manual operation.

5.4 Frequency Downshift

When performing an ultrasonic inspection of a material, the frequency of the ultrasonic beam is of key importance as it defines resolution and sensitivity. In the case of conventional single compression probes, the transducer crystal is effectively in direct contact with the test piece. In such a scenario, the ultrasound generated by the crystal propagates directly into the

test piece. However, in the case of angle, twin crystal compression and delay line probes, the ultrasound generated by the crystal must first travel through a shoe or wedge material (usually Perspex or Rexolite) before entering the test piece. This subjects the ultrasound to a degree of attenuation. Attenuation has been shown in this and other studies [Krautkramer, 1983, Salgueiro da Silva et al, 1992, Smith, 1998] to have a greater effect on amplitude at higher frequencies, therefore imparting an overall downshift in signal frequency. In practical terms this means that an ultrasound beam of required frequency A in the test piece material, must be generated by a transducer of a higher frequency B. The difference between A and B being dependant on the characteristic 'frequency downshift' of the material of the shoe or wedge, which is in turn dependant on its thickness.

5.4.1 Assessment and Results

Therefore, the frequency downshift of hydrophilic polymers must be established before they can be utilised in an ultrasonic probe arrangement for critical inspections. This has been assessed practically, via the following steps:

1. Capture the backwall echo of a hydrophilic sample of known thickness,
2. Transfer of waveform data to a PC,
3. Calculation of frequency spectra, and
4. Determination of peak frequency value.

This process was repeated for different thicknesses of hydrophilic sample and for different hydrophilic batches. The peak frequency was plotted against the ultrasonic travel distance (twice the sample thickness) to enable the relationship to be assessed. The results are shown in Figure 5.14. It is appreciated that only three points have been collected for each polymer, which is the minimum useable when trying to identify a basic trend. However, the data does not appear to deviate significantly from the expected linear behaviour.

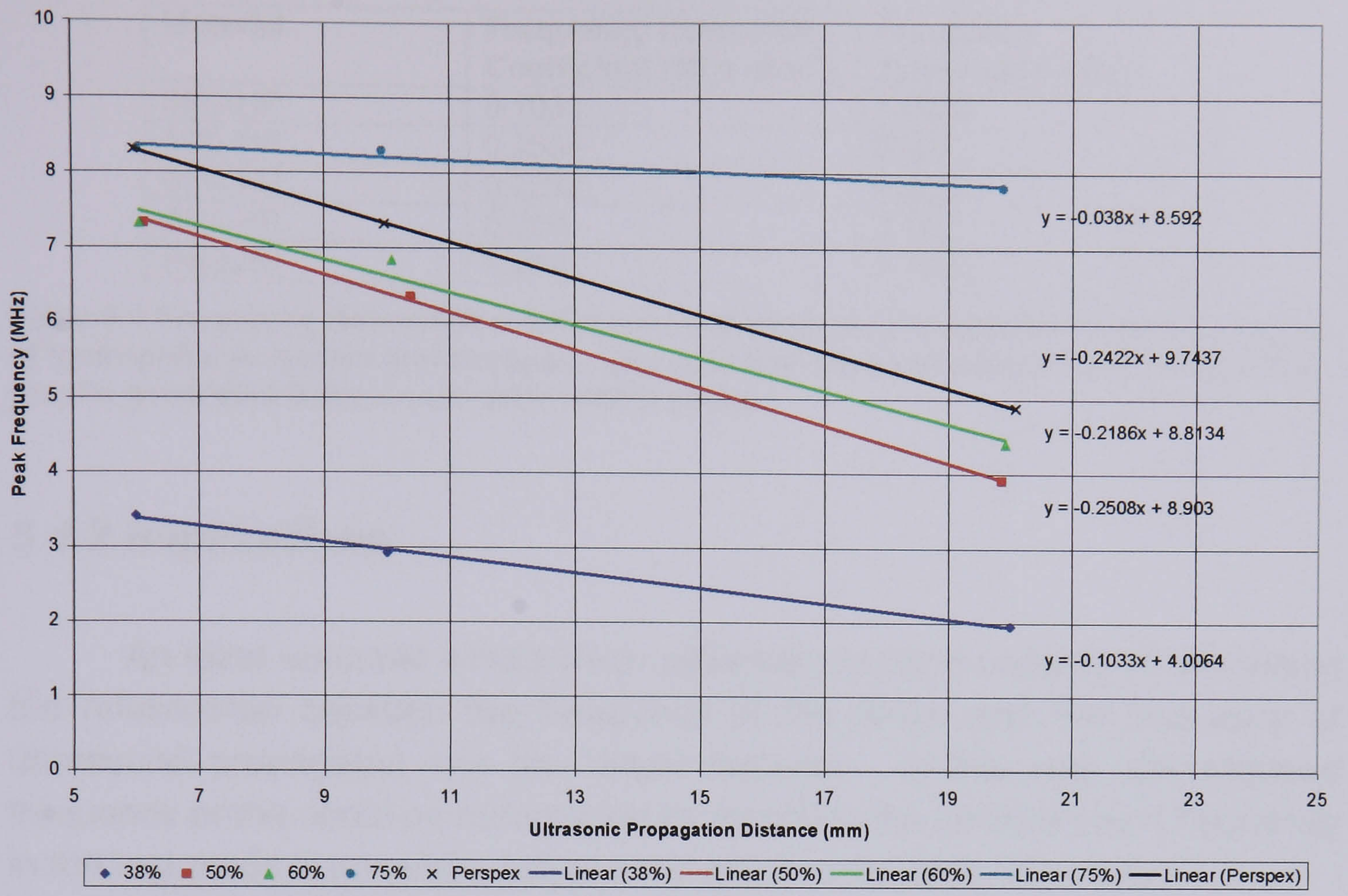

Figure 5.14 Peak frequency with respect to ultrasonic propagation distance for a number of hydrophilic polymers and Perspex. Data generated with a nominally 10MHz probe.

The linear relationships between frequency and propagation distance were expected as the attenuation of these hydrophilic materials has been shown to also be linear. Lines of best fit have been calculated and their equations determined, the gradients of which are the material specific frequency downshift coefficients with units of MHz mm^{-1}. In addition to this there is another factor corresponding to the effective frequency downshift at zero material thickness. This is described by the intercept of the straight line with the Y-axis. This has been termed here as the material specific 'frequency translation' with units of MHz.

The relationship between the data for the different materials is as expected; lower equilibrium water content polymers demonstrating lower frequencies over all sample thicknesses. The frequency downshift coefficients are very similar for Batch B and C hydrophilic polymers and Perspex. Batch D hydrophilic polymer demonstrates a much lower frequency downshift coefficient. Interestingly, the Batch A hydrophilic polymer demonstrates a lower frequency downshift coefficient than some higher water content polymers. Table 5.1 lists the results.

Material	Frequency Downshift Coefficient (MHz mm^{-1})	Frequency Translation (MHz)
38% HP	0.1033	4.0064
50% HP	0.2508	8.903
60% HP	0.2282	9.0298
75% HP	0.038	8.592
Perspex	0.2422	9.7437

Table 5.1 Frequency downshift coefficients and frequency translation data for a range of hydrophilic polymers and Perspex. The data has been calculated from straight line graphs generated from a nominally 10MHz probe.

5.4.2 Implications

An ideal outcome would be a universal equation capable of describing the relationship between the frequency of the probe and the frequency of ultrasound propagated into the target material. In this way, the required frequency probe could be determined by inputting the desired beam frequency in the test piece, hydrophilic polymer couplant material and thickness.

As an example the case of a specific probe will be considered. Firstly the frequency of the probe must be established. This may be done by analysing the frequency of a back wall echo from a material known not to impart any frequency downshift (i.e. a coefficient of zero). Investigations into attenuation in Chapter 2 showed that different thicknesses of aluminium returned the same peak frequency suggesting it as a candidate material for such probe frequency determination tests. The probe used in the generation of the data in Figure 5.14 was a TMP3, generating a peak frequency of 9.3MHz in aluminium. Therefore it is assumed that the equations determined in Figure 5.14 are valid for this particular probe or for a probe with this frequency at least.

The frequency of the sound beam generated in a target material from the TMP3 probe may be calculated for different hydrophilic polymers of different thicknesses used as couplant. If a Batch C hydrophilic polymer of 10mm thickness were used the frequency propagated into the target material may be calculated as follows:

$$F_B = F_D \times T + A \qquad \textbf{Equation 5.1}$$

where F_B is the peak frequency of the ultrasound generated in the target material, F_D is the material specific frequency downshift coefficient, T is the solid couplant thickness, and A is the frequency translation. This translates to

a peak frequency of 6.7MHz in this case. However, if a Batch D hydrophilic polymer were used instead, the peak frequency would be 8.2MHz.

In this way, the influence of the attenuation of the hydrophilic polymer may be correctly compensated for where particular inspection frequencies are required for critical applications. Ultimately it would be desirable for similar experimentation to be conduced using different frequency probes, for the determination of frequency downshift and translation coefficients. Should a trend be established between probe frequency and these coefficients, then it could be used to define a generic equation for beam frequency calculations. This would be an ideal work package for further investigation in this arena.

It is notable that coupling pressure, temperature and hydration condition also effect the frequency of the ultrasound propagated into the target material. In addition, the surface condition of the target material will also have an influence, making the issue of coupling pressure even more significant. An all-encompassing frequency prediction technique would need to take all of these factors into account. Although these factors have been investigated in this research and reported in prior Chapters, only the frequency downshift due to attenuation in individual hydrophilic polymer samples have been considered here for clarity and ease of interpretation.

5.5 Conclusions

An investigation has been conducted into the influence of temperature on the ultrasonic attenuation and velocity in a Batch C hydrated hydrophilic polymer. The temperature range employed was from -20 to +25°C. It was found that:

- Attenuation in the polymer is heightened when below 5°C.
- Attenuation is greatest over the range -5 to -10°C.
- The polymer becomes milky in appearance and very stiff below -5°C.
- The ultrasonic velocity in the polymer increases below 5°C.
- The rate of velocity increase with reducing temperature (below 0°C) is approximately $30ms^{-1}$ per °C.

The effect of applied pressure has been evaluated with respect to its influence on the ultrasonic properties of a Batch C hydrated hydrophilic polymer. This investigation proved that:

- The attenuation is independent of applied pressure over the range employed (0 – 2.4kg cm^{-2} i.e. up to 5.4kg applied load).

- Coupling efficiency via an interface saturated with free water was independent of applied pressure.

- The velocity of ultrasound reduces with increasing pressure by approximately 44ms^{-1} per kg cm^{-2} (23ms^{-1} per kg applied load).

A method has been described by which the frequency downshift imparted by different hydrophilic polymers of different thicknesses can be calculated for a specific probe. An example has been shown as proof of technique.

Chapter 6: Further Investigation of Ultrasonic Properties

6.1 Definition of Secondary Material Properties

At this point in the research project a range of hydrophilic polymers have been characterised in terms of their hydration, ultrasonic and basic mechanical wear properties. This has afforded considerable knowledge relevant to the ultimate utilisation of hydrophilic polymers as solid contact ultrasonic couplant. In this Chapter, the evaluation of additional properties that might be encountered in scenarios beyond those anticipated for 'normal' ultrasonic coupling applications is discussed and the results reported. Exploration of these properties, which include incomplete hydration, dehydration and the ability to support shear waves, have provided a broader knowledge of hydrophilic polymer behaviour.

Improvements in data analysis techniques made during the course of this research as a direct result of experience gained, enabled these additional investigations to be conducted. Without such advancements, the extent of data manipulation required would place unacceptable time demands on the project.

6.2 Incomplete Hydration

Thus far this research has considered hydrophilic polymers in saturated form. Of particular interest is how ultrasonic properties are modified by conditions of incomplete hydration during the hydration process. The presence of both rubbery and glassy regions has been identified but to date not explored in detail ultrasonically. Coincidentally, Maffezzolli [1998] has used ultrasound to characterise water sorption in HEMA. His research has been an excellent (and the only) source of reference for this area of hydrophilic polymer study. However, it has left many issues unanswered and is restricted to very thin specimens of HEMA (the oldest and least able hydrophilic material for use in ultrasonic coupling applications). Therefore, this study is the first to explore cross-linked hydrophilic copolymers with respect to specific ultrasonic properties under incomplete hydration conditions.

6.2.1 Sample Preparation

A 60% equilibrium water content cross-linked copolymer of MMA VP, was taken from Batch C for investigation. From the predefined expansion ratio of this polymer, thin discs of 2.30mm thickness were cut to hydrate to 3.00mm. Thin samples were used to minimise the time to full hydration enabling the complete process from dry to saturation to be observed in a single procedure. The faces of the discs were parallel and ground flat to ensure a good finish. The diameter was 15mm as a minimum, compared to the probe diameter of 6mm. Therefore the hydration fronts are assumed to be parallel to the surface of the probe.

6.2.2 Testing Procedure

A sample was submerged in distilled water to initiate the hydration process. At fixed time intervals the sample was removed, blotted dry and weighed. This was followed by two ultrasonic measurements involving coupling a TMP3 probe to the sample with a small amount of oil. Oil was used over water as it did not result in continued hydration during the measurement process. The ultrasonic flaw detector (using optimum broadband settings previously determined for the probe and described in Section 2.2.4.1.) performed a pulse echo analysis and stored the A-scan in its memory. The settings on the ultrasonic flaw detector were then adjusted[C] so that only the sample back wall echo was visible on the screen. The echo was captured and transferred to a PC for analysis in Microsoft Excel. The oil was then wiped from the surface of the sample and it was reintroduced to the water bath. The order of measurement taking was as follows:

1. Removal from water and blotting dry,
2. Weighing on a balance accurate to $1x10^{-3}$g,
3. Storage of pulse echo A-Scan for later analysis,
4. Capture of back wall echo and communication to a computer for later analysis, and
5. Sample wiped free of oil and replaced in water bath.

These measurements were performed as quickly as possible to avoid deviation from the hydration behaviour resulting from continuous submersion. In fact a velocity measurement and thickness measurement was also desirable to enable their modification to be examined with respect to

---

[C] Approximate settings were stored in the panel memory locations of the ultrasonic flaw detector for both the A-scan storage and back wall echo capture. This assisted with speeding up the measurement process, as only minor manual adjustments were required.

hydration. However, the time required to take the measurements, which would have involved further adjustment to the settings on the ultrasonic flaw detector, increasing the time the sample was out of contact with water to a significant level, risking interference with the hydration profile. Therefore, these measurements were not undertaken. Note that changes in ultrasonic velocity may be derived from the stored A-Scans by performing a further data analysis process. The expansion ration is known to be linear and so may be assumed to be directly proportional to the weight gain. In total, twenty sets of readings were taken over a twenty two hour period to interrogate the sample during hydration.

6.2.3 Preliminary Results

The pulse echo A-Scans of the sample during different stages of hydration were particularly pleasing. In the case of the completely dry sample, both the front and back wall echoes are clearly visible. Subsequent measurements (acquired after hydration had initiated) while both rubbery and glassy regions were in existence, showed two additional reflections from within the sample. These resulted from the discontinuity between the rubbery and glassy regions themselves. Hence the interface between the two regions is proven to be 'abrupt enough' to cause an interface from which ultrasound will be reflected. This enables the progression of the hydration fronts to be investigated ultrasonically during the hydration process. Figure 6.1 shows typical A-Scans of the sample in dry and part hydrated conditions.

The TMP3 probe used to interrogate the sample had a delay line fitted made of Rexolite (similar to Perspex). This was the case for reasons described in Appendix A, namely the ability to resolve discontinuities close to the sample surface, normally obscured by crystal ring-down. Therefore, the first (left most) echo seen in Figure 6.1 A-D represents the interface between the Rexolite and sample surface. The probe was 10MHz and highly damped affording a pulse length of approximately 0.5mm in the hydrophilic sample. This was sufficient for resolving the discontinuities in this investigation. Improved depth resolution could be achieved by shortening the pulse length by increasing frequency, increasing the crystal damping or both.

Figure 6.1 Pulse echo A-Scans of a Batch C hydrophilic polymer during different stages of hydration. A frequency of 10MHz was used to enable resolution of the interfaces. A) 0% water prior to submersion. B) 18.9% water after 35 minutes submersion. C) 32.7% water after 123 minutes submersion. D) 45.0% water after 281 minutes submersion.

6.2.4 Influence of Partial Hydration on Sound Velocity

Echoes from the rubbery-glassy interfaces could be observed from the first hydration measurement, taken only five minutes after submersion. At this time, the sample contained only 8.1% water. The reflections from the advancing hydration fronts were seen from the pulse echo A-Scans to be approaching each other during hydration. After 123 minutes submersion, the two echoes were on top of each other, indicating that the two fronts had met. No indication of internal interfaces was observed on any subsequent pulse echo A-Scan.

Of particular note is the apparent overall decrease in bulk ultrasonic velocity as hydration continued. This is indicated by the increase in time between the front and back wall echoes, seen on the A-Scans as an increased distance. The onscreen range of the ultrasonic unit was 3µs in

Figure 6.1A and increased to 4μs for Figure 6.1 B to D. The precise change in travel time through the sample was determined by analysing the A-scan data for the maximum amplitude in the front and back wall echoes and relating those to their corresponding time intervals. The difference between the two was the ultrasonic travel time through the sample. While this was seen to increase with continued submersion, it was also appreciated that the sample thickness was increasing also. This would counteract an apparent increase in velocity. To compensate for this, the following assumption was made. As cross-linked hydrophilic polymers are known to have a linear expansion ratio, the thickness was assumed to increase at the same rate as weight gain, reaching the final thickness upon saturation. The thickness change during hydration calculated via this method is plotted in Figure 6.2. The velocity was then determined for each measurement over the hydration process using the calculated thickness and time interval between the sample front and back wall echoes. The result is plotted in Figure 6.3.

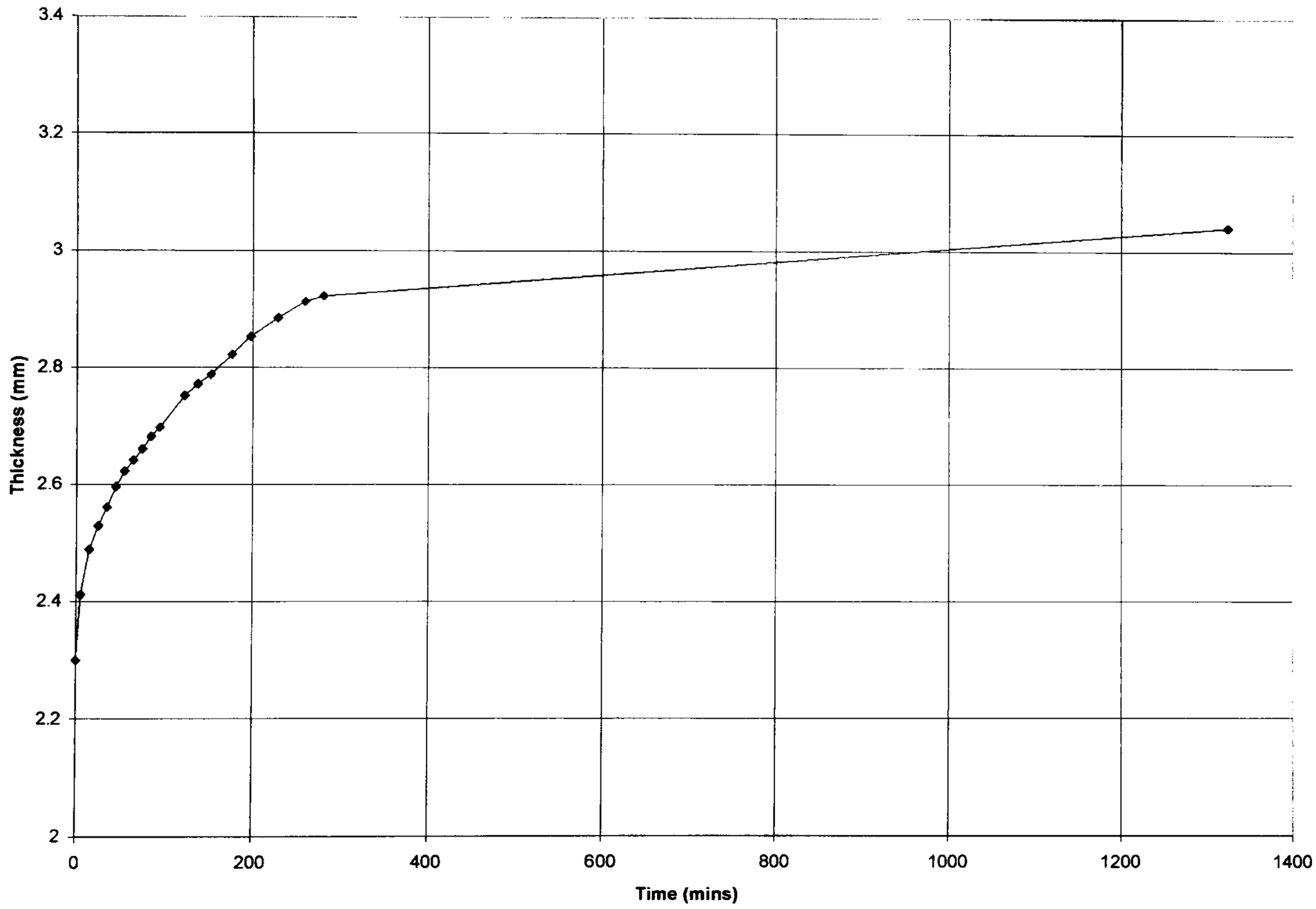

Figure 6.2 Calculated thickness of a Batch C hydrophilic polymer during hydration. Thickness was assumed to increase at an equal rate to water sorption.

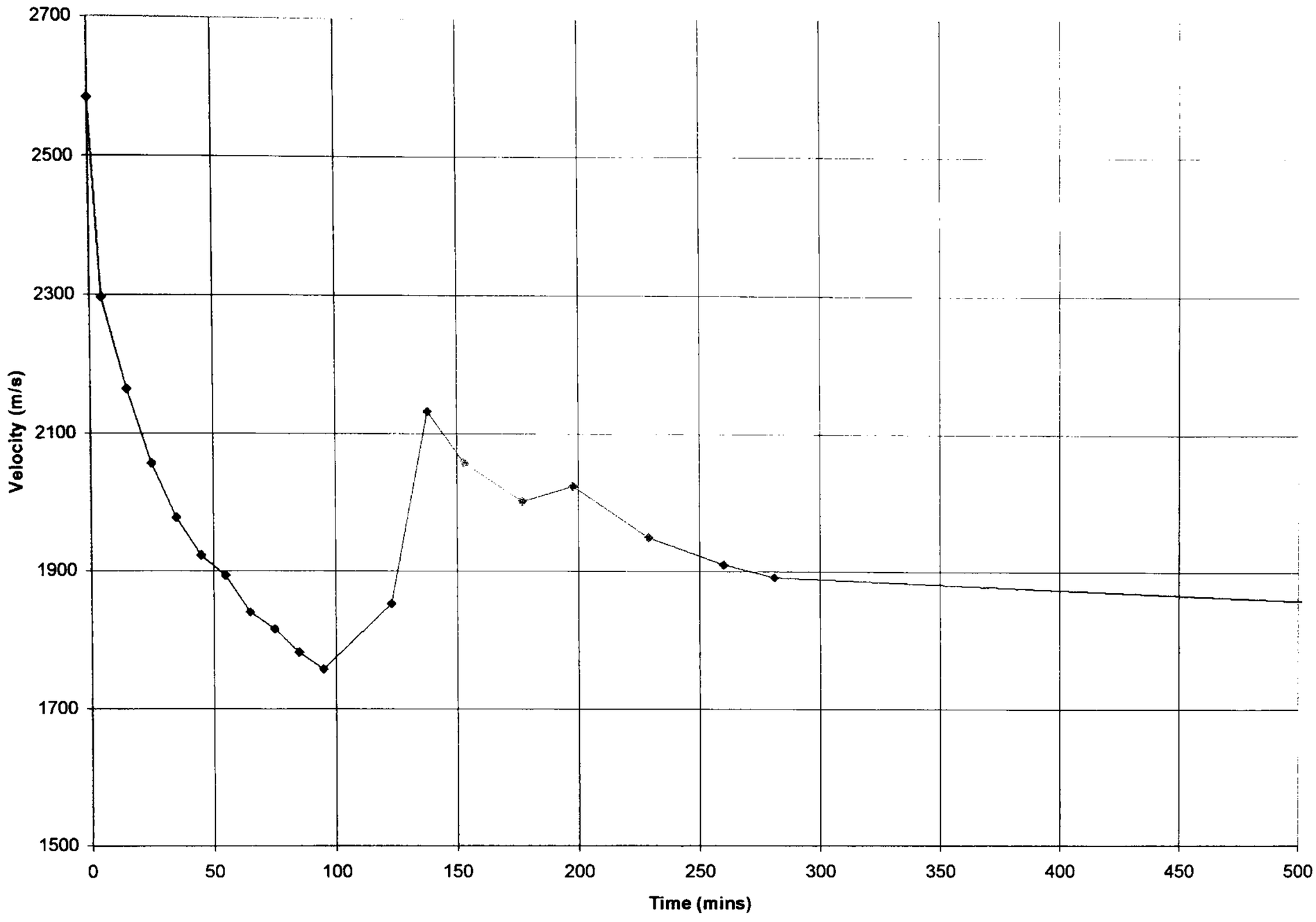

Figure 6.3 Calculated velocity of ultrasound transmission through a Batch C hydrophilic polymers during hydration.

The velocity can be seen to drop from 2584ms^{-1} when dry to 1757ms^{-1} after 95 minutes submersion at which point it begins to increase sharply to 2132ms^{-1} at 128 minutes. The velocity then gradually drops back to 1732ms^{-1} on saturation (which is consistent with measurements taken in Chapter 2). Interestingly, the first velocity increase data point was recorded at 123 minutes, the same time as the hydration fronts disappeared. It is feasible that this has affected the speed of sound through the sample in some way. It is more likely that when the glassy region disappears, at 123 minutes, the sample stiffness reduces markedly. Therefore, even minor changes in the pressure applied to the interrogating probe may have compressed the sample affecting an apparent velocity increase. It is noteworthy that Maffezzoli did not report a similar velocity upturn during hydration tests conducted on HEMA. A possible way to overcome this uncertainty would be to perform the hydration tests live in an immersion tank. In this way, no contact would be made with the sample and so the effect of sample compression may be ignored. This would be an interesting point for future investigation.

6.2.5 Influence of Partial Hydration on Attenuation

The back wall echoes captured during the hydration process were subjected to a fast Fourier Transform to establish their frequency spectra. The many spectra reveal an interesting trend. Figure 6.4 shows only those

acquired from the sample (i) prior to submersion, (ii) after 35 minutes, (iii) 123 minutes, and (iv) 1325 minutes submersion for ease of interpretation. It must again be noted that the interrogating probe was fitted with a delay-line. This will itself attenuate ultrasound resulting in lower amplitudes and some frequency down-shift.

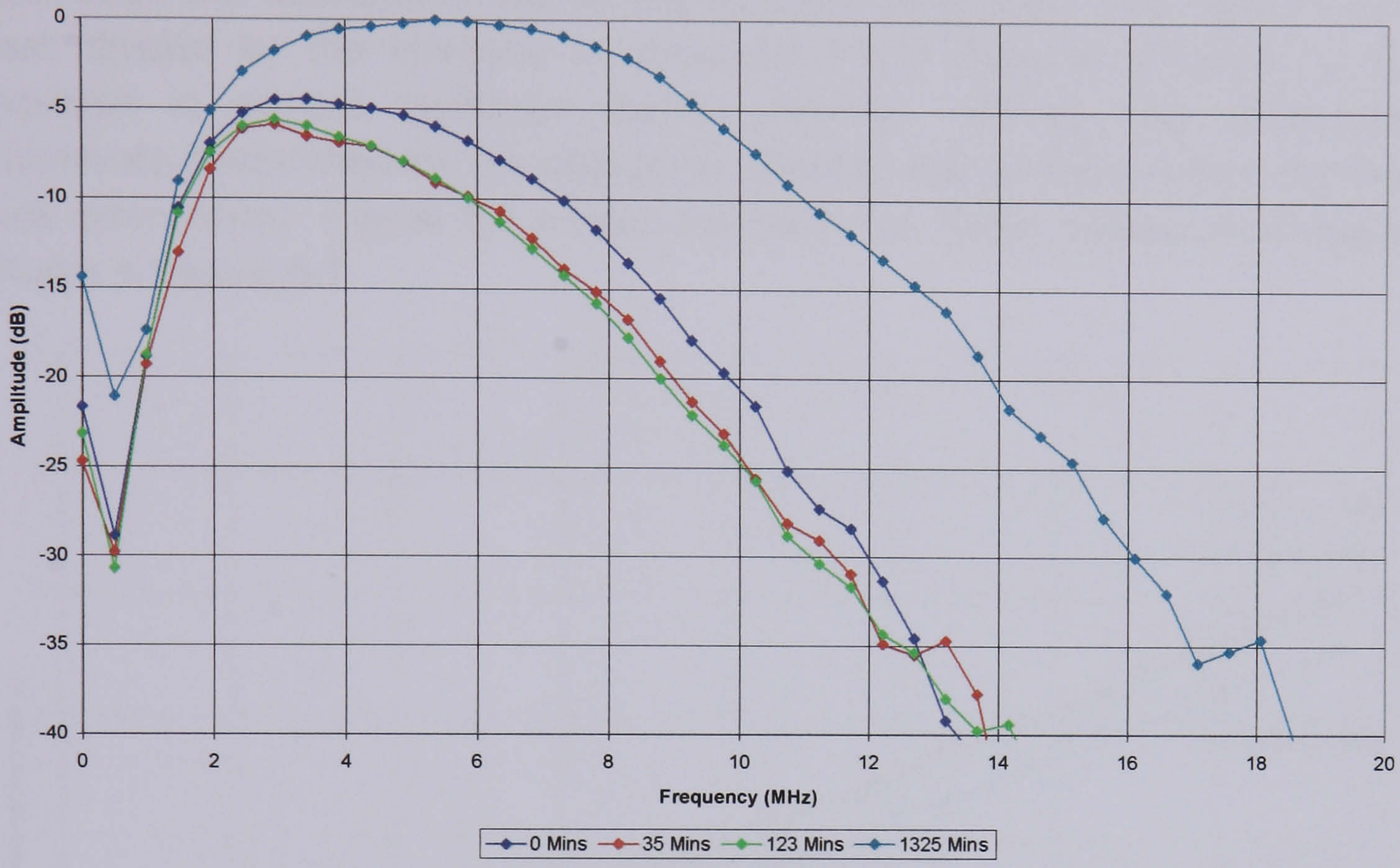

Figure 6.4 Frequency spectra of a Batch C hydrophilic polymer at different stages of hydration. The data was acquired with a 10MHz TMP3 probe with its delay line attached.

As expected, the frequency spectra of the sample after 1325 minutes submersion is higher in amplitude and peak frequency than that of the sample prior to submersion. It may be perceived that this is so because the former is completely saturated, while the latter contains no water. This is logical from studies performed in Chapter 2, which showed that the higher the water content of a hydrophilic polymer, the lower its attenuation [Bourne et al, 2001a]. However, previous investigations compared saturated polymers of different equilibrium water contents. Here we are effectively comparing samples of the same equilibrium water content, only containing different fractions of this amount as the polymer moves towards saturation. Figure 6.4 shows the frequency spectra from the sample after 35 minutes and 123 minutes submersion, having water contents of 18.9% and 32.7% respectively, both demonstrating lower amplitudes and peak frequencies than the frequency spectra of the sample when completely dry.

From this it may be concluded that the attenuation in the hydrophilic polymers firstly increases during hydration before decreasing to a level below its starting point as saturation is reached.

In order for this phenomenon to be explored further, attenuation figures were calculated for the sample at all twenty partial hydration stages measured in this study. These were determined by firstly subtracting the partial hydration frequency spectra from that of complete saturation to provide the attenuation increase over that of saturation. By happy coincidence this also eliminates the attenuation due to the Rexolite delay-line. The figures were then divided by the increase in ultrasonic travel distance affected by the increase in sample thickness during swelling. Finally, the attenuation previously determined for the saturated material was added to report the true bulk attenuation. Figure 6.5 shows the result for partial hydration situations shown in Figure 6.1.

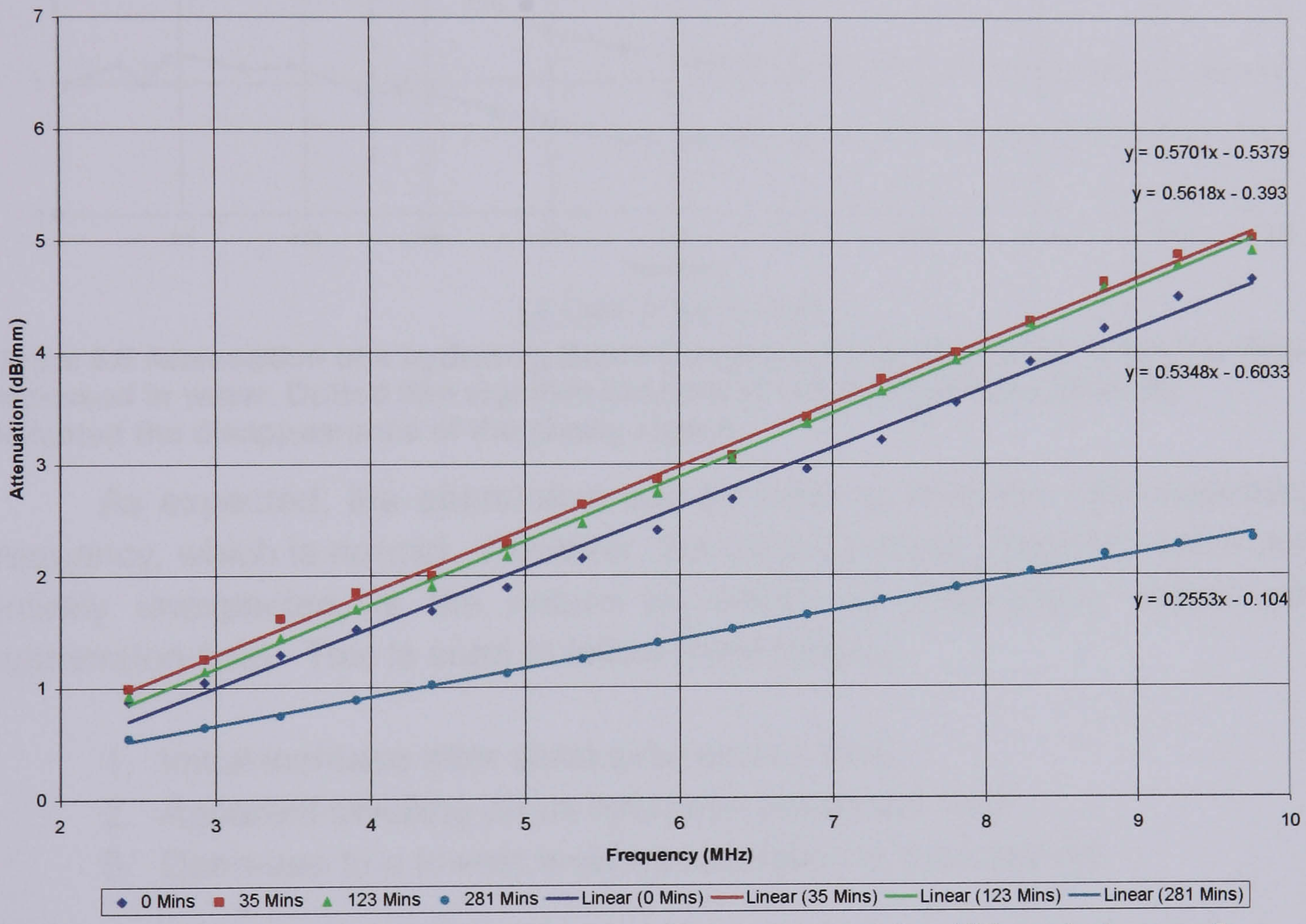

Figure 6.5 Attenuation in a Batch C hydrophilic polymer at the different stages of hydration shown in Figure 6.1 (0% water prior to submersion, 18.9% water after 35 minutes submersion, 32.7% water after 123 minutes submersion, and 45.0% water after 281 minutes submersion.

The data outside of the useable bandwidth of the ultrasound incident on the sample (i.e. non-reliable) was discarded to concentrate on the accurate attenuation data. This proved to be linear with frequency. Lines of best fit were plotted and their equations determined (as shown in Figure 6.5). With this procedure repeated for all data sets, the line equations could be used to calculate attenuation at any frequency and at all part hydration stages. Figure 6.6 shows the attenuation data at three different frequencies inside the useable range, permitting actual recorded data to be used.

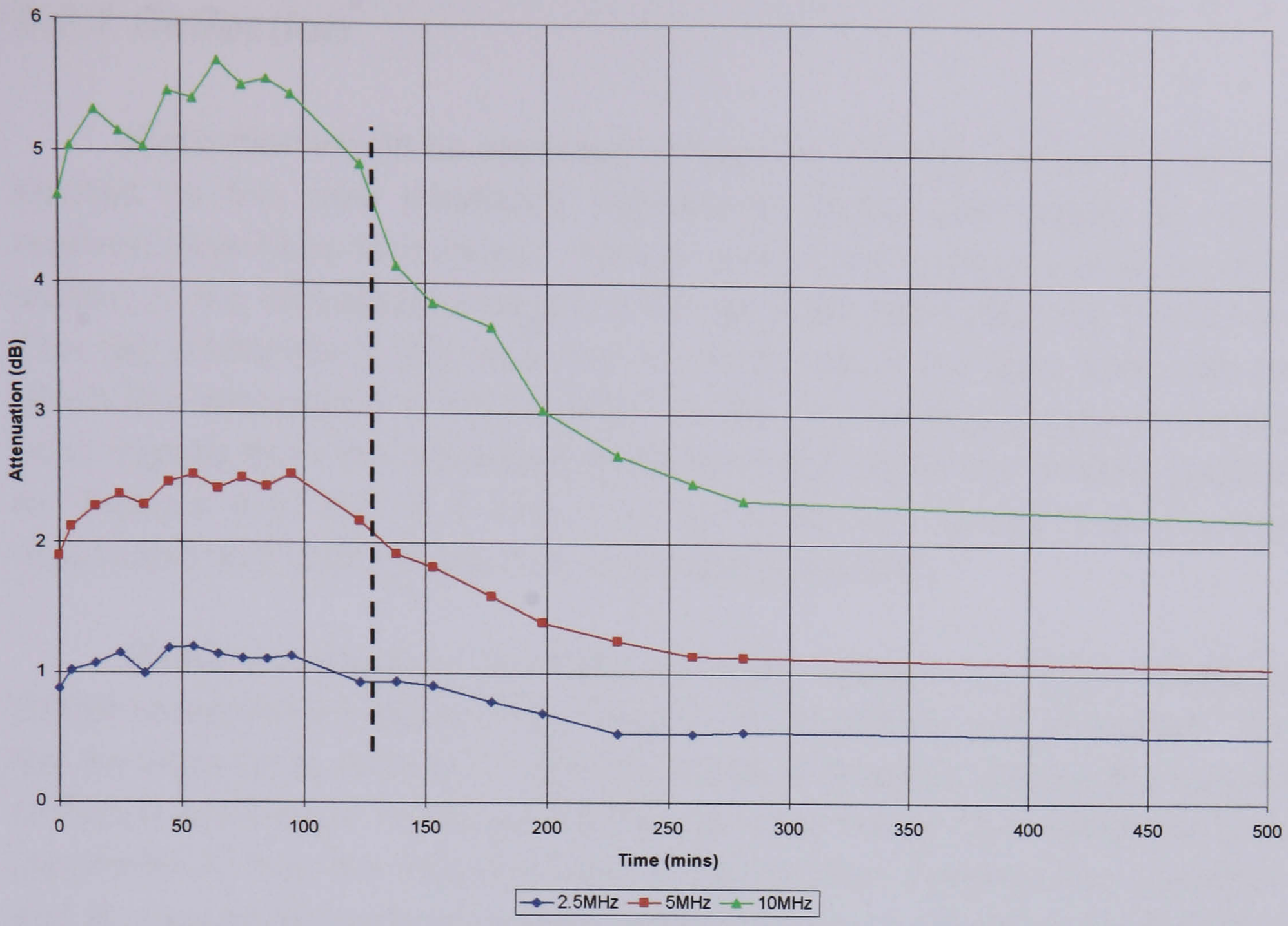

Figure 6.6 Attenuation of a hydrating Batch C hydrophilic polymer with respect to time immersed in water. Dotted line signifies the time at which pulse echo analysis indicated the disappearance of the glassy region.

As expected, the attenuation can be seen to increase with increasing frequency, which is normal. However, the most interesting feature, which was entirely unexpected, is the nature by which the attenuation varies with submersion time. This is seen to follow three stages:

1. Initial increase after short submersion time,
2. Apparent levelling off as hydration continues, and
3. Decrease to a lowest level as saturation is approached.

6.2.6 Discussion of Attenuation Results

In an attempt to explain the attenuation phenomenon observed in partially hydrated hydrophilic polymers, the nature of attenuation in materials will be briefly reconsidered. The measured attenuation of a material is known to represent loss in signal amplitude caused by reflection, scattering and absorption [Krautkramer, 1983]. Mode conversion can also contribute in cases where the sound beam is incident onto oblique interfaces [Smith, 1998]. However, in this study we are concerned with ultrasound incident normal to the sample and hence the effects of mode conversion may be ignored. The remaining contributions will be considered in turn.

6.2.7 Reflection

Reflection would be expected to have an influence on the part hydrated sample as two new interfaces (rubbery to glassy and glassy to rubbery regions) have been introduced. Indeed, pulse echo analysis has shown that a portion of the ultrasonic energy is reflected from each interface (Figure 6.1). This will contribute to the reduction in amplitude of the back wall echo from which the attenuation is determined. In fact, the disappearance of the pulse echo signals from the advancing hydration front within the sample (indicated on Figures 6.6, 6.7, 6.9 and 6.10 by a vertical dotted line) correlates reasonably well with the onset of attenuation reduction.

While investigating the case of water sorption in HEMA, Maffezzoli [1996] considered 3 states of hydration; dry, absorbing and saturated. From this he went on to attempt to quantify the loss of signal amplitude caused by reflection from these additional interfaces. It is known from ultrasonic theory (Appendix A) that the reflection due to an interface between two materials A and B, may be considered directly proportional to a reflection coefficient R_{AB} given by [Krautkramer, 1983]:

$$R_{AB} = \left| \frac{Z_B - Z_A}{Z_B + Z_A} \right| \qquad \textbf{Equation 6.1}$$

Z being the acoustic impedance of a material (product of density and acoustic velocity). The acoustic impedance of both dry (Z_d) and saturated (Z_s) hydrophilic polymer may be easily determined. The acoustic impedance of the hydrating portion (Z_r) will however, be dynamic, changing with respect to the quantity of water absorbed and hence time. Therefore, it will lie between the equilibrium values of dry and saturation. Maffezzoli sought to estimate the acoustic impedance of the absorbing region of the hydrophilic polymer by assuming a linear dependence between acoustic impedance and weight gain (W). This led to Equation 6.2 where W_{max} is the maximum water uptake of the polymer at equilibrium.

$$Z_r(t) = Z_d - \frac{(Z_d - Z_s)W}{W_{\max}} \qquad \textbf{Equation 6.2}$$

Applied to the data acquired in this study for a hydrophilic copolymer, the simulated change in acoustic impedance of the hydrating region is represented in Figure 6.7.

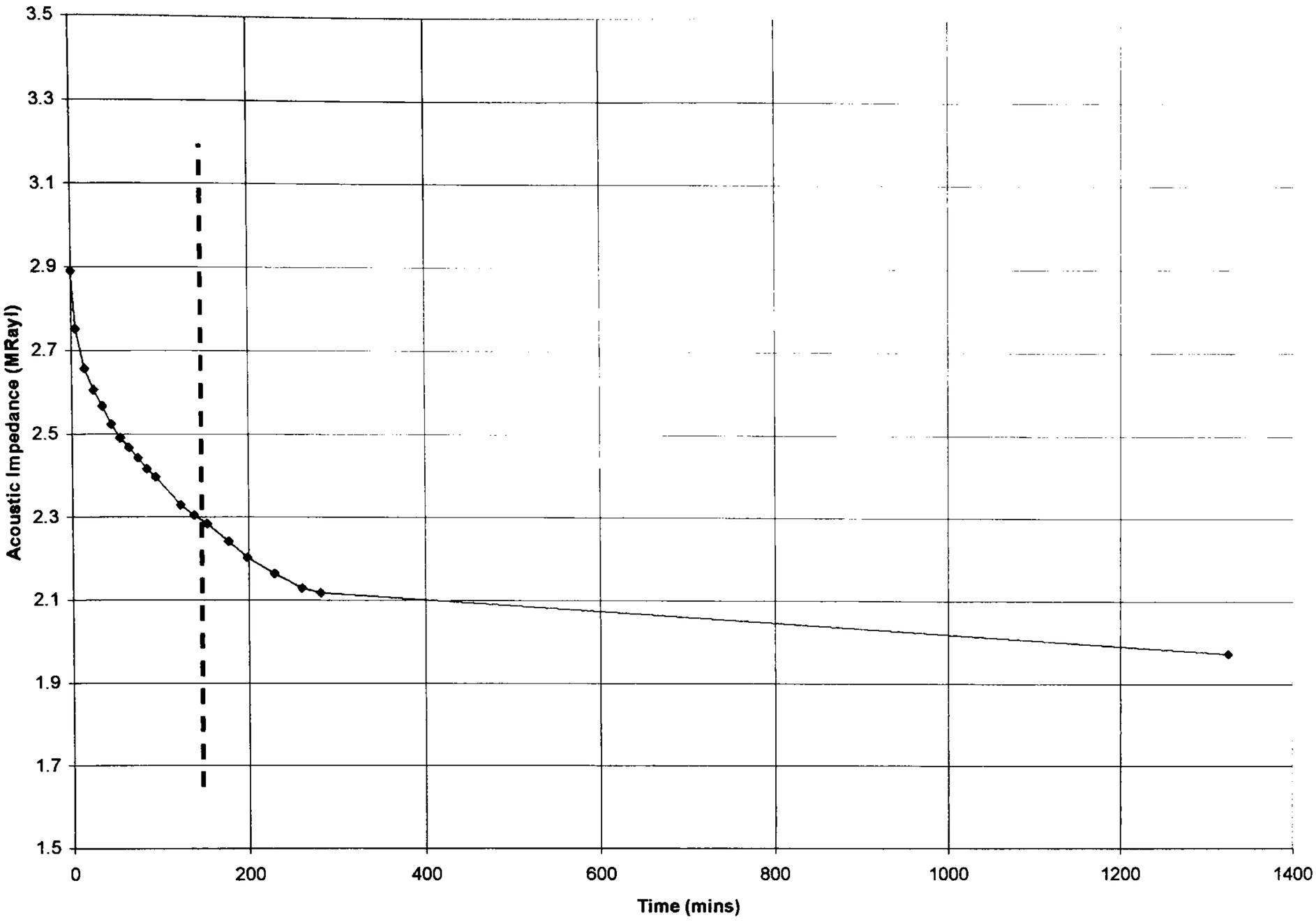

Figure 6.7 Simulated change in acoustic impedance of the water absorbing region of a hydrating hydrophilic polymer according to Maffezzoli's assumption of a linear relationship with water sorption. Dotted line signifies the time at which pulse echo analysis indicated the disappearance of the glassy region.

Maffezzoli writes that the contribution of the additional interfaces to the measured attenuation may be calculated based on their reflection coefficients determined from this simulated dynamic acoustic impedance.

$$R_{\text{int}} = R_{rd} + A + B + C \qquad \textbf{Equation 6.3}$$

where,

$$A = (1 - R_{rd})R_{dr} \qquad \textbf{Equation 6.4}$$

$$B = (1 - R_{rd} - A)R_{rd} \qquad \textbf{Equation 6.5}$$

$$C = (1 - R_{rd} - A - B)R_{dr} \qquad \textbf{Equation 6.6}$$

where R_{int} is the reflection coefficient from the internal interfaces for a pulse echo measurement, R_{rd} is the reflection coefficient from the hydrating region to the dry region and R_{dr} is the reflection coefficient from the dry to the hydrating region respectively.

However, the simpler approach explained by Smith [1999] may be adopted for this. Smith uses Equation 6.7 for the calculation of transmission loss due to double through transmission through a sample in an immersion tank. This represents the ultrasound beam crossing the interface between

water and the sample four times. By substituting the dynamic acoustic impedance values of the water absorbing region calculated by Equation 6.2 and that of the dry region into Equation 6.7, losses due to internal reflection will be calculated with respect to immersion time.

$$Loss = 40\log_{10}\left(\frac{4Z_{rd}Z_d}{(Z_{rd}+Z_d)^2}\right) \qquad \textbf{Equation 6.7}$$

However, after a period, the glassy region disappears. This has been confirmed by pulse echo analysis, see Figure 6.1 D. When this condition is achieved, the contribution of reflection to the measured attenuation should be eliminated. Application of Equation 6.7 to the hydration data achieved in this study results in a simulated attenuation contribution that is presented in Figure 6.8.

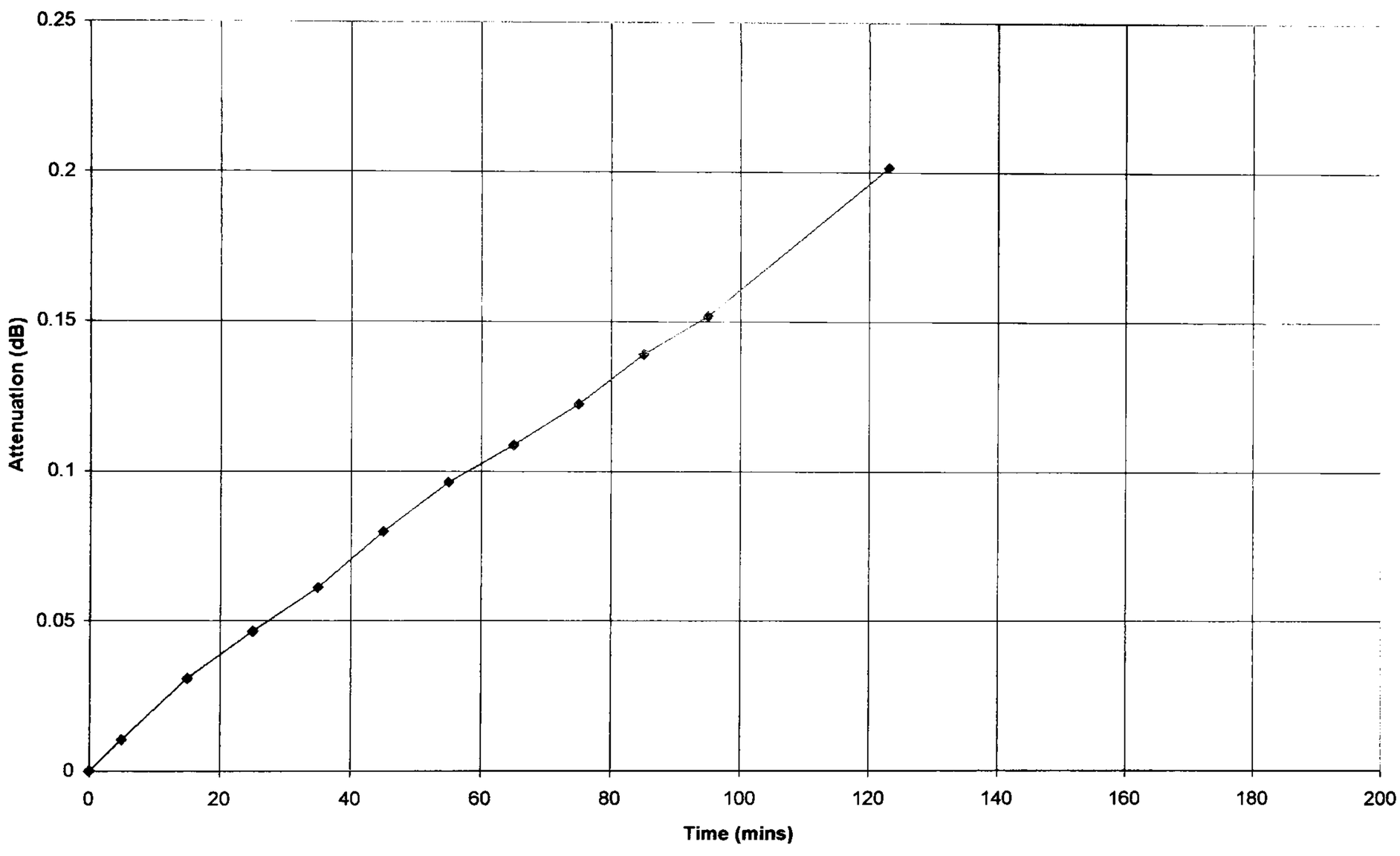

Figure 6.8 Simulated contribution of internal reflection to the measured attenuation of a hydrating hydrophilic polymer.

Removal of this contribution to attenuation from the data shown in Figure 6.6 modifies the overall attenuation to that displayed in Figure 6.9. It is quite obvious that the impact is minimal, making no obvious effect; Figure 6.10 shows the attenuation both prior and after correction for reflection at 5MHz for comparison. Therefore, it is concluded that the contribution of internal reflection from the interfaces between rubbery and glassy regions plays only a minor role in the overall material attenuation during hydration. In fact, so minor is its effect, that even if the simulated dynamic acoustic impedance of the hydrating region of the hydrophilic polymer deviated greatly from its assumed linear relationship with increasing water content, it could still not account for the phenomenon of firstly rising and then falling attenuation.

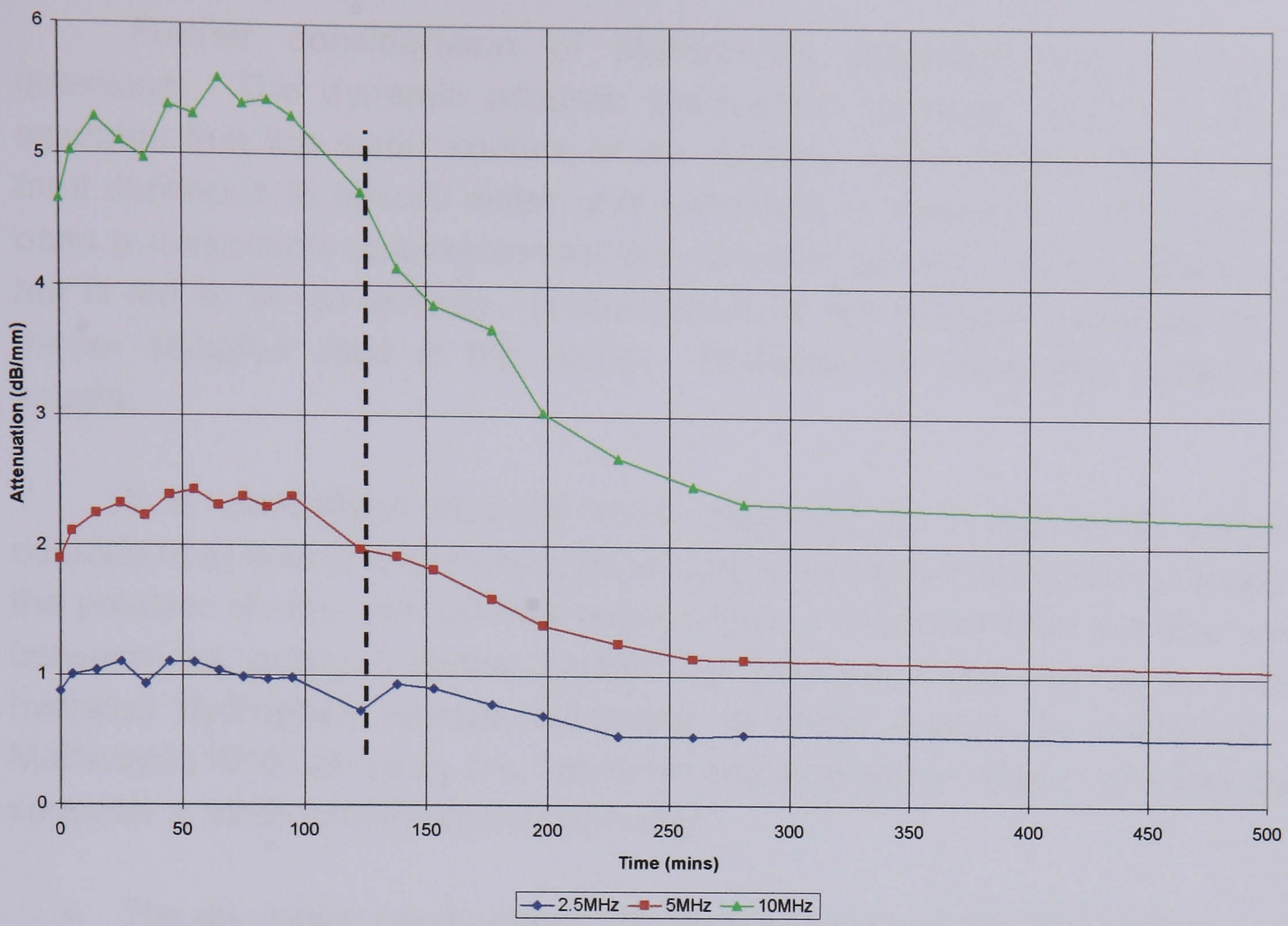

Figure 6.9 Attenuation in a Batch C hydrophilic polymer during hydration, compensated for internal reflections from rubbery-glassy interfaces. Assumes dynamic acoustic impedance for water sorbing region of the polymer, Maffezzolli [1996]. Dotted line signifies the time at which pulse echo analysis indicated the disappearance of the glassy region.

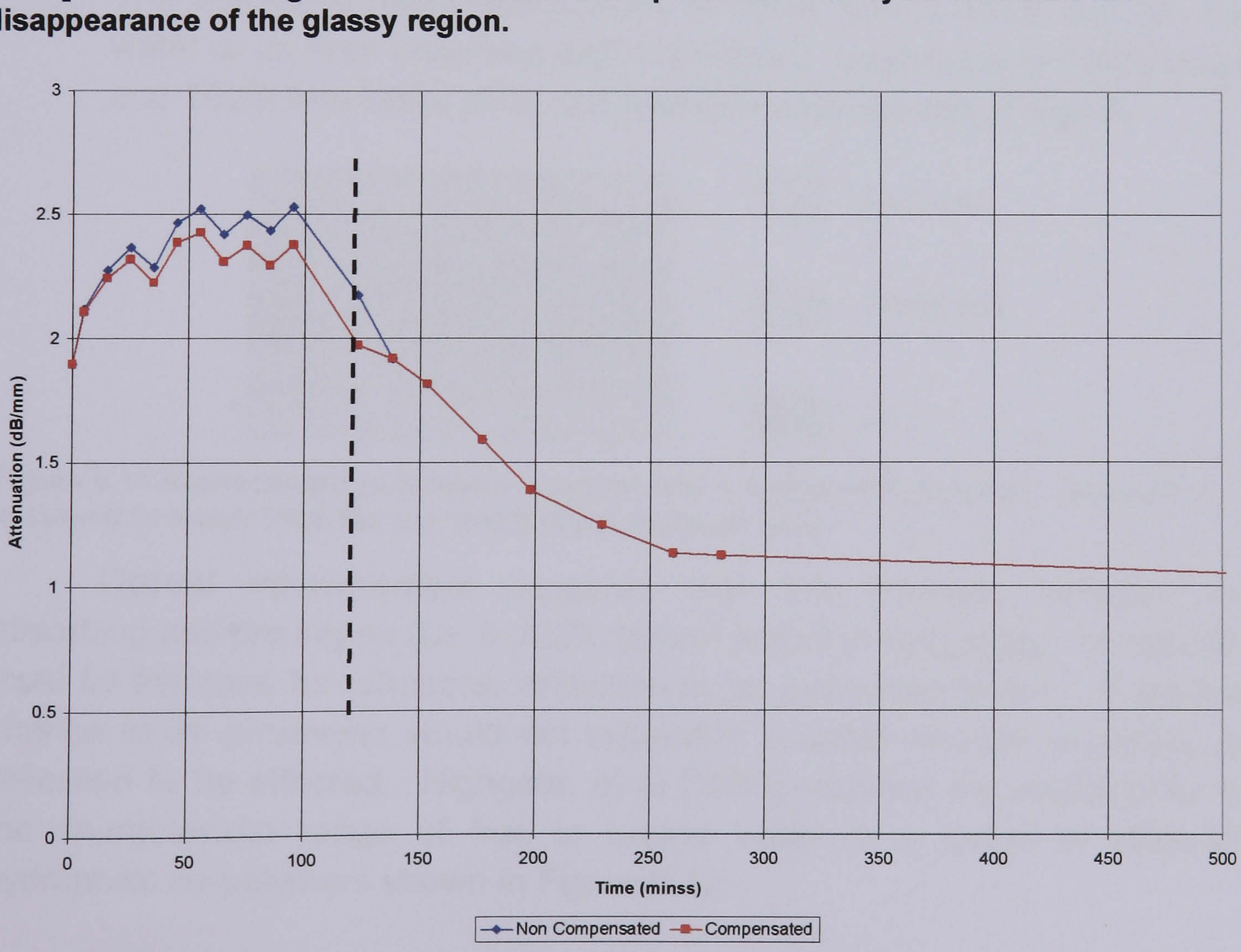

Figure 6.10 Attenuation in a Batch C hydrophilic polymer at 5MHz both prior and after correction for internal reflections. Dotted line indicates the time at which pulse echo analysis indicated the disappearance of the glassy region.

Further consideration of Maffezzoli's approach raises additional questions. The dynamic acoustic impedance calculated by Equation 6.2 assumes that the water content of the rubbery region behind the hydration front continues to absorb water until saturation is achieved. This may have been a reasonable assumption for the very thin samples used by Maffezzoli, but is felt to be an unlikely representation of the sorption behaviour of the thicker samples used in this study. Therefore an alternative model was sought.

It is understood that the water absorbed by a hydrophilic polymer consists of (i) bound water which penetrates the polymer first and is bonded to the polymer chains, and (ii) free water which is absorbed later into tiny voids between the polymer chains caused by swelling. This results in a part hydrated hydrophilic sample consisting of three regions as described by Maffezzoli [1996] as being dry, saturated and absorbing. Closer consideration suggests a more realistic model whereby:

- The dry region must contain 0% bound water and 0% free water.
- The saturated region in turn must consist of 100% bound water and 100% free water, and
- The absorbing region will consist of 100% bound water and 0% free water at its front (interface with dry region), graduating to 100% bound and 100% free water at its end (interface with saturated region).

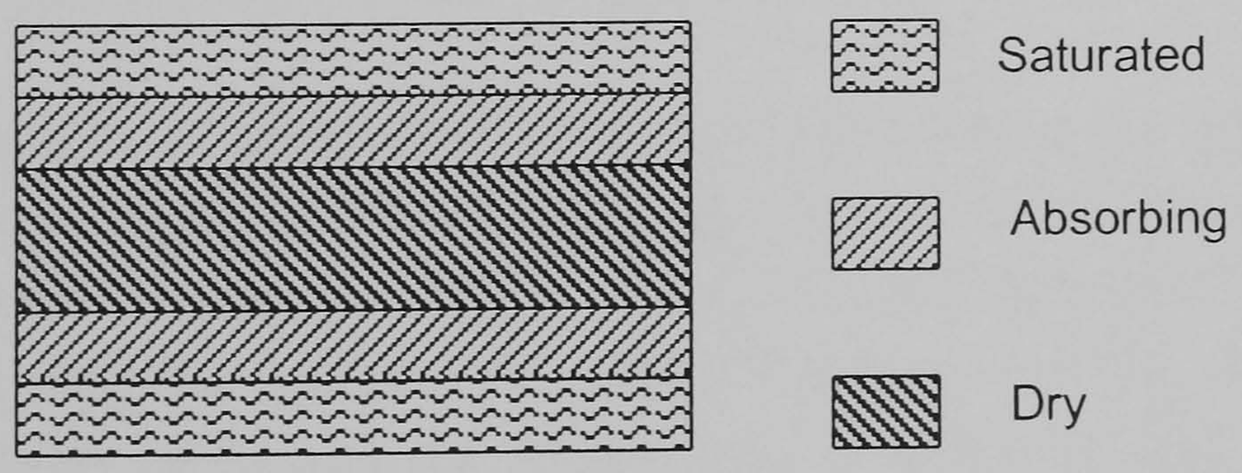

Figure 6.11 Representation of water sorption into a hydrophilic polymer. Sorption is assumed to occur from the top and bottom surfaces only.

Optical measurement suggests that the interface between the absorbing and dry region (i.e. 0-100% bound water) is very sharp. Indeed this must be the case for ultrasonic reflection to be generated from it. A gradual change in its properties would not represent a sharp enough boundary for reflection to be effected. Highgate, et al [1989] reported the relationship for the characteristic range of free to bound water in a range of MMA-VP hydrophilic co-polymers shown in Figure 6.12.

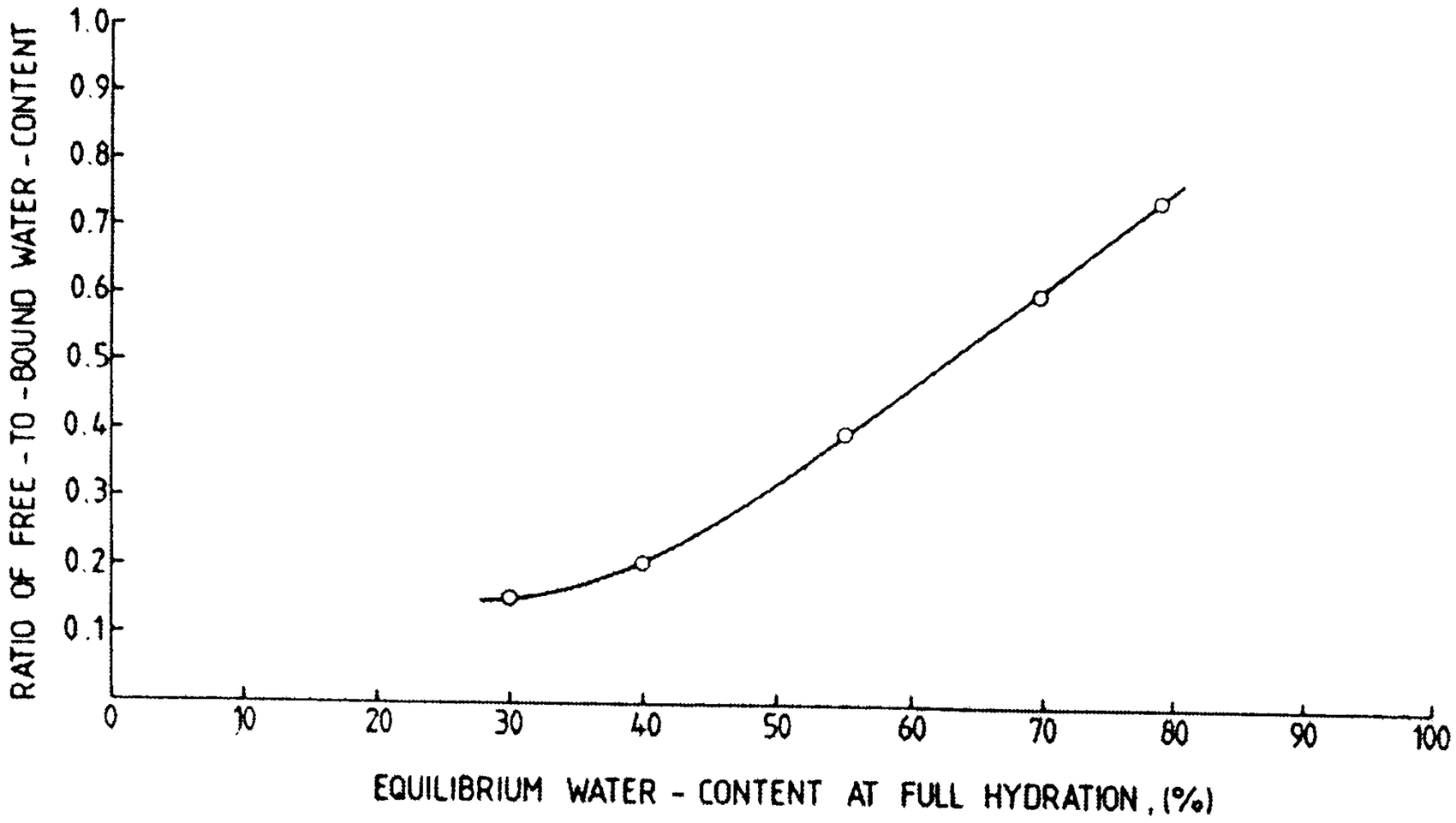

Figure 6.12 Relationship between bound to free water in hydrophilic polymers, Highgate [1989].

This data suggests that a 60% hydrophilic polymer such as the Batch C sample under investigation in this study has a free to bound water ratio of approximately 0.45. Therefore, at saturation, 45% of the water may be assumed to be free and 55% to be bound. Thus it is suggested that the water content at the hydration front is 55% of saturation equating to 33% water content by weight. By plotting the water content of the hydrophilic co-polymers investigated in Chapter 2 against their acoustic impedance, the data may be extrapolated back to a polymer containing approximately 33% water. This reveals an acoustic impedance of approximately 2.237MN s m^{-3}.

Therefore, it is suggested that the contribution of reflection from the rubbery to glass regions to overall attenuation is constant at 0.28dB as determined from Equation 6.7. It is clearly apparent that while this contribution is slightly greater than that imposed by the dynamic acoustic impedance model proposed by Maffezzoli, it still has little bearing on the overall attenuation measured for the hydrophilic polymer during hydration especially in the case of the higher frequency components. Indeed, with higher frequencies demonstrating greater increases in attenuation, the cause of attenuation must be frequency dependent. Reflection from interfaces between different acoustic impedance would have the same effect over all frequencies.

6.2.8 Scattering

With reflection, as one of the three contributors to attenuation considered, attention will now be shifted to scattering as an explanation for the non-linear attenuation behaviour recorded in hydrophilic polymers during

hydration. The initial increase in attenuation may be attributed to the formation of microvoids or crazes in the glassy matrix before transmission to the rubbery state. Early water penetration is considered to be bound water, which will exert a strong osmotic pressure on the glassy region feasibly strong enough to initiate the growth of crazes which in turn may scatter ultrasonic waves resulting in an increase in measured attenuation. Such scattering of ultrasonic waves may be caused by micro-discontinuities of as little of one twentieth of the wavelength [Brown, 1980]. This could explain why the attenuation at higher frequencies undergoes a more severe attenuation increase in the early stages of hydration. If this experiment were to be repeated, a high frequency broadband probe could be used without a delay line attached. This would propagate higher frequency ultrasound into the sample enabling the ultrasonic effects to be explored over a greater frequency range.

It is feasible that the levelling-off of attenuation after the initial rise may be achieved by the formation of a dynamic equilibrium as the rubber-glass interface moves across the sample. Scattering of ultrasonic waves increasing as crazes occur in the glassy matrix, while at the same time, attenuation decreases as more water is absorbed converting the glassy matrix to a rubbery polymer. This cannot be confirmed without examination with higher frequency ultrasound than that available in this study. Maffezzoli, et al [1996] suggested that following initial sorption of water, there would be a time delay before the onset of craze nucleation. This may be attributed to the time delay of attenuation increase, suggesting that scattering is the main contributor to the measured attenuation. If this were the case, one would expect the time delay to attenuation increase to be the same for all thicknesses of hydrophilic polymer of the same equilibrium water content. This was not the case for the tests performed by Maffezzoli.

6.2.9 Absorption

Finally the influence of absorption on the attenuation may be considered. During the transmission of ultrasonic waves, the host material is subjected to alternate compressive and expansive deformations. The response of the material is a function of its viscoelestic properties, characterised by a storage modulus and loss modulus proportional to the energy absorption occurring during the propagation of acoustic waves. While giving consideration to the phenomenon that may influence these moduli, it became apparent that a change of material state such as that observed during glass transition may be responsible.

Glass transition is usually associated with temperature (Tg), and is defined as the temperature at which a material changes from a glassy to a rubbery state. A hydrophilic co-polymer also undergoes a change from a glassy to rubbery state. It may therefore be considered to undergo a glass transition analogue, whereby extra degrees of freedom are attained via a hydraulic rather than temperature effect. This imparts the increase in flexibility observed when it absorbs water.

The acoustic waves travelling across the sample meet two material strata undergoing a glass transition analogue. McCrum, et al [1967] and Van Krevelen [1990] have written that a polymer undergoing a thermal glass transition peaks in the loss modulus, dielectric loss and also in the absorption of acoustic waves. Therefore, it is reasonable to suggest that a hydrophilic polymer undergoing a transformation from glassy to rubbery state owing to the absorption of water (glass transition analogue) may be responsible for absorption of ultrasound, imparting a large effect on the measured attenuation.

As discussed with respect to the contribution of scattering from crazes, absorption from the regions within the hydrating polymer also fit the peculiar attenuation trend. Initial water sorption and creation of two glass transition analogue regions close to the surfaces may cause the initial rise in attenuation seen after the sample is introduced to water. As more water is absorbed the glass transition analogue regions reach equilibrium thickness, causing a levelling off of attenuation. The attenuation remains constant as the two transition regions move from the surfaces towards the centre of the sample. Once the two fronts meet, the sample becomes a continuous rubbery medium and the attenuation begins to drop rapidly. Maffezzoli had noted a peak in attenuation during water sorption in very thin samples of HEMA as opposed to a levelling off of attenuation observed in these experiments. It is conceivable that this occurred via a route of (i) the setting up of two glass transition analogue regions causing the onset of an attenuation increase, (ii) the meeting of the two transition regions before they were able to grow to their equilibrium thickness. This would result in the disappearance of the glassy region and the onset of attenuation reduction.

All considered, it is not possible to categorically state which component of bulk attenuation; reflection, scatter or absorption is capable of explaining the overall attenuation behaviour of hydrophilic polymers during water sorption. Where there is genuine overlap with work undertaken by Maffezzoli who used ultrasound as a tool to investigate polymer-solvent systems, there is good agreement of results, suggesting that HEMA and MMA-VP copolymers behave in a similar way. Of the three contenders, the effect of reflection has

been well considered and reasonably accurately estimated through the exploration of two models. Although it does influence bulk attenuation, its influence is small and can be ruled out as a reason for attenuation increase during the onset of water sorption. The effects of scattering and absorption have been considered. However, there is no evidence from the literature that crazes are formed ahead of the hydration front from osmotic pressure causing scattering – this is purely logical speculation. In fact, owing to the low notch tare strength of hydrated hydrophilic polymers, the presence of crazes might be expected to result in breakage. As this is not observed in practice, the attenuation increases during hydration are felt more likely to result from the glass transition analogue. With both scattering and absorption coefficients influencing the bulk attenuation simultaneously, the two effects cannot be readily distinguished from each other. One thing is for certain, when a hydrophilic polymer undergoing hydration contains both rubbery and glassy regions simultaneously, an increase in bulk attenuation is observed. With the contribution of reflection accounted for, scattering or absorption (or both) from the rubbery glassy interfaces must explain the phenomenon.

6.3 Influence of Dehydration on Attenuation

It may be observed that when hydrophilic polymers are left out of contact with water, they dehydrate and reduce in size. Of particular interest is that distinct glassy and rubbery regions do not appear to form, the whole material appearing to remain homogenous but suffering a loss in flexibility. Pulse echo analysis during part dehydration stages has not shown the presence of internal interfaces such as those discovered during hydration caused by the interfaces between rubbery and glassy regions.

In order to investigate this effect on attenuation, three dry hydrophilic polymer samples from Batch C were sealed in separate watertight containers with sufficient water to allow them to reach 25, 50, and 75% saturation. For the Batch C hydrophilic polymer used, this translated to 15, 30 and 45 % water by wet weight. A fourth was placed in a water bath and allowed to reach saturation. A fifth was kept completely dry. The samples were left for two days to enable them to reach equilibrium. At this time, each was weighed to determine the exact amount of water each contained. In each case, all water in the sealed containers appeared to have been absorbed by the polymers. Allowing the polymers to equilibrate in this way achieved a situation whereby the continued absorption of water had been limited. The water present in the structure spread itself evenly throughout the polymer sample. This simulated a sample in a partially dehydrated stage.

Equally, the sample may be said to be similar to a partially hydrated sample only without the interfaces usually associated with the presence of rubbery and glassy regions, demonstrating a continuous water content through the section instead. Table 6.1 shows the final water contents after equilibrium had been reached.

Target Water Content (wt%)	Thickness (mm)	Weight (g)	Actual Water Content (wt%)
0.00	4.45	0.71	0.00
15.00	5.04	0.90	21.22
30.00	5.34	1.10	35.55
45.00	5.75	1.34	47.09
60.00	6.26	1.69	58.05

Table 6.1 Water content of simulated part dehydrated hydrophilic polymers from Batch C.

6.3.1 Results and Discussion

A TMP3 probe was used in broadband mode without its delay line to obtain frequency spectra for all five samples. Techniques already described in Chapter 2 were used to convert the frequency spectra into attenuation plots. These are presented in Figure 6.13 and Figure 6.14 respectively.

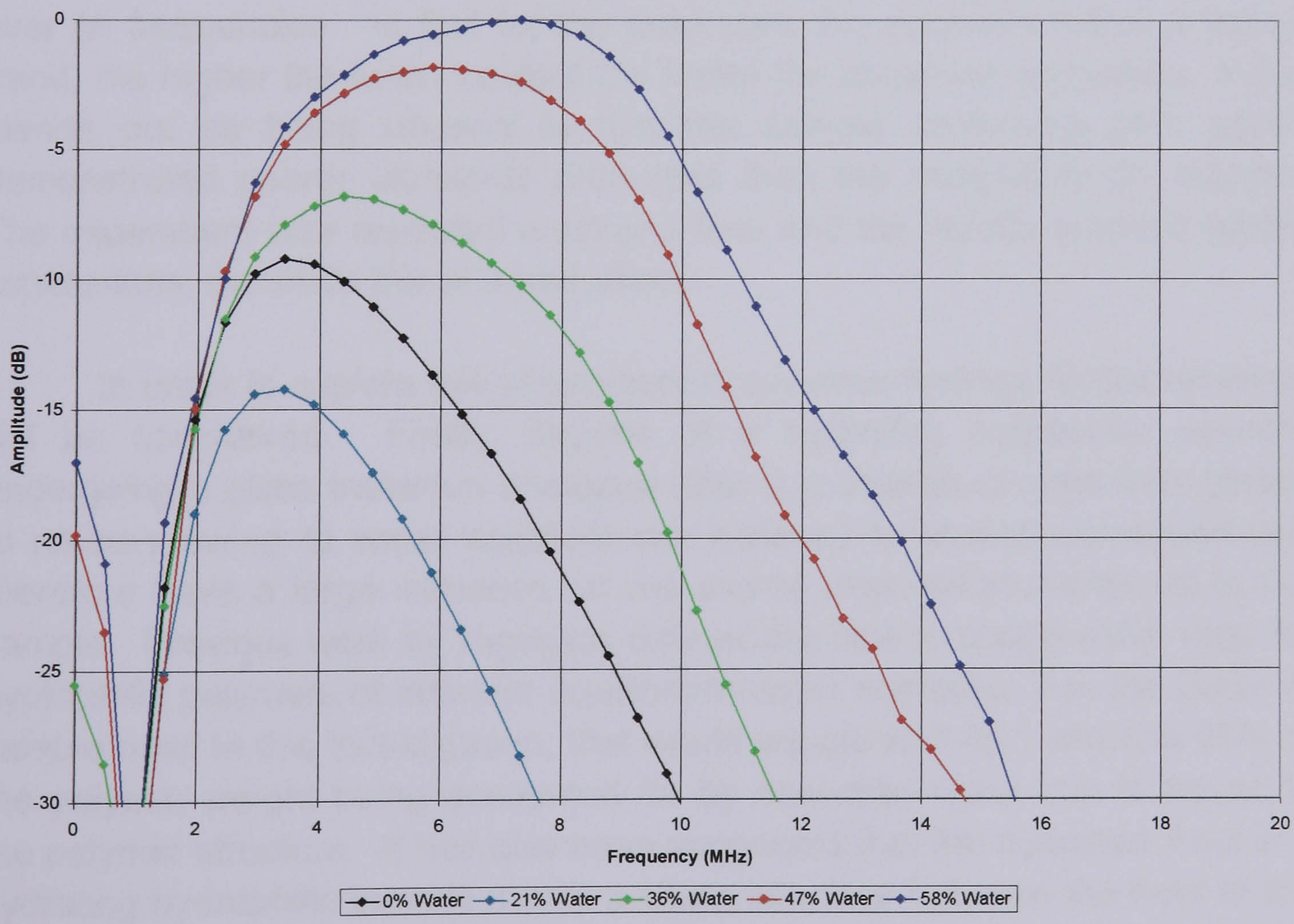

Figure 6.13 Frequency spectra through five Batch C hydrophilic polymers. Each is at equilibrium but containing different quantities of water. The legend represents the actual water content.

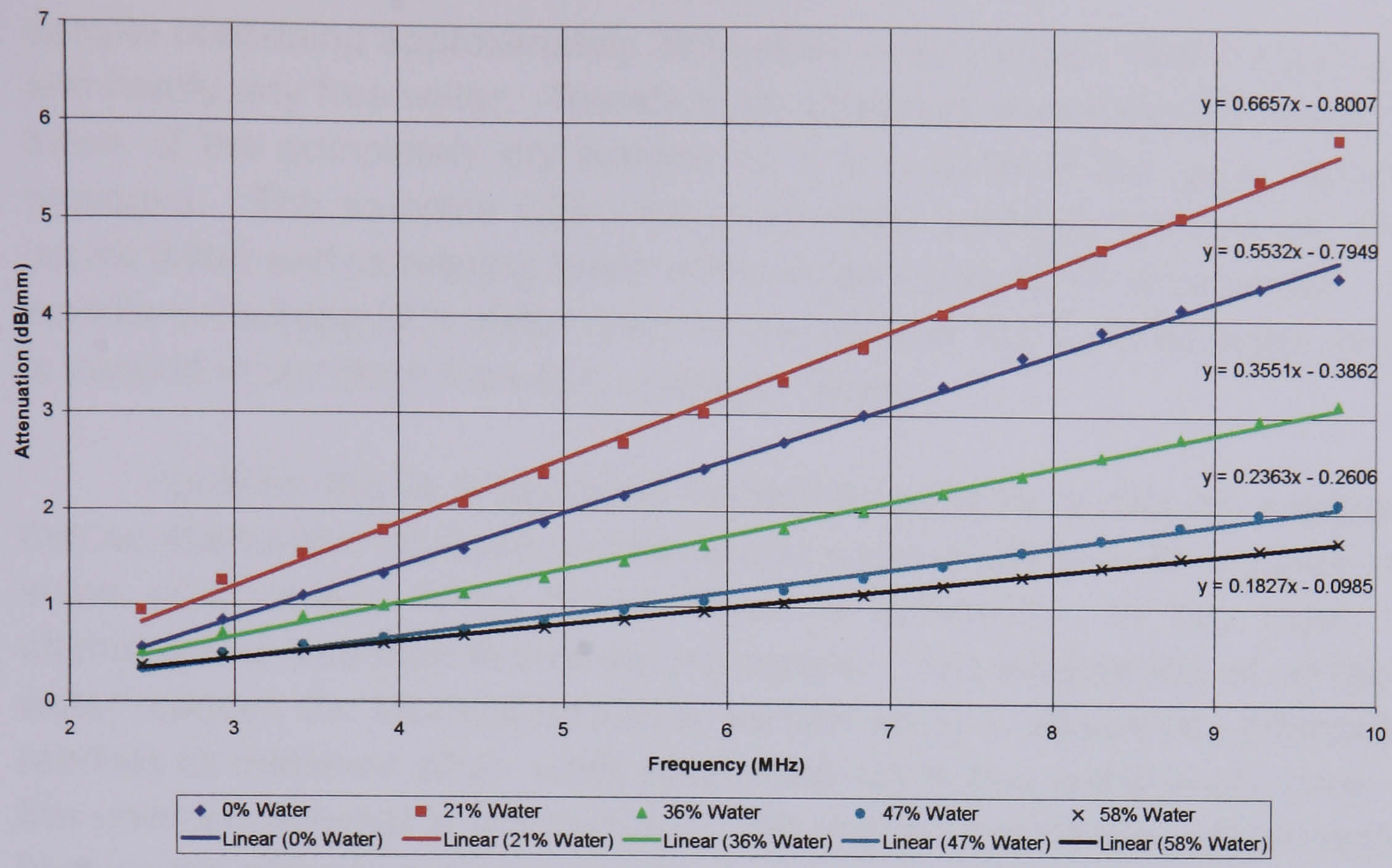

Figure 6.14 Attenuation plots of five Batch C hydrophilic polymers. Each is at equilibrium but containing different quantities of water. The legend represents the actual water content.

As expected, the saturated sample demonstrated the highest amplitude, peak frequency and bandwidth together with the lowest attenuation over all frequencies. In fact for the most part, the polymers follow a logical trend, the higher the water content the better the ultrasonic properties. What stands out as being unusual is that the sample containing 21% water, demonstrated poorer ultrasonic properties than the completely dry sample. The experiment was repeated a second time and the results reached similar conclusions, therefore this is a real effect.

In order to explain this phenomenon, previous findings of this research will be considered. Firstly, regions of a hydrating hydrophilic polymer undergoing a glass transition analogue (that is a change of state from glassy to rubbery owing to water sorption) are believed to absorb ultrasound and therefore have a large influence on the overall attenuation measured in the sample. Previous work by Highgate defined the free to bound water ratio for hydrophilic polymers of different equilibrium water contents. For the Batch C sample used in this investigation, that would equate to 0.45:1 which is 33% of the polymer weight being accounted for by absorbed water that is bound to the polymer structure. It has also been suggested that the hydration front in a hydrating hydrophilic sample marks a sharp interface between the front of the absorbing region containing 100% bound water and 0% free water (33% by weight) and 0% water in the dry region. This would involve a glass transition analogue occurring at a water content somewhere below 33%. If this theory is now applied to the homogeneous partially hydrated/dehydrated samples, the

sample containing approximately 36% water must contain 100% bound water and hardly any free water. Therefore, its ultrasonic properties are better than those of the completely dry sample as it is outside of the glass transition analogue. The samples with increasing water contents still contain 100% bound water and increasing levels of free water up to 100% at saturation. The sample containing 21% water does not yet contain 100% bound water and so is trapped in the glass transition analogue 'phase'.

Applying this to a hydrating hydrophilic polymer, it may be suggested that an attenuation increase is observed as water is added to the polymer until some point where 100% bound water is achieved. In this state, the attenuation is less than that of the dry sample. The introduction of additional water reduces the attenuation further as free water is absorbed. Attenuation reaches its minimum when 100% bound and 100% free water is achieved. At this point the polymer is at saturation. This implies that what has been termed here as the glass transition analogue may occur at different water contents in hydrophilic polymers of different equilibrium water contents.

6.4 Shear Wave Propagation

Solid materials are known to support the passage of shear waves. However, liquids do not. This is because liquids have either no or little shear strength. It is therefore interesting to raise the question of the potential for shear wave transmission in hydrated hydrophilic polymers. As these materials are solids yet consisting mainly of water, it is possible to conceive an argument for both scenarios; the ability to support (i) both compression and shear waves, and (ii) compression waves only.

In order to assess this experimentally, there was a need to establish a means for the theoretical propagation of a shear wave in a hydrated hydrophilic polymer. The generation of a shear wave from a conventional ultrasonic compression wave probe was desirable as this could be achieved with existing equipment. It would however necessitate introducing a compression wave into the hydrophilic sample surface at an oblique angle. Mode conversion would generate a refracted shear wave in the sample. However, it must be remembered that a compression wave may also be generated, making signal interpretation very difficult. To ensure the propagation of only the shear wave in the sample, the wedge material must have an ultrasonic propagation velocity less than that of the sample. In addition, the angle of incidence must be between the first and second critical angles. Either a second ultrasonic probe appropriately placed on the opposite side of the sample or a carefully positioned reflector within the sample (such

as a saw cut) to reflect the shear wave back to the transmitting probe would be required for detection and confirmation of shear wave propagation.

Three methods of generating shear waves in a hydrated hydrophilic polymer were considered, the first two utilising mode conversion and the third a development of a specialised ultrasonic probe.

6.4.1 Shear Wave Generation via Immersion

The first method was immersion based as it afforded the ability to easily change the angle of incidence (the angle of the probe in relation to the sample). Moreover, the velocity of a compression wave in water is slower than that in the hydrophilic samples investigated in this research, which is not the case for all suitable solid materials. Therefore, it is possible to achieve a situation whereby the refracted compression wave is totally internally reflected. The incidence angle at which this condition is satisfied is known as the first critical angle and results in the theoretical propagation of a single shear wave in the sample.

Obviously, the velocity of shear waves in hydrated hydrophilic polymers is not known. Therefore, the expected angle of refraction in the sample cannot be determined from the angle of incidence. However, the velocity of compression waves in the sample is known to be 1679ms^{-1} (Batch C hydrated hydrophilic polymer). This permitted Snell's Law to be used, calculating the first critical angle to be 36.6° in water. Therefore, an angle of incidence greater than 36.6°, should generate a refracted shear wave in the sample.

Rule of thumb states that in a given material, the shear wave velocity is normally half that of the compression wave velocity. This assumption would make the shear wave velocity in a hydrated Batch C hydrophilic polymer 840ms^{-1}. As this velocity is less than the compression velocity in water, a second critical angle cannot be achieved using the immersion technique. It also suggests that an angle of incidence of 57.4° would be required in order to generate a shear wave of 45° in the sample.

6.4.2 Shear Wave Generation via Internal Reflection

An alternative method considered for the generation of shear waves in hydrated hydrophilic polymers involves internal reflection. Shaping of a sample (most likely by machining when in its dry condition) to incorporate an angled face onto which a compression wave beam could be propagated

would set up a situation where mode conversion would be expected to occur. Again, as the shear velocity is unknown, its potential angle of reflection cannot be calculated, but instead may be estimated. Assuming a theoretical shear wave velocity of 840ms^{-1} in the sample, a compression wave beam incident on a surface inclined at 45° would theoretically generate a shear wave at 20°. Figure 6.15 illustrates a possible experimental set up of a single compression probe coupled to a large block of hydrophilic polymer. A second probe would be used to detect internally reflected waves. As shear wave velocity is slower than compression wave velocity, region A represents the theoretical detection point for shear waves and region B for compression waves.

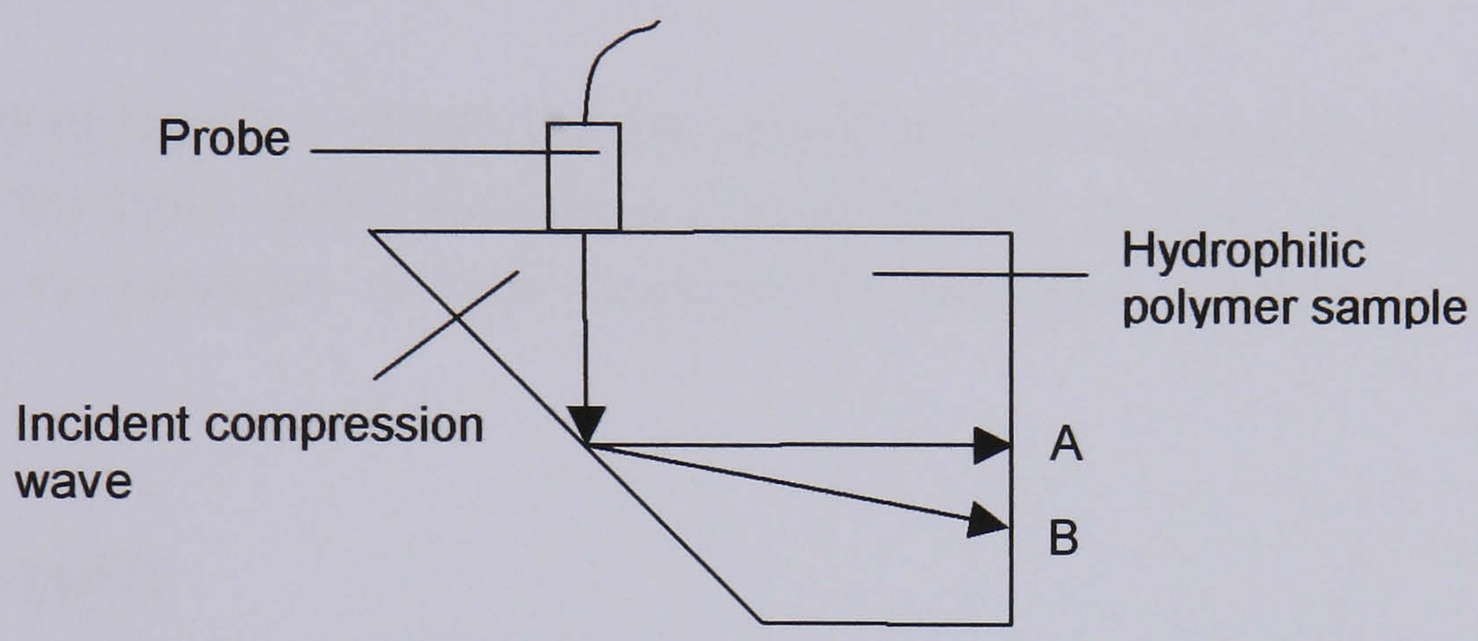

Figure 6.15 Possible experimental set up for the generation of shear waves in a solid material using a single compression wave ultrasonic probe. Regions A and B are detection regions for both shear and compression waves respectively.

6.4.3 Zero Degree Shear Wave Probe

The final method for shear wave generation in the sample involved the development of a dedicated ultrasonic probe. Conventional shear wave probes generate a refracted shear wave in the sample, in ways similar to that described in the immersion technique, only with Perspex being used as the wedge material rather than water. As a result, the shear waves are propagated into the sample at an angle. In order to generate shear waves in the sample, normal to the surface, a special transducer crystal must be used that distorts in a shear rather than thickness (compression) mode when placed within an electric field.

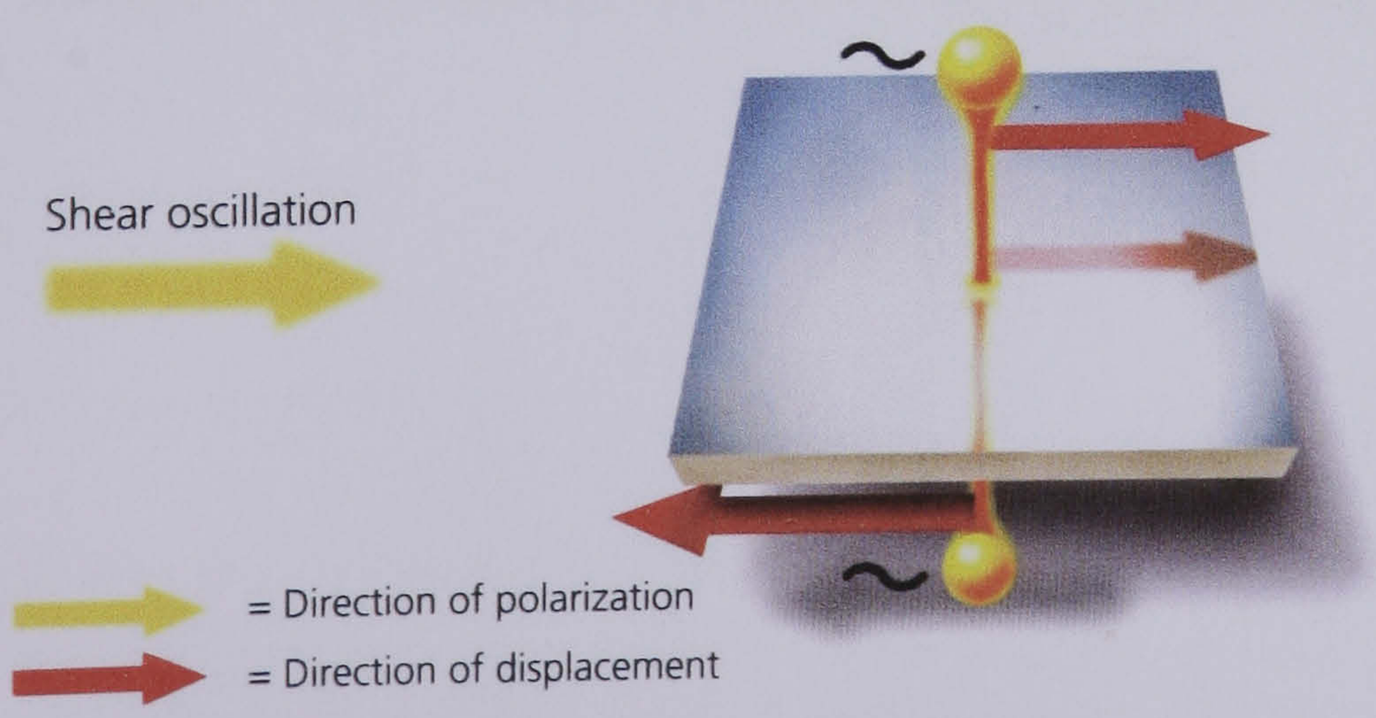

Figure 6.16 Schematic of transducer crystals vibrating in shear mode.

Manufacture of a probe containing such a crystal in place of the conventional type, enables a shear wave beam to be generated directly in the sample. Such devices require special consideration be given to the composition of the damping slug to so as not to excessively damp the resultant sound beam. Similarly, coupling into any test piece cannot be achieved via conventional couplants. This is because they (like water) do not support shear waves due to consisting largely of either water or oil. Viscous substances including honey and treacle are most commonly used in their place. As yet, no commercially available couplant is available for this application.

Use of a probe of this nature would enable hydrophilic polymers to be assessed for their ability to support shear waves quickly and easily, without the need to produce a large hydrophilic polymer sample or complicated geometry.

6.4.4 Results

The experimental methods involving attempts to generate shear waves via the immersion and internal reflection methods described above were not considered practical as in both cases, large hydrophilic polymer samples were required, which were not available at the time. After discussion with the sponsors, it was considered most beneficial if the third route was taken, the development of a zero degree shear wave probe. This offered the desirable spin off of a new range of ultrasonic probes for the sponsors, should the development be successful.

10mm diameter, 4MHz shear polarised piezoelectric crystals were used in manufacturing the device. These were commissioned by the sponsors from Morgan Electro Ceramics. Three prototypes were developed using different levels of back damping. The most efficient was used for the evaluation of the hydrophilic sample. A certificate of the probe (ZS5-10) may be seen In Appendix D.

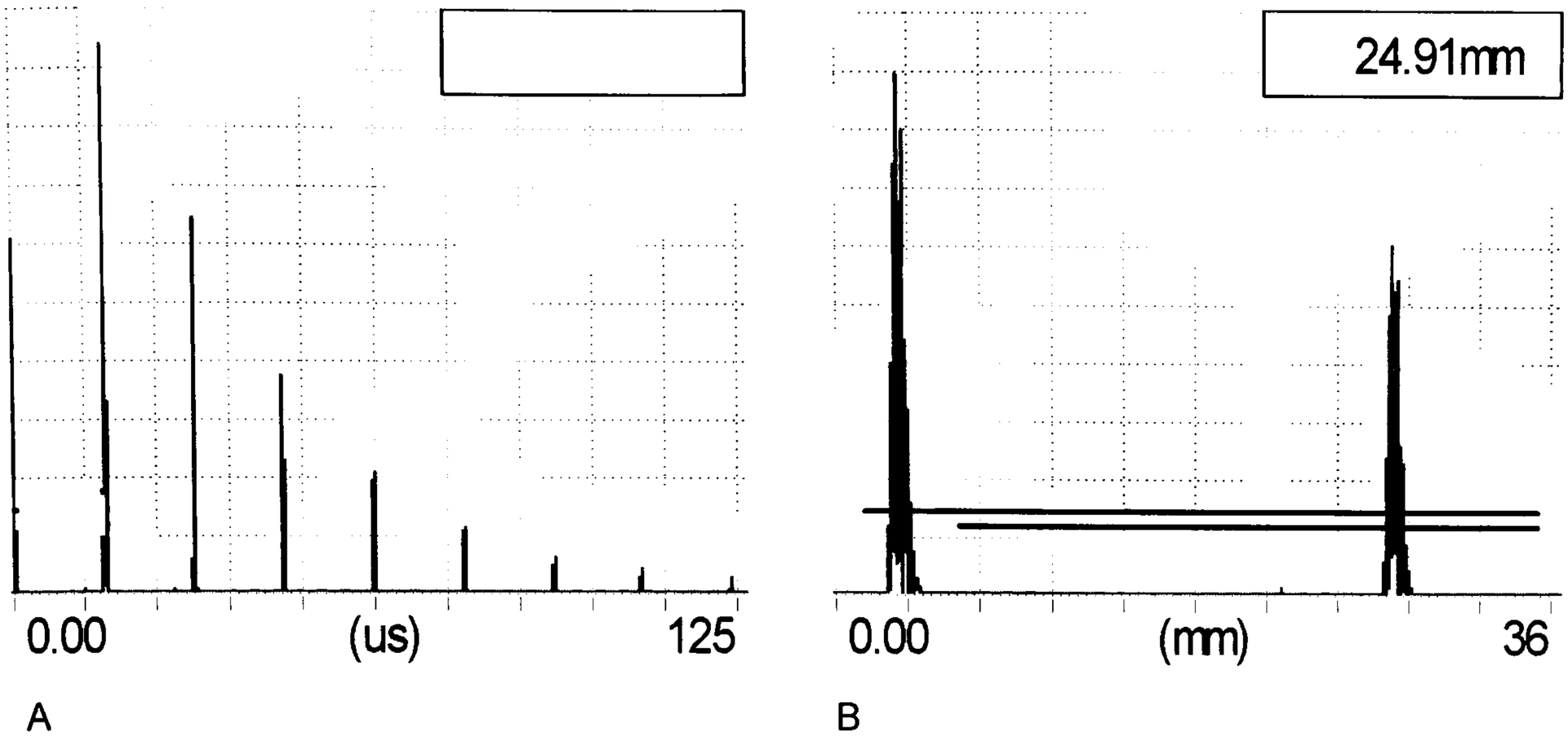

Figure 6.17 Example of shear waves propagated in steel. A) Multiple echoes. B) Distance measurement between two repeat echoes.

Honey was successfully used as a couplant when testing the probe on a steel component. Clear back wall echoes were detected, their positions along the base line of the flaw detector suggesting an ultrasonic travel time of 3230ms^{-1} (the text book velocity for shear waves in steel [Krautkramer, 1983]). The same honey was used, to couple the probe to the hydrophilic polymer sample. However, no back wall echo was observed when used in pulse echo mode, suggesting that the sample does not support shear waves. Further attempts to obtain a back wall echo were made by increasing the gain on the ultrasonic flaw detector to maximum and utilising lower frequency filterbands, to no avail.

Finally, an earlier prototype probe was used in tandem in a through transmission arrangement. In this way the sound beam would only pass through the sample thickness once, and should therefore be stronger in amplitude. However, still no signal was detected. In view of this it is concluded that hydrated hydrophilic samples of approximately 60% water content do not support the passage of shear waves. This may be used as a strong case to suggest that all hydrated hydrophilic samples support only compression waves. However, this would have to be confirmed by practical investigation with hydrophilic polymers of lower equilibrium water contents. There may be a threshold water content below which shear waves are supported. This would be a good research topic for future investigations into hydrophilic polymers.

This may be considered a positive outcome for the use of hydrophilic polymers in ultrasonic NDT. Often very complex wedge designs are used in angle probes to dissipate reverberated ultrasound from both shear and compression waves reflected from the shoe – test piece interface. A hydrophilic polymer used in place of Perspex as a wedge in an angle probe,

for example, would generate a more predictable reverberation profile and making dissipation easier and more controllable.

6.5 Conclusions

The influence of incomplete hydration on the ultrasound velocity and attenuation has been explored for a Batch C hydrophilic polymer. It was found that:

- The progression of hydration fronts may be monitored with pulse echo ultrasound.

- The ultrasonic velocity tends to decrease with increasing water sorption.

- Attenuation increases with increased water sorption, levels off as hydration continues, until the glassy region disappears, at which point it falls rapidly.

- The transition from glassy to rubbery state is believed to account for the majority of initial attenuation increase on water sorption.

The effect of dehydration on ultrasonic attenuation was investigated for a Batch C hydrophilic polymer. This was achieved by allowing polymers to equilibrate at part saturation levels in a sealed system. It was shown that:

- The sample having absorbed 21% water (i.e. approximately 25% saturation) was measured as having a greater attenuation than the sample containing 0% water.

- Other than this exception, the greater the water content, the lower the attenuation.

A Batch C hydrophilic polymer showed no sign of supporting shear wave propagation.

Chapter 7: Solid Couplant Application Design

7.1 Design Engineering

At this stage in the research project, hydrophilic polymers have been evaluated with respect to their application as novel solid contact ultrasonic couplant. In so doing a number of material properties key to their performance in a practical environment have been investigated. There is no evidence to suggest that hydrophilic polymers cannot be successfully employed as part of a novel ultrasonic probe for the inspection of materials and structures. Moreover, their measured ultrasonic performance has proven to be particularly attractive for such application.

Conditions are suitable for use of hydrophilic polymers in both manual and automated ultrasonic NDT. The simplest design might be to attach a disk of hydrophilic polymer to the tip of a conventional contact probe. This would be well suited for manual single-point applications such as thickness metering. However, a device capable of being scanned over a test piece, taking multi-point or continuous readings would be much more useful, addressing the limitations of current ultrasonic scanning methods discussed in Section 3.1.

At this stage it is worth reviewing the basic considerations for the design criteria of the novel prototype ultrasonic inspection device:

- Hydrophilic polymers are relatively weak materials.
- There are economic limitations to the maximum manufacture size.
- They must remain hydrated to operate most effectively.
- They shrink on dehydration.
- They are to be used to transmit and receive ultrasound into other materials.
- They will be in contact with and moved along the surface of other materials.

With respect to these considerations, a wheel probe design offers the most appropriate solution, whereby the hydrophilic polymer makes up the tyre. In this way, direct contact can be made with the test piece by means of rolling contact, minimising potentially harmful friction and scrubbing effects.

The issue of maintaining hydration of the hydrophilic polymer during use raised a number of design questions. Indeed, it was anticipated that this requirement would play a major role in the final design of the device.

7.2 Wheel Probe Design Logic

In designing the prototype wheel probe there were three main factors to consider, the practical ultrasonic physics, the mechanical and hydraulic properties of the hydrophilic polymer, and the mechanical assembly of all the required components. In all of these categories, design decisions were made with an appreciation of the environment in which the device is ultimately to be operated. The sponsors provided valuable assistance in this respect.

7.2.1 Ultrasonic Considerations

The principle design constraints were determined by analysis of different competing designs. This was a difficult process as a number of trade-offs existed between desirable ultrasonic outcomes. The ultimate performance of the device will largely be influenced by signal amplitude, frequency and ease of interpretation. These factors are discussed in the following sections in detail.

7.2.1.1 The Influence of Interfaces

It is understood that an ultrasonic beam incident on an interface between two dissimilar materials will be, at least partly, reflected. Therefore, the smaller the number of interfaces an ultrasonic beam must traverse inside a probe, the better. Similarly the lower the acoustic impedance mismatch between the two materials making up the interface, the better. The conventional wheel probes developed and manufactured by the sponsor have five internal interfaces between quite dissimilar materials, crystal-aluminium, aluminium-oil, oil-Perspex, Perspex-rubber and rubber-test piece. This is a very inefficient arrangement resulting in nearly 8dB loss in amplitude owing to internal interface reflection alone.

An important design objective was therefore to reduce the number of internal interfaces in the prototype. Two main approaches were used, both offering the potential for substantially less internal reflection than those currently under commercial manufacture. The first was an arrangement whereby the hydrophilic tyre would make direct contact with the probe and the

test piece. In this way only two interfaces would be present, probe-tyre and tyre-test piece. The second was an arrangement whereby the body of the probe would be filled with a coupling fluid (e.g. water), coupling the sound between the probe and inside of the tyre. In this scenario three interfaces would be encountered, probe-coupling fluid, coupling fluid-tyre, and tyre-test piece.

If considering signal loss due to reflection alone, the former design option was expected to be most efficient. The loss due to transmission from the probe crystal to a Batch C hydrophilic polymer is calculated as being 6.4dB due to the large acoustic impedance mismatch between the ceramic transducer crystal and the polymer. Now considering the later design option, the transmission from the same crystal into water may be calculated as being responsible for a 7.3dB drop in signal amplitude. This must be added to the loss due to the water-polymer interface, being a significantly lower 0.06dB, making approximately 7.4dB loss in total. This means that the former design option would be more efficient by approximately 1dB. This difference is very small and may be thought of as not very significant when considered alongside the attenuation imparted by the extra travel distance in the hydrophilic polymer required by the former design.

It is notable that use of a new technology piezocomposite transducer crystal in either of these arrangements would result in a decrease in signal loss owing to reduced acoustic impedance of the crystal. In the examples above, a PZT crystal with an acoustic impedance of 29MN s m^{-3} was assumed. Piezocomposite crystals are now available with acoustic impedance in the range of 3MN s m^{-3}. The difference in practical terms between the two options discussed would be a significant reduction in the reflection losses to 0.6 and 0.2dB respectively from 6.4 and 7.4dB.

7.2.1.2 The Influence of Attenuation

The thinner the tyre, the less attenuation will be imparted onto the ultrasound propagated to the test piece surface. This is beneficial in terms of both reduced frequency downshift and amplitude loss. This argument clearly shows the advantage of a fluid filled wheel as the attenuation in a fluid such as water would be significantly lower than in the hydrophilic polymer. For example, an ultrasonic delay line of 20mm consisting of Batch C hydrophilic polymer would result in a loss in amplitude of 16dB at 5MHz. If, however that delay line consisted of 10mm of water and 10mm of hydrophilic polymer, the loss due to attenuation would be 8.1dB at 5MHz, a significant saving. It must be borne in mind that the thinner the tyre the weaker it is likely to become. In

addition, there are important implications for the ease of signal interpretation resulting from the reduced ultrasonic travel time in a thinner tyre.

7.2.1.3 The Influence of Ultrasonic Travel Time

As the wheel probe is to operate in pulse echo mode, the echoes from the interfaces internal to the probe will influence the signal interpretation and maximum inspection depth into the test piece material. This is exactly the same principle as with single crystal delay line probes. The Perspex delay attached to the front of the probe will produce a repeat echo pattern. Reflections from the test piece appear in-between these repeat echoes. Therefore, the spacing of these echoes determines the maximum thickness of test piece examinable without the presence of delay line echoes which may be easily mistaken for defects or mask important signal characteristics.

Considering a fluid filled wheel probe, two sets of repeat echoes will be generated. The first will result from the water path between the probe and the inner surface of the tyre and the second from reverberations within the tyre itself. Therefore, the most efficient arrangement would involve a design which would cause both sets of repeat echoes to appear at the same time intervals and so ultimately maximising the distance between each repeat echo on the screen of the flaw detector.

To achieve this, the ultrasonic travel time in the water and tyre must be the same. This will be influenced by (i) the physical distance between the probe and the inner surface of the tyre, (ii) the thickness of the tyre, and (iii) the ratio of the ultrasonic velocities of the water and hydrophilic polymer. The ratio is approximately 1.12 in the case of Batch C polymers for example. On this basis a tyre of 10mm thickness would need a water path distance of approximately 11.2mm. This arrangement would generate repeat echoes every 6μs on the time base of the flaw detector. If the test piece is assumed to be steel, this equates to a repeat echo every 35mm beneath the surface, defining the maximum inspection depth as such. In this way a compromise can be made between signal amplitude, maximum inspection depth and mechanical strength. It is noteworthy that the velocity of sound in the test piece will also influence maximum inspection depth.

7.2.1.4 Tyre Footprint

The ultrasound must strike the outer surface of the tyre at a region that is in contact with the test piece, i.e. the footprint, in order for sound to be

transmitted into the test piece. In an effort to reduce the chance of the ultrasound beam interacting with an area of the tyre not in contact with the test piece, which would generate spurious echoes and reduce signal amplitude, it is advantageous to focus the probe. In this way, the beam diameter can be minimised at the tyre-test piece interface. As a happy coincidence, focussed probes are less influenced by misalignment.

7.2.2 Mechanical and Hydraulic Properties

Any design must take into account the special requirements of hydrophilic polymers, namely their relatively low mechanical strength and gradual dehydration behaviour. Hydrophilic polymers are known to be particularly weak in tension having poor notch-tear strength. Also, the thicker the tyre, the more robust it will be, giving itself a degree of support and resistance to puncture.

7.2.2.1 Hydrophilic Polymer Selection

With the benefit of data collected and analysed in this research, it is obvious that there is a direct trade off between mechanical resilience and ultrasonic performance. Polymers with higher water content have the best ultrasonic properties but suffer from poor mechanical strength and vice versa. It is felt that there is an application in ultrasonic inspection for all of the hydrophilic polymers evaluated in this research. However, for the challenging wheel probe approach embarked upon here, Batch C hydrophilic polymer is considered to exhibit the most attractive combination of properties. Containing approximately 60% water by wet weight, Batch C hydrophilic polymers sit centrally among the range materials investigated, demonstrating a good balance between physical flexibility and mechanical longevity. Therefore, for the purposes of this Chapter, referral to hydrophilic polymer will correspond to Batch C material.

7.2.2.2 Mechanical Considerations

The hydrophilic polymer must be kept (as much as is feasible) in compression. This will reduce the chance of potentially harmful tensile forces being set up. Similarly, designs involving delicate features on the tyre must be avoided, as these would be liable to premature damage. It is felt beneficial to have a simple geometrical shape for the tyre to avoid such situations.

7.2.2.3 Additional Considerations

To maintain the flexibility of the device it was decided that the probe should be interchangeable. This enables probes of different frequency and focal length to be evaluated.

The tyre must also be replaceable. This is essential should the tyre be damaged in any way, permitting testing to continue. Also, this approach provides scope for trying out different designs of tyre, for example flat or with different degrees of curvature.

A general point is that the larger the outer diameter of the wheel, the easier it should be for it to pass over undulations in the test piece surface.

A fluid filled wheel carries the possibility of air bubble inclusion. Should this occur it would interfere with operation where testing must be conducted upside-down.

7.3 Designs Philosophies

Key to the design will be the mechanism by which the tyre is kept hydrated. Deviation from full hydration will result in a reduction in ultrasonic performance and may introduce undesirable tensile stresses in the tyre. Alternative modes of continuous hydration have been considered and will be discussed in terms of their individual advantages and disadvantages with respect to four different design philosophies.

7.3.1 External Hydration

In this case, water would be applied to the external surface of the tyre, possibly by way of a drip feed, as the wheel rotates. This would be a simple design. It would rely on the ability of the hydrophilic tyre to absorb water at a rate equal to that at which it is lost during operation, and/or for the presence of water on the external surface to retard dehydration. This method could make very efficient use of the rehydration fluid as its slow release could be tailored to the rate of absorption of the tyre. Despite the obvious appeal to this solution, there is a drawback. An amount of free water will be introduced to the surface of the test piece, which would exclude the device from prolonged use on materials particularly sensitive to water.

Advantages	Disadvantages
No risk of air bubbles	Surface contact is wet
Scope for smaller design	Reduced signal amplitude

Table 7.1 Advantages and disadvantages of external hydration wheel probe design.

7.3.2 Internal Hydration

Hydration of the tyre may be maintained from the inside of the wheel via a supply of water to the body of the device. The success of this solution would hinge on the ability of the hydrophilic polymer to absorb water from its inner surface at a rate equal to that by which it is lost from its outer surface. Previous life tests have suggested that this may not be the case as tyres were seen to get stiff on the outside while the inside remained soft and flexible.

The water inside the tyre could be at low or medium pressure. Increasing the pressure of the water on the inside may encourage faster water absorption. However, this research has not sought to establish evidence of this.

An obvious advantage of this method of hydration maintenance would be the chance to keep the outer surface dry, thus permitting use on materials highly sensitive to water. A point worthy of consideration is that of a temperature gradient in the tyre itself. This could be the result of operation on a hot or cold test piece or simply due to frictional forces generated in the tyre during operation. The latter scenario would tend to make the outer surface warmer than the inner. This may work against rehydration of the tyre from the inside, as diffusion tends to run from hot to cold.

Advantages	Disadvantages
Potential for keeping surface contact dry	Less likely to maintain hydration
Scope for increased signal amplitude	Potential for fluid leakage
	Difficulty in replacing tyre
	Hydration working against diffusion gradient

Table 7.2 Advantages and disadvantages of internal hydration wheel probe design.

7.3.3 Composite

This method offers the chance to combine both internal and external hydration methods to potentially accelerate the rate of absorption (or prevent dehydration) by increasing the surface area of the polymer in contact with the rehydrating fluid. Although this again results in some free water on the outside of the tyre, it is logically the most likely method of maintaining hydration which in turn offers the scope for extended operational time. It

would be feasible to deactivate the external hydration supply in situations were free water cannot be tolerated.

Advantages	Disadvantages
Improved chance of full hydration	Potential for fluid leakage
Scope for increased signal amplitude	Difficulty in replacing tyre
Contact may be wet or dry	

Table 7.3 Advantages and disadvantages of combining both internal and external hydration.

7.3.4 Sacrificial

This approach would not require the application of any free water, therefore permitting use on water sensitive structures. The tyre would simply be run until it either destroys itself or degrades to an extent that it is no longer useful. At that point the old tyre would be discarded and a new one fitted. However, it is anticipated that a device operating on this principle would suffer from a significantly sorter life than the others discussed. There are also concerns over the potential for use of the tyre continuing beyond acceptable limits, encountering significant change in effective performance as an ultrasonic couplant.

Advantages	Disadvantages
Polymer contact dry	Short life
	Degrading ultrasonic properties
	Expensive running costs

Table 7.4 Advantages and disadvantages of applying no free water to the wheel probe tyre.

7.3.5 Summary of Design Considerations

The chosen design of the device takes the form of a wheel, the hydrophilic polymer making up the tyre. The body of the wheel is filled with water for two reasons:

i. To take advantage of the superior ultrasonic properties of water over hydrophilic polymer. This permits a reduction in tyre thickness, reducing the attenuation imparted on the ultrasound travelling between the probe and test piece by a significant amount.

ii. The water provides consistent coupling to the inner surface of the tyre promoting stable and reproducible signal amplitude, while permitting the wheel to turn freely.

Preceding discussion has identified a number of design constraints/requirements key to the practical application of the device. These are summarised below. It is important that these criteria are satisfied by the ultimate design.

- A delicate balance must be achieved between the ultrasonic and mechanical properties of the hydrophilic polymer tyre.
- The tyre must maintain full hydration to operate most effectively.
- Water must not leak from the body of the wheel.
- The thickness of the tyre is directly proportional to the maximum inspection depth into the test piece material.
- The tyre must be held in compression.
- The tyre must be replaceable.
- The ultrasonic probe must be interchangeable.
- Feed and bleed holes are required for the introduction of water to the body of the wheel after assembly.
- The ultrasonic travel time between the probe and inner surface of the tyre must match the travel time in the tyre itself.
- Perpendicular alignment between the probe and test piece surface must be maintained while the body of the wheel rotates.

7.4 Prototype Design

Two basic designs evolved out from consideration of the design requirement criteria and extensive discussion with the sponsors. Both enable the evaluation of all hydration modes described above. A brief description of each will now be given.

7.4.1 Slipping System

A large diameter axle would house an ultrasonic probe. A hydrophilic tyre would fit directly onto the axle. When the device is moved over a test

piece surface, the tyre would slip (with the assistance of a lubricant) around the axle. The axle itself must not revolve, as the face of the transducer must always be parallel to the plane of interrogation. This system is very novel and offers advantages for ease of tyre replacement and initial manufacture. There is also potential for both internal (water could be pumped through the axle, allowing contact with the inner surface of the tyre through small holes in the axle wall) and external (drip feed) hydration. A 3D representation was created (modelled on a simple pipe) to assist with visualisation. This is shown in Figure 7.1.

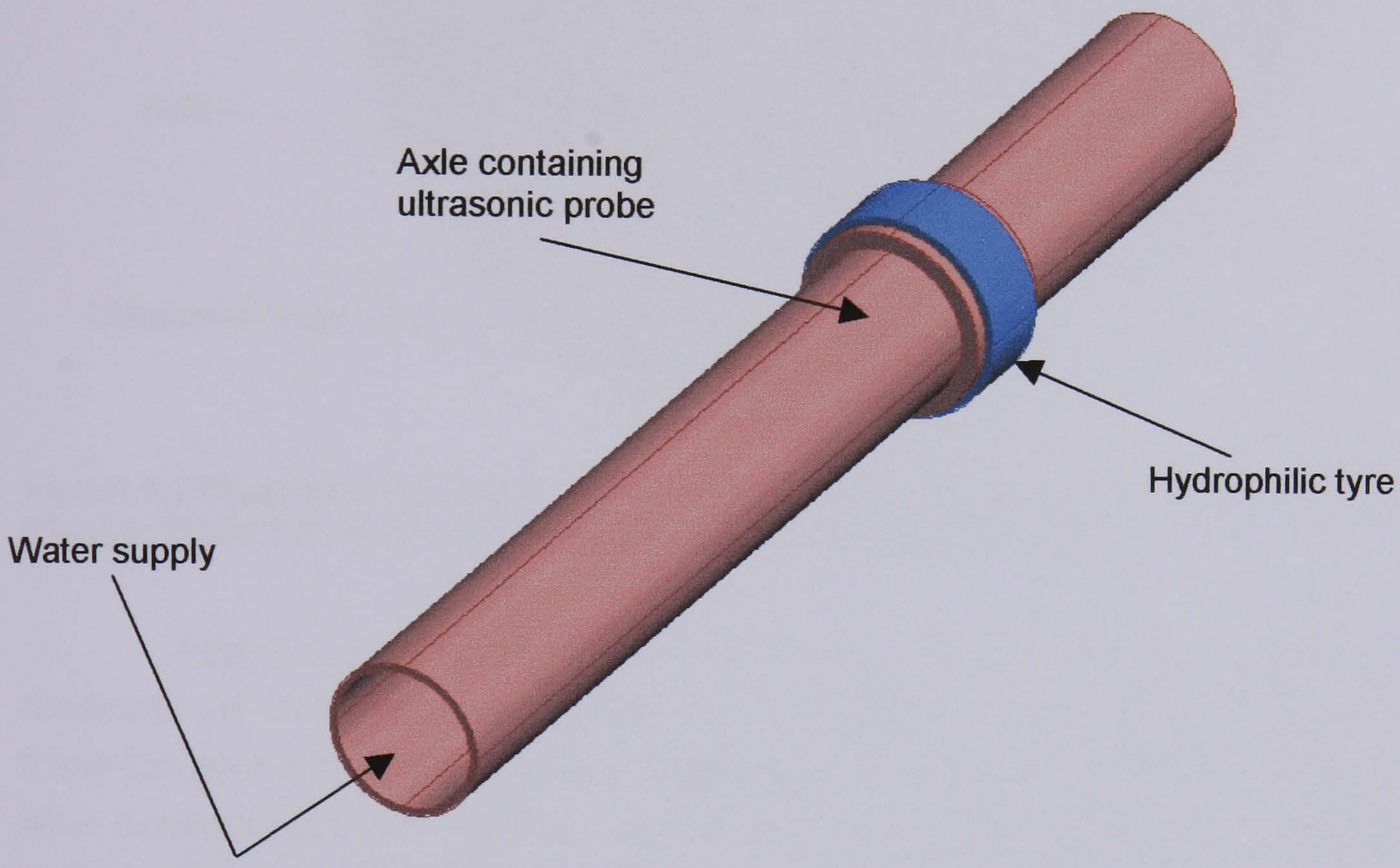

Figure 7.1 3D representation of slipping system design philosophy for a novel ultrasonic wheel probe (Design Wave 3D modelling package). Blue = Hydrophilic Tyre.

7.4.2 Immersion based

This design adopts a more traditional wheel form. A fixed axle would hold an ultrasonic probe (parallel to the plane of interrogation) effectively immersed in water. The walls of the wheel and the hydrophilic tyre itself would seal the water inside the body of the wheel. The tyre may or may not make contact with the probe. This design offers internal hydration with the potential for additional external hydration if required. Moreover, it is felt that it is more favourable in terms of ultrasonic transmission for reasons already explained, while the internal reservoir would assist in allowing free rotation of the wheel. The largest obstacle identified is the relative design complexity, which poses questions of how the polymer will seal against the wall of the wheel. Figure 7.2 illustrates the design philosophy.

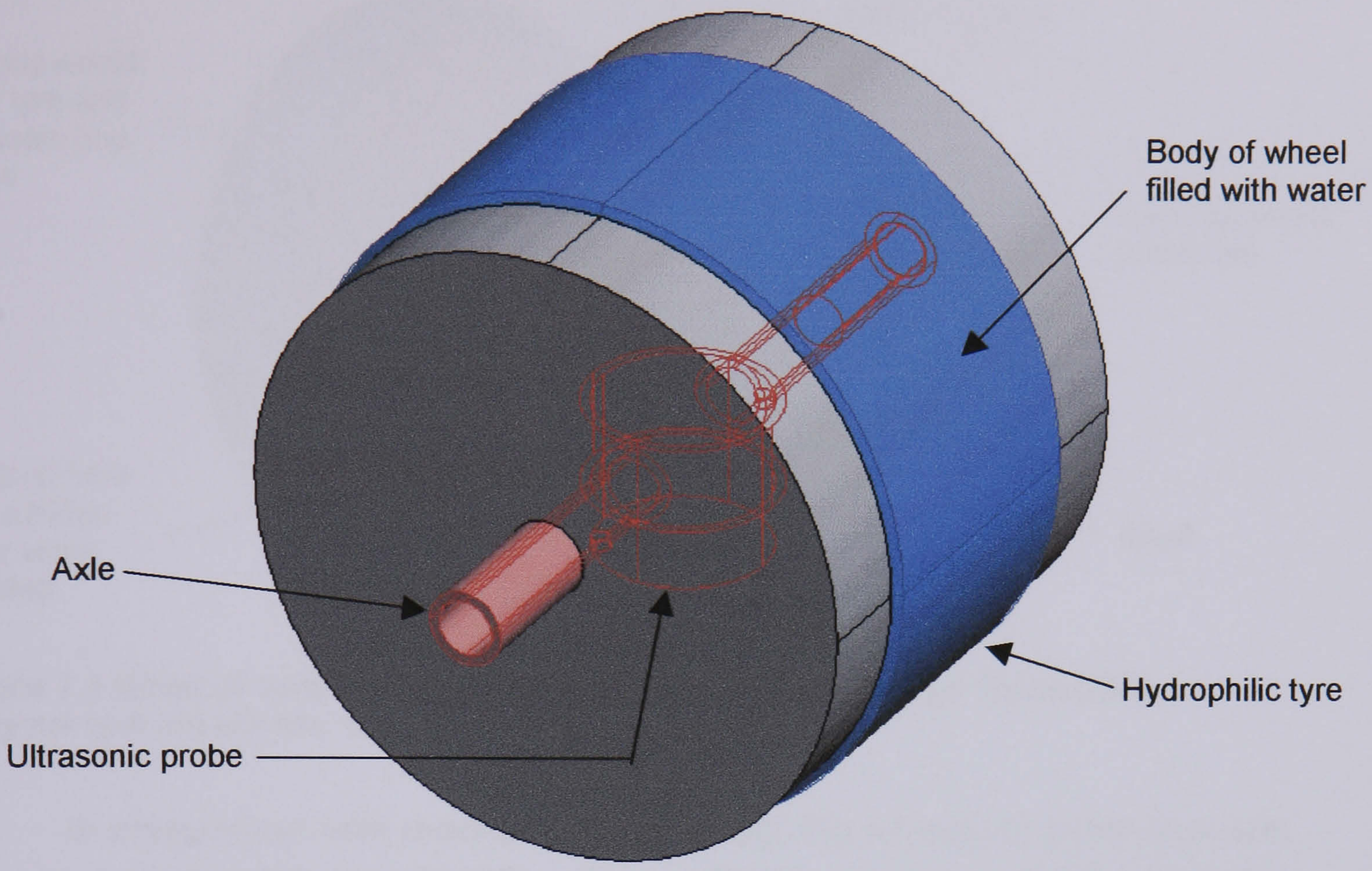

Figure 7.2 Illustration of immersion based ultrasonic wheel probe design philosophy (Design Wave 3D modelling package). Blue = Hydrophilic Tyre.

After lengthy consideration, the probe design incorporating an internal reservoir of water was preferred as it offered a more direct ultrasonic route from the probe to the test piece together with a lower risk of tyre wear. It was also appreciated that such an immersion-based prototype with careful design would offer great flexibility for the evaluation of many variants of both probe and tyre design. Likewise exploration of the slipping system principle should also be possible with this type of prototype device.

7.4.3 Development

The initial task involved identifying a source for all the necessary components required. With their dimensions known, the prototype device was modelled using DesignWave 3D. An early design is shown in Figure 7.3. This enabled different design variants to be explored.

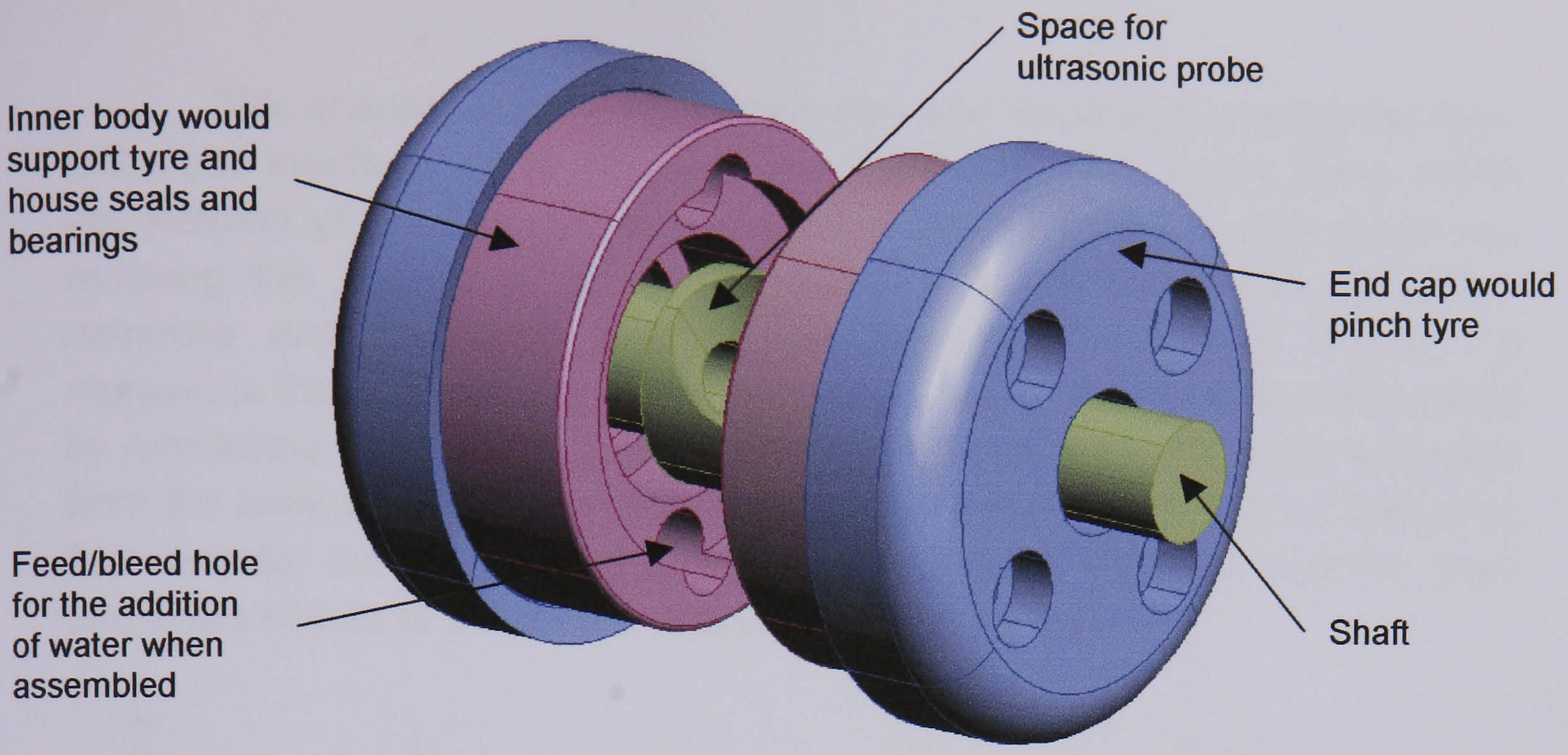

Figure 7.3 Model of early prototype ultrasonic wheel probe design. Hydrophilic Polymer tyre not shown. (DesignWave 3D).

In conjunction with mechanical modelling, the ultrasonic behaviour was also modelled using Imagine3D. This software is designed for ultrasonic technique development. The structure of the test piece may be modelled and ultrasonic properties assigned to the constituent materials. The software predicts an A-scan output generated by the probe. This was particularly useful when verifying that repeat echoes lined up with one another correctly.

The design of the tyre and wheel is such that the hydrophilic polymer is kept in compression. The body of the wheel provides support for when the tyre is pressed against the test piece. The outer end-caps are interchangeable to allow the evaluation of different size polymer tyres. They are also angled in such a way that they grip the tyre when not in contact with the test piece applying a restraining force, preventing the tyre 'popping out'. This design performs the sealing between the hydrophilic and the body of the wheel, preventing water loss. O-Rings are used in addition, as a back up sealing mechanism. Lip seals prevent water loss between the axle and the main body while still permitting rotation. The axle houses the interchangeable ultrasonic probe. The device handle holds the shaft fast preventing it from rotating with the main body. In this way, the direction of the ultrasonic beam is fixed with the orientation of the handle, providing a way of ensuring that it is always incident on the test piece. A spring is also incorporated into the handle to accommodate undulations in the test piece surface when scanning.

The first ultrasonic probe for use inside the device was designed and then passed over to the sponsors for manufacture. The crystal was 10mm in diameter and 5MHz. An epoxy lens was used to focus the beam at approximately 30mm in water.

This ensured that the beam diameter was small as it crossed the tyre-test piece interface. This increased the likelihood of the beam being inside the footprint of the tyre, therefore ensuring good transfer of ultrasound and reducing the chance of spurious echoes. Figure 7.4 shows the pulse response and frequency spectra generated by the device. Figure 7.5 represents the focal point of the transducer in water. This data was generated by monitoring the amount of receiver gain required to increase the reflection from the bottom of an immersion tank to 50% screen height on an ultrasonic flaw detector over a range of distances. The graph clearly shows the peak amplitude occurs at a distance of approximately 35mm.

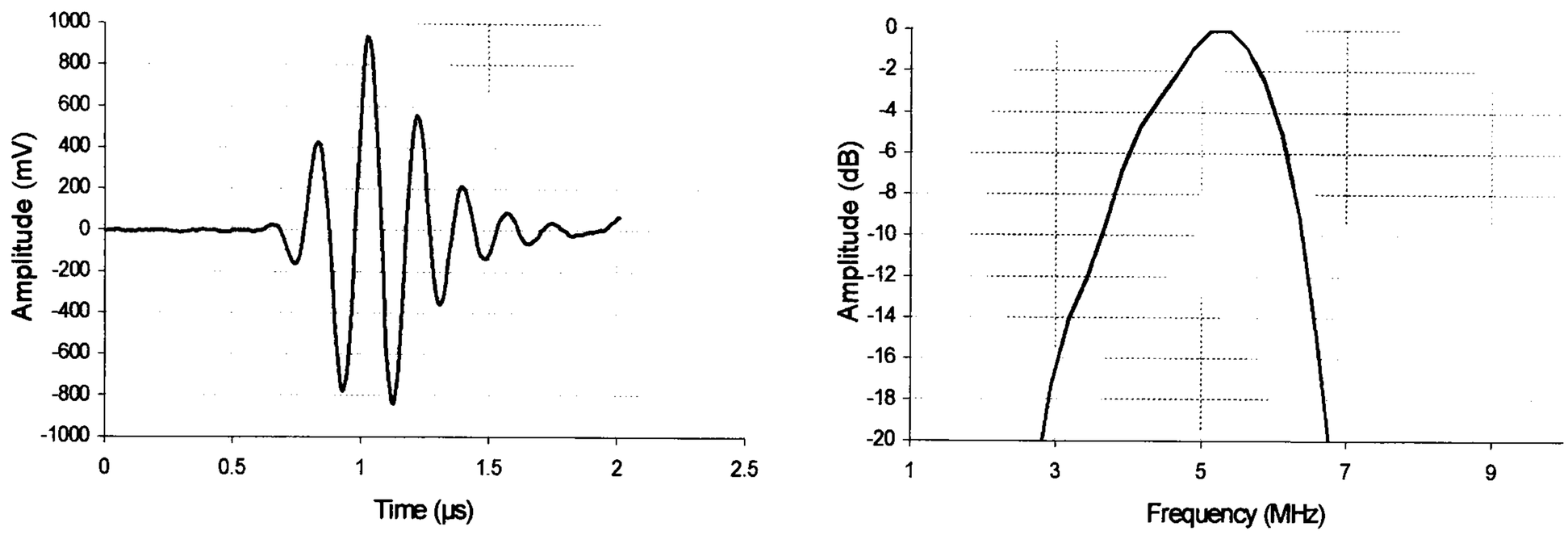

Figure 7.4 The ultrasonic pulse and corresponding frequency spectrum generated by the immersion probe designed specifically for use in the prototype wheel probe.

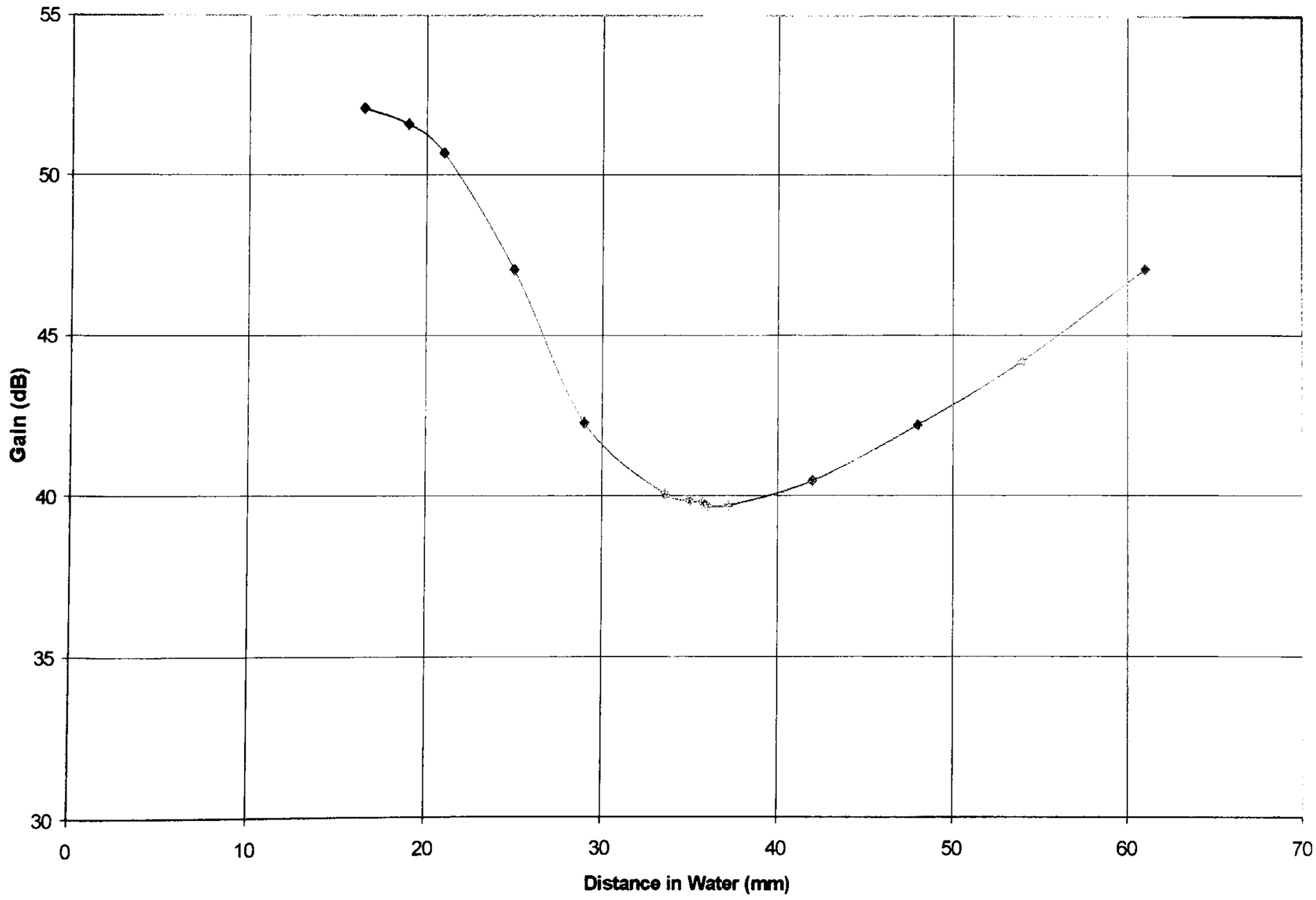

Figure 7.5 Representation of the focal distance of the immersion probe designed for use in the prototype wheel probe.

All other mechanical parts were designed around the probe and to fit with off-the-shelf components (including seals, bearings, fasteners, etc). Drawings were produced for each part, which were then passed onto the machine shop via the Design Office at Cranfield University. All components were machined from stainless steel to eliminate corrosion resulting from prolonged contact with water.

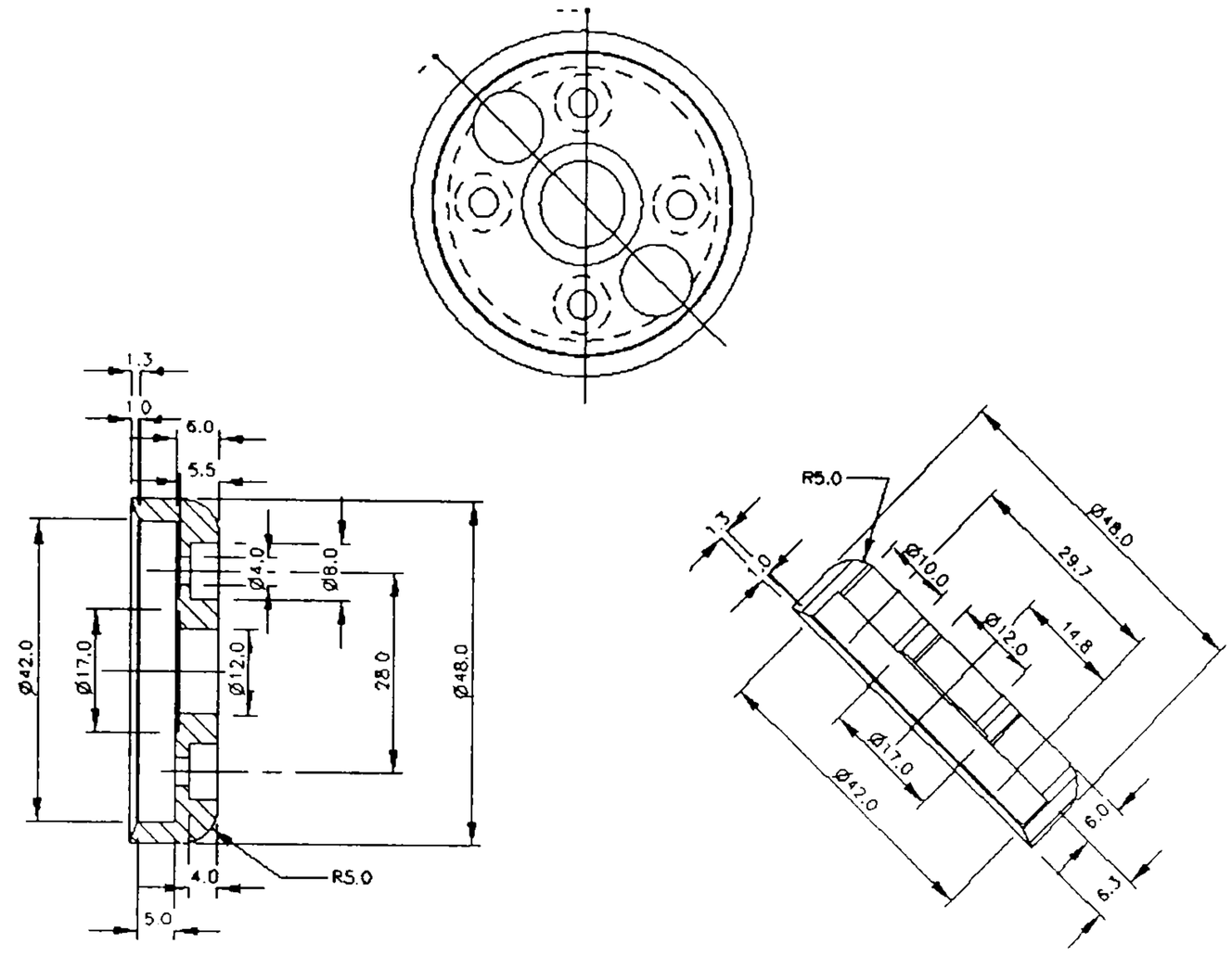

Figure 7.6 Representation of drawings produced for the manufacture of a prototype ultrasonic wheel probe.

One aspect of the design which proved particularly useful was the removable end-caps. These allow different size tyres to be used on the device without the need to re-machine the complete unit. This was especially beneficial as the supplier of the hydrophilic material experienced difficulties producing samples of hydrophilic polymer sufficiently large for machining into the size required for the tyre as air bubbles manifested themselves in the polymerisation phase of fabrication. Fortunately, these were close to the surface and so could be removed by machining down the outer diameter of the tyre. The result was a thinner tyre that did not protrude from the end-caps and so did not make contact with the test piece. Fortunately, the tyre could still be used as smaller diameter end-caps were quickly machined from Perspex for fitting directly onto the same prototype wheel. The new end-caps still gripped the tyre in compression, but ensured that a sufficient portion of the tyre protruded, enabling contact with the test piece.

After further experimentation with the polymerisation process, the suppliers were able to reproducibly fabricate the larger tyre. The technique centred on rapid removal of heat from the exothermic reaction which was

responsible for the bubble inclusions in the early prototypes. This was achieved by casting the polymer into a doughnut shaped sacrificial mould. In this way the distance between any point in the mould to a surface was minimised. By happy coincidence this also cut down on the quantities of raw materials used and the subsequent machining operations. Hydration is conducted slowly at low temperature (approximately 5°C) to reduce unwanted stresses caused by high-speed hydration of such large components.

7.5 Results and Discussion

Following assembly of the device, it put to the test in a number of different test situations. The first were manual inspections, where a portable ultrasonic flaw detector was used to present the A-scan generated by the wheel probe. A number of more advanced application trials were then conducted. Such tests incorporated a pulser/receiver linked directly to a computer along with a portable desktop scanner. The A-scan was shown on the screen of the computer through WinSpect software, supplied by UTEX Instruments. This more sophisticated system enabled the generation of full C-scan images. Figure 7.7 below shows the device being operated both manually and automatically.

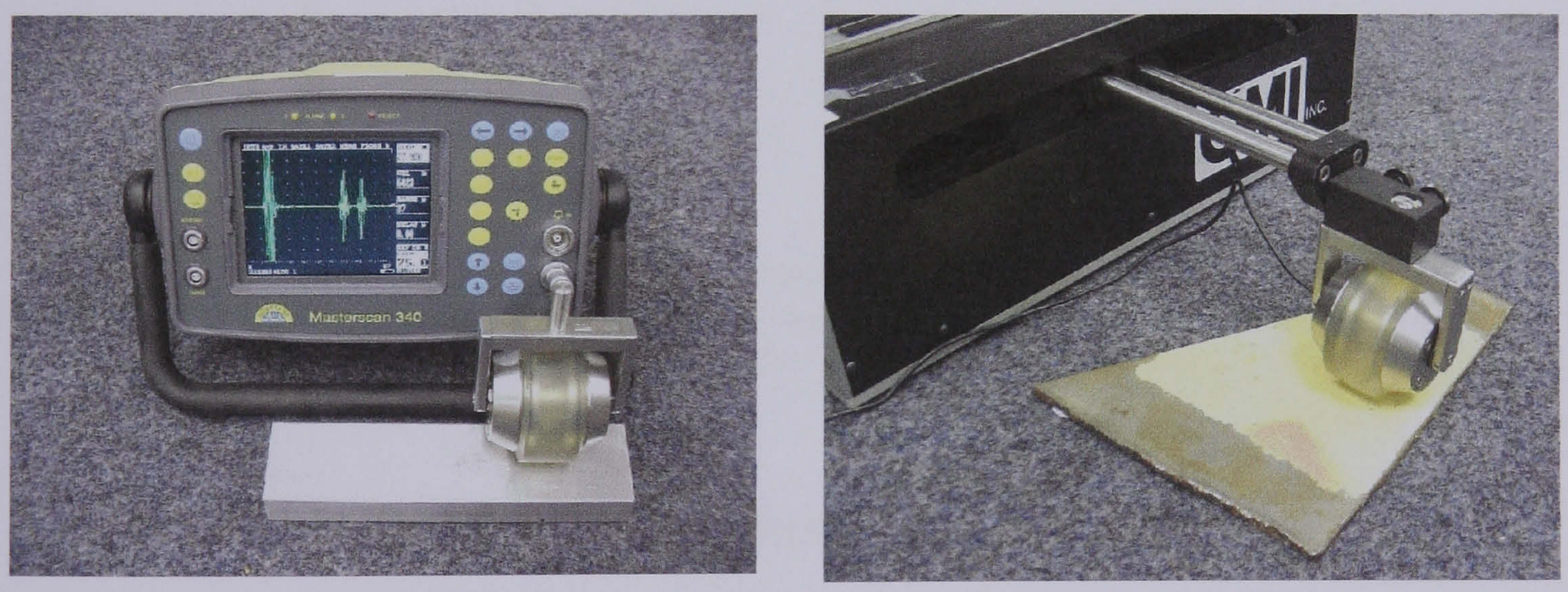

Figure 7.7 Examples of the prototype ultrasonic wheel probe being used both A) manually and B) automatically.

7.5.1 Signal Interpretation

In order to explore the signals generated by the wheel probe, it was connected to an ultrasonic flaw detector while not coupled to a test piece. The range was expanded from 0 to 100μs (which is the equivalent to 150mm in water) to permit observation of the A-scan from the probe through to repeat echoes from the hydrophilic polymer tyre. The receiver gain was increased to 53dB so the echoes were clearly seen. Figure 7.8A shows the fully rectified A-scan achieved. The left most peak is the transmitter pulse, the second is

the interface between the water-tyre interface and the third is the reflection from the outer surface of the tyre. The subsequent echoes are multiple reflections from these interfaces.

The excellent transmission of ultrasound between the hydrophilic polymer tyre and water is highlighted in Figure 7.8B where the probe is dipped into water while the settings on the ultrasonic flaw detector remained unchanged. The amplitude of the reflection from the outer surface of the tyre drops significantly as energy is transmitted into the water rather than being reflected back into the wheel. It is also notable that the multiple reflections disappear. This is a very good thing, suggesting that repeat echoes from the water path and tyre may not influence signal interpretation as much as was originally feared when inspecting materials of low acoustic impedance.

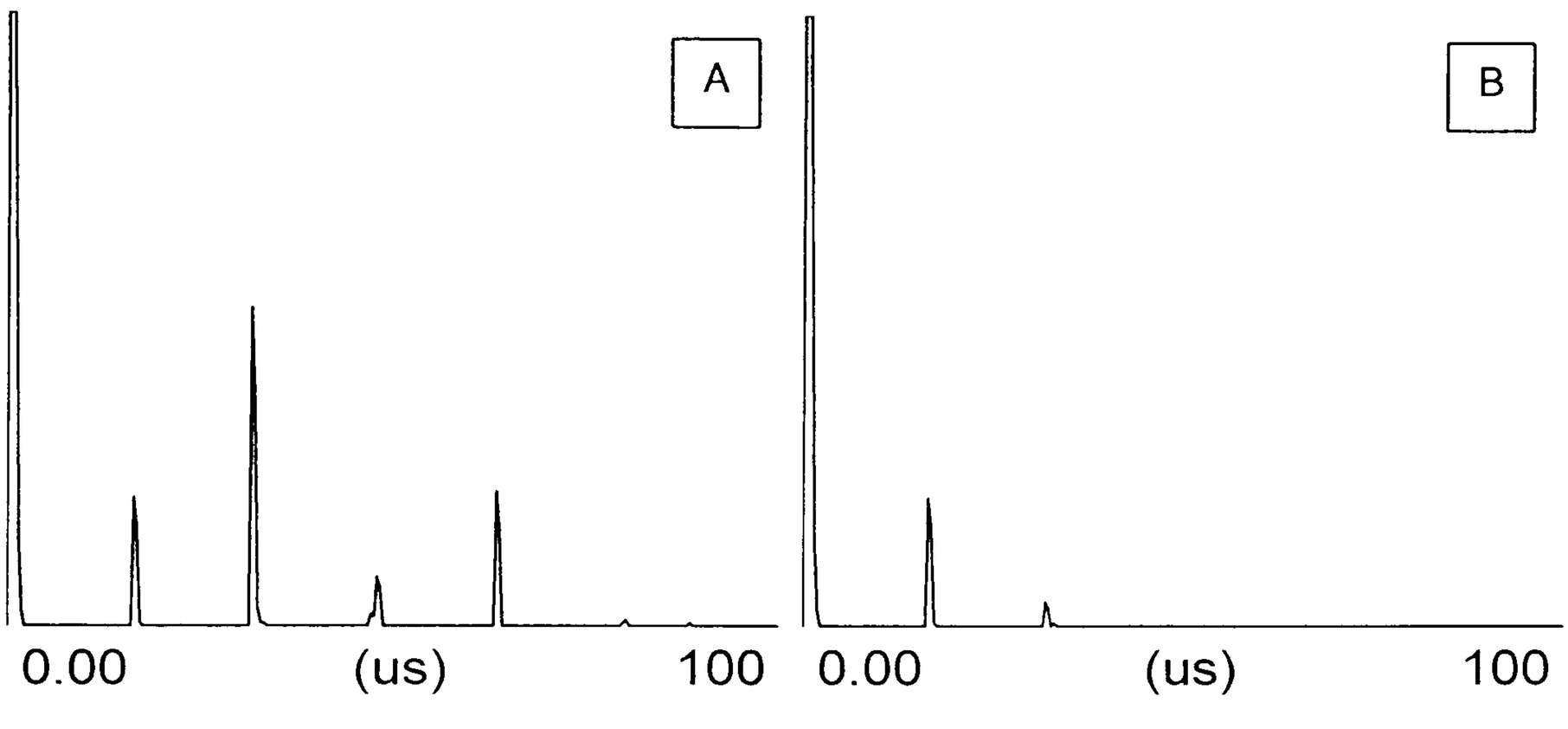

Figure 7.8. A) Signals from uncoupled wheel probe. B) Signals from wheel probe dipped into water. In both cases the gain on the ultrasonic flaw detector was set to 53dB and the screen delay was set to zero.

7.5.2 Manual Inspection Application

For normal application the flaw detector would be set up appropriately so that the reflection from the outer surface of the tyre was at the left of the screen and the range appropriate for the thickness of the test piece to be inspected. This is the case for both Figure 7.9 and Figure 7.10. The black trace in Figure 7.9 shows the flaw detector screen when set up for the inspection of a 6mm thick Perspex plate using the wheel probe. At this stage the wheel is not in contact with the Perspex and a small repeat echo from the tyre can be seen in the ninth graticule. The superimposed blue trace is the signal produced when the wheel probe is placed in contact with the Perspex sample.

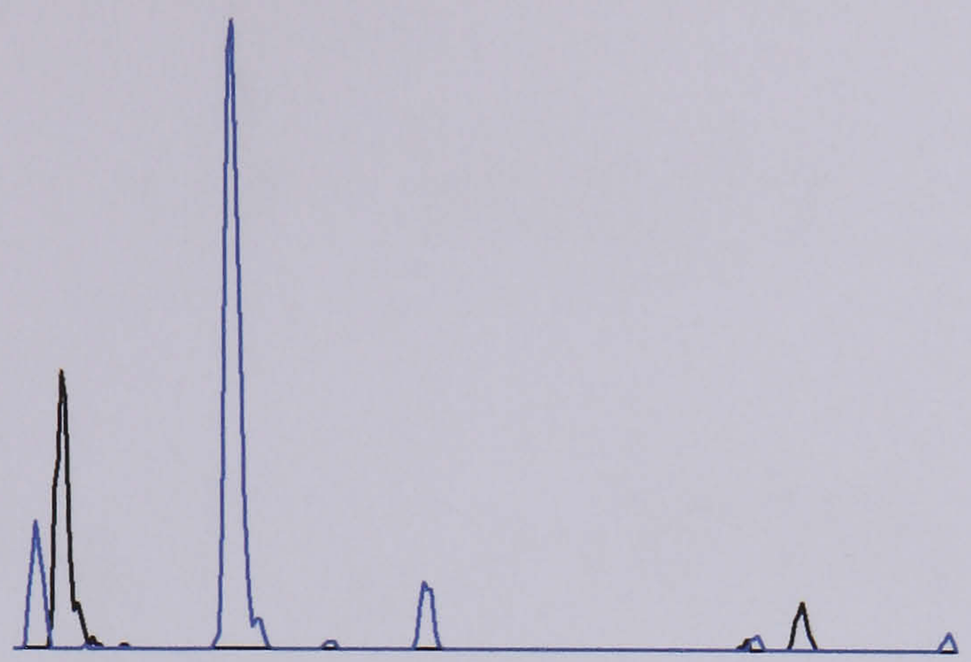

Figure 7.9 Black – trace from wheel probe with screen set-up appropriate for the inspection of Perspex plate. Blue – trace achieved when probe placed in contact with Perspex. The gain of the ultrasonic flaw detector remained constant at 53dB.

The initial interface echo between the tyre and the Perspex (left most black) can be seen to reduce in size and move slightly to the left when the probe was placed in contact with the Perspex sample. This is due to the slight compression of the tyre, reducing the ultrasonic travel time. The reduction in amplitude is caused by a reduction in the amount of energy reflected from the outer surface of the tyre as energy is transmitted into the Perspex. Of particular note is that the interface echo is lower in amplitude than the Perspex back wall echo. This is evidence of the excellent transmition achieved via this arrangement.

As the water path and tyre thickness are used as a delay, transducer dead zone effects are minimised making inspection very close to the test piece surface possible. Indeed when the wheel probe is held in contact with a test piece of good surface finish, the interface echo is typically of very low amplitude. Figure 7.10 shows the response from a 2mm flat bottomed hole 2mm below the surface of a Perspex sample. It is clear that the echo from the simulated defect is of higher amplitude than that from the sample surface. Even though the gain is only set to 53dB, a repeat echo from the defect is clearly visible.

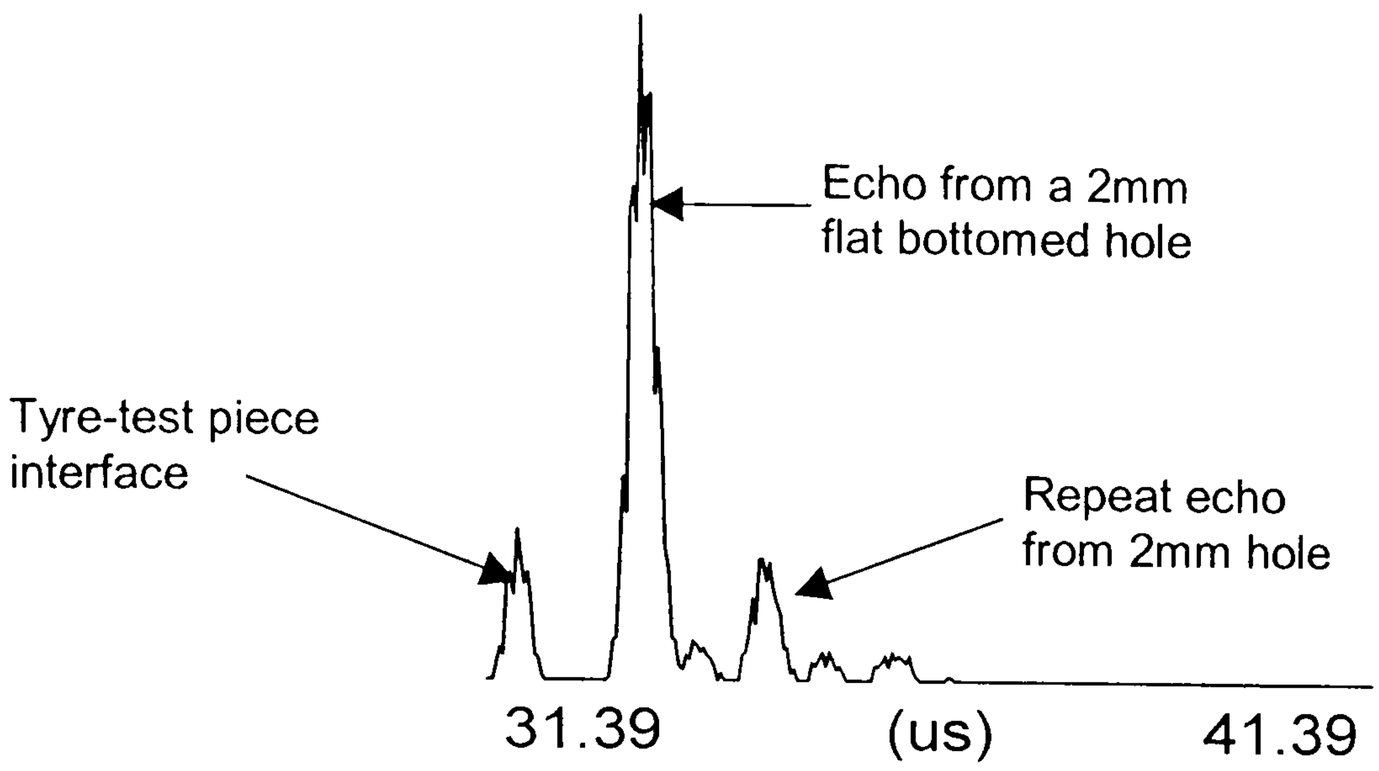

Figure 7.10 Signal from a 2mm flat-bottomed hole 2mm from the surface of a Perspex test piece achieved with the wheel probe.

7.5.3 Automated Inspection Application

With strong and clear signals being generated in pulse echo mode, there was great anticipation for implementing the wheel probe as part of an automated system towards the generation of C-scan images. The first test piece examined was a steel plate approximately 6mm thick (same one as shown in Figure 7.7). It was relatively smooth on one side, partly covered in paint. The underside was severely corroded with many pits and scratches. The wheel was scanned over the steel plate in a rectilinear raster with an ultrasonic reading being taken every 0.2mm. Similarly, the index was 0.2mm, which is considered to be very fine. The wheel rotated well as it passed along the length of the steel plate. When indexed sideways, the tyre slipped easily as anticipated. This was however a minor concern as the long term scuffing effect on the tyre was not known. Fortunately it proved not to be an issue, the original tyre being still in use nearly two years later.

The C-scan was set up so as to monitor the amplitude of the back wall echo. The scan was repeated a number of times, while the instrument settings were honed. Two ultimate tests were performed with the wheel probe. The first involved scanning the plate with two drops of water to aid coupling. The second was performed with the tyre blotted completely dry, coupling being provided solely by the hydrophilic polymer tyre. The results compared extremely well. The acid test however, still remained. The main aim of this device was to offer an alternative to immersion coupling. In order to investigate the respective performance, the probe was removed from the centre of the wheel and used to scan the steel plate in a conventional immersion tank. The distance between the probe and steel plate was carefully adjusted to be the same as it would be if the probe were inside the

wheel. On all three scans, the same index resolution was used to permit direct comparison.

Figure 7.11 shows the results achieved. The brighter the colour, the higher the amplitude of the back wall echo. It is clear that all of the features that were resolved with the conventional immersion test were also resolved with the wheel probe, whether operating with a small amount of water or completely dry. This is a very positive outcome. It was noticed that during the scan with a small quantity of free water, the water droplets clung to the footprint, leaving no trace of water on the test piece.

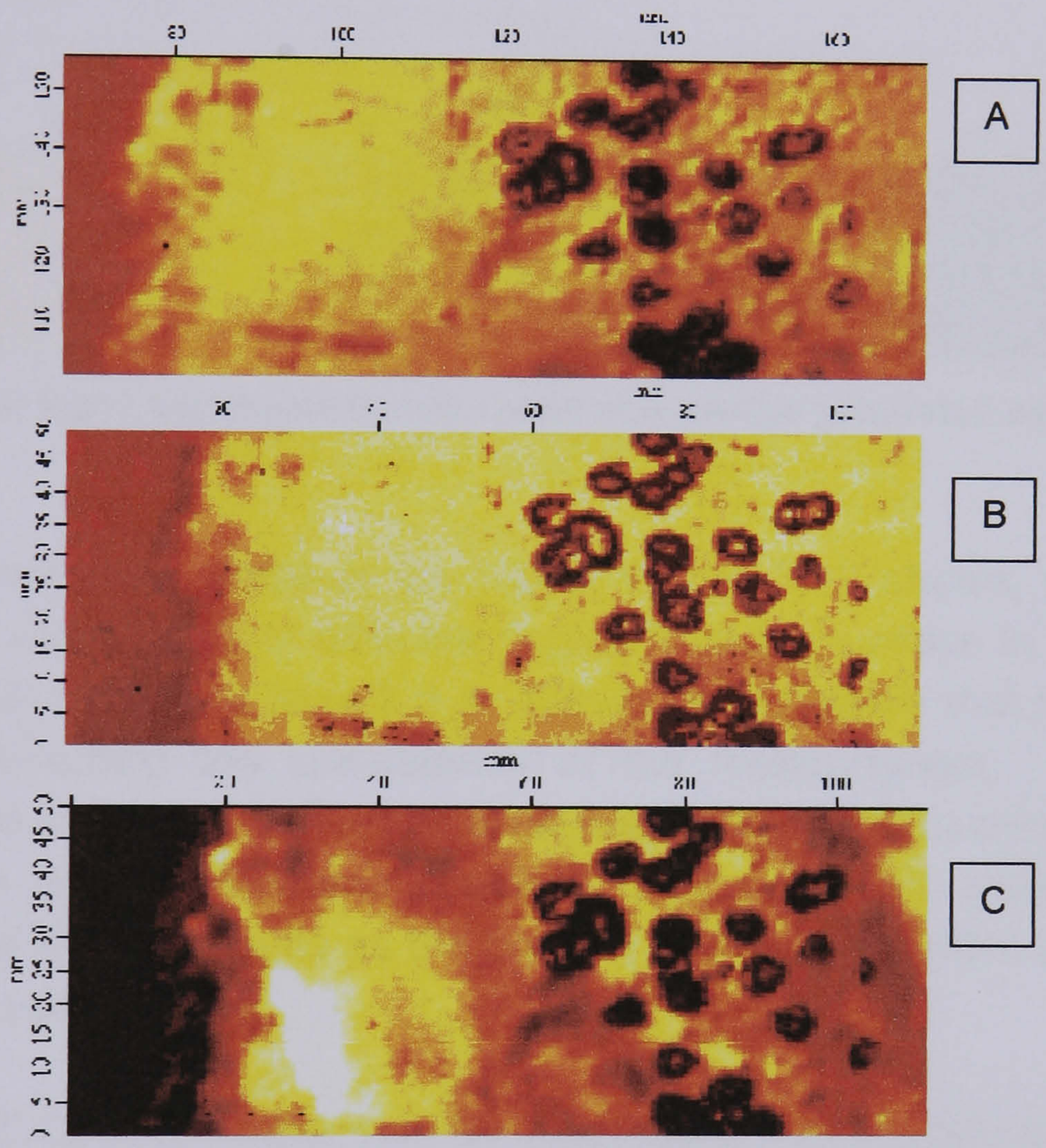

Figure 7.11 C-scans generated with A) a conventional immersion test, B) the wheel probe with two drops of water, and C) the wheel probe in the absence of surface water. Test piece is corroded steel. Probe is 10mm diameter and nominally 5MHz.

Stronger signals were achieved over areas of the plate with a covering of paint. These can be seen in Figure 7.11 as the brighter areas on the right hand side of the C-scans. This is most likely due to the smoother surface finish, affording an improved level of contact with the tyre. This contrast is more noticeable in Figure 7.11C, where the tyre was completely dry. In the left-hand region without paint, the image is very dark, caused by the respective low amplitude of the back wall echo. Logically, this is due to the reduced level of coupling caused by the higher surface roughness. Despite surface roughness, alignment of the probe to the test piece proved itself to be vital to repeatable performance.

Additional tests have been conducted to explore the wheel probe performance further. These have included 'time of flight' evaluations. This involves monitoring the time it takes for ultrasound to travel through the test piece and back to the probe, achieved in this case by monitoring the time difference between the echoes from the tyre-test piece interface and the test piece back wall. These time measurements are then converted into a distance representing a depth measurement which is then translated into a colour scale. Figure 7.12 shows the results of one such scan complete with a thickness profile.

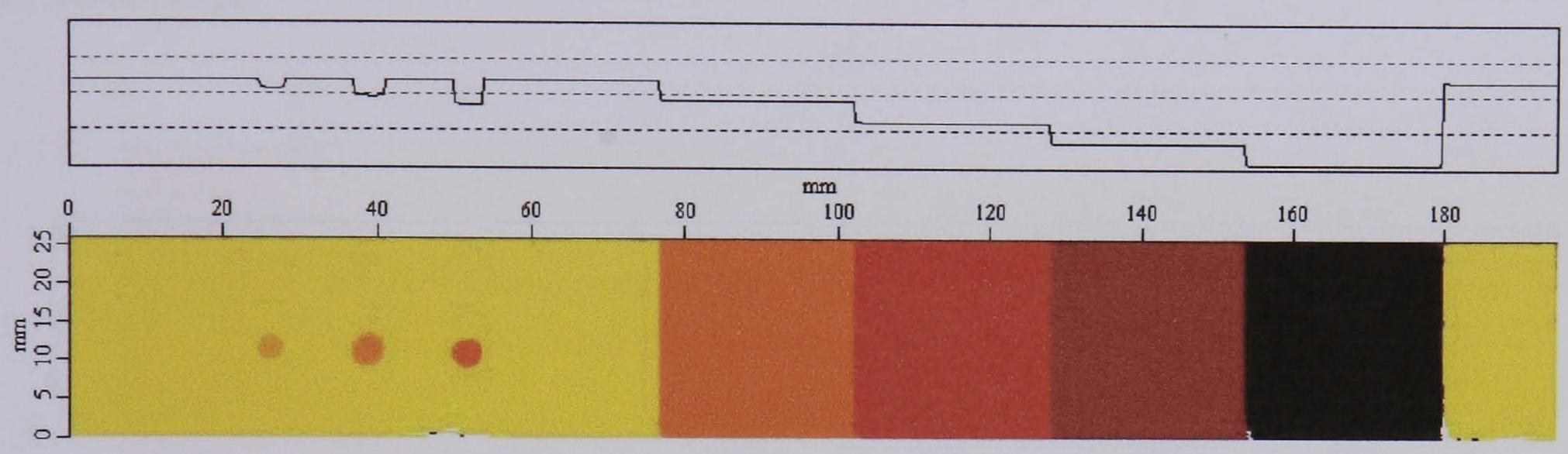

Figure 7.12 Time of flight representation of a steel step wedge generated with the wheel probe.

As the thickness profile at the top of Figure 7.12 shows, the wedge contained three small holes at different depths from the surface in addition to large variations in thickness from 2.5 to 13mm. It is notable that the scan is very uniform, reflecting the consistency of the measurement. No signal fluctuations were observed indicating a consistent level of coupling. This is vitally important as an ultrasonic couplant must have the ability to yield reproducible and reliable results as the coupling consistency often defines the sensitivity of an examination.

In figure 7.12 three holes may be clearly seen on the left-hand side at different depths from the surface. The diameters of the holes look to be different, but in reality, they are exactly the same. This is caused by the use of a focussed ultrasonic probe. The holes in the focal zone, where the beam is narrowest, appear to be smaller in diameter than those outside the focal zone where the beam diameter interrogates a larger area. In this sense the holes are evaluating the beam diameter rather than the beam evaluating the hole diameter. Inspection with non-focussed probes would significantly reduce this effect.

The wheel probe has been used by the sponsors to conduct research into solid coupled ultrasound inspection [Bourne et al, 2000b and 2001a,b]. Figure 7.13 shows a C-scan of a magnesium plate. The material is very sensitive to water corrosion and so cannot be inspected via conventional

immersion techniques. In this case, the prototype wheel probe developed as a result of this research was used in pulse echo mode at 5MHz. The sample was 30mm thick, containing three rows of five artificial defects in the form of flat-bottomed holes. The diameter of the holes was different on each row, the bottom middle and top being 5, 2 and 1mm in diameter respectively. In each row the holes were introduced at different depths, the remaining material being 20, 10, 5, 2 and 1mm respectively. The C-scan involved monitoring the amplitude of the back wall echo of the sample. It is clear that all 15 defects were detected including one that was genuinely not expected, seen on the left of the image.

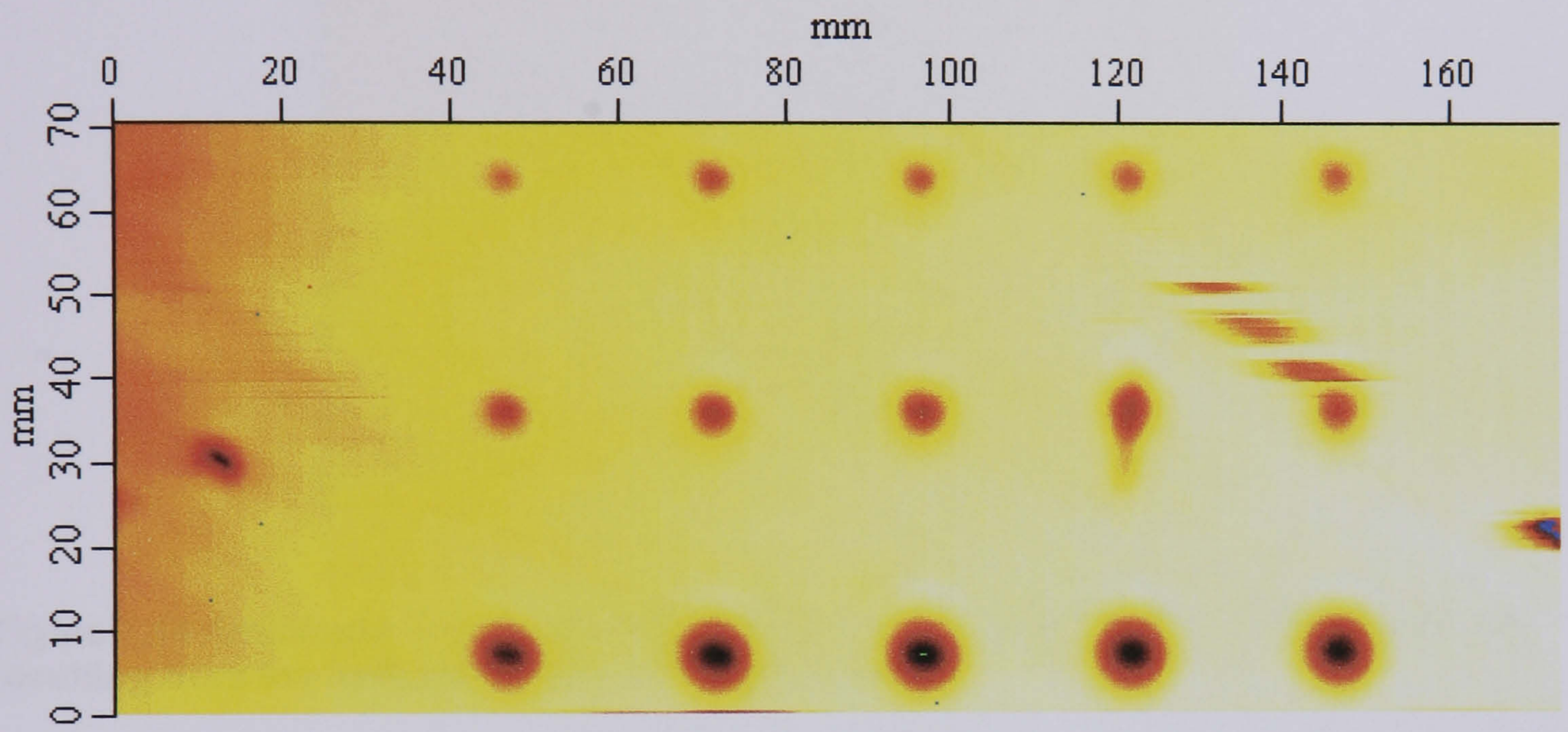

Figure 7.13 C-scan of Magnesium alloy containing artificial defects. Scan produced using the prototype wheel probe generated as a result of this research.

7.5.4 Reproducibility

Consider a contact probe scanning over the surface of a test piece. If the probe passes over a small defect, one could expect the amplitude of the back wall echo to drop momentarily – hence the defect is detected. If however, the level of coupling between the interrogating probe and test piece was not constant, the signal would vary in amplitude in any case as differing amounts of energy are transferred between the probe and test piece. Therefore, if the amplitude variations due to inconsistent coupling are greater than the variations due to the presence of a defect, the defect will go undetected.

It is therefore important to be able to quantify the ability of the wheel probe to maintain constant coupling efficiency while scanning. This was evaluated by practical measurement. The wheel probe was used to C-scan a uniform Perspex plate of 10mm thickness, the gate monitoring the amplitude of the back wall echo. The scan area was sufficiently large as to involve one

complete revolution of the tyre at an index of 0.5mm. As the Perspex was defect free, any fluctuations in signal amplitude must be a result of either coupling variations or non-uniform ultrasonic properties in the tyre. Figure 7.14 shows a section of the C-scan produced. The colour scale has been adjusted to highlight the differences in signal amplitude (greater amplitude is represented by brighter colours). The scanning time was approximately 20 minutes.

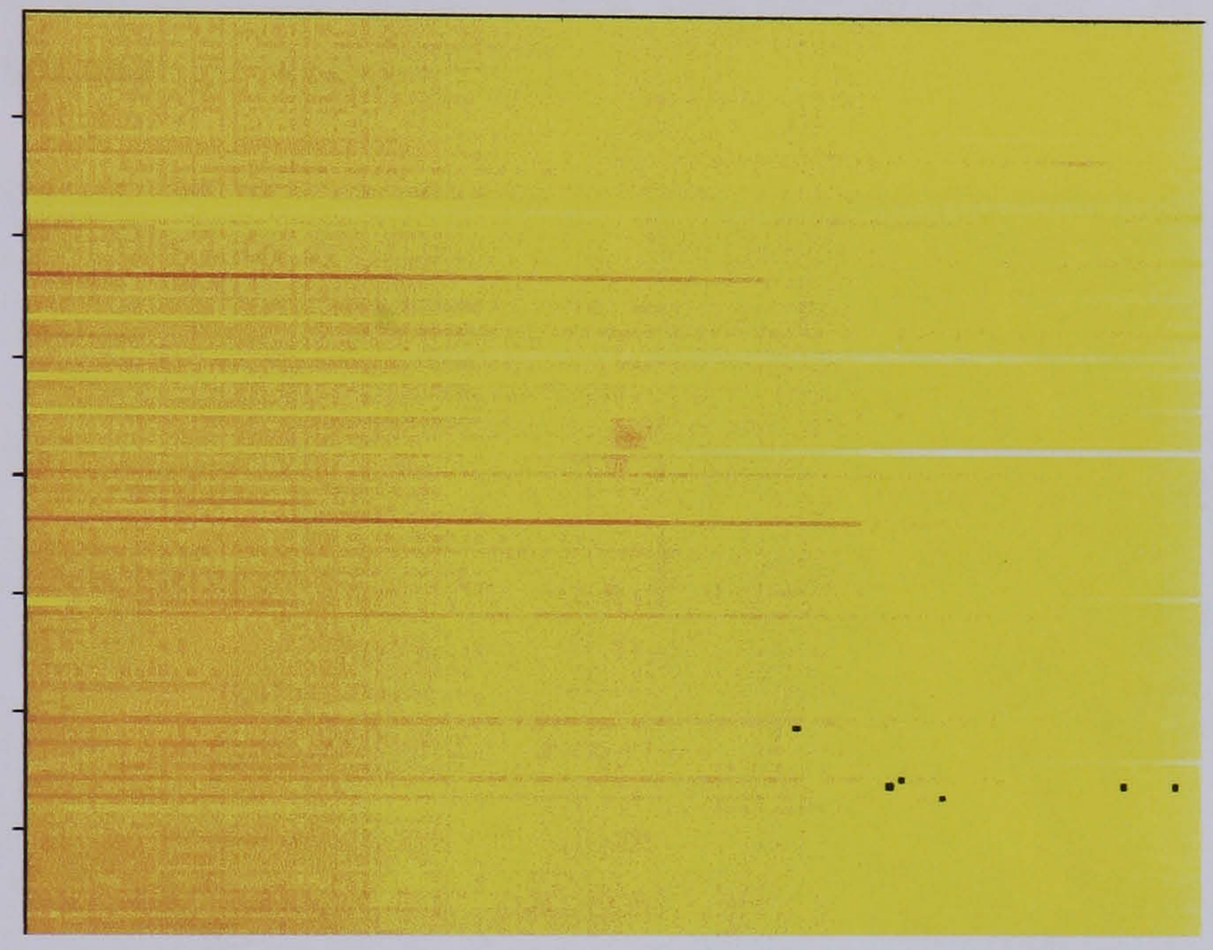

Figure 7.14 Amplitude C-scan of a uniform Perspex plate showing coupling variations resulting from the hydrophilic tyre of the wheel probe.

The difference between the maximum and minimum amplitudes over the entire scan was measured as being 1.8dB (i.e.±0.9dB). This proves that a very consistent level of coupling was achieved. Moreover, it is believed that much of the variation recorded in this investigation was as a result of probe misalignment as it was observed that the fixture attaching the wheel probe to the scanning arm was ill-fitting and beginning to work loose. Therefore, it is safe to state that the wheel probe is able to identify changes in signal amplitude of less than 2dB from a test piece with a smooth surface. This is a very impressive level of sensitivity.

Similar scans of this type were performed where drops of water were applied to the external surface of the tyre prior to testing. In these scenarios there was no sign of tyre dehydration. This suggested that if small quantities of free water could be tolerated on the surface of the test piece, the wheel probe could be reliable operated over significant periods of time without risk of tyre dehydration.

7.5.5 Final Design

With the prototype fully evaluated, the design was honed to satisfy the commercial needs of the sponsors. Modelling was performed in Solid Edge, one example being shown Figure 7.15a. The tyre was 13.5mm thick, which translates to a maximum inspection depth of 35mm in steel. The device was named the Hydro Probe and has resulted in patent application in the UK and USA [Bourne, et al, UK9921846.3 and US-09/396,435.]. A certificate of the Hydro Probe is shown in Appendix D.

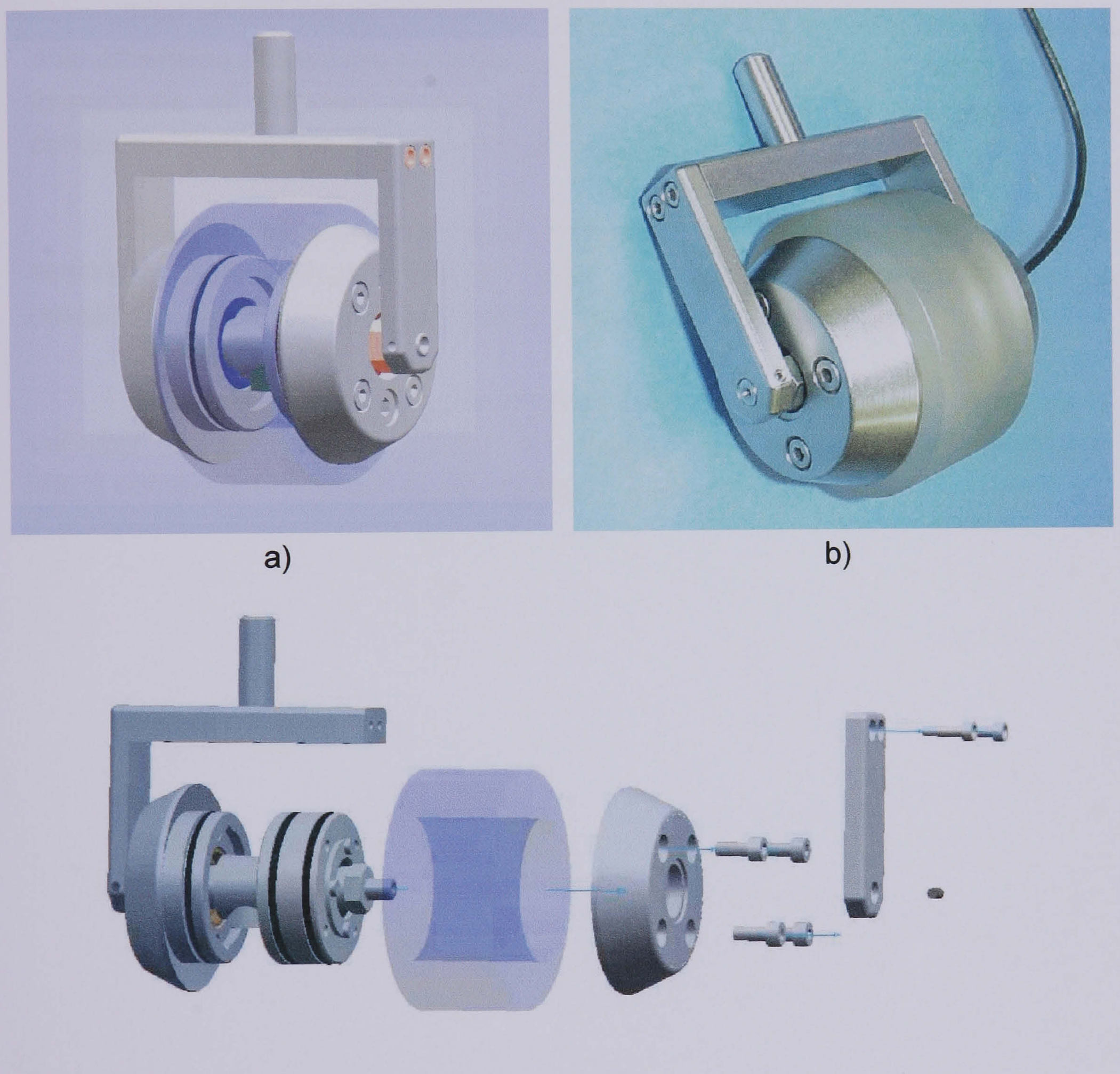

a) b)

c)

Figure 7.15 A) 3D model of commercialised wheel probe, generated in Solid Edge. B) First wheel probe manufactured commercially. C) Partly exploded view of wheel probe assembly.

7.6 Conclusions

A study into the design of a prototype ultrasonic device employing hydrophilic polymer as solid contact ultrasonic couplant has been conducted. This process involved consideration of ultrasonic, mechanical and hydration factors and resulted in the development of a prototype wheel probe, operating at 5MHz in pulse echo mode. The tyre consisted of a Batch C hydrophilic polymer with an equilibrium water content of approximately 60%.

Trial of the wheel probe has generated results of exceptional quality only otherwise obtainable by immersion testing. Both manual and automated inspections of different materials of various surface finishes have been conducted from which excellent results were achieved.

Coupling efficiency has been shown to remain within ±0.9dB during C-scanning of a uniform Perspex plate. Enhanced sensitivity is believed possible through maintaining improved beam alignment during scanning.

The sponsors have demonstrated their confidence in the device as a valuable tool for industrial ultrasonic inspection, by developing the prototype into a commercial product and investing in patent protection.

Chapter 8: Conclusions

8.1 The Problem

The requirement for ultrasonic NDT in many industries including aerospace, oil, power and construction is increasing. In particular, the use of composite materials is growing rapidly, demanding a similar growth in appropriate inspection tools and methods. Conventional approaches towards manual and automated inspection require either the application of coupling gel or the complete submersion of the test piece in water. This is often unacceptable as the presence of such substances can cause corrosion and degradation of the test piece material. In the case of automated testing the risk of water ingress into certain defects challenges the reliability of defect detection. Inspection in this way often necessitates the transportation of the test structure to the test laboratory, which is inconvenient and often not practical. There is therefore a need for a device enabling the manual and automated inspection of components without the need for liquid couplant application or submersion in water.

This project was proposed to (i) evaluate the concept of utilising hydrophilic polymers as novel solid contact ultrasonic couplant, (ii) verify ultrasonic properties by practical measurement, (iii) research prototype design options for an alternative device incorporating hydrophilic polymer.

8.2 Actions Taken

The key factors governing the efficient transfer of ultrasound from an ultrasonic probe into a target material for the purposes of ultrasonic NDT were identified. A range of hydrophilic polymers was evaluated against these factors towards the assessment of their suitability for employment as solid contact ultrasonic couplants. Initial practical investigation into these factors took on a three pronged approach focussing on (i) ultrasonic properties, (ii) modification of these properties due to factors likely to be encountered in practical application, and (iii) ultrasonic behaviour in conditions beyond those expected to be encountered in practical application.

i. For each polymer, the velocity of ultrasound propagation, acoustic impedance, and attenuation with respect to frequency were measured using state of the art ultrasonic equipment and custom designed software macros.

ii. A specially designed mechanical rig was built enabling the nature of ultrasonic transmission into steel to be evaluated over a range of contact pressures up to 2.5kg cm^{-2}. The change in ultrasonic attenuation and velocity were measured over a range of temperatures (from room temperature down to -20°C) and mechanical pressures.

iii. The influence of incomplete hydration and subsequent dehydration was measured with respect to ultrasonic attenuation and velocity.

Attention was also directed towards mechanical longevity through practical measurement in a simulated 'rolling contact' environment. Additional points of interest, which included assessment of shear wave support and frequency downshift caused by ultrasound propagation through different hydrophilic polymers, were also investigated.

The ultimate stage of this work involved the design and development of a prototype wheel probe device incorporating hydrophilic polymer as a novel solid contact ultrasonic couplant. Through this process, numerous design factors were considered towards the demonstration of the preferred operational arrangement. The device was assessed over a range of applications and the results presented.

8.3 Summary of Conclusions

8.3.1 Ultrasonic Properties

Ultrasonic attenuation, the ability to conform to a surface and acoustic impedance are all essential factors governing the efficient propagation of ultrasonic waves and their transfer across solid contacting interfaces. Therefore, these properties are crucial for ultrasonic coupling media. Unfortunately, high conformance usually equates to high attenuation in conventional materials, posing a difficult trade-off for practical application. This is not the case for hydrated cross-linked hydrophilic polymers, therefore suggesting themselves as excellent candidate materials for solid contact ultrasonic couplants. Samples of 38% equilibrium water content demonstrated attenuation of 1.8dB mm^{-1} at 5MHz compared to 0.58dB mm^{-1} in more compliant polymers containing 75% water. After considering the attenuation in natural rubber of 3.75dB mm^{-1}, a material often used in conventional solid coupled devices, hydrophilic polymers were seen to offer significantly superior ultrasonic properties.

Hydrophilic polymers are able to conform well to uneven surfaces. Optimal ultrasonic contact was achieved between a 50% equilibrium water content polymer and a smooth steel test block at a pressure of 0.4kg cm^{-2}. The acoustic impedance of all of the hydrophilic polymers evaluated in this research was demonstrated to be usefully greater than that of pure water and natural rubber.

8.3.2 Application Specific Properties

Thought was given to the practical application of hydrophilic polymers. Within this remit, the influence of temperature, contact pressure and frequency downshift were researched. Proof has been presented of a gradual deterioration of ultrasonic properties below 5°C, attenuation increasing from 1dB mm^{-1} to a maximum of 4dB mm^{-1} (5MHz) at -12°C. Ultrasonic velocity showed a similar trend, increasing from 1700ms^{-1} at 5°C to 2350ms^{-1} at -20°C. Both attenuation and velocity did not demonstrate significant change over the range 5-25°C.

Pressure of up to 2.5kg cm^{-2} was shown to have no influence on ultrasonic attenuation although it did affect a slight reduction in velocity of approximately 44ms^{-1} per kg cm^{-2}. The implications of maintaining an angled shear wave via hydrophilic polymers under a range of temperatures and pressures were discussed.

A reduction in peak frequency resulting from passage through hydrophilic material was measured. This was found to be specific to the equilibrium water content of the polymer, ranging from 0.04 to 0.25MHz mm^{-1} in the polymers investigated in this research. A process was outlined by which the extent of frequency downshift can be predicted for different hydrophilic polymers of different thicknesses.

8.3.3 Further Investigation of Ultrasonic Properties

The impact of the hydrophilic polymer hydration process on ultrasonic properties was monitored and showed changes in attenuation and velocity. In the case of a 60% water content polymer, attenuation increased from less than 2 to 2.5dB mm^{-1} (5MHz) after about 25 minutes submersion in water. This was followed by a brief levelling off after approximately 75 minutes, before a gradual reduction to a minimum level of 1dB mm^{-1} once saturation was reached. Velocity underwent a reduction from 2584ms^{-1} when completely dry, to 1757ms^{-1} after 95 minutes submersion in water, when the glassy core

disappeared. This was followed by an unexpected sharp increase to 2132ms^{-1} before a gradual decrease to 1732ms^{-1} as 100% hydration was approached. This was suspected to have resulted from sample compression as the sample underwent a stepped increase in flexibility. The main influence of attenuation increase during hydration was attributed to the plasticisation process occurring at the glassy-rubbery interface resulting from water sorption. The rational behind this hypothesis was explained.

Samples of hydrophilic polymer at different stages of dehydration were shown to exhibit different attenuation levels. Interestingly, a sample at 25% saturation demonstrated a higher attenuation than the same sample completely dry. Dehydration resulted in an increase in attenuation from 0.8dB mm^{-1} at 100% saturation, to 2.5dB mm^{-1} at 25% saturation and back down to 2dBmm^{-1} at 0% saturation.

Attempts were made to propagate shear waves in a sample of hydrated hydrophilic polymer. This involved the development of a new ultrasonic probe capable of delivering shear waves into the test piece at 90° to the surface. The experiments showed no sign of propagation, suggesting that shear wave support is not possible.

8.3.4 Prototype Device

The ultimate phase of this work included the design, development and trial of a prototype ultrasonic inspection device incorporating hydrophilic polymer as a novel solid contact ultrasonic couplant. Alternative design options were considered and discussed before deciding upon a wheel probe philosophy consisting of an interchangeable probe and hydrophilic tyre. The body of the device was fluid filled. A PMMA-VP cross-linked hydrophilic polymer with an equilibrium water content of approximately 60% by wet weight was believed best suited for application with this device. Results have been achieved for both manual and automated inspections at 5MHz in pulse echo mode. The resultant A-scans are similar in appearance to a single crystal delay line probe and immersion test. C-scan data has included defect scanning and time of flight measurement. Ultrasonic results were of equal quality to those achieved by conventional immersion testing, validating the design choices.

8.4 Contribution to Ultrasonic NDT

This research has introduced hydrophilic polymers to the industrial NDT arena. Their ultrasonic properties are highly attractive for utilisation in many application areas and may be easily tailored alongside mechanical properties by manipulation of equilibrium water content and chemical structure. The deployment of hydrophilic polymers as solid contact ultrasonic couplants for the scanning of test components is believed to offer the most benefits over conventional techniques. A prototype wheel probe inspection device has been produced to address this challenging requirement.

The high performance of the prototype has generated results equal in quality to those obtained via conventional immersion testing. Pulse echo operation has been demonstrated, offering inspection options where access is limited.

Employment of this device for both manual and automated inspection can eliminate the need for coupling fluids and their associated limitations. It is anticipated that further development work within the NDT community will generate additional devices incorporating hydrophilic polymers.

Hydrophilic polymers permit the use of higher frequencies than any other flexible solid couplant presently available and at lower contact pressures. This offers improved spatial and depth resolution while minimising risk of test piece damage due to excessive coupling forces. The roller probe design has resulted in patent application in both the UK and USA. The device is now commercially available from the sponsors of this work, units having been supplied into aerospace, space, manufacturing, oil and gas industries.

8.5 Further Research

Results from this research have been disseminated via conference presentation and publication. This has stimulated much interest in hydrophilic polymer application in a variety of ultrasonic applications both within and beyond the scope of this work. Continued research in this area is therefore desireable if the full potential of these materials is to be realised. Suggested topics for further research are discussed below.

8.5.1 Extension of Low Temperature Applications

The hydrophilic polymer evaluated below room temperature demonstrated an increase in attenuation below 5°C. This is believed to be caused by the freezing/thawing action taking place and limits the operational temperature range over which hydrophilic polymers may be used for ultrasonic coupling applications. Hydration of the polymer in an antifreeze solution may provide a route to the useful extension of this temperature range. This might also delay the onset of polymer stiffening, permitting good surface contact to be achieved at lower temperatures. This may be researched using the same measurement procedure employed in this thesis.

8.5.2 Coupling to Rough Surfaces

The ability of a range of hydrophilic polymers to couple effectively to a smooth steel test block was demonstrated in this research. The conformance to materials of defined surface roughness would be of further practical importance, assisting in appropriate hydrophilic polymer selection for particular applications. This may be evaluated ultrasonically with a mechanical rig similar to the one developed in this research.

8.5.3 Further Wheel Probe Development

With regard to the prototype wheel probe, there is a practical limitation to the maximum depth of test piece that may be interrogated without the unwanted occurrence of repeat echoes from the hydrophilic tyre. One method of overcoming this and permitting deeper inspections would be the use of a thicker tyre. This in turn would require a larger water path between the ultrasonic probe and the inner surface of the tyre. The result would be a significantly larger device, which may not be practical. A preferred approach would be to design a wheel probe based on a twin crystal probe. An acoustic curtain would be required extending from the probe itself out to the outer surface of the tyre. This would be a significant design challenge, but one that would generate an inspection device with wider application.

A further enhancement to the wheel probe would be the elimination of the internal water. The presence of the water leaves the chance that an air bubble may be introduced, which could have a detrimental effect on results. The most significant limitation should this occur, involves inspections necessitating the wheel to be used upside-down. In this scenario the bubble of air would be positioned directly in the ultrasound beam, interrupting

transmission. One route to countering this would be the employment of a solid material such as Perspex in place of the water. Such a design would require lubrication at the inner surface of the hydrophilic tyre. This is not an ideal solution as candidate solid materials exhibit significantly higher attenuation than water. A more innovative approach may involve the inclusion of a very high water content hydrophilic polymer, for example 75-85%, in place of the water. This would combine the advantage of the attractive ultrasonic properties of water without the risk of air bubble inclusion.

8.5.4 Frequency Downshift

Further exploration into the relationship between frequency downshift and probe frequency would be beneficial not only for hydrophilic materials but also other materials commonly used as wedges and delay-lines in conventional ultrasonic probes. This research has demonstrated a route by which the frequency propagated into a target material via hydrophilic polymers may be calculated from the known frequency of the ultrasonic probe. This is important for applications necessitating the use of a particular frequency for critical defect resolution. Identification of a relationship between probe frequencies and associated downshift coefficients would enable the generation of a generic equation valid over a wide range of frequencies and hydrophilic polymer thicknesses. This would be particularly useful for future development of new inspection devices incorporating hydrophilic polymers.

8.5.5 Shear Wave Propagation

It is known that pure water does not support the propagation of shear waves. A hydrophilic polymer having an equilibrium water content of 60% showed no evidence of shear wave support. It is feasible that this may not be the case for polymers of lower water contents. The presence of a refracted shear wave in a device incorporating hydrophilic polymers would influence the design as spurious echoes may be generated as a result. Trials conducted into shear wave propagation in polymers of less than 60% water may demonstrate a threshold water content below which shear waves are supported. This may be evaluated with a zero degree shear wave probe similar to those used in this research or by internal reflection techniques also explained.

Bibliography

1. Abd El-Malak, N.A "Ultrasonic Properties of Composites (Polymer – Fibre Glass)" Bull. Mater. Sci. Vol. 20, No. 7, (1997)
2. Achenbach, J.D. "Wave Propagation in Elastic Solids" (North Holland, 1973)
3. Arakawa, T. "A Study of the Transmission and Reflection of an Ultrasonic Beam at Machines Pressed Against each other" Materials Evaluation, 41, 714-719 (1983)
4. Ashbee, K.H.G "Polymer NDE" Proceedings of the European Workshop on Nondestructive Evaluation of Polymer and Polymer Matrix Composites (Technomic, 1986)
5. Baik, J.M. and Thompson, R.B. "Ultrasonic Scattering from Imperfect Interfaces: a Quasi-Static Model" Journal of NDE, Vol.4, 177-196 (1984)
6. Billson, D.R. and Hutchins, D.A. "Development of Novel Piezoelectric Ultrasonic Transducers for Couplant-Free Non-Destructive Testing" British Journal of NDT, 35 (1993)
7. Bankarendo, A.N., Drobot, Y.B. and Kruglov, S.V, Soviet Journal of NDT, Vol. 12 (1975)
8. Bourne, S.J., Newborough, M., Highgate, D.J. and Woodhead, W. "Ultrasound Probe Including Hydrophilic Couplant" Patent Application UK9921846.3 (1999)
9. Bourne, S.J., Newborough, M., Highgate, D.J. and Woodhead, W. "Ultrasound Probe Including Hydrophilic Couplant" Patent Application US-09/396,435 (1999)
10. Bourne, S.J., Buckley, J.M. and Kelly, P.M. "Applications of Air-Scan Technology to Ballistic Impact Protective Systems" Proc. Personal Armour Symposium, Defence Clothing and Textiles Agency (2000a)
11. Bourne, S.J., Newborough, M. and Highgate, D.J. "Novel Solid Contact Ultrasonic Polymers Based on Hydrophilic Polymers" Proc. 15th World Conference on NDT (2000b)
12. Bourne, S.J., Newborough, M. and Highgate, D.J. "High frequency ultrasonic wheel probe using hydrophilic polymers as novel solid couplant" Insight, Vol. 43, No.1 (2001a)
13. Bourne, S.J., Newborough, M. and Highgate, D.J. " An Introduction to Hydrophilic Polymers as High Frequency Solid contact Ultrasonic Couplant" Proc. 2nd Pan American Conference on NDT (2001b)
14. Bray, D.E. and Stanley, R.K. "Nondestructive Evaluation – A Tool for Design, Manufacturing and Service" (McGraw-Hill, 1989)
15. Brown, N. "Methods of Studying Crazing" Methods of Experimental Physics, Vol.16C, Academic Press, New York (1980)

16. Bruck, S.D. "Long-Term Stability of Intraocular Lenses – A Literature Review, Assessment and Testing Protocol" J. Long-Term Effects of Medical Implants 333-350 (1993)

17. BSi 90/70986 GME/23, 23/02 (1990)

18. Buchholz, F.L. and Peppas, N.A. "Superabsorbent Polymers" (ANSI, 1994)

19. Buckley, J.M. and Loertscher, H. "Frequency Considerations in Air Coupled Ultrasonic Inspection" Proc. 38th Conf. Of the British Institute of NDT (1999)

20. Bush, A.W., Gibson, R.D. and Thomas, T.R. "The Elastic Contact of a Rough Surface" Ware, 35, 87-113 (1975)

21. Cadler, C.A. and Wilcox, W.W. Materials Evaluation, Vol. 38, No. 86 (1980)

22. Cahalan, P.T., Coury, A.J., Jevne, A.H., Kallok, M.J. and Perrault, J.J. "Recent Developments in Hydrophilic Polymers" (MD&DI, 1984)

23. Canella, G. "The Effect of Couplant Thickness in Ultrasonic Contact Testing" British Journal of NDT, 179-182 (1974)

24. Cartz, L. "Nondestructive Testing" (ASM International, 1995)

25. Day, "PVDF and Array Transducers" NDT.net Vol.1 No.16 (1996)

26. Dawkins, J.V. "Developments in Polymer Characterisation – 4" (Applied Science Publishers, 1983)

27. Dickson, K.J. "Dry Coupling Ultrasonic Method of Inspection on Composite and Metallic Honeycomb Panels on Aircraft Structures" Pro 10th World Conf on NDT, 216-221 (1982)

28. Dixon, S., Edwards, C. and Palmer, S.B. "High-Temperature Thickness Gauging Using a Highly Deformable Dry Couplant Material" Insight, Vol.42, No.11, 734-736 (2000)

29. Drinkwater, B. and Cawley, P. "An Ultrasonic Wheel Probe Alternative to Liquid Coupling" Insight 36, 430-433 (1994)

30. Drinkwater, B., Dwyer-Joyce, R.S. and Cawley, P. "A Study of Interaction Between Ultrasound and a Partially Contacting Solid-Solid Interface" Proc. Royal Society of London, 452, 2613-2628 (1996a)

31. Drinkwater, B.W. and Cawley, P. "The Effect of Dust and Surface Roughness on the Efficiency of Solid Coupled Ultrasonic Transducers" Rev. Prog. Quant. NDE, 15, 955-962 (1996b)

32. Drinkwater, B., Dwyer-Joyce, R. and Cawley, P. "A Study of the Transmission of Ultrasound Across Solid-Rubber Interfaces" J. Acoust. Soc. Am., 102 (1997a)

33. Drinkwater, B. and Cawley, P. "The Practical Application of Solid Coupled Transducers" Materials Evaluation, 401-406 (1997b)

34. Drinkwater, B. and Cawley, P. "Measurement of the Frequency Dependence of the Ultrasonic Reflection Coefficient from Thin Interface Layers and Partially Contacting Interfaces" Ultrasonics, 479-488 (1997c)

35. Fleury, G. and Gondard, C. "Improvements of Ultrasonic Inspections Through the use of Piezocomposite Transducers" NDT.net, Vol.1, No.9 (1996)

36. Frost, H.M. "Electromagnetic Ultrasound Transducers – Principles, Practice and Applications" Physical Acoustics, 14, 179 (Academic Press, 1979)

37. Gehrke, S.H. "Synthesis, Equilibrium Swelling, Kinetics, Permeability and Applications of Environmentally Responsive Gels" Advances in Polymer Science, 110, 81-144 (1993)

38. Grandia, W.A., Grandia, B., Strycek, J. and Loertscher, H. "Airscan Transducers, Techniques and Applications" NDT.net (1994)

39. Greenwood, J.A. and Williamson, J.B.P. "Contact of Normally Flat Surfaces" Proc. R. Soc. Lond. 295, 300-319 (1966)

40. Haines, N.F. "The Theory of Sound Wave Transmission and Reflection at Contacting Surfaces" CEGB Berkeley Nuclear Laboratories, Rept RD-B-N4744 (1980)

41. Halmshaw, R. "Mathematics and Formula in NDT" (British Institute of NDT, 1978)

42. Halmshaw, R. "Non-Destructive Testing – Second Edition" (Edward Arnold, 1991)

43. Highgate, D.J. 'Relevant properties of hydrophilic polymers for lens performance' Optician, pp 12-19, Jan 4 (1974)

44. Highgate, D.J. and Frankland, J.D. 'The development of an improved hydrophilic contact lens material' Optician, June 13 (1975)

45. Highgate, Knight, C. and Probert, S.D. "Anomalous 'Freezing' of Water in Hydrophilic Polymeric Structures" J. Applied Energy, pp 243-259 (1989)

46. Highgate, D., Kay, D., Knight, C. and Probert, S.D. "Fluidised Beds as 'Coolth' Stores" J. Applied Energy, 39 (1991)

47. Hossack, J.A. and Hayward, G. "Finite-Element Analysis of 1-3 Composite Transducers" IEEE Trans Ultrason, Ferroelectrics, Freq Contr, UFFC-38, 618-629 (1991)

48. Hossack, J.A., Cach, M., Platte, M. and Reis, A. "Piezoelectric Materials for Ultrasonic Probes" NDT.net Vol.1, No.9 (1996)

49. Hsu, D.K., Kwang-Hee Im, and In-Young Yang, "Applications of Electromagnetic Acoustic Transducers in NDT of Non-Conducting Composite Materials", ASME International Journal, Vol.13, No.5, 403-413 (1999)

50. Hull, J.B., Langton, C.M., Barker, S. and Jones, A.R. "Identification and Characterisation of Materials by Broadband Ultrasonic Attenuation Analysis" Journal of Materials Processing Technology, 56, 148-157 (1996)

51. Hutchins, D.A. and Macphail, J.D. "A New Design of Capacitance Transducers for Ultrasonic Displacement Detection" J Phys E, 18, 69-73 (1985)

52. Hutchins, D.A. "Ultrasonic Generation by Pulsed Lasers" (Academic Press, 1988)

53. Hutchins, D.A., Breese, L.F. and Billson, D.R. "Resonance Studies of Bonded Aluminium Joints" Nondestr Test Eval, 10, 149-165 (1993)

54. Johnson, K.L. "Contact Mechanics" (Cambridge University Press, Cambridge, 1985)

55. Kalal, J. "Water Sensitive Chemically Cross-Linked Gels" Institute of Macromolecular Chemistry, Czechoslovak Academy of Sciences, Prague 6, Czechoslovakia. (Circa. 1980)

56. Kaye, G.W.C. and Laby, T.H. 'Tables of physical and chemical constants' Longman, 14th Edition (1975)

57. Kendall, K. and Tabor, D. "An Ultrasonic Study of the Area of Contact Between Stationary and Sliding Surfaces" Proc. R. Lond. 323, 321-340 (1971)

58. Kinsler, L.E. and Frey, P. "Fundamentals of Acoustics", 2nd Edition, Wiley, New York (1962)

59. Klein, M., Pouet, B. and Badur, G.D. "Recent Advances in Adaptive Receivers for Laser Generated Ultrasound" NDT.net, Vol.5, No.6 (2000)

60. Krautkramer, J. "Determination of the Size of Defects by the Ultrasonic Impulse Echo Method" British Journal of Applied Physics, Vol.10 (1959)

61. Krautkramer, J. and Krautkramer, H "Ultrasonic Testing of Materials" (Springer-Verlag, 1983)

62. Krehl, P., Schwirke, F. and Cooper, A.W. Journal of Applied Physics, Vol. 46 (1975)

63. Krolikowski, J., Szczepek, J. and Witczak, Z. "High Pressure in Ultrasonic Study of the Contact of Solids" Physica, 139B & 140B, 803-805 (1986)

64. Krolikowski, J. and Szczepek, J. "Prediction of Contact Parameters using Ultrasonic Method" Wear, 148, 181-195 (1991)

65. Kudela, V. "Encyclopaedia of Polymer Science and Technology" Ch. Hydrogels. Edited by Kroschwitz, J. (John Wiley, 1990)

66. Larson et al, "Coupling Sheath for Ultrasound Transducers" US patent No.US 6039694 (2000)

67. Latif, R "Ultrasonic Probe Calibration Software with Built in Database", MSc. In PC Interfacing and Software Applications, University of Central Lancashire, (2000)

68. Lecru, D. "Inspection of Bond Assemblies Using Roller-Type Ultrasonic Probes Without Coupling Fluid" Rev. of Progress in Quantitative NDE, Vol.6 1779-1785 (1987)

69. Luprano, V.A.M., Montagna, G. and Maffezzoli, A. "A Study of the Water Sorption Kinetic of Poly(HEMA) Hydrogels by SLAM and FT-IR Measurements" IEEE Transactions on Ultrasonics, Ferroelectrics, and Frequency Control, 43, 948-955 (1996)

70. Maffezzoli, A., Luprano, V.A., Montagna, G., Nicolais, L., and Esposito, F. " Ultrasonic Wave Attenuation During Water Sorption in Poly(2-hydroxyethyl methacrylate) Hydrogels" J. Polymer Engineering and Science, 36, 1832-1838 (1996)

71. Maffezzoli, A., Luprano, A.M., Montagna, G. and Nicolais, L. "Ultrasonic Characterization of Water Sorption in Poly (2-hydroxyethyl methacrylate) Hydrogels" J. Applied Polymer Science, 67, 823-831 (1998)

72. Manthey, W., Kroemer, N. and Magori, V. "Ultrasonic Transducers and Transducer Arrays for Applications in Air" Meas Sci Techni, 3, 249-261 (1992)

73. Maragatan, F.J., Thompson, R.B., Rose, J.H. and Gray, T.A. "The Interaction of Ultrasound with Imperfect Interfaces: Experimental Studies of Model Structures" J NDE, 11, 109 (1992)

74. Mason, W.P. and Thurston, R.N. "Physical Acoustics – Volume XV" (Academic Press, 1981)

75. Mathur, A.M. "Methods for Synthesis of Hydrogel Networks – A Review" J. Macromolecular Science – Reviews in Macromolecular Chemistry and Physics, C36, 2, 405-430 (1996)

76. Matthews, F.L and Rawlings, R. "Composite Materials: Engineering and Science" 415-423 (1994)

77. McCrum, B.E., Read, B.E. and Williams, G. "Anelastic and Dielectric Effects in Polymeric Solids", J. Wiley, London (1967)

78. McKie, A.D.W. and Addison, R.C. "Rapid Inspection of Composites using Laser Brushed Ultrasound" Rev Prog Quant NDE, 12, (Plenum Press. New York) 507-516 (1993)

79. Miller, G.F. and Pursey, H. Proceedings of the Royal Society of London, Vol.223 (1954)

80. Molyneux, P. "The Interface Between the Chemistry of Aqueous Polymer Solutions and their Application Technology" Department of Pharmacy, Chelsea College, UoL. P.1-20. (Circa 1980)

81. Monchalin, J.P. "Optical Detection of Ultrasound" "EEE Trans Ultras Ferr Freq Contr, UFFC-33, 485-493 (1986)

82. Monchalin, J.P. "Progress Towards the Application of Laser Ultrasonics in Industry" Rev Prog Quant NDE, 12 (Plenum Press. New York) 495-506 (1993)

83. Montecalvo, "Solid Multipurpose Ultrasonic Biomedical Couplant Gel in Sheet Form and Method" US patent No. US 5522878 (1996)

84. Morgan Electro Ceramics TP-224 "Piezoelectric Coupling" www.morgan-electroceramics.com

85. Morgan Electro Ceramics TP-226 "Properties of Piezoelectricity Ceramics" www.morgan-electroceramics.com

86. Morgan Electro Ceramics TP-234 "Piezoelectric Ceramics" www.morgan-electroceramics.com

87. Nagy, P.B., Rose, J.H. and Bilgen, M. "Excess Scattering Induced Loss at a Rough Surface Due to Partially Coherent Double-Reflection" Review of Progress in Quantitative Nondestructive Evaluation, 14, 1845-1852 (1995)

88. Nagy, P.B. "Ultrasonic Classification of Imperfect Interfaces" J NDE, 11, 127 (1992)

89. Nicoletti, D. and Sorli, B. "Measurement of Changes in Surface Roughness Using Ultrasonic Reflection Coefficient" Review of Progress in Quantitative Nondestructive Evaluation, 14, 1853-1860 (1995)

90. Okoroafor, E. "Novel Couplants for Ultrasonic Testing of Structural Materials: A Feasibility Study" (1996)

91. Orr, et al, "Ultrasound Medical Diagnostic Device Having a Coupling Medium Providing Self-Adherence to a Patient" US Patent No. US 5394877 (1995)

92. Peaker, F.W. and Robb, J.C. "Progress in High Polymers" (London Heywood & Company Ltd, 1961)

93. Petillion, O., Dupuis, J.P., Voillaume, H. and Tretout, H. "Application of Laser Based Ultrasonics for the Aerospace Industry" NDT.net, Vol.3 No.9 (1998)

94. Pipes, R.B. "Nondestructive Evaluation and Flaw Criticality for Composite Materials" (American Society for Testing Materials, 1979)

95. Ready, J.F. "Effects of High Power Laser Radiation" (New York: Academic, 1971)

96. Refojo, M.F. "Vapour Pressure and Swelling Pressure of Hydrogels for Medical and Related Applications, 31, 37-51 (1976)

97. Richardson et al, "Ultrasonic Transducer Coupling Medium" US patent No.US 4459854 (1984)

98. Rivera, O. and Vitale, E.V. "Airborne Ultrasonic Scanning" Materials Evaluation, 46, 614-615 (1988)

99. Robinson, A.M., Drinkwater, B.W. and Freemantle, R.J. "An Integrated Systems Approach to Automated Scanning and Analysis of Engineering Structures" Insight, Vol.42, No.11, 714-719 (2000)

100. Sachse, W. and Hsu, N.N. "Ultrasonic Transducers for Materials Testing and Their Characterisation" Physical Acoustics, Vol. XIV, (Academic Press, NY) 277-407 (1979)

101. Salgueiro da Silva, M., Eccleston, R.S., Bessa Sousa, J. and Palmer, S.B. "Automated Measurement of Ultrasound Velocity and Attenuation" Ultrasonics, Vol. 30 No. 6 (1992)

102. Schindell, D.W., Hutchins, D.A., Zou, L. and Sayer, M. "Capacitance Devices for the Generation of Air-borne Ultrasonic Fields" Proc IEE Ultrasonics Symp, 843-846 (1982)

103. Scruby, C.B., Dewhurst, R.J. Hutchins, D.A. and Palmer, S.B. Journal of Applied Physics, Vol. 51 (1981)

104. Semenova, S.I. "Hydrophilic Membranes for Pervaporation: An Analytical Review" J. Desalination, 110, 251-286 (1997)

105. Shah, K.R. " Hydrophilic Hydrophobic Domain Polymer Systems" ACS Symposium Series, 467, 468-483 (1991)

106. Sharpe, R.S. "Research Techniques in Nondestructive Testing – Vol. VIII" (Academic Press, 1985)

107. Sheffield Polytechnic, "Measurement of Ultrasonic Attenuation in Metals", School of Science, Division of Applied Physics (JDB:EXP-10.22)

108. Silk, M.G. "Ultrasonic Transducers for Nondestructive Testing" (Adam Hilger Ltd, 1984)

109. Smith, R.A., Marriott, A.B. and Jones, L.D. "Delamination Sizing in Fibre-Reinforced Plastics using Pulse-Echo Amplitude" Insight, Vol.39, No.5 (1997)

110. Smith, R.A., Jone, L.D., Zeqiri, B. and Hodnett, M. "Ultrasonic C-scan Standardisation for Fibre-Reinforced Polymer Composites – Minimising the Uncertainties in Attenuation Measurements" Insight, Vol. 40, No. 1, 34-43 (1998)

111. Smith, R.A "An Introduction to the Ultrasonic Inspection of Composites" Course Hand-out, Non-Destructive Evaluation of Composite Materials, DERA (1999)

112. Soloway, "Acoustic Couplant for use with an Ultrasonic Search Unit" US patent No.US 3921442 (1975)

113. Storer, R.A. "Compilation of ASTM Standard Definitions – 8th Edition" (American Society for the Testing of Materials, 1994)

114. Taylor, S. "Evaluation of the impact protection of UHMWPE" M.Sc. Thesis, Imperial College (1997)

115. Thavasimuthu, M., Palanichamy, P, Subramanian, C.V., Bhattacharya, D.K. and Raj, B. "Evaluation of Abrasive Wheels by an Ultrasonic Dry Couplant Technique" British Journal of NDT, Vol.31, No.7 (1989)

116. Thavaimuthu, M., Palanichamy, P, Subramanian, C.V., Bhattacharya, D.K., Raj, B. and Rao, J. "Inspection of Steam Turbine Rotor Blade-to-Shroud Rivets by Dry Couplant Ultrasonic Testing: A Case Study" British Journal of NDT, Vol. 32, No.2 131-133 (1990)

117. Thompson, R.B. "Physical Principles of Measurements with EMAT Transducers" (Academic Press, 1990)

118. Van Krevelen, D.W. "Properties of Polymers", Elsevier, Amsterdam (1990)

119. Vincent, A. "Influence of Wearplate and Coupling Layer Thickness on Ultrasonic Velocity Measurement" Ultrasonics, 25, 237-243 (1987)

120. Wagner, J.W. "Optical Detection of Ultrasound" Physical Acoustics, Vol. XIX (Academic Press, New York) 201-266 (1990)

121. Wokalek, "Method of Transmitting Ultrasound into a Body" US patent No.US 4905700 (1990)

122. Woo, K.L. and Thomas, T.R. "Contact of Rough Surfaces: A Review of Experimental Work" Wear, 58, 331-340 (1980)

123. Wooldridge, A.B. "The Effects of Compressive Stress on the Ultrasonic Response of Steel-Steel Interfaces and of Fatigue Cracks" CEGB North Western Region, Report No. NW/SSD/RR/42/79, (1979)

124. Yano, T., Tone, M., and Fukumoto, A. "Range Finding and Surface Characterisation Using High Frequency Air Transducers" IEEE Transactions in Ultrasonics, Ferroelectrics and Frequency Control, 34, 232-236, (1987)

125. Anon. "Hydrogels in Medicine and Pharmacy – Volume 1 Fundamentals" (Circa.1985)

Appendix A

Review of Ultrasonic Non Destructive Testing and Test Methods

Review of Ultrasonic Non Destructive Testing and Test Methods

A.1 Pulse Generation

Ultrasonic pulses are most commonly generated and detected via the piezoelectric effect. The phenomenon of piezoelectricity is well documented and is exhibited in a number of naturally occurring materials, perhaps the most well known example being quartz. The effect was discovered in 1880 by the Curie brothers, who observed that when certain materials are mechanically deformed, electrical charges are generated at their surfaces. The reverse effect was discovered the following year whereby the same materials deform when placed within an electric field. The former is used to detect ultrasound and the latter to transmit. Wood and Loomis (1927) conducted the pioneering work on the use of the piezoelectric effect for the generation of ultrasonic waves.

Stimulating a piezoelectric crystal at its natural frequency using a voltage generates pulses of sound. For typical ultrasonic testing applications, this might be between 500kHz and 10MHz. Backing the crystal with a material that absorbs sound readily makes the pulse of sound directional. Consider such a crystal in contact with (coupled to) a steel test piece. Excitation of the crystal would generate ultrasonic energy, which would be transmitted into the steel. As the pulse of waves travel through the steel, it undergoes a degree of spreading and suffers some attenuation. It will be reflected or scattered at any surface or discontinuity such as an internal flaw within the steel. A second piezoelectric crystal placed appropriately on the steel surface could detect the reflected ultrasound. This results in a voltage generated in that crystal directly proportional to the intensity of the returning ultrasound. The time interval between the transmitted and reflected pulses is a measure of how far the discontinuity is from the surface of the test piece, calculated from the known speed of sound in the material under examination. The amplitude of the returning pulse may be used as a guide to the thickness and size of the flaw/discontinuity. This system is known as pulse-echo testing and is the basis of ultrasonic flaw detection and thickness metering. One crystal can be used for alternately transmitting and receiving the sound, or two crystals can be used in a 'pitch catch' arrangement, one always transmitting and the other always receiving both scenarios are represented in Figure A.1. [Krautkramer 1983, Silk 1984, Halmshaw 1991 and Cartz 1995] The role of

the piezoelectric crystal transforming electrical to mechanical energy and vice versa, has led to the term transducer.

Through transmission is an alternative method of examination. This requires two transducer crystals (probes) on opposite sides of the test piece. This technique may be used where very small defects are present, too small to generate detectable echoes of their own. Instead, one probe transmits into the test piece and the other monitors the amplitude of the ultrasound detected on the other side. This will be sensitive to the presence of defects but unable to detect their distance from the surface. An alternative application would be the detection of large delaminations in composite materials. [Smith, 1999]

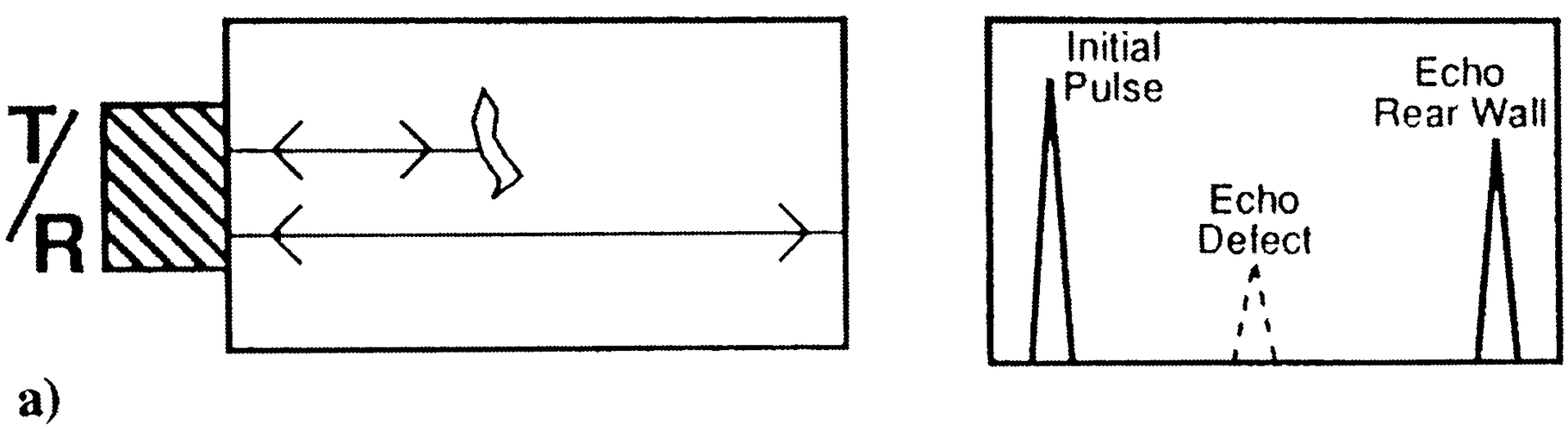

Figure A.1 Schematic representation of a) pulse echo operation and b) through transmission. Cartz [1995]

A.2 Waves – Longitudinal, Shear and Surface

The ultrasonic waves are mechanical vibrations and so have a different wavelength in different materials. They are possible because of the elastic properties of the material they pass through and are due to induced particle vibration in the material. If the particle vibration is sinusoidal, the waves can be assigned a single wavelength, λ, from the well-known formula below, where f is the frequency and V is the wave velocity.

$$f = \frac{V}{\lambda}$$ **Equation A.1**

A pulse of ultrasonic energy can be considered as the synthesis of a series of purely sinusoidal waves of different frequencies and amplitudes (Figure A.2). The narrower the pulse, the greater the number of frequency components, as is well known from Fourier analysis.

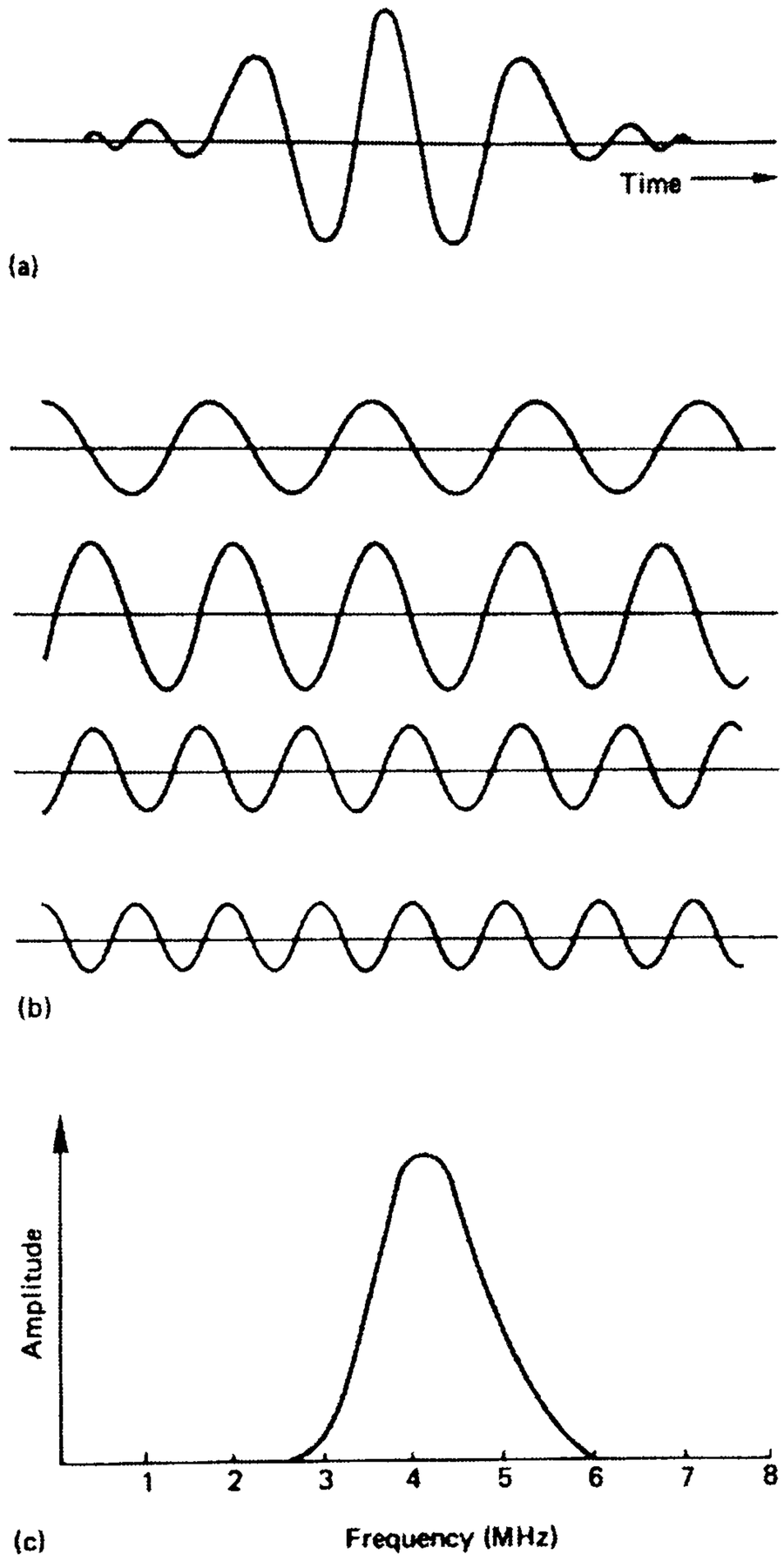

Figure A.2 Representation of the frequency components of an ultrasonic pulse. A) Ultrasonic pulse, B) Frequency components of different amplitudes, and C) Frequency Spectrum. Halmshaw [1991]

If the particle motion of a wave is along the line of the direction of travel of the wave, the resulting wave is called a compression wave (or sometimes a longitudinal wave). Such waves can be propagated in solids, liquids and gases. In solid materials it is also possible for the particle movement to be at right angles to the direction of travel of the wave. Such waves are usually called shear waves (or sometimes, transverse waves). These usually have a velocity of approximately half that of longitudinal waves in the same material and for practical purposes cannot be generated in liquids.

Various types of surface waves can also be generated in solid material. Rayleigh waves are one type of surface wave that can be generated on the

free surface of any solid material. In Rayleigh waves the particle movement is elliptical and such waves exist only in the surface layer of large solids. At greater depths than two wavelengths below the surface the particle motion is virtually zero. The surface velocity is usually about 0.9 times the shear wave velocity in most solids [Krautkramer, 1983]. Rayleigh waves on a solid surface are non-dispersive, but in a layered medium, dispersive Rayleigh waves (i.e. the wave velocity is frequency-dependent) are possible.

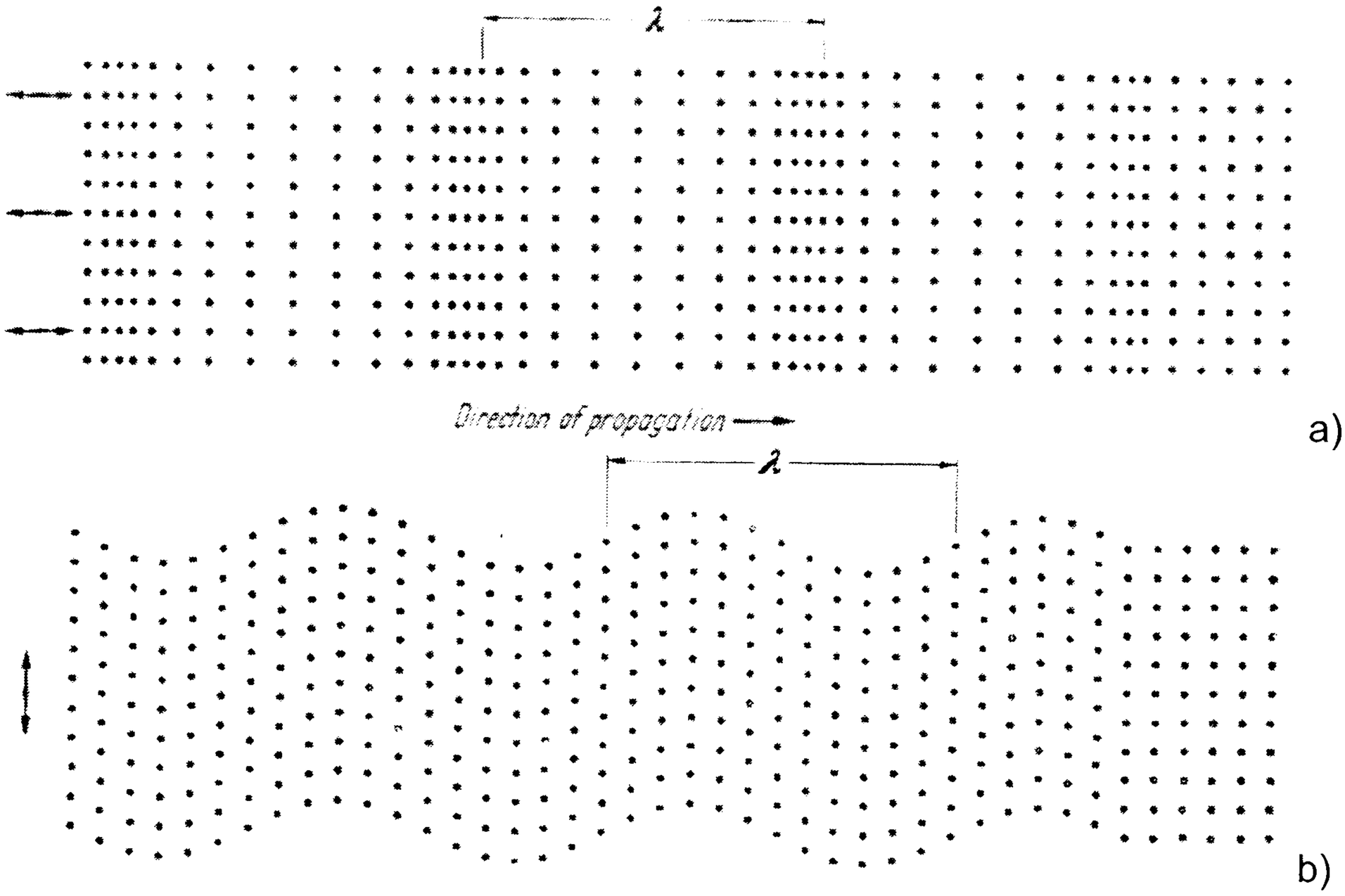

Figure A.3 Schematic representation of particle motion in a) compression and, b) shear waves. [Krautkramer. 1983]

In plate material, where the thickness is of the order of a few wavelengths, again, various forms of surface wave are possible, the most important forms for NDT being Lamb waves. These are a combination of longitudinal and shear waves, the proportion dependent on the frequency. With Lamb waves there is therefore a component of wave motion at right angles to the surface and so they may be regarded as complex resonances of the plate. The wave velocity depends on the plate thickness, the frequency, the mode order and the material. [Krautkramer, 1983]

Surface waves are used for special applications in ultrasonic testing of materials, but by far the most important types of waves for industrial ultrasonic applications are the compression and shear waves.

A.3 Wave Velocity

The velocity of various types of ultrasonic wave can be calculated from the elastic properties of the material through which it propagates [Krautkramer, 1983].

$$Vc = \left[\frac{E(1-\sigma)}{\rho(1+\sigma)(1-2\sigma)} \right]^{\frac{1}{2}}$$ **Equation A.2**

$$Vs = \left[\frac{E}{2\rho(1+\sigma)} \right]^{\frac{1}{2}}$$ **Equation A.3**

A.4 Waves at Boundaries

When an ultrasonic wave is perpendicularly incident at a plane boundary between two media, some ultrasonic energy will be transmitted through the boundary and some reflected. The percentages of energy transmitted and reflected depend on the specific acoustic impedance, Z, defined for each material as

$$Z = \rho V$$ **Equation A.4**

For two materials in theoretical perfect contact but of different acoustic impedances, Z_1 and Z_2, the percentage of energy transmitted, E_T, is given [Krautkramer, 1983] by

$$E_T = \frac{4Z_1Z_2}{(Z_1+Z_2)^2} \times 100$$ **Equation A.5**

and the reflected energy, E_R, by

$$E_R = \left(\frac{Z_1 - Z_2}{Z_1 + Z_2} \right)^2 \times 100$$ **Equation A.6**

These formulas are valid for both compression and shear waves, but as shear waves cannot be sustained in a liquid or gas, a shear wave is always completely reflected at a solid/liquid or solid/gas interface.

A common practical case is the water/steel (or steel/water) interface. Inserting suitable values, it can be calculated that at a water/steel interface, 12% of the incident energy is reflected and 88% is transmitted.

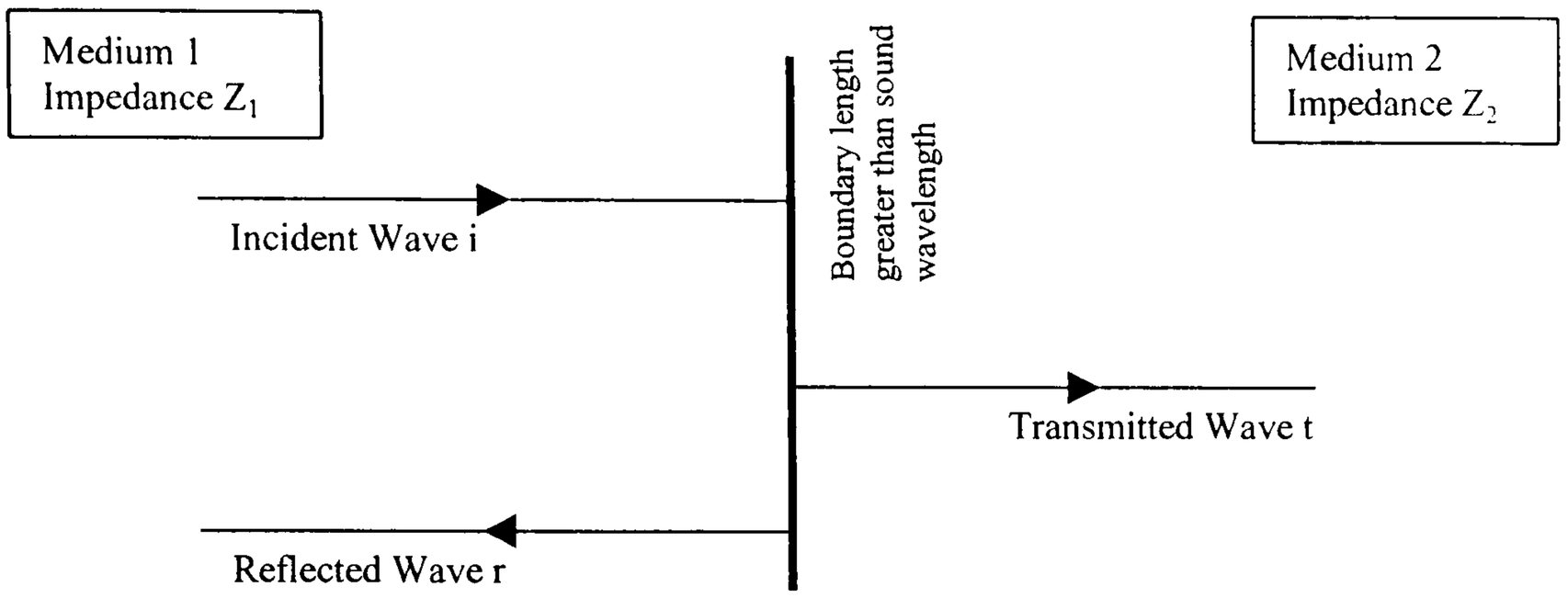

Figure A.4 Representation of ultrasound being transmitted and reflected from an interface between two materials of different acoustic impedance.

It should be noted that Equations A.5 and A.6 are for transmitted and reflected energies. For amplitude values, the square root is taken. These equations are for single, large area interfaces, but the double interface is also of practical importance (Figure A.5).

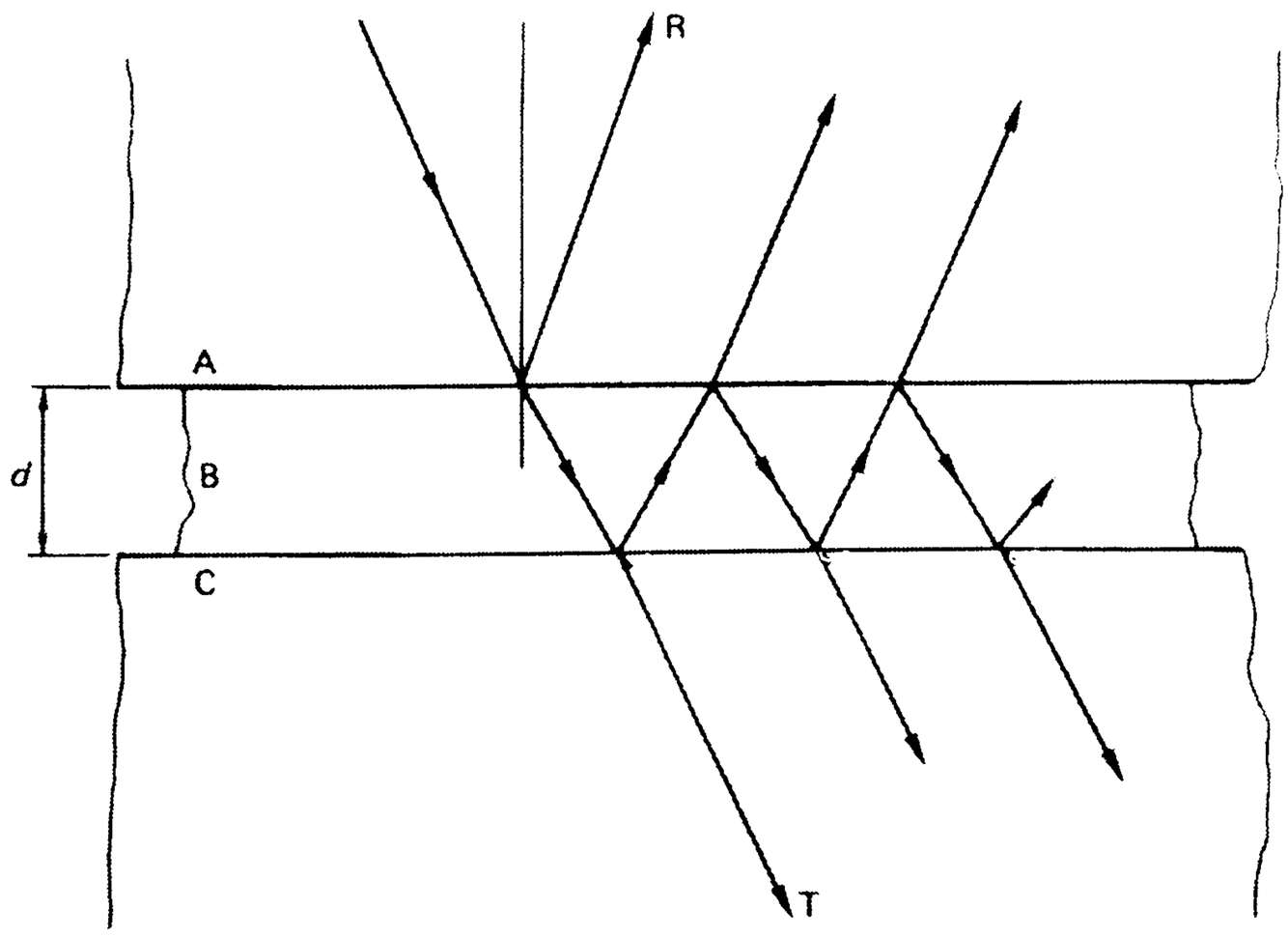

Figure A.5 Representation of ultrasound passing through a double interface (refraction effects re ignored). Halmshaw [1991]

The wave in material A is split at the interface between A and B into a transmitted and reflected wave. The transmitted component is again divided at the interface between B and C and so on. The result is a sequence of

reflected waves in both directions between A and C, and depending on the wave phases there may be interference in both the reflected and transmitted components. Note that the beam is shown entering material A at an angle. This is only to aid visualisation. Here we are considering a beam of normal incidence. The equation for transmission from A to C through B (a layer of thickness L) is given below [Billson and Hutchins, 1993 originally from Kinsler and Frey, 1962]:

$$E_{Plate} = \frac{4Z_3Z_1}{(Z_3+Z_1)^2\cos^2 k_2L + \left[Z_2 + \frac{Z_3Z_1}{Z_2}\right]^2 \sin^2 k_2L} \qquad \textbf{Equation A.7}$$

where k_2 is the wave-number in the layer medium at the particular frequency of interest, and is given by:

$$k_2 = \frac{2\pi}{\lambda_2} \qquad \textbf{Equation A.8}$$

where λ_2 is the wavelength in the layer.

Maximum transmission occurs when L is an integral number of half wavelengths and minimum transmission when L is an odd number of quarter wavelengths. The effect is of importance in determining the thickness of couplant used as an interface between the piezoelectric element of a probe and the specimen surface. For optimum transmission, the couplant should have a thickness of one half wavelength (or multiple thereof).

A.5 Reflection and Refraction at Oblique Incidence

When a compression wave hits an interface between two 'ultrasonically different' media (A and B) at an angle other than 90°, a portion is reflected back and a portion is transmitted across the interface as with normal incidence. The angle of reflection of the compressional wave in material A is equal to the angle of incidence. Snell's Law describes the relationship between the angle of incidence and the angle of refraction of the compressional wave in material B:

$$\frac{\sin\alpha_i}{\sin\beta_C} = \frac{V_{CA}}{V_{CB}} \qquad \textbf{Equation A.9}$$

Where α_i and β_C are the angles of incidence and refraction respectively and V_{CA} and V_{CB} are the compression wave velocities in the two materials A and B.

What also happens at the interface is that a component of the compression wave is converted into a shear wave, part of which is reflected in material A and part refracted in material B. As is the case with the compression waves, the shear waves have different velocities in the different materials either side of the interface. Again, Snell's Law describes the relationship between the angles:

$$\frac{\sin \alpha_S}{\sin \beta_S} = \frac{V_{SA}}{V_{SB}} \qquad \textbf{Equation A.10}$$

where α_S and β_S are the angles of reflected and refracted shear waves respectively. V_{SA} and V_{SB} are the shear wave velocities in materials A and B. These expressions hold for both incident compression and incident shear waves.

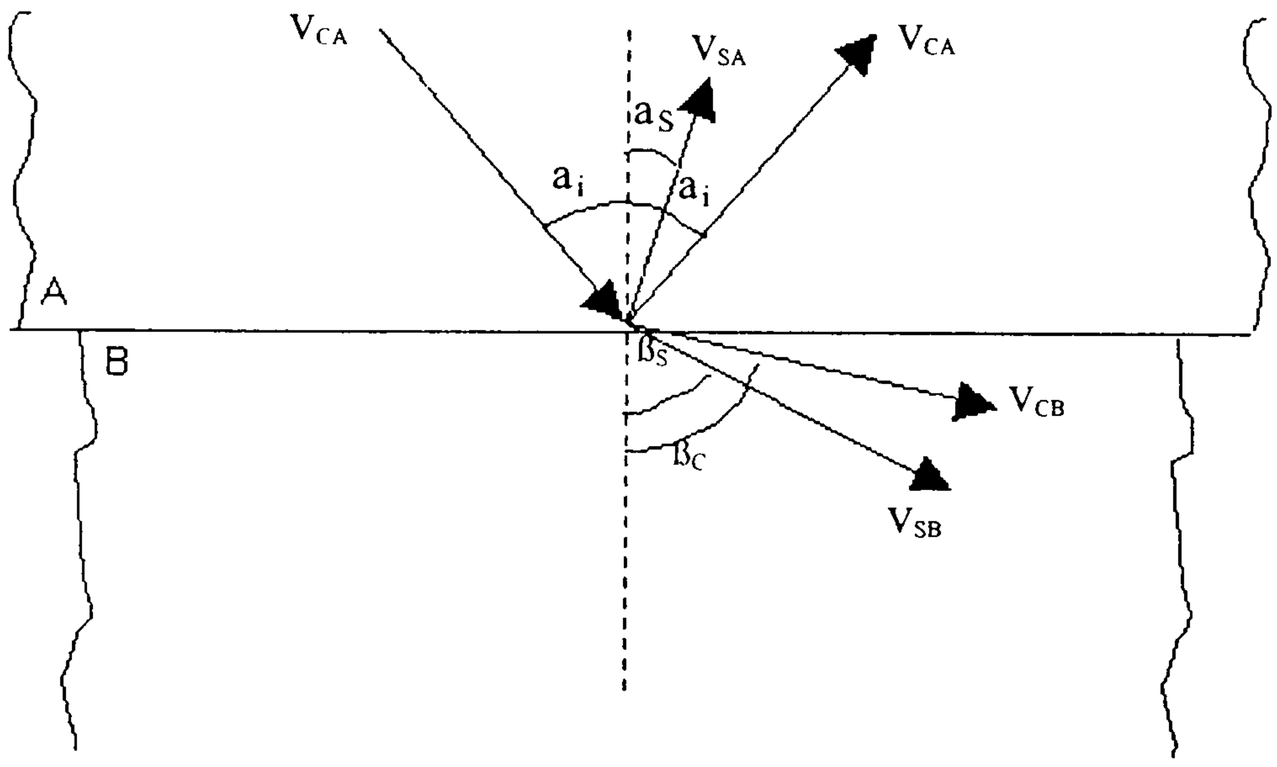

Figure A.6 Schematic of reflected and refracted ultrasound when incident on an interface at angle other than 90°.

As the velocity of compression waves is always greater than the velocity of shear waves in a given material, β_C will always be greater than β_S. It is also noteworthy that if $V_A > V_B$, the refracted waves will be bent towards the normal and if $V_B > V_A$, the refracted waves will be bent away from the normal (as is the case in Figure A.6). Therefore, in the latter scenario, an angle of incidence can be achieved where the angle of the refracted compressional wave (β_C) is equal to 90°, leaving only a refracted shear wave in material B. This angle of incidence is known as the first critical angle. The angle of incidence may be increased further until the shear wave is no longer present in material B. This is known as the second critical angle.

Critical angles are of importance in NDT for applications that require ultrasonic waves to be introduced into components at angles other than 90°, for example weld testing in steels. Indeed, angle probes for such applications incorporate a Perspex wedge, the ultrasonic velocity of which is lower than that of steel. Therefore, a compressional wave introduced to the wedge so as to strike the interface with the steel at an angle between the two critical angles will result in a single shear wave being generated in the steel. Varying the angle of incidence controls the angle of the refracted shear wave in the steel. The critical angles in this case (Perspex to steel) are 27° and 56° respectively. Figure A.7 is a schematic representing an angle beam probe being used to inspect a weld between two metal plates.

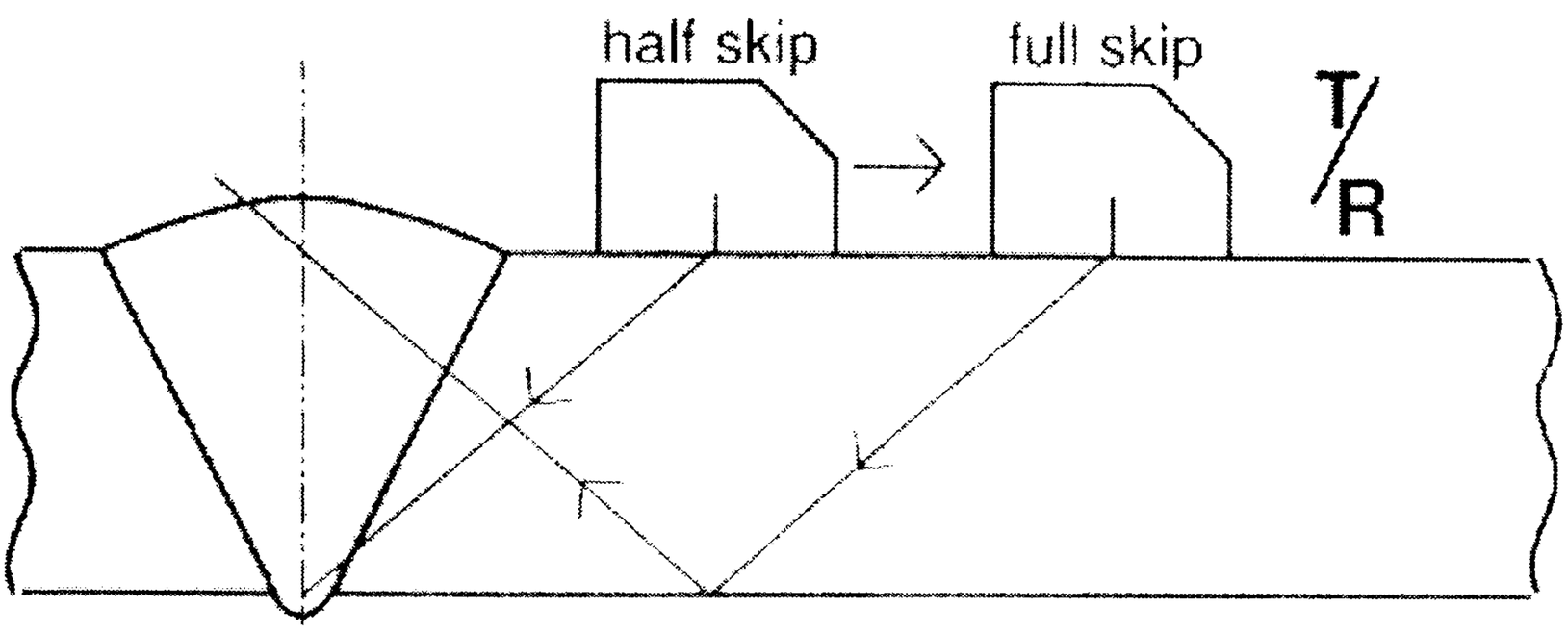

Figure A.7 Schematic of angle probe as used for the weld testing application. Cartz [1995]

A.6 Attenuation

As ultrasound passes through a solid, its intensity will reduce. This is due to reflection and scattering caused by discontinuities and absorption due to frictional forces of the particles of the solid. This reduction in beam strength can be expressed by:

$$I_X = I_O e^{-\mu X} \qquad \textbf{Equation A.11}$$

Where I is the intensity at a distance x from an initial intensity I_O. Generally, μ is taken as the sum of the true attenuation coefficient μ_T and the scatter coefficient μ_S.

Decibels (dB) are a convenient way of measuring changes in intensity or amplification. A decibel is one tenth of a bel, which is a unit based on

logarithms to the base 10. Thus, two powers P_1 and P_2 are said to differ by n bels if:

$$\frac{P_1}{P_2} = 10^n$$ **Equation A.12**

or

$$n = \log_{10}\left(\frac{P_1}{P_2}\right) bels$$ **Equation A.13**

$$n = 10\log_{10}\left(\frac{P_1}{P_2}\right) decibels \text{ (dB)}$$ **Equation A.14**

Acoustic power (or intensity) is proportional to (amplitude)^2, so for comparison of amplitudes A_1 and A_2, the equation can be rewritten,

$$n = 10\log_{10}\left(\frac{A_1^2}{A_2^2}\right) = 20\log_{10}\left(\frac{A_1}{A_2}\right) decibels$$ **Equation A.15**

It should be noted that the attenuation coefficient is also a function of frequency. According to Mason and McSkimin [quoted in Halmshaw, 1991], there is a true absorption, which is proportional to frequency and a scatter coefficient which, is dependent on the relationship between the probe diameter (D) and the wavelength of the ultrasound (λ).

A.7 Beam Shape

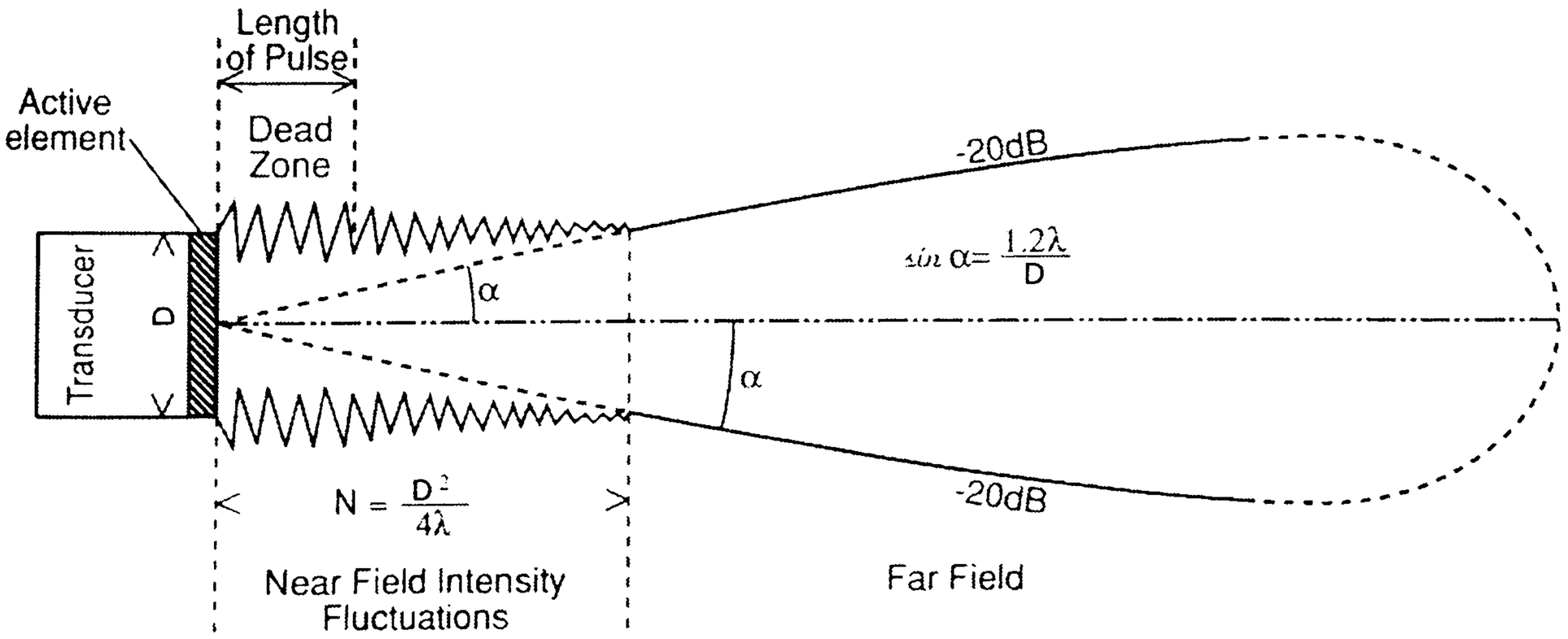

Figure A.8 Representation of an ultrasonic beam generated by a piezoelectric transducer showing the dead zone, near field length and beam divergence angle. Cartz [1995]

The ultrasonic beam generated by a piezoelectric transducer can be split up into two regions, the near field and far field, alternatively known as the Fresnel and Fraunhofer zones respectively. Figure A.8 illustrates a common representation of the beam shape with the near and far fields marked on it. The near field length may be calculated as,

$$N = \frac{\left(D^2 - \lambda^2\right)}{4\lambda}$$

Equation A.16

which is often abbreviated to

$$N = \frac{D^2}{4\lambda}$$

Equation A.17

Consider the ultrasonic beam at a very small distance from the transducer crystal. There would be many local pressure variations across the width of the beam. As we move away, the beam width would remain fairly constant while the beam profile would undergo modification, passing through a central minimum at half the nearfield length before reaching a central maximum at the nearfield length. This is represented pictorially in Figure A.9a. As we continue to move away from the transducer crystal, past the nearfield length, the beam width would begin to increase and the beam profile would become more constant. This is represented in Figure A.9b.

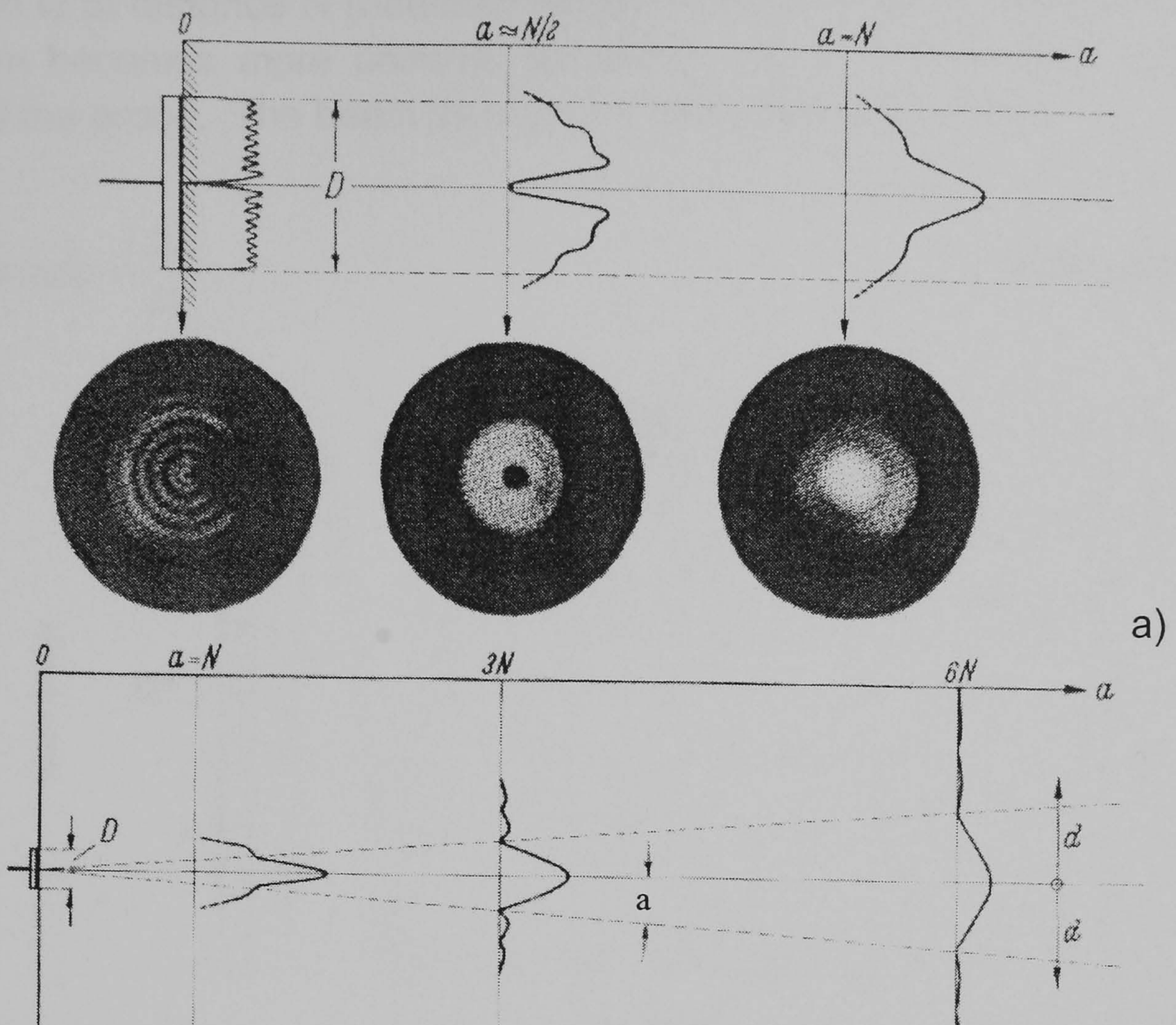

Figure A.9 Representation of ultrasonic beam profile simulated for an ideal piston oscillator A) at distances short of, and B) beyond the nearfield length, Krautkramer [1983]

Indeed, if the piezoelectric crystal is considered to be a simple piston, the acoustic pressure may be calculated at any position along the acoustic axis (according to Krautkramer, 1983 and Halmshaw, 1991) by the following equation,

$$P_R = P_0 2\sin\left\{\frac{\pi}{\lambda}\left[\left(\frac{D^2}{4}+R^2\right)^{\frac{1}{2}}-R\right]\right\} \qquad \textbf{Equation A.18}$$

where P_R is the acoustic pressure at a distance R along the acoustic axis and D is the diameter of the crystal. This may be plotted as relative amplitude against distance from the crystal as illustrated in Figure A.10. The last

maximum is at distance N (nearfield length) from the crystal. After this point, the beam becomes more uniform, spreading out as if originating from the centre of the probe. The beam divergence half angle is given by

$$\sin(\alpha) = \frac{1.2\lambda}{D}. \qquad \textbf{Equation A.19}$$

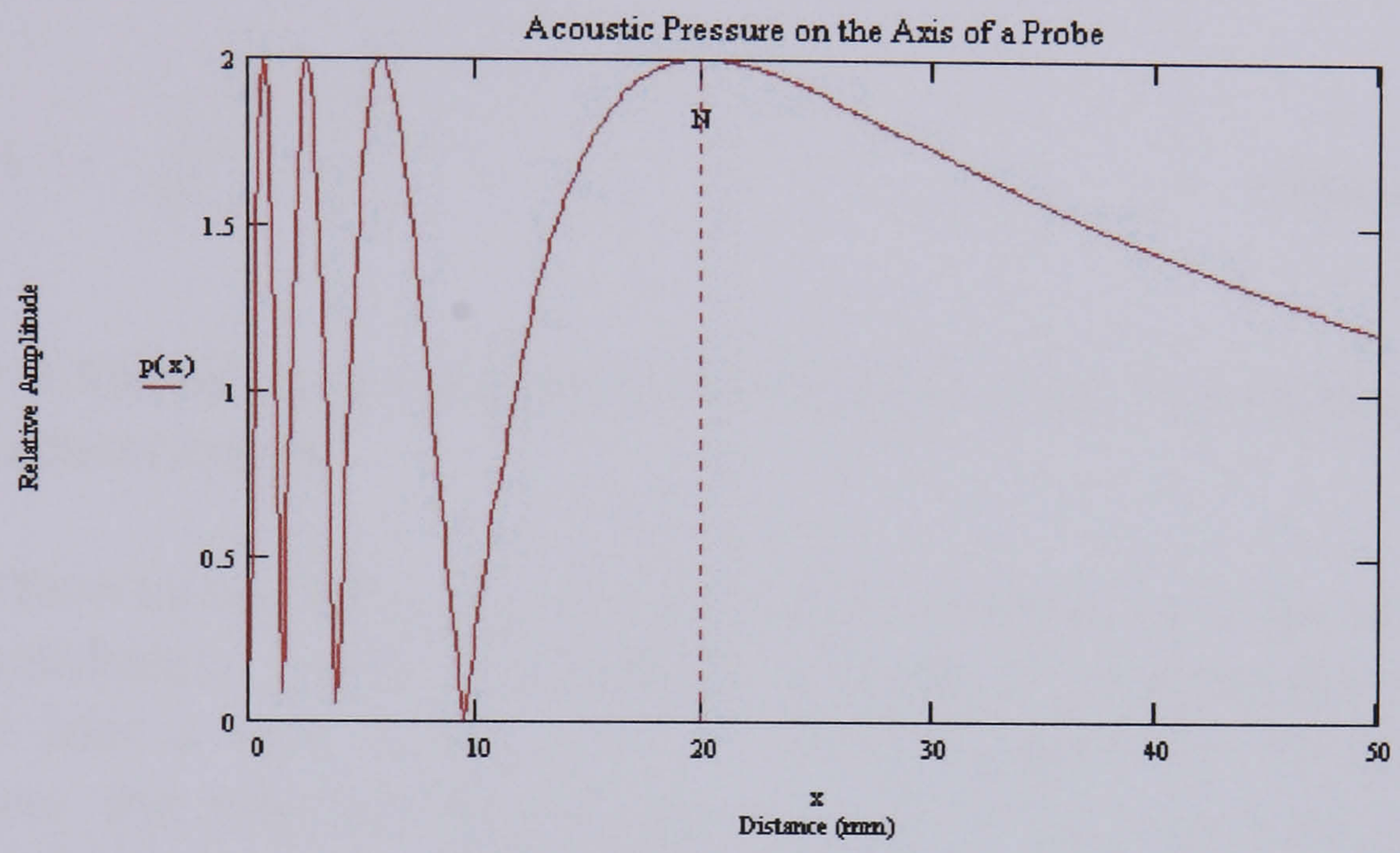

Figure A.10 Representation of sound pressure along the acoustic axis of a 10mm diameter, 5MHz transducer transmitting into steel. Plot generated by a Mathcad program specially developed during the course of this work.

It is important to remember that Figure A.10 represents the acoustic pressure on the axis only and in practice the acoustic pressure over an area must be considered. For example, if a second transducer crystal were placed at a distance N/2 from the first, according to Equation A.18 the acoustic pressure would be zero. However, it would be the sound pressure over the area of the transducer that would determine the amplitude received.

A.7.1 Focussing

The near field length is the natural focal point of a plane transducer crystal, being the region of the ultrasonic beam with the smallest diameter. However, the shape of the beam can be modified to focus as either a line or a spot at a specified distance from the crystal, within the near field length. The most common way of doing this for a single crystal probe is to use a lens (usually Perspex or Rexolite) that is bonded onto the crystal face. Since the size of the transducer crystal is relatively small compared with the wavelength, diffraction phenomenon rather than geometric optics define the sound field for focussed probes. Equation 20 [Krautkramer, 1983] describes the sound pressure along the axis in the case of a spherically focussed probe.

$$p = p_0 \left| \frac{2}{1 - \frac{a}{r}} \right| \left| \sin\left[\frac{\pi}{\lambda} \left(\sqrt{(a-h)^2 + \frac{D^2}{4}} - a \right) \right] \right| \qquad \textbf{Equation A.20}$$

with

$$h = r - \sqrt{r^2 - \frac{D^2}{4}} \qquad \textbf{Equation A.21}$$

where r is the radius of curvature of the probe lens and a is the distance from the transducer crystal.

Plane transducers may also be forced to focus within the near field by using collimators. This is effectively a baffle of ultrasonically absorbent material with a hole in the middle. When attached to the face of the transducer, the hole defines the effective size of the transducer so the last axial maximum will move closer. The advantage of focussing a transducer or attaching a collimator is that the width of the beam is reduced enabling the good penetration of a low frequency to be combined with the improved spatial resolution of a small transducer in the near field. Twin crystal transducers may also be 'focussed' by angling the shoe to induce a cross-beam situation. Such an angle is referred to as a toe-in angle.

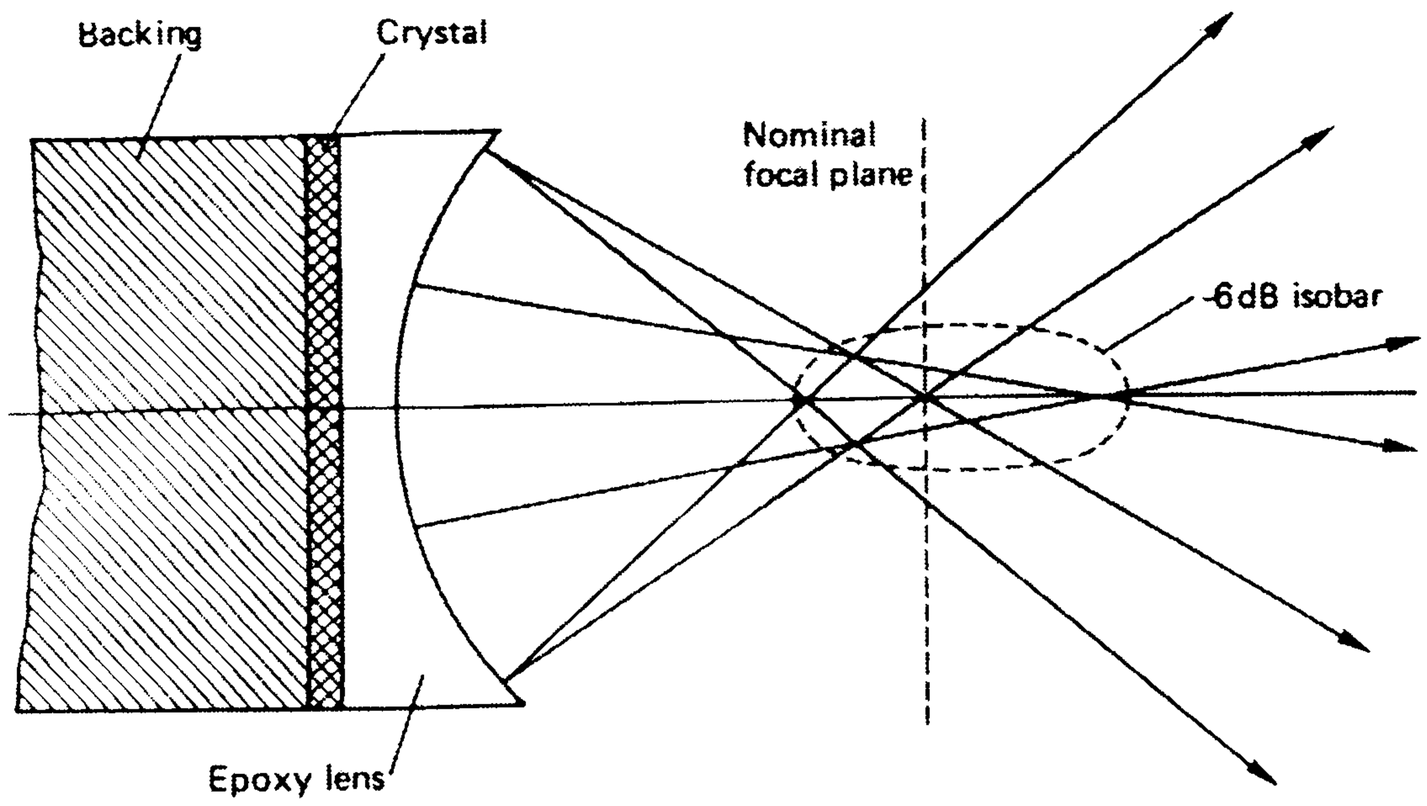

Figure A.11 Representation of the ultrasound generated by a focussed ultrasonic transducer. Halmshaw [1991]

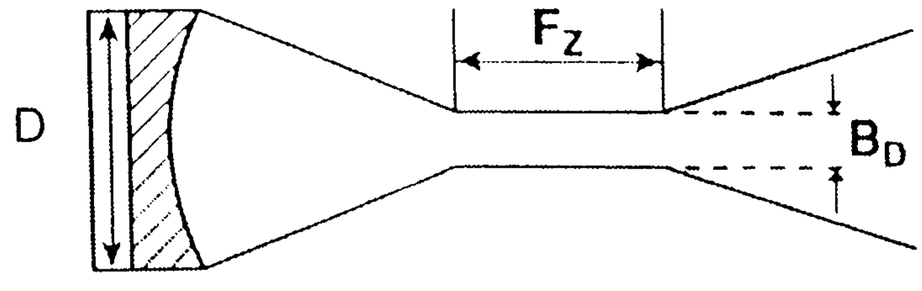

Figure A.12 Representation of the focal zone of a focussed transducer. Cartz [1995]

The beam diameter (B_D) to a 6dB drop at the focal zone according to Cartz is:

$$B_D = \frac{1.02FV}{fD}$$ **Equation A.22**

The length of the focal zone F_Z (depth of field) is:

$$F_Z = NS_F{}^2\left[\frac{2}{1+0.5S_F}\right]$$ **Equation A.23**

where,

$$S_F = \frac{F}{N}$$ **Equation A.24**

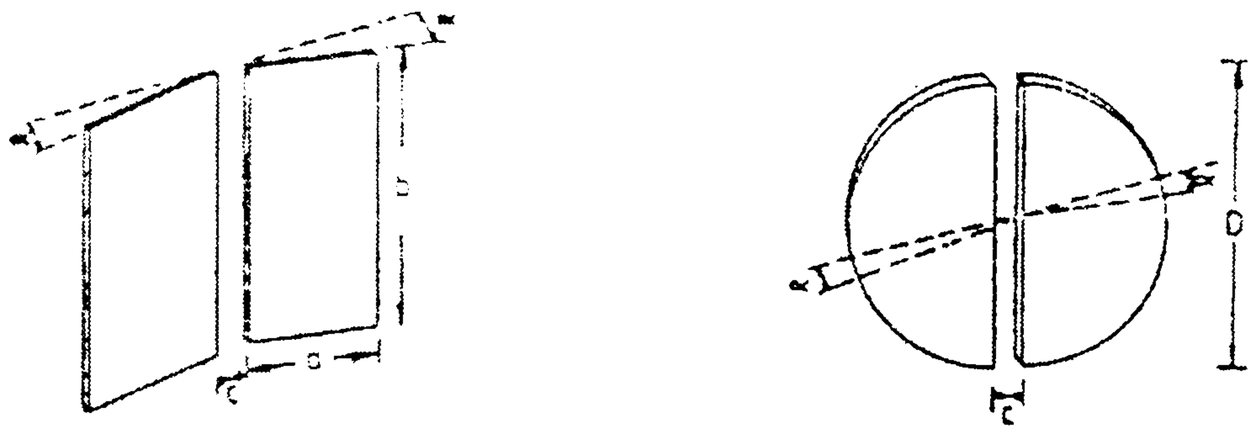

(a)
Rectangular crystals

(b)
Circular crystal : use a = 0.4D

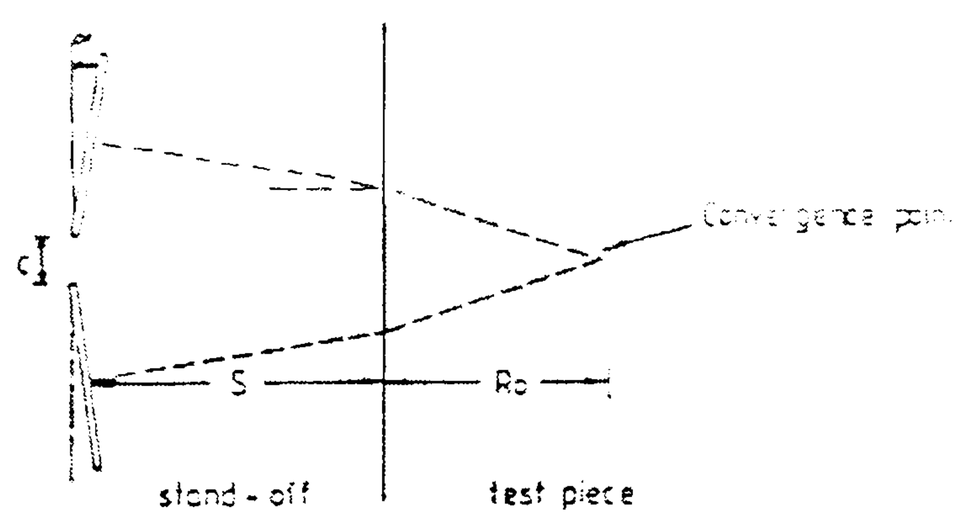

Figure A.13 Schematic representation of beam focussing in a twin crystal transducer. BSi 90/70986 GME/23 23 Feb, 1990.

$$R_0 = \left\{ \frac{(a+c)}{2\alpha} - S \right\} \frac{V_1}{V_2}$$ **Equation A.25**

where a is the width of the transducer crystal, c is the separation distance between the two crystals, a is the toe-in angle, S is the thickness of the shoe, and V_1 and V_2 are the sound velocities in both the shoe and test piece material respectively.

Single crystal focussed probes are most commonly used for immersion testing, where the ultrasound passes from the crystal into the lens, through a water path and into the test piece. The distance of water path Wp required between the test piece and a focussed compression probe in order to achieve focus at a test piece material depth of M_d is defined in Equation A.26 and illustrated in Figure A.14.

$$W_P = F - M_d \left(\frac{V_1}{V_2} \right)$$ **Equation A.26**

where F is the focal length in water, V_1 and V_2 are the velocities of sound in the test piece material and water respectively.

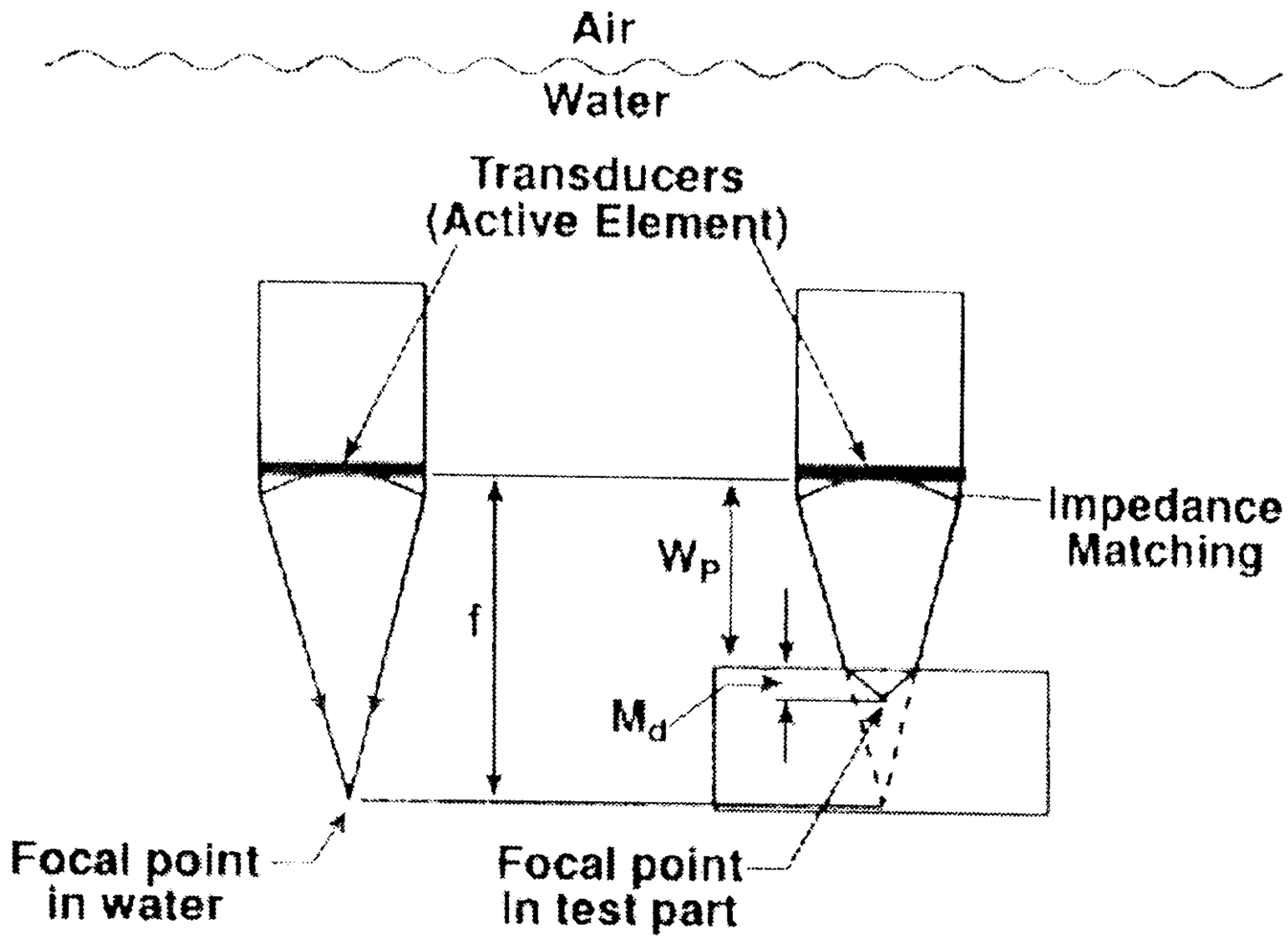

Figure A.14 Schematic representation of relationship between water path distance and focal point depth within a test piece during immersion testing. Cartz [1995]

A.7.2 Transducer Dead Zone

The dead zone is an effect noticed when a single crystal is functioning as both the transmitter and receiver and represents a certain time, or depth into the test material in which nothing can be detected. This is illustrated in Figure A.8. It results from the time taken for the crystal to stop ringing after firing. In other words, there is a finite time after sending out a pulse when the crystal is not ready to receive. Reflections from discontinuities in this zone are confused with the tail of the initial pulse or 'TX'.

Common steps taken to combat the dead zone for single element probes include, using a shorter pulse. This can be achieved by using a shorter driving pulse in conjunction with a more highly damped transducer. This enables the crystal to recover quicker, ready for detection. Attaching a 'delay material' to the face of the contact probe (often made of Perspex or Rexolite) is an alternative method. The sound travels slower in the delay material than in the test piece, effectively 'using up' the dead zone. The output display can be adjusted so that the test piece echoes arrive in between two repeat echoes from the delay/test piece interface. Immersion testing is another option. Here the water path between the transducer and the test piece material acts as a variable delay so that the dead zone is in the water path rather than in the test piece. There will always be a small dead zone however, owing to the relatively large amplitude of the echo from the water/test piece interface.

A.8 Ultrasonic Probe Design

The typical design for a single crystal compression wave probe is shown in Figure A.15. The piezoelectric element (or crystal) would be of suitable thickness to produce the desired resonant frequency. The crystal would be metalised on both faces and typically be between 5 and 35mm in diameter, of frequencies between 0.5 and 20MHz. The crystal would be backed with a highly attenuative backing material often made from a mixture of tungsten powder and epoxy resin. This would be pressed onto the back of the crystal under pressure to form a 'slug'. The slug would be of similar acoustic impedance to the crystal itself, ensuring that ultrasound reverberating internally in the probe passes into it readily, minimising the risk of spurious echoes. Thin wires that pass through the backing material make electrical contacts with the crystal and the connector (positioned on the top of the probe in the Figures below).

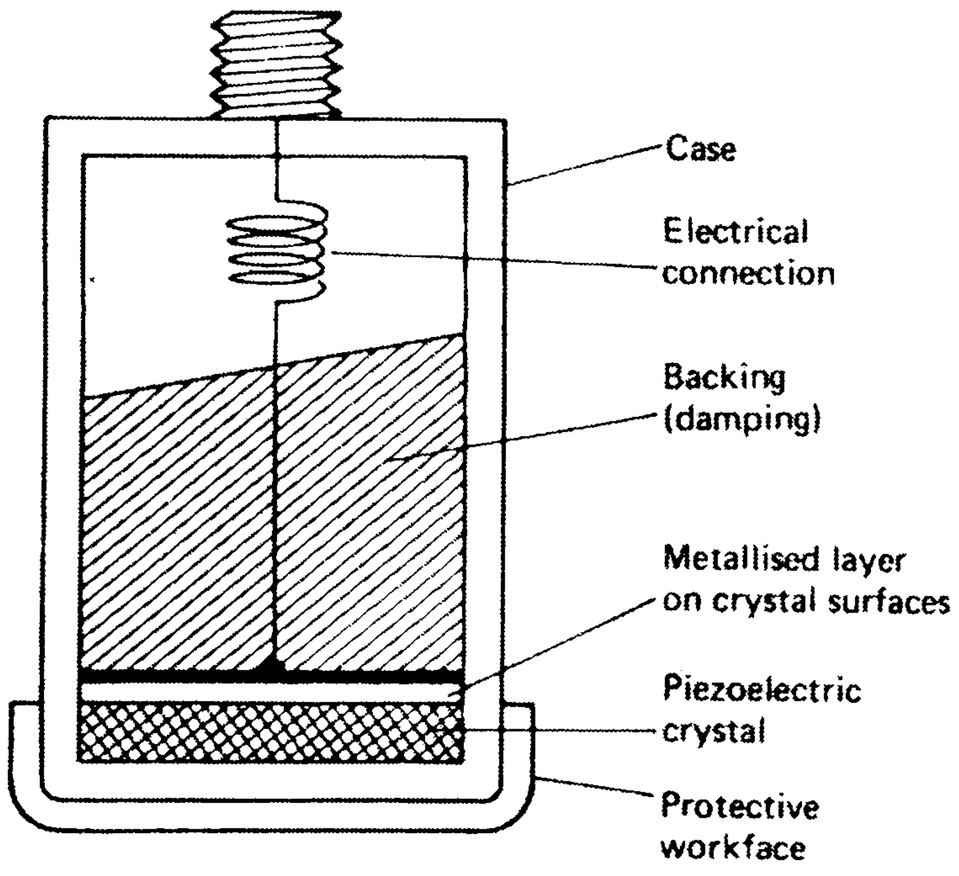

Figure A.15 Schematic of an ultrasonic probe designed for the generation of compressional waves. This particular example has a protective workface to reduce probe wear. The design of immersion probes is essentially the same only without the protective workface.

Another common probe design is the twin crystal compression wave probe. Such devices incorporate two crystals, one that always transmits and one that always receives. It is usual for these to incorporate Perspex 'delays' which retard the arrival of ultrasound reflected from near surface defects, overcoming the dead zone effects associated with single crystal probes. An 'acoustic curtain' made from a cork-like material called Nebar is sandwiched between both delay blocks preventing cross-talk between the crystals. Figure A.16 illustrates one such probe, whose crystals are parallel to the specimen surface. It is also common for the crystals to be angled inwards slightly, to encourage a degree of natural focussing of the beam.

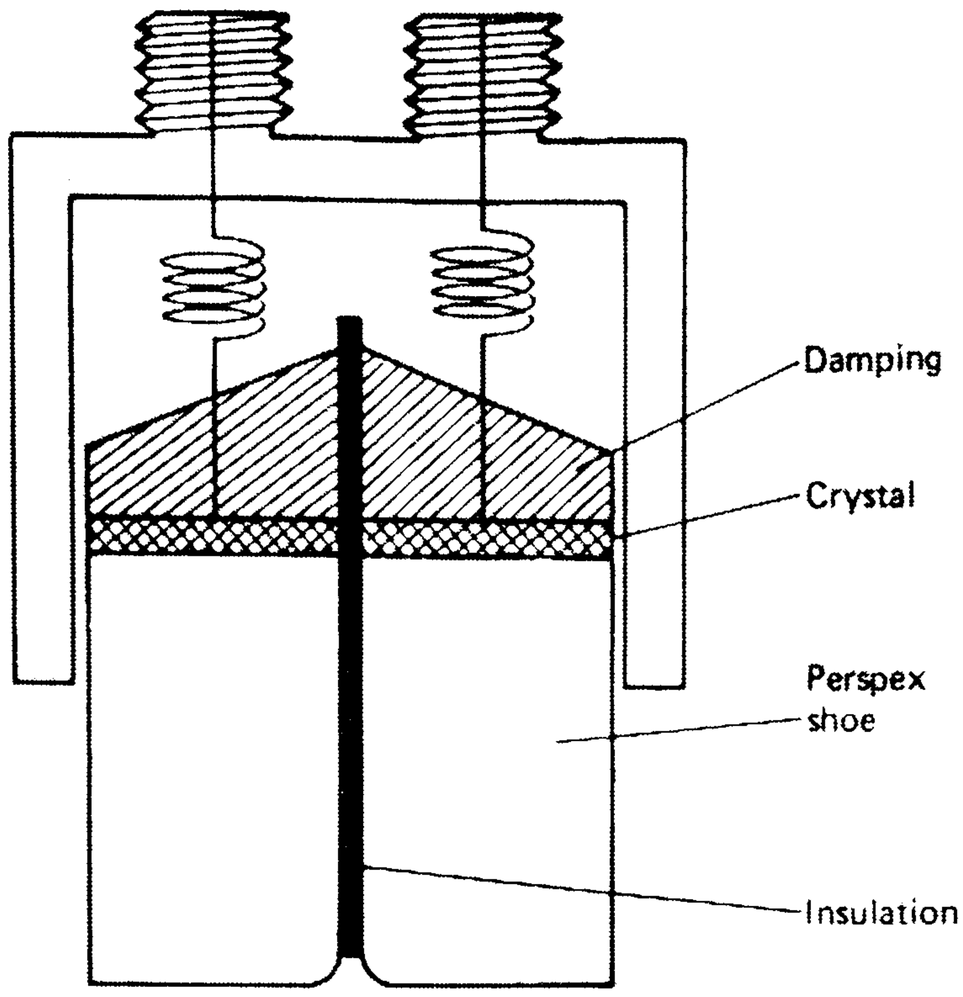

Figure A.16 Schematic of a twin crystal delay line probe.

A common shear wave (or angle beam) probe is shown in Figure A.17. It essentially consists of a standard compression probe bonded onto a Perspex wedge. The angle of the face onto which the crystal is bonded is such that mode conversion is observed at the interface between the Perspex and the test piece, generating a refracted shear wave at a known angle (usually 45, 60 or 70°) in the test piece. This angle depends on the velocity of ultrasound in the test piece and so it is usual for the angle to be specified for use in steel. The wedge is shaped to dissipate internally reflected ultrasound, minimising spurious echoes.

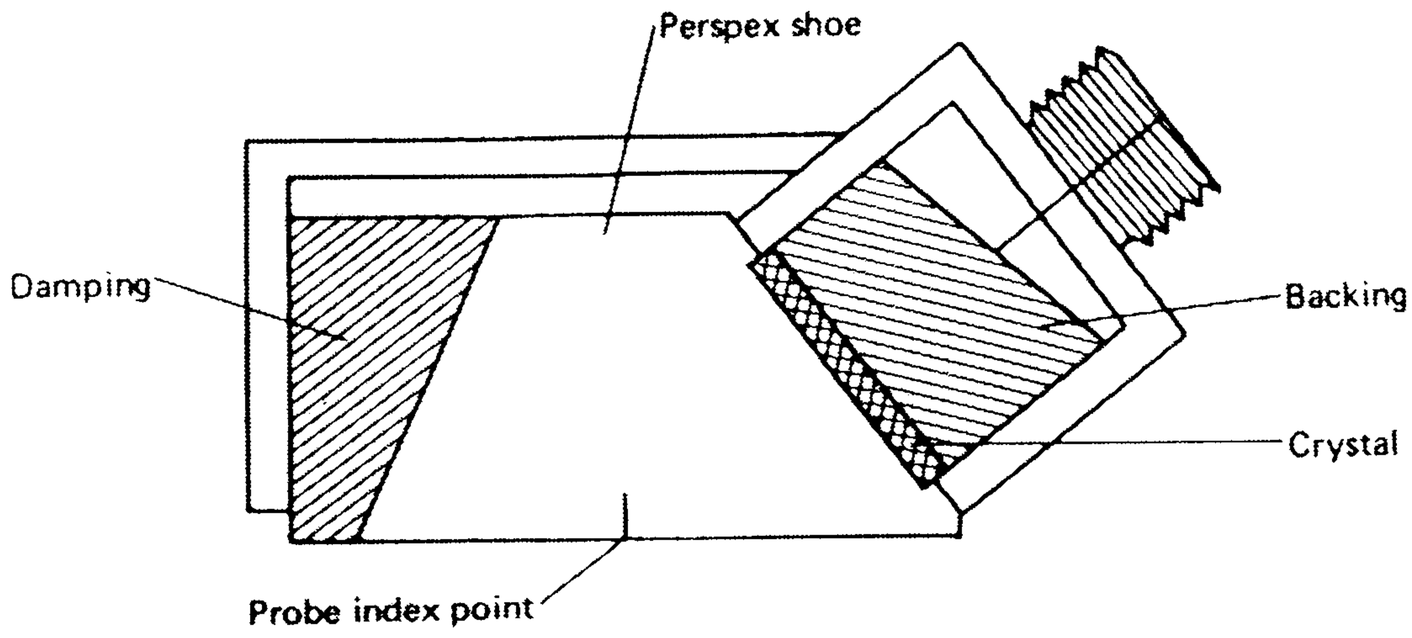

Figure A.17 Schematic of an angle probe.

A.9 Choice of Transducer

A.9.1 Frequency Considerations

The optimum choice of frequency for a particular inspection depends on a trade-off between two conflicting factors:

- The need for good penetration, which decreases with increasing frequency, and
- The spatial resolution and depth resolution which increases with increasing frequency.

It is therefore necessary to decide on the minimum detectable defect size required. This determines the maximum beam size (which limits the spatial resolution) and maximum pulse length (which limits the depth resolution) to be used. Then the lowest frequency transducer capable of achieving this beam size and pulse length should be selected in order to maximise penetration. [Smith, 1999]. Much work has been done concerned with the sizing of defects using ultrasound. This is a large topic that is well documented and so it will not be addressed here. The following references are offered for further information on defect sizing in composites and metals. [Krauthramer, 1959 and Smith et al, 1997].

It is possible to go through this procedure and end up with a transducer that does not give sufficient penetration. In these instances, the selection of an appropriately focussed transducer may help. Alternatively, informed selection of transducer material can yield many improvements.

A.9.2 Material Considerations

The vast majority of industrial ultrasonic transducers have ceramic elements (e.g. lead metaniobate or lead zirconate titanate). Such materials are accepted as having very good 'source' characteristics. However, being ceramics they have high acoustic impedance which makes them poor transmitters into water and water based couplants. By controlling the level of damping applied to the back of the crystal, the pulse length may be modified – the higher the damping, the shorter the pulse length and the better the depth resolution. [Silk, 1984 and Morgan Electro Ceramics TP-224, TP-226, TP-234]

Polymer film (e.g. poly-vinylidene fluoride, PVDF) transducers are particularly suited to immersion testing as they are acoustically well matched to water. They have poor source characteristics but are very efficient

receivers. They naturally produce short pulses of wide-bandwidth, but suffer from poor penetration. [Day, 1996]

More recently piezocomposite materials have been increasingly used in industrial NDT. These materials consist of tiny pillars of piezoceramic such as PZT, surrounded by a polymer matrix. This system has the advantage of the good source characteristics of the ceramic combined with the overall lower acoustic impedance afforded by the polymer filler. This makes for a more efficient transmitter into many materials particularly those of low acoustic impedance such as water and composites. A further advantage is the high internal damping of the piezocomposite. This results in a shorter pulse length without the need for the high level of damping required by conventional ceramics. The lower level of damping affords a higher amplitude ultrasonic signal. By achieving this piezocomposites go some way towards tacking the resolution-penetration trade off. For practical reasons piezocomposite transducers are limited to use at approximately 5MHz and below. [Fleury and Gondard, 1995 & Hossack et al, 1991]. This is due to the fragile nature of the structure.

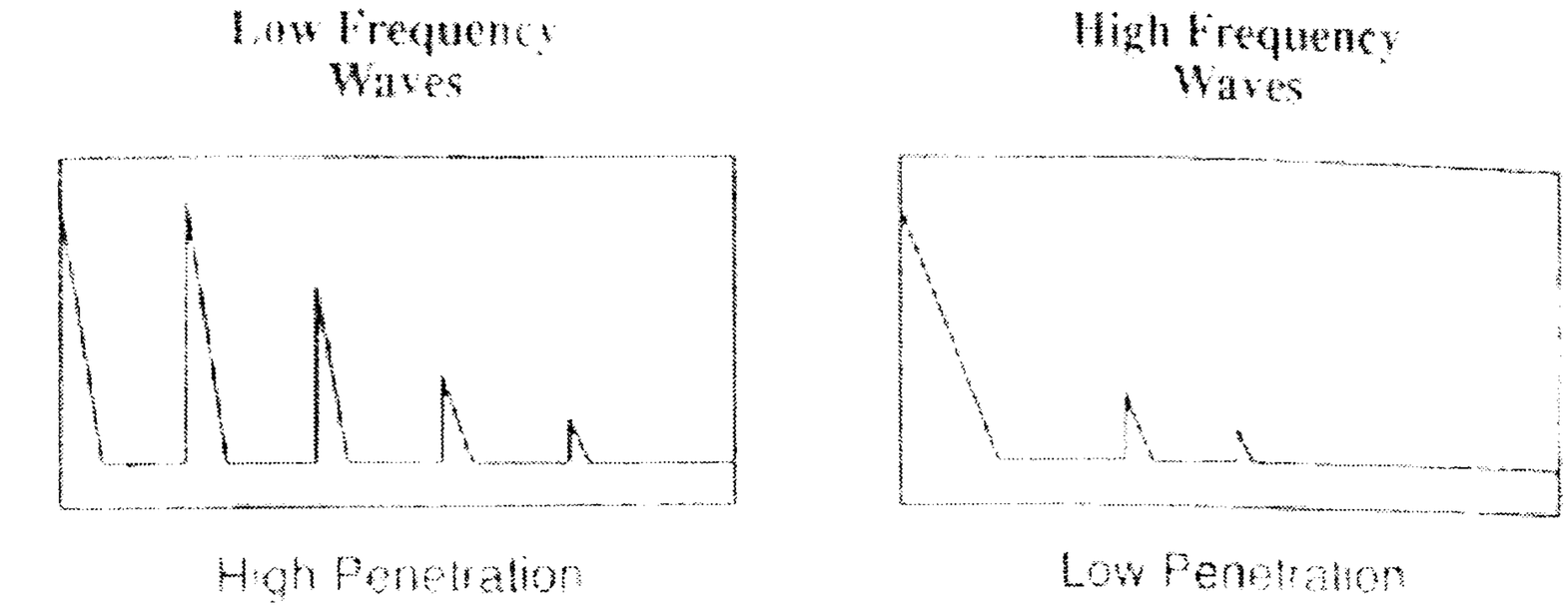

Figure A.18 Illustration of oscilloscope displays using transducers of a) high or low penetration (ability to detect defects at distances within the solid) and b) high or low resolution (ability to separate echoes from closely spaced defects). Cartz, 1995.

A.10 Data Presentation – A, B & C-Scans

Ultrasonic data can be displayed in a number of formats. The simplest and perhaps most common representation is the A-Scan, an illustration of which can be seen in Figure A.19. Central to the generation of such data is the ultrasonic flaw detector. This contains the necessary electronics to (i) produce signals that cause an ultrasonic transducer to generate sound in the test piece, (ii) receive electrical signals from a transducer representing any reflected sound, and (iii) amplify and display the information on an oscilloscope screen. The amplitudes of the ultrasonic waves received by the transducer are converted into electrical signals and rectified before being displayed as the vertical deflection on the oscilloscope screen. The horizontal deflection corresponds to time. The display typically consists of a number of vertical spikes, whose position along the screen can be calibrated in terms of depth in the test piece. This allows the depth of a particular reflector to be measured. The amplitude of each echo gives an indication of the size and nature of the reflector. An A-Scan is a representation of a single point only.

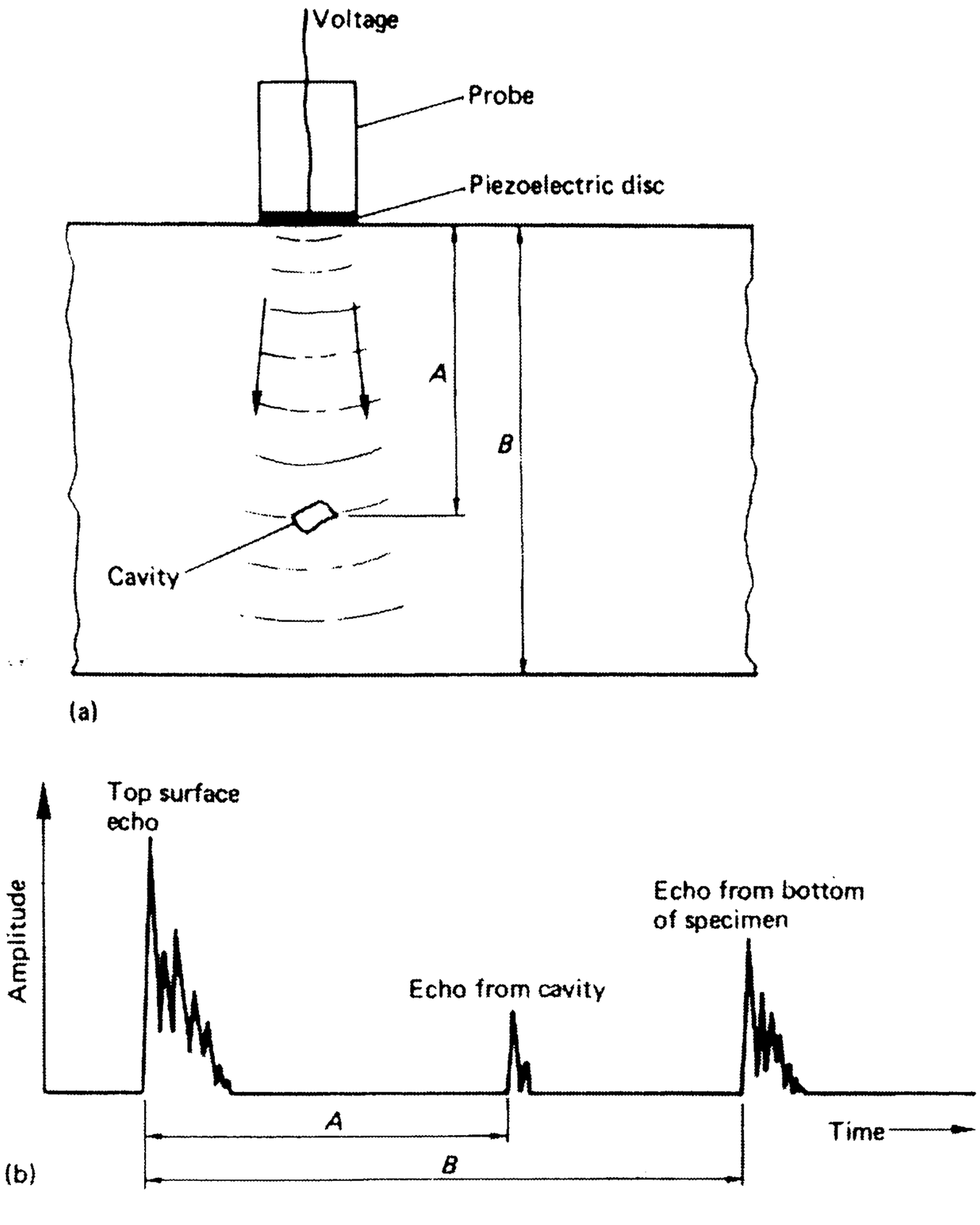

Figure A.19 The basic principle of ultrasonic testing with a compression wave probe operating in pulse echo mode – a) set-up of probe on test piece, and b) standard A-scan display on screen. Halmshaw [1991]

If the probe used for recording A-scans is moved linearly, often by motor control, in a plane parallel to that of the test piece a number of A-scans can be recorded corresponding to different locations across the test piece. The basic principle is illustrated in Figure A.20. The A-scans can be combined on a display device such as a storage oscilloscope where the horizontal deflection is proportional to the transducer position and the vertical deflection is proportional to time (or depth through the test piece) and the stored intensity is modulated by the amplitude of the received reflections. This type of display is called a B-scan (brightness scan) and corresponds to a slice taken through the test piece, normal to the surface. It should be noted that, as with the A-scan technique, the 'shadow' region behind a large area defect will not be inspected and this must be remembered when interpreting B-scans.

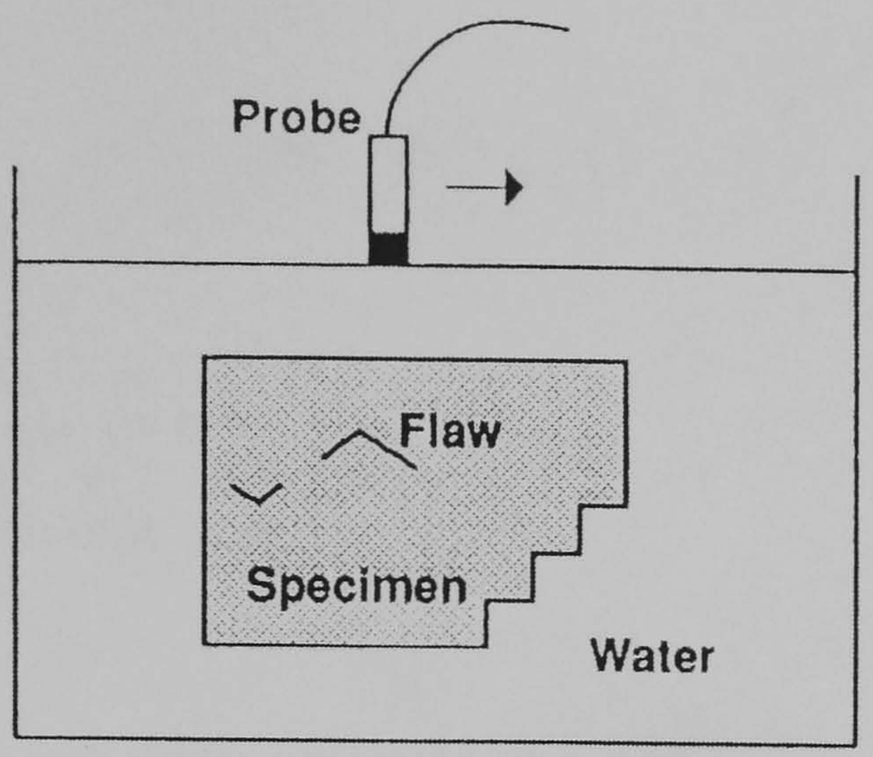

Experimental Arrangement

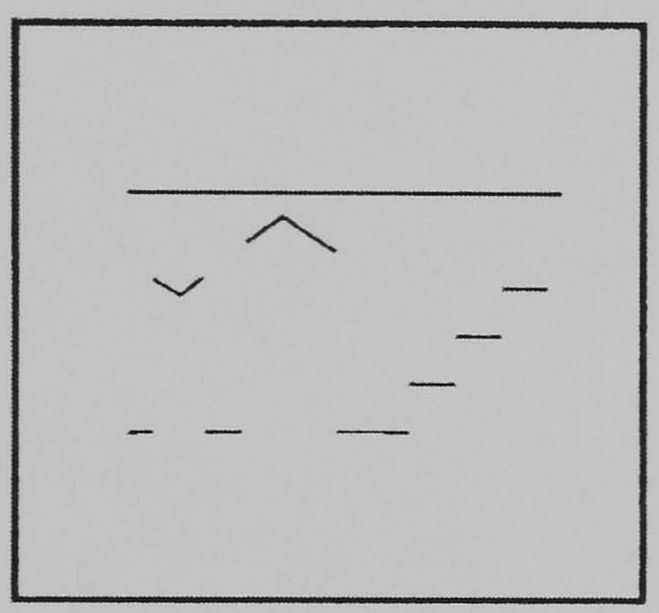

Oscilloscope Display

Figure A.20 Representation of a B-scan. Cartz [1995]

A third technique for the representation of ultrasonic data is the C-scan. In this mode, the transducer is scanned over the test piece surface in a rectilinear raster as illustrated in Figure A.21. This us usually performed under computer control.

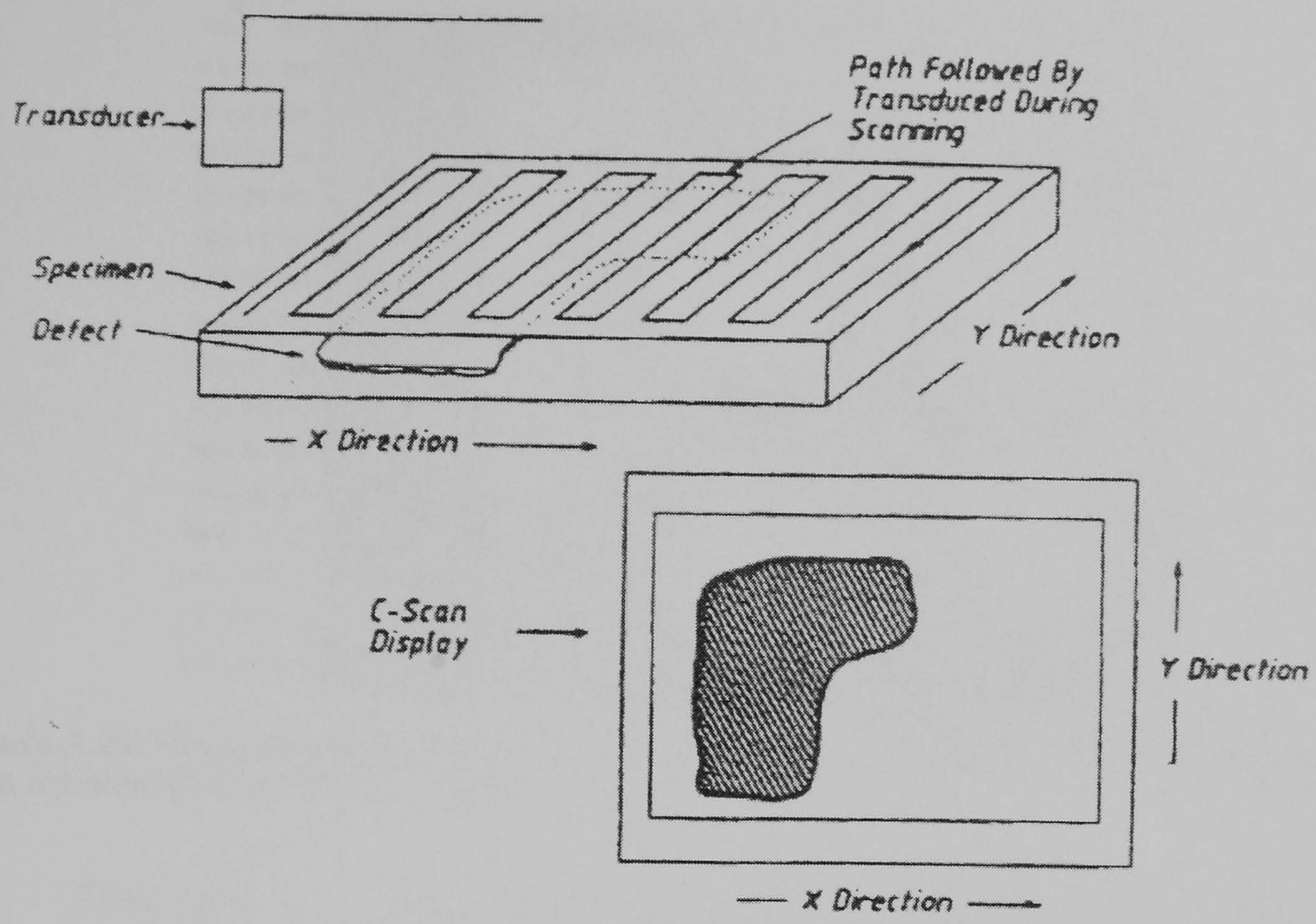

Figure A.21 Representation of probe motion in relation to test piece during C-scan acquisition. Smith [1999]

Most ultrasonic flaw detectors employ a system of 'gates' or defined time windows, which can be positioned on the time-base to coincide with particular parts of the received ultrasonic waveform. The ultrasonic flaw detector measures the peak amplitude within the gate and stores it with the probe location information in the PC. It is easy to set the gate appropriately around a particular reflection of interest such as the back wall echo. If the reflector position varies within the test piece or the water path distance varies owing to sample geometry, the gate can be 'locked' to an 'interface trigger' such as the reflection from the front of the test piece. In this way the gate may start at a defined distance behind or in front of the interface trigger guaranteeing collection of amplitude data from the region of interest.

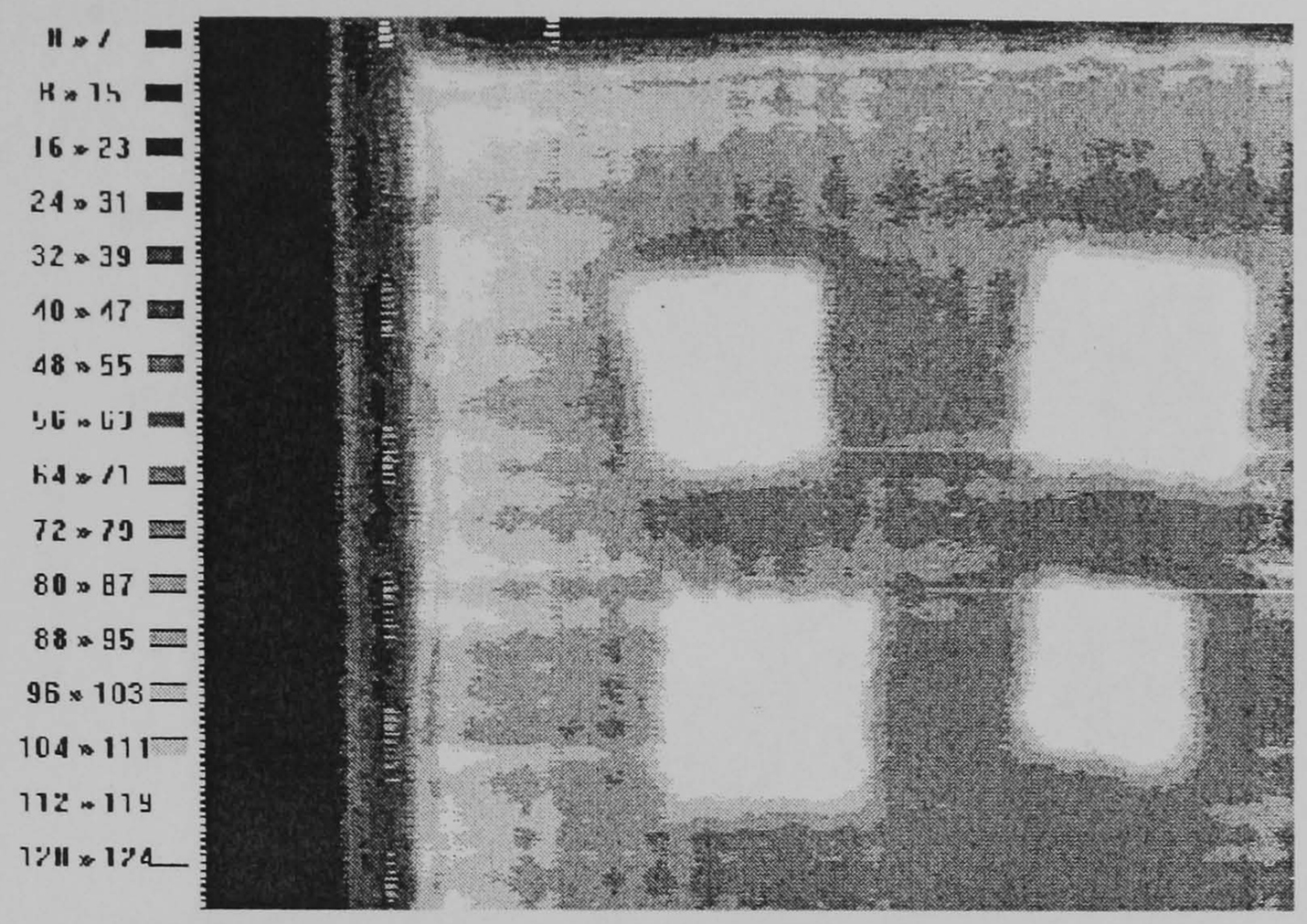

Figure A.22 Through transmission C-scan of an ultra high weight polyethylene panel with artificial (folded PTFE) defects.

There are a number of common gate positions that include (i) the back wall, where the attenuation in the test piece is monitored, (ii) a reflector beyond the test piece (double through transmission) and (iii) defect location where the gate is positioned such that it starts just after the front surface and ends just before the back surface. In this latter scenario, if an echo is generated from a defect within the body of the test piece the amplitude measured in the gate will increase. On the resulting C-scan of that area, the defect will appear in its correct plan position and its colour will indicate the amplitude of the defect reflection. This gives a very good indication of the defects lateral extent and allows rapid interpretation.

A depth scan (or time of flight –TOF) is also represented in C-scan form. In this case rather than measuring the amplitude of an echo, the time (distance) from either the transducer transmitter pulse to a particular echo or indeed the time interval between two echoes may be monitored. In this way, a scan can be produced representing the defect depth or material thickness.

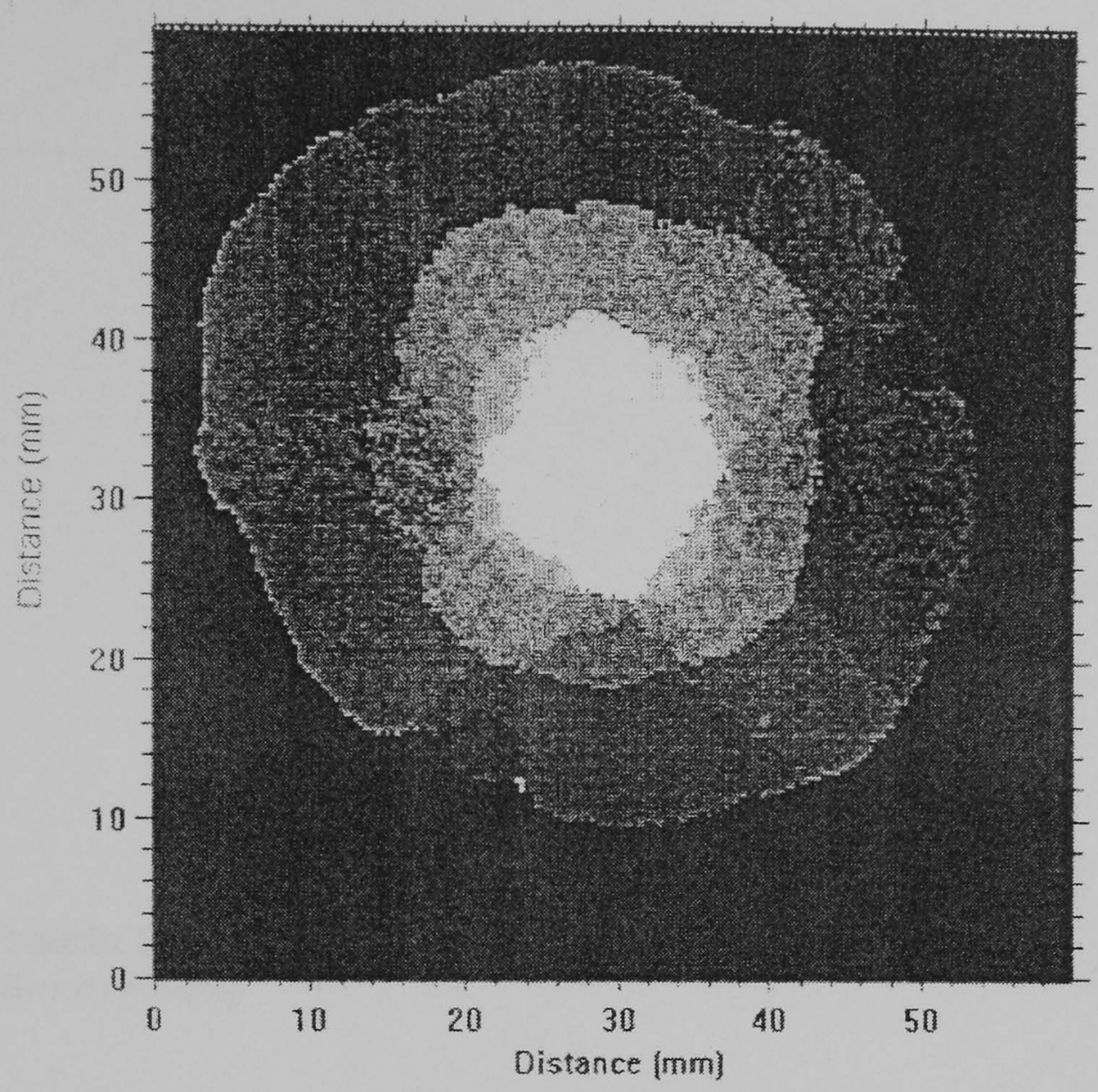

Figure A.23 Time of flight C-scan of impact damage in a composite material. Different shades represent depths of the reflections from the different delaminations. Smith [1999]

Work has been carried out at DERA Farnborough by Smith [1999] into the 'pseudo-3D' imaging of ultrasonic data. The focus was on representing as much ultrasonic information as possible in one hit. The first step was to display depth scan data as a 3-D image. This enabled the observer to rotate the component and view it from any angle. Usually, the colour of the scan represents either depth or amplitude data. However, when the 3-D image is being rotated, the observer can determine which components of the scan are closest due to parallax effects. This frees up the use of the scan colour to be used to represent reflection amplitude data. In this way four dimensions can be displayed in one go. However, it must be noted that this technique only works when the 3-D image is being rotated. Otherwise the observer is unable to determine depth. This method of ultrasonic data presentation is believed to be the current state of the art.

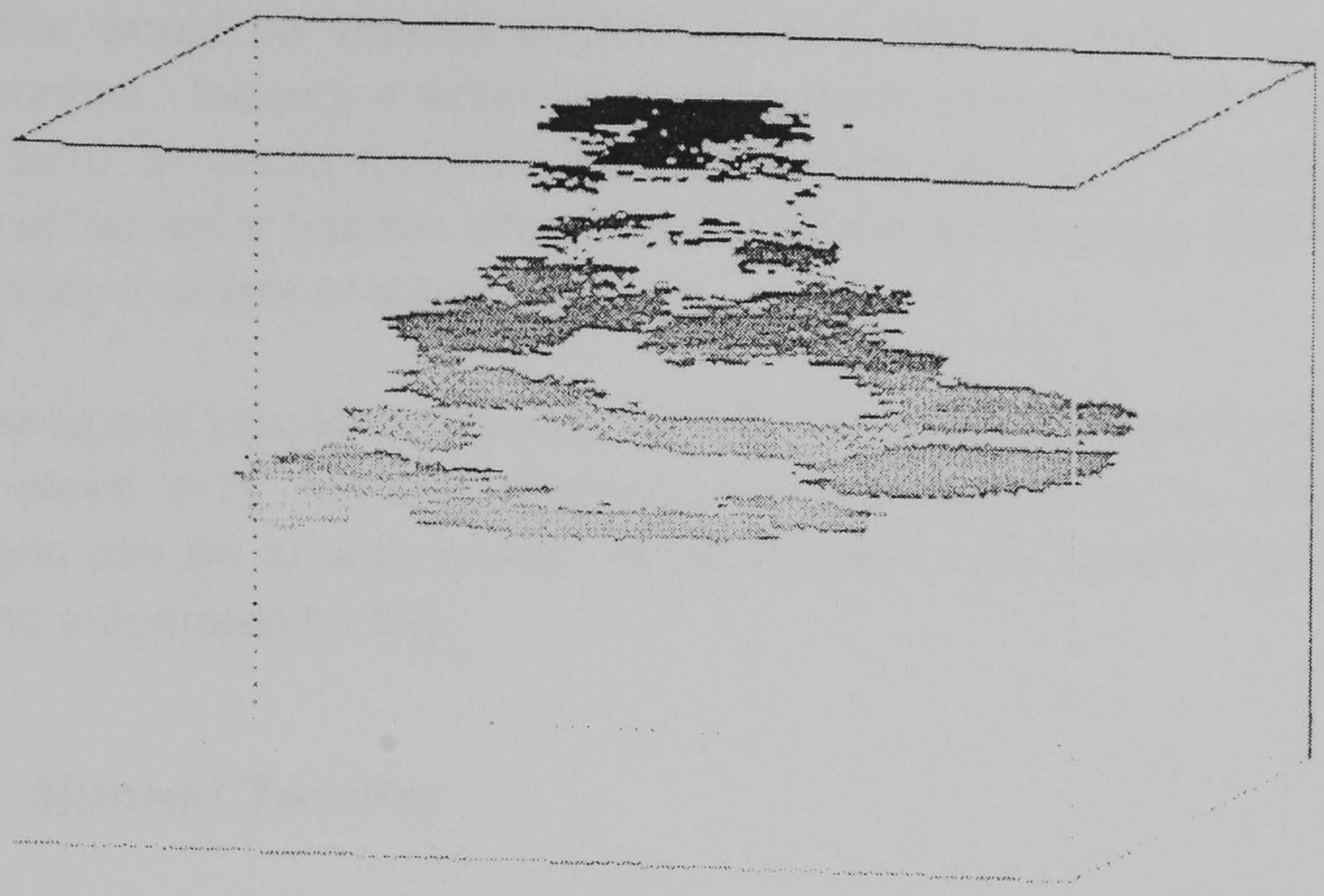

Figure A.24 Pseudo 3D C-scan of the same region of impact in the composite shown in Figure A.23. Smith [1999]

A.11 Ultrasonic Couplant

Ultrasonic couplant is arguably the most vital part of any ultrasonic inspection, for it is the means by which energy is transferred between the interrogating probe and the test piece. It is designed to compensate for imperfect contact between both of these surfaces, caused by curvature and/or surface roughness. If for example, a flat probe were placed in pressed contact with a seemingly smooth metal surface, most of the interface would be occupied by air, contact only being made over a few very small areas. As the acoustic impedance mismatch between air and solid materials is so great, almost no ultrasound would be propagated into the test piece in this scenario. The application of couplant to the interface between the probe and test piece would ensure good contact and hence eliminate air, making for good ultrasound transmission. No couplant, no ultrasound.

In fact an impression of the influence of a small air gap between a probe and test piece on the transmission of ultrasound may be gained by considering Equation A.7. Here the transmission from one material to another via a small plate is evaluated. Assuming an acoustic impedance of 33MN s m^{-3} for the probe (being that of PZT a common transducer crystal material) for the first material and standard values for air and steel [Cartz, 1995] to represent the plate and second material respectively, transmission across an air gap may be estimated. This shows that while a theoretical air gap of zero would transmit 97% of the ultrasonic energy, an air gap of only $1x10^{-11}$m would transmit just 1%. If that same gap were filled with water, the

transmission would be virtually unchanged from that achieved by perfectly intimate contact. Indeed, a water-filled gap between the probe and steel test piece of $2x10^{-7}$m would transmit 1% of the sound energy. Therefore, the presence of the water has the effect of reducing the effective gap thickness by approximately 4 orders of magnitude.

The type of couplant used depends on the application and the nature of the test piece (e.g. surface roughness and susceptibility to corrosion). Applications can be broadly broken down into two main categories, manual testing and automated testing.

A.11.1 Manual Testing

Manual testing encompasses thickness metering, condition monitoring and weld testing. It requires an operator to manually place a single probe on a test piece, usually making single point measurements with a portable ultrasonic flaw detector (see Figure A.25). The unit would typically show A-Scan data or simply a thickness reading. A small degree of scanning is also performed by rubbing the probe along the surface of the test piece. This is particularly the case for weld testing. Historically, oil was one of the most commonly used coupling media for such contact tests. Low viscosity oils being used for very smooth surfaces, where rough surfaces necessitated more viscous oil. Non-dripping couplant such as grease was preferred for overhead testing. Even wallpaper paste, toothpaste and washing up liquid have been frequently used in the past, chosen for convenience but often displayed very bad ultrasonic properties. Nowadays there is a wide range of oil and water based gel-type couplants produced commercially for manual contact testing over a range of temperatures [Krautkramer, 1983]. Appendix E contains data sheets for typical oil and water based couplants.

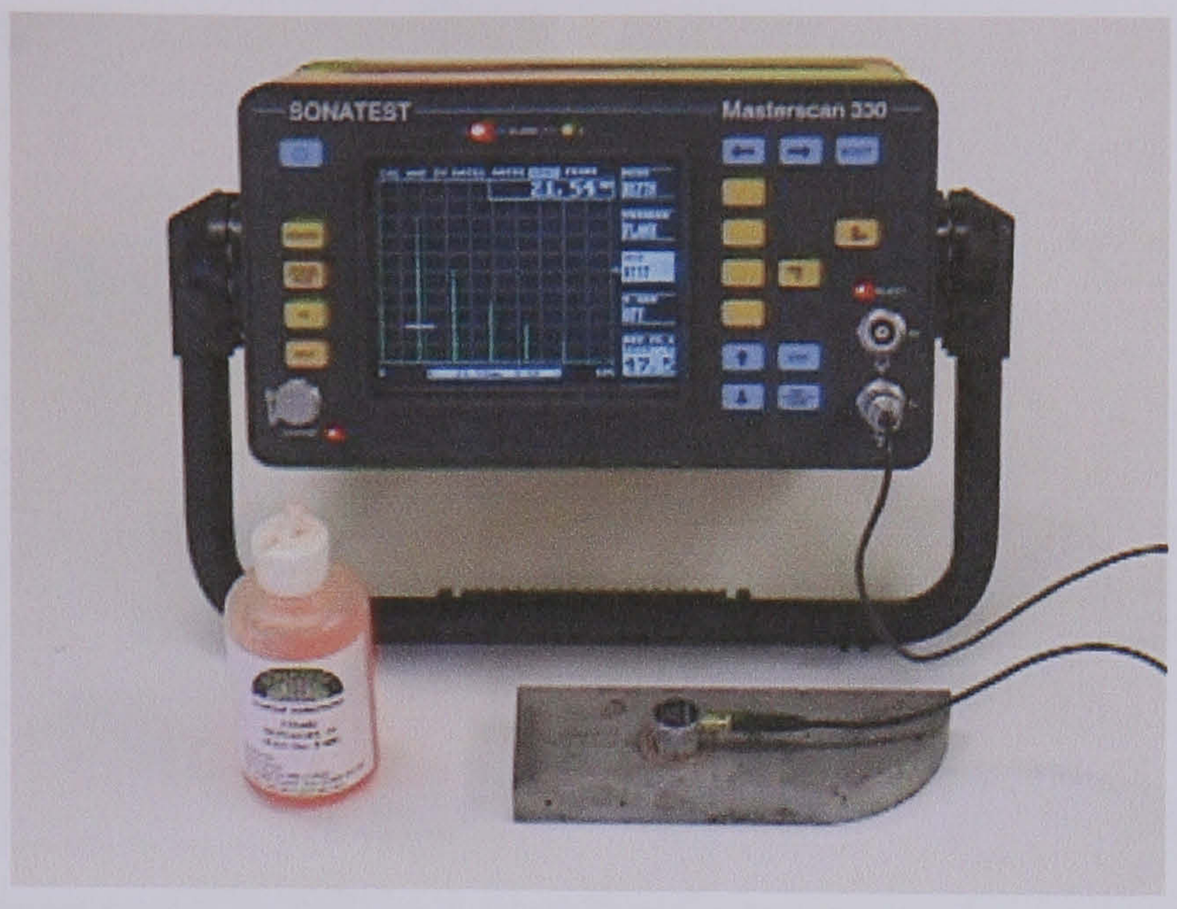

Figure A.25 Example of equipment used to conduct manual (static) contact testing.

For applications that necessitate a greater area to be covered by the probes, there is an alternative probe design loosely termed the 'wheel probe'. Such wheel probes utilise solid coupling media, most commonly in the form of a rubber tyre. This allows the probe to be tracked over larger distances more practically. Such devices tend not to be capable of providing the same consistency of results as conventional manual probes (as described above) and until recently must be used in pairs, in through transmission mode, owing mainly to the undesirable ultrasonic properties of the coupling rubbers employed. This is an issue that is discussed in more detail in Chapter 3.

A characteristic application of such wheel probes would be the detection of delaminations in composite material. This would typically involve tracking the probes manually over the panel while observing a real time A-scan display for sound transmission. Where the boding in the panel is good, sound will be readily transmitted. If however, the probes are passed over an area containing a delamination, sound transmission would be blocked. The difference between these two characteristic A-scans can be readily made. B and even C-scans may be generated from such devices provided more sophisticated scanning apparatus is available. A great limitation of the through transmission technique is that the location of the defect in relation to the test piece surface cannot be established. This would require a pulse echo measurement.

Figure A.26 The Dryscan UFD 200 unit and wheel probes secured in scanning callipers. This equipment was developed at Sonatest with much input from John Dickson, circa 1980.

There are alternative methods designed for the manual ultrasonic scanning of small areas using a conventional contact probe. Such systems typically require the face of the probe to be irrigated with water to provide coupling (commonly known as bubbler probe). An example of such a system incorporates an R-Theta Arm one of which has been developed by DERA, Farnborough and commercialised by Krautkramer and another by Inspection Solutions (Cymru). Here a probe held in a free moving scanning arm is connected to a laptop via a portable ultrasonic flaw detector. As the probe is manually tracked over the surface of the test piece, encoders in the arm tell the laptop the position of the probe while the current reading on the flaw detector is recorded on the laptop screen at the correct location. The result is manually 'painting' a C-scan of the test piece. Such equipment has a limited range of inspection as very long arms demonstrate an unacceptable positional hysteresis. However, recent work conducted by the RAF at St Athan has shown that data can be stitched together to generate an image of an entire aeroplane wing hence going some way towards overcoming the scan range issues. The arm is usually secured in place by four suction cups.

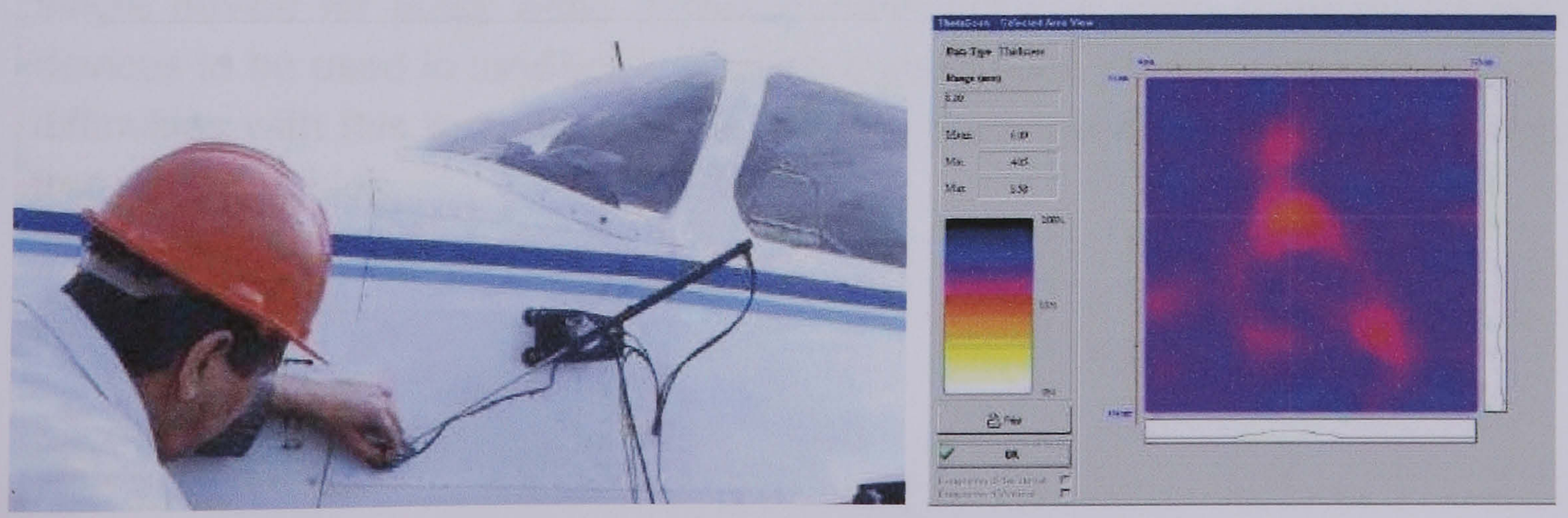

Figure A.27 Example of R Theta scanning arm and software developed by Inspection Solutions Cymru.

A.11.2 Automated Testing

One of the most commonly used automated techniques is immersion testing. This involves submerging the test piece and, either one probe for pulse echo, or two probes for through transmission, in a tank of water. Hence a continuous water path is established between the probe and test piece, along which the ultrasound can propagate. Thus, water is the coupling media. The probe(s) are usually moved over the test piece surface via computer control according to a predefined scanning programme. Data may be presented in either A, B or C-scan format, the latter being most common. Immersion testing maintains the most constant level of coupling achievable for all ultrasonic applications, providing consistent sensitivity while scanning.

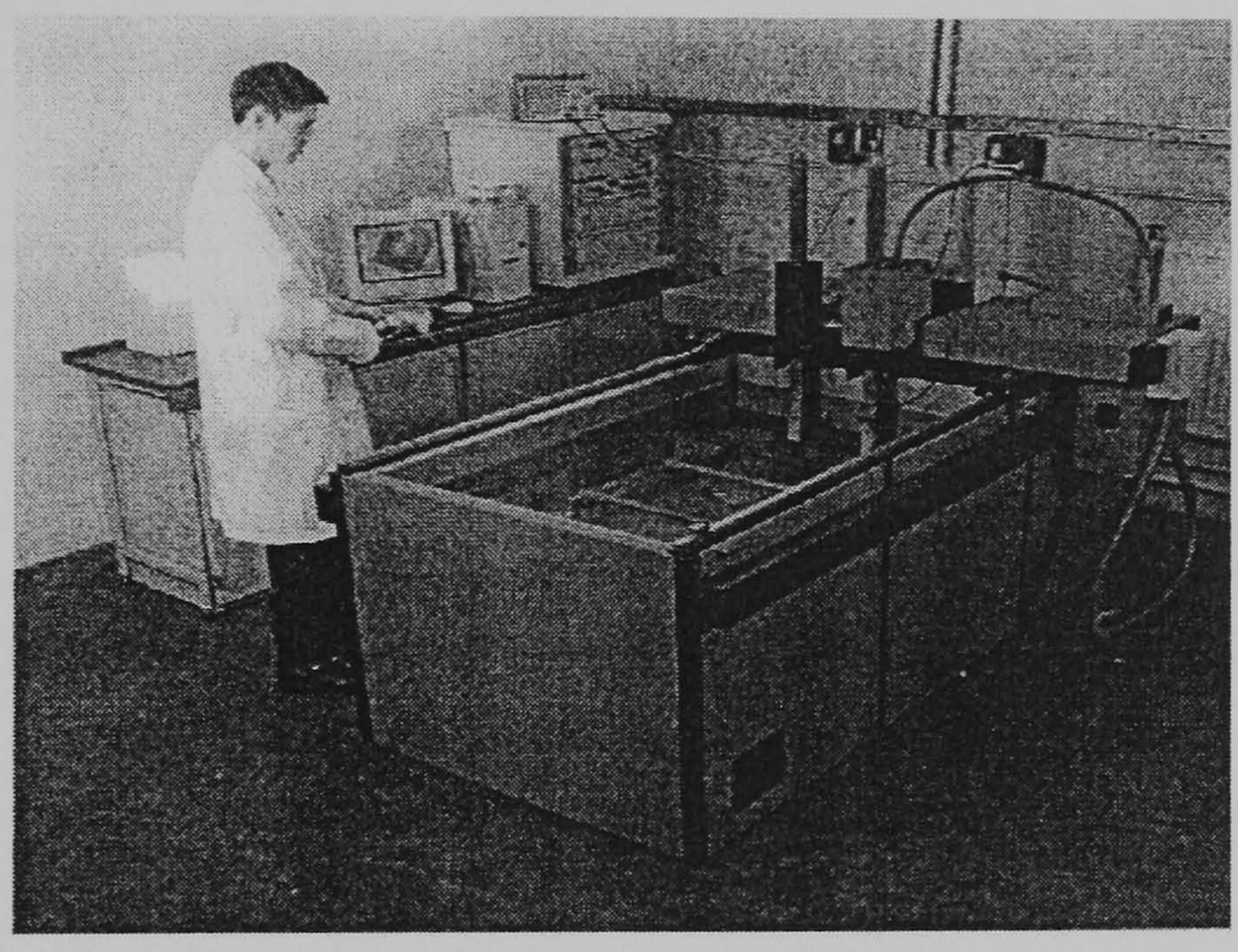

Figure A.28 A computer controlled ultrasonic immersion tank used by the Defence Clothing and Textiles Agency, Colchester.

Jet probe testing is an alternative technique whereby the probe itself squirts a jet of water at the test piece at high pressure. This again establishes a continual water path for ultrasound transmission. It is possible to use a single device for pulse echo measurements but it is more common for two devices to be used in tandem in through transmission mode. One of the main difficulties with this technique is the need to keep the water flow laminar and free of air bubbles.

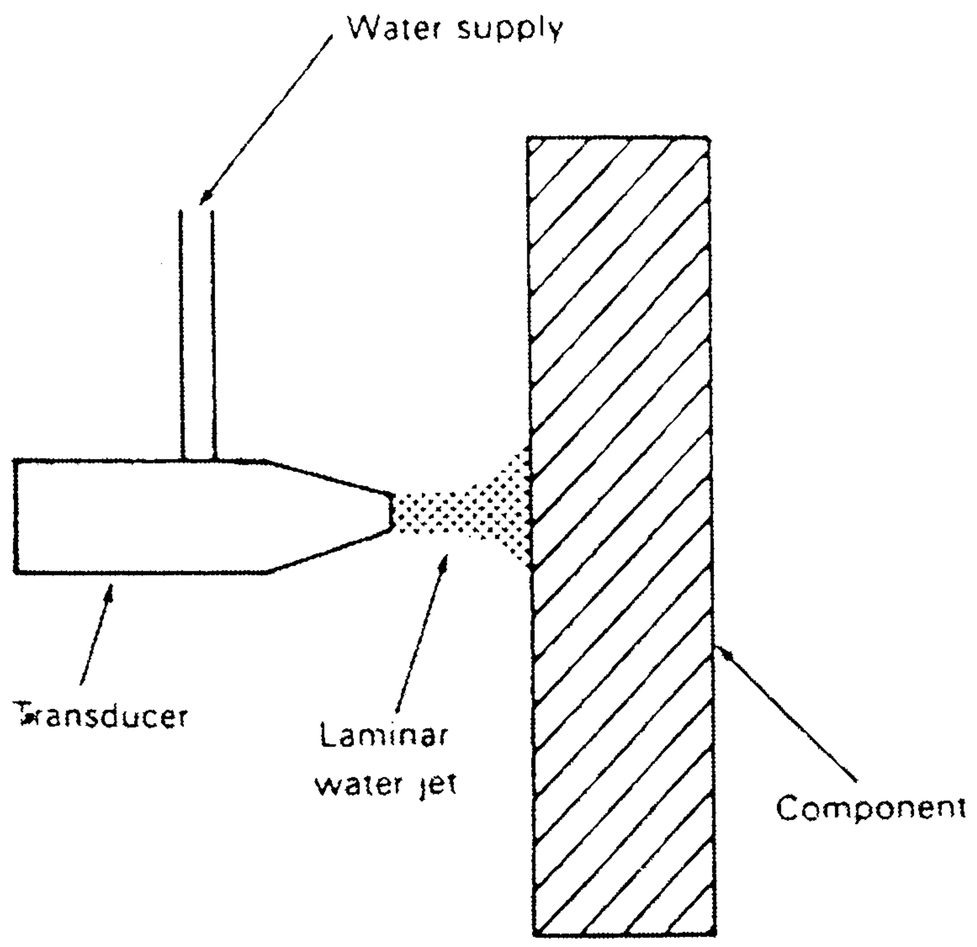

Figure A.29 Schematic of a jet probe. Matthews and Rawlings [1994]

Appendix B

Instrument List

Instrument List

Instrument	Description	Supplier
Masterscan 330	High specification digital ultrasonic unit used for manual inspection	Sonatest PLC
UTEX UT340	Desktop pulser receiver system	UTEX Scientific
QMI DAS-10	Desktop X-Y scanner	QMI INC
Honda HA-701S	High precision desktop scanner (X-Y-Z)	Honda
Mettler Toledo BD6000	Balance	Sonatest PLC
Precisa 510C	High resolution balance	Sonatest PLC
Callipers	Digital vernier callipers	Sonatest PLC
Newport Thermometer	Digital Thermometer	Cranfield University
TMP3	10MHz delay-line ultrasonic probe	Sonatest PLC
SLH10-10	10MHz highly damped probe	Sonatest PLC
ZS5-10	5MHz zero degree shear wave probe	Sonatest PLC

Software	Description	Supplier
Mathcad V.5.0	Mathematical design software	Sonatest PLC
Wavestore	Communications software between MS330 and PC	Sonatest PLC
WinDFD	Advanced communications software for MS330 and PC	Sonatest PLC
SDMS	Sonatest Data Management Software	Sonatest PLC
Optimum Pulse Finder	Prototype Probe evaluation software	Sonatest PLC
Probe Tester	Advanced probe evaluation and reporting system	Sonatest PLC
WinSpect	Data Acquisition software required for C-scanning	UTEX Scientific
Imagine 3D	Ultrasonic Modelling package	UTEX Scientific
Design Wave 3D	3D Modelling package	Sonatest PLC
Solid Edge	3D Modelling package	Sonatest PLC

Appendix C

Analysis Programs and Macros

```
Sub FFTAlpha()
'
' FFTAlpha Macro
' Macro recorded 17/08/01 by Simon Bourne
'
' Keyboard Shortcut: Ctrl+a
'
' Assumes RF amplitude data in range B2:B255
' Assumes range data (time) in range A2:A256

' Program written for use with a Sonatest Masterscan 330
'
    Sheets("Sheet1").Select
    Rows("1:1").Select
    Selection.Insert Shift:=xlDown
    Range("A1").Select
    ActiveCell.FormulaR1C1 = "Frequency Analysis"
    Range("A1").Select
    With Selection.Font
        .Name = "Arial"
        .Size = 16
        .Strikethrough = False
        .Superscript = False
        .Subscript = False
        .OutlineFont = False
        .Shadow = False
        .Underline = xlUnderlineStyleNone
        .ColorIndex = xlAutomatic
    End With
    Range("A2").Select
    ActiveCell.FormulaR1C1 = "Time (us)"
    Range("B2").Select
    ActiveCell.FormulaR1C1 = "Vpp (mV)"
    Range("B257").Select
    ActiveCell.FormulaR1C1 = "0"
    Selection.AutoFill Destination:=Range("B257:B514"), Type:=xlFillDefault
    Range("B257:B514").Select
    ActiveWindow.ScrollRow = 1
    Range("C2").Select
    ActiveCell.FormulaR1C1 = "FFT"
    Range("C3").Select
    AddIns("Analysis ToolPak").Installed = False
    AddIns("Analysis ToolPak - VBA").Installed = False
    AddIns("Analysis ToolPak").Installed = True
    AddIns("Analysis ToolPak - VBA").Installed = True
    Application.Run "ATPVBAEN.XLA!Fourier", ActiveSheet.Range("$B$3:$B$514"), _
      ActiveSheet.Range("$C$3:$C$514"), False, False
    ActiveWindow.ScrollRow = 1
    Range("G2").Select
    ActiveCell.FormulaR1C1 = "Vector"
    Range("G3").Select
    ActiveCell.FormulaR1C1 = "=IMABS(RC[-4])"
    Range("G3").Select
    Selection.AutoFill Destination:=Range("G3:G514"), Type:=xlFillDefault
    Range("G3:G514").Select
    ActiveWindow.ScrollRow = 1
    Range("H2").Select
    ActiveCell.FormulaR1C1 = "Max Amp"
    Range("H3").Select
    ActiveCell.FormulaR1C1 = "=MAX(RC[-1]:R[511]C[-1])"
```

```
Range("H4").Select
ActiveWindow.ScrollRow = 1
Range("I2").Select
ActiveCell.FormulaR1C1 = "Amplitude (dB)"
Range("I3").Select
ActiveCell.FormulaR1C1 = "=20*LOG(RC[-2]/R3C8)"
Range("I3").Select
Selection.AutoFill Destination:=Range("I3:I514"), Type:=xlFillDefault
Range("I3:I514").Select
ActiveWindow.ScrollRow = 1
Columns("I:I").Select
Selection.Insert Shift:=xlToRight
Range("I2").Select
ActiveCell.FormulaR1C1 = "Frequency(MHz)"
Range("I3").Select
ActiveCell.FormulaR1C1 = "0"
Range("I4").Select
ActiveCell.FormulaR1C1 = "=250/(512*R[249]C[-8])"
Range("I5").Select
ActiveWindow.SmallScroll Down:=-4
ActiveCell.FormulaR1C1 = "=R[-1]C+R4C9"
Range("I5").Select
Selection.AutoFill Destination:=Range("I5:I514"), Type:=xlFillDefault
Range("I5:I514").Select
ActiveWindow.ScrollRow = 1
Columns("I:J").Select
Columns("I:J").EntireColumn.AutoFit
Range("I3:J514").Select
Charts.Add
ActiveChart.ChartType = xlXYScatterLines
ActiveChart.SetSourceData Source:=Sheets("Sheet1").Range("I3:J514"), PlotBy _
    :=xlColumns
ActiveChart.Location Where:=xlLocationAsNewSheet, Name:="Frequency Spectra"
With ActiveChart
    .HasTitle = True
    .ChartTitle.Characters.Text = "Frequency Spectra"
    .Axes(xlCategory, xlPrimary).HasTitle = True
    .Axes(xlCategory, xlPrimary).AxisTitle.Characters.Text = "Frequency (MHz)"
    .Axes(xlValue, xlPrimary).HasTitle = True
    .Axes(xlValue, xlPrimary).AxisTitle.Characters.Text = "Amplitude (dB)"
End With
With ActiveChart.Axes(xlCategory)
    .HasMajorGridlines = True
    .HasMinorGridlines = False
End With
With ActiveChart.Axes(xlValue)
    .HasMajorGridlines = True
    .HasMinorGridlines = False
End With
ActiveChart.HasLegend = False
Sheets("Frequency Spectra").Select
ActiveChart.PlotArea.Select
With Selection.Border
    .ColorIndex = 16
    .Weight = xlThin
    .LineStyle = xlContinuous
End With
Selection.Interior.ColorIndex = xlNone
ActiveChart.Axes(xlValue).Select
With ActiveChart.Axes(xlValue)
```

```
    .MinimumScale = -20
    .MaximumScaleIsAuto = True
    .MinorUnitIsAuto = True
    .MajorUnitIsAuto = True
    .Crosses = xlCustom
    .CrossesAt = -20
    .ReversePlotOrder = False
    .ScaleType = xlLinear
End With
ActiveChart.Axes(xlCategory).Select
With ActiveChart.Axes(xlCategory)
    .MinimumScaleIsAuto = True
    .MaximumScale = 20
    .MinorUnitIsAuto = True
    .MajorUnitIsAuto = True
    .Crosses = xlAutomatic
    .ReversePlotOrder = False
    .ScaleType = xlLinear
  End With
End Sub
```

FFT of captured waveform from DFD's DFDFFT.mcd 18Mar98

$b := READPRN(DFDDATA) - 100$ $r := rows(b)$ $r = 258$

$range := (b_0 + 100) \cdot 10^{-3}$ (converts to metres) $velocity := b_1 + 100$ $Gain := b_2 + 100$

$range = 0.002$ $velocity = 2 \cdot 10^3$ $Gain = 37.5$

$tpp := \frac{range \cdot 2}{velocity \cdot 250}$ $fsample := \frac{1}{tpp}$ $tpp = 8 \cdot 10^{-9}$ $fsample = 1.25 \cdot 10^8$

$Vpp := (300 \cdot 10^{-3}) \cdot 10^{\left(\frac{110 - Gain}{20}\right)}$ Peak to peak voltage (mV)

$c := 0..254$ $d_c := b_{c+3}$ $Vpp = 1.265 \cdot 10^3$

$d_{511} := 0$ $c := 0..511$ $e := CFFT(d)$ $f := \overrightarrow{|e|}$

FFT of complete waveform (padded out to get finer frequency resolution)

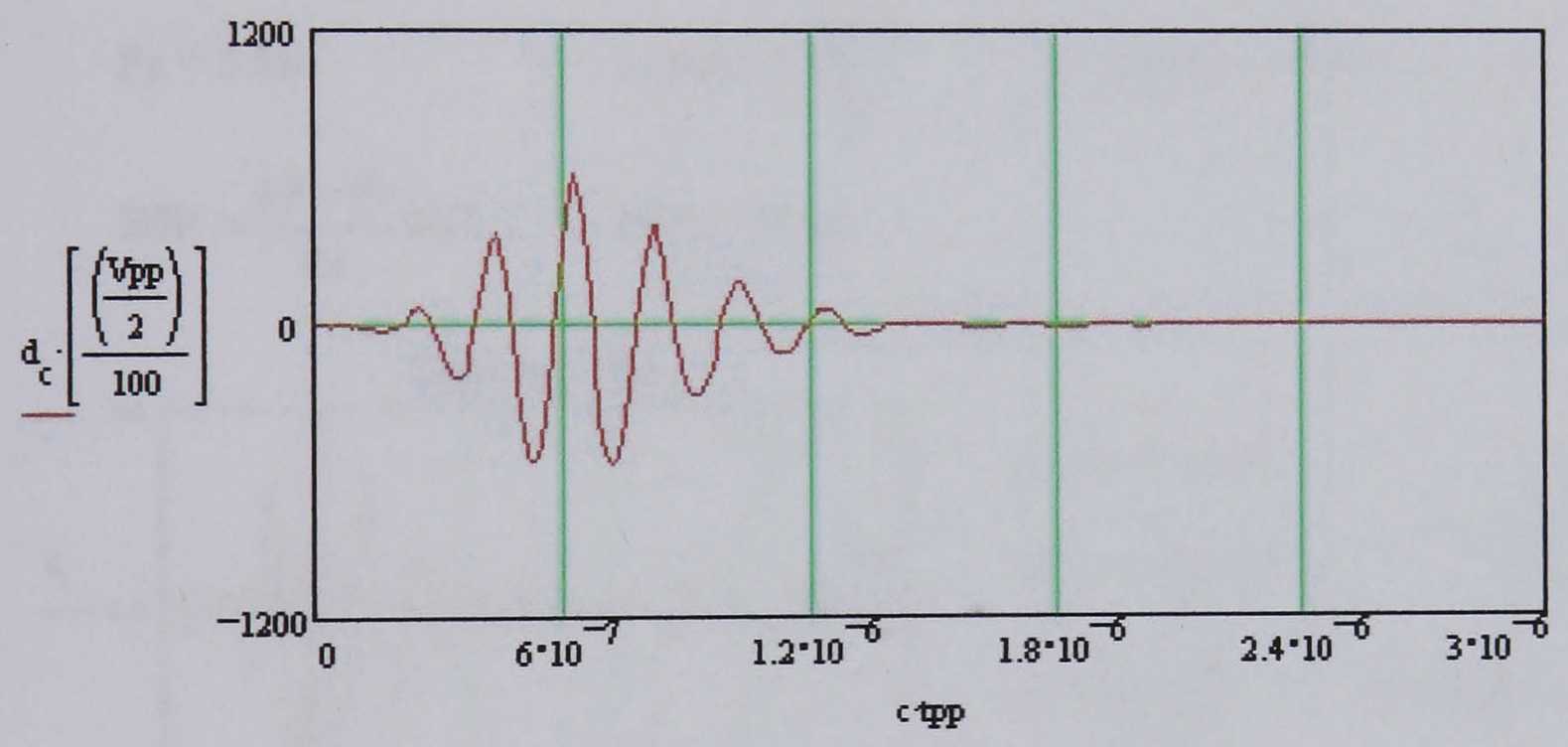

$ffreq := \frac{1}{tpp \cdot length(d)}$

$ffreq = 2.441 \cdot 10^5$

$db(x) := 20 \cdot \log(x)$ $f := \overrightarrow{(db(f) - 0)}$ Convert to log scale...

$biggest := max(f)$ $biggest = 16.022$ $f := \overrightarrow{(f - biggest)}$ Find the peak value and normalise

FFT of complete waveform

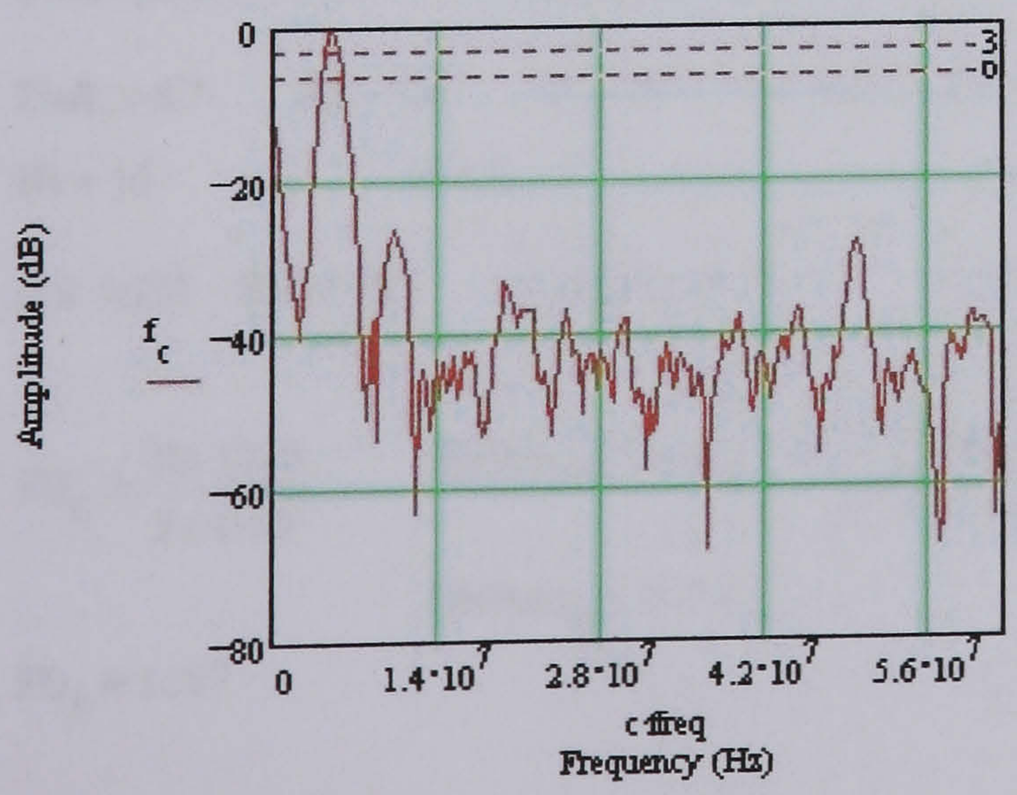

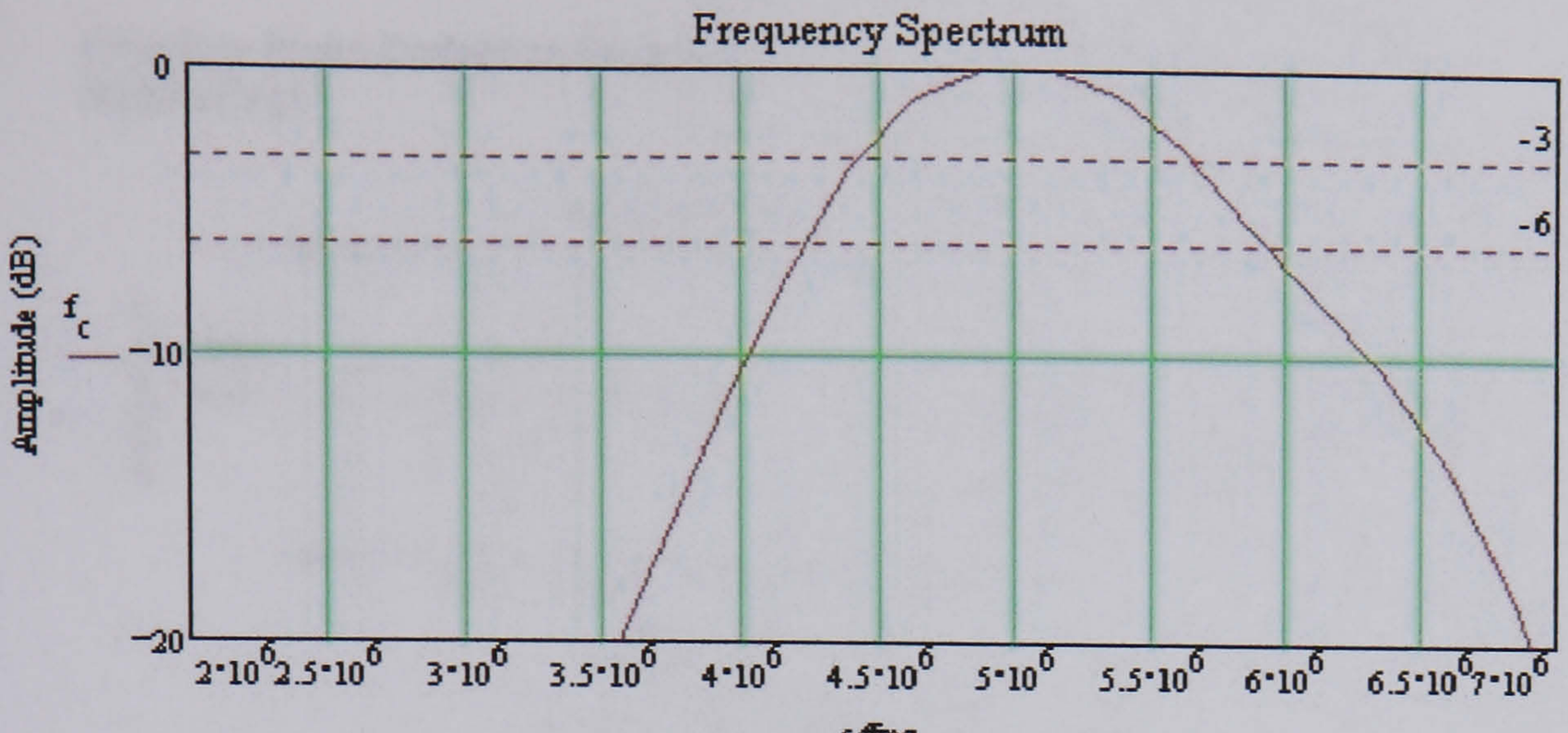

-6dB frequency and peak frequency points measured using cross hairs and inserted in to formulas

Enter data from FFT

$$Ff := \frac{5.96552\cdot10^6}{10^6} \qquad Fi := \frac{4.26601\cdot10^6}{10^6} \qquad Fc := \frac{Ff + Fi}{2} \qquad Fp := \frac{5.02956\cdot10^6}{10^6}$$

$$Fc = 5.116 \qquad Lamda := \frac{3.250}{Fc} \qquad Lamda = 0.635$$

$$BW := \frac{Ff - Fi}{Fc}\cdot100 \qquad BW = 33.221$$

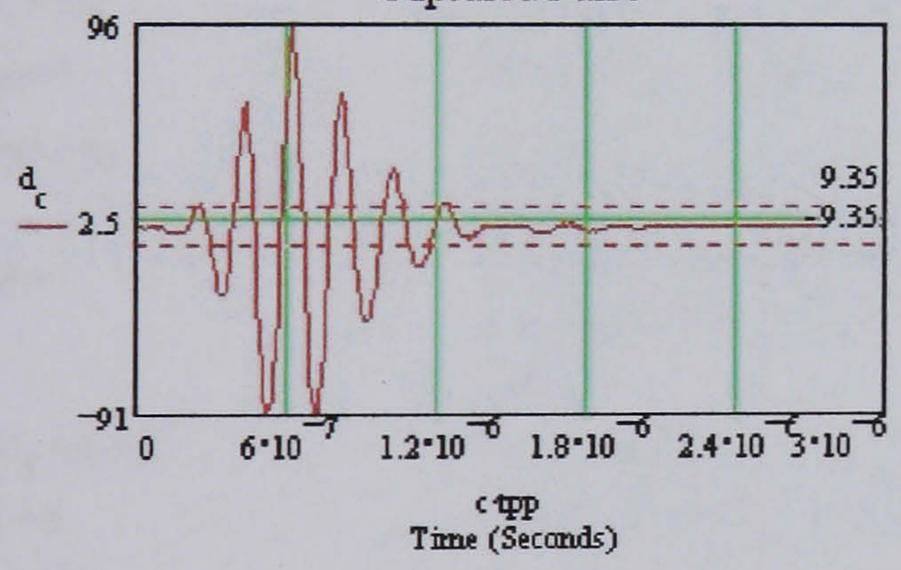

$pl := 2.47826\cdot10^{-7}$

$pu := 1.26522\cdot10^{-6}$

Pulse length mesured at 10% of maximum deflection

$$Pd := \frac{pu - pl}{1\cdot10^{-6}} \qquad Pd = 1.017$$

Enter probe data $Za := 15$ $\delta := 0$ $\beta := 70$

$Deff := 6.7$ $Dp := 10$ $N := 6$ $Nt := (N + Dp)$ $D := 10$

$Nt = 16$ $N = 6$

$Zel := 231$ $SN := 30.5$ $Damping := 50$ $\phi := -2$ $V := 69.5$ $TX := 40$

$$FD_6 := \frac{Nt\cdot3.250}{Fc\cdot Deff} \qquad DivAng_6 := \operatorname{asin}\left[0.51\cdot\left(\frac{Lamda}{Deff}\right)\right]\cdot\frac{180}{\pi} \qquad DivAng_{20} := \operatorname{asin}\left[0.87\cdot\left(\frac{Lamda}{Deff}\right)\right]\cdot\frac{180}{\pi}$$

$DivAng_6 = 2.772$ $DivAng_{20} = 4.732$

$FD_6 = 1.517$

Prototype Probe Evaluation Program
Results Page

Master Scan 330

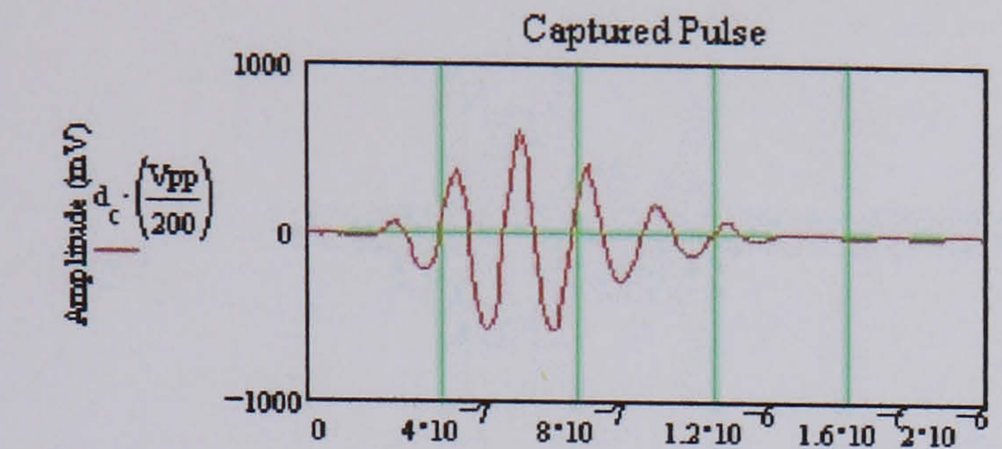

Captured using MS330 1MHz narrow band setting.

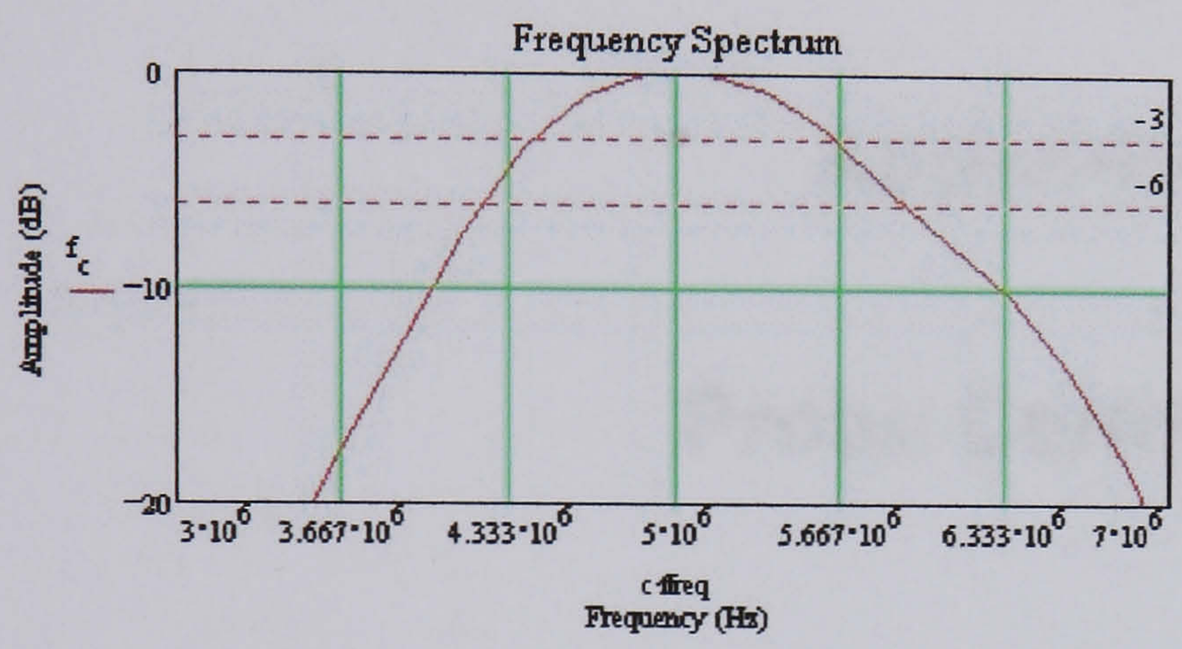

$\beta = 70$	The angle between the main beam and the normal to the test surface (+/- 2 Degrees)
Fc = 5.1	Centre Frequency +/-10% (MHz)
Fp = 5	Peak frequency (MHz)
BW = 33	The range of frequencies in the echo pulse whose amplitude, at the most, is 6 dB less than the centre frequency (%)
Pd = 1	Pulse duration, the time interval over which the modulus of the unrectified pulse amplitude exceeds 10% of its maximum amplitude (μs)
$FD_6 = 1.517$	Focal diameter of the beam to a 6 dB drop (mm)
N = 6	Near field length - excluding delay path (+/-1.3mm)
Dp = 10	Delay path (+/-1mm)
D = 10	Diameter of crystal (mm)
Deff = 6.7	Effective diameter of crystal (+/-0.2mm)
$DivAng_6 = 2.772$ $DivAng_{20} = 4.732$	Divergence angle of beam for a 6 and 20 dB drop (Degrees)
$\delta = 0$	Angle of squint (+/- 1.5 Degrees)
Za = 15	Index point (+2/-1mm)
Zel = 231	Electrical impedance at Peak Frequency (Ω)
$\phi = -2$	Phase angle at Peak Frequency (Degrees)
SN = 30.5	Signal to noise ratio - narrow band (dB)
V = 69.5	Gain reserve - narrow band (dB)
Damping = 50	Damping setting of MS330 (Ω)
TX = 40	Transmitter width of MS330 (ns)

Appendix D

Probe Certificates

TRANSDUCER CERTIFICATE

- *Sound Solutions* -

Date stamp

TMP3 TEST

Type of probe	Single Compression
Serial number	127/04
Frequency ± 10% (MHz)	10
Crystal shape	Circular
Crystal size (mm)	6
Crystal material	Lead Metaniobate
Probe dimensions (mm)	Ø13x22
Probe weight (g)	9
Connector type	Microdot
Connector position	Side
Wear face material	Rexolite

Signal Waveform

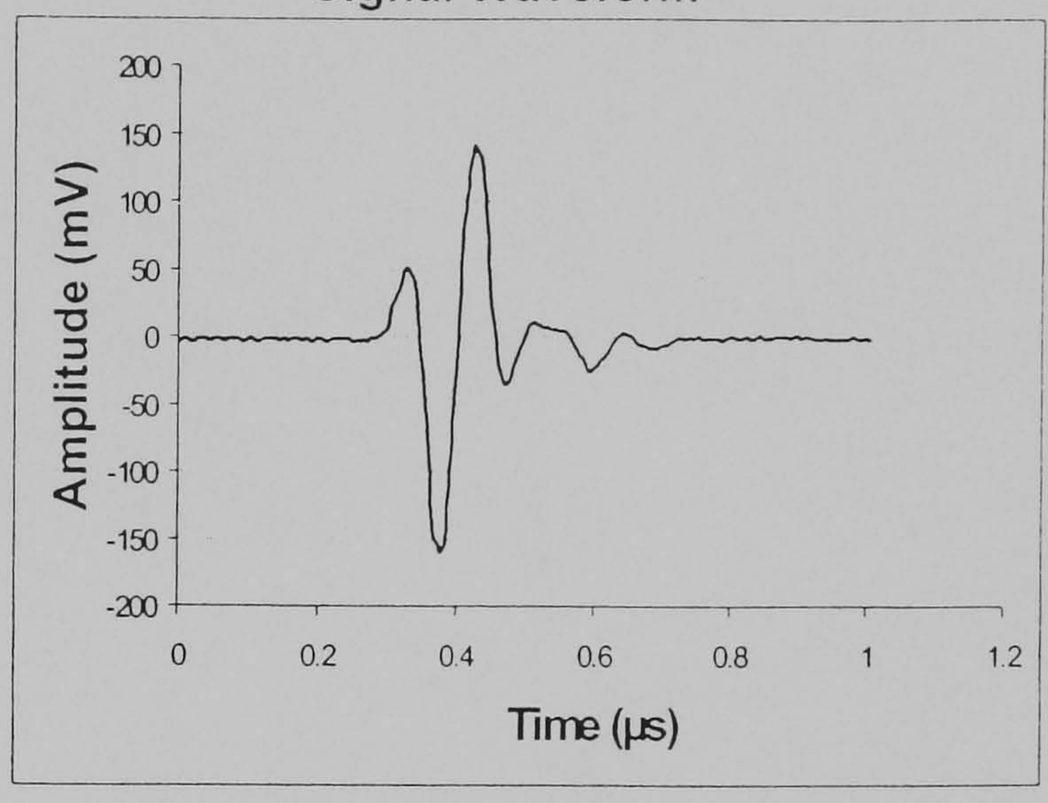

Frequency Spectrum

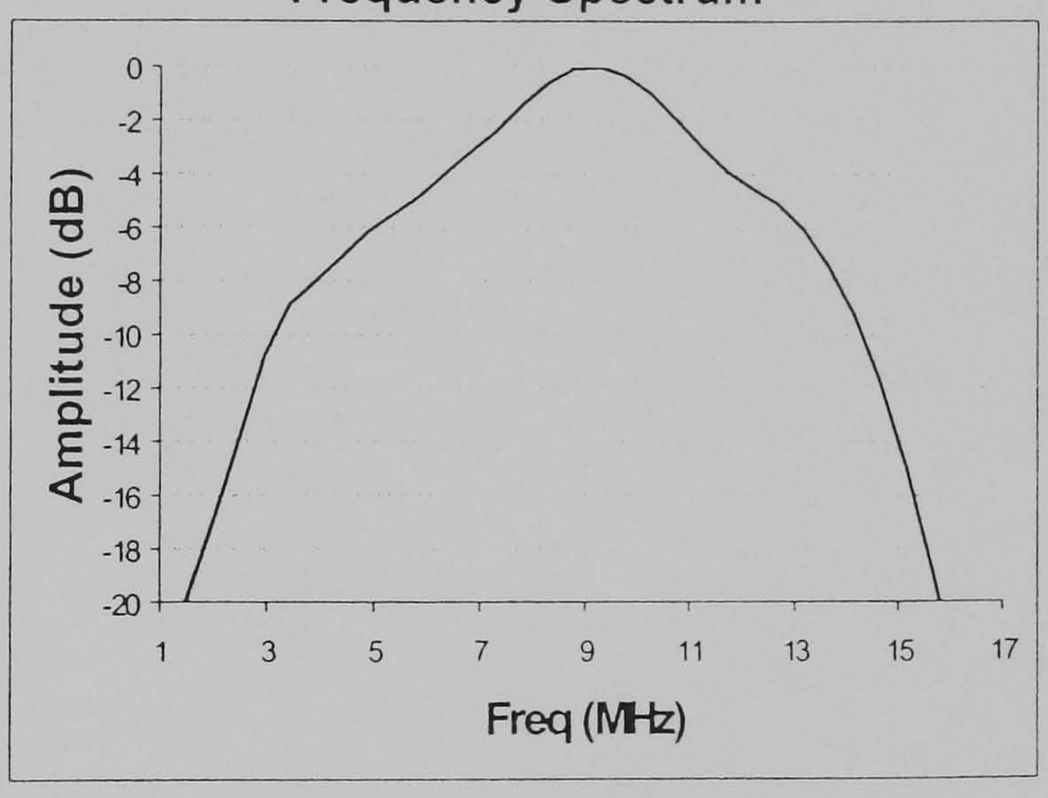

Test Results

Peak frequency	9.28 MHz	**Pulse duration**	0.31 µs	**-6dB upper**	13.14 MHz
Centre frequency	8.09 MHz	**Peak to peak voltage**	300.8 mV	**-6dB lower**	4.98 MHz
Near field length	13.9 mm			**Bandwidth**	8.17 MHz

Test Conditions

Instrument used	Masterscan 330
Pulse width	110 ns
Pulse impedance	50 Ohms
Inspector name	Simon Bourne

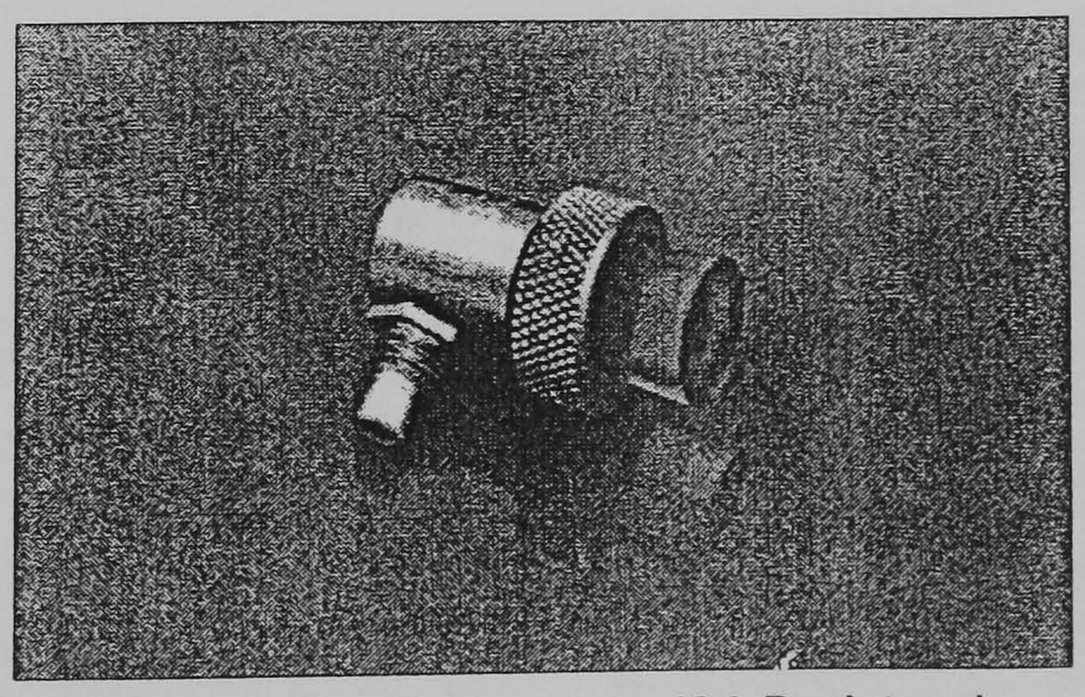

INVESTOR IN PEOPLE

Dickens Road, Old Wolverton, Milton Keynes, MK12 5QQ, England.

Registered in England No. 1961000

ISO Registered

Certificate No. Q5056

Tel: + 44 (0) 1908 316345 **Web: www.sonatest-plc.com** **Fax: + 44 (0) 1908 321323**

TRANSDUCER CERTIFICATE

- *Sound Solutions* -

Date stamp

SLP10-10 TEST

Type of probe	Single Compression
Serial number	PhD
Frequency ± 10% (MHz)	10
Crystal shape	Circular
Crystal size (mm)	10
Crystal material	Lead Metaniobate
Probe dimensions (mm)	Ø17x15
Probe weight (g)	20
Connector type	Subvis
Connector position	Side
Wear face material	N/A

Signal Waveform

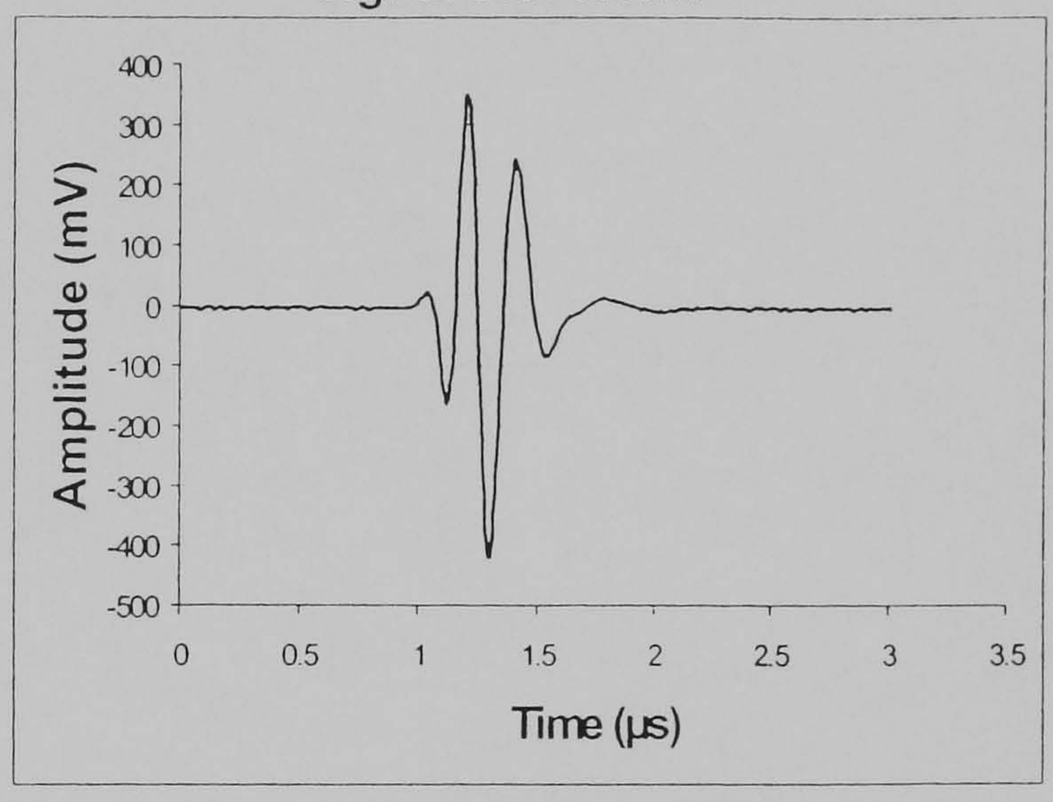

Frequency Spectrum

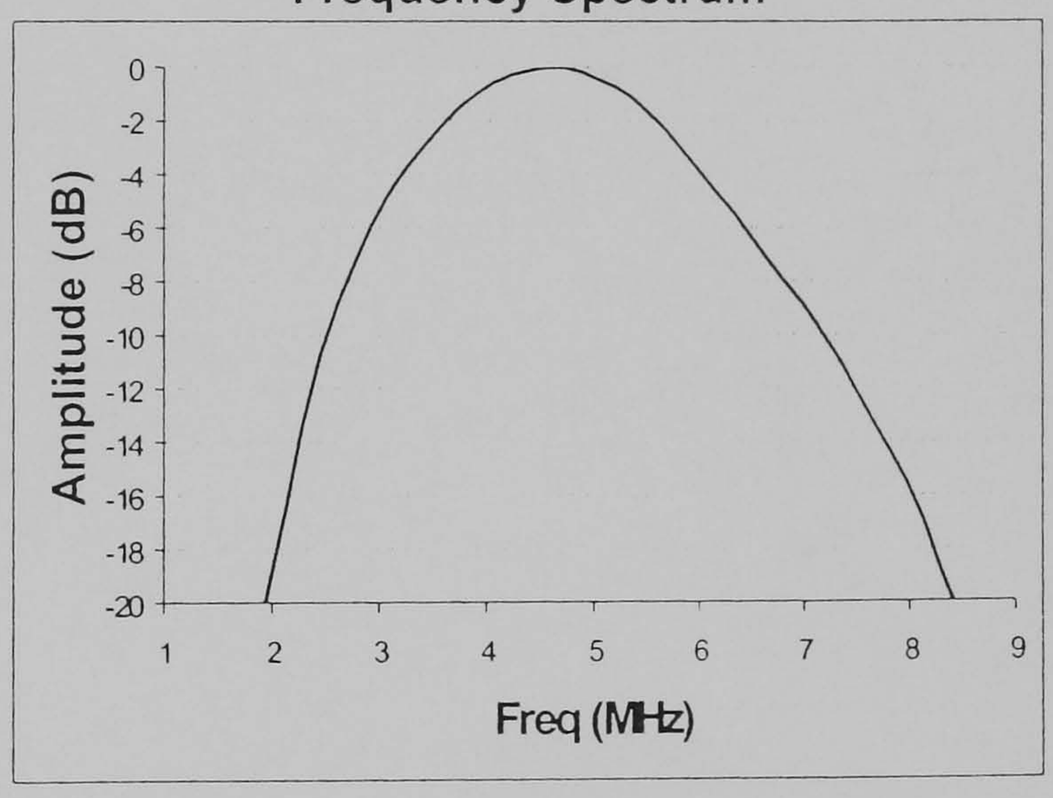

Test Results

Peak frequency	4.72 MHz	Pulse duration	0.53 µs	-6dB upper	6.44 MHz
Centre frequency	4.34 MHz	Peak to peak voltage	769.9 mV	-6dB lower	2.92 MHz
Near field length	19.6 mm			Bandwidth	3.52 MHz

Test Conditions

Instrument used	Masterscan 330
Pulse width	100 ns
Pulse impedance	400 Ohms
Inspector name	Simon Bourne

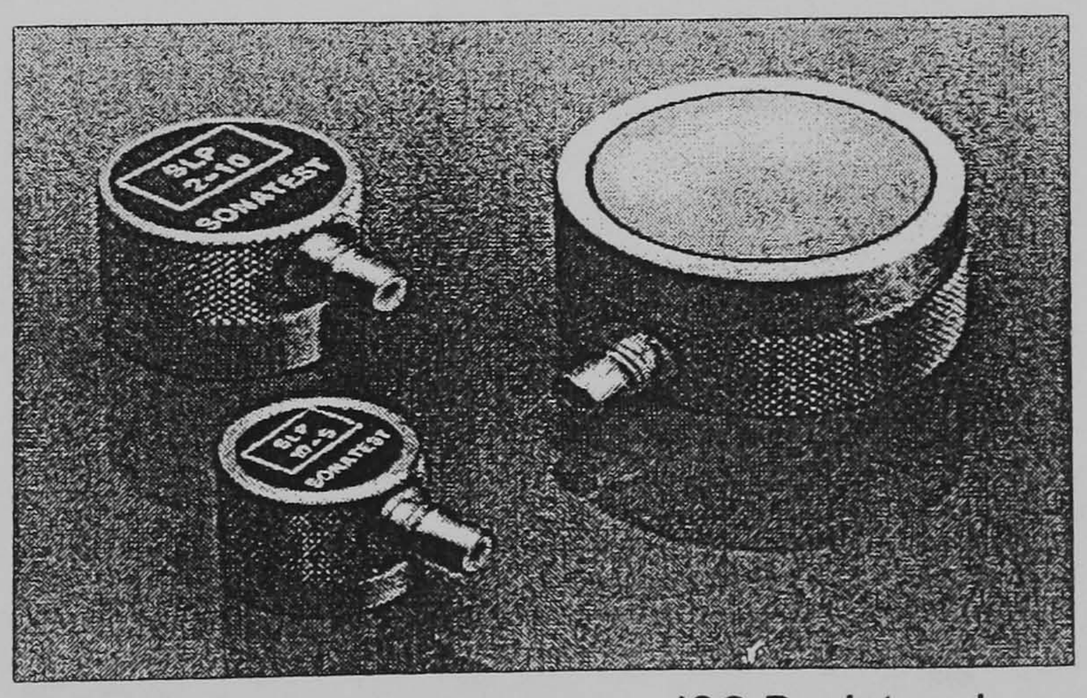

INVESTOR IN PEOPLE

Dickens Road, Old Wolverton, Milton Keynes, MK12 5QQ, England.

Registered in England No. 1961000

ISO Registered

Certificate No. Q5056

Tel: + 44 (0) 1908 316345 Web: www.sonatest-plc.com Fax: + 44 (0) 1908 321323

TRANSDUCER CERTIFICATE

- *Sound Solutions* -

Date stamp

SLP10-10

Type of probe	Single Compression
Serial number	PhD
Frequency ± 10% (MHz)	9
Crystal shape	Circular
Crystal size (mm)	10
Crystal material	Lead Metaniobate
Probe dimensions (mm)	Ø17x15
Probe weight (g)	20
Connector type	Subvis
Connector position	Side
Wear face material	N/A

Signal Waveform

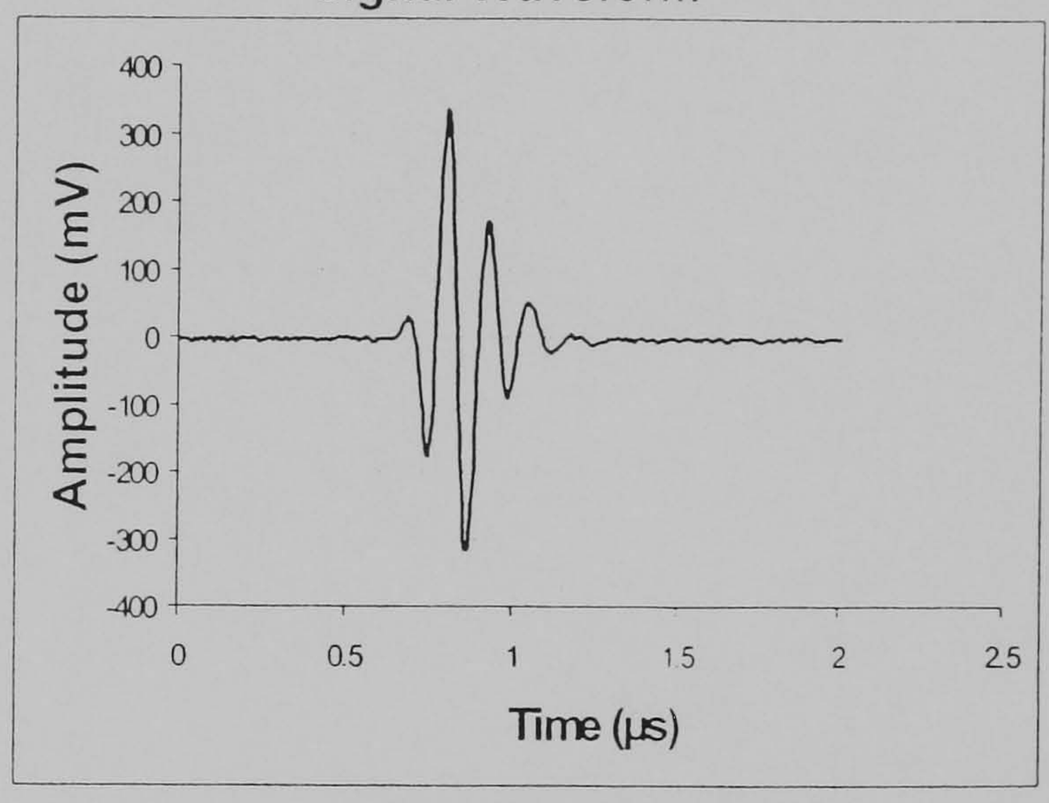

Frequency Spectrum

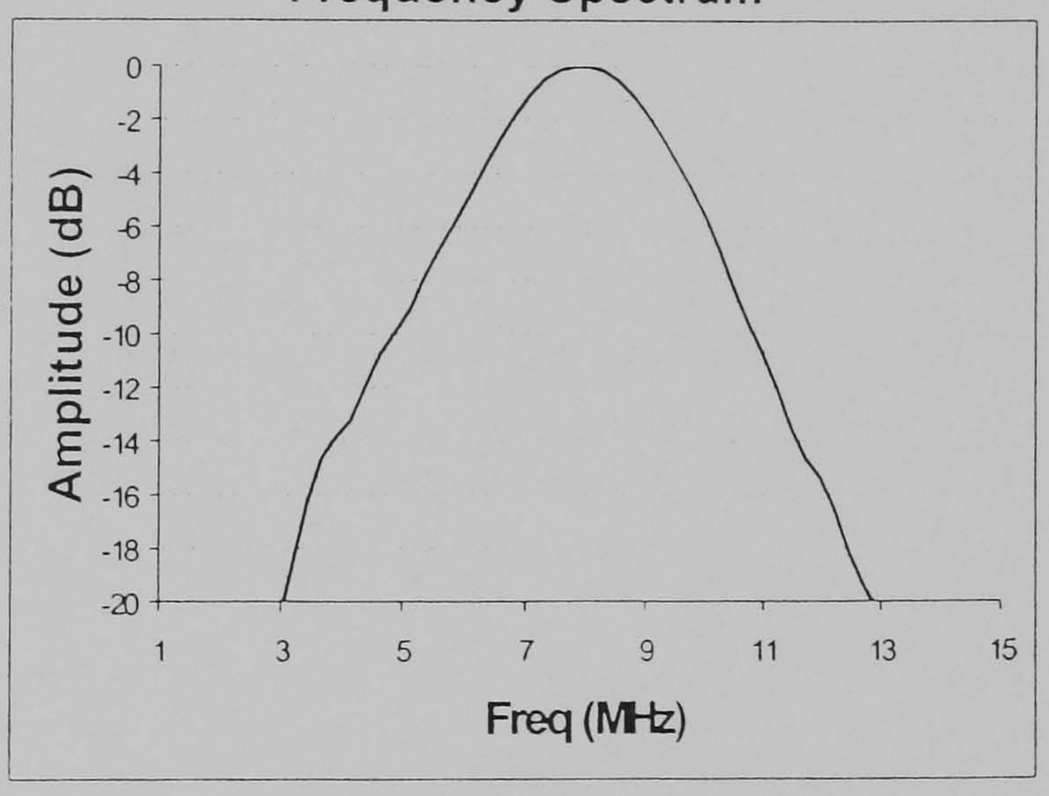

Test Results

Peak frequency	8.06 MHz	**Pulse duration**	0.35 µs	**-6dB upper**	10.09 MHz
Centre frequency	7.66 MHz	**Peak to peak voltage**	651.8 mV	**-6dB lower**	5.81 MHz
Near field length	33.8 mm			**Bandwidth**	4.28 MHz

Test Conditions

Instrument used	Masterscan 330
Pulse width	50 ns
Pulse impedance	400 Ohms
Inspector name	Simon Bourne

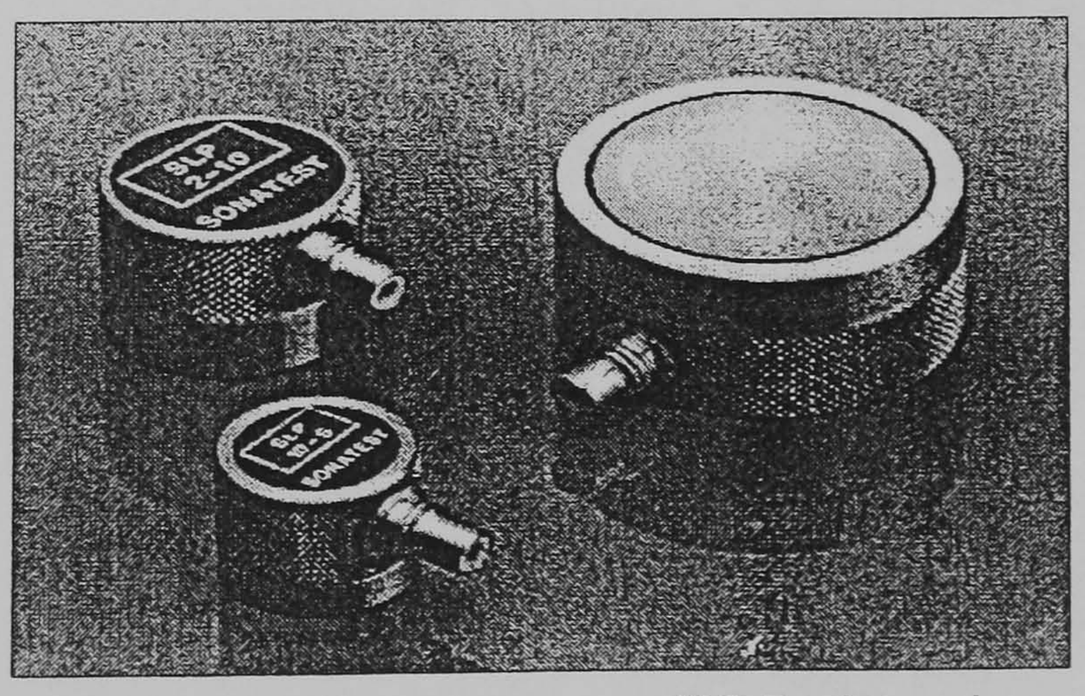

INVESTOR IN PEOPLE

Dickens Road, Old Wolverton, Milton Keynes, MK12 5QQ, England.

Registered in England No. 1961000

ISO Registered

Certificate No. Q5056

Tel: + 44 (0) 1908 316345 **Web: www.sonatest-plc.com** **Fax: + 44 (0) 1908 321323**

TRANSDUCER CERTIFICATE

- *Sound Solutions* -

Date stamp

ZS5-10

Type of probe	Zero Degrees Shear
Serial number	06/03/2001
Frequency ± 10% (MHz)	5
Beam angle ± N/A (°)	N/A
Crystal shape	Circular
Crystal size (mm)	10
Crystal material	N/A
Probe dimensions (mm)	Ø
Probe weight (g)	65
Connector type	Flying Lead
Connector position	N/A
TR Interchangable	N/A
Wedge/delay material	N/A
Focal type	N/A
Focal lengtht (mm)	N/A
Index point	N/A

Signal Waveform

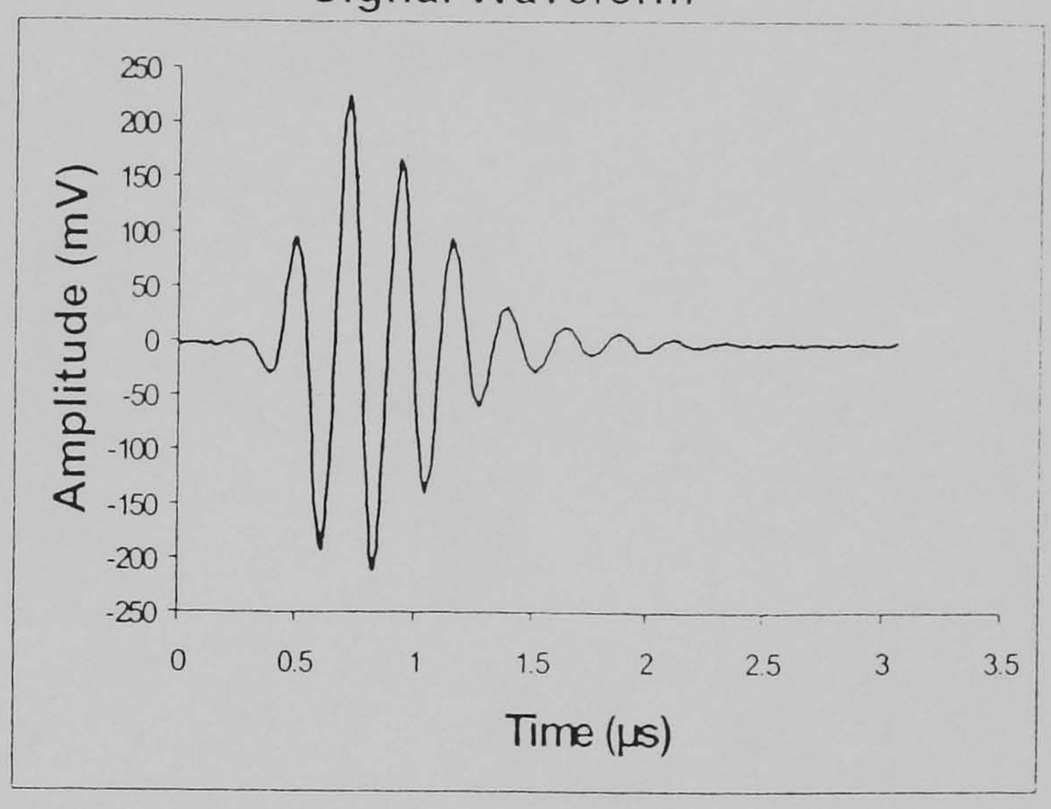

Frequency Spectrum

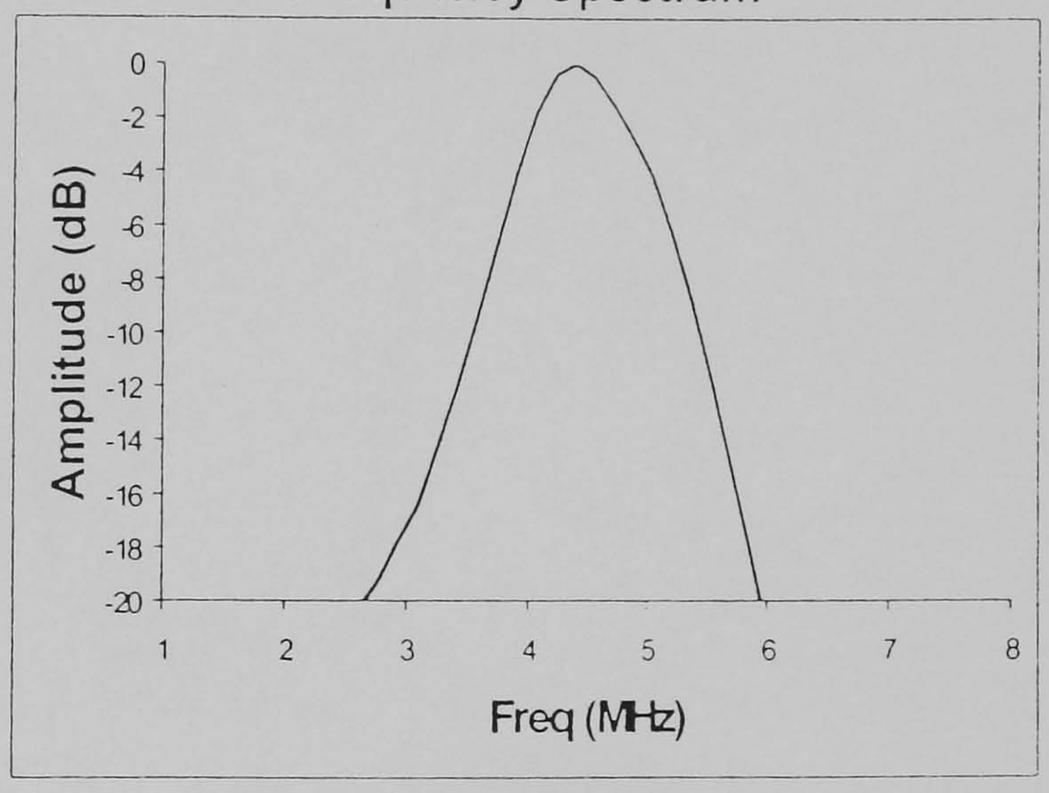

Test Results

Peak frequency	4.39 MHz	Pulse duration	1.18 µs	-6dB upper	5.20 MHz
Centre frequency	4.44 MHz	Peak to peak voltage	437 mV	-6dB lower	3.79 MHz
Near field length	33.8 mm	Angle	N/A	Bandwidth	1.41 MHz

Test Conditions

Instrument used	Masterscan 330
Pulse width	100 ns
Pulse impedance	400 Ohms
Inspector name	David Waller

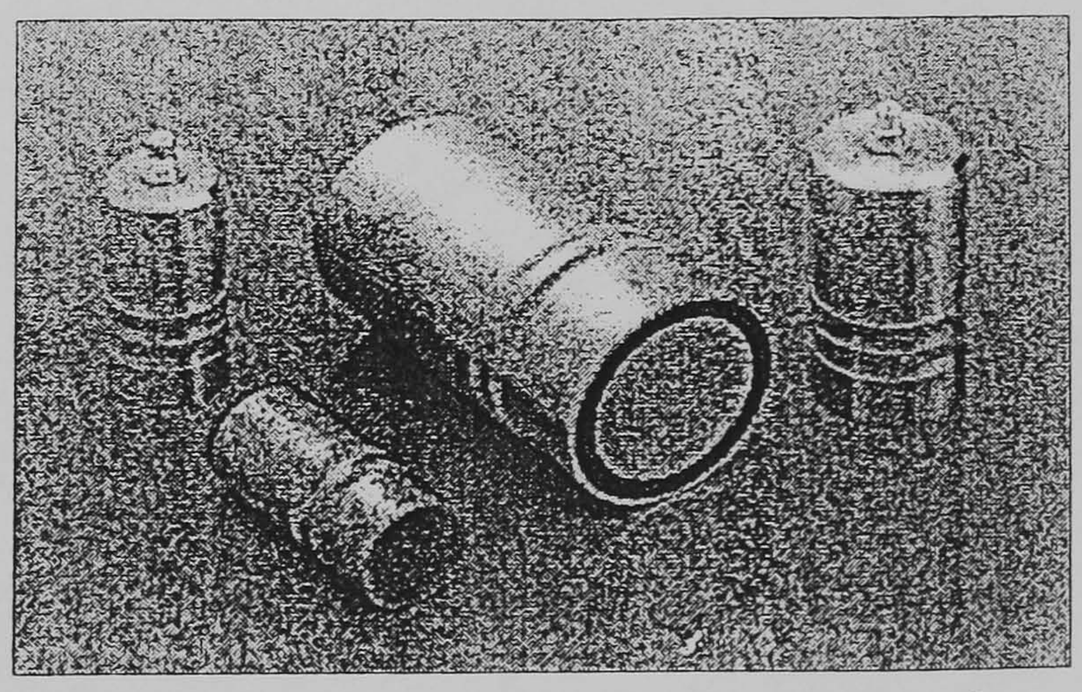

ISO Registered

Dickens Road, Old Wolverton, Milton Keynes, MK12 5QQ, England.

Registered in England No. 1961000

Certificate No. Q5056

INVESTOR IN PEOPLE

Tel: + 44 (0) 1908 316345 Web: www.sonatest-plc.com Fax: + 44 (0) 1908 321323

TRANSDUCER CERTIFICATE

- *Sound Solutions* -

Date stamp

HP5-10

Type of probe	Roller Probe
Serial number	108/01
Frequency ± 10% (MHz)	5
Beam angle ± N/A (°)	N/A
Crystal shape	Circular
Crystal size (mm)	10
Crystal material	Lead Metaniobate
Probe dimensions (mm)	Ø67x85
Probe weight (g)	880
Connector type	BNC
Connector position	Side
TR Interchangable	N/A
Wedge/delay material	Hydrophilic Polymer
Focal type	N/A
Focal lengtht (mm)	N/A
Index point	N/A

Signal Waveform

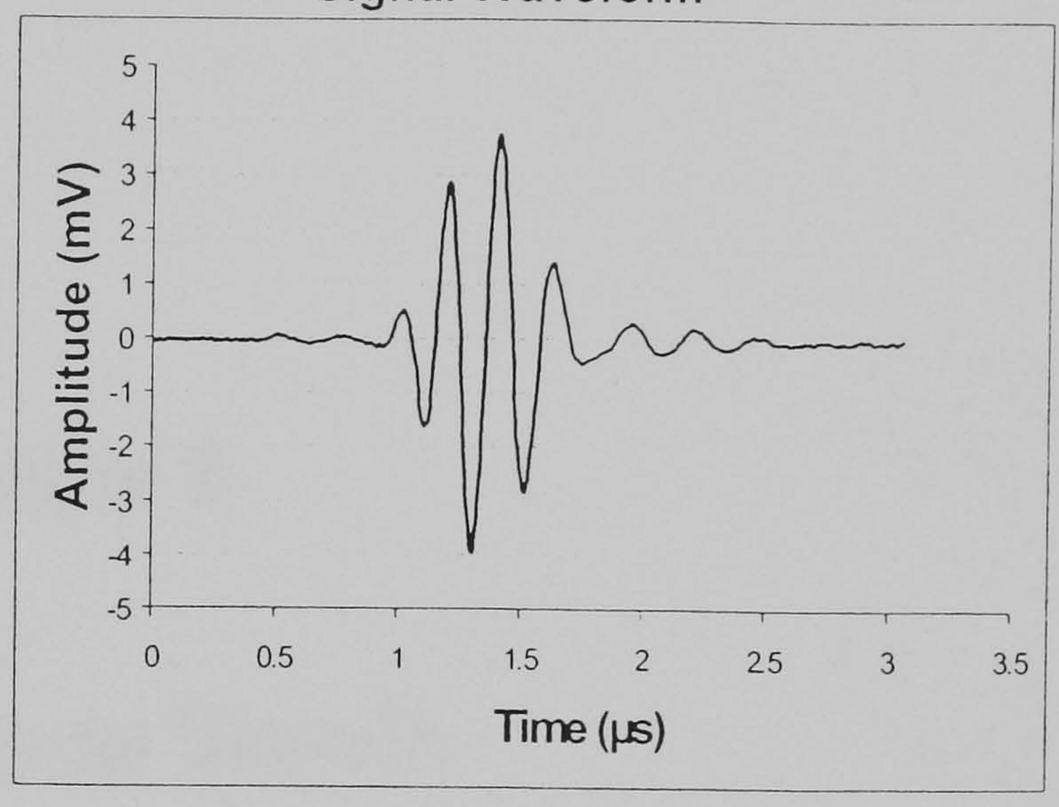

Frequency Spectrum

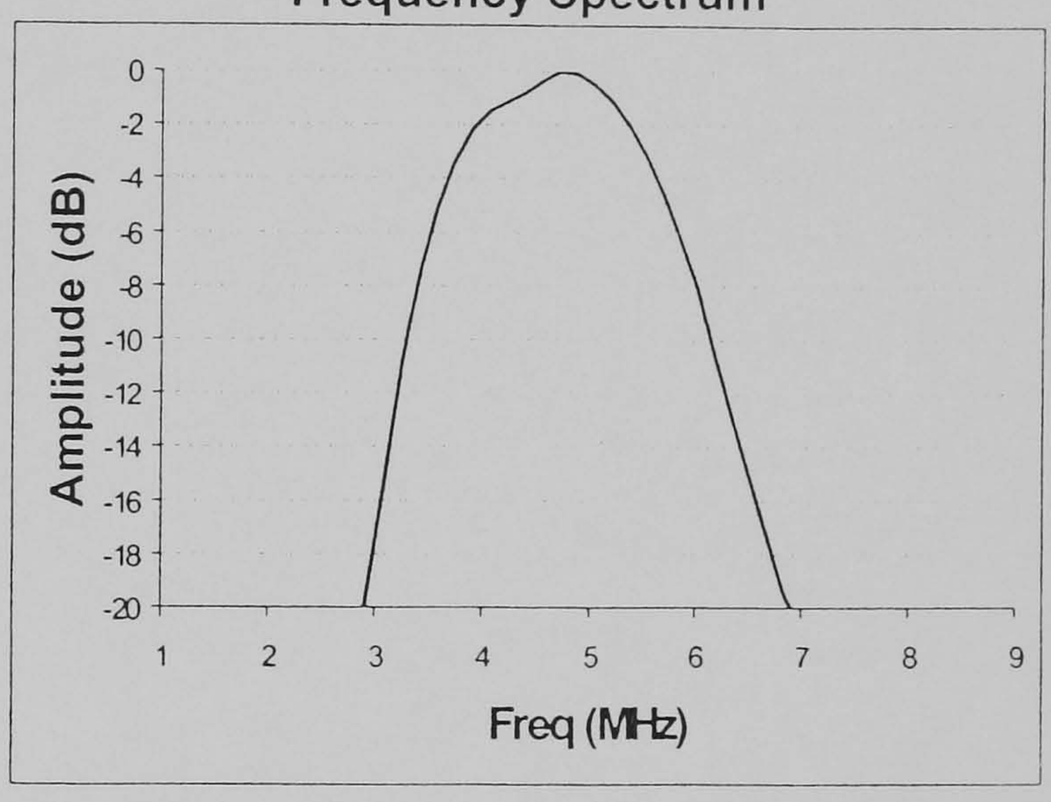

Test Results

Peak frequency	4.72 MHz	**Pulse duration**	0.77 µs	**-6dB upper**	5.84 MHz
Centre frequency	4.53 MHz	**Peak to peak voltage**	8 mV	**-6dB lower**	3.52 MHz
Near field length	19.6 mm	**Angle**	N/A	**Bandwidth**	2.33 MHz

Test Conditions

Instrument used	Masterscan 330
Pulse width	100 ns
Pulse impedance	50 Ohms
Inspector name	Simon Bourne

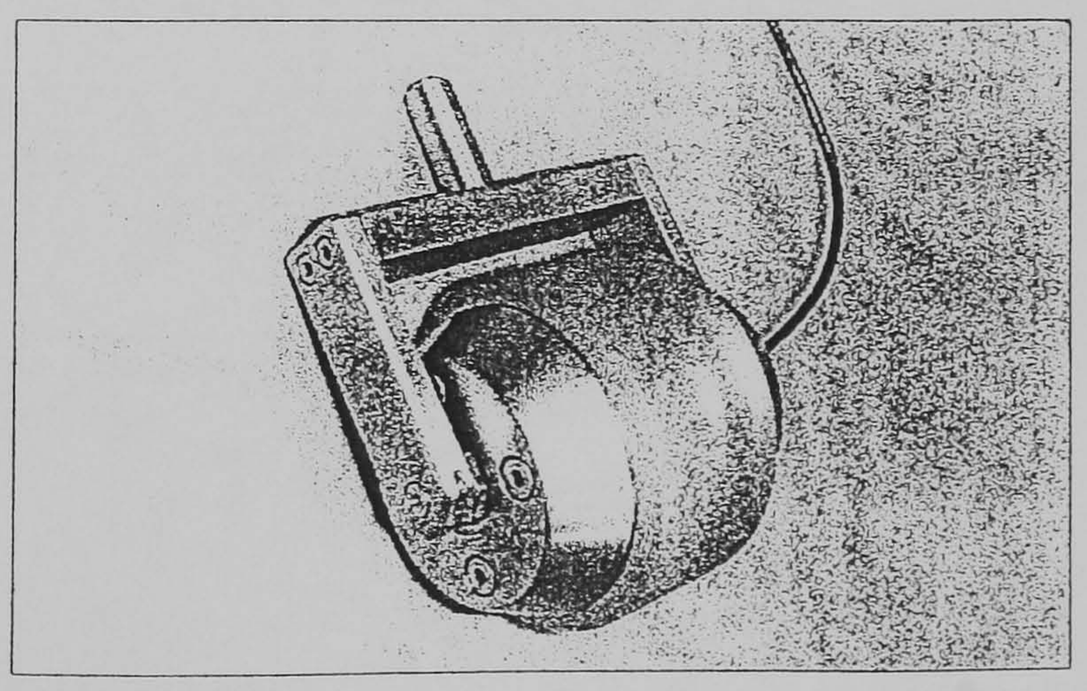

INVESTOR IN PEOPLE

Dickens Road, Old Wolverton, Milton Keynes, MK12 5QQ, England.

Registered in England No. 1961000

ISO Registered

Certificate No. Q5056

Tel: + 44 (0) 1908 316345 Web: www.sonatest-plc.com Fax: + 44 (0) 1908 321323

Appendix E

Couplant Data Sheets

- *Sound Solutions* -

)ATA SHEET

SONAGEL O

JLTRASONIC COUPLANT

APPEARANCE:	Orange Gel
DENSITY @ 20°C:	0.94 grams/cc
FLASH POINT (PM):	175°C
PH VALUE:	N/A
SOLUBILITY:	Insoluble in water. Soluble in solvents.
SULPHUR:	<50 P.P.M.
HALOGENS:	<50 P.P.M
CORROSION:	Non-corrosive to most metals
TEMPERATURE RANGE:	-10°C to 160°C
REMOVABILITY:	Water, alcohol or similar solvent

onagel O is a stable semi-transparent orange gel specifically designed for ultrasonic inspection and it is non-
xic and safe for the environment. It is intended as a replacement for mineral oils and greases; and it retains its
el state without causing corrosion or drying on the test surface.

his product is designed for use on all types of metallic surface and is especially suited to solving the problems
rough, pitted, uneven surfaces allowing smooth probe movement during testing. The thixotropic properties of
is couplant give excellent wetting and acoustic transmission and do not allow the product to flow all over the
st area. This makes it very economical to use as you only cover the working area not the whole piece, and is
specially suitable for vertical and overhead surfaces.

onagel O incorporates chemicals which allow very slow drying even at elevated temperatures, whilst being free
VOC's and other hazardous materials. However, it does contain a special tracer dye to enable areas to be
ecked for coverage but the couplant is still easily removed with gentle water washing or solvent wipes.

onagel O is available in easy to use 125 mls applicator bottles as well as in plastic 1 litre and 25 litre bulk
ntainers (both with suitable carrying handles).

onatest Plc
ckens Road
lton Keynes
K12 5QQ
l: +44(0)1908 316345
x: +44(0)1908 321323
nail: sales@sonatest-plc.com

- *Sound Solutions* -

DATA SHEET

SONAGEL W

ULTRASONIC COUPLANT

APPEARANCE:	Bright Yellow Gel
DENSITY @ 20°C:	1.06 grams/cc
FLASH POINT (PM):	Non-flammable*
PH VALUE:	7.5 – 8.5
SOLUBILITY:	Water Soluble
SULPHUR:	<50 P.P.M.
HALOGENS:	<50 P.P.M
CORROSION:	Non-corrosive to most metals
TEMPERATURE RANGE:	-10°C to 60°C
REMOVABILITY:	Water, alcohol or similar solvent

*NB: This product will have a flash point of 160°C(PM) when used for long periods at elevated temperatures.

Sonagel W is a stable clear yellow gel specifically designed for ultrasonic inspection and it is non-toxic and safe for the environment.

This product is designed for use on all types of metallic surface and is especially suited to solving the problems of rough, pitted, uneven surfaces allowing smooth probe movement during testing. The thixotropic properties of this couplant give excellent wetting and acoustic transmission and do not allow the product to flow all over the test area. This makes it very economical to use as you only cover the working area not the whole piece.

Sonagel W incorporates chemicals which allow very slow drying even at elevated temperatures, whilst being free of VOC's and other hazardous materials. However, it does contain a special tracer dye to enable areas to be checked for coverage but the couplant is still easily removed with water or solvent wipes. A full safety data sheet is available upon request.

Sonagel W is available in easy to use 125 mls applicator bottles, 250 mls bottles, as well as in plastic 1 litre, 5 litre and 25 litre bulk containers (with suitable carrying handles).

Oil based Sonagel-0 and high temperature Sonagel-HT are also available as standard. Other couplants may also be supplied upon request.

Sonatest Plc
Dickens Road
Milton Keynes
MK12 5QQ
Tel: +44(0)1908 316345
Fax: +44(0)1908 321323
e-mail: sales@sonatest-plc.com